



HAL
open science

Contribution to the study of combustion instabilities in cryotechnic rocket engines : coupling diffuse interface models with kinetic-based moment methods for primary atomization simulations

Pierre Cordesse

► To cite this version:

Pierre Cordesse. Contribution to the study of combustion instabilities in cryotechnic rocket engines : coupling diffuse interface models with kinetic-based moment methods for primary atomization simulations. Mathematical Physics [math-ph]. Université Paris-Saclay, 2020. English. NNT : 2020UP-ASC016 . tel-02948195

HAL Id: tel-02948195

<https://theses.hal.science/tel-02948195v1>

Submitted on 24 Sep 2020

HAL is a multi-disciplinary open access archive for the deposit and dissemination of scientific research documents, whether they are published or not. The documents may come from teaching and research institutions in France or abroad, or from public or private research centers.

L'archive ouverte pluridisciplinaire **HAL**, est destinée au dépôt et à la diffusion de documents scientifiques de niveau recherche, publiés ou non, émanant des établissements d'enseignement et de recherche français ou étrangers, des laboratoires publics ou privés.

Contribution to the study of combustion
instabilities in cryotechnic rocket engines:
coupling diffuse interface models with
kinetic-based moment methods for primary
atomization simulation

Thèse de doctorat de l'université Paris-Saclay

École doctorale n°574, mathématiques Hadamard (EDMH)
Spécialité de doctorat: Mathématiques appliquées
Unité de recherche: École Polytechnique, Centre de Mathématiques Appliquées,
91128, Palaiseau, France
Réfèrent: CentraleSupélec

Thèse présentée et soutenue à Palaiseau, le 23 juin 2020, par

Pierre CORDESSE

Composition du Jury

Pauline LAFITTE Professeur, MICS, CentraleSupélec	Présidente
Nicolas SEGUIN Professeur, IRMAR, Université de Rennes	Rapporteur & Examineur
Gretar TRYGGVASON Professeur, Johns Hopkins University	Rapporteur & Examineur
Grégoire ALLAIRE Professeur, CMAP, École polytechnique	Examineur
Sergey GAVRILYUK Professeur, IUSTI, Université Aix-Marseille	Examineur
Marica PELANTI Professeur assistante, IMSIA, ENSTA	Examinatrice
Marc MASSOT Professeur, CMAP, École polytechnique	Directeur de thèse
Angelo MURRONE Ingénieur, ONERA	Encadrant
Didier BRESCH Directeur de recherche, LAMA, Université Savoie Mont Blanc	Invité
Marie THERON Ingénieur, CNES	Invitée

Titre : Contribution à l'étude des instabilités de combustion dans les moteurs cryotechniques : couplage entre modèles à interface diffuses et modèles cinétiques pour la simulation de l'atomisation

Mots clés : Modèles diphasiques d'ordre réduit, thermodynamique multi-fluide, dynamique à deux échelles de l'interface, calcul variationnel, solveurs de Riemann approchés, simulations numériques

Résumé : Gardiens de l'espace, les lanceurs sont soumis à des améliorations intenses et compétitives, par le biais de campagnes de tests expérimentaux et numériques. Les simulations numériques prédictives sont devenues obligatoires pour améliorer notre compréhension de la physique. Ajustables, elles se prêtent parfaitement à la conception et l'optimisation, en particulier de la chambre de combustion, pour garantir la sûreté et maximiser l'efficacité. L'un des principaux phénomènes physiques impliqués dans la combustion du combustible et de l'oxydant est l'atomisation du jet, qui pilote à la fois les distributions de gouttelettes et les instabilités potentielles à haute fréquence dans des conditions sous-critiques. Elle englobe un large spectre de topologies d'écoulement diphasiques, des phases séparées à la phase dispersée, avec une région mixte où la physique et la topologie de l'écoulement à petite échelle sont très complexes. Les modèles d'ordre réduit sont de bons candidats pour réaliser des simulations prédictives et relativement peu coûteuses en ressource de calcul sur des configurations industrielles. Cependant, jusqu'à présent ils ne décrivent correctement que la dynamique des grandes échelles et doivent donc être couplés à des modèles de phase dispersée nécessitant un réglage minutieux de paramètres pour prédire la formation du spray. Afin de décrire à la fois les régions mixte et dispersée, l'amélioration de la hiérarchie de modèles d'ordre réduit repose sur quelques principes clefs au cœur de la thèse ci-présente et fournit des problèmes interdisciplinaires faisant appel tant à l'analyse mathématique et la modélisation physique de ces systèmes d'EDP qu'à leur discrétisation numérique et leur implémentation dans des codes de CFD à des fins industriels.

Grâce d'une part à l'extension de la théorie des équations de conservation supplémentaires à des systèmes impliquant des termes non-conservatifs et d'autre part à un formalisme de thermodynamique multi-fluide tenant compte des effets non-idéaux, nous proposons de nouvelles pistes pour définir une entropie de mélange strictement convexe et consistante avec le système d'équation et les lois de pression, dans le but de permettre la symétrisation entropique des modèles diphasiques, de prouver leur hyperbolicité et d'obtenir des termes sources généraux. De plus, en rompant avec la vision géométrique de l'interface, nous proposons une description multi-échelle de l'interface pour décrire un mélange multi-fluide comportant une dynamique interfaciale complexe. Le Principe de Moindre Action a permis de dériver un modèle bifluide à une vitesse couplant grandes et petites échelles de l'écoulement. Nous avons ensuite développé une stratégie de séparation d'opérateurs basée sur la discrétisation par Volumes Finis, et nous avons implémenté le nouveau modèle dans le logiciel industriel multiphysique de CFD, CEDRE, de l'ONERA afin d'évaluer numériquement ce dernier. Enfin, nous avons construit et analysé les fondations d'une hiérarchie de cas tests accessibles à la DNS tout en étant au plus proche de configurations industrielles, dans le but d'évaluer les résultats de simulations du nouveau modèle ou de tout autre modèle à venir.

Title : Contribution to the study of combustion instabilities in cryotechnic rocket engines: coupling diffuse interface models with kinetic-based moment methods for primary atomization simulations

Keywords : Reduced-order two-phase flow models, multi-fluid thermodynamics, dual-scale interface dynamics, variational calculus, approximate Riemann solvers, numerical simulations

Abstract : Gatekeepers to the open space, launchers are subject to intense and competitive enhancements, through experimental and numerical test campaigns. Predictive numerical simulations have become mandatory to increase our understanding of the physics. Adjustable, they provide early-stage optimization processes, in particular of the combustion chamber, to guarantee safety and maximize efficiency. One of the major physical phenomena involved in the combustion of the fuel and oxidizer is the jet atomization, which pilots both the droplet distributions and the potential high-frequency instabilities in subcritical conditions. It encompasses a large spectrum of two-phase flow topologies, from separated phases to disperse phase, with a *mixed region* where the small scale physics and topology of the flow are very complex. Reduced-order models are good candidates to perform predictive but low CPU demanding simulations on industrial configurations but have only been able so far to capture large scale dynamics and have to be coupled to disperse phase models through adjustable and weakly reliable parameters in order to predict spray formation. Improving the hierarchy of reduced order models in order to better describe both the mixed region and the disperse region requires a series of building blocks at the heart of the present work and gives on to complex problems in the mathematical analysis and physical modelling of these systems of PDE as well as their numerical discretization and implementation in CFD codes for industrial uses.

Thanks to the extension of the theory on supplementary conservative equations to system of non-conservation laws and the formalism of the multi-fluid thermodynamics accounting for non-ideal effects, we give some new leads to define a strictly convex mixture entropy consistent with the system of equations and the pressure laws, which would allow to recover the entropic symmetrization of two-phase flow models, prove their hyperbolicity and obtain generalized source terms. Furthermore, we have departed from a geometric approach of the interface and proposed a multi-scale rendering of the interface to describe multi-fluid flow with complex interface dynamics. The Stationary Action Principle has returned a single velocity two-phase flow model coupling large and small scales of the flow. We then have developed a splitting strategy based on a Finite Volume discretization and have implemented the new model in the industrial CFD software CEDRE of ONERA to proceed to a numerical verification. Finally, we have constituted and investigated a first building block of a hierarchy of test-cases designed to be amenable to DNS while close enough to industrial configurations in order to assess the simulation results of the new model but also to any up-coming models.

NNT : 2020UPASCo16

THÈSE DE DOCTORAT
DE L'UNIVERSITÉ PARIS-SACLAY

PRÉPARÉE À L'ÉCOLE POLYTECHNIQUE

ÉCOLE DOCTORALE N°574
ÉCOLE DOCTORALE DE MATHÉMATIQUES HADAMARD (EDMH, ED 574)
SPÉCIALITÉ DE DOCTORAT : MATHÉMATIQUES APPLIQUÉES

PAR

PIERRE CORDESSE

CONTRIBUTION TO THE STUDY OF COMBUSTION
INSTABILITIES IN CRYOTECHNIC ROCKET ENGINES: COUPLING
DIFFUSE INTERFACE MODELS WITH KINETIC-BASED MOMENT
METHODS FOR PRIMARY ATOMIZATION SIMULATIONS

Thèse présentée et soutenue à l'École polytechnique le 3 avril 2020.
Composition du Jury :

PAULINE LAFITTE	(Professeur, MICS, CentraleSupélec)	PRÉSIDENTE
NICOLAS SEGUIN	(Professeur, IRMAR, Université de Rennes)	RAPPORTEUR, EXAMINATEUR
GRETAR TRYGGVASON	(Professeur, Johns Hopkins University)	RAPPORTEUR, EXAMINATEUR
GRÉGOIRE ALLAIRE	(Professeur, CMAP, École polytechnique)	EXAMINATEUR
SERGEY GAVRILYUK	(Professeur, IUSTI, Université Aix-Marseille)	EXAMINATEUR
MARICA PELANTI	(Professeur assistant, IMSIA, ENSTA)	EXAMINATRICE
MARC MASSOT	(Professeur, CMAP, École polytechnique)	DIRECTEUR DE THÈSE
ANGELO MURRONE	(Ingénieur, ONERA)	ENCADRANT
DIDIER BRESCH	(Directeur de recherche, LAMA, Université Savoie Mont Blanc)	INVITÉ
MARIE THÉRON	(Ingénieur, CNES)	INVITÉE

REMERCIEMENTS

La thèse de doctorat fut avant tout une aventure scientifique et humaine d'une très grande intensité. Elle m'a demandé en effet d'aller puiser patience, persévérance et rigueur à tout instant. Chaque problème posé devient un projet obnubilant, auquel on ne se dérobe que lorsque l'on trouve une solution. Cette dernière n'est jamais évidente, elle sédimente lentement aux détours de conversation, dans le métro, autour d'un verre entre ami, voire parfois au milieu de la nuit. Espoirs, déceptions et jubilations, le quotidien du chercheur est rythmé par de puissants ascenseurs émotionnels, et je pense que c'est l'une des grandes qualités de ce métier.

Loin d'être une démarche individuelle, la recherche est synonyme de rencontres de personnes passionnées et inspirantes. Nombreuses furent-elles durant ma thèse, et les lignes ci-après témoigneront de ma reconnaissance.

Aussi, je tiens d'abord à remercier le jury de ma thèse et en particulier Nicolas Seguin et Gretar Tryggvason pour votre rapport approfondi et vos multiples questions à la soutenance, témoignant de votre intérêt pour mes travaux. Merci à Pauline Lafitte pour la présidence du jury. Merci à Marica Pelanti, Marie Théron, Grégoire Allaire, Didier Bresch et Sergey Gavrilyuk pour votre présence et nos échanges ce jour et à l'occasion de revues de projets ou conférences.

Ensuite, je souhaite remercier mon équipe encadrante, Marc, Angelo et toi aussi Samuel. Vous avez été pour moi une force d'inspiration, vous m'avez soutenu en tout temps et m'avez transmis votre goût profond de la recherche. Angelo, merci pour ta bienveillance et nos discussions. Samuel, merci pour toute ta pédagogie, tes relectures et ces innombrables calculs que nous avons fait ensemble sur un tableau à Mountain View ou sur le coin d'une petite table de café au Luxembourg ou à Alésia. Marc, merci de m'avoir proposé durant ma troisième année d'école de faire une thèse et d'avoir été aussi convaincant pour que j'ose relever le défi. Tu as toujours su m'insuffler la volonté d'aller plus loin, de me dépasser. Merci pour ton exigence en toutes circonstances, tu as toujours su placer la barre où il fallait. Merci aussi pour ta compréhension et ta sympathie, et pour toutes nos discussions dépassant largement les sujets de la thèse.

La multiplicité des institutions qui m'ont financé ou accueilli durant ce projet de thèse m'a permis de travailler dans un cadre très diversifié. L'ONERA à Châtillon et Palaiseau, l'EM2C à CentraleSupélec, le CMAP à l'École polytechnique, le CNES à Paris, l'EDMH et aussi la NASA Ames Research Center à Mountain View. Quelle chance d'avoir pu découvrir tous ces lieux ! Merci aux équipes administratives et informatiques régulièrement sollicitées qui m'ont permis de travailler dans de très bonnes conditions où que je sois.

À l'ONERA, je souhaite remercier mon co-bureau Adrien. Merci pour ton aide lors de mes

débuts, ta patience pour m'expliquer toutes tes astuces gnuplot et inkscape. Merci Nicolas pour ton humour, ta bonne humeur presque infaillible, ton soutien sur la dernière ligne droite et merci à ton cochon d'Inde d'avoir été le sujet de tant de blagues. Merci Bastien d'avoir toujours su solutionner mes casse-têtes mathématiques et pour ces nombreuses pauses sportives du midi qui ont toujours été l'occasion de partager un peu de nos vies. Merci Nicolas pour ta franchise, ton attention et ton inspirant record de la thèse la plus vite bouclée de tous les temps. Merci Clément pour tout ce que tu m'as appris, pour la confiance que tu m'as accordée et le courage que tu m'as apporté sur les six derniers mois lorsque nous bataillions ensemble pour construire MF5, 6, 7,..euh 12 ?! Merci Luc-Henry pour ta joie au quotidien et ton amour de la Nature. Merci Pascale pour toutes tes anecdotes et le goût que tu as réussi à m'insuffler pour le trail (pas qu'à moi j'en suis sûr). Merci Daniel pour tous nos échanges et ton partage d'expérience. Merci aussi à Lionel, Aymeric, Dominique, Lionel, Julien, Jean-Michel, Éric, Gilles, Antoine, Bernard, Alain, Philippe, François, Gérard, et tous les collègues du département.

Merci aussi à Ruben, Marc-Arthur et Quentin. Tous les quatre nous avons eu la chance de vivre des moments magiques, pleins de rires et des projets motivants ici, ou de l'autre côté de l'Atlantique. Merci aussi Alberto, Léa et mes co-bureaux du CMAP.

Au delà des travaux scientifiques de la thèse, j'ai eu la chance de découvrir diverses associations de l'industrie aéronautique et spatiale, en particulier ONERA Alumni et la 3AF, offrant un cadre propice à une implication bénévole. Bruno et Gérard merci pour votre confiance et tout ce que vous avez à coeur de transmettre *aux jeunes* comme vous dites. Les projets intergénérationnels que nous avons entrepris ont été fortement épanouissants, je vous en remercie.

Merci aussi à tous mes amis qui ont suivi de près ou de loin cette aventure. Merci Francine, Alex, Igor et Thomas. Merci à la coloc, Sophie, Christian, Thomas, Bob et Quentin. Merci Jérôme, Arnaud, Florian, Gaëtan, Valentin, la promo S&M8, Grégoire, Fany et Flo. Merci aussi à toute ma famille pour votre soutien et votre écoute. Merci Anne d'avoir pu particulièrement échanger sur nos péripéties de publications. Merci Estelle pour ta patience, ton intérêt pour mes travaux et ton soutien infaillible, qui m'ont été plus d'une fois salutaires.

ABSTRACT

Gatekeepers to the open space, launchers are subject to intense and competitive enhancements, through experimental and numerical test campaigns. Predictive numerical simulations have become mandatory to increase our understanding of the physics. Adjustable, they provide early-stage optimization processes, in particular of the combustion chamber, to guarantee safety and maximize efficiency. One of the major physical phenomena involved in the combustion of the fuel and oxidizer is the jet atomization, which pilotes both the droplet distributions and the potential high-frequency instabilities in subcritical conditions. It encompasses a large spectrum of two-phase flow topologies, from separated phases to disperse phase, with a *mixed region* where the small scale physics and topology of the flow are very complex. Reduced-order models are good candidates to perform predictive but low CPU demanding simulations on industrial configurations but have only been able so far to capture large scale dynamics and have to be coupled to disperse phase models through adjustable and weakly reliable parameters in order to predict spray formation.

Improving the hierarchy of reduced order models in order to better describe both the mixed region and the disperse region requires a series of building blocks at the heart of the present work and gives on to complex problems in the mathematical analysis and physical modelling of these systems of PDE as well as their numerical discretization and implementation in CFD codes for industrial uses.

Thanks to the extension of the theory on supplementary conservative equations to system of non-conservation laws and the formalism of the multi-fluid thermodynamics accounting for non-ideal effects, we give some new leads to define a strictly convex mixture entropy consistent with the system of equations and the pressure laws, which would allow to recover the entropic symmetrization of two-phase flow models, prove their hyperbolicity and obtain generalized source terms.

Furthermore, we have departed from a geometric approach of the interface and proposed a multi-scale rendering of the interface to describe multi-fluid flow with complex interface dynamics. The Stationary Action Principle has returned a single velocity two-phase flow model coupling large and small scales of the flow. We then have developed a splitting strategy based on a Finite Volume discretization and have implemented the new model in the industrial CFD software CEDRE of ONERA to proceed to a numerical verification.

Finally, we have constituted and investigated a first building block of a hierarchy of test-cases designed to be amenable to DNS while close enough to industrial configurations in order to assess the simulation results of the new model but also to any up-coming models.

RÉSUMÉ

Gardiens de l'espace, les lanceurs sont soumis à des améliorations intenses et compétitives, par le biais de campagnes de tests expérimentaux et numériques. Les simulations numériques prédictives sont devenues obligatoires pour améliorer notre compréhension de la physique. Ajustables, elles se prêtent parfaitement à la conception et l'optimisation, en particuliers de la chambre de combustion, pour garantir la sûreté et maximiser l'efficacité. L'un des principaux phénomènes physiques impliqués dans la combustion du combustible et de l'oxydant est l'atomisation du jet, qui pilote à la fois les distributions de gouttelettes et les instabilités potentielles à haute fréquence dans des conditions sous-critiques. Elle englobe un large spectre de topologies d'écoulement diphasiques, des phases séparées à la phase dispersée, avec une région mixte où la physique et la topologie de l'écoulement à petite échelle sont très complexes. Les modèles d'ordre réduit sont de bons candidats pour réaliser des simulations prédictives et relativement peu coûteuses en ressource de calcul sur des configurations industrielles. Cependant, jusqu'à présent ils ne décrivent correctement que la dynamique des grandes échelles et doivent donc être couplés à des modèles de phase dispersée nécessitant un réglage minutieux de paramètres pour prédire la formation du spray. Afin de décrire à la fois les régions mixte et dispersée, l'amélioration de la hiérarchie de modèles d'ordre réduit repose sur quelques principes clefs au cœur de la thèse ci-présente et fournit des problèmes interdisciplinaires faisant appel tant à l'analyse mathématique et la modélisation physique de ces systèmes d'EDP qu'à leur discrétisation numérique et leur implémentation dans des codes de CFD à des fins industriels.

Grâce d'une part à l'extension de la théorie des équations de conservation supplémentaires à des systèmes impliquant des termes non-conservatifs et d'autre part à un formalisme de thermodynamique multi-fluide tenant compte des effets non-idéaux, nous proposons de nouvelles pistes pour définir une entropie de mélange strictement convexe et consistante avec le système d'équation et les lois de pression, dans le but de permettre la symétrisation entropique des modèles diphasiques, de prouver leur hyperbolicité et d'obtenir des termes sources généraux. De plus, en rompant avec la vision géométrique de l'interface, nous proposons une description multi-échelle de l'interface pour décrire un mélange multi-fluide comportant une dynamique interfaciale complexe. Le Principe de Moindre Action a permis de dériver un modèle bifluide à une vitesse couplant grandes et petites échelles de l'écoulement. Nous avons ensuite développé une stratégie de séparation d'opérateurs basée sur la discrétisation par Volumes Finis, et nous avons implémenté le nouveau modèle dans le logiciel industriel multiphysique de CFD, CEDRE, de l'ONERA afin d'évaluer numériquement ce dernier. Enfin, nous avons construit et analysé les fondations d'une hiérarchie de cas tests accessibles à la DNS tout en étant au plus proche de configurations industrielles, dans le but d'évaluer les résultats de simulations du nouveau modèle ou de tout autre modèle à venir.

OUTLINE

ACKNOWLEDGMENTS	i
ABSTRACT	iii
RÉSUMÉ	v
GENERAL INTRODUCTION	1
INTRODUCTION GÉNÉRALE	15
1 TWO-VELOCITY FLOW MODELLING	37
2 DERIVATION OF A MULTI-FLUID THERMODYNAMICS ACCOUNTING FOR NON-IDEAL EFFECTS	97
3 DERIVATION OF TWO-SCALE KINEMATICS AND CAPILLARY TWO-PHASE FLOW MODEL TO DESCRIBE THE INTERFACE DYNAMICS	139
4 IMPLEMENTATION OF A FINITE VOLUME NUMERICAL STRATEGY FOR THE DUAL-SCALE TWO-PHASE FLOW MODEL	189
5 NUMERICAL SIMULATIONS TO COMPARE AND VALIDATE REDUCED-ORDER MODEL HIERARCHY	237
CONCLUSION AND PERSPECTIVES	275

GENERAL INTRODUCTION

SPACE PROPULSION

During the last decades, the global launch system payload market has experienced a strong growing demand and the trend should continue in the coming years. The number of launches has indeed jumped from 85 in 2016 to 114 in 2018 worldwide, putting into orbits satellites of various size serving scientific, military and booming commercial means. Since launchers are the gatekeepers to the open space, nations and private companies seeking space independency and sovereignty must pursue their efforts into the development of competitive rockets.

Most of today's rockets use chemical propulsion, which are air-independent. Thrust is generated from the chemical reaction of an oxidizer and a fuel in a combustion chamber. The hot gases produced by the combustion are then accelerated through a convergent-divergent nozzle, converting chemical energy into kinetic energy, and eventually providing thrust for the rocket.

Two main space propulsion technologies coexist, pure solid rocket and liquid propulsion systems. Pure solid rocket engines are made of a mixture that combines solid oxidizer and fuel packed in a cylinder. An axisymmetric hole is dug inside and serves as a combustion chamber. When igniting the inner surface of the propellant, a flame produces hot burnt gases, which are then accelerated through the nozzle, generating thrust. Simple and cheap, this type of engine produces a high thrust justifying its use at take-off. Nevertheless, the combustion rate is hardly flexible and can not be stopped once started. In liquid propulsion systems, fuel and oxidizer are stored away from the combustion chamber in vessels at a liquid state to minimize occupancy. Liquid propellants are pumped into the combustion chamber where they mix and burn, hot burnt gases being accelerated through a nozzle leading to thrust generation. Storable propellants such as Rocket Propellant One (RP-1), Mono-Metil Hydrazine (MMH) or Unsymmetrical dimethylhydrazine (UDMH), are stored at ambient pressure whereas cryogenic propellants like oxygen (LOX), hydrogen (LH₂) or methane (LCH₄) must be maintained at very low temperature to stay liquid. More efficient than solid rocket engines in terms of specific impulse¹, liquid rocket engines offer flexible thrust and reignition at the price of more complexity. These advantages have led to the selection of two cryogenic engines in the upcoming European launcher, Ariane 6, as sketched in [Figure 0.1](#), and of reusable cryogenic engines for future launchers after Ariane 6 e.g. Prometheus engine for THEMIS, Ariane Next program [Patureau de Mirand et al. \(2020\) \[171\]](#). Cryogenic rocket engines must operate over a large range of combustion chamber pressure from atmospheric pressure at take-off up to high pressure at

¹Specific impulse is a time defined as the ratio of thrust generated to the propellant mass flow rate. The more thrust and the less propellants used the better, thus the higher the specific impulse the more efficient the engine is.

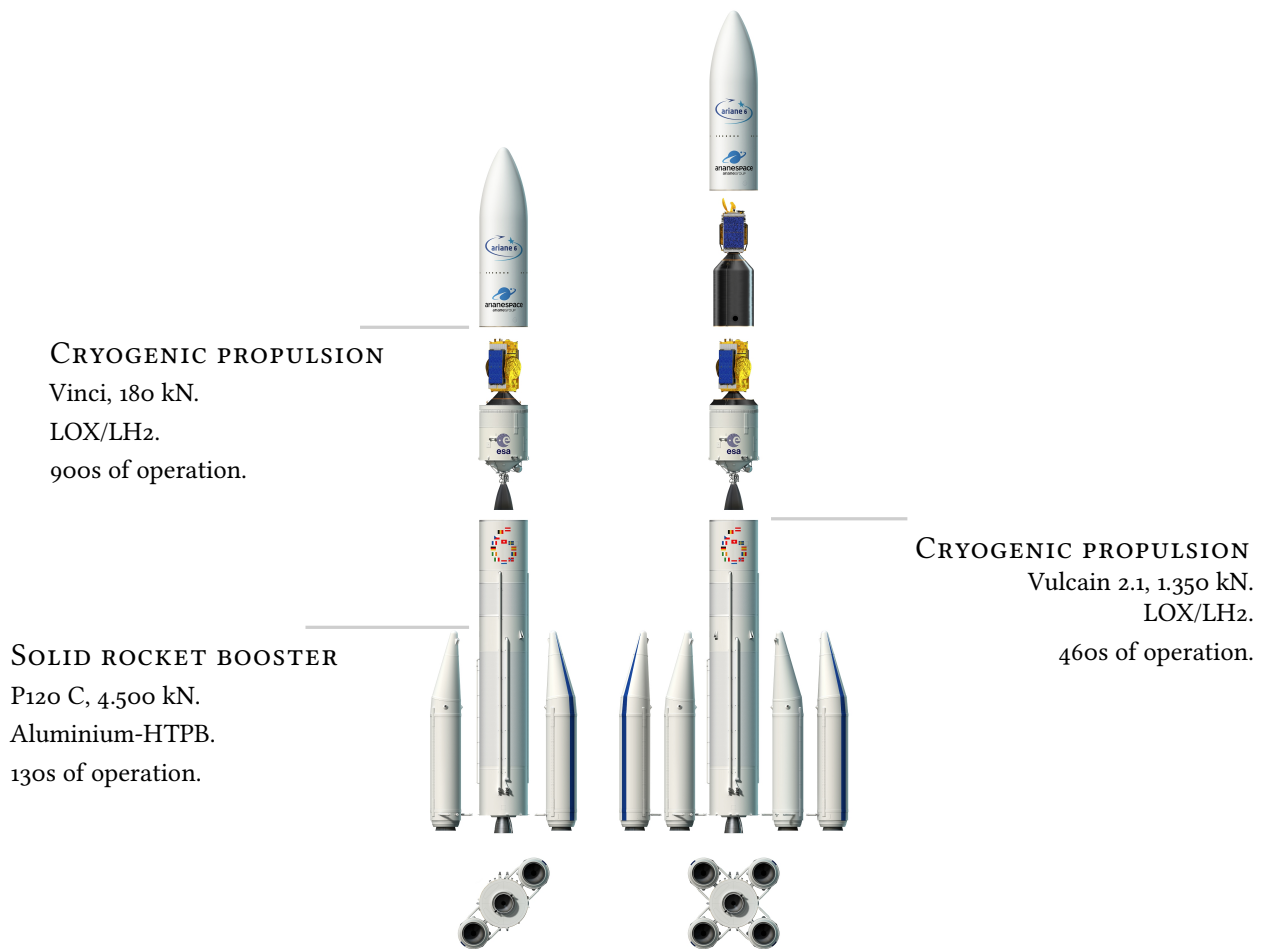


FIGURE 0.1: Artist view of the two configurations of Ariane 6 (©SESA–David Ducros, 2018).

nominal operational point. Since the thermodynamics state of the propellants is characterized by their critical temperature and critical pressure, the propellants are injected either as liquid or gas depending on combustion chamber thermodynamics state. For Vulcain 2.1, Vinci and Prometheus, the fuel (LH₂ or LCH₄ in future version), stored at very low temperature, serves as a coolant of the combustion chamber wall before injection, heating it above its critical temperature, such that it always penetrates the chamber in a gaseous state. However, the oxidizer (LOX) is injected below its critical temperature such that we distinguish two injection regimes, sub-critical and trans-critical regimes, depending on the combustion chamber pressure. At sub-critical regime, the pressure of the chamber is less than the critical pressure of the oxidizer, 50 bar for LOX. The latter is then injected at a liquid state. This regime is encountered at ignition on-ground, re-ignition in outer-space, but corresponds also to the nominal operating point of the cryogenic engine HM7B thrusting the upper-stage of Ariane 5. Sub-critical injection encompasses various flow topologies during jet atomization. At trans-critical regime, the pressure of the chamber exceeds the critical pressure of the fuel, the latter being injected at a trans-critical state. Surface tension is thus negligible and the jet atomization is only driven by hydrodynamics, turbulence and diffusion. Trans-critical regimes are nominal operating conditions of Vulcain 2.1, Vinci and Prometheus.

Engines safety and efficiency are two of the main priorities given to the space industry. These two requirements are directly prescribed by multi-scale and multi-physics phenomena occurring and interacting in the combustion chamber. Principal physical processes are the co-current injection of fuel and oxidizer, the atomization and evaporation of the latter, turbulence and flame combustion, heat radiation and acoustics. They animate a large research domain. When the engine operates at sub-critical conditions, the fuel atomization plays a crucial part in the combustion process, thus must be thoroughly studied to understand its impact on the generation of droplets evaporating and eventually reacting with the gaseous flow field and on High-Frequency (HF) combustion instabilities. The former is nowadays a key concern for reignition and performance issues. The latter, the HF combustion instabilities, ensue from an energy transfer of the propellant combustion to the acoustic field, resulting in growing pressure oscillations which can reach resonance modes and lead to critical damages of the rocket.

Accidents in the 80's occurring in the cryogenic engines of the Ariane launchers due to combustion instabilities urged the need of a better understanding of the flow in the combustion chamber. As a consequence the national research program (GDR), "Combustion dans les moteurs fusées", was launched in 1993. In 1994 the Office National d'Études et de Recherches Aérospatiales (ONERA) first operated the Mascotte experimental test bench for cryogenic combustion to acquire experimental data and study the cryogenic combustion. Test campaigns showed the essential role of the primary atomization, but also the strong interactions of the various phenomena [Habiballah et al. \(1997\) \[101\]](#). These advances led to the reconduction of the program in 1997 for further investigation [Vingert et al. \(1999\) \[217\]](#). Even though these experimentations have led to better understanding of the observed physical phenomena and helped design safe and efficient engines, they faced limitations due to very high operating and instrumenting costs, a restricted ranges of operating conditions and the complexity of the collected data accounting for strongly interacting phenomena.

As a result, predictive numerical simulations have become mandatory, at least as a complementary tool in order to increase our understanding of the physics. Adjustable, they provide early-stage optimization processes, thus accelerating developments while reducing the costs. In particular these numerical methods guaranty safe and efficient combustion chambers by predicting droplet distributions and instabilities they may generate in a given configuration.

The present thesis is supported by the Centre National d'Études Spatiales (CNES) and ONERA as part of the CNES Launchers Directorate Liquid Propulsion R&D program program in order to contribute to the enhancement of the European space industry. The focus is thus laid on the jet atomization in cryogenic rocket engines operating at sub-critical regimes.

JET ATOMIZATION PROCESS IN SUB-CRITICAL REGIME

Fuel and oxidizer are introduced into the combustion chamber through several injectors at different thermodynamics state. The oxidizer is liquid while the fuel is gaseous. There are several types of injector, but the most commonly used is the shear-coaxial injector. At its exit starts the atomization of the oxidizer, also called jet atomization, which encompasses in sub-critical conditions various two-phase flow topologies. The two phases are first separated by a smooth interface, the characteristic length scale being that of the injector diameter, $10^{-3} m$.

Then, shear stress caused by strong velocity gradients tears the liquid core apart and ligaments are formed. This process is called primary atomization. The ligaments get thinner and thinner until they break into droplets. During the secondary atomization process, the droplets fragments and downstream, we observe a polydisperse spray of droplets carried by the gaseous phase. The droplet diameter is then typically on the order of $10^{-7} m$. Figure 0.2 describes the various flow topologies in the specific case of cryogenic engines equipped with shear-coaxial injectors where the fuel is gaseous hydrogen, $H_2(g)$, and the oxidizer is liquid oxygen, $O_2(l)$.

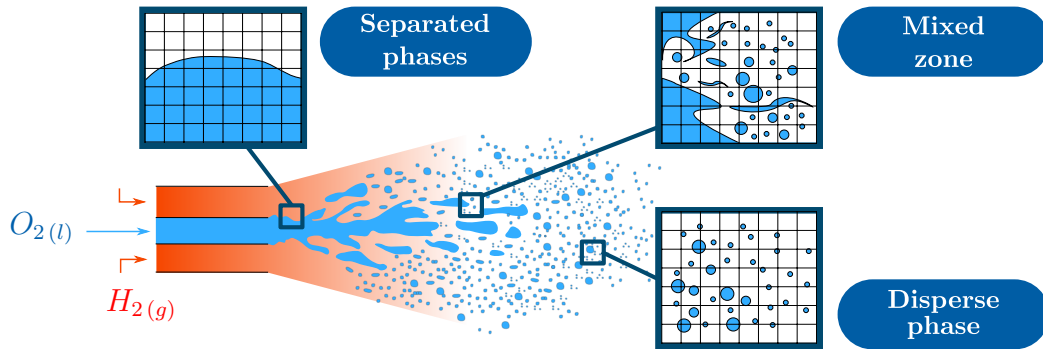


FIGURE 0.2: Description of the various regimes and flow topologies in jet atomization for cryogenic injectors in sub-critical conditions.

In the so-called *mixed region* where primary and secondary atomizations occur, the sub-scale physics and topology of the flow are very complex. The typical range of flow numbers in sub-critical cryogenic cylindrical jet in real configurations are $Re_L = 10^5$ for the liquid Reynolds number and $We_H = 10^5$ for the hydrodynamic Weber number, whose definitions can be found in Lasheras et al. (1998) [129].

The complex and various flow topologies encountered in the jet atomization in sub-critical conditions are not limited to cryogenic rocket engines. Other combustion processes such as fuel injection in automotive engines, or aeronautical simplex atomizers employed on mid-range engines rely on jet atomizations. In the latter, the jet atomization occurs at lower flow numbers, the typical liquid Reynolds number of the liquid sheet flowing out from the atomizer is of the order of $Re_L = 10^3$, while the hydrodynamic Weber number is $We_H = 10^1 - 10^2$. But jet atomization goes far beyond combustion processes. Applications range from biological and agricultural sprays to industrial deposition processes and coating.

Therefore, the present thesis, even if aiming at the better understanding of jet atomization in sub-critical cryogenic applications, will naturally bring out new ideas in order to tackle a large class of two-phase flows involving complex interface dynamics and strong phase thermodynamics off-equilibrium.

DIRECT NUMERICAL SIMULATION LIMITATIONS

Direct Numerical Simulations (DNS) are employed to accurately describe turbulent single-phase flows – flows with fluctuating velocities at large Reynolds number – by solving the incompressible Navier-Stokes equations from the largest scale down to the Kolmogorov scale of the flow, under which all the turbulent kinetic energy is dissipated into heat. Such approach

is not directly applicable to two-phase flows due to the presence of an interface, which has to be accounted for and modelled. Several approaches exist to describe the interface, but they all split into two categories. The interface is either described as a spreaded region of strongly heterogeneous composition, involving a characteristic finite physical lengthscale, or the interface is assumed as a zero-thickness surface. Hereafter, we will rely on this latter strong conceptual assumption. Since velocity fluctuations are compounded by interface fluctuations in two-phase flows, no smallest length scale such as the Kolmogorov scale exists to fix the grid size owing to the fact the interface fluctuations may tend to zero.

Two-phase flow DNS often refers in the community to solving the incompressible Navier-Stokes equations accounting for surface tension and reconstructing accurately the interface through two principal approaches. First, the interface can be tracked explicitly in a Lagrangian way with marker particles identifying either one of the two fluids, originally called Marker and Cell (MAC) method [Harlow and Welch \(1965\) \[102\]](#), or directly the interface itself, referred as Front-Tracking method [Glimm et al. \(2001\) \[89\]](#), [Tryggvason et al. \(2001\) \[213\]](#). The interface can also be implicitly captured with an Eulerian approach through an advected marker function. The latter is either a distance function for the Level set method introduced in [Osher and Sethian \(1988\) \[169\]](#) and coupled later on with the Ghost Fluid Method developed in [Fedkiw et al. \(1999\) \[69\]](#), [Liu et al. \(2003\) \[143\]](#), [Liu et al. \(2005\) \[142\]](#), whose zero determinates the interface locus. The advected marker function can also be the liquid volume fraction for the Volume Of Fluid (VOF) method [Hirt and Nichols \(1981\) \[108\]](#), whose variation from 0 to 1 locates the interface. Both approaches require to treat jump conditions at the interface to accurately solve discontinuous variables. Recent advances propose compressible VOF techniques as in [Jemison et al. \(2014\) \[114\]](#), [Kuila et al. \(2015\) \[123\]](#), [Duret et al. \(2018\) \[63\]](#).

The accuracy of two-phase flow DNS relies mainly on the mesh size, which in the case of jet atomization is required to be extremely small to capture the smallest scales of the interface dynamics, with approximately 10^9 cells, making the cost in computing resources – central processing units (CPU) time, memory usage and disk space – extremely high. Even if they have already provided impressive results in this field such as in [Tomar et al. \(2010\) \[209\]](#), [Tryggvason et al. \(2011\) \[214\]](#), [Desjardins et al. \(2013\) \[51\]](#), [Chen et al. \(2013\) \[26\]](#), [Ling et al. \(2015\) \[140\]](#), [Zandian et al. \(2018\) \[225\]](#) or [Vaudor et al. \(2017\) \[216\]](#) as shown in [Figure 0.3](#), they remain too costly in terms of computing resources to be applied in an industrial context due to the high Reynolds and Weber numbers of the applications.

Therefore, reduced-order models must still be developed despite the fact they usually discard the smallest scales of the interface dynamics by averaging the transport equations. Instead of implicitly filtering all the scales of the flow below the grid size in the case of DNS, reduced-order models introduce a characteristic lengthscale to explicitly filter the scales of the flow, leading to a separation of the large scales, which are fully resolved and the *subscals* of the flow, which require modelling if to be accounted for.

REDUCED-ORDER MODELS STRATEGIES

Among the approaches found in the literature to build reduced-order models for jet atomization, two of them consist in 1) coupling specific models, each of them suited to a given flow topology, 2) using a unified model encompassing all the flow topologies of the given application at the

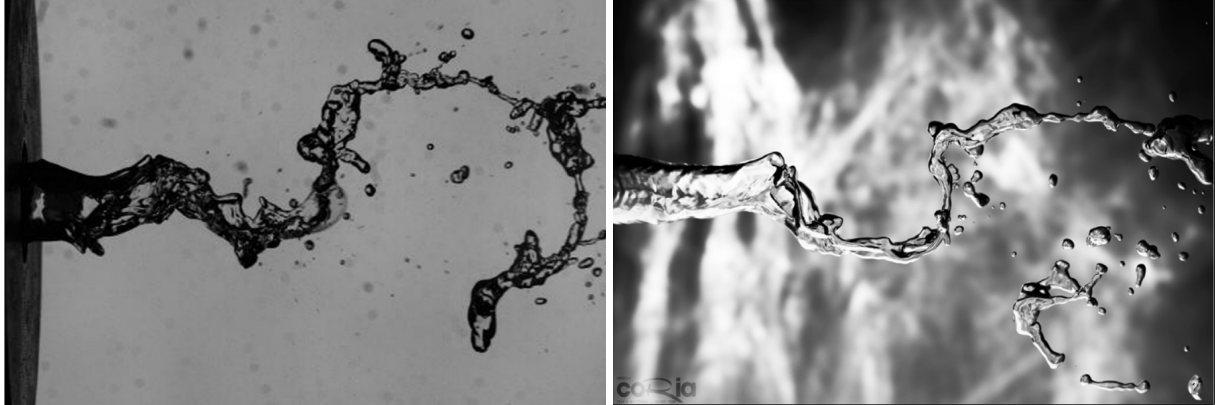


FIGURE 0.3: Qualitative comparison of a liquid jet atomization between (left) experimental results obtained on the LEGI test bench [Delon et al. \(2013\) \[50\]](#) and (right) the level set obtained from DNS simulation with ARCHER code [Vaudor et al. \(2017\) \[216\]](#).

cost of *subscale* modelling.

Coupling methods rely mainly on employing a specific model in the separated phases zone and a second in the disperse phase zone (see [Figure 0.2](#)). In the separated phases zone, two-phase flow models are derived by diffuse interface or interface tracking methods. The former uses a statistical averaging of the instantaneous Navier-Stokes equations for each phase [Drew \(1983\) \[57\]](#) and offer a hierarchy of models [Drui \(2017\) \[59\]](#), [Drui et al. \(2019\) \[60\]](#) among which stands the Baer-Nunziato [Baer and Nunziato \(1986\) \[5\]](#) model accounting for full off-equilibrium of the phases. The latter includes space filtering as done by [Herrmann \(2013\) \[106\]](#), [Hecht \(2016\) \[105\]](#). As for the disperse phase, the particles are tracked either in a Lagrangian way [Ling et al. \(2015\) \[140\]](#), [Zamansky et al. \(2016\) \[224\]](#), or by an Eulerian approach where the droplets distribution is rebuilt thanks to the Kinetic-Based-Moment-Method (KBMM) as proposed by [Sabat \(2016\) \[187\]](#), [Sibra et al. \(2017\) \[202\]](#), [Dupif \(2018\) \[62\]](#), who treat polydisperse droplets in size, velocity and temperature. Usually, the methods applied to the separated phases zone are extended to the mixed region. However, to remain predictive it implies either a high level of description of both the phases off-equilibrium and the interface dynamics or an extremely refined mesh. Finally, since both models employ a different set of variables and are two-way coupled through source terms, the two-way coupling strategy is not straightforward and not necessarily intrinsic. A first referent implementation of the coupling approach can be found in [Herrmann \(2013\) \[106\]](#) where the author couples a dual-scale interface tracking method with a Lagrangian description of the particles. Nevertheless, the coupling suffers from a lack of consistency in terms of statistics and mass and momentum transfer. A second referent implementation has been built in [Le Touze \(2015\) \[132\]](#), with a diffuse interface model coupled to a KBMM element. Nonetheless, the description of the disequilibrium of the two-phase flow is very limited and the prediction of the polydispersity of the generated spray still relies on some arbitrary parameters, which have to be evaluated.

Having a unified model encompassing any flow topology is sought after by the two-phase flow community. Many authors have proposed various means to enrich the existing reduced-order models by introducing additional flow parameters that are reminiscent of small scale features, which can not be described by the bulk variables. New geometric variables

are transported such as the density of interfacial area M Devassy (2013) [149], M Devassy et al. (2015) [148] or local curvature of the interface to account for small scale dynamics connected to capillary effects Herrmann (2013) [106]. Works in this direction are also found in Drui (2017) [59], Drui et al. (2019) [60] where a unified model accounting for micro-inertia and micro-viscosity associated to bubble pulsation is proposed. These dual-scale two-phase flow reduced-order models lead the way to include more subscale description of the interface dynamics into a full out-of-equilibrium two-phase flow which would degenerate into a predictive spray model in the disperse flow area as suggested in Essadki et al. (2018) [68], Essadki et al. (2019) [67].

The strategy retained at ONERA is to perform numerical simulations of the primary atomization from the injection to the combustion of the spray by coupling reduced-order models. One leading course of action consists in coupling Eulerian models, more specifically Kinetic-Based-Moment Methods (KBMM) to describe the disperse flow and diffuse interface models (DIM) to reproduce the separated phases and the *mixed region*. These models are implemented in the industrial CFD code CEDRE Refloch et al. (2011) [184], Gaillard et al. (2016) [76]. While the predictiveness of KBMM solvers in dispersed flow have already been demonstrated Sabat et al. (2019) [188], it is not yet the case for the diffuse interface models (DIM) which are meant to handle the challenging *mixed region*. In this context, this thesis was initiated in order to contribute to the study of combustion instabilities in cryogenic rocket engines through the coupling of diffuse interface models with kinetic-based moment methods for primary atomization simulations. Nevertheless, even if at first sight, the method applied for each approach is significantly different, they both face the same challenge, which consists in accurately describing the *mixed region* where the flow is the most complex due to the high thermodynamics disequilibrium between the phases and the rich interface dynamics. Focusing on the most complex part of the flow, the present thesis naturally aims at contributing to both approaches.

DIFFUSE INTERFACE MODELS AND THEIR CHALLENGES

Among the hierarchy of DIM, well-known models such as the multi-species compressible Navier-Stokes, referred to as the *four equation* model have been massively adopted in the industry (Le Touze (2015) [132]) but have shown their limitations as they neglect the fluids thermodynamics disequilibrium in the mixing zones and can not capture the complex dynamics of the interface especially in the *mixed region*. Therefore, recent efforts have led to first increase the disequilibrium description of the phases by implementing and testing the so-called *five-equation* model Kapila et al. (2001) [115] accounting for two temperatures on real configurations Murrone et al. (2018) [163] or even the Baer-Nunziato model Baer and Nunziato (1986) [5], also called *seven-equation model*, whereby two temperatures, two pressures and two velocities are solved. Secondly, supplementary evolution equations of geometric variables describing the dynamics of the interface are proposed, such as for the interfacial density area as in M Devassy et al. (2015) [148].

Nevertheless, building and using these models eventually as assessment numerical tools is challenging since it involves a large spectrum of scientific disciplines, from 1) the partial differential equations (PDE) analysis, 2) the related mathematical and physical modelling and 3) the postulated thermodynamics, to 4) the numerical discretization and implementation in computational fluid dynamics codes, as well as 5) the verification and validation of the proposed

models on test cases providing analytical solutions or DNS data, or on real configurations to compare with experimental results. In each of these fields, problems arise and we summarize them hereinafter.

1) *PDE analysis*: For systems of conservation laws, the theory developed in [Godunov \(1961\) \[91\]](#), [Friedrichs and Lax \(1971\) \[73\]](#) provides a specific supplementary conservation equation for smooth solution, namely the *entropy equation*. Such systems of PDEs are locally hyperbolic at any point where a locally convex entropy function exists [161], and when they are equipped with a strictly convex entropy, they can be symmetrized [73] [104] and thus are globally hyperbolic. These properties have been at the heart of the mathematical theory of existence and uniqueness of smooth solutions [Kawashima and Shizuta \(1988\) \[118\]](#) [Giovangigli and Masot \(1998\) \[85\]](#), but they are also a corner stone for the study of weak solutions for which the work of [Kruřkov \(1970\) \[122\]](#) proves the well-posedness of Cauchy problem for a single equation in multi-space dimensions. Nonetheless, to derive the diffuse interface models of interest, we employ rational thermodynamics and Stationnary Action Principle (SAP), that often lead to system that can not be written in a conservative form. It is the case of the Baer-Nunziato model, that allows to account for hydrodynamical, mechanical and thermal desiquilibria, and thus the best candidate for the present thesis. The presence of non-conservative terms in the system of PDE prevents the use of the above theory. Still some key advances exist. The Baer-Nunziato model has been shown to be symmetrizable by [Coquel et al. \(2014\) \[31\]](#) – not in the sense of Godunov-Mock – far from the resonance condition for which hyperbolicity degenerates. In [Forestier and Gavriljuk \(2011\) \[71\]](#), assuming that resonance does not occur, the model is proved to be partially symmetrizable in the sense of Godunov-Mock. Nonetheless, a unifying theory extending the standard approach for systems of conservations laws to systems including non-conservative terms is still missing and impedes unveiling key properties of these systems such as entropy supplementary conservation law, entropic symmetrization and hyperbolicity.

2) *Mathematical and physical modelling*: Deriving DIM from a microscopic analysis of the smallest scales of the interface dynamics is not straightforward since the change of scale that is involved introduces unclosed terms, thus it does not allow to trace back macroscopic closure of interfacial quantities such as the interfacial velocity or the interfacial pressure. Therefore numerous closures have been proposed, based on wave-type considerations and the entropy inequality as in [Embid and Baer \(1992\) \[65\]](#), [Coquel et al. \(2002\) \[28\]](#), [Gallouët et al. \(2004\) \[78\]](#) for the Baer-Nunziato model. Nevertheless, they highly rely on the associated thermodynamics of the system, which always assumes non-miscible phases, discards any potential non-ideal effects and impacts the Riemann invariants of the system. Moreover, the dissipative structure is not provided by the SAP and must be postulated according to the second principle of thermodynamics. Adequate source terms allowing for the thermodynamics relaxation of the pressure, the velocity and the temperature of the phase towards equilibrium as well as mass transfer have been proposed, based on a separation of the phenomena [Lochon \(2016\) \[144\]](#), [Lorenzo et al. \(2017\) \[146\]](#), [De lorenzo \(2018\) \[45\]](#), but no generalized source terms have been derived yet based on the entropic variables. Furthermore, while the diffuse interface models offer a hierarchy of models with respect to the level of thermodynamical and hydrodynamical equilibrium between the phases, they provide a poor description of the interface dynamics, limited to the transport of the volume fraction of each phase in each computational cells. In separated phases, the gradient of the volume fraction is a good indicator of the normal to the interface, thus of the local curvature. Nonetheless, as soon as subscale surface phenomena

occur, the volume fraction prediction smooths out all the details of the flow and its gradient can no longer provide meaningful information regarding the topology of the interface. So called dual-scale approaches have been emerging in the framework of VOF methods. It consists in fully resolving, on an auxiliary refined grid, the sub-grid dynamics of the interface using a refined level set approach [Herrmann \(2013\) \[106\]](#). However, such an approach is not directly applicable to the diffuse interface models, since the interface representation is not necessarily sharp. For diffuse interface models, advances rely on supplementary evolution equations of geometric quantities, such as the transport of large and small scale interfacial density areas in the work of [M Devassy et al. \(2015\) \[148\]](#). This approach is very appealing, but there is no mathematical formalism available at the moment for solid and consistent interface scale separation.

3) *Thermodynamics*: The reduced-order models have to be equipped with a postulated thermodynamics. Most multi-fluids thermodynamics approaches are based on the assumption of no interactions between the fluids, resulting in equipping each fluid with its own thermodynamics and then defining mixing thermodynamics quantities by taken arithmetic average of each phase contribution. Nevertheless, in interface region, non-ideal effects such as compaction or surface tension occur and should be taken into account in the thermodynamics, questioning the validity of having an isolated phase thermodynamics approach. Moreover, an accurate description of the subscale dynamics of the interface can only rely on interacting thermodynamics, as for instance in disperse zones where the acoustic properties of the mixture can not be predicted by an isolated fluid thermodynamics approach. While a thorough thermodynamics formalism has been developed to account for non-ideal effects in multi-species gas, it is not yet the case for multi-fluid flows.

4) *Numerical methods*: While the mathematical properties of these Eulerian models are still under current investigation, even the most basic element of the hierarchy of models, that is the Bear-Nunziato model, gives rise to numerical challenges. The models require numerical schemes that are robust and efficient to cope with the strong discontinuities and high gradients encountered in the targeted applications, but also in adequacy with the closures of the interfacial terms. The presence of non-conservative terms in the system of equations usually complexify the definition of weak solutions in the sense of distributions, and Rankine-Hugoniot jump conditions, which allow to solve accurately the local Riemann problems, can not be unambiguously defined. No general theory exists for these models, making the derivation of efficient numerical schemes challenging. The influence on shock solutions of the non-conservative products have been investigated for instance for the multicomponent fluid modelling of plasma flows out of thermal equilibrium in [Wargnier et al. \(2018\) \[219\]](#). It showed that numerical treatments are necessary to prevent non-physical shocks for the solution. In the case of the Baer-Nunziato model, it has been proven that the solution across one wave is not unique [Andrianov and Warnecke \(2004\) \[3\]](#). Furthermore, since the non-conservative terms can not be written in a divergence form, they are not treated as numerical fluxes but as source terms. The most simplest way to handle the non-conservative terms is to assume local constancy of the interfacial pressure and velocity on each interface at each time integration ([Saurel and Abgrall \(1999\) \[190\]](#), [Zein et al. \(2010\) \[226\]](#), [Furfaro and Saurel \(2015\) \[74\]](#)) allowing a simple discretization. Nonetheless, the non-conservative products, usually present in the phasic equations, cancel each other when deriving the mixture equations. It has led to the development of several numerical strategies, from the Exact Riemann solvers [Andrianov and Warnecke \(2004\) \[3\]](#), [Schwendeman et al. \(2006\) \[199\]](#), [Deledicque and Papalexandris \(2007\) \[47\]](#)

to approximate Riemann solvers Saurel and Abgrall (1999) [190], Saurel et al. (2009) [195], Ambroso and Chalons (2012) [1] including correction techniques based on mixture conservative equations. In addition, exact solver of the linearized Riemann problem have been also developed since they are able to include the non-conservative terms into the discretization Sainsaulieu (1995) [189], Gallouët et al. (2004) [78], Pelanti and Shyue (2014) [172]. Finally, an entropy-satisfying relaxation scheme has been proposed for the Baer-Nunziato model in Coquel et al. (2014) [32], Coquel et al. (2017) [29] for which a discrete entropy inequality is proven, guarantying the nonlinear stability of the numerical method. Nevertheless these rich developments apply mostly for the basic elements of the diffuse interface models, which discard subscale modelling and use non-interacting thermodynamics. Accounting for these two main advances requires new numerical schemes.

5) *Numerical simulation*: The applications we are seeking are characterized by strong gradients and discontinuities, thus need also to be assessed numerically to highlight their promising predictiveness before being widely deployed in the industry. Therefore, we first need to implement the numerical methods in CFD codes, able to scale massively to reach realistic configurations. At ONERA, the multiphysics computational fluid dynamics software CEDRE Refloch et al. (2011) [184] works on general unstructured meshes and is organized as a set of solvers. Two of them are Eulerian solvers. The CHARME solver is used for fluids and postulates multispecies Navier-Stokes equations and offers either LES or RANS turbulence models as well as chemical reactions. The SPIREE solver is dedicated to disperse phase flow and is built on KBMM, that proposes either a size sampling approach, also referred as to the Multi-Class methods, or Eulerian Multi Fluid models, also called *sectional* methods Laurent and Massot (2001) [130]. CHARME provides only the simplest model in the hierarchy of the diffuse interface models, for which an equilibrium with respect to velocity, pressure and temperature is assumed between both phases. Since CEDRE aims at describing a wider range and more ambitious applications, such as reacting multiphase flow applications, next generations models must be implemented in it. This thesis contributes directly to this objective. Secondly, in order to validate the reduced-order models, we need to be able to assess the simulation results. Usually some experimental data are at disposal, but they are often limited in terms of applications ranges and data collections. DNS data could thus provide precise elements of comparisons on elementary test cases while increasing step by step the complexity of the flow. It is very attractive, but solid and exhaustive benchmarks have not been established yet for two-phase flow. Furthermore, even if some well-known test cases exist, it is not clear how to compare the results of reduced-order models with DNS due to the difference of the modelling approaches.

CONTRIBUTION AND MANUSCRIPT OVERVIEW

These various fields have been examined in the present work in order to set some solid background to contribute in an original manner to solving some of the missing elements described in the previous section.

In Chapter 1, we first introduce the existing methods to derive two-velocity two-phase flow diffuse interface models. Then, we propose a derivation from variational calculus of a two-velocity two-phase flow model along with an equation on the entropy piloting the relaxation phenomena. We highlight how the average interfacial pressure and velocity are closed

and the consequences of their closures based first on waves types and Riemann invariants, but then thanks to an extension of the existing theory of supplementary conservative equations to system of non-conservation laws. This result has been published in [Cordesse and Massot \(2020\) \[41\]](#). As first step to extend the theory of Godunov-Mock to non-conservative systems, this contribution has brought about entropy supplementary conservative equations for the Baer-Nunziato model together with constraints on both the interfacial quantities and the definition of the thermodynamics. In particular, introducing some level of mixing of the two phases into the definition of the mixing entropy has raised incompatibility issues between the existence of a mixing process in the thermodynamics of the mixture and an interfacial pressure, questioning the way to account consistently for interactions in the thermodynamics and the system of PDE it equips.

In [Chapter 2](#), we introduce a formalism to build a multi-fluid thermodynamics, based on a reference state and pressure law, accounting for non-ideal effects. It allows to highlight the impact on the mathematical structure of the system derived from the SAP and gives hints on how to recover the phase evolution equations. This work has been submitted in [Cordesse et al. \(2020\) \[35\]](#).

In [Chapter 3](#), relying on a probability density function (pdf), we depart from a geometric approach of the interface and propose a multi-scale rendering of the interface without any postulate on its location nor its shape. This novel multi-scale modelling tool is thus not relying on any two-phase flow topology assumption and seems to bridge the gap between the diverse approaches, in particular diffuse and sharp interface models, to describe multi-fluid flow. From the pdf, we recover classic geometric variables as well as a natural decomposition into a filtered and fluctuating contributions. Based on these quantities, we extend the definition of the Lagrangian describing the barotropic two-phase flow medium adding dual-scale kinetic and potential contributions to account for small-scale kinematics and surface tension. The Stationary Action Principle returns a system of PDE showing a coupling between large and small scales. We finally extend the system to two-parameter equations of state of each phase, leading to a single-velocity six-equation model in the same spirit as [Saurel et al. \(2009\) \[195\]](#). This Chapter is the results of three proceedings, [Cordesse et al. \(2020\) \[37\]](#), [Cordesse et al. \(2019\) \[40\]](#), [Cordesse et al. \(2019\) \[33\]](#) and an article submitted to the International Journal of Multiphase Flow [Cordesse et al. \(2020\) \[34\]](#).

In [Chapter 4](#), we make supplementary assumptions on the thermodynamics and neglect the pulsation to alleviate some difficulties related to the original model and obtain a primary block, from which we derive an asymptotic system when assuming instantaneous pressure relaxation. We proceed then to the mathematical analysis of the homogeneous form of the primary block. In order to include the large scale capillary terms in the mathematical analysis, we add a supplementary equation on the volume fraction gradient. The model is found to be weakly hyperbolic. We then present a splitting strategy leading to three sub-systems corresponding respectively to the hydrodynamics and acoustics convection, then the large and small capillary fluxes and finally the relaxation procedure, and proceed to their mathematical analysis. Later on, we detail the numerical method applied on each sub-system based on a Finite Volume discretization and finally we proceed to a numerical verification of the implemented model by reproducing classic one and two dimensional test cases selected to test Euler and large capillary fluxes as well as the pressure relaxation. The results attests the reliability of the splitting strategy.

Chapter 5 includes first a qualitative and quantitative comparisons of some elements of the hierarchy of diffuse interface models, the single-velocity and single-pressure and two-velocity two-pressure models, with or without coupling with a KBMM element. The numerical simulations have been performed on challenging cryogenic jet atomization configurations as a demonstration of feasibility and a first step towards genuine validation. Then, we have constituted and investigated a first building block of a hierarchy of test-cases designed to be amenable to DNS while close enough to industrial configurations, for which we propose a comparison of two-fluid compressible simulations with DNS data-bases. It has also led to a better understanding of the main conceptual differences between the two modelling approaches. This chapter is the result of three proceedings Cordesse et al. (2018) [36], Murrone et al. (2018) [163], Cordesse et al. (2019) [38], a technical report Cordesse et al. (2020) [37] and finally, an article Cordesse et al. (2019) [42] submitted to the journal Flow, Turbulence and Combustion (FTaC).

SCIENTIFIC OUTREACH

The present thesis has led to the following contributions,

IN PREPARATION

- P. Cordesse, S. Kokh, M. Massot, *Derivation of a two-phase flow model with two-scale kinematics and surface tension by means of variational calculus*, in preparation for International Journal of Multiphase Flow.
- P. Cordesse, C. Le Touze, A. Murrone, S. Kokh, M. Massot, *Finite volume numerical strategy for dual-scale two-phase flow model*, in preparation for Journal of Computational Physics.

PAPERS AND PREPRINTS

- P. Cordesse, L. Matuszewski, M. Massot, *Multi-fluid thermodynamics from a pressure law approach*, submitted to Continuum Mechanics and Thermodynamics, 2020, 1–20.
- P. Cordesse, R. Di Battista, Q. Chevalier, L. Matuszewski, T. Ménard, S. Kokh, M. Massot, *A diffuse interface approach for disperse two-phase flows involving dual-scale kinematics of droplet deformation based on geometrical variables*, submitted to ESAIM: Proceedings and Surveys, 2019, 1–20.
- P. Cordesse, A. Remigi, B. Duret, A. Murrone, T. Ménard, F-X. Demoulin, M. Massot, *Validation strategy of reduced-order two-fluid flow models based on a hierarchy of direct numerical simulations*, submitted to Flow, Turbulence and Combustion, 2019, 1–20 [HAL-02350200](#).
- P. Cordesse, M. Massot, *Entropy supplementary conservation law for non-linear systems of PDEs with non-conservative terms: application to the modelling and analysis of complex fluid flows using computer algebra*, Communications in Mathematical Sciences, 2019, 1–23, [HAL-01978949](#) in Press.

BOOK CHAPTERS

- P. Cordesse, A. Murrone, T. Ménard, M. Massot, *Comparative study of jet atomization simulations: direct numerical simulations and diffuse interface models coupled with kinetic-based moment methods*, Proceedings of the NASA Summer Program, 2020, 1–12, [HAL-02349534](#).
- P. Cordesse, S. Kokh, R. Di Battista, F. Drui, M. Massot, *Derivation of a two-phase flow model with two-scale kinematics, geometric variables and surface tension by mean of variational calculus*, Proceedings of the NASA Summer Program, 2020, 1–12, [HAL-02336996](#).

CONFERENCE PROCEEDINGS

- P. Cordesse, A. Murrone, T. Ménard, M. Massot, *Validation strategy of reduced-order two-fluid flow models based on a hierarchy of direct numerical simulations*, Proceedings of the 2019 ICMF 10th International Conference on Multiphase Flow, Rio de Janeiro, Brazil, 2019, 1–8, [HAL-02194973](#).
- P. Cordesse, R. Di Battista, S. Kokh, M. Massot, *Derivation of a two-phase flow model with two-scale kinematics and surface tension by means of variational calculus*, Proceedings of the 2019 ICMF 10th International Conference on Multiphase Flow, Rio de Janeiro, Brazil, 2019, 1–6, [HAL-02194951](#).
- P. Cordesse, A. Murrone, M. Massot, *Coupling a hierarchy of diffuse interface model with kinetic-based moment methods for spray atomization simulations in cryogenic rocket engines*, Proceedings of the 2018 ICLASS 14th International Conference on Liquid Atomization and Spray Systems, Chicago, IL, USA, 2018, 1–8, [HAL-01888477](#).
- P. Cordesse, M. Massot, A. Murrone, *Mathematical modelling of multi-phase flow using entropy symmetrization*, Proceeding of the ECCM-ECFD, Glasgow, UK, 2018, 1–12, [HAL-01888513](#).
- A. Murrone, A. Boucher, P. Cordesse, *A five-equation model for the simulation of the two-phase flow in cryogenic coaxial injector*, Proceeding of the Space Propulsion, Seville, Spain, 2018, 1–12, [HAL-02195012](#).

POSTER AND ORAL PRESENTATIONS

- P. Cordesse, *Two-fluid model hierarchy - thermodynamics, non-conservative terms and hyperbolicity/entropic symmetrization*, Invited speaker at the Second Workshop on Compressible Multiphase Flows, IRMA, université de Strasbourg, France, 2019.
- P. Cordesse, M. Massot, A. Murrone, *Multi-phase flow with two velocities modelling for jet atomization simulations*, Poster Session at the 44th Congrès National d'Analyse Numérique CANUM, Cap d'Agde, France, 2018.
- P. Cordesse, M. Massot, and A. Murrone, *Multi-phase flow modeling using entropy symmetrization and variational calculus for jet atomization simulations*, Oral presentation at the Dispersed two-phase flows conference, Toulouse, France, 2018.

- P. Cordesse, A. Murrone, M. Massot, C. Le Touze, A. Boucher, *Coupling a hierarchy of diffuse interface model with kinetic-based moment methods for primary atomization simulations in liquid propulsion*, Oral presentation at the 3rd International Conference on Numerical Methods in Multiphase Flows, Tokyo, Japan, 2017.

SUMMER PROGRAM

Participation in the Summer program at the NASA Ames Research Center, Advanced Supercomputing Division and Heliophysics, July 2018, *Large scale description of interfacial two-phase flows for the construction of a unified Eulerian model from injection to polydisperse spray using geometrical properties for subscale modeling: theoretical derivation, numerical implementation and DNS assessment*. The project was lead by Marc Massot and hosted by Nagi N. Mansour.

ADVISORS AND COLLABORATORS

The present thesis has been founded by a Phd Grant from ONERA, CNES and Initiative HPC@Maths (École polytechnique). It has been initiated with ONERA and CNES at the Laboratoire Énergétique Moléculaire et Macroscopique, Combustion (EM2C) at CentraleSupélec, but has quasi-entirely been prepared at the Centre de Mathématiques APpliquées (CMAP) at École polytechnique and ONERA.

The thesis has benefited from a large collaboration of people from different backgrounds. Have been involved into the PhD thesis as advisors and collaborators,

- ONERA: Clément Le Touze, Lionel Matuszewski,
- CORIA: Thibaut Ménard, François-Xavier Demoulin,
- CEA: Samuel Kokh,
- CMAP: Ruben Di Battista, Alberto Remigi,

and fruitful discussions with Frédéric Coquel, Daniel Lhuillier and Vincent Giovangigli have enlarged the vision of the present work.

INTRODUCTION GÉNÉRALE

PROPULSION SPATIALE

Au cours des dernières décennies, le marché mondial des charges utiles des systèmes de lancement a connu une forte croissance de la demande et cette tendance devrait se poursuivre dans les années à venir. Le nombre de lancements au niveau mondial est en effet passé de 85 en 2016 à 114 en 2018, mettant en orbite des satellites de tailles diverses au service de missions scientifiques, militaires et commerciales en plein essor. Les lanceurs étant les gardiens de l'Espace, les nations et les entreprises privées recherchant indépendance et souveraineté spatiale doivent poursuivre leurs efforts dans le développement de fusées compétitives.

La plupart des fusées actuelles utilisent la propulsion chimique anaérobie. La poussée est générée à partir de la réaction chimique entre un oxydant et un combustible dans une chambre de combustion. Les gaz chauds produits par la combustion sont ensuite accélérés par une tuyère convergente-divergente qui convertit l'énergie chimique en énergie cinétique, et fournit finalement la poussée de la fusée.

Deux technologies principales de propulsion spatiale coexistent, les fusées à propergol solide et les systèmes de propulsion liquide. Les moteurs fusée à propergol solide sont constitués d'un mélange d'oxydant et de carburant conditionné dans un cylindre à l'état solide. Un trou axisymétrique est creusé au centre et fait office de chambre de combustion. Lors de l'allumage de la surface intérieure du propergol, une flamme produit des gaz brûlés chauds, qui sont ensuite accélérés par la tuyère, générant une poussée. Simple et peu coûteux, ce type de moteur produit une forte poussée justifiant son utilisation au décollage pour s'arracher de l'atmosphère terrestre. Néanmoins, la vitesse de combustion n'est guère flexible et le phénomène ne peut pas être arrêté une fois démarrée. Dans les systèmes de propulsion liquide, le combustible et l'oxydant sont stockés dans des réservoirs séparés à l'écart de la chambre de combustion et à l'état liquide afin de minimiser l'encombrement. Les propergols liquides sont pompés dans la chambre de combustion où ils sont mélangés et brûlés, les gaz chauds brûlés sont accélérés par une tuyère, générant la poussée. Les propergols stockables tels que Rocket Propellant One (RP-1), Mono-Metil Hydrazine (MMH) ou Unsymmetrical dimethylhydrazine (UDMH), sont stockés à pression ambiante, alors que les propergols cryogéniques tels que l'oxygène (LOX), l'hydrogène (LH₂) ou le méthane (LCH₄) doivent être maintenus à une température très basse pour rester liquides. Plus efficaces que les moteurs solides de fusées en terme d'impulsion spécifique², les moteurs de fusée à propergol liquide offrent une poussée flexible et un réallumage possible au prix d'une plus grande complexité. Ces avantages ont

²L'impulsion spécifique est un temps défini comme le ratio de la poussée générée et le débit massique du propergol consommé. Plus la poussée est importante et moins les propergols sont consommés, meilleure est l'impulsion spécifique et donc meilleure est l'efficacité du moteur.

conduit à la sélection de deux moteurs cryogéniques pour le lanceur européen Ariane 6 à venir, tel que représenté dans la [Figure 0.4](#), et des moteurs cryogéniques réutilisables pour les futurs lanceurs suivant Ariane 6, comme le moteur Prometheus pour les programmes THEMIS et Ariane Next [Patureau de Mirand et al. \(2020\) \[171\]](#). Les moteurs de fusée cryogéniques doivent

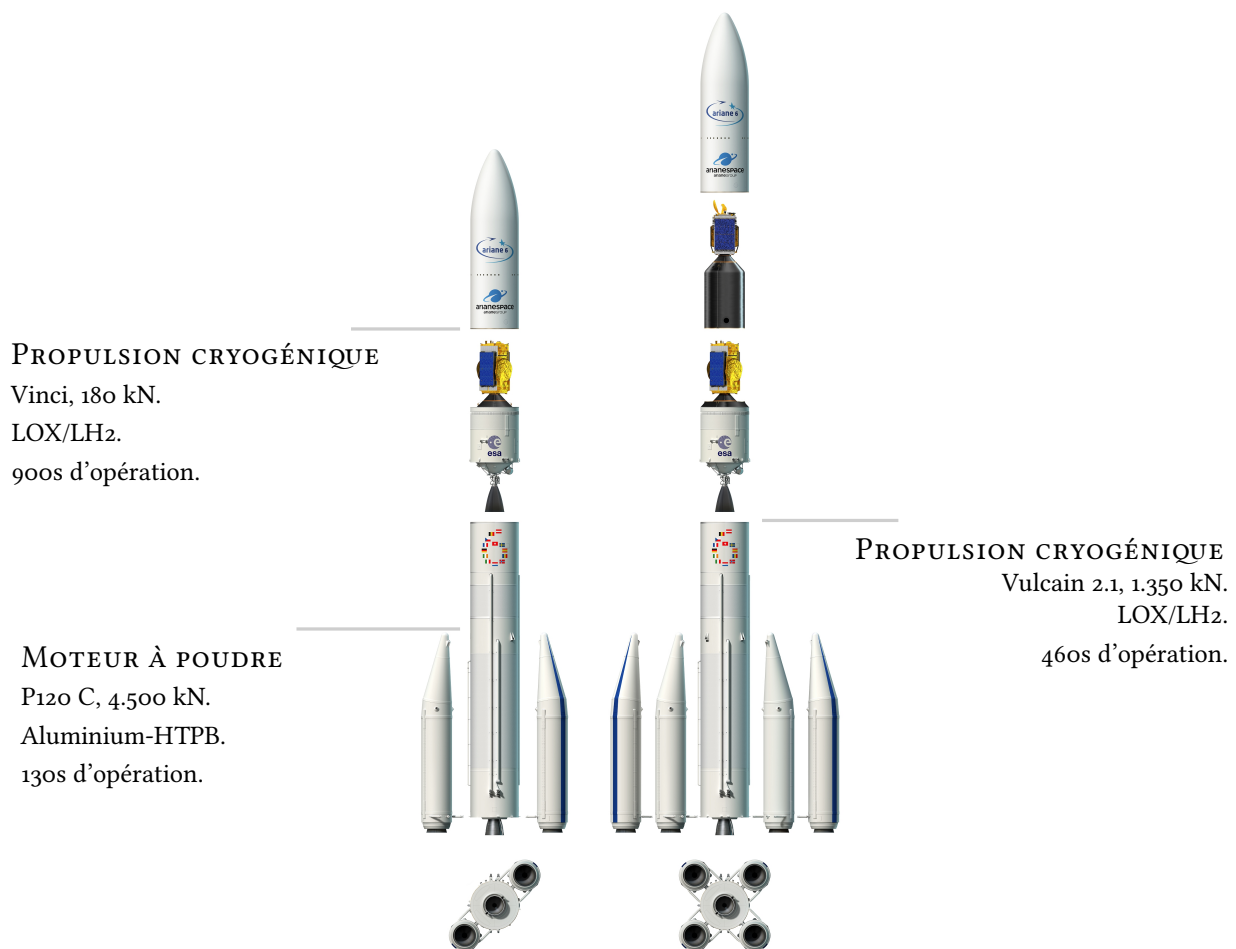


FIGURE 0.4: Vue d'artiste des deux configurations d'Ariane 6 (©SESA–David Ducros, 2018).

fonctionner sur une large gamme de pression dans la chambre de combustion, de la pression atmosphérique au décollage à la haute pression au point de fonctionnement nominal. L'état thermodynamique des propergols étant caractérisé par leur température critique et leur pression critique, les propergols sont injectés sous forme liquide ou gazeuse selon la pression et la température de la chambre de combustion. Pour Vulcain 2.1, Vinci et Prometheus, le carburant (LH₂ ou probablement LCH₄ dans une version future d'Ariane 6), stocké à très faible température, sert de réfrigérant des parois de la chambre de combustion avant injection, qui en retour le chauffe au-dessus de sa température critique, de sorte qu'il pénètre dans la chambre toujours à l'état gazeux. L'oxydant (LOX) est quant à lui injecté en dessous de sa température critique, de sorte que l'on distingue deux régimes d'injection, le régime sous-critique et le régime trans-critique, en fonction de la pression de la chambre de combustion. En régime sous-critique, la pression de la chambre est inférieure à la pression critique de l'oxydant qui est de 50 *bar* pour le LOX. Ce dernier est alors injecté à l'état liquide. Ce régime se rencontre à l'allumage au sol,

au réallumage dans l'espace, mais correspond aussi au point de fonctionnement nominal du moteur cryotechnique HM7B qui pousse l'étage supérieur d'Ariane 5. L'injection sous-critique donne lieu à un écoulement diphasique et de topologies diverses lors de l'atomisation par jet. En régime transcritique, la pression de la chambre dépasse la pression critique du combustible, ce dernier étant injecté en état transcritique. La tension superficielle est donc négligeable et l'atomisation du jet n'est entraînée que par l'hydrodynamique, la turbulence et la diffusion. Les régimes trans-critiques sont des conditions de fonctionnement nominales de Vulcain 2.1, Vinci et Prometheus.

La sécurité et l'efficacité des moteurs constituent deux des principales priorités accordées à l'industrie spatiale. Ces deux exigences sont dictées par des phénomènes multi-échelles et multi-physiques qui se produisent et interagissent dans la chambre de combustion. Les principaux processus physiques sont l'injection à co-courant de carburant et d'oxydant, l'atomisation et l'évaporation de ce dernier, la turbulence et la combustion de la flamme, le rayonnement thermique et l'acoustique. Ils animent un vaste domaine de recherche. Lorsque le moteur fonctionne dans des conditions sous-critiques, l'atomisation du carburant joue un rôle crucial dans le processus de combustion. Elle doit donc être étudiée en profondeur pour comprendre son impact sur la génération de gouttelettes s'évaporant et finissant par réagir avec le champ d'écoulement gazeux, et sur les instabilités de combustion à haute fréquence (HF). La génération de gouttelettes s'évaporant et réagissant avec le champ d'écoulement gazeux est aujourd'hui une préoccupation majeure pour les questions de réallumage et de performance moteur. Les instabilités de combustion HF résultent d'un transfert d'énergie de la combustion du propergol vers le champ acoustique, ce qui entraîne des oscillations de pression croissantes pouvant atteindre des modes de résonance et conduire à des dommages critiques de la fusée.

Les accidents survenus dans les années 80 dans les moteurs cryogéniques des lanceurs Ariane en raison d'instabilités de combustion ont souligné la nécessité de mieux comprendre l'écoulement fluide au sein de la chambre de combustion. En conséquence, le programme national de recherche (PNR), "Combustion dans les moteurs fusées", a été lancé en 1993. En 1994, l'Office National d'Études et de Recherches Aérospatiales (ONERA) a exploité pour la première fois le banc expérimental de combustion cryogénique Mascotte pour acquérir des données expérimentales et étudier la combustion cryogénique. Les campagnes d'essais ont montré le rôle essentiel de l'atomisation primaire, mais aussi les fortes interactions des différents phénomènes [Habiballah et al. \(1997\) \[101\]](#). Ces progrès ont amené la reconduction du programme en 1997 pour une étude plus approfondie [Vingert et al. \(1999\) \[217\]](#). Même si ces expérimentations ont permis de mieux comprendre les phénomènes physiques observés et ont contribué à la conception de moteurs fiables et efficaces, elles se sont heurtées à des limites de coûts d'exploitation et d'instrumentation très élevés, à une gamme restreinte de conditions de fonctionnement et à la complexité des données recueillies de phénomènes en forte interaction.

Par conséquent, les simulations numériques prédictives sont devenues indispensables, au moins à titre d'outil complémentaire, afin d'accroître notre compréhension de la physique. Ajustables, elles fournissent des procédés d'optimisation amonts, accélérant ainsi les développements tout en réduisant les coûts. En particulier, ces méthodes numériques garantissent des chambres de combustion fiables et efficaces en prédisant les distributions de gouttelettes et les instabilités qu'elles peuvent générer dans une configuration donnée.

La présente thèse est soutenue par le Centre National d'Études Spatiales (CNES) et l'ONERA dans le cadre du programme de recherche et développement sur la propulsion liquide porté par

la Direction des lanceurs afin de contribuer au renforcement de l'industrie spatiale européenne. L'accent est ainsi mis sur l'atomisation des jets dans les moteurs de fusées cryogéniques fonctionnant à des régimes sous-critiques.

ATOMISATION PAR JET EN RÉGIME SOUS-CRITIQUE

Le combustible et l'oxydant sont introduits dans la chambre de combustion par plusieurs injecteurs à différents états thermodynamiques. L'oxydant est liquide alors que le combustible est gazeux. Il existe plusieurs types d'injecteurs, mais le plus couramment utilisé est l'injecteur à cisaillement coaxial. À sa sortie commence l'atomisation de l'oxydant, qui englobe en condition sous-critique diverses topologies d'écoulement diphasiques. Les deux phases sont d'abord séparées par une interface lisse, l'échelle de longueur caractéristique étant celle du diamètre de l'injecteur, $10^{-3} m$. Ensuite, une contrainte de cisaillement causée par de forts gradients de vitesse déchire le coeur liquide et des ligaments se forment. Ce processus est appelé atomisation primaire. Les ligaments deviennent de plus en plus fins jusqu'à ce qu'ils se brisent en gouttelettes. Au cours du processus d'atomisation secondaire, les gouttelettes se fragmentent et en aval, on observe une pulvérisation polydispersée de gouttelettes portées par la phase gazeuse. Le diamètre des gouttelettes est alors généralement de l'ordre de $10^{-7} m$. La [Figure 0.5](#) décrit les différentes topologies d'écoulement dans le cas spécifique des moteurs cryogéniques équipés d'injecteurs cisailés coaxiaux où le carburant est l'hydrogène gazeux, $H_2(g)$, et l'oxydant l'oxygène liquide, $O_2(l)$.

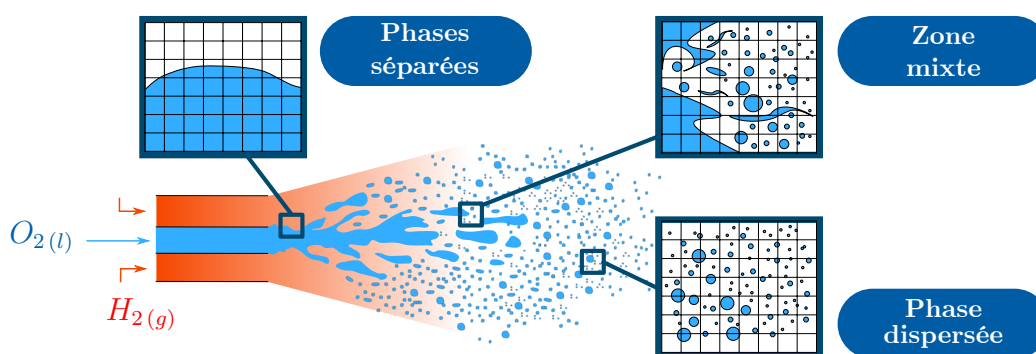


FIGURE 0.5: Illustration des régimes et topologies d'écoulement survenant dans l'atomisation d'un jet issu d'un injecteur cryogénique en condition sous-critique.

Dans la région dite *mixte* où se produisent les atomisations primaire et secondaire, la physique en sous-échelle et la topologie de l'écoulement sont très complexes. Les nombres sans dimension caractérisant un jet cylindrique cryogénique sous-critique en configuration réelle sont de l'ordre de $Re_L = 10^5$ pour le nombre de Reynolds liquide et $We_H = 10^5$ pour le nombre de Weber hydrodynamique, dont les définitions sont présentes dans [Lasheras et al. \(1998\) \[129\]](#).

Les topologies d'écoulement complexes et variées rencontrées dans l'atomisation de jet en conditions sous-critiques ne se limitent pas aux moteurs de fusée cryogéniques. D'autres processus de combustion, tels que l'injection de carburant dans les moteurs automobiles ou les atomiseurs simplex aéronautiques utilisés sur les moteurs moyen courrier, reposent également sur l'atomisation de jet. Dans ce dernier, l'atomisation par jet se produit à des nombres carac-

téristiques inférieurs, le nombre de Reynolds liquide typique de la nappe liquide s'écoulant de l'atomiseur est de l'ordre de $Re_L = 10^3$, tandis que le nombre de Weber hydrodynamique est de $We_H = 10^1 - 10^2$. Mais l'atomisation par jet va bien au-delà des processus de combustion. Les applications s'étendent aux pulvérisations biologiques et agricoles ainsi qu'aux procédés de dépôt industriel et de revêtement.

Par conséquent, la thèse ci-présente, même si elle vise à mieux comprendre l'atomisation des jets dans les applications cryogéniques sous-critiques, fera naturellement émerger de nouvelles idées permettant d'aborder une grande classe d'écoulements diphasiques impliquant une dynamique d'interface complexe et une thermodynamique de phases hors-équilibre.

LIMITES DES SIMULATIONS NUMÉRIQUES DIRECTES

Les simulations numériques directes (DNS) sont utilisées pour décrire avec précision les écoulements monophasiques turbulents - des écoulements caractérisés par la présence de fluctuations de vitesse par grand nombre de Reynolds - en résolvant les équations incompressibles de Navier-Stokes, de la plus grande échelle à l'échelle de Kolmogorov en deçà de laquelle toute l'énergie cinétique turbulente est dissipée en chaleur. Cette approche n'est pas directement applicable aux écoulements diphasiques en raison de la présence d'une interface, qui doit être prise en compte et modélisée. Il existe plusieurs approches pour décrire l'interface, mais elles se divisent toutes en deux catégories. Soit l'interface est décrite comme une région étalée de composition fortement hétérogène, impliquant une échelle de longueur caractéristique physique finie, soit l'interface est supposée être une surface d'épaisseur nulle. Nous nous appuyons ci-après sur cette dernière hypothèse conceptuelle forte. Comme aux fluctuations de vitesse s'ajoutent les fluctuations d'interface dans les écoulements diphasiques, il n'existe pas de plus petite échelle de longueur comme l'échelle de Kolmogorov pour fixer la taille du maillage, car les fluctuations d'interface peuvent tendre vers zéro.

Les DNS des écoulements diphasiques font référence souvent dans la communauté à la résolution des équations incompressibles de Navier-Stokes tenant compte de la tension de surface et à la reconstruction précise de l'interface par deux approches. Une première approche consiste à suivre explicitement de manière lagrangienne avec des particules marqueurs identifiant soit l'un des deux fluides, appelé à l'origine méthode MAC (Marker and Cell) [Harlow and Welch \(1965\) \[102\]](#), soit directement l'interface elle-même, appelée méthode Front-Tracking [Glimm et al. \(2001\) \[89\]](#), [Tryggvason et al. \(2001\) \[213\]](#). L'interface peut également être reconstruite implicitement avec une approche eulérienne grâce à une fonction advectée. Cette dernière est soit une fonction de distance pour la méthode Level set introduite dans [Osher and Sethian \(1988\) \[169\]](#) et couplée ultérieurement avec la méthode Ghost Fluid développée dans [Fedkiw et al. \(1999\) \[69\]](#), [Liu et al. \(2003\) \[143\]](#), [Liu et al. \(2005\) \[142\]](#), dont le zéro détermine le lieu de l'interface. Elle peut être également définie par la fraction volumique de liquide dans la méthode Volume Of Fluid (VOF) [Hirt and Nichols \(1981\) \[108\]](#), dont les variations entre 0 et 1 déterminent le lieu de l'interface. Les deux approches nécessitent de traiter les conditions de saut à l'interface pour résoudre avec précision les variables discontinues. Des avancées récentes proposent des techniques VOF compressibles comme dans [Jemison et al. \(2014\) \[114\]](#), [Kuila et al. \(2015\) \[123\]](#), [Duret et al. \(2018\) \[63\]](#).

La précision des DNS d'écoulement diphasique repose principalement sur la taille du

maillage qui, dans le cas de l’atomisation de jet, doit être extrêmement petite pour capturer les plus petites échelles de la dynamique de l’interface, avec environ 10^9 cellules, ce qui rend le coût en ressources informatiques – temps des unités centrales de traitement (UCT), utilisation de la mémoire et espace disque – extrêmement élevé. Même si elles ont déjà donné des résultats impressionnants dans ce domaine comme dans Tomar et al. (2010) [209], Tryggvason et al. (2011) [214], Desjardins et al. (2013) [51], Chen et al. (2013) [26], Ling et al. (2015) [140], Zandian et al. (2018) [225] ou Vaudor et al. (2017) [216] comme le montre Figure 0.6, elles restent trop coûteuses en termes de ressources de calcul pour être appliquées dans un contexte industriel en raison des nombres de Reynolds et de Weber élevés des applications visées.

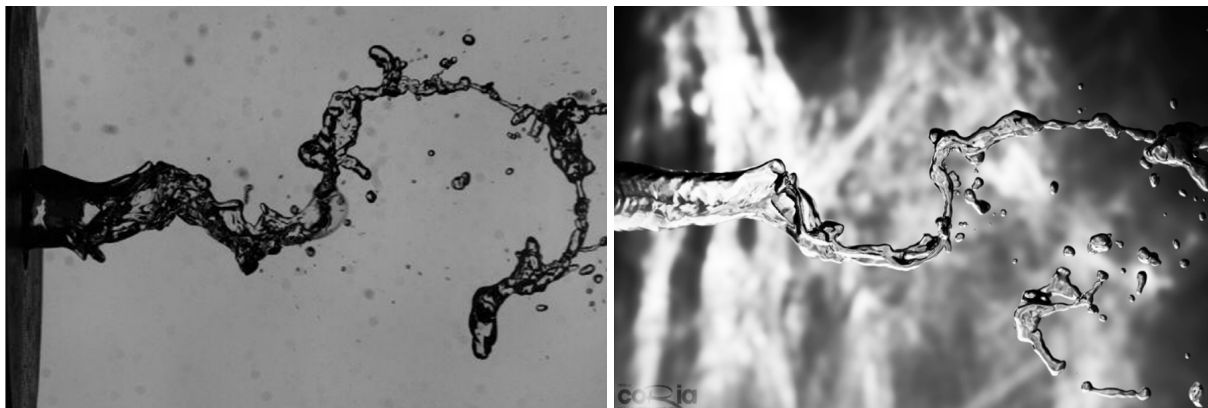


FIGURE 0.6: Comparaison qualitative d’une atomisation de jet liquide entre (à gauche) les résultats expérimentaux obtenus sur le banc d’essai LEGI Delon et al. (2013) [50] et (à droite) l’ensemble des niveaux obtenus par DNS avec le code ARCHER Vaudor et al. (2017) [216].

Par conséquent, les modèles d’ordre réduit doivent encore être développés malgré le fait qu’ils négligent généralement les plus petites échelles de la dynamique d’interface en moyennant les équations de transport. Au lieu de filtrer implicitement toutes les échelles de l’écoulement en dessous de la taille de maille dans le cas de DNS, les modèles d’ordre réduit introduisent une échelle de longueur caractéristique pour filtrer explicitement les échelles de l’écoulement, ce qui conduit à une séparation des grandes échelles, qui sont entièrement résolues et des *petites échelles* de l’écoulement, qui nécessitent un modèle de fermeture si l’on veut en tenir compte.

STRATÉGIE DES MODÈLES D’ORDRE RÉDUIT

Parmi les approches de la littérature pour construire des modèles d’ordre réduit pour l’atomisation de jet, deux d’entre elles consistent à 1) coupler des modèles spécifiques, chacun adapté à une topologie d’écoulement donnée, 2) utiliser un modèle unifié englobant toutes les topologies d’écoulement de la configuration étudiée au prix d’une modélisation des *petites échelles*.

Les méthodes de couplage reposent principalement sur l’utilisation d’un modèle spécifique dans la zone de phases séparées et d’un second dans la zone de phase dispersée (voir Figure 0.5). Dans la zone de phases séparées, les modèles d’écoulement à deux phases sont dérivés par des méthodes d’interface diffuse ou de suivi d’interface. La première utilise

une moyenne statistique des équations instantanées de Navier-Stokes pour chaque phase Drew (1983) [57] et offre une hiérarchie de modèles Drui (2017) [59], Drui et al. (2019) [60] parmi lesquels se trouve le modèle Baer and Nunziato (1986) [5] de Baer-Nunziato qui tient compte du déséquilibre complet des phases. Ce dernier inclut un filtrage spatial comme fait dans Herrmann (2013) [106], Hecht (2016) [105]. Quant à la phase dispersée, les particules sont suivies soit de manière Lagrangienne Ling et al. (2015) [140], Zamansky et al. (2016) [224], soit par une approche Eulérienne où la distribution des gouttelettes est reconstruite grâce à la Kinetic-Based-Moment-Method (KBMM) telle que proposée par Sabat (2016) [187], Sibra et al. (2017) [202], Dupif (2018) [62], qui traite les gouttelettes polydispersées en taille, vitesse et température. Habituellement, les méthodes appliquées à la zone de phases séparées sont étendues à la *région mixte*. Cependant, pour rester prédictive, elle implique soit un haut niveau de description des phases hors équilibre et de la dynamique de l'interface, soit un maillage extrêmement fin. Enfin, comme les deux modèles utilisent un ensemble différent de variables et sont couplés par des termes sources, la stratégie de couplage fort n'est pas simple et pas nécessairement intrinsèque. Une première implémentation de référence de l'approche par couplage se trouve dans Herrmann (2013) [106] où l'auteur couple une méthode de suivi d'interface à double échelle avec une description lagrangienne des particules. Néanmoins, le couplage souffre d'un manque de cohérence en termes de traitements statistiques et de transfert de masse et de moment. Une deuxième implémentation de référence a été élaborée dans Le Touze (2015) [132], avec un modèle d'interface diffuse couplé à un élément de la méthode KBMM. Néanmoins, la description du déséquilibre de l'écoulement diphasique est très limitée et la prédiction de la polydispersité du spray généré repose encore sur certains paramètres arbitraires, qui doivent être évalués.

La communauté de recherche sur les écoulements diphasiques aspire à un modèle unifié couvrant toute topologie d'écoulement. De nombreux auteurs ont proposé divers moyens d'enrichir les modèles d'ordre réduit existants en introduisant des paramètres d'écoulement supplémentaires qui réintroduisent les caractéristiques des petites échelles, ces dernières ne pouvant pas être décrites par les variables fluides du mélange. De nouvelles variables géométriques sont transportées, telles que la densité d'aire interfaciale M Devassy (2013) [149], M Devassy et al. (2015) [148] ou la courbure locale de l'interface pour tenir compte de la dynamique à petite échelle liée aux effets capillaires Herrmann (2013) [106]. On trouve également des travaux dans ce sens dans Drui (2017) [59], Drui et al. (2019) [60] où un modèle unifié prenant en compte la micro-inertie et la micro-viscosité associées à la pulsation des bulles est proposé. Ces modèles d'ordre réduit d'écoulement diphasique à double échelle ouvrent la voie à l'inclusion d'une description des petites échelles de la dynamique de l'interface dans un écoulement diphasique totalement hors équilibre qui dégèrerait en un modèle de spray prédictif dans la zone d'écoulement dispersé comme suggéré dans Essadki et al. (2018) [68], Essadki et al. (2019) [67].

La stratégie retenue à l'ONERA est de réaliser des simulations numériques de l'atomisation primaire depuis l'injection jusqu'à la combustion du spray en couplant des modèles d'ordre réduit. Une des pistes d'action principales consiste à coupler des modèles Eulériens, plus précisément des méthodes cinétiques de type KBMM pour décrire l'écoulement dispersé et des modèles à interface diffuse (MID) pour reproduire les phases séparées et la *région mixte*. Ces modèles sont implémentés dans le code industriel de CFD CEDRE Refloch et al. (2011) [184], Gaillard et al. (2016) [76]. Si la prédictibilité des solveurs KBMM en écoulement dispersé a déjà été démontrée Sabat et al. (2019) [188], ce n'est pas encore le cas pour les modèles à interface

diffuse qui sont utilisés pour traiter la *région mixte* très difficile. Dans ce contexte, cette thèse a été initiée afin de contribuer à l'étude des instabilités de combustion dans les moteurs de fusées cryogéniques par le couplage de modèles à interface diffuse avec des modèles cinétiques pour la simulation de l'atomisation. Néanmoins, même si à première vue, la méthode appliquée pour chaque approche est significativement différente, elles font toutes deux face au même défi, qui consiste à décrire précisément la *région mixte* où l'écoulement est le plus complexe en raison du fort déséquilibre thermodynamique entre les phases et de la riche dynamique d'interface. En se concentrant sur la partie la plus complexe de l'écoulement, la présente thèse vise naturellement à contribuer aux deux approches.

DÉFIS DES MODÈLES À INTERFACE DIFFUSE

Dans la hiérarchie des modèles à interface diffuse, des modèles bien connus tels que le modèle compressible multi-espèces Navier-Stokes, appelé modèle *quatre équations*, ont été massivement adoptés dans l'industrie (Le Touze (2015) [132]) mais ont montré leurs limites car ils négligent le déséquilibre thermodynamique des fluides dans les zones de mélange et ne peuvent pas capturer la dynamique complexe de l'interface en particulier dans la *région mixte*. C'est pourquoi des efforts récents ont permis d'accroître la description du déséquilibre des phases en mettant en oeuvre et en testant le modèle *cinq-équation* Kapila et al. (2001) [115] qui transporte deux températures sur des configurations réelles Murrone et al. (2018) [163] ou encore le modèle Baer-Nunziato Baer and Nunziato (1986) [5], également appelé *sept-équation*, qui permet de résoudre deux températures, deux pressions et deux vitesses. Par la suite, des équations d'évolution supplémentaires des variables géométriques décrivant la dynamique de l'interface ont été proposées, comme pour la densité d'aire interfaciale dans M Devassy et al. (2015) [148].

Néanmoins, la construction et l'utilisation de ces modèles en tant qu'outils numériques de validation est un défi car elle implique un large spectre de disciplines scientifiques, allant de 1) l'analyse des équations aux dérivées partielles (EDP), 2) la modélisation mathématique et physique associée et 3) la thermodynamique postulée, à 4) la discrétisation numérique et l'implémentation dans les codes de CFD, ainsi que 5) la vérification et la validation des modèles proposés sur des cas tests fournissant des solutions analytiques ou des données DNS, ou sur des configurations réelles à comparer avec les résultats expérimentaux. Dans chacun de ces domaines, des problèmes se posent et nous les résumons ci-après.

1) *Analyse des EDP* : Pour les systèmes de lois de conservation, la théorie développée dans Godunov (1961) [91], Friedrichs and Lax (1971) [73] fournit une équation de conservation supplémentaire spécifique pour une solution régulière, à savoir l'*équation d'entropie*. Ces systèmes d'EDP sont localement hyperboliques en tout point où il existe une fonction d'entropie localement convexe [161], et lorsqu'ils sont dotés d'une entropie strictement convexe, ils peuvent être symétrisés [73] [104] et sont donc globalement hyperboliques. Ces propriétés ont été au coeur de la théorie mathématique de l'existence et de l'unicité des solutions régulières Kawashima and Shizuta (1988) [118] Giovangigli and Massot (1998) [85], mais ils sont aussi une pierre angulaire pour l'étude des solutions faibles pour lesquelles les travaux de Kružkov (1970) [122] prouvent le caractère bien posé du problème de Cauchy pour une unique équation en trois dimension spatiale. Néanmoins, pour dériver les modèles à interface diffuse d'intérêt, nous avons recours à la thermodynamique rationnelle et le principe de moindre action (PMA), con-

duisant souvent à des systèmes qui ne peuvent pas être écrits sous forme conservative. C'est le cas du modèle Baer-Nunziato, qui permet de prendre en compte les déséquilibres hydrodynamiques, mécaniques et thermiques, et donc le meilleur candidat pour la présente thèse. La présence de termes non conservatifs dans le système d'EDP empêche l'utilisation de la théorie décrite ci-dessus. Toutefois, quelques avancées importantes ont émergé. Le modèle de Baer-Nunziato s'est avéré symétrisable [Coquel et al. \(2014\) \[31\]](#) – pas dans le sens de Godunov-Mock – loin de la condition de résonance pour laquelle l'hyperbolicité dégénère. Dans [Forestier and Gavriluyk \(2011\) \[71\]](#), en supposant qu'il n'y ait pas de résonance, le modèle s'avère partiellement symétrisable au sens de Godunov-Mock. Néanmoins, une théorie unificatrice étendant l'approche standard des systèmes de lois de conservation aux systèmes incluant des termes non conservatifs fait toujours défaut et permettrait de révéler des propriétés clés de ces systèmes telles que la loi de conservation supplémentaire de l'entropie, la symétrisation entropique et l'hyperbolicité.

2) *Modélisation mathématique et physique* : Dériver un modèle à interface diffuse à partir d'une analyse microscopique des plus petites échelles de la dynamique d'interface ne coule pas de source puisque le changement d'échelle impliqué introduit des termes non fermés, empêchant de récupérer la fermeture macroscopique des quantités interfaciales telles que la vitesse interfaciale ou la pression interfaciale. C'est pourquoi de nombreuses fermetures ont été proposées, sur la base de considérations relatives au type d'onde et à l'inégalité d'entropie, comme dans [Embid and Baer \(1992\) \[65\]](#), [Coquel et al. \(2002\) \[28\]](#), [Gallouët et al. \(2004\) \[78\]](#) pour le modèle Baer-Nunziato. Néanmoins, ils s'appuient fortement sur la thermodynamique associée du système, qui repose toujours sur l'hypothèse de phases non miscibles, écartant tout effet potentiel non idéal et impactant les invariants de Riemann du système. De plus, la structure dissipative ne peut pas être obtenue par le PMA et doit être postulée selon le deuxième principe de la thermodynamique. Des termes sources adéquats permettant la relaxation thermodynamique de la pression, de la vitesse et de la température des phases ainsi que le transfert de masse ont été proposés, basés sur une séparation des phénomènes [Lochon \(2016\) \[144\]](#), [Lorenzo et al. \(2017\) \[146\]](#), [De lorenzo \(2018\) \[45\]](#), mais aucun terme source généralisé n'a encore été dérivé sur la base des variables entropiques. En outre, si les modèles à interface diffuse offrent une hiérarchie de modèles en ce qui concerne le niveau d'équilibre thermodynamique et hydrodynamique entre les phases, ils fournissent une mauvaise description de la dynamique d'interface, limitée au transport de la fraction volumique de chaque phase dans chaque cellule de calcul. Dans les phases séparées, le gradient de la fraction volumique est un bon indicateur de la normale à l'interface, donc de la courbure locale. Néanmoins, dès que des phénomènes de surface de sous-échelle se produisent, la prédiction de la fraction volumique lisse tous les détails de l'écoulement et son gradient ne peut plus fournir d'informations significatives sur la topologie de l'interface. Des approches dites à double échelle ont fait leur apparition dans le cadre des méthodes VOF. Elles consistent à résoudre entièrement, sur une grille raffinée auxiliaire, la dynamique sous-échelle de l'interface à l'aide d'une Level Set supplémentaire [Herrmann \(2013\) \[106\]](#). Toutefois, une telle approche n'est pas directement applicable aux modèles à interface diffuse, car la représentation de l'interface n'est pas nécessairement discontinue. Pour les modèles à interface diffuse, les avancées reposent sur des équations d'évolution supplémentaires de grandeurs géométriques, comme le transport de la densité d'aire interfaciale grande et petite échelle dans les travaux de [M Devassy et al. \(2015\) \[148\]](#). Cette approche est très séduisante, mais il n'existe actuellement aucun formalisme mathématique permettant une séparation consistante et cohérente des échelles de l'interface.

3) *Thermodynamique* : Les modèles d'ordre réduit doivent être équipés d'une thermodynamique postulée. La plupart des approches de la thermodynamique multi-fluides sont basées sur l'hypothèse d'une absence d'interactions entre les fluides, ce qui a pour conséquence de doter chaque fluide de sa propre thermodynamique, puis de définir les quantités thermodynamiques de mélange en prenant la moyenne arithmétique de la contribution de chaque phase. Toutefois, dans la région interfaciale, des effets non idéaux tels que la compaction ou la tension superficielle se produisent et doivent être pris en compte dans la thermodynamique, ce qui remet en question la validité d'une approche de thermodynamique de phase isolée. De plus, une description précise de la dynamique de l'interface ne peut reposer que sur une thermodynamique d'interaction, comme par exemple dans les zones dispersées où les propriétés acoustiques du mélange ne peuvent pas être prédites par une approche thermodynamique de fluides isolés. Si un formalisme thermodynamique approfondi a été développé pour tenir compte des effets non idéaux dans les gaz multi-espèces, ce n'est pas encore le cas pour les écoulements multi-fluides.

4) *Méthodes numériques* : Alors que les propriétés mathématiques de ces modèles réduits Eulériens sont encore en cours d'investigation, même l'élément le plus riche de la hiérarchie des modèles dénués de toute complexité liée à la thermodynamique de mélange ou l'enrichissement de la description de l'interface, à savoir le modèle Baer-Nunziato, pose des problèmes numériques. Les modèles nécessitent des schémas numériques robustes et efficaces pour faire face aux fortes discontinuités et aux gradients élevés rencontrés dans les applications ciblées, mais aussi en adéquation avec les fermetures des termes interfaciaux. La présence de termes non conservatifs dans le système d'équations complexifie généralement la définition des solutions faibles au sens des distributions. Les conditions de saut de Rankine-Hugoniot, qui permettent de résoudre avec précision les problèmes de Riemann locaux, ne peuvent être définies sans ambiguïté. Il n'existe pas de théorie générale pour ces modèles, ce qui rend difficile la construction de schémas numériques efficaces. L'influence des produits non conservatifs sur les solutions discontinues incluant des chocs a été étudiée, par exemple pour la modélisation multi-composantes des écoulements plasmas hors équilibre thermique dans [Wargnier et al. \(2018\) \[219\]](#). Cette étude a montré que des traitements numériques sont nécessaires pour éviter les chocs non physiques dans la solution. Dans le cas du modèle Baer-Nunziato, il a été prouvé que la solution au travers d'une onde n'est pas unique [Andrianov and Warnecke \(2004\) \[3\]](#). En outre, comme les termes non conservatifs ne peuvent pas être écrits sous forme de divergence, ils ne sont pas traités comme des flux numériques mais comme des termes sources. La façon la plus simple de traiter les termes non conservatifs est de supposer localement que la pression et la vitesse interfaciales sur chaque interface à chaque intégration temporelle sont constantes ([Saurel and Abgrall \(1999\) \[190\]](#), [Zein et al. \(2010\) \[226\]](#), [Furfaro and Saurel \(2015\) \[74\]](#)) permettant une discrétisation simple. Néanmoins, les produits non conservatifs, généralement présents dans les équations phasiques, s'annulent mutuellement lors de la dérivation des équations de mélange. Cela a conduit au développement de plusieurs stratégies numériques allant des solveurs de Riemann exacts [Andrianov and Warnecke \(2004\) \[3\]](#), [Schwendeman et al. \(2006\) \[199\]](#), [Deledicque and Papalexandris \(2007\) \[47\]](#) aux solveurs de Riemann approchés [Saurel and Abgrall \(1999\) \[190\]](#), [Saurel et al. \(2009\) \[195\]](#), [Ambroso and Chalons \(2012\) \[1\]](#), y compris des techniques de correction basées sur des équations de mélange conservatives. De surcroît, des solveurs exacts du problème de Riemann linéarisé ont également été développés puisqu'ils sont capables d'inclure les termes non conservatifs dans la discrétisation [Sainsaulieu \(1995\) \[189\]](#), [Gallouët et al. \(2004\) \[78\]](#), [Pelanti and Shyue \(2014\) \[172\]](#). Enfin, un schéma de relaxation entropique a été proposé pour le modèle Baer-Nunziato dans Co-

quel et al. (2014) [32], Coquel et al. (2017) [29] pour lequel une inégalité d'entropie discrète est prouvée, garantissant la stabilité non linéaire de la méthode numérique. Néanmoins, ces développements complexes s'appliquent principalement aux éléments de base des modèles à interface diffuse, qui négligent la modélisation sous-échelle et utilisent la thermodynamique absente d'interaction. La prise en compte de ces deux principales avancées nécessiterait de nouveaux schémas numériques.

5) *Simulations numériques* : Les applications que nous visons sont caractérisées par de forts gradients et des discontinuités, les modèles réduits doivent donc aussi être évalués numériquement pour mettre en évidence leur prédictibilité prometteuse avant d'être largement déployées dans l'industrie. Nous devons donc d'abord mettre en oeuvre les méthodes numériques dans des codes CFD, capables d'être déployées sur des ressources massives de calcul pour atteindre des configurations réalistes. A l'ONERA, le logiciel de calcul multiphysique de CFD CEDRE Refloch et al. (2011) [184] fonctionne sur des maillages généraux non structurés et est organisé en un ensemble de solveurs. Deux d'entre eux sont des solveurs Eulériens. Le solveur CHARME est utilisé pour les fluides, postule des équations de Navier-Stokes multi-espèces et propose des modèles de turbulence LES ou RANS ainsi que des modèles de réactions chimiques. Le solveur SPIREE est dédié à l'écoulement en phase dispersée et est construit sur des modèles cinétiques de type KBMM, qui propose soit une approche d'échantillonnage par taille, également appelée méthodes multi-classe, soit des modèles Eulériens multi-fluides, également appelés méthodes *sectionnelles* Laurent and Massot (2001) [130]. CHARME ne fournit que le modèle le plus simple dans la hiérarchie des modèles à interface diffuse, pour lequel on suppose un équilibre en ce qui concerne la vitesse, la pression et la température des deux phases. Comme CEDRE vise une gamme plus large et ambitieuse d'applications, telles que des écoulements multiphasiques réactifs, les nouvelles générations de modèles doivent y être implémentées. Cette thèse contribue directement à cet objectif. Deuxièmement, afin de valider les modèles d'ordre réduit, nous devons être en mesure d'évaluer les résultats de la simulation. Habituellement, certaines données expérimentales sont disponibles, mais elles sont souvent limitées en termes de gammes d'applications et de collecte de données. Les données DNS pourraient ainsi fournir des éléments de comparaison précis sur des cas de tests élémentaires tout en augmentant pas à pas la complexité de l'écoulement. Cette approche semble très intéressante, mais des éléments de comparaison référents et exhaustifs n'ont pas encore été établis pour les écoulements diphasiques. En outre, même si certains cas tests bien connus existent, il n'est pas évident de comparer les résultats des modèles d'ordre réduit avec ceux de la DNS en raison de la différence des approches de modélisation.

CONTRIBUTION ET TOUR D'HORIZON DU MANUSCRIT

De nombreuses problématiques ont été examinées dans ce travail afin de disposer de bases solides pour contribuer de manière originale à la résolution de certains des éléments manquants décrits dans la section précédente.

Dans [Chapter 1](#), nous présentons tout d'abord les méthodes existantes pour dériver des modèles à interface diffuse d'écoulement diphasique à deux vitesses. Ensuite, nous proposons une dérivation à partir du calcul variationnel d'un modèle d'écoulement diphasique à deux vitesses contenant une équation sur l'entropie pilotant les phénomènes de relaxation. Nous mettons en évidence comment la pression et la vitesse interfaciale moyenne sont fermées et

les conséquences de leur fermeture en nous basant d’abord sur les types d’ondes et les invariants de Riemann, puis par une extension de la théorie existante des équations conservatives supplémentaires au système de lois non-conservatives. Ce résultat a été publié dans [Cordesse and Massot \(2020\) \[41\]](#). Première étape pour étendre la théorie de Godunov-Mock aux systèmes non conservatifs, cette contribution a permis d’obtenir des équations conservatives supplémentaires d’entropie pour le modèle de Baer-Nunziato ainsi que des contraintes sur les quantités interfaciales et la définition de la thermodynamique. En particulier, l’introduction d’un certain niveau de mélange des deux phases dans la définition de l’entropie de mélange a soulevé des problèmes d’incompatibilité entre l’existence d’un processus de mélange dans la thermodynamique et une pression interfaciale, remettant en question la manière de prendre en compte de manière cohérente les interactions dans la thermodynamique et le système d’EDP qu’elle équipe.

Dans [Chapter 2](#), nous introduisons un formalisme pour construire une thermodynamique multi-fluides, basée sur un état de référence et une loi de pression, prenant en compte les effets non idéaux. Il permet de mettre en évidence l’impact sur la structure mathématique du système dérivé du PMA et donne des indications sur la manière de récupérer les équations d’évolution de phase. Ce travail a été soumis dans [Cordesse et al. \(2020\) \[35\]](#).

Dans [Chapter 3](#), s’appuyant sur une fonction de densité de probabilité, nous nous écartons d’une approche géométrique de l’interface et proposons une approche multi-échelle de l’interface sans aucun postulat sur sa localisation ni sa forme. Ce nouvel outil de modélisation multi-échelle ne repose donc sur aucune hypothèse de topologie d’écoulement diphasique et semble faire converger les diverses approches, en particulier des modèles à interface diffuse et à interface discontinue, pour décrire l’écoulement multi-fluides. A partir de la fonction de densité de probabilité, nous reconstruisons les variables géométriques classiques et obtenons une décomposition naturelle en une partie filtrée et la fluctuation associée. Sur la base de ces quantités, nous étendons la définition du Lagrangien décrivant le milieu en écoulement diphasique barotrope en ajoutant des contributions cinétiques et potentielles à double échelle pour tenir compte de la cinématique et de la tension superficielle à petite échelle. Le PMA renvoie un système d’EDP montrant un couplage entre les grandes et les petites échelles. Nous étendons finalement le système à des équations d’état à deux paramètres pour chaque phase, conduisant à un modèle à une seule vitesse à six équations dans le même esprit que [Saurel et al. \(2009\) \[195\]](#). Ce chapitre est le résultat de trois travaux, [Cordesse et al. \(2020\) \[37\]](#), [Cordesse et al. \(2019\) \[40\]](#), [Cordesse et al. \(2019\) \[33\]](#) et d’un article soumis à *International Journal of Multiphase Flow* [Cordesse et al. \(2020\) \[34\]](#).

Dans [Chapter 4](#), nous faisons des hypothèses supplémentaires sur la thermodynamique et négligeons la pulsation pour réduire certaines difficultés liées au modèle original et obtenir un bloc primaire, à partir duquel nous dérivons un système asymptotique en supposant une relaxation instantanée de la pression. Nous procédons ensuite à l’analyse mathématique de la forme homogène du bloc primaire. Afin d’inclure les termes capillaires à grande échelle dans l’analyse mathématique, nous ajoutons une équation supplémentaire sur le gradient de la fraction volumique. Nous constatons que le modèle est faiblement hyperbolique. Nous présentons ensuite une stratégie de splitting d’opérateur conduisant à trois sous-systèmes correspondant respectivement à l’hydrodynamique et à la convection acoustique, puis aux flux capillaires de grande et de petite échelles et enfin à la procédure de relaxation des pressions, et nous procédons à leur analyse mathématique. Ensuite, nous détaillons la méthode numérique appliquée à chaque sous-système sur la base d’une discrétisation de type Volumes Finis et

enfin nous procédons à une vérification numérique du modèle mis en oeuvre en reproduisant des cas de test classiques en une et deux dimensions sélectionnés pour tester les flux d'Euler et les flux capillaires de grande échelle ainsi que la relaxation de la pression. Les résultats attestent de la fiabilité de la stratégie de splitting.

Chapter 5 comprend tout d'abord une comparaison qualitative et quantitative de certains éléments de la hiérarchie des modèles à interface diffuse, à savoir les modèles à vitesse et pression uniques et à deux vitesses et deux pressions, avec ou sans couplage avec un élément KBMM. Les simulations numériques ont été réalisées sur des configurations d'atomisation de jet cryogénique difficiles, en tant que démonstration de la faisabilité et représentent une première étape vers une véritable validation. Ensuite, nous avons constitué et étudié un premier ensemble d'une hiérarchie de cas tests conçus pour être compatibles avec la DNS tout en étant suffisamment proches des configurations industrielles, pour lesquels nous proposons une comparaison des simulations compressibles diphasiques avec les données issues de la DNS. Cette démarche a également permis de mieux comprendre les principales différences conceptuelles entre les deux approches de modélisation. Ce chapitre est le résultat de trois actes de conférence [Cordesse et al. \(2018\) \[36\]](#), [Murrone et al. \(2018\) \[163\]](#), [Cordesse et al. \(2019\) \[38\]](#), d'un rapport technique [Cordesse et al. \(2020\) \[37\]](#) et enfin d'un article [Cordesse et al. \(2019\) \[42\]](#) soumis à la revue *Flow, Turbulence and Combustion (FTaC)*.

PORTÉE SCIENTIFIQUE

La présente thèse a donné lieu aux contributions suivantes,

ARTICLE EN PRÉPARATION

- P. Cordesse, S. Kokh, M. Massot, *Derivation of a two-phase flow model with two-scale kinematics and surface tension by means of variational calculus*, in preparation for *International Journal of Multiphase Flow*.
- P. Cordesse, C. Le Touze, A. Murrone, S. Kokh, M. Massot, *Finite volume numerical strategy for dual-scale two-phase flow model*, in preparation for *Journal of Computational Physics*.

ARTICLE AVEC COMITÉ DE RELECTURE PUBLIÉ OU EN RELECTURE

- P. Cordesse, L. Matuszewski, M. Massot, *Multi-fluid thermodynamics from a pressure law approach*, submitted to *Continuum Mechanics and Thermodynamics*, 2020, 1–20.
- P. Cordesse, R. Di Battista, Q. Chevalier, L. Matuszewski, T. Ménard, S. Kokh, M. Massot, *A diffuse interface approach for disperse two-phase flows involving dual-scale kinematics of droplet deformation based on geometrical variables*, submitted to *ESAIM: Proceedings and Surveys*, 2019, 1–20.
- P. Cordesse, A. Remigi, B. Duret, A. Murrone, T. Ménard, F-X. Demoulin, M. Massot, *Validation strategy of reduced-order two-fluid flow models based on a hierarchy of direct*

numerical simulations, submitted to Flow, Turbulence and Combustion, 2019, 1–20 [HAL-02350200](#).

- P. Cordesse, M. Massot, *Entropy supplementary conservation law for non-linear systems of PDEs with non-conservative terms: application to the modelling and analysis of complex fluid flows using computer algebra*, Communications in Mathematical Sciences, 2019, 1–23, [HAL-01978949](#) in Press.

CHAPITRE DE RAPPORT TECHNIQUE

- P. Cordesse, A. Murrone, T. Ménard, M. Massot, *Comparative study of jet atomization simulations: direct numerical simulations and diffuse interface models coupled with kinetic-based moment methods*, Proceedings of the NASA Summer Program, 2020, 1–12, [HAL-02349534](#).
- P. Cordesse, S. Kokh, R. Di Battista, F. Drui, M. Massot, *Derivation of a two-phase flow model with two-scale kinematics, geometric variables and surface tension by mean of variational calculus*, Proceedings of the NASA Summer Program, 2020, 1–12, [HAL-02336996](#).

ACTE DE CONFÉRENCE

- P. Cordesse, A. Murrone, T. Ménard, M. Massot, *Validation strategy of reduced-order two-fluid flow models based on a hierarchy of direct numerical simulations*, Proceedings of the 2019 ICMF 10th International Conference on Multiphase Flow, Rio de Janeiro, Brazil, 2019, 1–8, [HAL-02194973](#).
- P. Cordesse, R. Di Battista, S. Kokh, M. Massot, *Derivation of a two-phase flow model with two-scale kinematics and surface tension by means of variational calculus*, Proceedings of the 2019 ICMF 10th International Conference on Multiphase Flow, Rio de Janeiro, Brazil, 2019, 1–6, [HAL-02194951](#).
- P. Cordesse, A. Murrone, M. Massot, *Coupling a hierarchy of diffuse interface model with kinetic-based moment methods for spray atomization simulations in cryogenic rocket engines*, Proceedings of the 2018 ICLASS 14th International Conference on Liquid Atomization and Spray Systems, Chicago, IL, USA, 2018, 1–8, [HAL-01888477](#).
- P. Cordesse, M. Massot, A. Murrone, *Mathematical modelling of multi-phase flow using entropy symmetrization*, Proceeding of the ECCM-ECFD, Glasgow, UK, 2018, 1–12, [HAL-01888513](#).
- A. Murrone, A. Boucher, P. Cordesse, *A five-equation model for the simulation of the two-phase flow in cryogenic coaxial injector*, Proceeding of the Space Propulsion, Seville, Spain, 2018, 1–12, [HAL-02195012](#).

POSTER ET PRÉSENTATION ORAL EN CONFÉRENCE

- P. Cordesse, *Two-fluid model hierarchy - thermodynamics, non-conservative terms and hyperbolicity/entropic symmetrization*, Invited speaker at the Second Workshop on Compressible Multiphase Flows, IRMA, université de Strasbourg, France, 2019.

- P. Cordesse, M. Massot, A. Murrone, *Multi-phase flow with two velocities modelling for jet atomization simulations*, Poster Session at the 44th Congrès National d'Analyse Numérique CANUM, Cap d'Agde, France, 2018.
- P. Cordesse, M. Massot, and A. Murrone, *Multi-phase flow modeling using entropy symmetrization and variational calculus for jet atomization simulations*, Oral presentation at the Dispersed two-phase flows conference, Toulouse, France, 2018.
- P. Cordesse, A. Murrone, M. Massot, C. Le Touze, A. Boucher, *Coupling a hierarchy of diffuse interface model with kinetic-based moment methods for primary atomization simulations in liquid propulsion*, Oral presentation at the 3rd International Conference on Numerical Methods in Multiphase Flows, Tokyo, Japan, 2017.

PROGRAMME D'ÉTÉ

Participation au programme d'été au NASA Ames research center, Advanced Supercomputing Division and Heliophysics, juillet 2018, *Large scale description of interfacial two-phase flows for the construction of a unified Eulerian model from injection to polydisperse spray using geometrical properties for subscale modeling: theoretical derivation, numerical implementation and DNS assessment*. Le projet a été dirigé par Marc Massot et nous avons été accueilli par Nagi N. Mansour.

CONSEILLERS ET COLLABORATEURS

La thèse a été financée par une bourse de doctorat de l'ONERA, du CNES et de l'Initiative HPC@Maths (École polytechnique). Elle a été initiée avec l'ONERA et le CNES au Laboratoire d'Energétique Moléculaire et Macroscopique, Combustion (EM2C) de CentraleSupélec, mais a été préparée en quasi-totalité au Centre de Mathématiques APpliquées (CMAP) de l'École polytechnique et à l'ONERA.

La thèse a bénéficié d'une large collaboration de personnes d'horizons différents. Ont été impliqués dans la thèse de doctorat en tant que conseillers et collaborateurs,

- ONERA : Clément Le Touze, Lionel Matuszewski,
- CORIA : Thibaut Ménard, François-Xavier Demoulin,
- CEA : Samuel Kokh,
- CMAP : Ruben Di Battista, Alberto Remigi,

et des discussions fructueuses avec Frédéric Coquel, Daniel Lhuillier et Vincent Giovangigli ont permis d'élargir la vision du travail présenté.

CONTENT

ACKNOWLEDGMENTS	i
ABSTRACT	iii
RÉSUMÉ	v
GENERAL INTRODUCTION	1
Space propulsion	1
Jet atomization process in sub-critical regime	3
Direct numerical simulation limitations	4
Reduced-order models strategies	5
Diffuse interface models and their challenges	7
Contribution and manuscript overview	10
Scientific outreach	12
INTRODUCTION GÉNÉRALE	15
Propulsion spatiale	15
Atomisation par jet en régime sous-critique	18
Limites des simulations numériques directes	19
Stratégie des modèles d'ordre réduit	20
Défis des modèles à interface diffuse	22
Contribution et tour d'horizon du manuscrit	25
Portée scientifique	27
1 TWO-VELOCITY FLOW MODELLING	37
1.1 Review of the derivation methods	40
1.1.1 Averaging approach	40
1.1.1.1 From a local instant formulation ...	40
1.1.1.2 ... to a macroscopic description	41
1.1.1.3 Examples on two-velocity two-phase flow model	45
1.1.1.4 Conclusion	46
1.1.2 Landau approach	46
1.1.3 Variational Principle and irreversible thermodynamics	48
1.1.3.1 Review of the evolution of the variational principle applied to compressible two-phase flow	48

	1.1.3.2	The question of the thermodynamics constraints	50
	1.1.3.3	Irreversible thermodynamics	52
1.1.4		Hierarchy of diffuse interface models	53
	1.1.4.1	Pressure and velocity relaxations	54
	1.1.4.2	Pressure, velocity and temperature relaxations	54
1.1.5		Conclusion	54
1.2		Derivation of a two-velocity two-phase flow model by means of the variational principle	55
	1.2.1	Decomposition of the infinitesimal variations of the action of a two-phase flow	55
	1.2.1.1	Notations	55
	1.2.1.2	Variations of the trajectories and of the action	56
	1.2.1.3	Stationary Action Principle	58
	1.2.2	Derivation of a two-velocity two-phase flow model	58
	1.2.2.1	Assumptions	59
	1.2.2.2	Transformations under constraints	59
	1.2.2.3	Action first infinitesimal variations	60
	1.2.2.4	Action second infinitesimal variations	61
	1.2.2.5	Final set of equations - simplified approach with two Gibbs equations	62
	1.2.2.6	From mixture equations to phase equations	63
	1.2.3	Conclusion	63
1.3		Mathematical analysis and closure of the seven-equation model	64
	1.3.1	Hyperbolicity study	64
	1.3.1.1	Primitive variables equations	64
	1.3.1.2	Eigenvalues and eigenvectors	66
	1.3.1.3	Non-resonance condition	67
	1.3.2	Wave types and interfacial velocity closure	67
	1.3.3	Riemann invariants and the interfacial pressure closure	68
	1.3.3.1	Riemann invariants	68
	1.3.3.2	Interfacial pressure closure	69
	1.3.4	Conclusion	70
1.4		Entropy supplementary conservation law for non-linear systems of PDEs with non-conservative terms: application to the modelling and analysis of complex fluid flows using computer algebra	71
	1.4.1	Abstract	71
	1.4.2	Introduction	71
	1.4.3	Supplementary conservation law	74
	1.4.3.1	First-order nonlinear conservative systems.	74
	1.4.3.2	Extension to systems involving non-conservative terms.	75
	1.4.3.3	Design or analysis of physical models using computer algebra.	77
	1.4.3.4	Methodology.	80
	1.4.4	Application to the Baer-Nunziato model	80
	1.4.4.1	Context and presentation of the model.	80
	1.4.4.2	Methodology and decomposition.	82

1.4.4.3	Non-miscible phases entropy.	82
1.4.4.4	Partially miscible phases entropy.	84
1.4.4.5	Interfacial closures impacting thermodynamics.	85
1.4.4.6	Thermodynamics impacting interfacial term closures.	85
1.4.4.7	Link with dispersed phase flow.	86
1.4.5	Application to the plasma model	87
1.4.5.1	Decomposition.	88
1.4.5.2	Ideal Gas entropy.	88
1.4.6	Conclusion	90
Appendices		91
1.A	Mixture entropy constraint for the SAP	91
1.B	System with stiff relaxation	91
1.B.1	Constraint manifold and projection assumptions	91
1.B.2	Relaxed system	94
1.B.3	Chapman-Enskog reduced model	94
1.C	Variational calculus: general overview	94
1.C.1	First variation of the action	95
1.C.2	Eulerian and Lagrangian coordinates	96
1.C.3	Eulerian and Lagrangian variations	96
1.C.4	Least Action Principle	96

2 DERIVATION OF A MULTI-FLUID THERMODYNAMICS ACCOUNTING FOR NON-IDEAL EFFECTS 97

2.1	A consistent Multi-Fluid thermodynamics formalism including non-ideal effects and interface geometry	99
2.1.1	Abstract	99
2.1.2	Introduction	100
2.1.3	Extensivity of a fluid mixture entropy	103
2.1.3.1	Thermodynamics challenges raised from the multi-fluid modeling	103
2.1.3.2	Recovering the extensivity of the mixture entropy at subscale	105
2.1.3.3	Choice of extensive and intensive set of variables to characterize a multifluid mixture	107
2.1.4	Building a multi-fluid thermodynamics	109
2.1.4.1	Assumptions and set of variables	109
2.1.4.2	Fundamental equation of thermodynamics and entropy	110
2.1.4.3	The pressure law approach	112
2.1.5	Implications of the new formalism	117
2.1.5.1	Gibbs equation hierarchy	118
2.1.5.2	Adding supplementary variables to the thermodynamics: illustration with the interfacial density area	119
2.1.5.3	Isothermal thermodynamics	120
2.1.5.4	Thermodynamics potentials of two-phase flow	121
2.1.6	Applications to two-phase flow modeling and impact of non-ideal effects	122
2.1.6.1	Stationary Action Principle and entropy closure	122

2.1.6.2	Impact of the non-ideal effects on the mathematical wave structure	123
2.1.6.3	The interest of the Gibbs equation hierarchy under partial entropy constraints	124
2.1.7	Shedding some lights on identified systems of the literature with non-ideal effects	125
2.1.7.1	Stagnation pressure in a dispersed phase	125
2.1.7.2	Osmotic pressure in a solute/solvent mixture	125
2.1.7.3	Modification of the thermodynamics potentials	127
2.1.7.4	Interface thermodynamics in bubbly flow	128
2.1.8	Conclusion	131
	Appendices	133
2.A	Isothermal thermodynamics	133
2.B	Recovering the mixture entropy extensivity	134
2.B.1	From subsystems to <i>many fluid</i>	134
2.B.2	From <i>many fluid</i> to multi fluid	137

3	DERIVATION OF TWO-SCALE KINEMATICS AND CAPILLARY TWO-PHASE FLOW MODEL TO DESCRIBE THE INTERFACE DYNAMICS	139
3.1	Review of surface description in two-phase flow modelling	141
3.1.1	What is a two-phase flow interface ?	141
3.1.2	Review of existing modelling approach of a two-phase interface	141
3.1.3	Review of existing models based on a surface approach of the interface	142
3.1.3.1	Interface tracking or capturing models	143
3.1.3.2	Diffuse interface models	143
3.1.3.3	Surface density function	144
3.1.3.4	Dispersed flow	145
3.1.3.5	Mean and Gauss curvatures	145
3.1.3.6	Interfacial closures	146
3.1.3.7	Scale separation	146
3.1.4	Going somewhere else with diffuse interface models	147
3.2	Two-scale description of an interface by means of a pdf	148
3.2.1	Definition of the pdf	148
3.2.2	Interfacial area density	148
3.2.3	Two-scale interface description	149
3.3	Deriving a two-scale two-phase interface model	151
3.3.1	Two-phase medium kinetic energy	151
3.3.2	Two-phase medium interfacial energy	152
3.3.3	Lagrangian energy of the two-phase system	152
3.3.4	Hamilton's stationnary action principle	152
3.3.5	Final form of the system	155
3.3.6	Dissipation	156
3.3.7	A hierarchy of models	157
3.4	Extending the two-scale two-phase interface model to a complete EOS	159
3.4.1	Stationary Action principle	159

3.4.2	Final form of the system	162
3.4.3	Dissipation	163
Appendices		165
3.A	Normal perturbation of a regular closed surface	165
3.B	A diffuse interface approach for disperse two-phase flows involving dual-scale kinematics of droplet deformation based on geometrical variables	166
3.B.1	Oscillating inclusion subscale modelling	168
3.B.1.1	Oscillating inclusion literature review	168
3.B.1.2	Analytical energy balance of an isolated oscillating inclusion	168
3.B.1.3	Direct Numerical Simulation Comparison and Validation . .	170
3.B.2	Two-scale kinematics Two-phase flow model	173
3.B.2.1	Hypotheses related to the small scale kinematics	174
3.B.2.2	Lagrangian energy of the two-phase system	175
3.B.2.3	Extremization of the action	176
3.B.2.4	Companion Conservation Equation	177
3.B.2.5	Final system	177
3.B.2.6	Dissipation	178
3.B.2.7	Properties of the system	180
3.B.3	Conclusion	180
3.B.4	Appendices	181
3.B.4.1	Energy analytical calculation of a deformed droplet	181
3.B.4.2	Approximation of the droplet deformation	181
3.B.4.3	Kinetic energy	183
3.B.4.4	Potential energy	185
3.B.4.5	Mean curvature	186

4	IMPLEMENTATION OF A FINITE VOLUME NUMERICAL STRATEGY FOR THE DUAL-SCALE TWO-PHASE FLOW MODEL	189
4.1	Selection of numerical schemes for the two-scale two-phase flow model	191
4.1.1	Simplified system to be implemented as a primary block	191
4.1.1.1	Thermodynamics closure	191
4.1.1.2	Micro-inertia free	192
4.1.1.3	Geometric variables	193
4.1.1.4	Final system of equations	194
4.1.2	Mathematical analysis of the models	195
4.1.2.1	Operator splitting	197
4.1.3	Numerical method	199
4.1.3.1	First sub-system: euler flux with HLLC Solver	201
4.1.3.2	Second sub-system: capillary flux	204
4.1.3.3	Third sub-system: pressure relaxation procedure	205
4.1.3.4	Second-order extension	207
4.1.3.5	Summary of the numerical procedure	207
4.2	CEDRE Implementation of the two-scale two-phase flow model	208
4.3	Numerical verification of the two-scale two-phase flow model	210
4.3.1	Verification tests of the Euler flux and the relaxation procedure	210

4.3.1.1	Pure interface advection	210
4.3.1.2	Water-air shock tube with moderate density ratio	211
4.3.1.3	Water-air shock tube with high density ratio	211
4.3.1.4	Two-phase flow problem: comparison with the <i>five equation</i> model	212
4.3.2	Verification tests of the capillary flux	218
4.3.2.1	Static capillary effects	218
4.3.2.2	Dynamic capillary effects: oscillating ellipsoidal drop	220
4.3.2.3	Dynamic capillary effects: uniform velocity flow	222
4.3.2.4	Dynamic capillary effects: water shock interaction	223
4.3.3	Verifications tests on the new geometric terms	226
Appendices		230
4.A	Model Analysis	230
4.A.1	Euler with capillary flux	230
4.A.2	Sub-system 1: Euler system	230
4.A.3	Sub-system 2: Capillary system	231
4.B	Energy equations	233
5	NUMERICAL SIMULATIONS TO COMPARE AND VALIDATE REDUCED- ORDER MODEL HIERARCHY	237
5.1	Qualitative comparison of a hierarchy of diffuse interface model with and with- out atomization	239
5.1.1	Numerical strategy: coupling a DIM with a KBMM element	239
5.1.2	Description of the configuration	241
5.1.3	Case 1: five-equation model with and without atomization	242
5.1.4	Case 2: five-equation model and instantaneously relaxed seven-equation model without atomization	244
5.1.5	Case 3: instantaneously relaxed seven-equation model and non-instantaneously relaxed seven-equation model with atomization	245
5.2	Validation strategy of reduced-order two-fluid flow models based on a hierar- chy of direct numerical simulations	247
5.2.1	Numerical methods employed	248
5.2.1.1	CEDRE (SEQUOIA) Solver	248
5.2.1.2	ARCHER Solver	249
5.2.2	First test case: an air-assisted water atomization using a coaxial injector	249
5.2.2.1	Description of the LEGI experiment	250
5.2.2.2	Numerical set-up	251
5.2.2.3	Qualitative comparison	252
5.2.2.4	Quantitative comparison	253
5.2.3	Second test case: an air-assisted water atomization using a flat injector	254
5.2.3.1	Description of the configuration	254
5.2.3.2	Identification of the DNS region of validity	259
5.2.3.3	Evaluation of the atomization global characteristics of both numerical approaches	260
5.2.3.4	Statistical analysis	263

5.2.4 Conclusion	272
CONCLUSION AND PERSPECTIVES	275
BIBLIOGRAPHY	279

TWO-VELOCITY TWO-PHASE FLOW MODEL | 1

DERIVATION AND ANALYSIS

Among the hierarchy of diffuse interface models (DIM)¹, well-known models such as the multi-species compressible Navier-Stokes, referred as the four-equation model have been massively adopted in the industry but have shown their limitations as they neglect the fluids thermodynamics non-equilibrium in the mixing zones. Therefore, recent efforts have been done to increase the non-equilibrium description of the phases by implementing and testing the so-called five-equation model accounting for two temperatures or even the Baer-Nunziato model, also called seven-equation model, whereby two temperatures, two pressures and two velocities are solved. The latter is the model of interest of this thesis, thus we will mainly focus on these two-phase flow models in this chapter.

The primary goal of this chapter is to introduce the existing methods to derive two-velocity two-phase flow diffuse interface models, which account for the highest level of thermodynamics non-equilibrium of the phases. First, we will provide a concise literature review of the first two methods, the averaging approach and the Landau approach, based on the original contributions found in the literature. Then, we will give an exhaustive description of the origins, the evolutions and the difficulties of the third method, the Stationary Action Principle (SAP), since it will be the method we will employ in the rest of the thesis to derive models. We conclude on recalling the hierarchy of diffuse interface models these methods provide and the technique to yield these systems of equations.

In the next section, we will derive a new two-velocity two-phase flow model from the variational calculus along with an equation on the entropy driving the relaxation phenomena. This derivation is based on an orthogonal decomposition of the infinitesimal variations and a set of unusual constraints. This work is still in progress.

Stemming from rational thermodynamics or SAP, the complexity of these non-equilibrium reduced-order models are threefold: 1) the macroscopic set of equations of these models often include non-conservative terms, 2) these models are hardly derived from physics at small scale of interface dynamics, they thus require closure of interfacial quantities such as the interfacial velocity or the interfacial pressure, 3) the thermodynamics has to be postulated and relies on a set of assumptions. Therefore, we will investigate the mathematical properties of these models by proposing a mathematical analysis of the well-known two-velocity two-phase flow model, the Baer-Nunziato model, by means of dedicated tools based on computer algebra to ease and enhance the mathematical analysis. In particular, we will highlight how the average interfacial pressure and velocity are closed and the consequences of their closures based on waves types and Riemann invariants.

¹Since the signification of *diffuse interface models* vary in the scientific community, DIM refer in the present thesis to any averaged model which allows locally the presence of each phase. These models can be obtained by a statistical averaging process for instance. The definition will be detailed in [Chapter 3](#)

The presence of the non-conservative terms prohibits the use of the existing Mock-Godunov theory only valid for conservative systems. We will therefore provide an extension of the existing theory of supplementary conservative equations to system of non-conservation laws and will apply it in particular to the Baer-Nunziato model by means of computer algebra. It will bring about entropy supplementary conservative equations for the Baer-Nunziato model together with constraints on the interfacial quantities and the definition of the thermodynamics. In particular, we will show that introducing some level of mixing of the two phases into the definition of the mixing entropy raises incompatibility issues between the existence of a mixing process in the thermodynamics of the mixture and the interfacial terms, questioning the way to account consistently for interactions in the thermodynamics and the system of PDE it equips. The outcomes of this last section have been published in Cordesse and Massot (2020) [41].

1.1	Review of the derivation methods	40
1.1.1	Averaging approach	40
1.1.1.1	From a local instant formulation ...	40
1.1.1.2	... to a macroscopic description	41
1.1.1.3	Examples on two-velocity two-phase flow model	45
1.1.1.4	Conclusion	46
1.1.2	Landau approach	46
1.1.3	Variational Principle and irreversible thermodynamics	48
1.1.3.1	Review of the evolution of the variational principle applied to compressible two-phase flow	48
1.1.3.2	The question of the thermodynamics constraints	50
1.1.3.3	Irreversible thermodynamics	52
1.1.4	Hierarchy of diffuse interface models	53
1.1.4.1	Pressure and velocity relaxations	54
1.1.4.2	Pressure, velocity and temperature relaxations	54
1.1.5	Conclusion	54
1.2	Derivation of a two-velocity two-phase flow model by means of the variational principle	55
1.2.1	Decomposition of the infinitesimal variations of the action of a two-phase flow	55
1.2.1.1	Notations	55
1.2.1.2	Variations of the trajectories and of the action	56
1.2.1.3	Stationary Action Principle	58
1.2.2	Derivation of a two-velocity two-phase flow model	58
1.2.2.1	Assumptions	59
1.2.2.2	Transformations under constraints	59
1.2.2.3	Action first infinitesimal variations	60
1.2.2.4	Action second infinitesimal variations	61
1.2.2.5	Final set of equations - simplified approach with two Gibbs equations	62
1.2.2.6	From mixture equations to phase equations	63
1.2.3	Conclusion	63

1.3	Mathematical analysis and closure of the seven-equation model	64
1.3.1	Hyperbolicity study	64
1.3.1.1	Primitive variables equations	64
1.3.1.2	Eigenvalues and eigenvectors	66
1.3.1.3	Non-resonance condition	67
1.3.2	Wave types and interfacial velocity closure	67
1.3.3	Riemann invariants and the interfacial pressure closure	68
1.3.3.1	Riemann invariants	68
1.3.3.2	Interfacial pressure closure	69
1.3.4	Conclusion	70
1.4	Entropy supplementary conservation law for non-linear systems of PDEs with non-conservative terms: application to the modelling and analysis of complex fluid flows using computer algebra	71
1.4.1	Abstract	71
1.4.2	Introduction	71
1.4.3	Supplementary conservation law	74
1.4.3.1	First-order nonlinear conservative systems.	74
1.4.3.2	Extension to systems involving non-conservative terms.	75
1.4.3.3	Design or analysis of physical models using computer algebra.	77
1.4.3.4	Methodology.	80
1.4.4	Application to the Baer-Nunziato model	80
1.4.4.1	Context and presentation of the model.	80
1.4.4.2	Methodology and decomposition.	82
1.4.4.3	Non-miscible phases entropy.	82
1.4.4.4	Partially miscible phases entropy.	84
1.4.4.5	Interfacial closures impacting thermodynamics.	85
1.4.4.6	Thermodynamics impacting interfacial term closures.	85
1.4.4.7	Link with dispersed phase flow.	86
1.4.5	Application to the plasma model	87
1.4.5.1	Decomposition.	88
1.4.5.2	Ideal Gas entropy.	88
1.4.6	Conclusion	90
	Appendices	91
1.A	Mixture entropy constraint for the SAP	91
1.B	System with stiff relaxation	91
1.B.1	Constraint manifold and projection assumptions	91
1.B.2	Relaxed system	94
1.B.3	Chapman-Enskog reduced model	94
1.C	Variational calculus: general overview	94
1.C.1	First variation of the action	95
1.C.2	Eulerian and Lagrangian coordinates	96
1.C.3	Eulerian and Lagrangian variations	96
1.C.4	Least Action Principle	96

1.1 REVIEW OF THE DERIVATION METHODS

Numerous two-phase flow models are found in the literature and only some of them will be presented hereafter. Their derivations mainly come from three methods: the averaging approach, the Landau methods of conservation laws and the Hamiltonian approach. Each method are based on different assumptions and leads to different modelling closure, which makes interesting the comparisons of the methods to understand the diversity of the existing closures.

We will first proceed to a short review of the averaging approach and the Landau method, referring explicitly to the original works they emanate from. Then, we will review the third method, SAP, which is of prior concern for the present thesis. Indeed, it will be applied to derive models. As a consequence we will give an exhaustive description of its origin and evolutions as well as the barriers encountered today with respect to the question of the entropy closure. Finally, we will recall the hierarchy of the diffuse interface models and how we obtain them.

1.1.1 AVERAGING APPROACH

As opposed to a single phase homogeneous flow, a multi-phase flow is composed of interfaces separating homogeneous phases. Each interface will be modeled in this chapter as a moving discontinuity preventing to address the heterogeneous flow as whole continuum, and thus one fails at applying conservation laws in the *mixed regions*. In [Chapter 3](#), we will revisit this axiom and depart from a geometric approach of the interface. Nonetheless, the conservation laws can still be applied in each homogeneous sub-regions. In [Ishii \(1975\) \[110\]](#), the author proposed to first describe locally each sub-regions, to extend equations across the interfaces and then apply an averaging procedure to obtain a macroscopic description of the flow.

1.1.1.1 FROM A LOCAL INSTANT FORMULATION ...

Given a multi-phase flow, where the position of the interface is assumed to be known, we assume that each sub-region constitutes a homogeneous medium, accurately described by the continuum approach. Thus, we can write for each phase k the continuity equation,

$$\partial_t \rho_k + \nabla \cdot [\rho_k \mathbf{v}_k] = 0, \quad (1.1a)$$

the momentum equation,

$$\partial_t (\rho_k \mathbf{v}_k) + \nabla \cdot [\rho_k \mathbf{v}_k \otimes \mathbf{v}_k + p_k \mathcal{I}_d] = \nabla \cdot \mathbf{D}_k + \rho_k \mathbf{f}_k^b, \quad (1.1b)$$

and the energy equation,

$$\partial_t (\rho_k E_k) + \nabla \cdot [(\rho_k E_k + p_k) \mathbf{v}_k] = \nabla \cdot [\mathbf{D}_k \cdot \mathbf{v}_k - \mathbf{q}_k] + \rho_k \mathbf{v}_k \cdot \mathbf{f}_k^b + \dot{\mathbf{q}}_k, \quad (1.1c)$$

where ρ_k , \mathbf{v}_k , p_k are the density, the velocity and the pressure of fluid k , \mathbf{D}_k the viscous tensor, \mathbf{f}_k^b any body force acting upon fluid k , \mathbf{q}_k the heat flux, $\dot{\mathbf{q}}_k$ any external energy source term and e_k the total energy, $E_k = \mathbf{v}_k^2/2 + e_k$ with e_k the internal energy.

These equations are then closed by three types of constitutive equations. The mechanical constitutive equations determine the viscous tensor and the body forces, the energetic constitutive equations yield a form to the heat flux and heat source term, and finally the constitutive equation of state relates the thermodynamics to the system of equations.

Furthermore, we need to add jump conditions across the interfaces where mass, momentum and energy exchanges between each sub-regions happen. Let \mathbf{n}_k be the outward pointing normal vector with respect to phase k of a mathematical surface $\mathcal{S}(\mathbf{x}, t) = 0$, $\mathbf{x} \in \mathbb{R}^3$, $t \in \mathbb{R}$ separating two fluids. By means of an integral balance equation of the conserved quantities $\varphi_k \in (\rho_k, \rho_k \mathbf{v}_k, \rho_k E_k)$ on a control volume of a portion of \mathcal{S} , neglecting diffusion, we obtain

$$\sum_{k=1,2} \int (\mathbf{f}(\varphi_k) - \mathbf{f}_I) \cdot \mathbf{n}_k \, d\mathcal{S} = 0, \quad (1.2)$$

with $\mathbf{f}(\varphi_k)$ the conservative flux of φ_k , \mathbf{f}_I the corresponding interfacial flux. When accounting for surface tension, it yields three jump conditions

$$\sum_{k=1,2} [\rho_k (\mathbf{v}_k - \mathbf{v}_I)] \cdot \mathbf{n}_k = 0, \quad (1.3a)$$

$$\sum_{k=1,2} [\rho_k \mathbf{v}_k \otimes (\mathbf{v}_k - \mathbf{v}_I) + p_k \mathcal{I}_d - \mathbf{T}] \cdot \mathbf{n}_k = 2\sigma H, \quad (1.3b)$$

$$\sum_{k=1,2} [\rho_k E_k (\mathbf{v}_k - \mathbf{v}_I) + (p_k - \mathbf{T}) \mathbf{v}_k] \cdot \mathbf{n}_k = 2\sigma H \mathbf{v}_I \cdot \mathbf{n}, \quad (1.3c)$$

$$(1.3d)$$

where the normal interfacial velocity \mathbf{v}_I is defined as the surface displacement velocity

$$\mathbf{v}_I \cdot \mathbf{n} = \partial_t \mathcal{S} / \|\nabla \mathcal{S}\|, \quad (1.4)$$

with $\|\bullet\|$ is the L^2 norm, σ is the surface tension coefficient and H is the local curvature of the interface with respect to fluid $k = 1$. The definition of the interfacial velocity is for the moment purely geometric.

These equations (1.1) are only valid in pure phase and jump relations (1.3) are appropriate for sharp interfaces. This set of equations could be directly solved through direct numerical simulations regardless the flow topology and many techniques exist such as Volume of Fluid combined with a Level Set methods recently applied in Vaudor et al. (2017) [216]. However, in industrial context, the time computation cost to solve all the flow details is too high, and sometimes not necessary. A macroscopic description of the flow might be sufficient as long as it is still predictive. Therefore, averaging procedure have been applied to the microscopic set of equations, to obtain a macroscopic formulation.

1.1.1.2 ... TO A MACROSCOPIC DESCRIPTION

We now want to re-establish a macroscopic description of a multiphase flow. Through the application of an averaging process on the microscopic equations, continuum mechanical equations are obtained. The procedure is summarized here. Shall $X_k(\mathbf{x}, t)$ the compact support phase function be defined as

$$X_k(\mathbf{x}, t) = \begin{cases} 1, & \text{if } \mathbf{x} \text{ is in phase } k \text{ at time } t \\ 0, & \text{if otherwise} \end{cases} \quad (1.5)$$

and is advected at the interfacial speed

$$\partial_t X_k + \mathbf{v}_I \cdot \nabla X_k = 0, \quad (1.6)$$

with $\nabla X_k = -\mathbf{n}_k \delta_k$, δ_k being the Dirac distribution of the interface associated to phase k .

We then multiply the conservative equations (1.1) by X_k and use an averaging operator $\langle \cdot \rangle$, which can be a time, space, weighted space or ensemble average, to obtain macroscopic equations. Each of these averaging processes embodies a vision of a mixture zone and will only influence the closure of interfacial source terms. Their effectiveness depends on the type of the flow. Time averaging is recommended Ishii (1975) [110] for turbulent two-phase flow and dispersed two-phase flow to smooth out local fluctuations. Space averaging is however more familiar since it gives a natural definition of the volume fraction α_k of phase k

$$\alpha_k \hat{=} \langle X_k \rangle. \quad (1.7)$$

Let us introduce the phase average and Favre average of a variable φ

$$\bar{\varphi} = \frac{\langle X_k \varphi \rangle}{\alpha_k}, \quad \tilde{\varphi} = \frac{\langle X_k \rho_k \varphi \rangle}{\alpha_k \bar{\rho}_k}. \quad (1.8)$$

Our prior interest is to understand the essence of the interfacial pressure and velocity terms employed in diffuse interface models. Therefore, we can neglect the body forces, the turbulence due to velocity fluctuations, the heat flux and heat source in the conservative equations (1.1), which do not play a role in their definition. Multiply Equations (1.1) by X_k and average them leads to

$$\partial_t (\alpha_k \bar{\rho}_k) + \nabla \cdot (\alpha_k \bar{\rho}_k \tilde{\mathbf{v}}_k) = \Gamma_k, \quad (1.9a)$$

$$\partial_t (\alpha_k \bar{\rho}_k \tilde{\mathbf{v}}_k) + \nabla \cdot [\alpha_k \bar{\rho}_k \tilde{\mathbf{v}}_k \otimes \tilde{\mathbf{v}}_k + \alpha_k (\tilde{p}_k \mathcal{I}_d - \tilde{\mathbf{T}}_k)] = M_k, \quad (1.9b)$$

$$\partial_t (\alpha_k \bar{\rho}_k \tilde{E}_k) + \nabla \cdot [\alpha_k (\bar{\rho}_k \tilde{E}_k + \tilde{p}_k - \tilde{\mathbf{T}}_k) \tilde{\mathbf{v}}_k] = p_{I,k}, \quad (1.9c)$$

where the quantities Γ_k , M_k and $p_{I,k}$ are the interfacial source terms defined by

$$\Gamma_k = \langle \rho_k (\mathbf{v}_k - \mathbf{v}_I) \cdot \nabla X_k \rangle, \quad (1.10a)$$

$$\mathbf{M}_k = \underbrace{\langle \rho_k (\mathbf{v}_k - \mathbf{v}_I) \otimes \mathbf{v}_k \nabla X_k \rangle}_{(1)} + \underbrace{\langle p_k \nabla X_k \rangle}_{(2)} - \underbrace{\langle \mathbf{D}_k \nabla X_k \rangle}_{(3)}, \quad (1.10b)$$

$$p_{I,k} = \underbrace{\langle \rho_k E_k (\mathbf{v}_k - \mathbf{v}_I) \cdot \nabla X_k \rangle}_{(1)} + \underbrace{\langle p_k \mathbf{v}_k \cdot \nabla X_k \rangle}_{(2)} - \underbrace{\langle \mathbf{D}_k \mathbf{v}_k \cdot \nabla X_k \rangle}_{(3)} \quad (1.10c)$$

with the jump conditions (accounting for surface tension)

$$\sum_{k=1,2} \Gamma_k = 0, \quad (1.11a)$$

$$\sum_{k=1,2} \mathbf{M}_k = 2\sigma \langle H \nabla X_1 \rangle, \quad (1.11b)$$

$$\sum_{k=1,2} p_{I,k} = \sum_{k=1,2} \langle \sigma H \mathbf{v}_I \cdot \nabla X_k \rangle. \quad (1.11c)$$

Remark 1. *It is to be noticed that the new jump conditions do not stem from the multiplication of the microscopic jump condition followed by the averaging procedure, but naturally from calculations. Nonetheless they are compatible.*

The source terms can be interpreted as follow: Γ_k corresponds to the mass transfer to phase k . (1) are the momentum and energy transfer due to mass transfer. (2) represents the pressure force and energy at the interface and (3) model the shear stress and its associated energy at the interface.

The system of equations obtained along with jump conditions contains many terms to model, and this gives birth to various closures. As discussed by Drew (1983) [57], some authors prefer to assume directly continuous conservative equations for each phase and then model the mass, momentum and energy transfer terms directly, bypassing the averaging process which leads to several unclosed terms. Nonetheless, this averaging process keeps a record on the microscopic terms, and thus offers guidelines for modelling.

Introduction of interfacial quantities Along the lines of Drew (1983) [57], we define the averaged interfacial velocity of phase k , $\langle \mathbf{v}_{I,k} \rangle$ as

$$\Gamma_k \langle \mathbf{v}_{I,k} \rangle \hat{=} \langle [\rho_k (\mathbf{v}_k - \mathbf{v}_I)] \otimes \mathbf{v}_k \nabla X_k \rangle, \quad (1.12)$$

to obtain a simple closure of the momentum transfer due to mass transfer. The interfacial pressure of phase k , $p_{I,k}$ is decomposed into its average and fluctuation parts $p_{I,k} = \langle p_{I,k} \rangle + p'_{I,k}$. We propose the following definition of the averaged interfacial pressure $\langle p_{I,k} \rangle$,

$$\langle p_{I,k} \rangle \nabla \alpha_k \hat{=} \langle p_k \nabla X_k \rangle - \langle p'_{I,k} \nabla X_k \rangle, \quad (1.13)$$

As a consequence, since we have neglected the velocity fluctuations, we have

$$\langle p_k \mathbf{v}_k \nabla X_k \rangle = \langle p_{I,k} \rangle \langle \mathbf{v}_{I,k} \rangle \cdot \nabla \alpha_k + \langle p'_{I,k} \nabla X_k \rangle \cdot \langle \mathbf{v}_{I,k} \rangle. \quad (1.14)$$

It leads to the following identification of the interfacial force density, $\mathbf{F}_{d,k}$

$$\mathbf{F}_{d,k} = \langle (p'_{I,k} - \mathbf{D}_k) \nabla X_k \rangle, \quad (1.15)$$

which is usually modelled as a drag force, the interfacial energy $E_{d,k}$

$$E_{d,k} = \langle (p'_{I,k} - \mathbf{D}_k) \nabla X_k \rangle \cdot \langle \mathbf{v}_{I,k} \rangle, \quad (1.16)$$

and the average interfacial energy due to mass transfert, $\langle E_{I,k} \rangle$

$$\langle E_{I,k} \rangle \Gamma_k \hat{=} \langle [\rho_k E_k (\mathbf{v}_k - \mathbf{v}_I)] \cdot \nabla X_k \rangle. \quad (1.17)$$

Finally the mean curvature H splits into

$$H = \langle H \rangle + H' \quad (1.18)$$

but we propose to neglect the fluctuating part to simplify the calculations. Equations (1.9) take now the form

$$\partial_t (\alpha_k \bar{\rho}_k) + \nabla \cdot (\alpha_k \bar{\rho}_k \tilde{\mathbf{v}}_k) = \Gamma_k, \quad (1.19a)$$

$$\partial_t (\alpha_k \bar{\rho}_k \tilde{\mathbf{v}}_k) + \nabla \cdot \left[\alpha_k \bar{\rho}_k \tilde{\mathbf{v}}_k \otimes \tilde{\mathbf{v}}_k + \alpha_k (\tilde{p}_k \mathcal{I}_d - \tilde{\mathbf{T}}_k) \right] = \Gamma_k \langle \mathbf{v}_{I,k} \rangle + \langle p_{I,k} \rangle \nabla \alpha_k + \mathbf{F}_{d,k} \quad (1.19b)$$

$$\partial_t(\alpha_k \bar{\rho}_k \tilde{E}_k) + \nabla \cdot [\alpha_k (\bar{\rho}_k \tilde{E}_k + \tilde{p}_k - \tilde{\mathbf{T}}_k) \tilde{\mathbf{v}}_k] = \Gamma_k \langle E_{I,k} \rangle + \langle p_{I,k} \rangle \langle \mathbf{v}_{I,k} \rangle \cdot \nabla \alpha_k + E_{d,k} \quad (1.19c)$$

with the jump conditions

$$\sum_{k=1,2} \Gamma_k = 0, \quad (1.20a)$$

$$\Gamma_1 (\langle \mathbf{v}_{I,1} \rangle - \langle \mathbf{v}_{I,2} \rangle) + (\langle p_{I,1} \rangle - \langle p_{I,2} \rangle) \nabla \alpha_1 + \sum_{k=1,2} \mathbf{F}_{d,k} = 2\sigma \langle H \rangle \nabla \alpha_1, \quad (1.20b)$$

$$\Gamma_1 (\langle E_{I,1} \rangle - \langle E_{I,2} \rangle) + (\langle p_{I,1} \rangle \langle \mathbf{v}_{I,1} \rangle - \langle p_{I,2} \rangle \langle \mathbf{v}_{I,2} \rangle) \nabla \alpha_1 + \sum_{k=1,2} E_{d,k} = \sigma \langle H \rangle (\langle \mathbf{v}_{I,1} \rangle - \langle \mathbf{v}_{I,2} \rangle) \nabla \alpha_1. \quad (1.20c)$$

Remark 2. The interfacial force density does not contain the force on the interface due to the average interfacial pressure $-\langle p_{I,k} \rangle \nabla \alpha_k$ called sometimes buoyant force or nozzling term as for instance in [Bdzil et al. \(1999\) \[7\]](#).

Interfacial quantity closures If the interface is assumed to have no proper mass, it seems reasonable to postulate

$$\langle \mathbf{v}_{I,1} \rangle = \langle \mathbf{v}_{I,2} \rangle = \langle \mathbf{v}_I \rangle, \quad (1.21)$$

as done in [Saurel and Abgrall \(1999\) \[190\]](#). Regarding the interfacial pressures, many closures are possible

- When no surface tension is accounted for,

$$\langle p_{I,1} \rangle = \langle p_{I,2} \rangle = \langle p_I \rangle, \quad (1.22a)$$

and many closure for $\langle p_I \rangle$ can be found in the literature and will be listed later on in this chapter.

- When surface tension is accounted for,

$$\langle p_{I,1} \rangle - \langle p_{I,2} \rangle = \sigma \langle H \rangle. \quad (1.22b)$$

- When accounting for both surface tension and packing in a dispersed flow where the dispersed phase is phase 2,

$$\langle p_{I,1} \rangle - \langle p_{I,2} \rangle = \sigma \langle H \rangle - p_c(\alpha_2). \quad (1.22c)$$

The contact pressure p_c is null for α_2 under a certain α_c , called the random close packing $\alpha_{RCP} \approx 0.65$ for spheres [Lhuillier et al. \(2013\) \[139\]](#), and then increases drastically when $\alpha_2 \rightarrow \alpha_c$.

For now on, we drop the averaging symbols \sim , $-$ and $\langle \rangle$ for sake of clarity.

The volume fraction equation The final step towards a complete two-phase flow model is to derive an evolution equation for the volume fraction. We could either simply approximate Equation (1.6) by

$$\partial_t \alpha_k + \mathbf{v}_I \cdot \nabla \alpha_k = 0, \quad (1.23)$$

or include the volume fraction as a thermodynamics variable and derive a compatible evolution equation ensuring the quasi-hyperbolicity of the system as proposed for the first time by Baer and Nunziato (1986) [5] and then by Saurel and Abgrall (1999) [190] as shown in Section 1.1.2.

1.1.1.3 EXAMPLES ON TWO-VELOCITY TWO-PHASE FLOW MODEL

Many models have been derived using the averaging approach. In 1983, Drew derived a dispersed two phase flows model. In 1984, Ransom and Hicks derived two different hyperbolic two-pressure models to find out the plausible causes of ill-posed Cauchy problems in the derivation of single pressure models leading to complex characteristics values [181]. Furthermore, Saurel and Abgrall (1999) [190] used the closure (1.21) and (1.22a) and defined an interfacial averaged energy $E_I = E_{I,1}/2 = E_{I,2}/2$, to close Equation (1.19)

$$\partial_t(\alpha_k \rho_k) + \nabla \cdot (\alpha_k \rho_k \mathbf{v}_k) = \epsilon_k \Gamma, \quad (1.24a)$$

$$\partial_t(\alpha_k \rho_k \mathbf{v}_k) + \nabla \cdot [\alpha_k \rho_k \mathbf{v}_k \otimes \mathbf{v}_k + \alpha_k p_k] = \epsilon_k \Gamma \mathbf{v}_I + p_I \nabla \alpha_k + \epsilon_k \mathbf{F}_d, \quad (1.24b)$$

$$\partial_t(\alpha_k \rho_k E_k) + \nabla \cdot [\alpha_k (\rho_k E_k + p_k) \mathbf{v}_k] = \epsilon_k \Gamma E_I + p_I \mathbf{v}_I \cdot \nabla \alpha_k + \epsilon_k \mathbf{v}_I \cdot \mathbf{F}_d, \quad (1.24c)$$

$$\partial_t \alpha_2 + \mathbf{v}_I \cdot \nabla \alpha_2 = 0, \quad (1.24d)$$

with $\epsilon_k = (-1)^{k+1}$, Γ the mass transfer to be determined empirically, the drag force \mathbf{F}_d defined as $\mathbf{F}_d = \lambda \mathbf{v}_d$ with \mathbf{v}_d the slip velocity $\mathbf{v}_d = \mathbf{v}_2 - \mathbf{v}_1$ and λ a positive parameter with a priori finite value, which can be interpreted as a velocity relaxation parameter controlling the rate at which velocities tends towards equilibrium, and the two interfacial closures

$$\mathbf{v}_I = \sum_{k=1,2} y_k \mathbf{v}_k, \quad p_I = \sum_{k=1,2} \alpha_k p_k, \quad (1.25)$$

with y_k the mass fraction of phase k defined as $y_k = \alpha_k \rho_k / \rho$, ρ being the mixture density defined as $\rho = \sum_{k=1,2} \alpha_k \rho_k$. System (1.24) is now symmetric with respect to each phase.

However, Saurel and Abgrall pointed out the need of a relaxation pressure process since behind two shock waves propagating in a separated two-phase flow, the model as it is (1.24) predicts a pressure discontinuity at the interface, each fluid having its own pressure, whereas physically both phases should relax towards an equilibrium pressure thanks to a multidimensional interface motion. The mean interfacial velocity given by Equation (1.25) cannot take into account this multidimensional interface motion. Hence, Saurel and Abgrall proposed to model the pressure relaxation process by a volume fraction variation and an energy variation

$$\partial_t \alpha_k = -\epsilon_k \mu p_d, \quad \partial_t \alpha_k \rho_k E_k = -\epsilon_k \mu p_I p_d, \quad (1.26)$$

with $p_d = p_2 - p_1$. The term μp_d expresses the rate of expansion of the volume fraction α_k such that pressures tend towards equilibrium. The variable μ controls the rate at which the

equilibrium is reached. In [Saurel and Le Metayer \(2001\) \[192\]](#), a mass flow rate term is added to the volume fraction transport equation. System (1.24) finally reads

$$\partial_t(\alpha_k \rho_k) + \nabla \cdot (\alpha_k \rho_k \mathbf{v}_k) = \epsilon_k \Gamma, \quad (1.27a)$$

$$\partial_t(\alpha_k \rho_k \mathbf{v}_k) + \nabla \cdot [\alpha_k \rho_k \mathbf{v}_k \otimes \mathbf{v}_k + \alpha_k p_k] = \epsilon_k \Gamma \mathbf{v}_I + p_I \nabla \alpha_k + \epsilon_k \lambda \mathbf{v}_d, \quad (1.27b)$$

$$\partial_t(\alpha_k \rho_k E_k) + \nabla \cdot [\alpha_k (\rho_k E_k + p_k) \mathbf{v}_k] = \epsilon_k \Gamma E_I + p_I \mathbf{v}_I \cdot \nabla \alpha_k + \epsilon_k \mathbf{v}_I \cdot \lambda \mathbf{v}_d - \epsilon_k \mu p_I p_d, \quad (1.27c)$$

$$\partial_t \alpha_2 + \mathbf{v}_I \cdot \nabla \alpha_2 = -\mu p_d + \epsilon_k \frac{\Gamma}{\rho_k}. \quad (1.27d)$$

System (1.27) has seven real eigenvalues not necessarily distinct

$$S_p = \{\mathbf{v}_1 - a_1, \mathbf{v}_1, \mathbf{v}_1 + a_1, \mathbf{v}_2 - a_2, \mathbf{v}_2, \mathbf{v}_2 + a_2, \mathbf{v}_I\}, \quad (1.28)$$

where a_k is the sound speed of phase k defined as $a_k^2 = \partial p_k / \partial \rho_k|_{s_k}$ with s_k the fluid entropy. The system is hyperbolic but some of the eigenvalues may collapse, in which case, as we will show in the mathematical analysis, the eigenvectors do not form a free basis. This phenomenon is called resonance. More importantly, the system contains first-order non-conservative terms, causing two mathematical issues: neither the theory of distribution used for conservation laws nor the Rankine-Hugoniot jump conditions can be used directly.

1.1.1.4 CONCLUSION

Averaging approach tries to bridge the gap between the precise microscopic description of fluids and a macroscopic approach of a two-phase flow. Nevertheless after averaging, many terms need to be closed, leading to a large variety of models. Moreover, the closures proposed are also usually based on the sub-scale topology of the interface, which circumscribes the utility of the derived models to a given flow topology, such as dispersed flow or granular flow.

1.1.2 LANDAU APPROACH

This second method consists of first postulating averaged conservation equations for each phase supplemented with unknown mass, momentum and energy exchange terms [Landau and Lifshitz \(1987\) \[207\]](#) according to the continuum mechanics theory [Truesdell \(1969\) \[212\]](#),

$$\partial_t(\alpha_k \rho_k) + \nabla \cdot (\alpha_k \rho_k \mathbf{v}_k) = \Gamma_k, \quad (1.29a)$$

$$\partial_t(\alpha_k \rho_k \mathbf{v}_k) + \nabla \cdot [\alpha_k \rho_k \mathbf{v}_k \otimes \mathbf{v}_k + p_{I,k}] = m_k^+, \quad (1.29b)$$

$$\partial_t(\alpha_k \rho_k E_k) + \nabla \cdot [(\alpha_k \rho_k E_k + p_{I,k}) \mathbf{v}_k + \mathbf{q}_k] = E_k^+ \quad (1.29c)$$

with $p_{I,k}$ the phase pressure, Γ_k , m_k^+ , E_k^+ the mass, momentum and energy exchange terms to be modelled. The body forces being out of interest in the discussion are neglected. Then, the conservation of mass, momentum and energy of the mixture constrain the unclosed terms of interactions, such that

$$\sum_{k=1,2} \Gamma_k = \sum_{k=1,2} m_k^+ = \sum_{k=1,2} E_k^+ = 0. \quad (1.30)$$

Finally, the second principle of thermodynamics is applied to the mixture, each phase being equipped with its own thermodynamics as if the phases were not seeing each other. Doing so, specific expressions for the exchange terms are obtained.

This method has been first implemented for two-phase flow by [Baer and Nunziato \(1986\) \[5\]](#), who proposed to add the volume fraction as an internal variable of the solid phase thermodynamics. The motivation of such novelty was to account for solid phase compaction since the model was derived to describe the deflagration-to-detonation (DDT) in gas-permeable, reactive granular materials.

The mixture entropy inequality derived from the second principle leads to an evolutionary equation for the volume fraction, consistent with the thermodynamics, and the system obtained in [Baer and Nunziato \(1986\) \[5\]](#) reads

$$\partial_t(\alpha_k \rho_k) + \nabla \cdot (\alpha_k \rho_k \mathbf{v}_k) = \Gamma, \quad (1.31a)$$

$$\partial_t(\alpha_k \rho_k \mathbf{v}_k) + \nabla \cdot [\alpha_k \rho_k \mathbf{v}_k \otimes \mathbf{v}_k + \alpha_k p_k] = \epsilon_k p_1 \nabla \alpha_k + \epsilon_k \lambda \mathbf{v}_d + \epsilon_k \Gamma \mathbf{v}_d, \quad (1.31b)$$

$$\begin{aligned} \partial_t(\alpha_k \rho_k E_k) + \nabla \cdot [\alpha_k (\rho_k E_k + p_k) \mathbf{v}_k + \mathbf{q}_k] = & \epsilon_k p_1 \mathbf{v}_d \cdot \nabla \alpha_k + \epsilon_k \lambda \|\mathbf{v}_d\|^2 + \epsilon_k h T_d \\ & + \epsilon_k \hat{p}_2 \frac{\alpha_1 \alpha_2}{\mu_c} (\hat{p}_2 - p_1) + \epsilon_k \Gamma E_d, \end{aligned} \quad (1.31c)$$

$$\partial_t \alpha_2 + \mathbf{v}_2 \cdot \nabla \alpha_2 = \hat{p}_2 \frac{\alpha_1 \alpha_2}{\mu_c} (\hat{p}_2 - p_1) + \frac{\Gamma}{\rho_2} \quad (1.31d)$$

with E_d and T_d are respectively the energy and the temperature differences between the phases $E_d = E_2 - E_1, T_d = T_2 - T_1$, the phase pressure has been identified to $p_{1,k} = \alpha_k p_k$. Accounting for the compaction of the granular phase, we notice the introduction of an extended pressure $\hat{p}_2 = p_2 - \beta_c$ with β_c the contact pressure of the grains. For the first time, an evolution equation for the volume fraction is obtained naturally from the thermodynamics closure. To fulfill the entropy inequality and sign all the terms, four coefficients have been introduced corresponding to four relaxations processes, namely

- a mass relaxation driven by the solid grain chemical reactions, hidden in the definition of Γ ,
- a velocity relaxation triggered by a drag force, driven by the coefficient λ ,
- a temperature relaxation thanks to conducto-convective heat transfer, whose coefficient is h ,
- a pressure relaxation driven by a compaction viscosity μ_c .

When comparing System (1.31) with System (1.27), we could interpret System (1.27) as a generalization of System (1.31) whereby the mean interfacial pressure is defined as the pressure of the most compressible phase, the gaseous phase, $p_I = p_1$ and the mean interfacial velocity is defined as the velocity of the most inertial phase, the grains, $\mathbf{v}_I = \mathbf{v}_2$. The pressure relaxation stemming from the thermodynamics found by [Baer and Nunziato \(1986\) \[5\]](#) has probably guided the pressure relaxation proposed by [Saurel and Abgrall \(1999\) \[190\]](#).

This model contains also non-conservative terms as in System (1.27). Embid and Baer studied the mathematical structure of the homogeneous BN model omitting source terms Embid and Baer (1992) [65]. The system yields six eigenvalues and one is doubled, \mathbf{v}_2 ,

$$S = \{\mathbf{v}_1 - a_1, \mathbf{v}_1, \mathbf{v}_1 + a_1, \mathbf{v}_2 - a_2, \mathbf{v}_2, \mathbf{v}_2 + a_2\} \quad (1.32)$$

with a_k the sound speed of phase k , whose expression depends on the equation of state. The velocity \mathbf{v}_2 is both responsible for entropy waves and compaction waves. The system is hyperbolic except in the case $\mathbf{v}_1 \pm a_1 = \mathbf{v}_2$ where resonance occurs. The authors refer this event to the choked flow condition.

1.1.3 VARIATIONAL PRINCIPLE AND IRREVERSIBLE THERMODYNAMICS

The third and last method to obtain a two-phase flow model is the variational principle. The variational approach uses Hamilton's principle of stationary action. General notations are introduced in Appendix 1.C. It states that any system will follow the physical path that minimizes its action \mathcal{A} , which is the integral over time and space of the energy of the system, the Lagrangian L , defined as the difference between the kinetic energy \mathcal{K} and the potential energy \mathcal{U} of the system. The equation

$$\delta_\lambda \mathcal{A} = 0, \quad (1.33)$$

returns a conservative system of partial differentiating equations describing the evolution of the system under arbitrary constraints.

Its advantage against other method is that the non-dissipative part of the model is obtained from the knowledge of only one scalar function, the Lagrangian of the system L . It can also account for specific effects, such as the microstructure of the flow or sub-scale effects, one just needs to introduce additional variables describing the phenomena to be accounted for Bedford and Drumheller (1978) [8]. For example, to model a bubbly flow, one needs to introduce variables to describe the volume and shape variations of the bubbles and the corresponding energies into the Lagrangian. If a certain effect is needed to be included, the variational approach consistently includes it in the mass, momentum and energy conservative equations. Still finding an explicit form of the Lagrangian that encompasses any flow topology remains a challenging task. SAP seems an appropriate candidate to derive two-phase flow models and will be the main methodology employed in this thesis (see Section 1.2 and Chapter 3). Therefore we propose a detailed review of this method, before applying it in the next section to derive a new model.

Last but not least, the dissipative part of the system must be added afterwards by exploiting the second principle of thermodynamics. As we will see later on, while for barotropic materials, the derivation is straightforward, it is still an open question when equipping the fluids with complete equations of state.

1.1.3.1 REVIEW OF THE EVOLUTION OF THE VARIATIONAL PRINCIPLE APPLIED TO COMPRESSIBLE TWO-PHASE FLOW

There are two equivalent methods to calculate the variation of Hamilton's action Serrin (1959) [200]: 1) the d'Alembert-Lagrange principle which uses Lagrangian multipliers to take into account constraints, and 2) the Hamilton's Principle based on an eulerian formalism which includes

the constraints into the virtual displacements. Geurst (1986) [83] proved that Euler and Lagrangian approaches are equivalents, both yield the same two-fluid equations and the latter can be transformed into the former by means of a canonical transformation. In the following, we will mainly focus on the Eulerian formulation.

Bedford and Drumheller (1978) [8] proposed the first application of the variational principle to obtain the equations of motion of a mixture in a continuum approach, reconnecting to the work done earlier with the averaging approach or later with the Landau approach described in the previous sections. Focusing on bubbly flow, he proposed to model the Lagrangian of compressible *non miscible* fluids as

$$L(\alpha_1\rho_1, \alpha_2\rho_2, \mathbf{v}_1, \mathbf{v}_2, \alpha_1) = \sum_{k=1,2} \left(\frac{1}{2}\alpha_k\rho_k\|\mathbf{v}_k\|^2 + b_k(\alpha_k, \mathbf{v}_d) - \alpha_k\rho_k\epsilon_k(\alpha_k, \rho_k) \right), \quad (1.34)$$

under the volume occupation and mass conservation constraints,

$$\sum_{k=1,2} \alpha_k = 1, \quad \partial_t(\alpha_k\rho_k) + \nabla \cdot (\alpha_k\rho_k\mathbf{v}_k) = 0, \quad (1.35)$$

where ϵ_k is the specific barotropic energy of each phase depending on the volume fraction to account for surface tension. The term b_k models the momentum supply from the interactions between phase k and the other constituents due to shear stress, thus function of the slip velocity and the volume fraction. Importantly, the derivation is done on a single reference space, i.e. with a single parameter family of virtual motion, considering the two-phase flow as a mixture, each phase staying independent due to the *immiscibility* assumption. Further works with the same methodology but with new terms have been done such as in Geurst (1985) [84] where a term was introduced into the kinetic energy to account for virtual mass still in the case of a bubbly flow reading $\rho_2 m(\alpha_2) \mathbf{v}_d^2/2$ where $m(\alpha_2)$ is called the virtual-mass coefficient and equals $m(\alpha_2) = \frac{1}{2}\alpha_2$ for spherical gas bubbles at low concentration, and under partial mass conservation constraints.

Later on, one major change has been put forward by Gouin (1990) [93]. The author decided to use a reference space for each component and thus to apply the variational principle with a two-parameter family of virtual motions of the mixture so that virtual displacements of *miscible* fluid mixtures can be considered. Gouin also pointed out that the potential energy does not always divide into internal energies related to each constituent of the mixture since interactions can occur. This idea has been carried on in Gavriljuk et al. (1997) [80], where they derived the conservative momentum equations. Then, using the Noether's theorem, they also retrieved a total energy and momentum equations in Gavriljuk et al. (1998) [82]. They also obtained Rankine-Hugoniot conditions and proved the hyperbolicity of the governing system in the one-dimensional case. In Gavriljuk et al. (1997) [80] the authors justified the dependence of the internal energy of a mixture on the relative motion of the components saying that since each phase has its own velocity, one shall not disregard their motions within the mixture. They proposed an extended form for the Lagrangian for a two-velocity system

$$L(\alpha_1\rho_1, \alpha_2\rho_2, \mathbf{v}_1, \mathbf{v}_2, \alpha_1) = \sum_{k=1,2} \frac{1}{2}\alpha_k\rho_k\|\mathbf{v}_k\|^2 - W(\alpha_1\rho_1, \alpha_2\rho_2, \mathbf{v}_d) \quad (1.36)$$

under the constraints

$$\partial_t(\alpha_k\rho_k) + \nabla \cdot (\alpha_k\rho_k\mathbf{v}_k) = 0, \quad k = 1, 2 \quad (1.37)$$

where $W(\alpha_1\rho_1, \alpha_2\rho_2, \mathbf{v}_d)$ is the potential energy and a simple case is given

$$W(\alpha_1\rho_1, \alpha_2\rho_2, \mathbf{v}_d) = \epsilon(\alpha_1\rho_1, \alpha_2\rho_2) - \frac{1}{2}g(\alpha_1\rho_1, \alpha_2\rho_2) \mathbf{v}_d^2, \quad (1.38)$$

g is a positive function and can be associated to an added mass effect. Further work on the same Lagrangian are done by [Gavrilyuk and Gouin \(1999\) \[79\]](#) and [Gouin and Gavrilyuk \(1999\) \[94\]](#).

In [Gavrilyuk and Saurel \(2002\) \[81\]](#), the authors obtained a two-phase compressible flow with two velocities taking into account micro-inertia for bubbly flow. The SAP has yielded a momentum equation for each fluid. Then the Noether's Theorem has led to the total energy equation. Finally they built the dissipative part of the system using the entropy inequality. The final system of equations is reminiscent of the Baer-Nunziato model [Baer and Nunziato \(1986\) \[5\]](#), but includes supplementary terms due to the micro-inertia.

1.1.3.2 THE QUESTION OF THE THERMODYNAMICS CONSTRAINTS

In this paragraph, we would like to point out the fact that the Stationary Action Principle does not always provide a closed system of equations. Indeed, as mentioned in the previous paragraph, for compressible two-phase flow, it yields the momentum equations together with the assumed constraints imposed on the flow. The latter are always composed at least of the mass conservation, which seems natural, but usually also of the partial entropy conservations $D_{k,t}S_k = 0$ as in [Gouin and Gavrilyuk \(1999\) \[94\]](#). These latter constraints are questionable in the sense that they prohibit any interaction between the fluids and prevent a thermodynamics relaxation of the phases, which must be added *a posteriori* by exploiting the second thermodynamics principle and postulating relaxation source terms. However these entropy closures are very accommodating since we can infer from them the phase internal energy transport equations given a Gibbs equation for each phase, and thus the system of equations is closed. Nevertheless if we want to allow exchange of entropy among the phases to reach for example thermodynamics equilibrium among the phases, we can no more assume the partial entropy conservations, and therefore the Stationary Action Principle fails at generating a closed system of equations. One needs to model the entropy closure of the system and several approaches can be found in the literature.

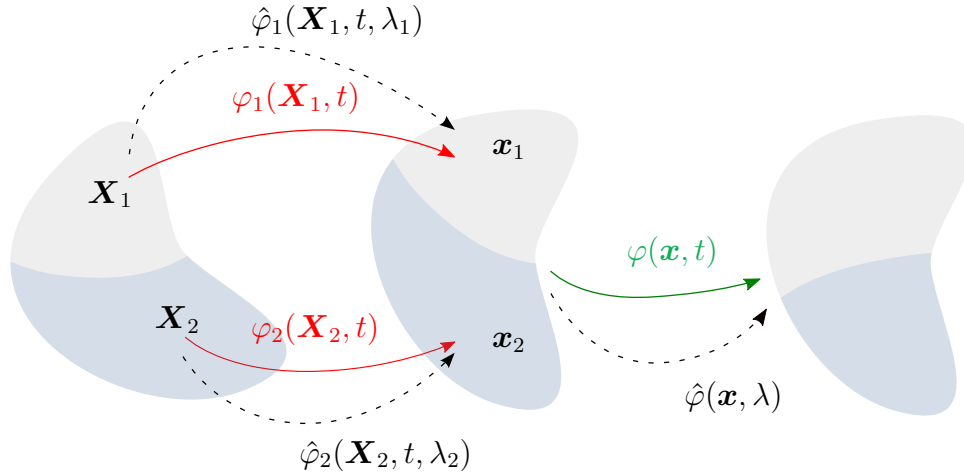
A first attempt to avoid the partial entropy conservation hypotheses has been proposed by [Gouin and Ruggeri \(2009\) \[95\]](#), where two virtual motions as shown in [Figure 1.1](#) are successively applied on the fluid mixture described by the following Lagrangian

$$L(\alpha_1\rho_1, \alpha_2\rho_2, \mathbf{v}_1, \mathbf{v}_2, s_1, s_2) = \sum_{k=1,2} \frac{1}{2} \alpha_k \rho_k \|\mathbf{v}_k\|^2 - \eta(\alpha_1\rho_1, \alpha_2\rho_2, \mathbf{v}_d, s_1, s_2) \quad (1.39)$$

where η denotes the volumetric potential energy of the mixture, being the sum of the internal energy and the extraneous force potentials.

- A first virtual motion defined by a two-parameter family $\hat{\varphi}_k(\mathbf{X}_k, t, \lambda_k)$ under partial masses and specific entropies conservation constraints, leads to the partial momentum equations.
- A second virtual motion defined by an one-parameter family $\hat{\varphi}(\mathbf{x}, \lambda)$ under partial masses conservation, associated with the time parameter, exploits the invariance with

respect to time of the system not to generate the total energy equation, as the Noether's theorem would do, but rather a transport equation linking the two specific entropies. Among all the variables of the system only the internal variables are assumed to be affected by this second virtual motion, and the authors considered only the entropies s_k as internal variables.



$$\text{constraints} \begin{cases} \partial_t(\alpha_k \rho_k) + \nabla \cdot [\alpha_k \rho_k \mathbf{v}_k] = 0, \\ D_{k,t} s_k = 0 \end{cases}, \quad \begin{cases} \partial_t(\alpha_k \rho_k) + \nabla \cdot [\alpha_k \rho_k \mathbf{v}_k] = 0 \end{cases}$$

FIGURE 1.1: Schematic representation of transformations applied to a portion of a two-phase flow and constraints.

The second virtual motion leads to the following equation

$$\alpha_1 \rho_1 T_1 \frac{D_1 s_1}{Dt} + \alpha_2 \rho_2 T_2 \frac{D_2 s_2}{Dt} = 0, \quad (1.40)$$

and the latter replaces the advection equations on the specific entropies, which were set as constraints in the first virtual motion. Nonetheless, this new equation (1.40) links both entropies and does not permit to recover an equation for each phase. Thus the system obtained is not closed yet since one needs the evolution equation of each entropy s_k . Further assumptions are needed.

For specific flows, such as quantum fluids, it is reasonable to assume that the mixture entropy s is convected along one of the two components trajectory [Landau and Lifshitz \(1987\) \[207\]](#), and identifying $s = s_1, s_2 = 0$ in Equation (1.40) closes the system.

In [Gouin and Ruggeri \(2009\) \[95\]](#), the authors finally assumed that the mixture is weakly out of equilibrium, $|\mathbf{v}_d| \ll 1$. Considering this last assumption, they approximate the potential energy to the internal energy of the mixture

$$\eta(\alpha_1 \rho_1, \alpha_2 \rho_2, \mathbf{v}_d, s_1, s_2) \approx \rho e(\alpha_1 \rho_1, \alpha_2 \rho_2, s_1, s_2). \quad (1.41)$$

Furthermore, they introduce an averaged temperature T , implicitly defined as the solution of

$$e(\rho, \rho_1/\rho, T) = e(\alpha_1 \rho_1, \alpha_2 \rho_2, s_1, s_2), \quad (1.42)$$

where the internal specific energy $e(\rho, \rho_1/\rho, T)$ satisfies the following mixture Gibbs equation

$$T ds = de(\rho, \rho_1/\rho, T) - \frac{p(T)}{\rho^2} d\rho + (g_2 - g_1) d(\rho_1/\rho) \quad (1.43)$$

where $p(T)$ is the equilibrium pressure at temperature T and g_k is the gibbs potential of phase k . After some calculations based on a first-order expansion near thermal equilibrium, the final system obtained takes the form

$$\partial_t(\alpha_k \rho_k) + \nabla \cdot [\alpha_k \rho_k \mathbf{v}_k] = 0 \quad (1.44a)$$

$$\partial_t(\alpha_k \rho_k \mathbf{v}_k) + \nabla \cdot [\alpha_k \rho_k \mathbf{v}_k \otimes \mathbf{v}_k] + \nabla(\alpha_k p_k) = p_k \nabla \alpha_k \quad (1.44b)$$

$$\rho_k T(T_{k'} - T_k) D_{k,t} s_k = T_{k'} \Lambda \nabla \cdot (\mathbf{v}_h)^2 \quad (1.44c)$$

where $k' = k + 1[2]$, $p - p(T) = -\Lambda \nabla \cdot (\mathbf{v}_h)$, and $p = \alpha_1 p_1 + \alpha_2 p_2$. Details of the calculations have not been reported here, the main point is to see they obtained a closure under supplementary assumptions on the flow.

An appealing alternative would be to put a constraint not on the phasic entropies but rather on the mixture entropy of the system s , removing the need of assuming independent thermodynamics for each fluid. Nonetheless, assuming this constraint alone leads to a temperature equilibrium of the phase [Gouin \(1990\) \[93\]](#). Details of the calculations are reported in [Appendix 1.A](#).

To conclude, the Stationary Action Principle is a powerful tool to derive the non-dissipative part of two-phase flow models from a unique scalar function, the Lagrangian. Yet as we have seen, the constraints applied on the flow have a high impact on the final model. Furthermore, when accounting for phase thermodynamics interactions, one cannot assume phase entropy advections, preventing the system to be closed. In the next [Section 1.2](#), we will provide an original derivation inspired from [Gouin and Ruggeri \(2009\) \[95\]](#) based on two ingredients: 1) an orthogonal decomposition of the infinitesimal variations, justifying the two successive infinitesimal variations used in [Gouin and Ruggeri \(2009\) \[95\]](#), and 2) novel set of constraints.

Before moving on to [Section 1.2](#), where we will apply the SAP to derive a new two-velocity two-phase flow model in an innovative manner, we would like to introduce the hierarchy of DIM these three methods offer. This brief review details how the most non-equilibrium two-phase flow model can yield some elements of the hierarchy of DIM. This review seems important since some of these elements are more frequently used in CFD codes, as more simple or adequate depending on the applications. Moreover we will conduct numerical simulations with some of them in [Chapter 5](#).

1.1.3.3 IRREVERSIBLE THERMODYNAMICS

The Stationary Action Principle always returns a non-dissipative system of equation, which may include relaxation phenomena that are reversible. An example of reversible relaxation phenomenon is the micro-inertia proposed in [Gavrilyuk and Saurel \(2002\) \[81\]](#) and revisited in [Drui et al. \(2019\) \[60\]](#). Irreversible thermodynamics must be added a posteriori through the second principle of thermodynamics, which states that the evolution equation of the entropy must be signed. It thus consists in adding dissipative effects through sources terms to the system of equation, while verifying the second principle of thermodynamics. Examples of irreversible effects are mechanical, hydrodynamical and thermal relaxation process, which allow the phases to reach equilibrium.

1.1.4 HIERARCHY OF DIFFUSE INTERFACE MODELS

While the assumptions and mathematical tools differ from one another, the three methods introduced hereinbefore can yield a hierarchy of reduced-order models based on reversible and irreversible relaxation phenomena.

A hierarchy of diffuse interface models based on both reversible and irreversible relaxation phenomena has been carefully built and examined in the PhD thesis of Florence Drui [Drui \(2017\) \[59\]](#) and published in [Drui et al. \(2019\) \[60\]](#). We refer the reader to these works. We propose in this section to draw the hierarchy of diffuse interface models based only on irreversible relaxation terms.

We thus go back to System (1.27) where the source terms describe the mechanical, hydrodynamic and thermal relaxations between the two phases. Introducing $\mathbf{q} \in \mathbb{R}^7 \mapsto \mathbf{r}(\mathbf{q}) \in \mathbb{R}^7$, an application describing the mechanical, hydrodynamic and thermal relaxations between the two phases, the condition $\mathbf{r}(\mathbf{q}) = 0_{\mathbb{R}^7}$ imposes three constraints, namely pressure, velocity and temperature equilibria, and defines the constrained manifold

$$\mathcal{E} = \left\{ \mathbf{q} \in \mathbb{R}^7, \mathbf{r}(\mathbf{q}) = 0_{\mathbb{R}^7} \right\}. \quad (1.45)$$

Remark 3. *In the present thesis, we will not account for mass and heat transfer. Such effects have been widely investigated in the recent PhD theses of [Lochon \(2016\) \[144\]](#), [De lorenzo \(2018\) \[45\]](#).*

When only pressure and velocity relaxations are accounted for, System (1.27) takes the form,

$$\partial_t \mathbf{q} + \mathcal{A}(\mathbf{q}) \partial_x \mathbf{q} = \mathbf{r}(\mathbf{q}), \quad (1.46a)$$

with $\mathcal{A}(\mathbf{q}) = \partial_{\mathbf{q}} \mathbf{f}(\mathbf{q}) + \mathcal{N}(\mathbf{q})$ and

$$\partial_{\mathbf{q}} \mathbf{f}(\mathbf{q}) = \begin{pmatrix} 0 & \mathbf{0} & \mathbf{0} \\ \mathbf{0} & \partial_{\mathbf{q}_2} \mathbf{f}_2(\mathbf{q}_2) & \mathbf{0} \\ \mathbf{0} & \mathbf{0} & \partial_{\mathbf{q}_1} \mathbf{f}_1(\mathbf{q}_1) \end{pmatrix}, \quad \mathcal{N}(\mathbf{q}) = \begin{pmatrix} v_I & \mathbf{0} & \mathbf{0} \\ \mathbf{n}_2 & \mathbf{0} & \mathbf{0} \\ \mathbf{n}_1 & \mathbf{0} & \mathbf{0} \end{pmatrix}, \quad (1.46b)$$

$$\mathbf{q}_k = \begin{pmatrix} \alpha_k \rho_k \\ \alpha_k \rho_k v_k \\ \alpha_k \rho_k E_k \end{pmatrix}, \quad \mathbf{f}_k(\mathbf{q}_k) = \begin{pmatrix} \alpha_k \rho_k v_k \\ \alpha_k (\rho_k v_k^2 + p_k) \\ \alpha_k (\rho_k E_k + p_k) v_k \end{pmatrix}, \quad \mathbf{n}_k(\mathbf{q}) = \epsilon_k \begin{pmatrix} 0 \\ p_I \\ p_I v_I \end{pmatrix}, \quad (1.46c)$$

where the column vector $\mathbf{q} \in \mathbb{R}^7$ is defined by $\mathbf{q}^t = (\alpha_2, \mathbf{q}_2^t, \mathbf{q}_1^t)$, the conservative flux $\mathbf{f} : \mathbf{q} \in \Omega \mapsto \mathbb{R}^7$ reads $\mathbf{f}(\mathbf{q})^t = (0, \mathbf{f}_2(\mathbf{q}_2)^t, \mathbf{f}_1(\mathbf{q}_1)^t)$ and $\mathcal{N} : \mathbf{q} \in \Omega \mapsto \mathbb{R}^{7 \times 7}$ is the matrix containing the non-conservative terms. Concerning the relaxation source term, $\mathbf{r}(\mathbf{q})$, it decomposes into

$$\mathbf{r} = \lambda \mathbf{r}^v + \mu \mathbf{r}^p, \quad \mathbf{r}^v = \begin{pmatrix} 0 \\ \mathbf{r}_2^v \\ \mathbf{r}_1^v \end{pmatrix}, \quad \mathbf{r}^p = \begin{pmatrix} p_d \\ \mathbf{r}_2^p \\ \mathbf{r}_1^p \end{pmatrix}, \quad (1.47a)$$

$$(\mathbf{r}_k^v)^t = -\epsilon_k (0, v_d, v_I v_d), \quad (\mathbf{r}_k^p)^t = -\epsilon_k (0, 0, p_I p_d) \quad (1.47b)$$

An expression for the relaxation parameters λ and μ have been derived for example using the DEM technic in [Saurel et al. \(2003\) \[191\]](#).

1.1.4.1 PRESSURE AND VELOCITY RELAXATIONS

Relaxing the pressure and the velocity can be interpreted as projecting the out-of-equilibrium state $\mathbf{q} \in \mathbb{R}^7$ on the constraint manifold \mathcal{E} where the relaxation $\mathbf{r}(\mathbf{q}) = 0_{\mathbb{R}^7}$ occurs. Details of the derivation method can be found in [Appendix 1.B](#).

One can thus look for reduced model by projecting $\mathbf{q} \in \mathbb{R}^7$ on multiple spaces \mathbb{R}^p , $p \leq 7$, and derive a hierarchy of reduced-order models. The hydrodynamical instantaneous relaxation leads to the *six-equation model* [Saurel et al. \(2009\) \[195\]](#). Relaxing both pressures and velocities, we obtain a *five-equation model* [Kapila et al. \(2001\) \[115\]](#).

In [Murrone and Guillard \(2005\) \[164\]](#), the authors interpret the reduced model as the asymptotic limit of the *seven-equation model* when $\mu \rightarrow 0$ and $\lambda \rightarrow 0$. Following their lines, the *five-equation model* reads

$$\partial_t \mathbf{q} + \mathcal{A}(\mathbf{q}) \partial_x \mathbf{q} = \tilde{\mathbf{r}}(\mathbf{q}) \quad (1.48)$$

with the conservative variables $\mathbf{q} = (\alpha_2, \mathbf{q}_2^t, \mathbf{q}_1^t)^t$, $\mathbf{q}_k = (\alpha_k \rho_k, \alpha_k \rho_k \mathbf{v}, \alpha_k \rho_k E_k)^t$, $\mathcal{A}(\mathbf{q})$ as in Equation (1.85) but with $v_1 = v_1 = v_2 = v$, $p_1 = p_1 = p_2$. The relaxation source term, $\tilde{\mathbf{r}}(\mathbf{q})$, is derived by taking the Taylor series of the $\mathbf{r}(\mathbf{q})$ with respect to μ and λ . It yields

$$v_1 = v + o(\lambda), \quad p_1 = p + o(\mu), \quad (1.49a)$$

$$\lambda v_d = \rho y_1 y_2 \left(\frac{1}{\rho_1} - \frac{1}{\rho_2} \right) \partial_x p + o(\lambda), \quad \mu p_d = \alpha_1 \alpha_2 \frac{\rho_1 a_1^2 - \rho_2 a_2^2}{\sum_{k=1,2} \alpha_{k'} \rho_k a_k^2} \partial_x v + o(\mu). \quad (1.49b)$$

The zero order terms are injected into Equation (1.47a) to define $\tilde{\mathbf{r}}$. For the *five-equation model*, the two partial momentum and energy equations are summed and replaced by an equation on the total momentum ρv and an equation on the total energy ρE respectively. Only one relaxing term remains in the system of equation, in the volume fraction equation, which becomes

$$D_t \alpha = \alpha_1 \alpha_2 \frac{\rho_1 a_1^2 - \rho_2 a_2^2}{\sum_{k=1,2} \alpha_{k'} \rho_k a_k^2} \partial_x v. \quad (1.50)$$

Thus the only difference in terms of equations between the *five-equation model* and the *instantaneously relaxed seven-equation model* lies in the volume fraction equation.

1.1.4.2 PRESSURE, VELOCITY AND TEMPERATURE RELAXATIONS

Finally, when relaxing also the temperatures [Zein et al. \(2010\) \[226\]](#), one obtains the multi-species compressible Navier-Stokes equations, called also *four-equation model*. This last model, associated with the previous ones, defines a hierarchy of diffuse interface models.

1.1.5 CONCLUSION

To conclude, diffuse interface models may be derived from three main methods and offer a large panel of elements obtained through relaxation phenomena. In particular, the projection on constrain manifolds of the *seven-equation model* leads to some of the well-known two-phase flow models. We will propose a numerical comparison of some elements of this hierarchy in [Chapter 5](#).

1.2 DERIVATION OF A TWO-VELOCITY TWO-PHASE FLOW MODEL BY MEANS OF THE VARIATIONAL PRINCIPLE

In the previous section, [Section 1.1.3](#), we have reviewed the SAP methodology, introduced the mathematical formalism and risen some crucial questions related to the thermodynamics constraints.

In this section, we want to apply the variational principle in an original way to obtain a compressible two-velocity two-phase flow model as well as a transport equation on the mixture entropy. This derivation is based on two ingredients: 1) we propose an orthogonal decomposition of infinitesimal variations as well as 2) a set of original constraints affiliated to each infinitesimal variation. This work has not yet been published but might be if some difficulties were to be lifted.

1.2.1 DECOMPOSITION OF THE INFINITESIMAL VARIATIONS OF THE ACTION OF A TWO-PHASE FLOW

The decomposition of the infinitesimal variations proposed by Gouin seems very appealing but its mathematical ground is not completely clear. In particular, no justification of the choice of the internal variables that vary during the temporal variation is given. In this section, we would like to prove the existence of a base of decomposition of the infinitesimal variations which could at least further justify the work of Gouin. These developments are based on the mathematical presentation of the variational principle in the books of [Bérest \(1997\) \[12\]](#) and [Bourguignon \(2007\) \[15\]](#).

1.2.1.1 NOTATIONS

Let \mathcal{V}_t be the volume occupied by a particle containing two phases at time $t_0 \leq t \leq t_1$. Each phase k of the mixture moves from an initial position \mathbf{X}_k in \mathcal{V}_{t_0} to the position \mathbf{x}_k in \mathcal{V}_t along a smooth path $\varphi_k(\mathbf{X}_k, t)$. It means that $\mathbf{x}_k = \varphi_k(\mathbf{X}_k, t)$ and $\varphi_k(\mathbf{X}_k, t_0) = \mathbf{X}_k$. The vector \mathbf{X}_k denotes the Lagrangian coordinates of phase k , while \mathbf{x}_k the Eulerian coordinates. For any field ψ , its Eulerian form will be written $\psi = \psi(t, \mathbf{x}_1, \mathbf{x}_2)$ while its Lagrangian form $\overset{\circ}{\psi} = \psi(t, \mathbf{X}_1, \mathbf{X}_2)$. By definition, $\psi(t, \mathbf{x}_1, \mathbf{x}_2) = \overset{\circ}{\psi}(t, \mathbf{X}_1, \mathbf{X}_2)$ whenever $\mathbf{x}_k = \varphi_k(\mathbf{X}_k, t)$ for each phase k , thus when variable dependencies are explicitly mentioned, the field will be written ψ . We note then

$$\mathcal{V}_t = \left\{ (\varphi_1(\mathbf{X}_1, t), \varphi_2(\mathbf{X}_2, t)) \in \mathbb{R}^3 \times \mathbb{R}^3 \mid (\mathbf{X}_1, \mathbf{X}_2) \in \mathcal{V}_{t_0}^2 \right\}, \quad (1.51a)$$

and introduce the space \mathcal{V} corresponding to all the spatial locations of the two-phase medium over a given period of time,

$$\mathcal{V} = \left\{ \mathcal{V}_t \subset \mathbb{R}^3 \times \mathbb{R}^3 \mid t_0 \leq t \leq t_1 \right\}. \quad (1.51b)$$

For sake of conciseness, we introduce the space Ω defined as $\Omega = \mathcal{V} \times [t_0, t_1]$. The trajectory of the portion of two-phase medium evolves in the manifold² \mathbb{R}^7 and is defined by the function

²Since we are seeking a two-velocity, two-pressure, two-temperature model, the state vector is defined by seven variables, such as $(\alpha_1 \rho_1, \alpha_2 \rho_2, \mathbf{v}_1, \mathbf{v}_2, s_1, s_2, \alpha_1) \in \mathbb{R}^7$

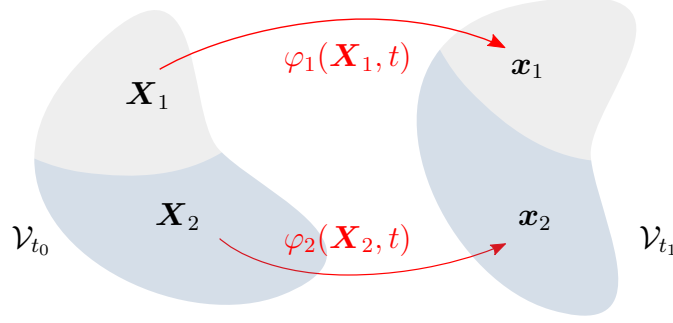


FIGURE 1.2: Illustration of a two-phase medium particle following its fluid paths φ_k over time.

γ

$$\gamma \left(\begin{array}{ccc} \Omega & \rightarrow & \mathbb{R}^7 \\ (\mathbf{x}_1, \mathbf{x}_2, t) & \mapsto & \gamma(\mathbf{x}_1, \mathbf{x}_2, t) \end{array} \right), \quad (1.52a)$$

describing the state vector of the mixture. We further introduce the space C of the smooth curves γ defined on Ω evolving in \mathbb{R}^7 and the tangent vector of a curve, $\dot{\gamma} \in \mathbb{R}^{7 \times 7}$, defined by

$$\forall \gamma \in C, \forall \omega \in \Omega, \dot{\gamma}(\omega) = \frac{\partial}{\partial \omega} \gamma(\omega). \quad (1.52b)$$

The Lagrangian, L , and the action, \mathcal{A} , associated with the portion of two-phase medium are finally defined as

$$L \left(\begin{array}{ccc} \mathcal{TM} & \rightarrow & \mathbb{R} \\ (\gamma, \dot{\gamma}) & \mapsto & L(\gamma, \dot{\gamma}) \end{array} \right), \quad \mathcal{A} \left(\begin{array}{ccc} C & \rightarrow & \mathbb{R} \\ \gamma & \mapsto & \int_{\Omega} L(\gamma, \dot{\gamma}) d\omega \end{array} \right), \quad (1.53)$$

where \mathcal{TM} is the tangent bundle defined by pairs of trajectories $\gamma \in C$ and their tangent vector $\dot{\gamma} \in \mathbb{R}^{7 \times 7}$.

1.2.1.2 VARIATIONS OF THE TRAJECTORIES AND OF THE ACTION

Since we can affect each of the trajectory coordinates, which are in Ω , we propose to define variations applied on these trajectories by affecting either the space or the time coordinates. We therefore assume these variations independent. Two independent variations of the action \mathcal{A} are thus possible and will be expressed through the definition of the corresponding variations of the trajectory γ .

The first trajectory variation is composed of two trajectory sub-variations γ_{λ_k} , $k = 1, 2$, defined as

$$\gamma_{\lambda_k} \left(\begin{array}{ccc} \Omega_{\lambda_k} & \rightarrow & \mathcal{M} \\ \hat{\omega} = (\hat{\varphi}_k(\mathbf{X}_k, t, \lambda_k), \varphi_{k'}(\mathbf{X}_{k'}, t), t) & \mapsto & \gamma_{\lambda_k}(\hat{\omega}) \end{array} \right), \quad (1.54)$$

where $k' = k + 1$ [2]. The vector $\hat{\varphi}_k$ is a family of paths parametrized by the scalar $\lambda_k \in]-\epsilon, \epsilon[$, with $\epsilon \in \mathbb{R}$ small, such that $\hat{\varphi}_k(\mathbf{X}_k, t, 0) = \varphi_k(\mathbf{X}_k, t)$ and the space Ω_{λ_k} is defined as

$$\Omega_{\lambda_k} = \left\{ (\hat{\varphi}_k(\mathbf{X}_k, t, \lambda_k), \varphi_{k'}(\mathbf{X}_{k'}, t), t) \subset \mathbb{R}^3 \times \mathbb{R}^3 \times [t_0, t_1] \mid (\mathbf{X}_1, \mathbf{X}_2) \in \mathcal{V}_{t_0}^2, \lambda_k \in]-\epsilon, \epsilon[\right\}. \quad (1.55)$$

The second trajectory variation γ_λ , which is independent to the first two sub-variations γ_{λ_k} , is given by

$$\gamma_\lambda \left(\begin{array}{ccc} \Omega_\lambda & \rightarrow & \mathcal{M} \\ \omega = (\varphi_1(\mathbf{X}_1, f(t, \lambda)), \varphi_2(\mathbf{X}_2, f(t, \lambda)), f(t, \lambda)) & \mapsto & \gamma_\lambda(\omega) \end{array} \right) \quad (1.56)$$

where f is a function of the time t parametrized by the scalar $\lambda \in]-\epsilon, \epsilon[$, such that $f(t, \lambda = 0) = t$. This parametrized function modifies the time coordinate. We do not specify the expression of f , but it could be defined as a time dilatation, $f(t, \lambda) = t/(\lambda + 1)$, or a time shift, $f(t, \lambda) = t + \lambda$. The space Ω_λ is defined as

$$\Omega_\lambda = \{(\varphi_1(\mathbf{X}_1, f(t, \lambda)), \varphi_2(\mathbf{X}_2, f(t, \lambda)), f(t, \lambda)) \in \mathcal{V}_t \times]t - \epsilon, t + \epsilon[\mid (\mathbf{X}_1, \mathbf{X}_2) \in \mathcal{V}_{t_0}^2, \lambda \in]-\epsilon, \epsilon[\} \quad (1.57)$$

Figure 1.3 illustrates the decomposition of the trajectory variations parametrized by the scalars λ_k , $k = 1, 2$ and λ .

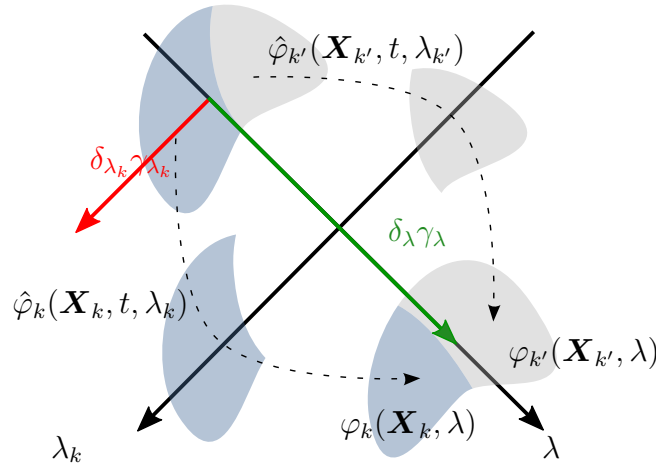


FIGURE 1.3: Schematic representation of transformations applied to a two-phase medium particle.

These two groups of variation must be understood as followed:

- γ_{λ_k} : at any time t each phase k can evolve within the two-phase medium, independently from one another, along a family of path $\hat{\varphi}_k$ parametrized by λ_k and the SAP determines along which path they indeed flow, which is φ_k . Each sub-variation affects one phase only and not the mixture.
- γ_λ : each phase of the two-phase medium follows its own path φ_k , so its spatial trajectory is determined. However, it can reach a given position on the given path φ_k at any time $f(t, \lambda)$ given by the time variation parametrized by λ . This variation affects thus the whole mixture and not just one of the two phases. The SAP yields the correct time at which the mixture occupies a given spatial position. Since through γ_{λ_k} , the two phases can evolve separately, they are not necessarily maintained at thermodynamics equilibrium. The time variation along the path γ_λ will force the two phases to evolve together and thus gain a new thermodynamics equilibrium. Thus, γ_λ can be seen as a relaxation process on the mixture to force the two phases to be always be at thermodynamics equilibrium.

Remark 4. These different variations are similar to those introduced in [Gouin and Ruggeri \(2009\) \[95\]](#), but with a sound mathematical origin that proves the independency of these infinitesimal variations.

The corresponding variations of the action are defined either using Lagrangian coordinates or Eulerian coordinates. Since we are interested in the Eulerian form of the motion equations, we consider variations of the Action expressed in terms of the Eulerian variables. They take the form

$$\delta_{\lambda_k} \mathcal{A} = \int_{\Omega_{\lambda_k}} \frac{\partial}{\partial \lambda_k} L(\gamma_{\lambda_k}, \dot{\gamma}_{\lambda_k}) \Big|_{\substack{t, \omega_i \text{ fixed} \\ \lambda_k=0}} d\omega, \quad (1.58a)$$

$$\delta_{\lambda} \mathcal{A} = \int_{\Omega_{\lambda}} \frac{\partial}{\partial \lambda} L(\gamma_{\lambda}, \dot{\gamma}_{\lambda}) \Big|_{\substack{t, \omega_i \text{ fixed} \\ \lambda=0}} d\omega. \quad (1.58b)$$

[Figure 1.4](#) illustrates the infinitesimal variations of the Action in the space $]-\epsilon, \epsilon[\times \mathcal{V} \times \mathbb{R}^7$. $\delta_{\lambda_k} \gamma_{\lambda_k}$ is always orthogonal to the trajectory γ and represents locally the infinitesimal spatial

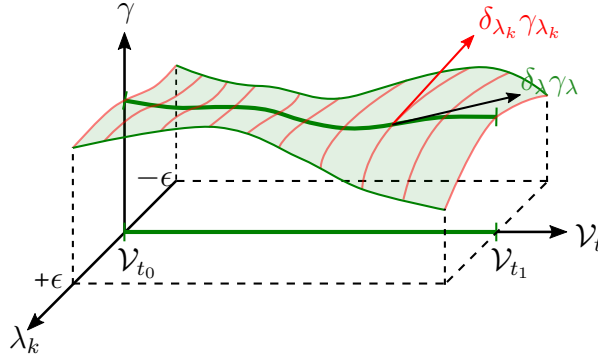


FIGURE 1.4: Representation of the Action first variations in the space $]-\epsilon, \epsilon[\times \mathcal{V} \times \mathbb{R}^7$.

variation of the point $\gamma(\omega)$ by the variation λ_k . The red lines embodies all the possible positions at a given time of the point $\gamma(\omega)$ due to the variation λ_k . Then, δ_{λ} is always tangent to the trajectory γ and corresponds locally to a variation of time of the point $\gamma(\omega)$ by the variation λ . [Figure 1.4](#) emphasizes the independency of the two variations.

1.2.1.3 STATIONARY ACTION PRINCIPLE

Hamilton's Least Action Principle returns the following system of equations

$$\delta_{\lambda_k} \mathcal{A} = 0, \quad k = 1, 2, \quad \delta_{\lambda} \mathcal{A} = 0. \quad (1.59)$$

As we will shortly see later on, the first two equations yielded by the infinitesimal variations γ_{λ_k} are momentum equations. The last one obtained from the infinitesimal variations γ_{λ} will bring in the evolution equation on the mixture entropy.

1.2.2 DERIVATION OF A TWO-VELOCITY TWO-PHASE FLOW MODEL

Having defined the infinitesimal variations, we still need to define the constraints under which the system evolves. Then the Least Action Principle will return governing equations. This method depicts a coherent mathematical system of equations and the resulting system will be compared to the Baer-Nunziato seven equations model.

1.2.2.1 ASSUMPTIONS

Let the system be a compressible two-phase flow out of equilibrium, such that it is described by the following set of variables

$$\mathbf{u} = (\mathbf{u}_1, \mathbf{u}_2, \alpha_1)^t, \quad \mathbf{u}_k = (\alpha_k \rho_k, \mathbf{v}_k, s_k)^t, \quad (1.60)$$

where s_k is the phasic entropy per unit of mass. The volume fractions are not independent and fulfill the constraint $\sum_{k=1,2} \alpha_k = 1$.

Remark 5. *It is possible to choose another set of variables $\mathbf{u}_2 = (\rho, \mathbf{u}_1, \mathbf{v}_h, \mathbf{v}_d, s_1, s_2, \alpha_1)^t$ and derive an equivalent system of equations.*

The internal energy e of the mixture is expressed as

$$e(\mathbf{u}) = \sum_{j \in \mathcal{N}_s(k)} y_k e_k(\rho_k, s_k) + \Delta e(\mathbf{u}). \quad (1.61)$$

where the first term of the RHS corresponds to the internal energy of each phase in a pure state and the second term accounts for mixing effects. The quantity y_k is the mass fraction of phase k and is related to the mixture density, the phase density and the volume fraction by $y_k = \alpha_k \rho_k / \rho$. The mixture entropy s is assumed to be defined by

$$s(\mathbf{u}) = \sum_{k=1,2} y_k s_k(\rho_k, p_k) + \Delta s(\mathbf{u}). \quad (1.62)$$

No phase transition is accounted for, thus mass and partial masses are conserved. The reader is invited to refer to [Chapter 2](#) to understand such definitions or to [Cordes et al. \(2020\) \[35\]](#) on which the referred chapter is based.

The Lagrangian is defined as

$$L(\mathbf{u}) = \sum_{k=1,2} L_k(\mathbf{u}_k, \alpha_k) - \Delta e(\mathbf{u}), \quad L_k(\mathbf{u}_k, \alpha_k) = \frac{1}{2} \alpha_k \rho_k \|\mathbf{v}_k\|^2 - \alpha_k \rho_k \epsilon_k \left(\frac{\alpha_k \rho_k}{\alpha_k}, s_k \right). \quad (1.63)$$

1.2.2.2 TRANSFORMATIONS UNDER CONSTRAINTS

The mixture undergoes two different transformations as depicted in [Figures 1.3](#) and [1.4](#): one corresponding to infinitesimal spatial variation, $\delta_{\lambda_k} \gamma_{\lambda_k}$ allowing the phases to remain out-of-equilibrium, a second, δ_{λ} , impacting the whole mixture, letting it reach full equilibrium as we will see. For each infinitesimal variation, one needs to define the underlying constraints. There is not a universal set of constraints, it depends on what we want to describe.

For the first transformation, we will assume that each variation δ_{λ_k} conserves mass and entropy and transports the volume fraction along the trajectory defined by the path $\hat{\varphi}_k(\mathbf{X}_k, t, \lambda_k)$, leading to the following set of constraints

$$\partial_t(\alpha_k \rho_k) + \nabla \cdot [\alpha_k \rho_k \mathbf{v}_k] = 0, \quad D_{k,t}(s_k) = 0, \quad D_{k,t}(\alpha_k) = 0, \quad (1.64)$$

where $D_{k,t}(\bullet) = \partial_t(\bullet) + \mathbf{v}_k \nabla \cdot (\bullet)$. The two phases evolve independently at their own velocity \mathbf{v}_k . Each phase undergoes an independent variation, and thus $\delta_{\lambda_1} \mathbf{x}_1 \neq \delta_{\lambda_2} \mathbf{x}_2$. It seems reasonable to assume the phase entropies to remain constant since no interaction occurs between

the two phases, thus no relaxation can occur. Hence we obtain the following equations for the infinitesimal variations of the variables

$$\delta_{\lambda_k}(\alpha_k \rho_k) = -\nabla \cdot (\alpha_k \rho_k \delta_{\lambda_k} \mathbf{x}_k), \quad \delta_{\lambda_k} \mathbf{v}_k = D_{k,t}(\delta_{\lambda_k} \mathbf{x}_k) - (\delta_{\lambda_k} \mathbf{x}_k \cdot \nabla) \mathbf{v}_k, \quad (1.65a)$$

$$\delta_{\lambda_k} b = -\nabla b \cdot \delta_{\lambda_k} \mathbf{x}_k, \quad b \in \{s_k, \alpha_k\}, \quad \delta_{\lambda_k} \mathbf{u}_{k'} = \mathbf{0}. \quad (1.65b)$$

For the first two-sub variations, each variable variation is related to the variation of the Euler coordinate \mathbf{x}_k .

The second transformation γ_λ corresponding to a time variation affects the mixture, which is allowed to reach thermodynamics equilibrium. While we still force mass conservation, we remove the constraints on both the entropies and the volume fraction, these variables, being internal variables, are naturally involved in the relaxation. Therefore, the constraints take the form

$$\partial_t \rho + \nabla \cdot [\rho \mathbf{v}] = 0, \quad D_{k,t}(y_k) = 0, \quad (1.66)$$

where \mathbf{v} is the mass averaged mixture velocity, $\mathbf{v} = \sum_{k=1,2} y_k \mathbf{v}_k$. Regarding the infinitesimal variations of the variables, the second transformation does not induce a virtual spatial displacement such that,

$$\delta_\lambda \mathbf{x}_k = \mathbf{0}, \quad k = 1, 2. \quad (1.67)$$

The direct consequence of Equation (1.67) is that

$$\delta_{\lambda_k} \mathbf{v}_k = \mathbf{0}, \quad \delta_{\lambda_k} \alpha_k \rho_k = 0. \quad (1.68)$$

Thus, the only remaining infinitesimal variations are those related to the remaining independent variables, namely the volume fraction and the partial entropies. Finally, as suggested by [Gouin and Ruggeri \(2009\) \[95\]](#), the infinitesimal Eulerian variation of any mixture variable ψ ,

$$\delta_\lambda \psi = \left. \frac{\partial \psi(\varphi_1(\mathbf{X}_1, \lambda), \varphi_2(\mathbf{X}_2, \lambda), \lambda)}{\partial \lambda} \right|_{\substack{\mathbf{x}_1, \mathbf{x}_2 \text{ fixed} \\ \lambda=t}} \quad (1.69)$$

can be identified as a material derivative of the mixture, such that

$$\delta_\lambda s = \partial_t s + \mathbf{v} \nabla \cdot s, \quad \delta_\lambda \alpha_k = \partial_t \alpha_k + \mathbf{v} \nabla \cdot \alpha_k. \quad (1.70)$$

Remark 6. *It would seem incorrect to use the material derivative related to the phase velocities, since the variation impacts the mixture as a whole.*

1.2.2.3 ACTION FIRST INFINITESIMAL VARIATIONS

For the first variations of the action \mathcal{A} , each one being independent, it yields

$$\delta_{\lambda_k} \mathcal{A} = \delta_{\lambda_k} \mathcal{A}_{(\alpha_k \rho_k)} + \delta_{\lambda_k} \mathcal{A}_{(\mathbf{v}_k)} + \sum_{b|D_{k,t} b=0} \delta_{\lambda_k} \mathcal{A}_{(b)} = 0, \quad (1.71a)$$

with

$$\delta_{\lambda_k} \mathcal{A}(\alpha_k \rho_k) = \int_{\hat{\Omega}_{\lambda_k}} \alpha_k \rho_k \nabla \left(\frac{\partial L}{\partial(\alpha_k \rho_k)} \right) \delta_{\lambda_k} \mathbf{x}_k \, d\hat{\omega}, \quad (1.71b)$$

$$\delta_{\lambda_k} \mathcal{A}(\mathbf{v}_k) = - \int_{\hat{\Omega}_{\lambda_k}} (\partial_t \mathbf{K}_k + \nabla \cdot [\mathbf{K}_k \otimes \mathbf{v}_k] + \nabla(\mathbf{v}_k) \mathbf{K}_k)^t \cdot \delta_{\lambda_k} \mathbf{x}_k \, d\hat{\omega}, \quad (1.71c)$$

$$\delta_{\lambda_k} \mathcal{A}(b) = - \sum_{b|D_{k,t} b=0} \int_{\hat{\Omega}_{\lambda_k}} \partial_b L \nabla(b) \cdot \delta_{\lambda_k} \mathbf{x}_k \, d\hat{\omega}, \quad (1.71d)$$

with $\mathbf{K}_k = (\partial_{\mathbf{v}_k} L)^t$. We introduce the Legendre transform of the partial density of the fluid,

$$L_k^* = \alpha_k \rho_k \frac{\partial L_k}{\partial(\alpha_k \rho_k)} - L_k. \quad (1.72)$$

Noticing that

$$\alpha_k \rho_k \nabla \left(\frac{\partial L}{\partial(\alpha_k \rho_k)} \right) = \nabla(L_k^*) + \nabla(L_k) - \frac{\partial L_k}{\partial(\alpha_k \rho_k)} \nabla(\alpha_k \rho_k) + \alpha_k \rho_k \nabla \left(\frac{\partial \Delta e}{\partial(\alpha_k \rho_k)} \right), \quad (1.73a)$$

$$\nabla(\mathbf{v}_k) \mathbf{K}_k = \nabla(\mathbf{v}_k) \left(\frac{\partial L_k}{\partial \mathbf{v}_k} \right)^t, \quad (1.73b)$$

$$\sum_{b|D_{k,t} b=0} \partial_b L \nabla(b) = \sum_{b|D_{k,t} b=0} \partial_b L_k \nabla(b) + \partial_{\alpha_k} L_{k'} \nabla(\alpha_k) + \sum_{b|D_{k,t} b=0} \partial_b \Delta e \nabla(b), \quad (1.73c)$$

we obtain from Equation (1.71a),

$$\begin{aligned} \partial_t \mathbf{K}_k + \nabla \cdot [\mathbf{K}_k \otimes \mathbf{v}_k] - \nabla(L_k^*) &= - \frac{\partial L_{k'}}{\partial \alpha_k} \nabla(\alpha_k) + \text{terms}(\Delta e) \\ \text{with terms}(\Delta e) &= \nabla \left(\alpha_k \rho_k \frac{\partial \Delta e}{\partial(\alpha_k \rho_k)} \right) - \sum_{b=\alpha_k, s_k, \alpha_k \rho_k} \frac{\partial \Delta e}{\partial b} \nabla(b). \end{aligned} \quad (1.74)$$

Evaluating \mathbf{K}_k and L_k^* yields a momentum equation

$$\partial_t(\alpha_k \rho_k \mathbf{v}_k) + \nabla \cdot \left[\alpha_k \rho_k \mathbf{v}_k \otimes \mathbf{v}_k + \alpha_k \rho_k^2 \frac{\partial e_k}{\partial \rho_k} \right] = \rho_{k'}^2 \frac{\partial e_{k'}}{\partial \rho_{k'}} \nabla(\alpha_k) + \text{terms}(\Delta e). \quad (1.75)$$

1.2.2.4 ACTION SECOND INFINITESIMAL VARIATIONS

For the second variation of the action \mathcal{A} , we have

$$\delta_{\lambda} \mathcal{A} = \delta_{\lambda} \mathcal{A}(\alpha_k) + \delta_{\lambda} \mathcal{A}(s) = 0, \quad (1.76a)$$

with

$$\delta_{\lambda} \mathcal{A}(\alpha_k) = \int_{\hat{\Omega}_{\lambda}} \frac{\partial L}{\partial \alpha_k} D_t \alpha_k \, d\hat{\omega}, \quad (1.76b)$$

$$\delta_{\lambda_k} \mathcal{A}(s) = - \int_{\hat{\Omega}_{\lambda}} \frac{\partial L}{\partial s} D_t s \, d\hat{\omega}. \quad (1.76c)$$

We obtain the mixture entropy evolution equation

$$\frac{\partial L}{\partial \alpha_k} D_t \alpha_k + \frac{\partial L}{\partial s} D_t s = 0. \quad (1.77)$$

In the standard framework of SAP, all derived equations are conservative, no dissipative process is accounted for. Nonetheless, here, we have explicitly allowed the mixture to undergo dissipative processes through thermodynamics relaxation. Therefore, Equation (1.77) must fulfill the second principle of thermodynamics, thus all entropy source terms should be signed.

1.2.2.5 FINAL SET OF EQUATIONS - SIMPLIFIED APPROACH WITH TWO GIBBS EQUATIONS

Going further requires to postulate the thermodynamics associated to each phase. Doing so, we will be able to express the partial derivatives of the internal energy e . As a first attempt, to simplify the approach, we assume that each phase has its own thermodynamics, as if each phase was isolated from one another. Thus they both obey a Gibbs equation,

$$T_k ds_k = de_k - p_k / \rho_k^2 d\rho_k. \quad (1.78)$$

Remark 7. Assuming that the phase Gibbs equation holds implies some constraints on the mixing terms and the transport equations as we will see in [Chapter 2](#).

Thus, from the definition (1.61) of the mixture energy e , we obtain

$$\alpha \rho_k^2 \frac{\partial e_k}{\partial(\alpha \rho)} = p_k, \quad \frac{\partial L}{\partial \alpha_k} = p_k - p_{k'} - \partial_{\alpha_k} \Delta e, \quad \frac{\partial L}{\partial s} = \frac{\partial e}{\partial s}. \quad (1.79)$$

The partial derivative of the total energy with respect to the total entropy is homogeneous to a temperature. We thus assume the inverse of this partial derivative is defined. The total entropy equation reads

$$D_t s = \left(\frac{\partial e}{\partial s} \right)^{-1} (p_2 - p_1 + \partial_{\alpha_1} \Delta e) D_t \alpha_1. \quad (1.80)$$

A way to sign the right hand side of the entropy equation is to assume the following evolution equation for the volume fraction,

$$D_t \alpha_1 = \mu (p_2 - p_1 + \partial_{\alpha_1} \Delta e), \quad (1.81)$$

with μ a constant parameter. Equation (1.81) is similar to a pressure relaxation term inferring that μ is the pressure relaxation coefficient.

We finally obtain the following set of equations, for $k = 1, 2$,

$$\partial_t (\alpha_k \rho_k) + \nabla \cdot [\alpha_k \rho_k \mathbf{v}_k] = 0, \quad (1.82a)$$

$$\partial_t (\alpha_k \rho_k \mathbf{v}_k) + \nabla \cdot [\alpha_k \rho_k \mathbf{v}_k \otimes \mathbf{v}_k + \alpha_k p_k] = p_{k'} \nabla (\alpha_k) + \text{terms}(\Delta e), \quad (1.82b)$$

$$D_t s = (\partial_e s)^{-1} \mu (p_2 - p_1 + \partial_{\alpha_1} \Delta e)^2, \quad (1.82c)$$

$$D_t \alpha_1 = \mu (p_2 - p_1 + \partial_{\alpha_1} \Delta e). \quad (1.82d)$$

Recovering the notion of interfacial pressure In [Gavrilyuk and Saurel \(2002\) \[81\]](#), the authors have proposed to identify the interfacial pressure expliciting the mixture energy terms and assuming Δe only depends on α_k . In this particular case, $\text{terms}(\Delta e)$ reduce to

$$\Delta e = - \frac{\partial \Delta e}{\partial \alpha_k} \nabla \alpha_k, \quad (1.83)$$

and we recover the interfacial pressure p_1 defined in [Gavrilyuk and Saurel \(2002\) \[81\]](#) as

$$p_{k'} - \frac{\partial \Delta e}{\partial \alpha_k} = p_1. \quad (1.84)$$

Mixture energy equation From System (1.82), we should be able to derive the mixture energy equation. It has not been done so far.

1.2.2.6 FROM MIXTURE EQUATIONS TO PHASE EQUATIONS

System (1.82) requires a closure relation. As in [Gouin and Ruggeri \(2009\) \[95\]](#) where Equation (1.40) links both partial entropies, here Equation (1.82c) does not permit to retrieve an equation for each phase entropy. Further assumptions based for instance on the flow topology, the physical properties of the fluids or symmetry considerations, are needed to split the total entropy equation into two equations, one for each phase entropy, and close the system of equations.

1.2.3 CONCLUSION

To conclude, the derivation based on the independent decomposition of the infinitesimal variations has led to an original two-velocity two-pressure system of equations, including an evolution equation on the mixture entropy as well as on the volume fraction. The second infinitesimal variation involving the internal variables can be interpreted as a relaxation of the mixture. So far, we have assumed the mixture entropy and the volume fraction were the only internal variables affected, yielding to a pressure relaxation term in the evolution equation of the volume fraction.

Future works could consist in extending the set of internal variables subject to the second infinitesimal variation, by adding for example additional geometric variables. Furthermore, another decomposition of the infinitesimal variations may exist, which could bring out new relaxation processes, more sophisticated than only hydrodynamical, mechanical or thermal relaxations. The latter are simple in the sense they isolate each variable under relaxation, but there is no reason these relaxations should be decoupled. This search for generalized source terms is intimately linked to the symmetrization in the sense of Mock-Godunov, which, when successfully applied on a model, yields the correct variables to relax. As we will see in the last section of this chapter, the Baer-Nunziato model for instance can not be symmetrized in the sense of Mock-Godunov due to the lack of strict convexity of the entropy. Hence, obtaining generalized source terms is still an active field of research.

In the next section, we would like to assess the well-posedness of two-velocity two-phase flow models such as System (1.82) we obtained. Since it is still ongoing work, we will not directly examine System (1.82) but the Baer-Nunziato model (1.27) introduced in [Section 1.1](#). In future work, we will also provide the mathematical study of System (1.82).

1.3 MATHEMATICAL ANALYSIS AND CLOSURE OF THE SEVEN-EQUATION MODEL

Examining the mathematical well-posedness of the systems we would like to use is mandatory. As emphasized in [Drew and Passman \(1998\) \[58\]](#), "*a model that is not properly formulated mathematically cannot describe physical phenomena correctly. While mathematical correctness does not imply physical validity, the latter cannot be obtained without the former.*" In this spirit, the community has always sought for a hyperbolic two-phase flow model. In [Lhuillier et al. \(2013\) \[139\]](#), the authors came up with a clear picture of the latest advances and hurdles in the quest for hyperbolicity, and gave some leads to achieve it.

We therefore proceed in this section to a mathematical analysis of the extended Baer-Nunziato model [\(1.27\) Saurel and Abgrall \(1999\) \[190\]](#), for which the interfacial quantities p_I and v_I still need to be closed. We will rely on self-developed tools based on computer algebra to ease and enhance the calculations, thus proposing original results. We will see that the choice of the interfacial quantities have a strong influence on the mathematical properties of the system, in particular on the Riemann invariants.

1.3.1 HYPERBOLICITY STUDY

Due to the rotational invariance of System [\(1.27\)](#), we can analyze its homogeneous form in the one-dimensional case. From Equation [\(1.46\)](#), we obtain the quasi linear form of the homogeneous system,

$$\partial_t \mathbf{q} + \mathcal{A}(\mathbf{q}) \partial_x \mathbf{q} = \mathbf{0} \quad (1.85)$$

where $\mathcal{A}(\mathbf{q}) = \partial_{\mathbf{q}} \mathbf{f}(\mathbf{q}) + \mathcal{N}(\mathbf{q})$ defined as in [\(1.46\)](#). A two-parameter equation of state will be used hereafter.

1.3.1.1 PRIMITIVE VARIABLES EQUATIONS

Manipulating System [\(1.85\)](#), we can derive equations on primitive variables

$$\text{density } D_{k,t} \rho_k = -\rho_k \partial_x v_k + \epsilon_k \frac{\rho_k}{\alpha_k} (v_k - v_I) \partial_x \alpha_2, \quad (1.86a)$$

$$\text{speed } D_{k,t} v_k = -\frac{1}{\rho_k} \partial_x (p_k) + \epsilon_k \frac{p_k - p_I}{\alpha_k \rho_k} \partial_x \alpha_2, \quad (1.86b)$$

$$\text{kinetic energy } D_{k,t} \frac{v_k^2}{2} = -\frac{v_k}{\rho_k} \partial_x (p_k) + \epsilon_k v_k \frac{p_k - p_I}{\alpha_k \rho_k} \partial_x \alpha_2, \quad (1.86c)$$

$$\text{total energy } D_{k,t} E_k = -\frac{1}{\alpha_k \rho_k} \partial_x (\alpha_k p_k v_k) - \epsilon_k \frac{p_I v_I}{\alpha_k \rho_k} \partial_x \alpha_2, \quad (1.86d)$$

$$\text{internal energy } D_{k,t} \epsilon_k = -\frac{p_k}{\rho_k} \partial_x v_k - \epsilon_k \frac{p_I}{\alpha_k \rho_k} (v_I - v_k) \partial_x \alpha_2. \quad (1.86e)$$

To derive the equations on the partial entropies, we need to define the thermodynamics associated to each phase. For simplicity, we will assume Gibbs equation valid for each phase and introduce the following notations

$$\kappa_k = \left. \frac{\partial \epsilon_k}{\partial p_k} \right|_{\rho_k}, \quad \chi_k = \left. \frac{\partial \epsilon_k}{\partial \rho_k} \right|_{p_k}, \quad a_k^2 = \left. \frac{\partial p_k}{\partial \rho_k} \right|_{s_k} = \frac{1}{\kappa_k} \left(\frac{p_k}{\rho_k^2} - \chi_k \right). \quad (1.87)$$

It leads to the two supplementary equations,

$$\text{pressure } D_{k,t}p_k = -\rho_k a_k^2 \partial_x v_k - \epsilon_k \frac{v_k - v_1}{\alpha_k} \left[-\rho_k a_k^2 + \frac{p_k - p_1}{\rho_k \kappa_k} \right] \partial_x \alpha_2 = 0, \quad (1.88a)$$

$$\text{entropy } D_{k,t}v_k = \frac{(-1)^k}{\alpha_k \rho_k T_k} (p_k - p_1) (v_k - v_1) \partial_x \alpha_2 = 0. \quad (1.88b)$$

Defining the set of variables $\mathbf{u} \in \mathbb{R}^7$ by $\mathbf{u}^t = (\alpha_2, \mathbf{u}_2^t, \mathbf{u}_1^t)$ with $\mathbf{u}_k^t = (\rho_k, v_k, p_k)$, we obtain the system found in [Saurel and Abgrall \(1999\)](#) [190] and [Andrianov et al. \(2003\)](#) [2]

$$\partial_t \mathbf{u} + \mathcal{A}(\mathbf{u}) \partial_x \mathbf{u} = \mathbf{0}, \quad (1.89a)$$

$$\mathcal{A}(\mathbf{u}) = \begin{pmatrix} v_1 & 0 & 0 \\ \mathcal{A}_{\mathbf{u},\alpha_2} & \mathcal{A}_{\mathbf{u}_2}(\mathbf{u}_2) & 0 \\ \mathcal{A}_{\mathbf{u},\alpha_1} & 0 & \mathcal{A}_{\mathbf{u}_1}(\mathbf{u}_1) \end{pmatrix}, \quad \mathcal{A}_{\mathbf{u},\alpha_k} = \epsilon_k \begin{pmatrix} \frac{\rho_k}{\alpha_k} (v_1 - v_k) \\ p_1 - p_k \\ \alpha_k \rho_k \\ \frac{\rho_k}{\alpha_k} (v_1 - v_k) a_{I,k}^2 \end{pmatrix}, \quad (1.89b)$$

$$\mathcal{A}_{\mathbf{u}_k}(\mathbf{u}_k) = \begin{pmatrix} v_k & \rho_k & 0 \\ 0 & v_k & \frac{1}{\rho_k} \\ 0 & \rho_k a_k^2 & v_k \end{pmatrix} \quad (1.89c)$$

and $a_{I,k}^2 = a_k^2 - \frac{p_k - p_1}{\rho_k^2 \kappa_k}$.

Theorem 1. *Given the two state vectors, $\mathbf{q} = (\alpha_2, \alpha_2 \rho_2, \alpha_2 \rho_2 v_2, \alpha_2 \rho_2 E_2, \alpha_1 \rho_1, \alpha_1 \rho_1 v_1, \alpha_1 \rho_1 E_1)^t \in \mathbb{R}^7$ and $\mathbf{u} = (\alpha_2, \rho_2, v_2, p_2, \rho_1, v_1, p_1)^t \in \mathbb{R}^7$, the following statements are equivalent,*

- (C₁) *The mapping $\mathbf{u} \mapsto \mathbf{q}$ is diffeomorph.*
- (C₂) *$\partial_{\mathbf{u}} \mathbf{q}$ is invertible.*
- (C₃) *$\alpha_k \neq 0, \rho_k \neq 0$ and $\kappa_k \neq 0$.*

Proof. One has

$$\partial_{\mathbf{u}} \mathbf{q} = \begin{pmatrix} 1 & 0 & 0 \\ (\partial_{\mathbf{u}} \mathbf{q})_{\alpha_2} & \partial_{\mathbf{u}_2} \mathbf{q}_2 & 0 \\ (\partial_{\mathbf{u}} \mathbf{q})_{\alpha_1} & 0 & \partial_{\mathbf{u}_1} \mathbf{q}_1 \end{pmatrix}, \quad \partial_{\mathbf{u}_k} \mathbf{q}_k = \begin{pmatrix} \alpha_2 & 0 & 0 \\ \alpha_2 v_2 & \alpha_2 \rho_2 & 0 \\ \alpha_2 (E_2 + \rho_2 \chi_2) & \alpha_2 \rho_2 v_2 & \alpha_2 \rho_2 \kappa_2 \end{pmatrix},$$

with $(\partial_{\mathbf{u}} \mathbf{q})_{\alpha_k}^t = -\epsilon_k (\rho_k, \rho_k v_k, \rho_k E_k)$. The determinant $\det(\partial_{\mathbf{u}} \mathbf{q}) = \alpha_2^3 \rho_2^2 \kappa_2 \alpha_1^3 \rho_1^2 \kappa_1$ gives the result. Assuming these conditions holds, we obtain

$$\partial_{\mathbf{q}} \mathbf{u} = \begin{pmatrix} 1 & 0 & 0 \\ (\partial_{\mathbf{q}} \mathbf{u})_{\alpha_2} & \partial_{\mathbf{q}_2} \mathbf{u}_2 & 0 \\ (\partial_{\mathbf{q}} \mathbf{u})_{\alpha_1} & 0 & \partial_{\mathbf{q}_1} \mathbf{u}_1 \end{pmatrix},$$

and

$$\partial_{\mathbf{q}_k} \mathbf{u}_k = (\partial_{\mathbf{u}_k} \mathbf{q}_k)^{-1} = \begin{pmatrix} \frac{1}{\alpha_k} & 0 & 0 \\ -\frac{\alpha_k}{v_k} & \frac{1}{\alpha_k \rho_k} & 0 \\ -\frac{E_k + \chi_k \rho_k - v_k^2}{\alpha_k \rho_k \kappa_k} & -\frac{\alpha_k \rho_k}{v_k} & \frac{1}{\alpha_k \rho_k \kappa_k} \end{pmatrix},$$

with $(\partial_{\mathbf{q}} \mathbf{u})_{\alpha_k}^t = \epsilon_k \left(\frac{\rho_k}{\alpha_k}, 0, -\frac{\rho_k \chi_k}{\alpha_k \kappa_k} \right)$. □

1.3.1.2 EIGENVALUES AND EIGENVECTORS

The mathematical properties of the 7 equations model have been studied by [Embid and Baer \(1992\) \[65\]](#), [Coquel et al. \(2002\) \[28\]](#), [Gallouët et al. \(2004\) \[78\]](#) among others. It admits 7 eigenvalues $\lambda_n \in \mathbb{R}$

$$\text{Sp}(\mathcal{A}_{\mathbf{u}}) = \{v_I, \{\text{Sp}(\mathcal{A}_{\mathbf{u}_k})\}_{k=2,1}\} = \{v_I, \{v_k, v_k \pm a_k\}_{k=2,1}\} \quad (1.90)$$

and the n corresponding right eigenvectors $\mathbf{r}_n \in \mathbb{R}^7$, $n \in [1, 7]$ which coordinates are $\mathbf{r}_n = (x_n, \mathbf{y}_n^2, \mathbf{y}_n^1)^t$ with $\mathbf{y}_n^k = (x_n^{k,1}, x_n^{k,2}, x_n^{k,3})^t$, $k = 1, 2$. Thus, the eigenvectors are solution of the following system

$$(\mathcal{A}(\mathbf{u}) - \lambda_n \mathcal{I}_7) \mathbf{r}_n = 0, \quad (1.91a)$$

inducing two systems of equations

$$\begin{cases} \lambda_1 = v_I, \\ \mathcal{A}_{\mathbf{u}, \alpha_2} x_1 = -(\mathcal{A}_{\mathbf{u}_2}(\mathbf{u}_2) - v_I \mathcal{I}_3) \mathbf{y}_1^2, \\ \mathcal{A}_{\mathbf{u}, \alpha_1} x_1 = -(\mathcal{A}_{\mathbf{u}_1}(\mathbf{u}_1) - v_I \mathcal{I}_3) \mathbf{y}_1^1, \end{cases} \text{ and } \forall n \in [2, 7] \begin{cases} x_n = 0, \\ 0 = (\mathcal{A}_{\mathbf{u}_2}(\mathbf{u}_2) - \lambda_n \mathcal{I}_3) \mathbf{y}_n^2, \\ 0 = (\mathcal{A}_{\mathbf{u}_1}(\mathbf{u}_1) - \lambda_n \mathcal{I}_3) \mathbf{y}_n^1. \end{cases} \quad (1.91b)$$

One finds then easily the six eigenvectors which are composed of the Euler eigenvectors for each system $\mathcal{A}_{\mathbf{u}_k}(\mathbf{u}_k)$,

$$\lambda_2 = v_2 \quad \mathbf{r}_2 = \begin{pmatrix} 0 & 1 & 0 & 0 & 0 & 0 & 0 \end{pmatrix}^t \quad (1.92a)$$

$$\lambda_3 = v_2 - a_2 \quad \mathbf{r}_3 = \begin{pmatrix} 0 & 1 & -\frac{a_2}{\rho_2} & a_2^2 & 0 & 0 & 0 \end{pmatrix}^t \quad (1.92b)$$

$$\lambda_4 = v_2 + a_2 \quad \mathbf{r}_4 = \begin{pmatrix} 0 & 1 & +\frac{a_2}{\rho_2} & a_2^2 & 0 & 0 & 0 \end{pmatrix}^t \quad (1.92c)$$

$$\lambda_5 = v_1 \quad \mathbf{r}_5 = \begin{pmatrix} 0 & 0 & 0 & 0 & 1 & 0 & 0 \end{pmatrix}^t \quad (1.92d)$$

$$\lambda_6 = v_1 - a_1 \quad \mathbf{r}_6 = \begin{pmatrix} 0 & 1 & 0 & 0 & 1 & -\frac{a_1^2}{\rho_1} & a_1^2 \end{pmatrix}^t \quad (1.92e)$$

$$\lambda_7 = v_2 + a_1 \quad \mathbf{r}_7 = \begin{pmatrix} 0 & 1 & 0 & 0 & 1 & +\frac{a_1^2}{\rho_1} & a_1^2 \end{pmatrix}^t \quad (1.92f)$$

The first eigenvector r_1 is more complex and its coordinates depend on the interfacial terms v_I and p_I ,

$$\lambda_1 = v_I, \quad \mathbf{r}_1 = \left(\alpha_1 \alpha_2 \sigma_1 \sigma_2 \quad (\mathbf{y}_1^2)^t \quad (\mathbf{y}_1^1)^t \right)^t, \quad (1.92g)$$

$$\text{with } \mathbf{y}_1^k = -\epsilon_k \alpha_{k'} \sigma_{k'} \begin{pmatrix} \rho_k (a_{I,k}^2 - \sigma_k) + p_I - p_k \\ (v_k - v_I) \frac{p_k - p_I - \rho_k a_{I,k}^2}{\rho_k} \\ \rho_k a_{I,k}^2 (v_k - v_I)^2 - a_k^2 (p_k - p_I) \end{pmatrix} \quad (1.92h)$$

with $\sigma_k = a_k^2 - (v_k - v_I)^2$.

1.3.1.3 NON-RESONANCE CONDITION

From Equations (1.92), the eigenvectors $(\mathbf{r}_n)_{n \in \{1,7\}}$ form a free basis if and only if

$$\alpha_1 \alpha_2 \sigma_1 \sigma_2 \neq 0. \quad (1.93)$$

Thus the only condition leading to hyperbolic degeneracy is

$$(v_k - v_1)^2 = a_k^2 \Leftrightarrow v_k \pm a_k = v_1. \quad (1.94)$$

This condition is called the *non-resonance condition* in Coquel et al. (2014) [31].

1.3.2 WAVE TYPES AND INTERFACIAL VELOCITY CLOSURE

As recalled in Embid and Baer (1992) [65], the waves of a non-linear system are classified between

$$\partial_{\mathbf{u}} \lambda_k \cdot \mathbf{r}_k = 0 \Rightarrow \lambda_k \text{ linearly degenerate}, \quad (1.95a)$$

$$\partial_{\mathbf{u}} \lambda_k \cdot \mathbf{r}_k \neq 0 \Rightarrow \lambda_k \text{ genuinely nonlinear}. \quad (1.95b)$$

Assuming two perfect gas equations of state, we show that

$$\partial_{\mathbf{u}} v_2 \cdot \mathbf{r}_2 = 0 \Rightarrow \lambda_2 = v_2 \text{ linearly degenerate}, \quad (1.96a)$$

$$\begin{aligned} \partial_{\mathbf{u}}(v_2 \pm a_2) \cdot \mathbf{r}_{3,4} &= \pm \partial_{\rho_2} a_2 \pm \frac{a_2}{\rho_2} \pm a_2^2 \partial_{p_2} a_2 \stackrel{PG}{=} \pm \frac{\gamma_2 + 1}{2\rho} \sqrt{\frac{\gamma_2 p_2}{\rho_2}} \\ &\Rightarrow \lambda_{3,4} = v_2 \pm a_2 \text{ genuinely nonlinear}, \end{aligned} \quad (1.96b)$$

$$\partial_{\mathbf{u}} v_1 \cdot \mathbf{r}_5 = 0 \Rightarrow \lambda_5 = v_1 \text{ linearly degenerate}, \quad (1.96c)$$

$$\begin{aligned} \partial_{\mathbf{u}}(v_1 \pm a_1) \cdot \mathbf{r}_{6,7} &= \pm \partial_{\rho_1} a_1 \pm \frac{a_1}{\rho_1} \pm a_1^2 \partial_{p_1} a_1 \stackrel{PG}{=} \pm \frac{\gamma_1 + 1}{2\rho_1} \sqrt{\frac{\gamma_1 p_1}{\rho_1}} \\ &\Rightarrow \lambda_{6,7} = v_1 \pm a_1 \text{ genuinely nonlinear}. \end{aligned} \quad (1.96d)$$

Thus, acoustic modes $v_k \pm a_k$ are genuinely non-linear and the entropy modes v_k are linearly degenerate. The latter are said entropic because the entropy jumps across them as we will see in the next paragraph.

Conditions have been sought to make the field λ_1 associated with v_1 linearly degenerate in order to obtain jump conditions and a maximum principle on the volume fraction. To preserve the symmetric structure of System (1.27), we seek a interfacial velocity with the form

$$v_1 = \beta v_1 + (1 - \beta) v_2, \quad (1.97)$$

with β an unknown function to be determined. If β is a function of $\beta = \beta(\alpha_2, \rho_1, \rho_2, p_1, p_2)$, then we have the following implication

$$\left\{ \begin{array}{l} v_1 = \beta v_1 + (1 - \beta) v_2 \\ \beta = \beta(\alpha_2, \rho_1, \rho_2, p_1, p_2) \\ \partial_{\mathbf{u}} v_1 \cdot \mathbf{r}_1 = 0 \end{array} \right\} \implies \beta \in \left\{ 0, 1, \frac{\alpha_1 \rho_1}{\alpha_1 \rho_1 + \alpha_2 \rho_2} \right\}. \quad (1.98)$$

This result can be found using any computing algebra tool and has been published in Coquel et al. (2002) [28].

1.3.3 RIEMANN INVARIANTS AND THE INTERFACIAL PRESSURE CLOSURE

Now that the interfacial velocity has been closed, the study of the Riemann invariants of System (1.27) gives some insights into the modelling of the interfacial pressure.

1.3.3.1 RIEMANN INVARIANTS

k -Riemann invariants $\psi_{k,j} \in \mathbb{R}$ for $j = \{1, 6\}$ are constants along the trajectories of the vector field \mathbf{r}_k such that

$$\partial_{\mathbf{u}_k} \psi_{k,j} \cdot \mathbf{r}_k = 0, j = \{1, 6\}. \quad (1.99)$$

As found in Coquel et al. (2002) [28], the Riemann invariants associated with the fields v_k and $v_k \pm a_k$ are not depending on the interfacial quantities and assuming two perfect gas equations of state, they read

$$\lambda_2 = v_2, \quad \psi_{2,j} = \{\alpha_2, v_2, p_2, \rho_1, v_1, p_1\} \quad (1.100a)$$

$$\lambda_3 = v_2 - a_2, \quad \psi_{3,j} = \left\{ \alpha_2, s_2, v_2 - \frac{2a_2}{\gamma_2 - 1}, \rho_1, v_1, p_1 \right\} \quad (1.100b)$$

$$\lambda_4 = v_2 + a_2, \quad \psi_{4,j} = \left\{ \alpha_2, s_2, v_2 + \frac{2a_2}{\gamma_2 - 1}, \rho_1, v_1, p_1 \right\} \quad (1.100c)$$

$$\lambda_5 = v_1, \quad \psi_{5,j} = \{\alpha_2, \rho_2, v_2, p_2, v_1, p_1\} \quad (1.100d)$$

$$\lambda_6 = v_1 - a_1, \quad \psi_{6,j} = \left\{ \alpha_2, \rho_2, v_2, p_2, s_1, v_1 - \frac{2a_1}{\gamma_1 - 1} \right\} \quad (1.100e)$$

$$\lambda_7 = v_1 + a_1, \quad \psi_{7,j} = \left\{ \alpha_2, \rho_2, v_2, p_2, s_1, v_1 + \frac{2a_1}{\gamma_1 - 1} \right\} \quad (1.100f)$$

There is only a jump of density ρ_k across the contact discontinuity $v_{k'}$, and the sonic waves $v_k \pm a_k$ are isoentropic.

As found in the work of Coquel et al. (2002) [28], assuming Equation (1.98), the first five 1-Riemann invariants can be obtained still without any closure on p_I .

$$\psi_{1,1} = v_I, \quad (1.101)$$

v_I is thus constant through the discontinuity.

$$\psi_{1,2} = \rho y_1 y_2 (v_1 - v_2), \quad (1.102)$$

$\psi_{1,2}$ looks like the mass weighted relative velocity in the local frame at the hydrodynamic velocity.

$$\psi_{1,3} = \alpha_1 p_1 + \alpha_2 p_2 + \psi_{1,2} (v_1 - v_2) = p + \rho y_1 y_2 (v_1 - v_2)^2 \quad (1.103)$$

with $p = \sum_{k=1,2} \alpha_k p_k$, $\psi_{1,3}$ is define as a total pressure (static pressure and the kinetic part evaluated at the relative velocity).

$$\psi_{1,5} = \epsilon_1 + \frac{p_1}{\rho_1} + \frac{1}{2(\alpha_1 \rho_1)^2} \psi_{1,2}^2 = h_1 + \frac{1}{2} y_2^2 (v_1 - v_2)^2, \quad (1.104)$$

$\psi_{1,5}$ is the total enthalpy of phase 1 (enthalpy and the kinetic part evaluated at the relative speed at the interface of the two phases).

$$\psi_{1,6} = \epsilon_2 + \frac{p_2}{\rho_2} + \frac{1}{2(\alpha_2\rho_2)^2}\psi_{1,2}^2 = h_2 + \frac{1}{2}y_1^2(v_1 - v_2)^2 \quad (1.105)$$

$\psi_{1,6}$ is the total enthalpy of phase 2 (enthalpy and the kinetic part evaluated at the relative speed at the interface of the two phases).

1.3.3.2 INTERFACIAL PRESSURE CLOSURE

Last but not the least, the key point in the Riemann invariant analysis is to find the last 1-Riemann invariant $\psi_{1,4}$. It depends directly on the closure of the interfacial pressure p_I .

Given a closure on the interfacial quantities, tedious calculations are needed to derive this last Riemann invariant due to the complexity of the first eigenvector \mathbf{r}_1 . Therefore, we have built a computing algebra script, helping us to solve Equation (1.99). Table 1.1 summarizes the results obtained for different closures. In Coquel et al. (2002) [28] and Gallouët et al. (2004) [78],

TABLE 1.1: $\psi_{1,4}$ Riemann invariant obtained by postulating p_I

p_I	general $\psi_{1,4}$	one particular solution $\psi_{1,4}$
p_k	$F\left(\frac{p_k}{\rho_k^{\gamma_k}}\right)$	s_k
$\alpha_k p_k$	$F\left(\frac{p_k}{\rho_k^{\gamma_k}} \exp\{(\gamma_k - 1)(-\alpha_k - \ln \alpha_{k'})\}\right)$	$s_k + (\gamma_k - 1)^2(-\alpha_k - \ln \alpha_{k'})$
$\sum_{k=1,2} \alpha_k p_k$?	?
$\frac{\sigma_1(1 - \beta)p_1 + \sigma_2\beta P_2}{\sigma_1(1 - \beta) + \sigma_2\beta}$?	$\frac{s_2}{s_1}$

the authors have proposed to define the interfacial pressure p_I as

$$p_I = \frac{\sigma_1(1 - \beta)p_1 + \sigma_2\beta P_2}{\sigma_1(1 - \beta) + \sigma_2\beta} \quad (1.106)$$

with $\sigma_k = \frac{1}{T_k s_k}$ for the perfect gas equation of state. In that case, we obtain

$$\psi_{1,4} = \frac{s_2}{s_1}. \quad (1.107)$$

The reader has probably noticed that for the closure $p_I = \alpha_1 p_1 + \alpha_2 p_2$, the last Riemann invariant could not be found by the computing algebra tool and no references has been found in the literature.

Since Riemann invariants play a crucial role in the jump conditions across the waves, one may choose the closure of p_I as a function of the Riemann invariant obtained. It is clear that $\psi_{1,4}$ is directly linked to the entropy of the system, more specifically to the entropy of the phase that imposes its pressure at the interface. For the closure $p_I = \alpha_1 p_1 + \alpha_2 p_2$, a good candidate for the missing Riemann invariant would be a function that depends on both phase entropies and the volume fraction.

1.3.4 CONCLUSION

We have carried out an exhaustive mathematical analysis of the Baer-Nunziato model relying on dedicated tools based on computer algebra and emphasized the close relation between the interfacial quantity closures and the Riemann invariants piloting the jump conditions across the waves. Since these tools are not specific to the Baer-Nunziato model, we will apply them in future work on System (1.82) we obtained in Section 1.2.

One of the main difficulty in the analysis conducted in this section is the presence of non-conservative terms in the system of equations. The study of hyperbolicity for conservative systems relies on the theory developed in Godunov (1961) [91], Friedrichs and Lax (1971) [73], which we thus cannot apply for the systems of interest. Therefore the next section is devoted to the extension of this theory in order to be able to apply to the *seven-equation* model in particular and hence further investigate the mathematical properties of the model.

1.4 ENTROPY SUPPLEMENTARY CONSERVATION LAW FOR NON-LINEAR SYSTEMS OF PDES WITH NON-CONSERVATIVE TERMS: APPLICATION TO THE MODELLING AND ANALYSIS OF COMPLEX FLUID FLOWS USING COMPUTER ALGEBRA

This section transcribes the results of a journal paper entitled *Entropy supplementary conservation law for non-linear systems of PDEs with non-conservative terms: application to the modelling and analysis of complex fluid flows using computer algebra*, written by Pierre Cordesse and Marc Massot and accepted in Communications in Mathematical Sciences [Cordesse and Massot \(2020\) \[41\]](#). It constitutes a building block into the mathematical study of the *seven-equation model*.

1.4.1 ABSTRACT

In the present contribution, we investigate first-order nonlinear systems of partial differential equations which are constituted of two parts: a system of conservation laws and non-conservative first order terms. Whereas the theory of first-order systems of conservation laws is well established and the conditions for the existence of supplementary conservation laws, and more specifically of an entropy supplementary conservation law for smooth solutions, well known, there exists so far no general extension to obtain such supplementary conservation laws when non-conservative terms are present. We propose a framework in order to extend the existing theory and show that the presence of non-conservative terms somewhat complexifies the problem since numerous combinations of the conservative and non-conservative terms can lead to a supplementary conservation law. We then identify a restricted framework in order to design and analyze physical models of complex fluid flows by means of computer algebra and thus obtain the entire ensemble of possible combination of conservative and non-conservative terms with the objective of obtaining specifically an entropy supplementary conservation law. The theory as well as developed computer algebra tool are then applied to a Baer-Nunziato two-phase flow model and to a multicomponent plasma fluid model. The first one is a first-order fluid model, with non-conservative terms impacting on the linearly degenerate field and requires a closure since there is no way to derive interfacial quantities from averaging principles and we need guidance in order to close the pressure and velocity of the interface and the thermodynamics of the mixture. The second one involves first order terms for the heavy species coupled to second order terms for the electrons, the non-conservative terms impact the genuinely nonlinear fields and the model can be rigorously derived from kinetic theory. We show how the theory allows to recover the whole spectrum of closures obtained so far in the literature for the two-phase flow system as well as conditions when one aims at extending the thermodynamics and also applies to the plasma case, where we recover the usual entropy supplementary equation, thus assessing the effectiveness and scope of the proposed theory.

1.4.2 INTRODUCTION

First-order nonlinear systems of partial differential equations and more specifically systems of conservation laws have been the subject of a vast literature since the second half of the twentieth century because they are ubiquitous in mathematical modelling of fluid flows and are used extensively for numerical simulation in applications and industrial context [Bissuel](#)

et al. (2018) [13], Gaillard et al. (2016) [76]. Such systems of equation can either be rigorously derived from kinetic theory of gases through various expansion techniques Ferziger and Kaper (1972) [70], Woods (1975) [221], or can be derived using rational thermodynamics and fluid mechanics including stationary action principle (SAP) Serrin (1959) [200], Landau and Lifshitz (1976) [127], Truesdell (1969) [212]. As far as Euler or Navier-Stokes equations are concerned for a gaseous flow field, the outcome of both approaches are similar and the mathematical properties of these systems have been thoroughly investigated for the past decades.

An interesting related problem is the quest for supplementary conservation laws. Noether's theorem Olver (1986) [168] leads, within the framework of SAP, to the derivation of supplementary conservation laws based on symmetry transformations of the variational problem under investigation³. Examples of such derivations on two-phase flow modelling can be found in Gavriluk and Saurel (2002) [81], Drui et al. (2019) [60]. However, to the authors knowledge, no symmetry transformations have been identified yielding a conservative law on the entropy of the system. In fact, SAP does not allow to reach a closed system of equations, and one has to provide a closure for the entropy (see Gouin and Ruggeri (2009) [95] for example). A specific type of supplementary conservation equation for smooth solution is especially important, namely the *entropy equation*, derived through the theory developed in Godunov (1961) [91], Friedrichs and Lax (1971) [73] for systems of conservation laws. Such systems of PDEs are hyperbolic at any point where a locally convex entropy function exists Mock (1980) [161], and when they are equipped with a strictly convex entropy, they can be symmetrized Friedrichs and Lax (1971) [73] Harten and Hyman (1983) [104] and thus are hyperbolic. These properties have been at the heart of the mathematical theory of existence and uniqueness of smooth solutions Kawashima and Shizuta (1988) [118] Giovangigli and Massot (1998) [85], but they are also a corner stone for the study of weak solutions for which the work of Kruřkov (1970) [122] proves the well-posedness of Cauchy problem for one-dimensional systems.

Nonetheless, for a number of applications, where reduced-order fluid models have to be used for tractable mathematical modelling and numerical simulations, be it in the industry or in other disciplines, micro-macro kinetic-theory-like approaches as well as rational thermodynamics and SAP approaches often lead to system of conservation laws involving *non-conservative terms*. Among the large spectrum of applications, we focus on two types of models, which exemplify the two approaches: 1- two phase flows models which rely on a hierarchy of diffuse interface models among which stands the Baer-Nunziato Baer and Nunziato (1986) [5] model used when full disequilibrium of the phases must be taken into account. Since this model is derived through rational thermodynamics, the macroscopic set of equations can not be derived from physics at small scale of interface dynamics and thus require closure of interfacial pressure and velocity, 2- multicomponent fluid modelling of plasmas flows out of thermal equilibrium, where the equations can be derived rigorously from kinetic theory using a multi-scale Chapman-Enskog expansion mixing a hyperbolic scaling for the heavy species and a parabolic scaling for the electrons Graille et al. (2009) [96]. Concerning the thermodynamics, whereas for the first model it has to be postulated and requires assumptions, it can be obtained from kinetic theory in the second model. In both cases, the models involve non-conservative terms, but these terms do not act on the same fields; linearly degenerate field is impacted for the two-phase flow model, whereas it acts on the genuinely nonlinear fields in

³Among the most well-known symmetry transformations, the time translation yields the conservation of the total energy of the system if the associated Lagrangian is invariant to time-shift and the space translation yields the conservation of the total momentum of the system if the Lagrangian is invariant to space-shift

the second Wagnier et al. (2018) [219]. Whereas hyperbolicity depends on the closure and is not guaranteed for the first class of models Gallouët et al. (2004) [78], the second is naturally hyperbolic Graille et al. (2009) [96] and also involves second-order terms and eventually source terms Magin et al. (2009) [150].

Thus, the presence of *non-conservative terms* encompasses several situations and requires a general theoretical framework. While Noether's theorem can still be applied to obtain some supplementary conservation laws, it does not permit to exhibit all of them and especially not an entropy supplementary conservation law. A unifying theory extending the standard approach for systems of conservation laws (entropy supplementary conservation law, entropic symmetrization, Godunov-Mock theorem, hyperbolicity) is still missing for such systems even if some key advances exist. The system has been shown to be symmetrizable by Coquel et al. (2014) [31] – not in the sense of Godunov-Mock – far from the resonance condition for which hyperbolicity degenerates. In Forestier and Gavrilyuk (2011) [71], the model is proved to be partially symmetrizable in the sense of Godunov-Mock.

The present paper first proposes an extension of the theory of supplementary conservation laws for system of conservation laws to first-order nonlinear systems of partial differential equations which are constituted of two parts: a system of conservation laws and *non-conservative first order terms*. We emphasize how the presence of non-conservative terms somewhat complexifies the problem since numerous combinations of the conservative and non-conservative terms can lead to supplementary conservation laws. We then identify a restricted framework in order to design and analyze physical models of complex fluid flows by means of computer algebra and thus obtain the entire ensemble of possible combination of conservative and non-conservative terms to obtain an entropy supplementary conservation law. The proposed theoretical approach is then applied to the two systems identified so far for their diversity of behaviour. Even if the whole theory is valid for any supplementary conservation law, we focus on obtaining an *entropy* supplementary conservation law. For the two-phase flow model, assuming a thermodynamics of non-miscible phases, we derive conditions to obtain an entropy supplementary conservative equation together with a compatible thermodynamics and closures for the non-conservative terms. Interestingly enough, all the closures proposed so far in the literature are recovered Baer and Nunziato (1986) [5], Kapila et al. (1997) [116], Bdzil et al. (1999) [7], Lochon (2016) [144], Saurel et al. (2003) [191]. The strength of the formalism lies also in the capacity to derive such conditions for some level of mixing of the phases. By introducing a mixing term in the definition of the entropy, the new theory brings out constraints on the form of the added mixing term. We recover not only the closure proposed to account for a configuration energy as in the context of deflagration-to-detonation Baer and Nunziato (1986) [5] or in Coquel et al. (2002) [28], but we also rigorously find new closures leading to a conservative system of equations⁴. We also prove that the theory encompasses the plasma case, where we recover the usual *entropy* supplementary equation assessing the effectiveness and scope of the proposed theory.

The paper is organized as follows. The extension of the theory for system of conservation laws to first-order nonlinear systems of partial differential equations including non-conservative terms, as well as the framework to apply the theory by means of computer algebra are introduced in Section 1.4.3. These results are then applied first to the Baer-Nunziato model

⁴Such closure is similar to the one used in Powers (1988) [176], Powers et al. (1990) [177] which led to a controversy Drew (1983) [57], Bdzil et al. (1999) [7], Andrianov et al. (2003) [2]

in [Section 1.4.4](#) and then to the plasma model in [Section 1.4.5](#) to obtain an entropy supplementary conservation law compatible with the model closure.

Notations: Let $\mathbf{a} \in \mathbb{R}^p$, $\mathbf{b} \in \mathbb{R}^p$, $\mathcal{B} \in \mathbb{R}^{p \times p}$, $\mathcal{C} \in \mathbb{R}^{p \times p}$, $\mathcal{D} \in \mathbb{R}^{p \times p \times p}$ be a p -component line first-order tensor, a p -component column first-order tensor, two p -square second-order tensor and a third-order tensor respectively. We introduce the following notations:

- $\mathbf{a}\mathcal{B}$ is a line first-order tensor in \mathbb{R}^p whose i component are defined by

$$(\mathbf{a}\mathcal{B})_i = \sum_{j=1,p} \mathbf{a}_j \mathcal{B}_{j,i}, \quad (1.108)$$

- $\mathcal{B}\mathbf{b}$ is a column first-order tensor in \mathbb{R}^p whose i component is defined by

$$(\mathcal{B}\mathbf{b})_i = \sum_{j=1,p} \mathcal{B}_{i,j} \mathbf{b}_j, \quad (1.109)$$

- $\mathcal{B} \times \mathcal{C}$ is p -square second-order tensor whose (i, j) component is defined by

$$(\mathcal{B} \times \mathcal{C})_{i,j} = \sum_{k=1,p} \mathcal{B}_{i,k} \mathcal{C}_{k,j}, \quad (1.110)$$

- $\mathbf{a} \otimes \mathbb{D}$ is a p -square second-order tensor whose (i, j) component is defined by

$$(\mathbf{a} \otimes \mathbb{D})_{(i,j)} = \sum_{k=1,p} \mathbf{a}_k \times \mathbb{D}_{k,i,j}. \quad (1.111)$$

Hereafter, we will name zero- first- and second-order tensors by scalar, vector and matrix respectively and for convenience we will use vector and matrix representations of functions. Moreover, given a scalar function S , the partial differentiation of S by a column vector \mathbf{a} , $\partial_{\mathbf{a}} S$ is a line vector in \mathbb{R}^p . Finally, \cdot denotes the Euclidean scalar product in \mathbb{R}^p .

1.4.3 SUPPLEMENTARY CONSERVATION LAW

First we recall the theory of the existence of a supplementary conservative equation for first-order nonlinear systems of conservation laws. Second, this notion is extended to systems containing first order non-conservative terms. Third, we introduce a framework to apply this new theory to design and analyze physical models using computer algebra.

A one-dimensional framework is adopted from now on, $x \in \mathbb{R}$, in order to simplify the derivation. Nonetheless, the results can easily be extended to the multi-dimensional approach as presented in [Godlewski and Raviart \(1996\) \[90\]](#) for systems of conservation laws.

1.4.3.1 FIRST-ORDER NONLINEAR CONSERVATIVE SYSTEMS.

The homogeneous form of a first-order nonlinear system of p conservation laws writes

$$\partial_t \mathbf{q} + \partial_x \mathbf{f}(\mathbf{q}) = \mathbf{0}, \quad (1.112)$$

where $\mathbf{q} \in \Omega \subset \mathbb{R}^p$ denotes the conservative variables with Ω an open convex of \mathbb{R}^p and $\mathbf{f} : \mathbf{q} \in \Omega \mapsto \mathbb{R}^p$ the conservative fluxes. Focusing on smooth solution of the system (1.112), its quasi-linear form is given by

$$\partial_t \mathbf{q} + \partial_{\mathbf{q}} \mathbf{f}(\mathbf{q}) \partial_x \mathbf{q} = \mathbf{0}. \quad (1.113)$$

Theorem 2. Let $H : \mathbf{q} \in \Omega \mapsto \mathbb{R}$ be a scalar function, not necessarily convex. The following statements are equivalent:

(C₁) System (1.112) admits a supplementary conservative equation

$$\partial_t H(\mathbf{q}) + \partial_x G(\mathbf{q}) = 0, \quad (1.114)$$

where $\mathbf{q} \in \mathbb{R}^p$ is a smooth solution of System (1.112) and $G : \mathbf{q} \in \Omega \mapsto \mathbb{R}$ is a scalar function.

(C₂) There exists a scalar function $G : \mathbf{q} \in \Omega \mapsto \mathbb{R}$ such that

$$\partial_{\mathbf{q}} H(\mathbf{q}) \partial_{\mathbf{q}} \mathbf{f}(\mathbf{q}) = \partial_{\mathbf{q}} G(\mathbf{q}). \quad (1.115)$$

(C₃) $\partial_{\mathbf{q}\mathbf{q}} H(\mathbf{q}) \times \partial_{\mathbf{q}} \mathbf{f}(\mathbf{q})$ is a p -square symmetric matrix.

Proof. The proofs of the theorem can be found in the literature. We would like to recall how the last statement is obtained. Assuming (C₂), differentiating Equation (1.115) leads to

$$\partial_{\mathbf{q}\mathbf{q}} H(\mathbf{q}) \times \partial_{\mathbf{q}} \mathbf{f}(\mathbf{q}) + \partial_{\mathbf{q}} H(\mathbf{q}) \otimes \partial_{\mathbf{q}\mathbf{q}} \mathbf{f}(\mathbf{q}) = \partial_{\mathbf{q}\mathbf{q}} G(\mathbf{q}), \quad (1.116)$$

where $\partial_{\mathbf{q}} H(\mathbf{q}) \otimes \partial_{\mathbf{q}\mathbf{q}} \mathbf{f}(\mathbf{q})$ is a p -square matrix defined as $\sum_i \partial_{\mathbf{q}_i} H(\mathbf{q}) \partial_{\mathbf{q}\mathbf{q}} \mathbf{f}_i(\mathbf{q})$ which is a linear combination of Hessian matrices and hence symmetric. Moreover, the RHS of Equation (1.116) $\partial_{\mathbf{q}\mathbf{q}} G(\mathbf{q})$ is symmetric. Therefore $\partial_{\mathbf{q}\mathbf{q}} H(\mathbf{q}) \times \partial_{\mathbf{q}} \mathbf{f}(\mathbf{q})$ is symmetric. □

Theorem 2 applies for any type of supplementary conservative equations and other formulations of Theorem 2 can be found in the literature Harten and Hyman (1983) [104], Godlewski and Raviart (1996) [90], Després and Dubois (2005) [52].

1.4.3.2 EXTENSION TO SYSTEMS INVOLVING NON-CONSERVATIVE TERMS.

Let us now consider the homogeneous form of a first-order nonlinear system of partial differential equations constituted of two parts: conservations laws and first-order non-conservative terms. Its quasi-linear form can be written as

$$\partial_t \mathbf{q} + [\partial_{\mathbf{q}} \mathbf{f}(\mathbf{q}) + \mathcal{N}(\mathbf{q})] \partial_x \mathbf{q} = 0, \quad (1.117)$$

where $\mathbf{q} \in \Omega \subset \mathbb{R}^p$ is a smooth solution with Ω an open convex of \mathbb{R}^p , $\mathbf{f} : \mathbf{q} \in \Omega \mapsto \mathbb{R}^p$ the conservative fluxes, $\mathcal{N} : \mathbf{q} \in \Omega \mapsto \mathbb{R}^{p \times p}$ the p -square matrix containing the first-order non-conservative terms.

In the following we extend the theory introduced in Section 1.4.3.1 to System (1.117). Given a scalar function $H : \mathbf{q} \in \Omega \mapsto \mathbb{R}$, multiplying System (1.117) by the line vector $\partial_{\mathbf{q}} H(\mathbf{q})$ yields

$$\partial_t H + \partial_{\mathbf{q}} H(\mathbf{q}) [\partial_{\mathbf{q}} \mathbf{f}(\mathbf{q}) + \mathcal{N}(\mathbf{q})] \partial_x \mathbf{q} = 0. \quad (1.118)$$

Compared to Equation (1.114), the presence of the non-conservative terms in Equation (1.118) complexifies the question of the existence of a supplementary conservative equation. Therefore we propose to decompose in a specific way the conservative and non-conservative terms in Definition 1.

Definition 1. Given a scalar function $H : \mathbf{q} \in \Omega \mapsto \mathbb{R}$ and a first-order nonlinear non-conservative system (1.117), let us define the four p -square matrices, $\mathcal{C}_1(\mathbf{q})$, $\mathcal{Z}_1(\mathbf{q})$, $\mathcal{C}_2(\mathbf{q})$ and $\mathcal{Z}_2(\mathbf{q})$ in $\mathbb{R}^{p \times p}$ such that

$$\partial_{\mathbf{q}}\mathbf{f}(\mathbf{q}) = \mathcal{C}_1(\mathbf{q}) + \mathcal{Z}_1(\mathbf{q}), \quad (1.119)$$

$$\mathcal{N}(\mathbf{q}) = \mathcal{C}_2(\mathbf{q}) + \mathcal{Z}_2(\mathbf{q}), \quad (1.120)$$

with the condition

$$\partial_{\mathbf{q}}H(\mathbf{q}) [\mathcal{Z}_1(\mathbf{q}) + \mathcal{Z}_2(\mathbf{q})] = \mathbf{0}. \quad (1.121)$$

In light of Definition 1, Theorem 2 can be extended as follows:

Theorem 3. Let $H : \mathbf{q} \in \Omega \mapsto \mathbb{R}$ be a scalar function, not necessarily convex. Given a first-order nonlinear system of non-conservation laws (1.117), if we introduce the decomposition as in Definition 1, then the following statements are equivalent:

(C₁) System (1.117) admits a supplementary conservative equation

$$\partial_t H(\mathbf{q}) + \partial_x G(\mathbf{q}) = 0, \quad (1.122)$$

where $\mathbf{q} \in \mathbb{R}^p$ is a smooth solution of System (1.117) and $G : \mathbf{q} \in \Omega \mapsto \mathbb{R}$ is a scalar function.

(C₂) There exists a scalar function $G : \mathbf{q} \in \Omega \mapsto \mathbb{R}$ such that

$$\partial_{\mathbf{q}}H(\mathbf{q}) [\mathcal{C}_1(\mathbf{q}) + \mathcal{C}_2(\mathbf{q})] = \partial_{\mathbf{q}}G(\mathbf{q}). \quad (1.123)$$

(C₃) $\partial_{\mathbf{q}\mathbf{q}}H(\mathbf{q}) \times [\mathcal{C}_1(\mathbf{q}) + \mathcal{C}_2(\mathbf{q})] + \partial_{\mathbf{q}}H(\mathbf{q}) \otimes \partial_{\mathbf{q}} [\mathcal{C}_1(\mathbf{q}) + \mathcal{C}_2(\mathbf{q})]$ is a p -square symmetric matrix.

Proof. Rewriting Equation (1.118) using the decomposition of the conservative and non-conservative terms as

$$\partial_t H(\mathbf{q}) + \partial_{\mathbf{q}}H(\mathbf{q}) [\mathcal{C}_1(\mathbf{q}) + \mathcal{C}_2(\mathbf{q})] \partial_x \mathbf{q} = -\partial_{\mathbf{q}}H(\mathbf{q}) [\mathcal{Z}_1(\mathbf{q}) + \mathcal{Z}_2(\mathbf{q})] \partial_x \mathbf{q} \quad (1.124)$$

outlines the result. □

Remark 8. Theorem 3 applies for any type of supplementary conservative equations. The usual symmetry condition on which relies the existence of a supplementary conservation equation is strongly modified when non-conservation terms are present. From Theorem 2 to Theorem 3 the condition

$$\partial_{\mathbf{q}\mathbf{q}}H(\mathbf{q}) \times \partial_{\mathbf{q}}\mathbf{f}(\mathbf{q}) \text{ symmetric,}$$

is modified into

$$\partial_{\mathbf{q}\mathbf{q}}H(\mathbf{q}) \times [\mathcal{C}_1(\mathbf{q}) + \mathcal{C}_2(\mathbf{q})] + \partial_{\mathbf{q}}H(\mathbf{q}) \otimes \partial_{\mathbf{q}} [\mathcal{C}_1(\mathbf{q}) + \mathcal{C}_2(\mathbf{q})] \text{ symmetric.}$$

In the context of systems of conservation laws, an interesting algebraic approach is proposed in Barros (2005) [6] based on the reinterpretation of the symmetric Condition (C₃) in Theorem 2 as a Frobenius problem. Nevertheless, when dealing with additional non-conservative terms, the above new symmetry condition prevents us from applying efficiently such an approach.

Remark 9. In Definition 1, the condition (1.121) implies that the conservative and non-conservative terms depend only on the variables \mathbf{q} , and not on their gradient. Some authors have allowed the matrices \mathcal{Z}_k to depend also on the gradients of the variables \mathbf{q} , then a more general condition for the decomposition can be written

$$\partial_{\mathbf{q}}H(\mathbf{q}) [\mathcal{Z}_1(\mathbf{q}, \partial_x \mathbf{q}) + \mathcal{Z}_2(\mathbf{q}, \partial_x \mathbf{q})] \partial_x \mathbf{q} \leq 0. \quad (1.125)$$

In Section 1.4.4, we will see that such a condition has been chosen to close the Baer-Nunziato model Saurel et al. (2003) [191]. However, since it changes the mathematical nature of the PDE under investigation, we will not include it in our study.

From a modelling perspective, System (1.117) under consideration is not necessarily closed. Therefore, the following corollary yields conditions on the model to obtain a supplementary conservative equation once we have postulated the thermodynamics.

Corollary 1. Let $H : \mathbf{q} \in \Omega \mapsto \mathbb{R}$ be a scalar function, not necessarily convex. Given a first-order nonlinear system of non-conservation laws (1.117) where $\mathbf{f} : \mathbf{q} \in \Omega \mapsto \mathbb{R}^p$ and $\mathcal{N} : \mathbf{q} \in \Omega \mapsto \mathbb{R}^{p \times p}$ are unknown functions to be modelled. If we introduce the decomposition as in Definition 1, then System (1.117) admits a supplementary conservative equation

$$\partial_t H(\mathbf{q}) + \partial_x G(\mathbf{q}) = 0, \quad (1.126)$$

where $\mathbf{q} \in \Omega \subset \mathbb{R}^p$ is a smooth solution of System (1.117) and $G : \mathbf{q} \in \Omega \mapsto \mathbb{R}$ a scalar function, if and only if the following conditions hold

(C₁) $\partial_{\mathbf{q}\mathbf{q}}H(\mathbf{q}) \times [\mathcal{C}_1(\mathbf{q}) + \mathcal{C}_2(\mathbf{q})] + \partial_{\mathbf{q}}H(\mathbf{q}) \otimes \partial_{\mathbf{q}}[\mathcal{C}_1(\mathbf{q}) + \mathcal{C}_2(\mathbf{q})]$ is a p -square symmetric matrix.

(C₂) $\partial_{\mathbf{q}}H(\mathbf{q}) [\mathcal{Z}_1(\mathbf{q}) + \mathcal{Z}_2(\mathbf{q})] = \mathbf{0}$.

1.4.3.3 DESIGN OR ANALYSIS OF PHYSICAL MODELS USING COMPUTER ALGEBRA.

We would like to apply the theory on first-order nonlinear non-conservative systems introduced in Section 1.4.3.2 to physical models such as the Baer-Nunziato model and the plasma model in order to design and analyze them. We recall that our prior interest is to obtain an *entropy* supplementary conservation law. However, the difficulty is manifold:

- The combination of the non-conservative terms and conservative terms proposed in Definition 1 to build a supplementary conservative equation is not unique and thus many degrees of freedom exist in defining the matrices \mathcal{C}_k and \mathcal{Z}_k .
- When the model is derived through rational thermodynamics, terms in the system of equations might need closure and the thermodynamics has to be postulated. Therefore, the matrices \mathcal{C}_k and \mathcal{Z}_k can contain unknowns related to the system and the definition of H .
- The calculations needed to derive a supplementary conservative equation are heavy and choice-based. Any change of \mathcal{C}_k and \mathcal{Z}_k that respects Definition 1, or any new postulated thermodynamics would require to derive again all the equations, and eventually a very limited range of possibilities would be examined.

These difficulties to apply the theory and examine all the possibilities makes computer algebra very appealing since it allows symbolic operations to be implemented and thus can derive equations systematically and quasi-instantaneously for any combinations of conservative and non-conservative terms as well as model closure and H definition.

Furthermore, the generic level handled by computer algebra is not unlimited and therefore Definition 1 requires further assumptions to circumscribe the number of degrees of freedom that can be accounted for.

Even if the theory proposed hereinbefore is valid to obtain any kind of supplementary conservation laws, we are mainly interested in obtaining an entropy supplementary conservation law. We thus need to define the notions of *entropy* and *entropic variables* in the following two definitions.

Definition 2. $H : \mathbf{q} \in \Omega \mapsto \mathbb{R}$ is said to be an entropy of the system (1.117) if $H(\mathbf{q})$ is a convex scalar function of the variables \mathbf{q} which fulfills Theorem 2. The supplementary conservative equation (1.114) is then named the entropy equation and $\mathbf{G} : \mathbf{q} \in \Omega \mapsto \mathbb{R}^p$ is the associated entropy flux.

Definition 3. Let $H : \mathbf{q} \in \Omega \mapsto \mathbb{R}$ be a scalar function, not necessarily convex. Given a first-order nonlinear conservative system (1.112), let us define the entropic variables $\mathbf{v} : \mathbf{q} \in \Omega \mapsto \mathbb{R}^p$ such that

$$\mathbf{v}(\mathbf{q}) = (\partial_{\mathbf{q}} H(\mathbf{q}))^t. \quad (1.127)$$

The entropic variables have been studied in [Giovangigli and Massot \(1998\) \[85\]](#) in order to obtain symmetric and normal forms of the system of equation and used in the framework of gaseous mixtures, where the mathematical entropy H is usually defined as the opposite of a physical entropy density per unit volume of the system [Giovangigli and Massot \(1998\) \[85\]](#).

Definition 4. Given a scalar function $H : \mathbf{q} \in \Omega \mapsto \mathbb{R}$, a first-order nonlinear non-conservative system (1.117), and the four p -square matrices $\mathcal{C}_1(\mathbf{q})$, $\mathcal{Z}_1(\mathbf{q})$, $\mathcal{C}_2(\mathbf{q})$ and $\mathcal{Z}_2(\mathbf{q})$ in $\mathbb{R}^{p \times p}$ defined in Definition 1, we introduce the unknown line vector $\mathbf{t} : \mathbf{q} \in \Omega \mapsto \mathbb{R}^p$ such that

$$\partial_{\mathbf{q}} H(\mathbf{q}) [\mathcal{C}_1(\mathbf{q}) + \mathcal{C}_2(\mathbf{q})] = \partial_{\mathbf{q}} H(\mathbf{q}) \partial_{\mathbf{q}} \mathbf{f}(\mathbf{q}) + \mathbf{t}(\mathbf{q}), \quad (1.128)$$

$$\partial_{\mathbf{q}} H(\mathbf{q}) [\mathcal{Z}_1(\mathbf{q}) + \mathcal{Z}_2(\mathbf{q})] = \partial_{\mathbf{q}} H(\mathbf{q}) \mathcal{N}(\mathbf{q}) - \mathbf{t}(\mathbf{q}). \quad (1.129)$$

The condition of Equation (1.121) rewrites into

$$\partial_{\mathbf{q}} H(\mathbf{q}) \mathcal{N}(\mathbf{q}) - \mathbf{t}(\mathbf{q}) = \mathbf{0}. \quad (1.130)$$

Remark 10. Since Definition 4 is a projection of the matrix equations of Definition 1 on the vector $\partial_{\mathbf{q}} H(\mathbf{q})$, it may be interesting to introduce an unknown matrix $\mathcal{T}(\mathbf{q}) \in \mathbb{R}^{p \times p}$ associated to the unknown line vector $\mathbf{t}(\mathbf{q})$ such that

$$\mathbf{t}(\mathbf{q}) = \partial_{\mathbf{q}} H(\mathbf{q}) \mathcal{T}(\mathbf{q}). \quad (1.131)$$

Thus, Definition 4 can be formulated as follows

$$\mathcal{C}_1(\mathbf{q}) + \mathcal{C}_2(\mathbf{q}) = \partial_{\mathbf{q}} \mathbf{f}(\mathbf{q}) + \mathcal{T}(\mathbf{q}), \quad (1.132)$$

$$\mathcal{Z}_1(\mathbf{q}) + \mathcal{Z}_2(\mathbf{q}) = \mathcal{N}(\mathbf{q}) - \mathcal{T}(\mathbf{q}), \quad (1.133)$$

with the condition

$$\partial_{\mathbf{q}} H(\mathbf{q}) [\mathcal{N}(\mathbf{q}) - \mathcal{T}(\mathbf{q})] = \mathbf{0}. \quad (1.134)$$

The unknown functional line vector $\mathbf{t}(\mathbf{q}) \in \mathbb{R}^p$ represents the transfer of non-conservative terms to the conservative terms. In the degenerate case where $\mathbf{t} = \mathbf{0}$, \mathcal{C}_k receives all the conservative terms and \mathcal{Z}_k all the non-conservative terms. Condition (1.130) forces all the non-conservative terms to vanish and System (1.117) is fully conservative, hence the theory of conservative system can be applied.

Definition 4 being more restrictive than Definition 1, computer algebra is now applicable to analyze the properties of a first-order nonlinear non-conservative system leading to a reformulation of Theorem 3.

Theorem 4. *Let $H : \mathbf{q} \in \Omega \mapsto \mathbb{R}$ be a scalar function, not necessarily convex. Consider a first-order nonlinear system of non-conservation laws (1.117). If we introduce the decomposition as in Definition 4, then the following statements are equivalent:*

(C₁) *System (1.117) admits a supplementary conservative equation*

$$\partial_t H(\mathbf{q}) + \partial_x G(\mathbf{q}) = 0, \quad (1.135)$$

where $\mathbf{q} \in \mathbb{R}^p$ is a smooth solution of System (1.117) and $G : \mathbf{q} \in \Omega \mapsto \mathbb{R}$ is a scalar function.

(C₂) *There exists a scalar function $G : \mathbf{q} \in \Omega \mapsto \mathbb{R}$ such that*

$$\partial_{\mathbf{q}} H(\mathbf{q}) \partial_{\mathbf{q}} \mathbf{f}(\mathbf{q}) + \mathbf{t}(\mathbf{q}) = \partial_{\mathbf{q}} G(\mathbf{q}). \quad (1.136)$$

(C₃) *$\partial_{\mathbf{q}\mathbf{q}} H(\mathbf{q}) \times \partial_{\mathbf{q}} \mathbf{f}(\mathbf{q}) + \partial_{\mathbf{q}} \mathbf{t}(\mathbf{q})$ is a p -square symmetric matrix.*

Proof. Injecting Definition 4 into Theorem 3 leads to these results. □

When H is the entropy of the system, Theorem 4 provides equations that relate the thermodynamics of the model through H , the model itself with possible terms to be closed in $\mathbf{f}(\mathbf{q})$ and $\mathcal{N}(\mathbf{q})$, and the unknown line vector $\mathbf{t}(\mathbf{q})$. Combined with the Definition 4, Theorem 4 brings out conditions on the model to obtain a supplementary conservative equation given a postulated thermodynamics and it leads to the following corollary.

Corollary 2. *Consider a first-order nonlinear system of non-conservation laws (1.117) where $\mathbf{q} \in \Omega \subset \mathbb{R}^p$ is a smooth solution with Ω an open convex of \mathbb{R}^p but $\mathbf{f} : \mathbf{q} \in \Omega \mapsto \mathbb{R}^p$ and $\mathcal{N} : \mathbf{q} \in \Omega \mapsto \mathbb{R}^{p \times p}$ are unknown functions to be modelled. Let $H : \mathbf{q} \in \Omega \mapsto \mathbb{R}$ be a scalar function, not necessarily convex. If we introduce the decomposition as in Definition 4, then System (1.117) admits a supplementary conservative equation*

$$\partial_t H(\mathbf{q}) + \partial_x G(\mathbf{q}) = 0, \quad (1.137)$$

where $G : \mathbf{q} \in \Omega \mapsto \mathbb{R}$ is a scalar function if and only if the following conditions hold

(C₁) *$\partial_{\mathbf{q}\mathbf{q}} H(\mathbf{q}) \times \partial_{\mathbf{q}} \mathbf{f}(\mathbf{q}) + \partial_{\mathbf{q}} \mathbf{t}(\mathbf{q})$ is symmetric.*

(C₂) *$\partial_{\mathbf{q}} H(\mathbf{q}) \mathcal{N}(\mathbf{q}) - \mathbf{t}(\mathbf{q}) = \mathbf{0}$.*

Remark 11. *The previous framework can be extended to the multi-dimensional case in a straightforward manner. If the original system is isotropic, such as for the applications we have in mind, then the previous conditions will be the same in the various directions. In the framework of more general non-isotropic systems, which satisfy Galilean and rotational invariances for example, we will obtain different conditions and we have to check that the decomposition we perform in the various directions satisfies some compatibility relations so that the obtained conservation law satisfies the original invariance properties of the system.*

1.4.3.4 METHODOLOGY.

Corollary 2 draws the methodology we have implemented in the Maple™ computer algebra software⁵ in order to obtain an *entropy* supplementary conservation law. Our methodology is the following:

(Step 1) We define the thermodynamics by postulating - if need be - an entropy function $H : \mathbf{q} \in \Omega \mapsto \mathbb{R}$.

(Step 2) We then use Condition (C_1) and (C_2) of Corollary 2 to ensure the existence of an entropy flux $G : \mathbf{q} \in \Omega \mapsto \mathbb{R}$ and solve

$$\begin{cases} \partial_{\mathbf{q}\mathbf{q}}H(\mathbf{q}) \times \partial_{\mathbf{q}}\mathbf{f}(\mathbf{q}) + \partial_{\mathbf{q}}\mathbf{t}(\mathbf{q}) \text{ symmetric,} \\ \partial_{\mathbf{q}}H(\mathbf{q}) \mathcal{N}(\mathbf{q}) - \mathbf{t}(\mathbf{q}) = \mathbf{0}. \end{cases} \quad (1.138)$$

In System (1.138), $\mathbf{t}(\mathbf{q})$ is systematically an unknown, $\mathbf{f}(\mathbf{q})$, $\mathcal{N}(\mathbf{q})$ as well as $H(\mathbf{q})$ can include unknown terms for which the variable dependency is specified. Maple™ generates then an exhaustive solution for $\mathbf{t}(\mathbf{q})$ and constraints on all the other unknown terms.

(Step 3) From that, the software derives the admissible entropy flux $G : \mathbf{q} \in \Omega \mapsto \mathbb{R}$ which gives then the supplementary conservative equation.

1.4.4 APPLICATION TO THE BAER-NUNZIATO MODEL

1.4.4.1 CONTEXT AND PRESENTATION OF THE MODEL.

The Baer-Nunziato model has been derived through rational thermodynamics in Baer and Nunziato (1986) [5] and describes a two-phase flow out of equilibrium. Extended by the work of Saurel and Abgrall (1999) [190] thanks to the introduction of interfacial quantities, the homogeneous form of the Baer-Nunziato model is

$$\partial_t \mathbf{q} + [\partial_{\mathbf{q}}\mathbf{f}(\mathbf{q}) + \mathcal{N}(\mathbf{q})] \partial_x \mathbf{q} = \mathbf{0}, \quad (1.139a)$$

$$\partial_{\mathbf{q}}\mathbf{f}(\mathbf{q}) = \begin{pmatrix} 0 & \mathbf{0} & \mathbf{0} \\ \mathbf{0} & \partial_{\mathbf{q}_2}\mathbf{f}_2(\mathbf{q}_2) & \mathbf{0} \\ \mathbf{0} & \mathbf{0} & \partial_{\mathbf{q}_1}\mathbf{f}_1(\mathbf{q}_1) \end{pmatrix}, \quad \mathcal{N}(\mathbf{q}) = \begin{pmatrix} v_I & \mathbf{0} & \mathbf{0} \\ \mathbf{n}_2 & \mathbf{0} & \mathbf{0} \\ \mathbf{n}_1 & \mathbf{0} & \mathbf{0} \end{pmatrix}, \quad (1.139b)$$

where the column vector $\mathbf{q} \in \mathbb{R}^7$ is defined by $\mathbf{q}^T = (\alpha_2, \mathbf{q}_2^T, \mathbf{q}_1^T)$, $\mathbf{q}_k^T = (\alpha_k \rho_k, \alpha_k \rho_k v_k, \alpha_k \rho_k E_k)$. The conservative flux $\mathbf{f} : \mathbf{q} \in \Omega \mapsto \mathbb{R}^7$ reads $\mathbf{f}(\mathbf{q})^T = (0, \mathbf{f}_2(\mathbf{q}_2)^T, \mathbf{f}_1(\mathbf{q}_1)^T)$ with

⁵Maple is a trademark of Waterloo Maple Inc.

$\mathbf{f}_k(\mathbf{q}_k)^T = (\alpha_k \rho_k v_k, \alpha_k (\rho_k v_k^2 + p_k), \alpha_k (\rho_k E_k + p_k) v_k)$. $\mathcal{N} : \mathbf{q} \in \Omega \mapsto \mathbb{R}^{7 \times 7}$ is the matrix containing the non-conservative terms with $\mathbf{n}_2(\mathbf{q})^T = -\mathbf{n}_1(\mathbf{q})^T = (0, -p_I, -p_I v_I)$. Then, α_k is the volume fraction of phase $k \in [1, 2]$, ρ_k the partial density, v_k the phase velocity, p_k the phase pressure, $E_k = e_k + v_k^2/2$ the total energy per unit of mass, e_k the internal energy, v_I the interfacial velocity and p_I the interfacial pressure.

Two levels of ingredients are still missing for this model. First, the macroscopic set of equations includes the interface dynamics through the interfacial terms v_I and p_I and thus needs closure on these terms. Second the thermodynamics has to be postulated.

The mathematical properties of the model have been studied by [Embid and Baer \(1992\)](#) [65], [Coquel et al. \(2002\)](#) [28], [Gallouët et al. \(2004\)](#) [78] among others and many closure have been proposed for the interfacial terms based on wave-type considerations and the entropy inequality.

Regarding the thermodynamics, for non-miscible phases, the entropy $H(\mathbf{q})$ is commonly defined by Equation (1.140) as in [Coquel et al. \(2002\)](#) [28], [Lochon \(2016\)](#) [144],

$$H(\mathbf{q}) = - \sum_{k=1,2} \alpha_k \rho_k s_k, \quad (1.140)$$

with $s_k = s_k(\rho_k, p_k)$ the phase entropy which takes for the Ideal Gas equation of state the form

$$s_k = c_{v,k} \ln \left(\frac{p_k}{\rho_k^{\gamma_k}} \right), \quad (1.141)$$

with $c_{v,k}$ the heat capacity, p_k the pressure, ρ_k the density and γ_k the isentropic coefficient of phase k .

If we were to account for partial miscibility between the two phases, we would have to add a mixing term to the definition of the non-miscible entropy. The mixing term could take the form proposed in [Gallouët et al. \(2004\)](#) [78], so that the entropy rewrites

$$H = - \sum_{k=1,2} \alpha_k \rho_k [s_k(\rho_k, p_k) - \psi_k(\alpha_k)], \quad (1.142)$$

with $\psi_k, k = \{1, 2\}$, two strictly convex nonlinear arbitrary functions depending on the volume fraction. Nevertheless, so far in the literature, no explicit expressions of these functions have been proposed. In [Gallouët et al. \(2004\)](#) [78], in order to obtain a supplementary conservative equation using the entropy defined in Equation (1.142), the authors show that the following condition has to be fulfilled

$$\psi_k(\alpha_k) = \psi_{k'}(\alpha_{k'}). \quad (1.143)$$

In this section, we apply to the Baer-Nunziato model the framework introduced in Section 1.4.3 by means of computer algebra. We will firstly assume the phases are non-miscible and derive an entropy supplementary conservative equation along with conditions on the interfacial terms. All the closures proposed in the literature will be recovered. Secondly, we will also apply the methodology in the case of a thermodynamics with partial miscibility and derive an entropy supplementary conservative equation together with conditions on both the

interfacial terms and the mixing terms of the entropy. Not only all the closures proposed in the literature are recovered but also new ones and we also propose explicit formulations of the mixing terms and show that depending on their expression, the condition expressed in Gallouët et al. (2004) [78] is not necessary.

1.4.4.2 METHODOLOGY AND DECOMPOSITION.

We start without any condition on (v_I, p_I) . We need initially to fix a decomposition of $\partial_{\mathbf{q}}\mathbf{f}(\mathbf{q})$ and $\mathcal{N}(\mathbf{q})$ including a certain degree of freedom as explained in Section 1.4.3.3.

Given an entropy $H : \mathbf{q} \in \Omega \mapsto \mathbb{R}$ of System (1.139a), by expressing the entropic variables as $\mathbf{v}(\mathbf{q})^T = (v_\alpha, \mathbf{v}_2^T, \mathbf{v}_1^T)$, we use the decomposition proposed in Definition (4). Since we do not want to generate other non-conservative terms, we choose to define the line vector $\mathbf{t} : \mathbf{q} \in \Omega \mapsto \mathbb{R}^p$ by $\mathbf{t}(\mathbf{q}) = (t_\alpha(\mathbf{q}), \mathbf{0}, \mathbf{0})$ where $t_\alpha : \mathbf{q} \in \Omega \mapsto \mathbb{R}$ is the unknown scalar function a priori of all the variables \mathbf{q} . We obtain the following decompositions

$$(\partial_{\mathbf{q}}H[\mathcal{C}_1 + \mathcal{C}_2])^T = \begin{pmatrix} t_\alpha(\mathbf{q}) \\ \mathbf{v}_2 \cdot \partial_{\mathbf{q}_2}\mathbf{f}_2(\mathbf{q}_2) \\ \mathbf{v}_1 \cdot \partial_{\mathbf{q}_1}\mathbf{f}_1(\mathbf{q}_1) \end{pmatrix}, \quad (1.144a)$$

$$(\partial_{\mathbf{q}}H[\mathcal{Z}_1 + \mathcal{Z}_2])^T = \begin{pmatrix} -t_\alpha(\mathbf{q}) + v_\alpha v_I + \sum_{k=1,2} \mathbf{v}_k \cdot \mathbf{n}_k \\ \mathbf{0} \\ \mathbf{0} \end{pmatrix}. \quad (1.144b)$$

t_α allows fractions of the non-conservative terms to feed the matrix \mathcal{C}_k .

Given this decomposition, we use the methodology proposed in Section 1.4.3.4. (*Step 2*) will be split here into two sub-steps.

(*Step 2.a*) Condition (C_1) on the symmetry of the matrix $\partial_{\mathbf{q}\mathbf{q}}H(\mathbf{q}) \times \partial_{\mathbf{q}}\mathbf{f}(\mathbf{q}) + \partial_{\mathbf{q}}\mathbf{t}(\mathbf{q})$ ensures the existence of an entropy flux $\mathbf{G}(\mathbf{q})$. It will determine $\mathbf{t}(\mathbf{q})$.

(*Step 2.b*) Knowing $\mathbf{t}(\mathbf{q})$, Condition (C_2), $\partial_{\mathbf{q}}H(\mathbf{q})\mathcal{N}(\mathbf{q}) - \mathbf{t}(\mathbf{q}) = \mathbf{0}$, will return an equation linking (v_I, p_I) and also ψ_k when miscibility is accounted for.

1.4.4.3 NON-MISCIBLE PHASES ENTROPY.

We start applying our method (*Step 1*) by postulating H as in Equation (1.140). The thermodynamics is entirely known and we use the Ideal Gas EOS. The entropic variables \mathbf{v} are then

$$\mathbf{v} = \begin{pmatrix} v_\alpha \\ \mathbf{v}_2 \\ \mathbf{v}_1 \end{pmatrix} \text{ with } v_\alpha = \frac{p_1}{T_1} - \frac{p_2}{T_2} \text{ and } \mathbf{v}_k = \frac{1}{T_k} \begin{pmatrix} g_k - v_k^2/2 \\ v_k \\ -1 \end{pmatrix}, \quad (1.145)$$

with g_k the Gibbs free energy, $g_k = e_k + p_k/\rho_k - T_k s_k$. We now apply the conditions to determine $t_\alpha(\mathbf{q})$ and derive the equation that links the interfacial quantities v_I and p_I .

Theorem 5. Consider System (1.139a). If the mixture entropy is defined as $H = -\sum_{k=1,2} \alpha_k \rho_k S_k$ then with the decomposition proposed in Equations (1.144)

$$\partial_{\mathbf{q}} H(\mathbf{q}) \times \partial_{\mathbf{q}} \mathbf{f}(\mathbf{q}) + \partial_{\mathbf{q}} \mathbf{t}(\mathbf{q}) \text{ symmetric} \Leftrightarrow t_\alpha(\mathbf{q}) = F(\alpha_2) + \frac{p_1}{T_1} v_1 - \frac{p_2}{T_2} v_2, \quad (1.146)$$

with F a strictly convex arbitrary function depending on the volume fraction α_2 . As a consequence the condition on $\partial_{\mathbf{q}} H(\mathbf{q}) [\mathcal{Z}_1(\mathbf{q}) + \mathcal{Z}_2(\mathbf{q})]$ gives

$$\begin{aligned} \partial_{\mathbf{q}} H(\mathbf{q}) [\mathcal{Z}_1(\mathbf{q}) + \mathcal{Z}_2(\mathbf{q})] &= 0 \\ \Leftrightarrow -F(\alpha_2) + \sum_{k=1,2} \frac{(-1)^k}{T_k} (p_I - p_k) (v_k - v_I) &= 0. \end{aligned} \quad (1.147)$$

Proof. The function t_α is found relying on symbolic computation and it holds as a proof. \square

As explained in (Step 2.a), Equation (1.146) guarantees the existence of an entropy flux G associated with the mixture entropy H chosen as in Equation (1.140) by defining the unknown function $t_\alpha(\mathbf{q})$.

Then as described in (Step 2.b), Equation (1.147) relates the interfacial terms (v_I, p_I) . By choosing $F(\alpha_2) = 0$, the condition on $\partial_{\mathbf{q}} H \times [\mathcal{Z}_1 + \mathcal{Z}_2]$ writes

$$\sum_{k=1,2} \frac{1}{T_k} (p_k - p_I) (v_I - v_k) = 0. \quad (1.148)$$

So now, to obtain a closed model along with a supplementary conservative equation, we can postulate an interfacial velocity v_I and derive the corresponding p_I . We will limit ourselves to defining v_I such that the field associated to v_I is linearly degenerate. In that case, the only admissible interfacial velocities are $v_I = \beta v_1 + (1 - \beta) v_2$ with $\beta \in [0, 1, \alpha_1 \rho_1 / \rho]$ [Coquel et al. \(2002\) \[28\]](#), [Lochon \(2016\) \[144\]](#). We will focus on the particular case where $F(\alpha_2) = 0$. We obtain the following results:

- If $v_I = v_k$, then Equation (1.148) returns $p_I = p_{k'}$. $(v_k, p_{k'})$ is the closure proposed first by [Baer and Nunziato \(1986\) \[5\]](#), [Kapila et al. \(1997\) \[116\]](#), [Bdzil et al. \(1999\) \[7\]](#), in the context of deflagration-to-detonation.
- If $v_I = \beta v_1 + (1 - \beta) v_2$ with $\beta = \alpha_1 \rho_1 / \rho$, then Equation (1.148) returns $p_I = \mu p_1 + (1 - \mu) p_2$ with $\mu(\beta) = (1 - \beta) T_2 / (\beta T_1 + (1 - \beta) T_2)$. It is the closure found in [Lochon \(2016\) \[144\]](#) among others.

We see that first these closures are a specific case where $F(\alpha_2)$ is chosen to be zero in Equation (1.147). Second, one could have chosen another interfacial velocity v_I and it would have led to another interfacial pressure p_I compatible with an entropy pair.

Remark 12. If we had used the extended condition expressed in Equation (1.125), then the condition on $\partial_{\mathbf{q}} H [\mathcal{Z}_1 + \mathcal{Z}_2]$ would be

$$\sum_{k=1,2} \frac{1}{T_k} [p_k - p_I(\mathbf{q}, \partial_x \mathbf{q})] [v_I(\mathbf{q}, \partial_x \mathbf{q}) - v_k] \partial_x \alpha_k \leq 0 \quad (1.149)$$

$$\Leftrightarrow -\sum_{k=1,2} \frac{1}{T_k} \frac{Z_k}{(Z_1 + Z_2)^2} [p_{k'} - p_k + \text{sgn}(\partial_x \alpha_1) (v_{k'} - v_k) Z_{k'}]^2 \leq 0, \quad (1.150)$$

where Z_k is defined by $Z_k = \rho_k a_k$ with the phase sound speed $a_k^2 = \partial p_k / \partial \rho_k|_{s_k}$. From Equation (1.149), one sees that the dependency on $\partial_x \mathbf{q}$ reduces to $\partial_x \alpha_2$ otherwise some terms would not be signable. Then closures such as the one found through Discrete Element Method (DEM) Saurel et al. (2003) [191] are obtained

$$v_I = \frac{Z_1 v_1 + Z_2 v_2}{Z_1 + Z_2} + \operatorname{sgn}(\partial_x \alpha_1) \frac{p_2 - p_1}{Z_1 + Z_2}, \quad (1.151)$$

$$p_I = \frac{Z_2 p_1 + Z_1 p_2}{Z_1 + Z_2} + \operatorname{sgn}(\partial_x \alpha_1) \frac{Z_1 Z_2}{Z_1 + Z_2} (v_2 - v_1). \quad (1.152)$$

1.4.4.4 PARTIALLY MISCIBLE PHASES ENTROPY.

Now, let us add a degree of freedom in the thermodynamics by introducing mixing terms in the definition of the entropy H as in Equation (1.142) to account for partial miscibility of the phases. The added terms, ψ_k , functions of the volume fraction α_k only, are to be determined.

The entropic variables \mathbf{v} are

$$\mathbf{v} = \begin{pmatrix} \sum_{k=1,2} (-1)^{k+1} \frac{p_k}{T_k} \left[1 - \frac{\alpha_k}{r_k} \psi'_k(\alpha_k) \right] \\ \mathbf{v}_2 \\ \mathbf{v}_1 \end{pmatrix} \text{ with } \mathbf{v}_k = \frac{1}{T_k} \begin{pmatrix} g_k - v_k^2/2 \\ v_k \\ -1 \end{pmatrix} \quad (1.153)$$

Theorem 6. Consider System (1.139a). If the mixture entropy is defined as $H = -\sum_{k=1,2} \alpha_k \rho_k [s_k - \psi_k(\alpha_k)]$ with ψ_k , $k = [1, 2]$, two strictly convex arbitrary functions depending on the volume fraction, then with the decomposition proposed in Equations (1.144), we have

$$\begin{aligned} & \partial_{\mathbf{q}\mathbf{q}} H \times \partial_{\mathbf{q}} \mathbf{f} + \partial_{\mathbf{q}} \mathbf{t} \text{ symmetric} \\ \Leftrightarrow t_\alpha(\mathbf{q}) &= F(\alpha_2) + \frac{p_1}{T_1} v_1 \left[1 - \frac{\alpha_1}{r_1} \psi'_1(\alpha_1) \right] - \frac{p_2}{T_2} v_2 \left[1 - \frac{\alpha_2}{r_2} \psi'_2(\alpha_2) \right] \end{aligned} \quad (1.154)$$

with F a strictly convex arbitrary function depending on the volume fraction. As a consequence the condition on $\partial_{\mathbf{q}} H[\mathcal{Z}_1 + \mathcal{Z}_2]$ gives

$$\begin{aligned} \mathbf{0} &= \partial_{\mathbf{q}} H(\mathbf{q}) [\mathcal{Z}_1(\mathbf{q}) + \mathcal{Z}_2(\mathbf{q})] \\ \Leftrightarrow 0 &= -F(\alpha_2) + \sum_{k=1,2} (-1)^{k+1} \alpha_k \rho_k \psi'_k(\alpha_k) (v_k - v_I) \\ &+ \sum_{k=1,2} \frac{(-1)^k}{T_k} (p_I - p_k) (v_k - v_I) \end{aligned} \quad (1.155)$$

Again, Equation (1.154) guarantees the existence of an entropy flux $G(\mathbf{q})$ conditioning the function $t_\alpha(\mathbf{q})$ (Step 2.a). The interfacial quantities (v_I, p_I) and ψ_k are linked by Equation (1.155) (Step 2.b).

The difference with the previous case for immiscible phases is that there are two supplementary unknowns ψ_k , $k = 1, 2$. We thus are free to either postulate first an interfacial velocity v_I and then derive the corresponding p_I and ψ_k or postulate first the functions ψ_k and see what choices we have for the interfacial terms. In the following we investigate the two approaches.

1.4.4.5 INTERFACIAL CLOSURES IMPACTING THERMODYNAMICS.

Let us postulate v_I and limit ourselves to the case $F(\alpha_2) = 0$. We will again seek a linearly degenerate field for v_I . In such case, the results in Table 1.2 are obtained.

TABLE 1.2: Admissible thermodynamics and model closures obtained by postulating v_I

	v_I	p_I	$(\psi_k, \psi_{k'})$
Case 1	v_k	$p_{k'}$	$(\psi_k, 0)$
Case 2	$\beta v_1 + (1 - \beta)v_2$ $\beta = \alpha_1 \rho_1 / \rho$	$\mu p_1 + (1 - \mu)p_2$ $\mu(\beta) = \frac{(1-\beta)T_2}{\beta T_1 + (1-\beta)T_2}$	$\psi_k(\alpha_k) = \psi_{k'}(\alpha_{k'})$

In Case 1 of Table 1.2, ψ_k can be interpreted as a configuration energy of phase k as in Baer and Nunziato (1986) [5], Kapila et al. (1997) [116], Bdzil et al. (1999) [7], in the context of deflagration-to-detonation. It is a term defining an interaction of one phase with itself only. More importantly, Equation (1.155) shows that it is not possible to include a configuration energy for each phase when choosing the closure $(v_I, p_I) = (v_k, p_{k'})$.

In Case 2 of Table 1.2, the condition on the mixing term introduced in Equation (1.143) by Gallouët et al. (2004) [78] is recovered and the closures are the one stated in Coquel et al. (2002) [28]. However, the condition on the mixing terms imposes a constraint on the volume fraction and thus on the flow topology. Since mixing of the phases should be able to occur disregarding the flow topology, these terms fail to introduce free mixing among the phases.

1.4.4.6 THERMODYNAMICS IMPACTING INTERFACIAL TERM CLOSURES.

Since Case 1 and Case 2 of Table 1.2 do not allow the phases to mix, let us choose first the thermodynamics of the system and induce the admissible interfacial terms.

It has been shown that the mixing entropy of an ideal compressible binary mixture is of the form $\sum_{k=1,2} \alpha_k \ln(\alpha_k)$. Therefore, we choose to define the functions ψ_k by $\psi_k(\alpha_k) = r_k \ln(\alpha_k)$. In this case, the entropy writes

$$H = - \sum_{k=1,2} \alpha_k \rho_k [s_k - r_k \ln(\alpha_k)], \quad (1.156)$$

with r_k the specific gas constant of phase k , we now account for quasi-miscibility between the phases.

The condition on t_α degenerates, $t_\alpha = F(\alpha_2)$ and the condition on $\partial_q H [\mathcal{Z}_1 + \mathcal{Z}_2]$ is now

$$-F(\alpha_2) + p_I \left(\frac{v_1 - v_I}{T_1} - \frac{v_2 - v_I}{T_2} \right) = 0. \quad (1.157)$$

It is no more possible to obtain the classic definition on v_I and p_I . In the case $F(\alpha_2) = 0$ two choices are possible to verify Equation (1.157) and summarized in Table 1.3.

Case 3 of Table 1.3 proposes a temperature-based averaged velocity for v_I , which does not seem to be physically reasonable. In Case 4, the interfacial pressure must vanish for the system

TABLE 1.3: Admissible thermodynamics and model closures obtained by postulating ψ_k

	v_I	p_I
Case 3	$\beta v_1 + (1 - \beta)v_2$ with $\beta = T_2/(T_2 - T_1)$	no constraint
Case 4	no constraint	o

to admit an entropy supplementary conservation equation and the Baer-Nunziato model becomes a conservative system if one assumes the field associated to v_I to be linearly degenerate. One knows how much it simplifies the problem in terms of numerical implementation. This result can be interpreted as an incompatibility between the existence of a mixing process in the thermodynamics of the mixture and an interfacial pressure, that stays meaningful as long as there is an interface between the two phases.

1.4.4.7 LINK WITH DISPERSED PHASE FLOW.

When the thermodynamics accounts for mixing (Case 4 Table 1.3), the existence of an entropy supplementary conservative equation is incompatible with the interfacial pressure, and thus the nozzling terms $p_I \partial_x \alpha k$ vanish.

In separated two-phase flows, these terms are known to be necessary to preserve uniformity in velocity and pressure of the flow during its temporal evolution [Andrianov et al. \(2003\) \[2\]](#) and are usually compared to the terms obtained in a single gas with a variable section [Saurel and Le Metayer \(2001\) \[192\]](#). Whereas these arguments seem valid for separated two-phase flows, one may question the role these terms play in a dispersed phase flows.

Taking the particular case $p_1 = 0$ and $p_2 = 0$ in the Baer-Nunziato model seems to lead to a system of equations similar to one that would describe a flow of incompressible suspended particles, where 1 would denote the carrier phase and 2 the dispersed phase. Doing so, one recovers not only the Marble model [Marble \(1963\) \[152\]](#), which proposes a pressureless gas dynamic equations for the particle phase, valid in the limit where $\alpha_2 < 10^{-3}$, but also the model obtained by Sainsaulieu [Sainsaulieu \(1995\) \[189\]](#) in the asymptotic limit where the volume fraction of the particles $\alpha_2 \rightarrow 0$.

Nevertheless, even if the partial differential equations are alike, the thermodynamics associated to Marble and Sainsaulieu models differ from the one we propose for the Baer-Nunziato model. The latter accounts for compressibility of the two phases and partial miscibility whereas the thermodynamics of the Marble model assumes incompressibility of the particles and non-miscibility between the two phases.

To conclude, if one aims at unifying the description of both separated phases and dispersed flow through a unique model, the thermodynamics must be treated together with the system modelling.

1.4.5 APPLICATION TO THE PLASMA MODEL

The multicomponent fluid modelling of plasma flows out of thermal equilibrium has been derived rigorously from kinetic theory using a multi-scale Chapman-Enskog expansion mixing a hyperbolic scaling for the heavy species with a parabolic scaling for the electrons [Graille et al. \(2009\) \[96\]](#). The system takes the form

$$\partial_t \mathbf{q} + [\partial_{\mathbf{q}} \mathbf{f}(\mathbf{q}) + \mathcal{N}(\mathbf{q})] \partial_x \mathbf{q} = \partial_x (\mathbf{D}(\mathbf{q}) \partial_x \mathbf{q}), \quad (1.158)$$

with

$$\partial_{\mathbf{q}} \mathbf{f}(\mathbf{q}) = \begin{pmatrix} 0 & 1 & 0 & 0 & 0 \\ (\kappa/2 - 1)v^2 & (2 - \kappa)v & \kappa & 0 & 0 \\ (\kappa/2v^2 - \frac{H}{\rho_h})v & \frac{H}{\rho_h} - \kappa v^2 & (1 + \kappa)v & 0 & 0 \\ -\frac{\rho_e}{\rho_h}v & \frac{\rho_e}{\rho_h} & 0 & v & 0 \\ -\frac{\rho_e \epsilon_e}{\rho_h}v & \frac{\rho_e \epsilon_e}{\rho_h} & 0 & 0 & v \end{pmatrix}, \quad (1.159)$$

$$\mathcal{N}(\mathbf{q}) = \begin{pmatrix} 0 & 0 & 0 & 0 & 0 \\ 0 & 0 & 0 & 0 & 0 \\ 0 & 0 & 0 & 0 & 0 \\ 0 & 0 & 0 & 0 & 0 \\ -\frac{\rho_e \epsilon_e}{\rho_h} \kappa v & \frac{\rho_e \epsilon_e}{\rho_h} \kappa & 0 & 0 & 0 \end{pmatrix}, \quad (1.160)$$

$$\mathbf{D}(\mathbf{q}) = \begin{pmatrix} 0 & 0 & 0 & 0 & 0 \\ 0 & 0 & 0 & 0 & 0 \\ 0 & 0 & 0 & -\frac{\lambda_e \kappa \epsilon_e}{\rho_e} & \frac{\lambda_e \kappa \epsilon_e}{\rho_e} + \gamma D \\ 0 & 0 & 0 & 0 & \frac{D \kappa}{T_e} \\ 0 & 0 & 0 & -\frac{\lambda_e \kappa \epsilon_e}{\rho_e} & \frac{\lambda_e \kappa \epsilon_e}{\rho_e} + \gamma D \end{pmatrix}, \quad (1.161)$$

where the column vector $\mathbf{q} \in \mathbb{R}^5$ is defined by $\mathbf{q}^T = (\rho_h, \rho_h v, E, \rho_e, \rho_e \epsilon_e)$ with ρ_h is the density of the heavy particles, v the hydrodynamic velocity, E the total energy defined by $E = \rho_h v^2/2 + \rho_h \epsilon_h + \rho_e \epsilon_e$, ϵ_h the internal energy of the heavy particles, ρ_e the density of the electrons, ϵ_e the internal energy of the electrons, H the total enthalpy defined by $H = E + p$ with $p = p_h + p_e$, T_e the temperature of the electrons, the constant κ defined by $\kappa = \gamma - 1$ with γ the isentropic coefficient, p_h is the pressure of the heavy particles and p_e is the pressure of the electrons. In the diffusive terms of the diffusion matrix $\mathbf{D} \in \mathbb{R}^{5 \times 5}$, λ_e is the electron thermal conductivity, D the electron diffusion coefficient.

Concerning the thermodynamics, it can be obtained from kinetic theory. The electrons and the heavy particles thermodynamics are defined by an ideal gas equation of state, and they share both the same isentropic coefficient: $p_h = \kappa \rho_h \epsilon_h$, $p_e = \kappa \rho_e \epsilon_e$ where p_h is the pressure of the heavy particles and p_e is the pressure of the electrons, r is the constant of the gas $r = c_v \kappa$ with c_v the calorific heat at constant volume, the model being adimensionalized $r = c_v(\gamma - 1) = 1$.

The model is naturally hyperbolic [Graille et al. \(2009\) \[96\]](#) and also involves second-order terms and eventually source terms [Magin et al. \(2009\) \[150\]](#). Here we considered the homogeneous form.

In this section, we would like to derive the usual entropy supplementary conservative equation found by [Graille et al. \(2009\) \[96\]](#) and show that it is unique, to attest the effectiveness of the theory.

1.4.5.1 DECOMPOSITION.

We need to proceed to the decomposition of the conservative and non conservative terms of System (1.158). We restrict ourselves again to the decomposition proposed in Definition (4) and we add a degree of liberty to each non-null non-conservative components by defining $\mathbf{t} : \mathbf{q} \in \Omega \mapsto \mathbb{R}^5$ as $\mathbf{t}(\mathbf{q})^T = (t_1(\mathbf{q}), t_2(\mathbf{q}), 0, 0, 0)$ such that the following decompositions are obtained

$$(\partial_{\mathbf{q}}H(\mathbf{q}) [\mathcal{C}_1(\mathbf{q}) + \mathcal{C}_2(\mathbf{q})])^T = \mathbf{v}(\mathbf{q}) \cdot \partial_{\mathbf{q}}\mathbf{f}(\mathbf{q}) + \begin{pmatrix} t_1(\mathbf{q}) \\ t_2(\mathbf{q}) \\ 0 \\ 0 \\ 0 \end{pmatrix}, \quad (1.162)$$

$$(\partial_{\mathbf{q}}H(\mathbf{q}) [\mathcal{Z}_1(\mathbf{q}) + \mathcal{Z}_2(\mathbf{q})])^T = \begin{pmatrix} -t_1(\mathbf{q}) - \frac{\rho_e}{\rho_h} \left(1 - \frac{T_e}{T_h}\right) v \\ -t_2(\mathbf{q}) + \frac{\rho_e}{\rho_h} \left(1 - \frac{T_e}{T_h}\right) \\ 0 \\ 0 \\ 0 \end{pmatrix}. \quad (1.163)$$

The unknown scalar functions $t_k(\mathbf{q})$ give the possibility to fractions of the non-conservative terms to be given to the matrix \mathcal{C}_k .

1.4.5.2 IDEAL GAS ENTROPY.

The entropy $H : \mathbf{q} \in \Omega \mapsto \mathbb{R}$ for two perfect gases is defined as

$$H = -\rho_h s_h - \rho_e s_e, \quad (1.164)$$

with the partial entropies defined by

$$s_h = c_v \ln \left(\frac{p_h}{\kappa \rho_h} \right), \quad s_e = c_v \ln \left(\frac{p_e}{\kappa \rho_e} \right). \quad (1.165)$$

This entropy includes mixing between the electrons and the heavy particles. Thus, we start applying our method (*Step 1*) by postulating H as in Equation (1.164). The entropic variables \mathbf{v} are then

$$\mathbf{v} = \begin{pmatrix} \frac{1}{T_h} (g_h - v^2/2) \\ \frac{1}{T_h} v \\ -\frac{1}{T_h} \\ \frac{1}{T_e} g_e \\ \frac{1}{T_h} - \frac{1}{T_e} \end{pmatrix}, \quad (1.166)$$

with g_k the Gibbs free energy, $g_k = e_k + p_k/\rho_k - T_k s_k$.

Remark 13. *In the fourth component of the entropic variable, the kinetic energy of the electrons has vanished. This is due to the low-Mach assumption made for the electrons.*

We now apply the conditions to determine $t_k(\mathbf{q})$.

Theorem 7. Consider System (1.158). If the mixture entropy is defined as $H = -\rho_h s_h - \rho_e s_e$, then with the decomposition proposed in Equations (1.162), we have

$$\begin{aligned} & \partial_{\mathbf{q}\mathbf{q}}H(\mathbf{q}) \times \partial_{\mathbf{q}}\mathbf{f}(\mathbf{q}) + \partial_{\mathbf{q}}\mathbf{t}(\mathbf{q}) \text{ symmetric} \\ \Leftrightarrow t_1(\mathbf{q}) &= \frac{\rho_e}{\rho_h} \left(1 - \frac{T_e}{T_h}\right) \mathbf{v}_S \text{ and } t_2(\mathbf{q}) = -\frac{\rho_e}{\rho_h} \left(1 - \frac{T_e}{T_h}\right), \end{aligned} \quad (1.167)$$

and the condition on $\partial_{\mathbf{q}}H(\mathbf{q}) [\mathcal{Z}_1(\mathbf{q}) + \mathcal{Z}_2(\mathbf{q})]$ is

$$\partial_{\mathbf{q}}H(\mathbf{q}) [\mathcal{Z}_1(\mathbf{q}) + \mathcal{Z}_2(\mathbf{q})] = (0, 0, 0, 0, 0). \quad (1.168)$$

Proof. Using Maple™, we find

$$\begin{aligned} & \partial_{\mathbf{q}\mathbf{q}}H(\mathbf{q}) \times \partial_{\mathbf{q}}\mathbf{f}(\mathbf{q}) + \partial_{\mathbf{q}}\mathbf{t}(\mathbf{q}) \text{ symmetric} \\ \Leftrightarrow t_1(\mathbf{q}) &= \frac{\rho_e}{\rho_h} \left(1 - \frac{T_e}{T_h}\right) v + \int [-v\partial_v F_1(\rho_h, v) + \rho_h \partial_{\rho_h} F_1(\rho_h, v)] dv + F_2(\rho_h) \\ \text{and } t_2(\mathbf{q}) &= -\frac{\rho_e}{\rho_h} \left(1 - \frac{T_e}{T_h}\right) + F_1(\rho_h, v), \end{aligned}$$

with F_1, F_2 two arbitrary functions and the condition on $\partial_{\mathbf{q}}H(\mathbf{q}) [\mathcal{Z}_1(\mathbf{q}) + \mathcal{Z}_2(\mathbf{q})]$ is

$$\begin{aligned} (\partial_{\mathbf{q}}H(\mathbf{q}) [\mathcal{Z}_1(\mathbf{q}) + \mathcal{Z}_2(\mathbf{q})])^T &= \begin{pmatrix} -\int [-v\partial_v F_1(\rho_h, v) + \rho_h \partial_{\rho_h} F_1(\rho_h, v)] dv - F_2(\rho_h) \\ -F_1(\rho_h, v) \\ 0 \\ 0 \\ 0 \end{pmatrix} \\ &= \mathbf{0}. \end{aligned}$$

One sees that the last equation imposes first $F_1 = 0$ and thus $F_2 = 0$. Reinjecting these terms into the first equation gives the result. \square

As explained in (Step 2.a), the Equation (1.167) guarantees the existence of an entropy flux $\mathbf{G} : \mathbf{q} \in \Omega \mapsto \mathbb{R}$ associated with the entropy H defined in Equation (1.164) by solving the unknown functions $t_1(\mathbf{q})$ and $t_2(\mathbf{q})$.

Therefore, for the entropy H defined in Equation (1.164), there is a unique decomposition which ensures the existence of a supplementary conservative equation which is given by

$$(\partial_{\mathbf{q}}H [\mathcal{C}_1 + \mathcal{C}_2])^T = \mathbf{v}^T \cdot \partial_{\mathbf{q}}\mathbf{f}(\mathbf{q}) + \begin{pmatrix} \frac{\rho_e}{\rho_h} \left(1 - \frac{T_e}{T_h}\right) v \\ \frac{\rho_e}{\rho_h} \left(1 - \frac{T_e}{T_h}\right) \\ 0 \\ 0 \\ 0 \end{pmatrix}, \quad (1.169)$$

$$\partial_{\mathbf{q}}H [\mathcal{Z}_1 + \mathcal{Z}_2] = \mathbf{0}. \quad (1.170)$$

It leads to the following entropy flux couple

$$H = -\rho_h s_h - \rho_e s_e, \quad (1.171)$$

$$G = -(\rho_h s_h + \rho_e s_e) v. \quad (1.172)$$

The theory recovers the supplementary conservative equation already found in the literature from the kinetic theory [Graille et al. \(2009\) \[96\]](#).

1.4.6 CONCLUSION

In the present contribution, we have proposed a theoretical framework for the derivation of supplementary conservation laws for systems of partial differential equation including first-order non-conservative terms - commonly encountered in modeling of complex flows - thus extending the standard approach for systems of conservation laws. Since our main objective is deriving an entropy supplementary conservation law, we have used this framework to make a first step to extend the theory of Godunov-Mock to such non-conservative systems.

Given a reasonable choice in the combination of the conservative and non-conservative terms, we have been able to show how to use the theory to design or analyze systems by means of computer algebra on two applications chosen for their numerous differences in terms of model and thermodynamics closure as well as the nature of the waves impacted by the non-conservative terms.

Firstly, applied to the Baer-Nunziato two-phase flow model derived from rational thermodynamics, the theory has brought about entropy supplementary conservative equations together with constraints on the interfacial quantities and the definition of the thermodynamics for non-miscible fluids and also when accounting for some level of mixing of the two phases. A new closure for the interfacial quantities has been proposed and leads to a conservative system. Secondly, for a plasma model obtained rigorously from the kinetic theory of gases, where the thermodynamics is also provided, the approach allows to recover as unique the supplementary conservation equation related to the kinetic entropy and is thus assessed.

The content of this section is a first step into studying the entropic symmetrization in the sense of Godunov-Mock and relation to source terms for two-phase flow modeling. Some partial symmetrization of the Baer-Nunziato model has been obtained in the classical framework by [Forestier and Gavriljuk \(2011\) \[71\]](#). Combining such symmetrization theory with source terms can then be envisioned such as in the case of plasma flows [Magin et al. \(2009\) \[150\]](#), even if the symmetrization is only partial in the framework of [Graille et al. \(2009\) \[96\]](#) where the electron are considered in a low-Mach limit.

Nevertheless, for such a study to be complete, several other steps have to be handled first: the question of the strict convexity of the entropy for the change of variable to be admissible and its relation to thermodynamics (a difficult question [Coquel et al. \(2002\) \[28\]](#), [Gallouët et al. \(2004\) \[78\]](#)). Since we wanted to investigate this loss of strict convexity in the framework of non-interacting thermodynamics, we have developed a new formalism to build a mixing thermodynamics for multi-fluids, and it is the objective of [Chapter 2](#). Based on this new developments, we hope that equipping the Baer-Nunziato system with an extended thermodynamics closure will lead to a strictly convex entropy and thus allow the study of entropic full symmetrization and source terms, in the spirit of [Giovangigli and Massot \(1998\) \[85\]](#), [Massot \(2002\) \[155\]](#), [Giovangigli and Massot \(2004\) \[86\]](#), [Magin et al. \(2009\) \[150\]](#).

APPENDIX 1.A MIXTURE ENTROPY CONSTRAINT FOR THE SAP

In Gouin (1990) [93], the author shows using Lagrangian multipliers that a constrain on the mixture entropy leads to thermal equilibrium. We detail here the proof using virtual displacements. Let us assume the mixture entropy is conserved during the second virtual displacement. Interpreted as the unique internal variable, only the mixture entropy is impacted by the second parametrized family, $\varphi_\lambda^L(\mathbf{x}, \lambda)$. It gives

$$\delta_\lambda (\alpha_1 \rho_1 s_1 + \alpha_2 \rho_2 s_2) = 0 \Leftrightarrow \alpha_1 \rho_1 \delta_\lambda s_1 = -\alpha_2 \rho_2 \delta_\lambda s_2. \quad (1.173)$$

Thus, calculating the Hamilton's action variation gives

$$\delta_\lambda \mathcal{A} = - \int_{t_0}^{t_1} \int_\Omega \frac{\partial \eta}{\partial s_1} \delta_\lambda s_1 + \frac{\partial \eta}{\partial s_2} \delta_\lambda s_2 \, dx dt = - \int_{t_0}^{t_1} \int_\Omega \alpha_1 \rho_1 (T_1 - T_2) \delta_\lambda s_1 \, dx dt = 0. \quad (1.174)$$

Equation 1.174 holds for any $\delta_\lambda s_1$, thus it imposes

$$\alpha_1 \rho_1 (T_1 - T_2) = 0, \quad (1.175)$$

implying thermal equilibrium.

APPENDIX 1.B SYSTEM WITH STIFF RELAXATION

In this section, we prove under some assumptions how a system of PDE with stiff relaxation terms can be projected on a constrain manifold yielding relaxed systems. Applied to the seven equation model, it yields a hierarchy of diffuse interface models. These developments are based on the works of Murrone and Guillard (2005) [164], Chen and Levermore (1994) [25] and on a thorough reading of Bourguignon (2007) [15].

A one-dimensional framework is adopted from now on, $x \in \mathbb{R}$, to simplify the derivation. Let us consider a system of partial differential equations with stiff relaxation terms $\mathbf{r} : \mathbf{u} \in \Omega \mapsto \mathbb{R}^N$, taking the form,

$$\partial_t \mathbf{u} + \mathcal{A}(\mathbf{u}) \partial_x \mathbf{u} = \mathbf{r}(\mathbf{u}), \quad (1.176)$$

where $\mathbf{u} = \mathbf{u}(x, t) \in \Omega \subset \mathbb{R}^N$ is the state vector defined on Ω an open convex of the manifold \mathbb{R}^N and $\mathcal{A} : \mathbf{u} \in \Omega \mapsto \mathbb{R}^N \times \mathbb{R}^N$ is a N -square matrix.

1.B.1 CONSTRAINT MANIFOLD AND PROJECTION ASSUMPTIONS

We want to build an orthogonal basis of \mathbb{R}^N by interpreting \mathbf{r} as a projection from the out-of-equilibrium space \mathbb{R}^N to the a constrain manifold where equilibrium is reached.

We first assume the following statements, illustrated in Figure 1.5:

- A1 : System (1.176) is hyperbolic.
- A2 : $\mathbf{r}(\mathbf{u})$ is a non-degenerated constrain defining p constraints.
- A3 : There is an application P defined by

$$P : \mathbb{R}^N \rightarrow \mathbb{R}^n \quad (1.177)$$

$$\forall \mathbf{u} \in \Omega, P\mathbf{r}(\mathbf{u}) = \mathbf{0}_{\mathbb{R}^n}.$$

A₄ : There exists for each $\mathbf{u} \in \mathcal{E}$ an admissible map of the constraint manifold \mathcal{E} , M , defined from a subset $\omega \subset \mathbb{R}^n$ on a neighbourhood of \mathbf{u} , $V_{\mathbf{u}}$, as

$$M \begin{pmatrix} \omega \subset \mathbb{R}^n & \rightarrow & V_{\mathbf{u}} \subset \mathcal{E} \subset \mathbb{R}^N \\ \tilde{\mathbf{u}} & \rightarrow & M(\tilde{\mathbf{u}}) \end{pmatrix}. \quad (1.178)$$

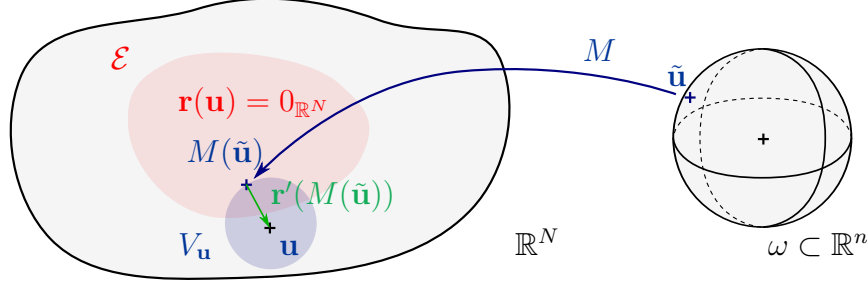


FIGURE 1.5: Constraint manifold \mathcal{E} and its admissible map M

From (A₂), considering $(\varphi_i)_{1 \leq i \leq p}$ the coordinates of $\mathbf{r}(\mathbf{u})$ using a map $(\mathbf{x}_i)_{1 \leq i \leq p}$ of \mathbb{R}^p , then the differentials $d\varphi_i$ are linearly independent. For instance, in the case of the seven equation model, $N = 7$, $\mathbf{r}(\mathbf{u})$ could impose up to $p = 3$ constraints to force full equilibrium of the fluids.

(A₃) infers that P can be interpreted in a certain basis as a projection onto a constraint manifold \mathcal{E} of dimension $N - p = n$ which contains the state vector at equilibrium defined as

$$\mathcal{E} = \{\mathbf{u} \in \Omega / \mathbf{r}(\mathbf{u}) = \mathbf{0}_{\mathbb{R}^N}\}, \quad \dim(\mathcal{E}) = n. \quad (1.179)$$

From (A₄), M is a diffeomorphism, thus the differential $dM_{\tilde{\mathbf{u}}}$ is a bijective application defined as

$$dM_{\tilde{\mathbf{u}}} \begin{pmatrix} T_{\tilde{\mathbf{u}}}\mathbb{R}^n = \mathbb{R}^n & \rightarrow & T_{M(\tilde{\mathbf{u}})}\mathcal{E} \\ X_{\tilde{\mathbf{u}}} & \rightarrow & \langle dM_{\tilde{\mathbf{u}}}|X_{\tilde{\mathbf{u}}} \rangle \end{pmatrix} \quad (1.180)$$

where $T_{\tilde{\mathbf{u}}}\mathbb{R}^n$ is the tangent space of \mathbb{R}^n at the point $\tilde{\mathbf{u}}$ and $T_{M(\tilde{\mathbf{u}})}\mathcal{E}$ the tangent space of \mathcal{E} at the point $M(\tilde{\mathbf{u}})$. $T_{\tilde{\mathbf{u}}}\mathbb{R}^n$ and \mathbb{R}^n are diffeomorph. $\langle \cdot | \cdot \rangle$ is the scalar product naturally defined in $T_{M(\tilde{\mathbf{u}})}\mathcal{E}$ since $T_{M(\tilde{\mathbf{u}})}\mathcal{E}$ and \mathbb{R}^n are diffeomorph. Since $dM_{\tilde{\mathbf{u}}}$ is a bijection, its column vectors $(dM_{\tilde{\mathbf{u}}}^1, \dots, dM_{\tilde{\mathbf{u}}}^n)$ are independent and form a basis of $T_{M(\tilde{\mathbf{u}})}\mathcal{E}$.

Since from (A₂), \mathbf{r} is a non-degenerated constraint, we introduce $\mathbf{r}'(M(\tilde{\mathbf{u}}))$, the Jacobian of the application \mathbf{r} evaluated at $M(\tilde{\mathbf{u}})$ defined by

$$\mathbf{r}'(M(\tilde{\mathbf{u}})) \begin{pmatrix} T_{M(\tilde{\mathbf{u}})}\mathbb{R}^N = \mathbb{R}^N & \rightarrow & T_{M(\tilde{\mathbf{u}})}\mathcal{E} = \mathbb{R}^n \\ X_{M(\tilde{\mathbf{u}})} & \rightarrow & \langle d\mathbf{r}_{M(\tilde{\mathbf{u}})}|X_{M(\tilde{\mathbf{u}})} \rangle \end{pmatrix}, \quad (1.181)$$

and the kernel of the application, $\text{Ker}(\mathbf{r}'(M(\tilde{\mathbf{u}})))$, reads

$$\text{Ker}(\mathbf{r}'(M(\tilde{\mathbf{u}}))) = \{M(\tilde{\mathbf{u}}) \in \mathcal{E} | \mathbf{r}'(M(\tilde{\mathbf{u}})) = \mathbf{0}_{\mathbb{R}^n}\}. \quad (1.182)$$

Under the above assumptions, we can prove that

$$\begin{aligned} \text{Ker}(\mathbf{r}'(M(\tilde{\mathbf{u}}))) &= \text{Ker}(T_{M(\tilde{\mathbf{u}})}\mathbb{R}^N) \\ &= \{X_{M(\tilde{\mathbf{u}})} \in T_{M(\tilde{\mathbf{u}})}\mathbb{R}^N | T_{M(\tilde{\mathbf{u}})}\mathbf{r}(X_{M(\tilde{\mathbf{u}})}) = \mathbf{0}_{\mathbb{R}^N}\} \\ &= T_{M(\tilde{\mathbf{u}})}\mathcal{E}. \end{aligned} \quad (1.183)$$

Hence $T_{M(\tilde{\mathbf{u}})}\mathcal{E}$ can be interpreted as

- The tangent space of \mathcal{E} at the point $M(\tilde{\mathbf{u}})$.
- All the bound vectors in \mathcal{E} whose direction is tangent at the point $M(\tilde{\mathbf{u}})$ with fixed initial point $M(\tilde{\mathbf{u}})$.
- All the critical points of the application \mathbf{r} on \mathcal{E} .

The basis $(dM_{\tilde{\mathbf{u}}}^1, \dots, dM_{\tilde{\mathbf{u}}}^n)$ of $T_{M(\tilde{\mathbf{u}})}\mathcal{E}$ is thus also a basis for $\text{Ker}(\mathbf{r}'(M(\tilde{\mathbf{u}})))$.

Last but not the least, in order to generate an interesting basis of \mathbb{R}^N from $(dM_{\tilde{\mathbf{u}}}^1, \dots, dM_{\tilde{\mathbf{u}}}^n)$, we assume the last following statement

A5 : $\text{Ker}(\mathbf{r}'(M(\tilde{\mathbf{u}}))) \oplus \text{Rng}(\mathbf{r}'(M(\tilde{\mathbf{u}}))) = \mathbb{R}^N$ which is not necessarily the case. It is a strong assumption implying that

$$\dim(\text{Rng}(\mathbf{r}'(M(\tilde{\mathbf{u}})))) = N - n \quad (1.184)$$

We can thus now build a complete basis of \mathbb{R}^N . Let us denote $I_{\text{Rng}} = (I^1, \dots, I^{N-n})$ a basis of $\text{Rng}(\mathbf{r}'(M(\tilde{\mathbf{u}})))$. Therefore, the family $B = (dM_{\tilde{\mathbf{u}}}^1, \dots, dM_{\tilde{\mathbf{u}}}^n, I^1, \dots, I^{N-n})$ forms a basis of \mathbb{R}^N . In this basis,

$$\forall \mathbf{u} \in \Omega \subset \mathbb{R}^N, \exists (a_i)_{1 \leq i \leq n} \in \mathbb{R}^n, \exists (b_i)_{1 \leq i \leq N-n} \in \mathbb{R}^{N-n} \mid \mathbf{u} = \sum_{i=1}^n a_i dM_{\tilde{\mathbf{u}}}^i + \sum_{i=1}^{N-n} b_i I^i \quad (1.185)$$

Using matrix notations, Equation 1.185 writes

$$\mathbf{u} = B \begin{pmatrix} a \\ b \end{pmatrix} \Leftrightarrow \begin{pmatrix} a \\ b \end{pmatrix} = B^{-1} \mathbf{u} = \begin{pmatrix} P\mathbf{u} \\ Q\mathbf{u} \end{pmatrix} \quad (1.186)$$

where P is the $n \times N$ matrix representing the application defined in Equation 1.177. It is thus the projection on the basis of $\text{Ker}(\mathbf{r}'(M(\tilde{\mathbf{u}})))$ in the direction of $\text{Rng}(\mathbf{r}'(M(\tilde{\mathbf{u}})))$. Q is the projection on the basis of $\text{Rng}(\mathbf{r}'(M(\tilde{\mathbf{u}})))$ in the direction of $\text{Ker}(\mathbf{r}'(M(\tilde{\mathbf{u}})))$.

The following properties are obtained

1. $PdM_{\tilde{\mathbf{u}}} = \mathcal{I}_n$
2. $(PdM_{\tilde{\mathbf{u}}})^2 = PdM_{\tilde{\mathbf{u}}}$
3. $PdM_{\tilde{\mathbf{u}}}$ is a projection
4. $(dM_{\tilde{\mathbf{u}}}P)^2 = dM_{\tilde{\mathbf{u}}}P$
5. $dM_{\tilde{\mathbf{u}}}P$ is a projection
6. $PM(\tilde{\mathbf{u}}) = \tilde{\mathbf{u}}$
7. $P\mathbf{r}'(M(\tilde{\mathbf{u}})) = \mathbf{0}_{\mathbb{R}^n}$

where \mathcal{I}_n is the $n \times n$ identity matrix. $dM_{\tilde{\mathbf{u}}}P$ is a $N \times N$ projection matrix onto the tangent space of $\text{Im}(M)$ (and not \mathcal{E}).

Proof. From previous definitions,

$$B^{-1} = \begin{pmatrix} P \\ Q \end{pmatrix} \Rightarrow B^{-1}B = \begin{pmatrix} P \\ Q \end{pmatrix} B \Rightarrow \mathcal{I}_N = \begin{pmatrix} PdM_{\tilde{\mathbf{u}}} \\ QI_{Rng} \end{pmatrix}$$

leading to property 1. Properties 2, 3, 4, 5 are straightforward. From property 1, we have $P = dM_{\tilde{\mathbf{u}}}^{-1}$ where $dM_{\tilde{\mathbf{u}}}^{-1}$ is the application that brings back any vector of $V_{\mathbf{u}}$ to ω . Thus, $PM(\tilde{\mathbf{u}}) = dM_{\tilde{\mathbf{u}}}^{-1}M(\tilde{\mathbf{u}}) = \tilde{\mathbf{u}}$. \square

1.B.2 RELAXED SYSTEM

Since we have built an orthogonal basis of \mathbb{R}^N based on the projection P , we can project System (1.176) by multiplying it by P onto $\text{Ker}(\mathbf{r}'(M(\tilde{\mathbf{u}})))$, leading to a system of n equations,

$$\partial_t(P\mathbf{u}) + P\mathcal{A}(\mathbf{u})\partial_x\mathbf{u} = P\mathbf{r}(\mathbf{u}) \quad (1.187)$$

Assuming the local equilibrium, $\mathbf{u} = M(\tilde{\mathbf{u}})$, using previous properties, it yields the reduced-model

$$\frac{\partial\mathbf{u}}{\partial t} + \tilde{\mathcal{A}}(\mathbf{u})\partial_x\mathbf{u} = \mathbf{0} \quad (1.188)$$

where $\tilde{\mathcal{A}}(\mathbf{u}) = Q\mathcal{A}(M(\tilde{\mathbf{u}}))$. While System (1.176) is assumed to be hyperbolic, [Chen and Levermore \(1994\)](#) [25] pointed out the fact that the resulting reduced-model has no reason to be hyperbolic.

1.B.3 CHAPMAN-ENSKOG REDUCED MODEL

Instead of assuming local equilibrium, another reduced model can be obtained using the Chapman-Enskog method. Assuming there is a characteristic relaxation parameter ϵ such that the stiff source terms takes the form \mathbf{r}/ϵ , then we look for a solution in the form

$$\mathbf{u} = M(\tilde{\mathbf{u}}) + \epsilon\mathbf{r}'(M(\tilde{\mathbf{u}})) + \frac{\epsilon^2}{2} ((\mathbf{r}'(M(\tilde{\mathbf{u}})))^t \mathbf{r}''(M(\tilde{\mathbf{u}}))\mathbf{r}'(M(\tilde{\mathbf{u}})) + o(\epsilon^2)), \quad (1.189)$$

where \mathbf{r}'' is the Hessian matrix of $\mathbf{r}(\mathbf{u})$. Injecting Equation 1.189 in system (1.176) gives

$$\begin{aligned} & \partial_t(M(\tilde{\mathbf{u}})) + \mathcal{A}(M(\tilde{\mathbf{u}}))\partial_x(M(\tilde{\mathbf{u}})) - \langle \mathbf{r}'(M(\tilde{\mathbf{u}})) | \mathbf{r}'(M(\tilde{\mathbf{u}})) \rangle \\ & + \epsilon [\partial_t(\mathbf{r}'(M(\tilde{\mathbf{u}}))) + \mathcal{A}(M(\tilde{\mathbf{u}}))\partial_x(\mathbf{r}'(M(\tilde{\mathbf{u}}))) + \langle \mathcal{A}(M(\tilde{\mathbf{u}})) | \mathbf{r}'(M(\tilde{\mathbf{u}})) \rangle \\ & \quad - 1/2 \langle \mathbf{r}''(M(\tilde{\mathbf{u}})) | \mathbf{r}'(M(\tilde{\mathbf{u}})) \rangle] \\ & \quad \quad \quad = O(\epsilon^2) \end{aligned} \quad (1.190)$$

Thus, multiplying by P system (1.190), and neglecting the terms of order ϵ , one finds the reduced model

$$\partial_t\tilde{\mathbf{u}} + P\mathcal{A}(M(\tilde{\mathbf{u}}))dM_{\tilde{\mathbf{u}}}\partial_x\tilde{\mathbf{u}} = 0. \quad (1.191)$$

APPENDIX 1.C VARIATIONAL CALCULUS: GENERAL OVERVIEW

Suppose a manifold \mathcal{M} . Each point \mathbf{q} in \mathcal{M} is referred by its position in time and space by the variable $\tau = (\mathbf{x}, t) \in \Omega \subset \mathbb{R}^3 \times \mathbb{R}_+$. Considering a fluid particle evolving in Ω , its trajectory

is defined by the function γ defined by Equation (1.192).

$$\gamma \begin{pmatrix} \Omega & \rightarrow & \mathcal{M} \\ \tau & \rightarrow & \gamma(\tau) \end{pmatrix} \quad (1.192)$$

$C = C^\infty(\Omega, \mathcal{M})$ contains all the curves γ defined on Ω evolving in \mathcal{M} .

A Lagrangian L is a differentiable scalar function, called observable, from the tangent bundle space $\mathcal{T}\mathcal{M}$ of a manifold \mathcal{M} onto \mathbb{R} . Any element of the tangent bundle $\mathcal{T}\mathcal{M}$ is a pair of a point \mathbf{q} in \mathcal{M} and a tangent vector $\dot{\mathbf{q}}$ of $T_q\mathcal{M}$. Suppose γ is a trajectory of a fluid particle in \mathcal{M} , then the Lagrangian associated with this fluid particle is defined as

$$L \begin{pmatrix} \mathcal{T}\mathcal{M} & \rightarrow & \mathbb{R} \\ (\mathbf{q}, \dot{\mathbf{q}}) & \rightarrow & L(\gamma(\tau), \dot{\gamma}(\tau)) \end{pmatrix} \quad (1.193)$$

The action \mathcal{A} of a Lagrangian L is an application defined as

$$\mathcal{A} \begin{pmatrix} C & \rightarrow & \mathbb{R} \\ \gamma & \rightarrow & \int_{\Omega} L(\gamma(\tau), \dot{\gamma}(\tau)) d\tau \end{pmatrix} \quad (1.194)$$

1.C.1 FIRST VARIATION OF THE ACTION

To define properly the first variation of the action \mathcal{A} , one needs to introduce a variation of γ . Suppose $\gamma \in C$. A variation γ_λ of γ is an application defined as

$$\gamma_\lambda \begin{pmatrix} (\Omega \times]-\epsilon, \epsilon[& \rightarrow & \mathcal{M} \\ (\tau, \lambda) & \rightarrow & \gamma_\lambda(\tau) = \gamma(\tau, \lambda) \end{pmatrix} \text{ with } \gamma_0(\tau) = \gamma(\tau) \quad (1.195)$$

Thus, the first variation of the action \mathcal{A} is

$$\frac{\partial}{\partial \lambda} \mathcal{A}(\gamma_\lambda) \Big|_{\substack{\tau \text{ fixed} \\ \lambda=0}} = \int_{\Omega} \frac{\partial}{\partial \lambda} L(\gamma_\lambda(\tau), \dot{\gamma}_\lambda(\tau)) \Big|_{\substack{\tau \text{ fixed} \\ \lambda=0}} d\tau \quad (1.196)$$

Usually, to shorten notation, the first variation of any field ψ is written $\delta_\lambda \psi$ and this notation will be used hereafter. Figure 1.6 illustrates the first variation of the action \mathcal{A} . δ_λ is the vector

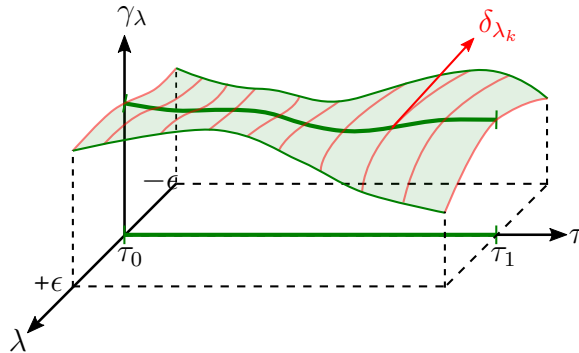


FIGURE 1.6: Action first variations

normal to the trajectories γ_λ and is tangent to the red curves each of which representing the infinitesimal variations of a point $\gamma(\tau)$. The green surface embodies the infinitesimal variations of γ .

1.C.2 EULERIAN AND LAGRANGIAN COORDINATES

In fluid dynamics, two systems of coordinates are used, namely the Eulerian coordinates \mathbf{x} and the Lagrangian coordinates \mathbf{X} . The former consists in observing at a given position in space \mathbf{x} the fluid particles flowing during a period of time, whereas the latter consists in tracking a given fluid particle from its initial position \mathbf{X} . There exists a bijective function, φ , such that $\mathbf{x} = \varphi(\mathbf{X}, t)$.

1.C.3 EULERIAN AND LAGRANGIAN VARIATIONS

In the next sections, the variation of the action will be expressed using Euler coordinates as an Euler model is sought. Therefore, we introduce here the distinction between a Lagrangian variation and an Eulerian variation of any field ψ .

$$\text{Lagrangian variation} \quad \delta_{\lambda}^{\circ} \psi = \left. \frac{\partial}{\partial \lambda} \psi(\gamma_{\lambda}(\mathbf{X}, t)) \right|_{\substack{t, \mathbf{X} \text{ fixed} \\ \lambda=0}} \quad (1.197)$$

$$\text{Eulerian variation} \quad \delta_{\lambda} \psi = \left. \frac{\partial}{\partial \lambda} \psi(\gamma_{\lambda}(\mathbf{x}, t)) \right|_{\substack{t, \mathbf{x} \text{ fixed} \\ \lambda=0}} \quad (1.198)$$

where \mathbf{X} are the Lagrangian coordinates whereas \mathbf{x} are the Eulerian coordinates. These two variations are linked by the following equation:

$$\delta_{\lambda}^{\circ} \psi = \left. \frac{\partial}{\partial \mathbf{x}} \psi(\gamma_{\lambda}(\mathbf{x}, t)) \right|_{t, \lambda \text{ fixed}} \cdot \delta_{\lambda} \mathbf{x} + \delta_{\lambda} \psi. \quad (1.199)$$

In the framework of two-phase medium, we will explicit the notation $\gamma_{\lambda}(\mathbf{x}, t)$ by using the path family $\hat{\varphi}(\mathbf{X}, t, \lambda)$ parametrized by the scalar λ such that $\hat{\varphi}(\mathbf{X}, t, \lambda = 0) = \varphi(\mathbf{X}, t) = \mathbf{x}$. Hence, we will denote $\gamma_{\lambda}(\mathbf{x}, t)$ by $\gamma_{\lambda}(\hat{\varphi}(\mathbf{X}, t, \lambda), t)$.

1.C.4 LEAST ACTION PRINCIPLE

Hamilton's Least Action Principle states that "*the true motion is the stationary point of the action \mathcal{A} on the set C of all paths γ beginning at point \mathbf{q}_0 at time t_0 and ending at point \mathbf{q}_1 at instant t_1* ". It leads to the following equation:

$$\delta_{\lambda} \mathcal{A} = 0 \quad (1.200)$$

DERIVATION OF A MULTI-FLUID THERMODYNAMICS ACCOUNTING FOR NON-IDEAL EFFECTS

2

*Chapter 2 is dedicated to the construction of a multi-fluid thermodynamics to equip the reduced-order systems of partial differentiating equations. These systems of PDE, stemming from rational thermodynamics or Stationary Action Principle, require to postulate their associated thermodynamics. The main contributions of this chapter are 1) to account for non-ideal effects in a consistent way with respect to both the thermodynamics variables and the investigated system, 2) to define a hierarchy of level of interactions between the fluids from isolated to interacting fluids and finally 3) to pave the way to adding supplementary variables to the thermodynamics such as geometric quantities. This work has been submitted in the journal *Continuum Mechanics and Thermodynamics Cordesse et al. (2020) [35]*.*

2.1	A consistent Multi-Fluid thermodynamics formalism including non-ideal effects and interface geometry	99
2.1.1	Abstract	99
2.1.2	Introduction	100
2.1.3	Extensivity of a fluid mixture entropy	103
2.1.3.1	Thermodynamics challenges raised from the multi-fluid modeling	103
2.1.3.2	Recovering the extensivity of the mixture entropy at subscale	105
2.1.3.3	Choice of extensive and intensive set of variables to characterize a multifluid mixture	107
2.1.4	Building a multi-fluid thermodynamics	109
2.1.4.1	Assumptions and set of variables	109
2.1.4.2	Fundamental equation of thermodynamics and entropy	110
2.1.4.3	The pressure law approach	112
2.1.5	Implications of the new formalism	117
2.1.5.1	Gibbs equation hierarchy	118
2.1.5.2	Adding supplementary variables to the thermodynamics: illustration with the interfacial density area	119
2.1.5.3	Isothermal thermodynamics	120
2.1.5.4	Thermodynamics potentials of two-phase flow	121
2.1.6	Applications to two-phase flow modeling and impact of non-ideal effects	122
2.1.6.1	Stationary Action Principle and entropy closure	122
2.1.6.2	Impact of the non-ideal effects on the mathematical wave structure	123

2.1.6.3	The interest of the Gibbs equation hierarchy under partial entropy constraints	124
2.1.7	Shedding some lights on identified systems of the literature with non-ideal effects	125
2.1.7.1	Stagnation pressure in a dispersed phase	125
2.1.7.2	Osmotic pressure in a solute/solvent mixture	125
2.1.7.3	Modification of the thermodynamics potentials	127
2.1.7.4	Interface thermodynamics in bubbly flow	128
2.1.8	Conclusion	131
Appendices		133
2.A	Isothermal thermodynamics	133
2.B	Recovering the mixture entropy extensivity	134
2.B.1	From subsystems to <i>many fluid</i>	134
2.B.2	From <i>many fluid</i> to multi fluid	137

2.1 A CONSISTENT MULTI-FLUID THERMODYNAMICS FORMALISM INCLUDING NON-IDEAL EFFECTS AND INTERFACE GEOMETRY : FROM THERMODYNAMIC POTENTIALS TO PRESSURE LAW AND THE IMPACT ON MULTIPHASE FLOW MODELING

This section transcribes the results of a journal paper entitled *Multi-fluid thermodynamics from a pressure law approach*, written by Pierre Cordesse, Lionel Matuszewski and Marc Masot and submitted to the Journal Continuum Mechanics and Thermodynamics [Cordesse et al. \(2020\) \[35\]](#).

2.1.1 ABSTRACT

In this contribution we propose a multi-fluid thermodynamics formalism describing a mixture of multi-component and multi-phase fluids. We follow a multi-fluid approach, that is we consider an averaging process, which allows to resolve large scale features of the flow above a threshold spatial scale and which provides a modeling of the details involving potentially small scale interface dynamics called subscale modeling. Since we cannot rely on local thermodynamic equilibrium at the fluid particle level, a thermodynamics has to be built. The first key issue is related to the property of extensivity of the mixture entropy, which can involve the geometry of the interface at subscale. We highlight a couple of configurations where this extensivity is recovered for some specific geometrical configuration of separated phases and disperse phase flow where the subscale geometry can be fully characterized. The formalism is then introduced and special attention is devoted to the proper choice of extensive and intensive variables for this multi-fluid description. Compatibility closures connecting the thermodynamics potential to pressure laws including non-ideal effects are obtained and allow, relying on the definition of a reference ideal state and well-chosen integration paths, to reconstruct all the thermodynamics potentials from the pressure laws. These results have key implications on multi-phase flow modeling and we examine the impact of the usual assumption of thermodynamics independence of the fluids in the classical multi-fluid models, as well as the introduction of supplementary geometrical variables describing the subscale structure of the interface. The presence of non-ideal effects on the thermodynamics constraints usually used in the Stationary Action Principle to derive two-phase flow models are revisited thanks to the present investigation and we highlight its impact on the mathematical structure and wave propagation of the resulting systems. The present formalism allows to shed some light on identified systems in the two-phase flow multi-fluid literature, where non-ideal effects are to be found, and to propose a unified point of view, which has the potential to alleviate the classical pitfalls such as the lack of convexity of the standard multi-fluid models entropy and the lack of consistency of the thermodynamics formalism.

Key-words: multi-fluid thermodynamics, non-ideal pressure laws, homogeneity, interface geometrical properties, mixing entropy and energy, two-phase flow.

2.1.2 INTRODUCTION

Continuum mechanics approach relies on a continuous description of fluids, the smallest element being a fluid particle [Truesdell \(1969\) \[212\]](#), [Woods \(1975\) \[221\]](#)¹. Fluid particles gather a large amount of molecules allowing for a statistical treatment of the parcel insuring homogeneous distribution at this scale and can even describe interfaces with the proper thermodynamics and equation of state. At this scale, we can model any multi-phase multi-component mixture as a single multi-species flow, with a potential transient zone where the fluid density changes drastically. Considering a liquid and its vapor, it has led to the development of thermodynamics accounting for phase transition through the Van der Waals equation of state [Van der Waals \(1894\) \[215\]](#) and extended through the inclusion of the gradients of composition quantities as thermodynamics internal variables to describe capillary effects [Korteweg, D.J. \(1901\) \[121\]](#), [Cahn and Hilliard \(1958\) \[16\]](#). When considering a multi-component fluid, it is possible to account for non-ideal effects and phase transitions through activity coefficients [Prausnitz et al. \(1998\) \[178\]](#), always assuming a local thermodynamics equilibrium. In [Giovangigli and Matuszewski \(2012\) \[87\]](#) a supercritical multi-component fluid thermodynamics is built from the Soave-Redlich-Kwong cubic equation of state, allowing phase separation due to non-ideal effects. Even if the physics is rich, such approaches, that we will refer to as *full-spectrum single fluid* approaches, have to rely on direct numerical simulations (DNS) to resolve the whole scale spectrum, which is out of reach of most of the realistic flow simulations.

The present contribution is part of a project supported by the Centre National d'Études Spatiales (CNES) and the Office National d'Études et de Recherches Aérospatiales (ONERA) within the scope of the Ariane program. The strategy retained at ONERA is to perform predictive numerical simulations of the primary atomization in cryogenic rocket engines from the injection to the combustion of the spray in order to provide early-stage optimization processes, thus accelerating developments while reducing the costs. Direct numerical simulations (DNS) remain too costly in terms of computing resources to be applied in an industrial context due to the high Reynolds and Weber numbers of the applications. Therefore, reduced-order models are still developed despite the fact they usually discard the smallest scales of the interface dynamics by averaging the transport equations. Instead of implicitly filtering all the scales of the flow below the grid size, reduced-order models introduce a characteristic lengthscale to explicitly filter the scales of the flow, leading to a separation of the large scales, which are fully resolved and the *subscales* of the flow, which require modeling if to be accounted for. The reduced-order models, often referred as *diffuse interface models* or *multi-fluid* models, offer a large levels of modeling and hierarchies are obtained through various dissipative or non-dissipative relaxation phenomena [Ishii \(1975\) \[110\]](#), [Drew \(1983\) \[57\]](#), [Baer and Nunziato \(1986\) \[5\]](#), [Saurel and Abgrall \(1999\) \[190\]](#), [Kapila et al. \(2001\) \[115\]](#), [Murrone and Guillard \(2005\) \[164\]](#), [Saurel et al. \(2009\) \[195\]](#), [Zein et al. \(2010\) \[226\]](#), [Drui et al. \(2019\) \[60\]](#), and some of simplest elements are massively adopted in the industry. Nevertheless they provide a poor description of the interface dynamics, limited to the transport of the volume fraction of each phase in each computational cells. In separated phases, the gradient of the volume fraction is a good indicator of the normal to the interface, thus of the local curvature. Nonetheless, as soon as subscale surface phenomena occur, the volume fraction prediction smooths out all the details of the

¹The kinetic theory allows to account for non-trivial interactions of molecules and provides a framework where the thermodynamics of the mixture can be identified [Chapman and Cowling \(1970\) \[24\]](#). Some challenges are still faced when accounting for compressibility effects in dense gases [Beijeren and Ernst \(1973\) \[9\]](#), [Beijeren and Ernst \(1973\) \[10\]](#), [Mareschal et al. \(1984\) \[153\]](#).

flow and its gradient can no longer provide meaningful information regarding the topology of the interface and the disperse phase description is out of reach [Essadki et al. \(2019\) \[67\]](#). Some advances rely on supplementary evolution equations of geometric quantities, such as the transport of large and small scale interfacial density areas in the work of [M Devassy et al. \(2015\) \[148\]](#) or quantities accounting for subscale effects such as micro-inertia [Gavrilyuk and Saurel \(2002\) \[81\]](#), [Drui et al. \(2019\) \[60\]](#).

A common characteristic of these reduced-order models is that they strongly rely on an isolated fluid thermodynamics², each fluid is equipped with its own thermodynamics. This has some major drawback in terms of mathematical structure as already noticed in several contributions [Coquel et al. \(2012\) \[30\]](#), [Cordesse and Massot \(2020\) \[41\]](#) as it implies the loss of convexity of the entropy, which prevents entropic symmetrization [Friedrichs and Lax \(1971\) \[73\]](#), [Harten \(1983\) \[103\]](#) and strict hyperbolicity. Yet these properties are key for the mathematical theory of existence and uniqueness of smooth solutions [Kawashima and Shizuta \(1988\) \[118\]](#), [Giovangigli and Massot \(1998\) \[85\]](#) but also for the study of weak solutions [Kruřkov \(1970\) \[122\]](#). Moreover, in terms of physics modeling, in interface regions, non-ideal effects such as compaction, osmotic pressure or surface tension occur and should be taken into account in the thermodynamics, questioning the validity of assuming an isolated phase thermodynamics approach. In addition, an accurate description of the subscale dynamics of the interface can only rely on interacting thermodynamics, as for instance in disperse zones where the acoustic properties of the mixture can not be predicted by an isolated fluid thermodynamics approach.

It is interesting to note that several attempts have been conducted in order to cope with this problem in very specific situations such as in suspension rheology [Lhuillier \(1995\) \[135\]](#), [Guazzelli and Pouliquen \(2018\) \[98\]](#) or polymers [Gujrati \(2003\) \[100\]](#). In a more mathematical way, non-ideal effects were added through the extension of thermodynamics potential with mixing terms such as [Coquel et al. \(2012\) \[30\]](#), [Cordesse and Massot \(2020\) \[41\]](#). However the consistency between the studied systems of equations and the chosen thermodynamics can be questioned. Another approach has been proposed and consists in introducing non-ideal effects directly in the pressure laws [Sainsaulieu \(1995\) \[189\]](#), [Guazzelli and Pouliquen \(2018\) \[98\]](#), but again without examining if it were consistent with the thermodynamics employed. An alternative almost systematically employed to circumvent the need of adding mixing terms in the thermodynamics is to include these effects as source terms in the system of equations even when these effects are not dissipative. Some recent work has been done to derive a consistent thermodynamics of three phase system [Mathis \(2017\) \[156\]](#) associated with a Baer-Nunziato type of three-phase flow model. Nevertheless the author still equip each phase with a Gibbs relation, which prevents inevitably the description of non-ideal effects.

It would then be desirable to propose a multi-fluid thermodynamics including general non-ideal effects. However several problems may appear when trying to define such a mixing thermodynamics. Back into the framework of full-spectrum single fluid models, where no averaging process is considered, an instructive example of the derivation of a consistent thermodynamics accounting for non-ideal effect can be found in [Giovangigli and Matuszewski \(2012\) \[87\]](#). The mathematical structure of the thermodynamics is based predominantly on the identification a unique ideal reference state, namely Perfect Gas, in accordance with which any non-ideal effect is added in a consistent way. The homogeneous properties of the mixture are clearly

²Some interactions, referred as compaction effects, are accounted for through the addition of the volume fraction as a internal variable on which depends the entropy [Baer and Nunziato \(1986\) \[5\]](#).

established and a strictly convex entropy is identified for system like Navier-Stokes equations leading to a symmetrization in the sense of Mock-Godunov. Firstly no such unambiguous reference state exists for a multi-fluid mixture and there is no consensual way of departing from ideality. Even the property of homogeneity of the thermodynamics potentials such as entropy of a multi-fluid flow encompassing a large range of scale is far from obvious.

In this contribution we propose a multi-fluid thermodynamics formalism describing a mixture of multi-component and multi-phase fluids. This thermodynamics is conceived to equip reduced-order models obtained through an averaging process, thus relying on a threshold length scale. All the details of the flow, ranging from the smallest scale dynamics of interfaces to the given threshold are denoted *subscale*; they are not resolved but rely on subscale modeling such as in [Gavrilyuk and Saurel \(2002\) \[81\]](#), [M Devassy et al. \(2015\) \[148\]](#), [Drui et al. \(2019\) \[60\]](#).

The first contribution consists in recovering the property of extensivity of the mixture entropy through a well-chosen set of variables involving both bulk and geometric quantities characterizing the geometry of the interface at subscale. We highlight a couple of configurations where this extensivity is recovered, leveraging from some specific geometrical configuration of separated phases and disperse phase flow where the subscale geometry can be fully characterized.

Then, compatibility closures connecting the thermodynamics potential to pressure laws including non-ideal effects are obtained and allow, relying on the definition of a reference ideal state and well-chosen integration paths, to reconstruct all the thermodynamics potentials from the pressure laws.

We emphasize the key implications on multi-fluid modeling of the formalism. First we draw a hierarchy based on three level of interaction of the fluids, from fully coupled multi-fluid mixture allowing for non-ideal effects to non-interacting multi-fluid flow where each phase is isolated from one another preventing any interaction. Then, we show that the formalism is adequate to add any supplementary variables to the thermodynamics, provided that the variable bears extensivity, allowing for instance to enrich the description of the interface, which makes it very convenient for multi-fluid flow modeling.

Furthermore, the presence of non-ideal effects on the thermodynamics constraints usually used in the Stationary Action Principle to derive two-phase flow models are revisited thanks to the present investigation and we highlight their impact on the mathematical structure and wave propagation of the resulting systems.

The proposed formalism allows to shed some light on identified systems in the two-phase flow multi-fluid literature, where non-ideal effects are to be found, and to propose a unified point of view. As first example, we propose to study the pressure law proposed by Sainsaulieu to reestablish the hyperbolicity of his two-phase flow model for dispersed flow [Sainsaulieu \(1995\) \[189\]](#) and show how it modifies the thermodynamics associated to the system. We also look at how the osmotic pressure in a solute/solvent mixture modifies the thermodynamics. Then we look at the phase compaction effect introduced in the context of deflagration-to-detonation modeling [Baer and Nunziato \(1986\) \[5\]](#), [Bdzil et al. \(1999\) \[7\]](#), [Saurel et al. \(2003\) \[191\]](#), and then used more generally in [Gallouët et al. \(2004\) \[78\]](#), where convex functions with respect to the volume fractions are added to the phase entropies. We provide a consistent pressure law which highlights how the system of equation is impacted by such

non-ideal effect. Finally, we reinterpret the surface tension in terms of pressure laws in the particular case of dispersed phase where the interfacial density area is a function of the volume fraction.

The paper is organized as follows. In the first [Section 2.1.3](#), we will address the question of the extensivity of the entropy of a multi-fluid mixture and define the right set of extensive and intensive variables. Then in [Section 2.1.4](#), we will build the thermodynamics of the mixture with respect to a reference ideal state and postulated pressure laws. In [Section 2.1.5](#) we will emphasize the implications of the formalism by exhibiting in particular the resulting hierarchy of interaction levels between the fluids and the strength of the formalism to easily extend to account for more thermodynamics variables by taking as an example the interfacial density area. Later on in [Section 2.1.6](#) we will highlight the impact of any non-ideal effects on both the thermodynamics and systems of partial differentiating equations of two-phase flow models obtained by means of the Stationary Action Principle. Finally in [Section 2.1.7](#), we will shed some lights on identified systems of the literature with non-ideal effects by means of the formalism.

2.1.3 EXTENSIVITY OF A FLUID MIXTURE ENTROPY

This section focuses on the thermodynamics challenges when considering multi-fluid models. The fact that all the scales of the flow are no more accessible as they are in the kinetic theory or in the full-spectrum single fluid approach questions the natural extensivity of the entropy of the mixture as well as the right set of variables to describe it. We will thus examine the consequences of the large scale modeling of the flow and show that the 1-homogeneity of the entropy can still be recovered under some assumptions for a carefully chosen set of bulk and geometric variables.

2.1.3.1 THERMODYNAMICS CHALLENGES RAISED FROM THE MULTI-FLUID MODELING

Deriving a fluid mixture system including non-ideal effects from kinetic theory is a difficult task [Chapman and Cowling \(1970\) \[24\]](#), [Beijeren and Ernst \(1973\) \[9\]](#), [Beijeren and Ernst \(1973\) \[10\]](#), [Mareschal et al. \(1984\) \[153\]](#). Thus relying on such an approach to build a thermodynamics for multi-fluid modeling does not seem to be the right path.

Continuum mechanics approach relies a continuous description of fluids, the smallest element being a fluid particle, its characteristic lengthscale ℓ_p large compared to the mean free path ℓ_{fr} but small with respect to any characteristic macroscopic length scale of the flow L , $L \gg \ell_p \gg \ell_{fr}$. Fluid particles gather a large amount of molecules allowing for a statistical treatment of the parcel insuring that the particles population is homogeneous at this scale and homogeneous thermodynamics at equilibrium applies.

In the full-spectrum single fluid approach, the entropy function displays 1-homogeneity properties with respect to the extensive variables of the system. These 1-homogeneity properties are closely related to the hypothesis of indiscernible particles which, allowing the correct Boltzmann counting, leads to analytic expression displaying extensivity with respect to the number of particle in the so-called *thermodynamic limit*, that is to say, the limit of numerous particle. This 1-homogeneity of entropy function is of tremendous importance since it allows to overcome the Gibbs paradox and thus insures that the second law of thermodynamics is not violated [Diu et al. \(1996\) \[55\]](#). To illustrate these features and introduce some useful notations,

we recall briefly the thermodynamical modeling of a single fluid with several species. Let us consider a m -species phase in a volume V of energy E and mass $M = \sum_{j=1,m} M_j$. The entropy S can be defined as an 1-homogeneous function of the extensive variables, the energy, E , the volume, V , and the masses M_j , $S(E, V, M_1, \dots, M_m)$. In terms of intensive variables, the entropy per unit of mass, s , is given by

$$s(e, v, y_1, \dots, y_m) \hat{=} S(e, v, y_1, \dots, y_m) = S\left(\frac{E}{M}, \frac{V}{M}, \frac{M_1}{M}, \dots, \frac{M_m}{M}\right) = \frac{S(E, V, M_1, \dots, M_m)}{M}, \quad (2.1)$$

with e is the energy per unit of mass, v the specific volume, y_j the mass fractions of species j . Naturally, s inherits the property of 1-homogeneity with respect to the intensive variables (e, v, y_1, \dots, y_m) , since we have

$$s(\lambda e, \lambda v, \lambda y_1, \dots, \lambda y_m) = \lambda s(e, v, y_1, \dots, y_m). \quad (2.2)$$

It is important to notice that the mono-species phase case is a degenerate case where $y_1 = M/M = 1$. In this case, the 1-homogeneity of the entropy is in theory lost since we have,

$$s(e, v, y_1) = s(e, v, 1). \quad (2.3)$$

Therefore, to avoid this singular situation, we remove the constraint on the mass fractions, $\sum_{k=1,N} y_k = 1$, and consider them independent variables, such that in the degenerate case of mono-species, we have

$$s(e, v, y_1) = S(e, v, y_1) = S\left(\frac{E}{M}, \frac{V}{M}, \frac{M}{M}\right) = \frac{S(E, V, M)}{M}, \quad (2.4)$$

and thus, s remains 1-homogeneous with respect to (e, v, y_1) .

This extensivity property of single fluid thermodynamics allows to build a mathematical formalism displaying symmetry with respect to the different chemical species and unambiguously defined specific properties for each species. Nevertheless, this property relies on the fact that all the scales of the flow down to the fluid particle lengthscale, $[\ell_p, L]$, are solved. In a multi-fluid approach, a second length-scale is introduced, ℓ_c , to proceed to a spatial averaging treatment of the flow. It allows to propose n_f very distinct models for each phases bounded to its own occupation volume whereas the full-spectrum single fluid approach would only require a single physical model, which complies with each element of the fluid. The multi-fluid approach is widely adopted to study multi-phase flows since it allows to use simplified thermodynamic models for each phase [Le Métayer and Saurel \(2016\) \[131\]](#), [Redlich and Kwong \(1949\) \[183\]](#), [Soave \(1972\) \[203\]](#), spinodal decomposition being considered as granted. However, whenever the interfacial effects are to be considered, the interfacial region has to be taken into account even in the simplest way.

Since all the subscales of the flow have been lost through the averaging process, we require to build a *fluid mixture thermodynamics*, which consists in describing the fluid mixture through a set of well chosen variables and establishing relationship among them and their derivatives accordingly to the fluid mixture evolution. The circumscription of the problem is achieved through the proposition of an entropy function reckoning the number of assumed isoprobable microscopic states complying with the descriptive variables.

The first difficulty is to choose the right set of variables and since extensivity property of single fluid thermodynamics allows to build a mathematical formalism displaying symmetry with respect to the different chemical species and unambiguously defined specific properties for each species, it is only natural to try to keep this homogeneity properties in the field of multi-fluid thermodynamics.

2.1.3.2 RECOVERING THE EXTENSIVITY OF THE MIXTURE ENTROPY AT SUBSCALE

Considering a volume $\Delta V \gg \ell_p^3$ big enough to harbor a vast number of fluid particles. A general derivation of the mixture entropy of this volume is proposed in Appendix 2.B, which infers the extensivity of the entropy with respect to both the phase volume occupation and the interfacial density area discarding any flow topology assumption but under given statistical hypotheses. These statistical hypotheses are somewhat similar to particle independence or particle short length correlation for classical single-fluid thermodynamics and are based on the assumption that there exists a thermodynamics lengthscale for which every strongly correlated configuration arises at much lower scale and thus may be treated from a statistical perspective. As pedagogical and illustrative examples, we propose to present hereafter the derivation on two specific flow topologies, a separated phases flow where the minimum length scale of the flow is captured, thus greater than ℓ_c , and a disperse phase flow, for which we recover easily the extensivity of the mixture entropy. For each of these examples, the subscale geometry is then fully characterized.

Separated phases flow Let us consider a separated phases flow, where all the scales of the interface are captured. In this case, depicted in Figure 2.1, the topology of the fluid volume V_k is fixed and invariant such that spatial extension does not induce more geometrical microscopic states. The global entropy homogeneity follows from the homogeneity of entropy for each

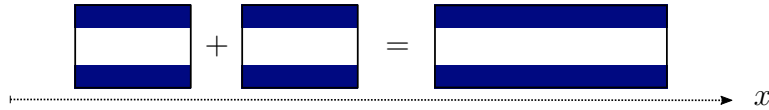


FIGURE 2.1: Illustration of the entropy extensivity in separated phases flow.

fluid since it takes the following form

$$S = \sum_{k \in \mathcal{N}_f} S_k + \sum_{k < l \in \mathcal{N}_f^2} S_{k < l}, \quad (2.5)$$

where S_k stands for the entropy of fluid k and $S_{k < l}$ is the entropy of each interface separating fluid k from fluid l , each entropy functional holding 1-homogeneity in its own subset of variables which is not described here Young (1995) [223]. The non-ideal effects are only related to the presence of the sharp interface, and are entirely described by the surface area of the interface, $\mathcal{S}_{k,l}$.

Disperse phase flow Let us assume this volume ΔV contains a collection of inclusions that we can sort with respect to their characteristic size as depicted in Figure 2.2. Let N_c be the number of inclusion classes, and N_{ci} be the number of inclusion in class ci . If steric

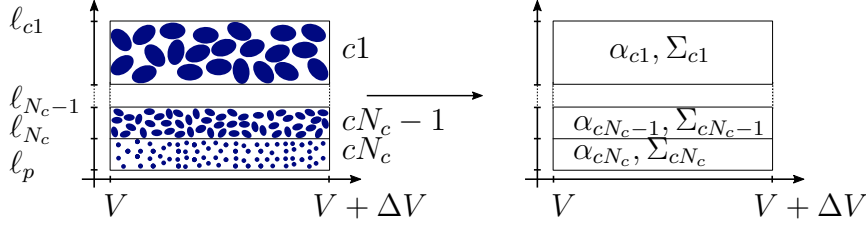


FIGURE 2.2: From a *many fluid* to a *multifluid* formulation to regain homogeneity properties of the entropy.

encumbrance related to the detail of inclusion class geometry is to be neglected, it is possible to approximate the number of geometrical configuration and thus the excess entropy for each class. For instance, sorting the classes by decreasing inclusion volume V_{ci} as depicted in [Figure 2.2](#), the number of geometrical configuration of the first class Ω_{c1} can be approximated by a Bernoulli counting process

$$\Omega_{c1} = \binom{N_{c1}^o}{N_{c1}} \left(\frac{V_{c1}}{\delta V} \right)^{N_{c1}} = \frac{(N_{c1}^o)!}{N_{c1}! (N_{c1}^o - N_{c1})!} \left(\frac{V_{c1}}{\delta V} \right)^{N_{c1}} = \frac{\left(\frac{V}{V_{c1}} \right)!}{(n_{c1} V)! \left(\frac{V}{V_{c1}} - n_{c1} V \right)!} \left(\frac{V_{c1}}{\delta V} \right)^{n_{c1} V}, \quad (2.6)$$

where $N_{c1}^o = V/V_{c1}$ is the maximum number inclusions of class $c1$, $\delta V \approx \ell_p^3$ is an elemental volume and $n_{c1} = N_{c1}/V$ is the density number of class 1 inclusions. Under the assumption of isoprobable configuration and using the Stirling formula $n! \simeq \sqrt{2\pi n} (n/e)^n$, the corresponding entropy then reads

$$S_{c1} = k_B \ln(\Omega_{c1}) \quad (2.7a)$$

$$\begin{aligned} &\simeq k_B n_{c1} V \ln \left(\frac{V_{c1}}{\delta V} \right) + k_B \ln \left[\left(2\pi n_{c1}^0 V \right)^{1/2} \left(\frac{n_{c1}^0 V}{e} \right)^{n_{c1}^0 V} \right] \\ &- k_B \ln \left[\left(2\pi n_{c1} V \right)^{1/2} \left(\frac{n_{c1} V}{e} \right)^{n_{c1} V} \right] \\ &- k_B \ln \left[\left(2\pi (n_{c1}^0 - n_{c1}) V \right)^{1/2} \left(\frac{(n_{c1}^0 - n_{c1}) V}{e} \right)^{(n_{c1}^0 - n_{c1}) V} \right] \end{aligned} \quad (2.7b)$$

$$\simeq k_B n_{c1} V \ln \left(\frac{V_{c1}}{\delta V} \right) - k_B V n_{c1}^0 [\alpha_{c1} \ln \alpha_{c1} + (1 - \alpha_{c1}) \ln (1 - \alpha_{c1})] - \frac{k_B}{2} \ln (\alpha_{c1} (1 - \alpha_{c1})). \quad (2.7c)$$

The first two terms are proportional to the number of inclusion in class $c1$, while the last term is not. In the thermodynamics limit, the latter term is negligible and we obtain

$$S_{c1} \simeq k_B n_{c1} V \ln \frac{V_{c1}}{\delta V} - k_B V n_{c1}^0 [\alpha_{c1} \ln \alpha_{c1} + (1 - \alpha_{c1}) \ln (1 - \alpha_{c1})], \quad (2.7d)$$

where the maximal density number $n_{c1}^0 = 1/V_{c1}$ and volume fraction $\alpha_{c1} = n_{c1}/n_{c1}^0 = N_{c1} V_{c1}/V$ of the class 1 have been introduced. If the following class of inclusion is such that $V_{c2} \ll V_{c1}$, the geometrical entropy related to class 2 can be approximated as

$$S_{c2} \simeq k_B n_{c2} V \ln \frac{V_{c2}}{\delta V} - k_B V (1 - \alpha_{c1}) n_{c2}^0 [\alpha_{c2} \ln \alpha_{c2} + (1 - \alpha_{c2}) \ln (1 - \alpha_{c2})], \quad (2.8)$$

and thus, by successively considering all classes, the configurational entropy of inclusion classes would sum up as

$$S_c \simeq k_B V \sum_{i=1}^{n_c} \left[n_{ci} \ln \frac{V_{ci}}{\delta V} - n_{ci}^0 \left(1 - \sum_{j < i} \alpha_{cj} \right) (\alpha_{ci} \ln \alpha_{ci} + (1 - \alpha_{ci}) \ln (1 - \alpha_{ci})) \right], \quad (2.9)$$

The mixture entropy S_c is thus 1-homogeneous with respect to the number of inclusion in class ci , N_{ci} , thus with respect to the phase volume occupation V_k . The non-ideal effects here are only due to the combinatory process rearranging the inclusions [Cordesse and Massot \(2020\) \[41\]](#), [Lhuillier \(2019\) \[138\]](#).

Since the flow is assumed monodisperse in the sense that there is one volume and one surface for all inclusions of a given class, the interfacial area is directly proportional to the volume occupation of each inclusion class. Thus, it inherits naturally the same properties in terms of homogeneity with respect to the entropy. The mixture entropy expression obtained in Equation (2.9) is only valid in this specific case but its derivation underline the requirement of the two following assumption to ensure extensivity, namely inclusion indiscernibility in a given class and numerous inclusion in each classes.

It is important to notice that if the distribution of classes is more complex, we would require additional variables to described it correctly, such as the mean Curvature or the Gauss Curvature. The extensivity of the entropy with respect to these additional variables would have to be examined.

To sum up, we see that the averaging process based on ℓ_c first re-establishes the meaning of volume fraction of fluid α_k . Secondly, it offers a non-usual approach of the interface whereby large and small scale surface dynamics are decoupled. At large scale, the entropy is naturally extensive, the interface dynamics being described by the gradient of any volumetric quantities such as the volume fraction. Small scale dynamics are captured by the small-scale variables, introduced to account for phase heterogeneity below the cut-off length ℓ_c . According to [2.1.3.2](#), considering $\Delta V = \ell_c^3$, we can assume that at this ℓ_c scale, the subscale configuration is sufficiently universal to assume the entropy homogeneous with respect to all the small-scale variables that allow to reconstruct a subscale representation. In particular, we presume the extensivity of the entropy with respect to the surface area of the interface.

2.1.3.3 CHOICE OF EXTENSIVE AND INTENSIVE SET OF VARIABLES TO CHARACTERIZE A MULTIFLUID MIXTURE

In a continuum mechanics approach, the set of bulk variables describing an out-of-equilibrium multiphase flow is circumscribed to the pressure, the temperature and the velocities of each phase. Regarding the description of the interface, in a diffuse interface model it is usually limited to the volume fraction accurately describing only the large scale dynamics of the interface. In the case of two-phase flow, the Baer-Nunziato model [Baer and Nunziato \(1986\) \[5\]](#) is a reference. Since the description of the interface dynamics at small scales can be enriched by transporting supplementary geometric variables such as the interfacial density area or the mean curvature as proposed in [Cordesse et al. \(2020\) \[34\]](#), we propose to first limit ourselves to the classic set of variable used by most mutlifluid models, but then we will show how to add supplementary extensive small scale variables in the case these variables are transported into the system of PDE.

Entropy of an isolated phase in a mixture In the limits introduced hereinbefore where the entropy recovers its homogeneity, we exhibit the entropy function and its properties with respect to extensive variables in the case of an isolated phase in a mixture.

Considering a mixture of $k \in \mathcal{N}_f = \{1, \dots, n_f\}$ fluids, each of them composed of $j \in \mathcal{N}_s(k) = \{1, \dots, m_k\}$ species of mass $M_{j,k}$, sharing a volume V of energy $E = \sum_{k \in \mathcal{N}_f} E_k$ and mass $M = \sum_{k \in \mathcal{N}_f} \sum_{j \in \mathcal{N}_s(k)} M_{j,k}$. Let us note m the total number of species, $m = \sum_{k \in \mathcal{N}_s(k)} m_k$. Each fluid occupies a volume V_k , its volume fraction α_k defines the volume occupation of fluid k with respect to the total volume V , $\alpha_k = V_k / \sum_{k \in \mathcal{N}_f} V_k$. In order to preserve symmetry when handling mass fractions, we assume each mass $M_{j,k}$ independent.

In the approach whereby each phase behaves independently and does not see each other, the entropy S_k of each fluid k is naturally 1-homogeneous with respect to the extensive variables $(E_k, V_k, M_{(j),k})$ with $M_{(j),k} = (M_{1,k}, \dots, M_{m_k,k})$ as a direct consequence of the single fluid case (2.1). The intensive quantities per phase are obtained by normalizing with the mass of each phase. The isolated fluid entropy per unit of mass s_k^o takes the form

$$s_k^o \left(e_k^o, v_k, \frac{y_{(j),k}}{y_k} \right) \hat{=} S_k \left(e_k^o, v_k, \frac{y_{(j),k}}{y_k} \right) = \frac{S_k(E_k, V_k, M_{(j),k})}{\sum_{j \in \mathcal{N}_s(k)} M_{j,k}}, \quad (2.10)$$

where e_k^o is the isolated fluid internal energy, v_k the fluid specific volume, $y_{j,k}$ the mass fraction of species j of phase k with respect to the mixture mass, $y_{j,k} = M_{j,k}/M$ and y_k is the mass fraction of phase k with respect to the fluid mixture mass defined as $y_k = \sum_{j \in \mathcal{N}_s(k)} M_{j,k}/M = M_k/M$.

For sake of clarity, we introduce the notation $\bar{y}_{j,k} = y_{j,k}/y_k$. Therefore, s_k^o remains 1-homogeneous with respect to the intensive variables $(e_k^o, v_k, \bar{y}_{(j),k}, v_k/\alpha_k)$. The Euler theorem yields

$$s_k^o \left(e_k^o, v_k, \bar{y}_{(j),k}, \frac{v_k}{\alpha_k} \right) = e_k^o \frac{\partial s_k^o}{\partial e_k^o} + v_k \frac{\partial s_k^o}{\partial v_k} + \sum_{j \in \mathcal{N}_s(k)} \bar{y}_{j,k} \frac{\partial s_k^o}{\partial \bar{y}_{j,k}}. \quad (2.11)$$

Entropy of a mixture Considering the whole mixture, in the thermodynamics limit discussed above, the mixture entropy S is 1-homogeneous with respect to the extensive variables $(E_{(k)}, V_{(k)}, M_{(j,k)}, \mathcal{S}_{(k,k')})$ where $E_{(k)} = (E_1, \dots, E_{n_f})$, $V_{(k)} = (V_1, \dots, V_{n_f})$, $M_{(j,k)} = (M_{1,k}, \dots, M_{m_k,k})_{k \in \mathcal{N}_f}$ and $\mathcal{S}_{(k,k')} = (\mathcal{S}_{k,k'} \mid (k, k') \in \mathcal{N}_f^2, k \neq k')$. The entropy per unit of mass of the whole mixture is given by

$$s \left(e_{(k)} y_{(k)}, v_{(k)} y_{(k)}, y_{(j,k)}, \Sigma_{(k,k')} v \right) = \frac{S(E_{(k)}, V_{(k)}, M_{(j,k)}, \mathcal{S}_{(k,k')})}{\sum_{k \in \mathcal{N}_f} \sum_{j \in \mathcal{N}_s(k)} M_{j,k}}, \quad (2.12)$$

with e_k the fluid internal energy, v the mixture specific volume and $\Sigma_{(k,k')}$ the interfacial density area separating fluid k and k' . s inherits the property of 1-homogeneity with respect to the intensive variables $(e_{(k)} y_{(k)}, v_{(k)} y_{(k)}, y_{(j,k)}, \dots, \Sigma_{(k,k')} v)$. Therefore, the Euler theorem leads to

$$s \left(e_{(k)} y_{(k)}, v_{(k)} y_{(k)}, y_{(j,k)}, \Sigma_{(k,k')} v \right) = \sum_{k \in \mathcal{N}_f} \left[e_k y_k \frac{\partial s}{\partial (e_k y_k)} + v_k y_k \frac{\partial s}{\partial (v_k y_k)} + \sum_{j \in \mathcal{N}_s(k)} y_{j,k} \frac{\partial s}{\partial y_{j,k}} \right] + \sum_{k < k' \in \mathcal{N}_f^2} v \Sigma_{k,k'} \frac{\partial s}{\partial (\Sigma_{k,k'} v)}. \quad (2.13)$$

Remark 14. Whereas for an isolated phase, the 1–homogeneity of the entropy s_k^o is carried directly by the energy e_k^o and the fluid specific volume v_k , for the mixture, the 1–homogeneity of the mixture entropy s is shifted to the fluid mass fraction y_k . In a sense, the case of the isolated phase is a degenerated case where $y_k = 1$, thus both dependencies are similar. Same remark holds for the mass fractions dependencies.

We recall that the mass fractions, the volume fractions and the specific volumes are connected through the relation $\forall k \in \mathcal{N}_f$, $y_k v_k = \alpha_k v$. Assuming a constraint on the volume occupation of the mixture, such that $\sum_{k \in \mathcal{N}_f} \alpha_k = 1$, we obtain that

$$v = \sum_{k \in \mathcal{N}_f} y_k v_k, \quad \alpha_k = \frac{y_k v_k}{\sum_{l \in \mathcal{N}_f} y_l v_l}, \quad (2.14)$$

which implies that v is 1–homogeneous and $\alpha_{(k)}$ 0–homogeneous.

We finally want to draw the reader’s attention to the final set of intensive variables bearing the 1–homogeneity with respect to the entropy. Neither the volume fraction α_k nor the interfacial density area $\Sigma_{k,k'}$ are found to be the right variables to work with. This is one of the key element on which relies the upcoming derivations.

2.1.4 BUILDING A MULTI-FLUID THERMODYNAMICS

To let the reader acquaint with the notations, we will first start by building a multi-fluid thermodynamics assuming the flow is described by a restricted set of variables. We thus discard the interfacial density area. At the end of the section we will show how the formalism allows a very simple extension to any supplementary variables chosen to described the mixture by taking the example of the interfacial density area.

2.1.4.1 ASSUMPTIONS AND SET OF VARIABLES

Assuming the mass fractions $y_{(j,k)}$ independent and the volume fractions constrained, we denote $\zeta = (T_{(k)}, v_{(k)} y_{(k)}, y_{(j,k)}) \in \mathcal{O}_\zeta$ the set of natural variables and $\xi = (e_{(k)} y_{(k)}, v_{(k)} y_{(k)}, y_{(j,k)}) \in \mathcal{O}_\xi$ the set of thermodynamics variables, where \mathcal{O}_ζ and \mathcal{O}_ξ are open sets defined on \mathbb{R}^{2n_f+m} . We assume the mappings $\zeta \mapsto \xi$ diffeomorph. We note $\tilde{\partial}_x$ any partial derivative of $x \in \zeta$, ∂_x any partial derivative of $x \in \xi$.

Furthermore, for any fluid $k \in \mathcal{N}_f$, let us introduce $\zeta_k = (T_k, v_k y_k, y_{(j),k}) \in \mathcal{O}_{\zeta_k}$ the fluid natural variables and $\xi_k = (e_k y_k, v_k y_k, y_{(j),k}) \in \mathcal{O}_{\xi_k}$ the fluid thermodynamics variables, where \mathcal{O}_{ζ_k} and \mathcal{O}_{ξ_k} are open sets defined on \mathbb{R}^{2+m_k} .

Finally, we define for any fluid $k \in \mathcal{N}_f$, $\bar{\zeta}_k = (T_k, v_k, \bar{y}_{(j),k}) \in \mathcal{O}_{\bar{\zeta}_k}$ the isolated fluid natural variables and $\bar{\xi}_k = (e_k, v_k, \bar{y}_{(j),k}) \in \mathcal{O}_{\bar{\xi}_k}$ the fluid thermodynamics variables, where $\mathcal{O}_{\bar{\zeta}_k}$ and $\mathcal{O}_{\bar{\xi}_k}$ are open sets defined on \mathbb{R}^{2+m_k} .

These set of variables have been carefully selected based on the results of the previous section.

2.1.4.2 FUNDAMENTAL EQUATION OF THERMODYNAMICS AND ENTROPY

The primary relation between the thermodynamics variables and their derivatives is the equation of thermodynamics, also called *Gibbs equation*. Once postulated, the Gibbs equation can eventually defines the expression of the entropy provided that we can employ the Euler theorem which exploits the 1–homogeneity of the entropy with respect to a given set of variables Gaillard (2015) [77].

Isolated phase in a mixture Given an identified set of variables for which the entropy of an isolated phase within a mixture is 1–homogeneous, we postulate a phase Gibbs equation, frequently assumed in two-phase flow modeling. We can then obtain the expression of the phase entropy, as well as compatibility closures between thermodynamics potentials and the pressure law. The following theorem is inspired from classic results found in the literature such as in Giovangigli and Matuszewski (2012) [87].

Theorem 8. *Given an isolated phase k in a mixture, assuming the Gibbs equation*

$$T_k ds_k^o(\bar{\zeta}_k) = de_k^o(\bar{\zeta}_k) + p_k^o(\bar{\zeta}_k) dv_k - \sum_{j \in \mathcal{N}_s(k)} g_{j,k}^o(\bar{\zeta}_k) d\bar{y}_{j,k}, \quad (2.15a)$$

where $p_k^o(\bar{\zeta}_k)$ is the fluid pressure, leads to an expression of the phase entropy per unit of mass $s_k^o(\bar{\zeta}_k)$

$$T_k s_k^o(\bar{\zeta}_k) = e_k^o(\bar{\zeta}_k) + p_k^o(\bar{\zeta}_k) v_k - \sum_{j \in \mathcal{N}_s(k)} g_{j,k}^o(\bar{\zeta}_k) \bar{y}_{j,k}, \quad (2.15b)$$

with $g_{j,k}^o(\bar{\zeta}_k)$ the phase gibbs potential defined by

$$g_{j,k}^o(\bar{\zeta}_k) = \tilde{\partial}_{\bar{y}_{j,k}} \left(e_k^o(\bar{\zeta}_k) - T_k s_k^o(\bar{\zeta}_k) \right), \quad (2.15c)$$

0–homogeneous with respect to $\bar{\zeta}_k$, and to the following compatibility closures

$$p_k^o(\bar{\zeta}_k) = \tilde{\partial}_{v_k} \left(T_k s_k^o(\bar{\zeta}_k) - e_k^o(\bar{\zeta}_k) \right), \quad \tilde{\partial}_{v_k} e_k^o(\bar{\zeta}_k) = T_k^2 \tilde{\partial}_{T_k} \left(\frac{p_k^o(\bar{\zeta}_k)}{T_k} \right). \quad (2.15d)$$

Proof. The results come from the Euler theorem written in Equation (2.11). \square

We introduce the definition of the isolated fluid free enthalpy per unit of mass $g_k^o(\bar{\zeta}_k) = e_k^o(\bar{\zeta}_k) + p_k^o(\bar{\zeta}_k) v_k - T_k s_k^o(\bar{\zeta}_k)$. Theorem (8) implies

$$g_k^o(\bar{\zeta}_k) = \sum_{j \in \mathcal{N}_s(k)} g_{j,k}^o(\bar{\zeta}_k) \bar{y}_{j,k}, \quad (2.16)$$

and $g_k^o(\bar{\zeta}_k)$ is 1–homogeneous with respect to $\bar{y}_{j,k}$.

Multi-fluid mixture We need now to generalize Theorem (8) to a multi-fluid mixture. The major difference lies in the fact that we can no more assume a Gibbs equation for each fluid, but we need to consider the mixture as a whole, and thus postulate a single Gibbs equation for the mixture. The second difference is the set of variables for which the entropy must be 1–homogeneous. From this mixture Gibbs equation, we can reconstruct the entropy of the system and exhibit compatibility closures as well as symmetry conditions among the thermodynamics potentials and the pressure laws.

Theorem 9. Given a multi-fluid mixture described by the set of variable ζ , let us assume the following Gibbs equation

$$ds(\zeta) = \sum_{k \in \mathcal{N}_f} \frac{1}{T_k} d(e_k(\zeta)y_k) + \sum_{k \in \mathcal{N}_f} \frac{p_k(\zeta)}{T_k} d(v_k y_k) - \sum_{k \in \mathcal{N}_f} \sum_{j \in \mathcal{N}_s(k)} \frac{G_{j,k}(\zeta)}{T_k} dy_{j,k}, \quad (2.17a)$$

where $p_k(\zeta)$ is the fluid pressure within the mixture. It infers an expression of the mixture entropy per unit of mass $s(\zeta)$

$$s(\zeta) = \sum_{k \in \mathcal{N}_f} \frac{1}{T_k} \left[e_k(\zeta)y_k + p_k(\zeta)v_k y_k - \sum_{j \in \mathcal{N}_s(k)} G_{j,k}(\zeta)y_{j,k} \right] \quad (2.17b)$$

with $G_{j,k}(\zeta)$ the mixture gibbs potential defined by

$$G_{j,k}(\zeta) = T_k \tilde{\partial}_{y_{j,k}} \left(\frac{e(\zeta)}{T} - s(\zeta) \right), \quad (2.17c)$$

where we have introduced two notations, an energy $e(\zeta)$ and a temperature T defined as $e(\zeta)/T = \sum_{k \in \mathcal{N}_f} e_k(\zeta)y_k/T_k$. Furthermore, we identify the following compatibility closures, for any $k \in \mathcal{N}_f$, we have

$$\frac{p_k(\zeta)}{T_k} = \tilde{\partial}_{v_k y_k} \left(s(\zeta) - \frac{e(\zeta)}{T} \right), \quad \forall l \in \mathcal{N}_f, \quad \tilde{\partial}_{v_l y_l} (e_k(\zeta)y_k) = T_k^2 \tilde{\partial}_{T_k} \left(\frac{p_l(\zeta)}{T_l} \right), \quad (2.17d)$$

and a symmetry condition

$$\tilde{\partial}_{v_l y_l} \left(\frac{p_k(\zeta)}{T_k} \right) = \tilde{\partial}_{v_k y_k} \left(\frac{p_l(\zeta)}{T_l} \right) \quad (2.17e)$$

Proof. The expression of s is derived using Equation (2.13) obtained from the Euler theorem. Then, we sum the total derivative of $e_{(k)}y_{(k)}$, in terms of ζ ,

$$\sum_{k \in \mathcal{N}_f} \frac{d(e_k(\zeta)y_k)}{T_k} = \sum_{k \in \mathcal{N}_f} \left(\left[\tilde{\partial}_{T_k} \left(\frac{e}{T} \right) + \frac{e_k y_k}{T_k^2} \right] dT_k + \tilde{\partial}_{v_k y_k} \left(\frac{e}{T} \right) d(v_k y_k) + \sum_{j \in \mathcal{N}_s(k)} \tilde{\partial}_{y_{j,k}} \left(\frac{e}{T} \right) dy_{j,k} \right).$$

Injecting it into the fundamental thermodynamics differential leads to

$$ds(\zeta) = \sum_{k \in \mathcal{N}_f} \left(\left[\tilde{\partial}_{T_k} \left(\frac{e}{T} \right) + \frac{e_k y_k}{T_k^2} \right] dT_k + \left[\frac{p_k}{T_k} + \tilde{\partial}_{v_k y_k} \left(\frac{e}{T} \right) \right] d(v_k y_k) + \sum_{j \in \mathcal{N}_s(k)} \left[\tilde{\partial}_{y_{j,k}} \left(\frac{e}{T} \right) - \frac{G_{j,k}(\zeta)}{T_k} \right] dy_{j,k} \right).$$

Consequently, the partial derivatives of the entropy read

$$\tilde{\partial}_{T_k} s = \tilde{\partial}_{T_k} \left(\frac{e}{T} \right) + \frac{e_k y_k}{T_k^2}, \quad \tilde{\partial}_{(v_k y_k)} s = \frac{p_k}{T_k} + \tilde{\partial}_{v_k y_k} \left(\frac{e}{T} \right), \quad \tilde{\partial}_{y_{j,k}} s = \tilde{\partial}_{y_{j,k}} \left(\frac{e}{T} \right) - \frac{G_{j,k}}{T_k},$$

and after some minor manipulations, we obtain

$$\frac{p_k(\zeta)}{T_k} = \tilde{\partial}_{v_k y_k} \left(s(\zeta) - \frac{e(\zeta)}{T} \right), \quad \tilde{\partial}_{v_k y_k} (e_k(\zeta)y_k) = T_k^2 \tilde{\partial}_{T_k} \left(\frac{p_k(\zeta)}{T_k} \right).$$

Furthermore, we see that for any $l \in \mathcal{N}_f$,

$$\frac{\tilde{\partial}}{\partial v_l y_l} \left(\frac{p_k}{T_k} \right) = \frac{\tilde{\partial}}{\partial v_l y_l} \left(\frac{\tilde{\partial}}{\partial v_l y_l} \left(s - \frac{e}{T} \right) \right) = \frac{\tilde{\partial}}{\partial v_l y_l} \left(\frac{\tilde{\partial}}{\partial v_l y_l} \left(s - \frac{e}{T} \right) \right),$$

assuming the partial derivatives commute. It results in the symmetry condition. Finally, noticing that

$$\tilde{\partial}_{(v_k y_k)} \left(\tilde{\partial}_{(v_l y_l)} (e_k y_k) \right) = \partial_{(v_k y_k)} \left(T_k^2 \tilde{\partial}_{T_k} (p_l / T_l) \right),$$

we can integrate with respect to $v_k y_k$,

$$\tilde{\partial}_{(v_l y_l)} (e_k y_k) = T_k^2 \frac{\tilde{\partial}}{\partial T_k} \left(\frac{p_l(\zeta^\tau)}{T_l} \right) + C_k$$

with C_k integration constant depending on $(T_{(l)}, v_{(l)} y_{(l)}, y_{(j,l)})$, $l \neq k$. Taking the particular case $l = k$ shows that the constant is null. □

We introduce the definition of the mixing free enthalpy per unit of mass

$$g(\zeta) = e(\zeta) + \sum_{k \in \mathcal{N}_f} p_k v_k y_k T / T_k - T s(\zeta). \quad (2.18)$$

Theorem (9) implies

$$g(\zeta) = \sum_{k \in \mathcal{N}_f} \sum_{j \in \mathcal{N}_s(k)} G_{j,k}(\zeta) y_{j,k} \frac{T}{T_k}. \quad (2.19)$$

It is important to notice that the thermodynamics potentials such as the entropy, s , the energy e and the mixing free enthalpy g are still not defined explicitly in terms of a given set of variables. We require further assumptions and propose in the next section to explicitly recover these potentials by assuming pressure laws.

2.1.4.3 THE PRESSURE LAW APPROACH

Following the lines of Giovangigli [Giovangigli and Matuszewski \(2012\) \[87\]](#), we propose to build the thermodynamics of a mixture starting from n_f stated pressure laws $p_k = p_k(\zeta)$ and then reconstruct the mixing energy, entropy and gibbs free energy by integrating the compatibility relations and using the symmetry conditions obtained in Theorem 9. This integration relies on the definition of a reference ideal state and well-chosen integration paths, which are unambiguous for multi-species single fluid (see [Giovangigli and Matuszewski \(2012\) \[87\]](#) for instance), but are not yet clearly identify for a mixture of fluids to the author's knowledge.

Compatibility closures connecting the thermodynamical potential to pressure laws including non-ideal effects are obtained and allow, relying on the definition of a reference ideal state and well-chosen integration paths, to reconstruct all the thermodynamical potentials from the pressure laws.

We choose to define n_f pressure laws by

$$p_k(\zeta) = p_k(\zeta_k) + \Delta p_k(\zeta), \quad (2.20)$$

where $p_k(\zeta_k)$ is the non-miscible not-interacting fluid pressure, as if the fluid were isolated from its neighbours, depending only on the fluid natural variables and Δp_k is a pressure correction term depending a priori on ζ accounting for interactions between the fluids. Since the pressure p_k is 0-homogeneous with respect to ζ , so are its decomposition terms. $p_k(\zeta_k)$ is thus 0-homogeneous with respect to ζ_k . Since $p_k^o(\overline{\zeta_k})$ is also 0-homogeneous with respect to $\overline{\zeta_k}$, we have

$$p_k(\zeta_k) = p_k^o(\zeta_k) = p_k^o(\overline{\zeta_k}). \quad (2.21)$$

Defining a reference state and the integration path The challenge now lies in the integration of the compatibility equations (2.17d) with respect to each specific volume $v_k y_k$ to obtain the natural definitions of the energy and entropy of mixing in terms of the pressure laws.

We first need to define a boundary condition. In the framework of supercritical fluid studied in [Giovangigli and Matuszewski \(2012\) \[87\]](#), the reference state is the Perfect Gas in the limit $v \mapsto +\infty$. We would also like to exploit the Perfect Gas state of the fluid mixture and will aim at integrating towards the Perfect Gas state of each fluid.

Secondly, since infinite directions of integration exist to reach the Perfect Gas state of a given mixture in the space $(v_k y_k)$, we need to ensure that we always integrate along the same direction each compatibility relation, which is not straightforward since they are expressed in terms of partial derivative with respect to the fluid quantity $v_k y_k$, preventing a direct integration along the mixing specific volume v . Given a quantity $\varphi : \zeta \in \mathcal{O}_\zeta \mapsto \mathbb{R}$, we introduce a family of the quantities $v_{(k)} y_{(k)}$ parametrized by n_f scalars $\beta_k \in \mathbb{R}$ and the variable $\tau \in \mathbb{R}$ to define the following mappings $(v_k y_k)(\tau) = (v_k y_k) + \beta_k \tau$. We propose to write ζ^τ the set of variables using these mappings, $\zeta^\tau = (T_{(k)}, v_{(k)} y_{(k)} + \beta_{(k)} \tau, y_{(j,k)})$. These mappings link together the partial derivative of φ with respect to the fluid specific volumes through the τ -derivative

$$\partial_\tau \varphi(\zeta^\tau) = \sum_{k \in \mathcal{N}_f} \beta_k \frac{\partial \varphi(\zeta^\tau)}{\partial (v_k y_k)}, \quad (2.22)$$

and to naturally integrate any quantity φ along the unique direction defined by the parameters β_k when τ varies from $0 \mapsto +\infty$.

In the limit, $\tau \mapsto +\infty$, $v_{(k)} y_{(k)} \mapsto +\infty$, $\forall k \in \mathcal{N}_f$. In this limit, each phase occupies an infinite volume and behaves as a Perfect Gas since there are no more molecular interaction. At this point, the directions of integration, β_k are not specified. We propose to maintain the notion of volume fraction while integrating towards the Perfect Gas state, thus we arbitrary choose $\beta_k = \alpha_k$. Therefore, we associate the limit $\tau \mapsto +\infty$ to the *Perfect Gas mixture* reference state where each phase behaves as a Perfect Gas at a given volume ratio dictated by the volume fractions.

We introduce the notation of superscript *PG* to denote this *Perfect Gas mixture* state of any quantity φ , such that integrating (2.22) over $\tau \in [0, +\infty[$ yields

$$\varphi(\zeta) = \varphi(T_{(k)}, y_{(j,k)})^{PG} - \sum_{k \in \mathcal{N}_f} \int_0^{+\infty} \alpha_k \frac{\partial \varphi(\zeta^\tau)}{\partial (v_k y_k)} d\tau. \quad (2.23)$$

Notably within this limit, we have

$$\forall k \in \mathcal{N}_f, \lim_{\tau \rightarrow +\infty} \Delta p_k(\zeta^\tau) = 0. \quad (2.24)$$

Finally, we will show in the construction of the thermodynamics potentials in the next paragraph that in the end the potentials do not depend on the direction of integration parametrized by β_k . This is an essential result and we therefore emphasize that the key element of the integration process is not the direction taken to reach the reference ideal state but rather to always use the same integration path to integrate each compatibility relation.

Reconstruction of the thermodynamics potentials Since we have now identified the integration paths and the reference ideal state, we can proceed to the integration of the compatibility equations (2.17d) in order to retrieve the definition of the thermodynamics potentials. Theorem (10) gives the definition of the mixing energy e , Theorem (11) the mixing entropy s and finally Theorem (12) the mixing gibbs free energy g .

We start by reconstructing the mixing energy, e .

Theorem 10. *Given n_f pressure laws defined by $p_k(\zeta) = p_k^o(\zeta_k) + \Delta p_k(\zeta)$ with p_k 0-homogeneous with respect to ζ . Assuming a Perfect Gas mixture reference state in the limit $\tau \mapsto +\infty$, the compatibility closures (2.17d) lead to a natural decomposition of the fluid energies as*

$$e_k(\zeta) = e_k(\zeta_k) + \Delta e_k(\zeta), \quad (2.25a)$$

$$e_k(\zeta_k) = e_k^{PG}(T_k, y_{(j,k)}) - \frac{T_k^2}{y_k} \int_{v_k y_k}^{+\infty} \tilde{\partial}_{T_k} \left(\frac{p_k^o(\zeta_k')}{T_k} \right) d(v_k' y_k') = e_k^o(\bar{\zeta}_k), \quad (2.25b)$$

$$\Delta e_k(\zeta) = - \frac{T_k^2}{y_k} \sum_{l \in \mathcal{N}_f} \int_0^{+\infty} \alpha_l \tilde{\partial}_{T_k} \left(\frac{\Delta p_l(\zeta^\tau)}{T_l} \right) d\tau. \quad (2.25c)$$

where $e_k(\zeta)$ is 0-homogeneous with respect to ζ . Furthermore, we also obtain a natural construction of the energy e as

$$\frac{e(\zeta)}{T} = \sum_{k \in \mathcal{N}_f} \frac{y_k}{T_k} [e_k(\zeta_k) + \Delta e_k(\zeta)], \quad (2.26)$$

with e 1-homogeneous with respect to ζ .

Proof. Using the family of transformations parametrized by α_k introduced in subSection 2.1.4.3, we want to integrate for each fluid k Equation (2.17d) along the direction $\tau \mapsto +\infty$ to reach the reference state. We have

$$\partial_\tau (e_k(\zeta^\tau) y_k) = \sum_{l \in \mathcal{N}_f} \alpha_l \tilde{\partial}_{(v_l y_l)} (e_k(\zeta^\tau) y_k) = \sum_{l \in \mathcal{N}_f} \alpha_l T_k^2 \frac{\tilde{\partial}}{\partial T_k} \left(\frac{p_l(\zeta^\tau)}{T_l} \right).$$

Integrating the previous expression along the direction $\tau \mapsto +\infty$, we obtain

$$(e_k y_k)(\zeta) = (e_k y_k)^{PG}(\zeta_k) - \sum_{l \in \mathcal{N}_f} T_k^2 \int_0^{+\infty} \alpha_l \frac{\tilde{\partial}}{\partial T_k} \left(\frac{p_l(\zeta^\tau)}{T_l} \right) d\tau,$$

where we have identified $e_k(T_{(k)}, v_{(l)}y_{(l)} \mapsto +\infty, y_{(j,l)})$ as the energy of perfect gas fluid, $e_k^{PG}(T_k, y_{(j,k)})$. Concerning the homogeneity of e_k^{PG} , we have

$$(e_k y_k)^{PG}(\zeta_k) = e_k^{PG}(\zeta_k) y_k = (e_k^o)^{PG}(\bar{\zeta}_k) y_k = (e_k^o)^{PG}(\zeta_k),$$

with $(e_k^o)^{PG}$ the perfect gas energy of the fluid k if it were isolated, which is 1-homogeneous with respect to $y_{(j,l)}$ [Giovangigli and Matuszewski \(2012\) \[87\]](#). Thus, $e_k^{PG}(\zeta_k)$ is naturally 0-homogeneous with respect to $y_{(j,l)}$. In the framework of multi-fluids, the 1-homogeneity is put at the mixture level rather than at each fluid level. Injecting the pressure laws leads finally to the result. □

As announced already in the previous paragraph, the construction of the energy does not depend on the parameters β_k , since deriving with respect to β_k the fluid energy $y_k e_k$ returns zero.

Proof. For any $m \in \mathcal{N}_f$, we have

$$\begin{aligned} \tilde{\partial}_{\beta_m}(y_k e_k) &= -T_k^2 \int_0^{+\infty} \frac{\tilde{\partial}}{\partial T_k} \left(\frac{\Delta p_m(\zeta^\tau)}{T_m} \right) d\tau - T_k^2 \sum_{l \in \mathcal{N}_f} \int_0^{+\infty} \beta_l \frac{\tilde{\partial}}{\partial \beta_m} \left(\frac{\tilde{\partial}}{\partial T_k} \left(\frac{\Delta p_l(\zeta^\tau)}{T_l} \right) \right) d\tau \\ &= -T_k^2 \int_0^{+\infty} \frac{\tilde{\partial}}{\partial T_k} \left(\frac{\Delta p_m(\zeta^\tau)}{T_m} \right) d\tau - T_k^2 \sum_{l \in \mathcal{N}_f} \int_0^{+\infty} \tau \beta_l \frac{\tilde{\partial}}{\partial v_m y_m} \left(\frac{\tilde{\partial}}{\partial T_k} \left(\frac{\Delta p_l(\zeta^\tau)}{T_l} \right) \right) d\tau \\ &= -T_k^2 \int_0^{+\infty} \frac{\tilde{\partial}}{\partial T_k} \left(\frac{\Delta p_m(\zeta^\tau)}{T_m} \right) d\tau - T_k^2 \int_0^{+\infty} \tau \sum_{l \in \mathcal{N}_f} \beta_l \frac{\tilde{\partial}}{\partial v_l y_l} \left(\frac{\tilde{\partial}}{\partial T_k} \left(\frac{\Delta p_m(\zeta^\tau)}{T_m} \right) \right) d\tau \\ &= -T_k^2 \int_0^{+\infty} \frac{\tilde{\partial}}{\partial T_k} \left(\frac{\Delta p_m(\zeta^\tau)}{T_m} \right) d\tau - T_k^2 \int_0^{+\infty} \tau \frac{\tilde{\partial}}{\partial \tau} \left(\frac{\tilde{\partial}}{\partial T_k} \left(\frac{\Delta p_m(\zeta^\tau)}{T_m} \right) \right) d\tau \\ &= -T_k^2 \left[\tau \frac{\tilde{\partial}}{\partial T_k} \left(\frac{\Delta p_m(\zeta^\tau)}{T_m} \right) \right]_{\tau=0}^{+\infty} \\ &= 0. \end{aligned}$$

□

We now reconstruct the mixing entropy, s .

Theorem 11. *Given n_f pressure laws defined by $p_k(\zeta) = p_k^o(\zeta_k) + \Delta p_k(\zeta)$ with p_k 0-homogeneous with respect to ζ . Assuming a Perfect Gas mixture reference state in the limit $\tau \mapsto +\infty$, the compatibility closures (2.17d) lead to a natural decomposition of the mixture entropy as*

$$s(\zeta) = \sum_{k \in \mathcal{N}_f} y_k [s_k(\zeta_k) + \Delta s_k(\zeta)], \quad (2.27a)$$

$$s_k(\zeta_k) = s_k^{PG}(T_k, y_{(j,k)}) - \frac{1}{y_k} \int_{v_k y_k}^{+\infty} \tilde{\partial}_{T_k} (p_k^o(\zeta'_k) - p_k^{PG}(T_k, y_{(j,k)})) d(v'_k y'_k) = s_k^o(\bar{\zeta}_k), \quad (2.27b)$$

$$\Delta s_k(\zeta) = -\frac{\alpha_k}{y_k} \int_0^{+\infty} \left[\tilde{\partial}_{T_k} (\Delta p_k(\zeta^\tau)) + \sum_{l \neq k \in \mathcal{N}_f} \frac{T_l}{T_k} \tilde{\partial}_{T_l} (\Delta p_k(\zeta^\tau)) \right] d\tau, \quad (2.27c)$$

where $s(\zeta)$ is 1-homogeneous with respect to ζ .

Proof. Using the family of transformations parametrized by α_k introduced in subSection 2.1.4.3, we want to integrate for each fluid k Equation (2.17d) along the direction $\tau \mapsto +\infty$ to reach the reference state. We have

$$\tilde{\partial}_\tau \left(s(\zeta^\tau) - \frac{e(\zeta^\tau)}{T} \right) = \sum_{k \in \mathcal{N}_f} \beta_k \tilde{\partial}_{(v_k y_k)} \left(s(\zeta^\tau) - \frac{e(\zeta^\tau)}{T} \right) = \sum_{k \in \mathcal{N}_f} \beta_k \frac{p_k(\zeta^\tau)}{T_k}.$$

Furthermore, we can express this compatibility closure in the case of a perfect mixture, and subtract it to the above relation, such that

$$\tilde{\partial}_\tau \left(s(\zeta^\tau) - \frac{e(\zeta^\tau)}{T} \right) - \tilde{\partial}_\tau \left(s^{PG}(\zeta^\tau) - \frac{e^{PG}(\zeta^\tau)}{T} \right) = \sum_{k \in \mathcal{N}_f} \beta_k \frac{p_k(\zeta^\tau) - p_k^{PG}(\zeta^\tau)}{T_k}.$$

We now integrate this relation over two states, τ' and τ'' ,

$$\left(s - \frac{e}{T} - s^{PG} + \frac{e^{PG}}{T} \right) (\zeta^{\tau'}) = \left(s - \frac{e}{T} - s^{PG} + \frac{e^{PG}}{T} \right) (\zeta^{\tau''}) - \sum_{k \in \mathcal{N}_f} \int_{\tau'}^{\tau''} \beta_k \frac{p_k(\zeta^\tau) - p_k^{PG}(\zeta^\tau)}{T_k} d\tau.$$

Taking the limit $\tau' = 0$ and $\tau'' \mapsto +\infty$ and choosing again the volume fractions constants during the integration, $\beta_k = \alpha_k$, to be consistent with the construction of the energy, it leads to

$$\left(s - \frac{e}{T} \right) (\zeta) = \left(s^{PG} - \frac{e^{PG}}{T} \right) (\zeta) - \sum_{k \in \mathcal{N}_f} \int_0^{+\infty} \alpha_k \frac{p_k(\zeta^\tau) - p_k^{PG}(\zeta^\tau)}{T_k} d\tau.$$

Reinjecting the n_f pressure laws and the definition of e from Theorem (10) leads to the results. □

Finally, let us reconstruc the mixing gibbs free energy g .

Theorem 12. *Given n_f pressure laws defined by $p_k(\zeta) = p_k^\circ(\zeta_k) + \Delta p_k(\zeta)$ with p_k 0-homogeneous with respect to ζ . Assuming a Perfect Gas mixture reference state in the limit $\tau \mapsto +\infty$, the definitions (2.17c),(2.19) and Theorems (10) (11) yield a natural decomposition of the gibbs potential energy*

$$G_{j,k}(\zeta) = g_{j,k}^\circ(\zeta_k) + \Delta g_{j,k}(\zeta), \quad (2.28)$$

$$\Delta g_{j,k}(\zeta) = T_k \tilde{\partial}_{y_{j,k}} \left(\sum_{l \in \mathcal{N}_f} \frac{y_l}{T_l} [\Delta e_l(\zeta) - T_l \Delta s_l(\zeta)] \right) = \sum_{l \in \mathcal{N}_f} \frac{T_k}{T_l} \int_0^{+\infty} \alpha_l \frac{\tilde{\partial}}{\partial y_{j,k}} (\Delta p_l(\zeta^\tau)) d\tau. \quad (2.29)$$

Thus, the mixing gibbs free energy takes the form

$$g(\zeta) = \sum_{k \in \mathcal{N}_f} \frac{T}{T_k} y_k [g_k(\zeta_k) + \Delta g_k(\zeta)], \quad (2.30a)$$

$$g_k(\zeta_k) = g_k^\circ(\bar{\zeta}_k), \quad (2.30b)$$

$$\Delta g_k(\zeta) = \sum_{l \in \mathcal{N}_f} \frac{T_k}{T_l} \int_0^{+\infty} \alpha_l \sum_{j \in \mathcal{N}_s(k)} \bar{y}_{j,k} \frac{\tilde{\partial}}{\partial y_{j,k}} (\Delta p_l(\zeta^\tau)) d\tau, \quad (2.30c)$$

where $g(\zeta)$ is 1-homogeneous and $g_k(\zeta_k)$ and $\Delta g_k(\zeta)$ are both 0-homogeneous.

Proof. Reinjecting the definitions of e and s into the definition of the mixture gibbs potential (2.17c), we have

$$G_{j,k}(\zeta) = T_k \tilde{\partial}_{y_{j,k}} \left(\frac{y_k e_k(\zeta_k)}{T_k} - y_k s_k(\zeta_k) \right) - T_k \tilde{\partial}_{y_{j,k}} \left(\sum_{l \in \mathcal{N}_f} \alpha_l \int_0^{+\infty} \left(T_l \tilde{\partial}_{T_l} \left(\frac{\Delta p_l(\zeta^\tau)}{T_l} \right) - \tilde{\partial}_{T_l}(\Delta p_l(\zeta^\tau)) \right) d\tau \right).$$

Disregarding the mixing terms for now, we have

$$T_k \tilde{\partial}_{y_{j,k}} \left(\frac{y_k e_k(\zeta_k)}{T_k} - y_k s_k(\zeta_k) \right) = \tilde{\partial}_{y_{j,k}} (e_k^o(\zeta_k) - T_k s_k^o(\zeta_k)) = g_{j,k}^o(\zeta_k) = g_{j,k}^o(\bar{\zeta}_k),$$

recalling that the phase gibbs potential $g_{j,k}^o$ is 0-homogeneous (see Equation (2.15c)). Thus, we have

$$\sum_{j \in \mathcal{N}_s(k)} G_{j,k}(\zeta_k) y_{j,k} = y_k \sum_{j \in \mathcal{N}_s(k)} g_{j,k}^o(\bar{\zeta}_k) \bar{y}_{j,k} = y_k g_k^o(\bar{\zeta}_k),$$

recalling the isolated fluid free enthalpy g_k^o defined in Equation (2.16) is 1-homogeneous. Again, we have shifted the 1-homogeneity to the mixture level rather than leaving it at each fluid level as it is done for multi-species gas. \square

We underline that the decomposition of the pressure laws in Equation (2.20) has naturally led to a decomposition of each thermodynamics potential. It permits to properly identify the role played by the mixing terms from the pressure law to the potentials.

Finally, we summarize the methodology employed and all the key ingredients to build the thermodynamics of a mixture of fluids:

- Choose the right set of variables for which the entropy is 1-homogeneous.
- Postulate a single mixture Gibbs equation.
- Obtain the compatibility closures and symmetry conditions relating the thermodynamics potentials and the pressure laws.
- Postulate the pressure laws.
- Define an integration path and a reference ideal state.
- Integrate the compatibility closures to obtain each thermodynamics potential.

2.1.5 IMPLICATIONS OF THE NEW FORMALISM

The new formalism introduced in the previous section has led to the definition of the thermodynamics of a multi-species multi-fluid mixture including non-ideal effects. We would like to point out some direct consequences of the formalism.

2.1.5.1 GIBBS EQUATION HIERARCHY

First, the formalism brings about three level of interaction of the fluids: 1) a fully coupled multi-fluid mixture based on a single Gibbs equation, 2) a weakly coupled multi-fluid flow where each fluid is equipped with an isolated Gibbs equation but still interact through a mixing Gibbs equation and 3) a non-interacting multi-fluid flow where each phase is isolated from one another, no interaction occurs.

From the fundamental equation of thermodynamics postulated for the mixture in Equation (2.17a), we can exhibit the fundamental equation of thermodynamics of each isolated phase and build a hierarchy of Gibbs equations.

We introduce $\Delta\text{FET}_k(\zeta) = T_k d(y_k \Delta s_k) - d(y_k \Delta e_k) - \Delta p_k d(y_k v_k) + \sum_{j \in \mathcal{N}_s(k)} \Delta g_{j,k} dy_{j,k}$ and $\text{FET}_k(\zeta_k) = T_k d(y_k s_k(\zeta_k)) - d(y_k e_k(\zeta_k)) - p_k(\zeta_k) d(y_k v_k) + \sum_{j \in \mathcal{N}_s(k)} g_{j,k}^0(\zeta_k) d\bar{y}_{j,k}$. From the construction of our thermodynamics variables, the Gibbs equation (2.17a) takes now the following form

$$\sum_{k \in \mathcal{N}_f} \frac{1}{T_k} \Delta\text{FET}_k(\zeta) + \sum_{k \in \mathcal{N}_f} \frac{1}{T_k} \text{FET}_k(\zeta_k) = 0. \quad (2.31)$$

Equation (2.31) exhibits the isolated phase fundamental equations of thermodynamics $\text{FET}_k(\zeta)$ along with $\Delta\text{FET}_k(\zeta)$, which looks like a Gibbs equation on the mixing part of all the thermodynamics variables.

Equation (2.31) enlightens the consequences of postulating a Gibbs equation for each phase of the mixture, $\text{FET}_k = 0$,

$$\forall k \in \mathcal{N}_f, \text{FET}_k = 0 \implies \sum_{k \in \mathcal{N}_f} \frac{1}{T_k} \Delta\text{FET}_k(\zeta) = 0. \quad (2.32)$$

It suggests, that when a Gibbs equation is assumed for each phase of a mixture, if mixing effects are added a posteriori, it must fullfill a Gibbs equation.

In light of Equations (2.31) and (2.32), the three levels of interactions are

1. The fully coupled multi-fluid mixture based on a single Gibbs equation

$$\sum_{k \in \mathcal{N}_f} \frac{1}{T_k} \Delta\text{FET}_k(\zeta) + \sum_{k \in \mathcal{N}_f} \frac{1}{T_k} \text{FET}_k(\zeta_k) = 0. \quad (2.33)$$

2. The weakly coupled multi-fluid flow based on a mixture Gibbs equation driving the interactions between the fluids

$$\sum_{k \in \mathcal{N}_f} \frac{1}{T_k} \Delta\text{FET}_k(\zeta) = 0, \quad (2.34a)$$

and a Gibbs equation for each fluid

$$\forall k \in \mathcal{N}_f, \text{FET}_k = 0. \quad (2.34b)$$

3. A non-interacting multi-fluid flow based on a Gibbs equation for each fluid

$$\forall k \in \mathcal{N}_f, \text{FET}_k = 0. \quad (2.35)$$

Furthermore, Equation (2.34a) has strong implication on the quest for the entropy transport equation of a mixture where each phase is assumed isolated from each other, as in the Least Action Principle derivation [Gouin and Ruggeri \(2009\) \[95\]](#), [Cordesse and Massot \(2020\) \[41\]](#). Assuming a hydrodynamical equilibrium where all phases flow at speed \mathbf{v} , if $D_t \bullet$ is the material derivative $\partial_t(\bullet) + \mathbf{v} \cdot \nabla \bullet$, we obtain a transport equation on the mixing entropy

$$\sum_{k \in \mathcal{N}_f} \frac{1}{T_k} \left[T_k D_t(y_k \Delta s_k) - D_t(y_k \Delta e_k) - \Delta p_k D_t(y_k v_k) + \sum_{j \in \mathcal{N}_s(k)} \Delta g_{j,k} D_t(y_{j,k}) \right] = 0. \quad (2.36)$$

This equation is then closed by injecting the conservation and momentum equations as well as the equation on the volume fraction of the investigated model.

2.1.5.2 ADDING SUPPLEMENTARY VARIABLES TO THE THERMODYNAMICS: ILLUSTRATION WITH THE INTERFACIAL DENSITY AREA

The formalism introduced is not circumscribed to the set of variable $\zeta_k = (T_k, v_k y_k, y_{(j),k}) \in \mathcal{O}_{\zeta_k}$, but encompasses any supplementary variable.

To illustrate this, let us add the interfacial density areas, which have been studied in [Section 2.1.4](#). We add the set of variables $\Sigma_{(k,k')} = (\Sigma_{k,k'} \mid (k, k') \in \mathcal{N}_f^2, k \neq k') \subset \mathbb{R}^{n_f(n_f-1)/2}$ to the set of variables ζ and ξ .

We have to assume a new Gibbs relation as we did in Equation (2.17a).

Theorem 13. *Given a multi-fluid mixture at thermal equilibrium, assuming the Gibbs equation*

$$\begin{aligned} ds(\zeta) = & \sum_{k \in \mathcal{N}_s(k)} \frac{1}{T_k} d(e_k(\zeta) y_k) + \sum_{k \in \mathcal{N}_s(k)} \frac{p_k(\zeta)}{T_k} d(v_k y_k) \\ & - \sum_{k \in \mathcal{N}_f} \sum_{j \in \mathcal{N}_s(k)} \frac{G_{j,k}(\zeta)}{T_k} dy_{j,k}, - \sum_{(k < k') \in \mathcal{N}_f^2} \frac{F_{k,k'}^\Sigma(\zeta)}{T_{k,k'}} d(\Sigma_{k,k'} v), \end{aligned} \quad (2.37a)$$

where $p_k(\zeta)$ is the fluid pressure within the mixture, $T_{k,k'}$ is the temperature at the interface between two adjacent fluids, k and k' , to be modelled. It leads to an expression of the mixture entropy per unit of mass $s(\zeta)$

$$s(\zeta) = \sum_{k \in \mathcal{N}_f} \frac{1}{T_k} \left[e_k(\zeta) y_k + p_k(\zeta) v_k y_k - \sum_{j \in \mathcal{N}_s(k)} G_{j,k}(\zeta) y_{j,k} \right] - \sum_{(k < k') \in \mathcal{N}_f^2} \frac{1}{T_{k,k'}} F_{k,k'}^\Sigma(\zeta) \Sigma_{k,k'} v \quad (2.37b)$$

with $G_{j,k}(\zeta)$ the mixture gibbs potential and $F_{k,k'}^\Sigma(\zeta)$ the interfacial density area potential defined by

$$G_{j,k}(\zeta) = T_k \tilde{\partial}_{y_{j,k}} \left(\frac{e(\zeta)}{T} - s(\zeta) \right), \quad F_{k,k'}^\Sigma(\zeta) = T_{k,k'} \tilde{\partial}_{(\Sigma_{k,k'} v)} \left(\frac{e(\zeta)}{T} - s(\zeta) \right), \quad (2.37c)$$

where we have introduced two notations, an energy $e(\zeta)$ and a temperature T defined as $e(\zeta)/T = \sum_{k \in \mathcal{N}_f} e_k(\zeta) y_k / T_k$. Furthermore, we identify the same compatibility closures and symmetry conditions as in [Theorem 9](#).

Proof. Same manipulations as in Theorem (9).

□

Adding the set of variables $(\Sigma_{(k,k')})$ does not impact the construction of the energy and the entropy from pressure laws. Therefore, Theorems (10), (11) still hold. Since the interfacial area effect is not included in the isolated phase thermodynamics, the sets ζ_k do not include it. Therefore, we obtain from the construction of the thermodynamics,

$$F_{k,k'}^{\Sigma}(\zeta) = \sum_{l \in \mathcal{N}_f} \frac{T_{k,k'}}{T_l} \frac{\tilde{\partial}}{\partial(\Sigma_{k,k'}v)} \int_0^{+\infty} \alpha_l \Delta p_l(\zeta^\tau) d\tau, \quad (2.38)$$

Furthermore, from the usual definition of the mixing free enthalpy per unit of mass $g(\zeta) = e(\zeta) + \sum_{k \in \mathcal{N}_f} p_k v_k y_k T/T_k - T s(\zeta)$, Theorem (13) gives a new expression of $g(\zeta)$

$$g(\zeta) = \sum_{k \in \mathcal{N}_f} \sum_{j \in \mathcal{N}_s(k)} \frac{T}{T_k} G_{j,k}(\zeta) y_{j,k} + \sum_{(k < k') \in \mathcal{N}_f^2} \frac{T}{T_{k,k'}} F_{k,k'}^{\Sigma}(\zeta) \Sigma_{k,k'} v, \quad (2.39)$$

which is not depending on the interfacial temperatures, and only the term Δg_k is altered and takes now the form

$$\Delta g_k(\zeta) = \sum_{l \in \mathcal{N}_f} \frac{T_k}{T_l} \left[\int_0^{+\infty} \alpha_l \sum_{j \in \mathcal{N}_s(k)} \bar{y}_{j,k} \frac{\tilde{\partial}}{\partial y_{j,k}} (\Delta p_l(\zeta^\tau)) d\tau \right] + \sum_{l \in \mathcal{N}_f} \frac{T_k}{T_l} \left[\sum_{(k < k') \in \mathcal{N}_f^2} \frac{\Sigma_{k,k'} v}{y_k} \frac{\tilde{\partial}}{\partial(\Sigma_{k,k'}v)} \int_0^{+\infty} \alpha_l \Delta p_l(\zeta^\tau) d\tau \right]. \quad (2.40)$$

We could have gone further, adding supplementary variables to the thermodynamics, either describing the interface such as the mean or the Gauss curvatures, or describing the flow disequilibrium such as the velocity fluctuations [Lhuillier \(1995\) \[135\]](#). The formalism can be applied straightforwardly to these variables, which makes it very convenient for multi-fluid flow modeling, provided that we can exhibit a related extensive variable.

2.1.5.3 ISOTHERMAL THERMODYNAMICS

So far, we have assume no relaxation process among the fluids and have obtained the most general mixing terms in the construction of the energy and the entropy. They involve mostly partial derivatives with respect to the temperatures. We also had to introduce a mixing temperature T in the definition of the energy e as well as interfacial temperatures $T_{k,k'}$ to account for the interfacial density area potentials, all to be modelled.

Thermal relaxation of the fluids should get rid of these unclosed temperatures. However, due to the complex temperature partial derivatives, the energy and the entropy definitions on this constraint manifold are not straightforward. Their expressions are given hereafter and detailed calculations can be found in [Appendix 2.A](#). Assuming thermal equilibrium, $T_{(k)} = T$,

the energy, the entropy and the Gibbs free energy take the form

$$e(\xi) = e^{PG}(\xi) - \sum_{k \in \mathcal{N}_f} T^2 \int_{y_k v_k}^{+\infty} \frac{\tilde{\partial}}{\partial T} \left(\frac{p_k^o(\zeta'_k)}{T} \right) dy'_k v'_k - \sum_{k \in \mathcal{N}_f} T^2 \int_0^{+\infty} \alpha_k \frac{\tilde{\partial}}{\partial T} \left(\frac{\Delta p_k(\zeta^\tau)}{T} \right) d\tau, \quad (2.41a)$$

$$s(\xi) = s^{PG}(\xi) - \sum_{k \in \mathcal{N}_f} \int_{y_k v_k}^{+\infty} \tilde{\partial}_T(p_k^o(\zeta'_k)) dy'_k v'_k - \sum_{k \in \mathcal{N}_f} \int_0^{+\infty} \alpha_k \tilde{\partial}_T(\Delta p_k(\zeta^\tau)) d\tau, \quad (2.41b)$$

$$g(\xi) = \sum_{k \in \mathcal{N}_f} \sum_{j \in \mathcal{N}_s(k)} g_{j,k}^o(\xi_k) y_{j,k} + \sum_{k \in \mathcal{N}_f} \sum_{l \in \mathcal{N}_f} \sum_{j \in \mathcal{N}_s(k)} \int_0^{+\infty} \alpha_k \tilde{\partial}_{y_{j,k}}(\Delta p_l(\zeta^\tau)) y_{j,k} d\tau \\ + \sum_{(k < k') \in \mathcal{N}_f^2} \sum_{l \in \mathcal{N}_f} \Sigma_{k,k'l} v \frac{\tilde{\partial}}{\partial \Sigma_{k,k'l} v} \left(\int_0^{+\infty} \alpha_k \Delta p_l(\zeta^\tau) d\tau \right). \quad (2.41c)$$

2.1.5.4 THERMODYNAMICS POTENTIALS OF TWO-PHASE FLOW

Since two-phase flow modeling is of prior concern and for sake of simplicity, we propose to specialize to the two-phase flow modeling, although the formalism can be applied to take into account more fluids. We thus propose to exhibit the thermodynamics variables obtained from two pressure laws and then emphasize how to add mixing effect in existing two-phase flow models in a consistent way regarding both the thermodynamics and the system of equations and analyze its consequences on the mathematical structure of the system.

The energy, the entropy and the Gibbs free energy of two phase flow simplify into

$$\frac{e(\zeta)}{T} = \sum_{k=1}^2 \frac{y_k e_k(\zeta_k)}{T_k} - \int_0^{+\infty} \left[\alpha_1 \left(T_1 \frac{\tilde{\partial}}{\partial T_1} \left(\frac{\Delta p_1(\zeta^\tau)}{T_1} \right) + \frac{T_2}{T_1} \frac{\tilde{\partial}}{\partial T_2} (\Delta p_1(\zeta^\tau)) \right) \right. \\ \left. + \alpha_2 \left(T_2 \frac{\tilde{\partial}}{\partial T_2} \left(\frac{\Delta p_2(\zeta^\tau)}{T_2} \right) + \frac{T_1}{T_2} \frac{\tilde{\partial}}{\partial T_1} (\Delta p_2(\zeta^\tau)) \right) \right] d\tau, \quad (2.42a)$$

$$s(\zeta) = \sum_{k=1}^2 y_k s_k(\zeta_k) - \int_0^{+\infty} \left[\alpha_1 \left(\frac{\tilde{\partial}}{\partial T_1} (\Delta p_1(\zeta^\tau)) + \frac{T_2}{T_1} \frac{\tilde{\partial}}{\partial T_2} (\Delta p_1(\zeta^\tau)) \right) \right. \\ \left. + \alpha_2 \left(\frac{\tilde{\partial}}{\partial T_2} (\Delta p_2(\zeta^\tau)) + \frac{T_1}{T_2} \frac{\tilde{\partial}}{\partial T_1} (\Delta p_2(\zeta^\tau)) \right) \right] d\tau, \quad (2.42b)$$

$$g(\xi) = \sum_{k=1}^2 \sum_{j \in \mathcal{N}_s(k)} g_{j,k}^o(\xi_k) y_{j,k} + \int_0^{+\infty} \sum_{j \in \mathcal{N}_s(1)} y_{j,1} \tilde{\partial}_{y_{j,1}} \left(\frac{T}{T_1} \alpha_1 \Delta p_1(\zeta^\tau) + \frac{T}{T_2} \alpha_2 \Delta p_2(\zeta^\tau) \right) d\tau \\ + \int_0^{+\infty} \sum_{j \in \mathcal{N}_s(2)} y_{j,2} \tilde{\partial}_{y_{j,2}} \left(\frac{T}{T_1} \alpha_1 \Delta p_1(\zeta^\tau) + \frac{T}{T_2} \alpha_2 \Delta p_2(\zeta^\tau) \right) d\tau \\ + \Sigma_{1,2} v \tilde{\partial}_{\Sigma_{1,2} v} \left(\int_0^{+\infty} \left(\frac{T}{T_1} \alpha_1 \Delta p_1(\zeta^\tau) + \frac{T}{T_2} \alpha_2 \Delta p_2(\zeta^\tau) \right) d\tau \right). \quad (2.42c)$$

Thermal equilibrium If we further assume thermal equilibrium, the energy and entropy simplify into

$$e(\zeta) = \sum_{k=1}^2 y_k e_k(\zeta_k) - \sum_{k=1}^2 \int_0^{+\infty} \left[\alpha_k T^2 \frac{\tilde{\partial}}{\partial T} \left(\frac{\Delta p_k(\zeta^\tau)}{T} \right) \right] d\tau, \quad (2.43a)$$

$$s(\zeta) = \sum_{k=1}^2 y_k s_k(\zeta_k) - \sum_{k=1}^2 \int_0^{+\infty} \left[\alpha_k \frac{\tilde{\partial}}{\partial T} (\Delta p_k(\zeta^\tau)) \right] d\tau. \quad (2.43b)$$

2.1.6 APPLICATIONS TO TWO-PHASE FLOW MODELING AND IMPACT OF NON-IDEAL EFFECTS

We would like to illustrate the strength of the formalism introduced in the previous section to highlight the impact of any non-ideal effects on both the thermodynamics and systems of partial differentiating equations of two-phase flow models obtained by means of the Stationary Action Principle.

2.1.6.1 STATIONARY ACTION PRINCIPLE AND ENTROPY CLOSURE

One major method to obtain a two-phase flow model is the Stationary Action Principle [Serin \(1959\) \[200\]](#), [Bedford and Drumheller \(1978\) \[8\]](#), [Geurst \(1985\) \[84\]](#), [Geurst \(1986\) \[83\]](#), [Gouin \(1990\) \[93\]](#). This variational approach uses Hamilton's principle of stationary action stating that any system under small perturbations will follow the physical path towards equilibrium that minimizes its action \mathcal{A} , the latter being the integral over time and space of the energy of the system, the Lagrangian L , defined as the difference between the kinetic energy \mathcal{K} and the potential energy \mathcal{U} of the system. The equation

$$\delta_\lambda \mathcal{A} = 0, \quad (2.44)$$

returns a system of partial differentiating equations describing the evolution of the system under arbitrary constraints. Examples of two-phase flow models obtained through SAP are found in [Gavrilyuk et al. \(1997\) \[80\]](#), [Gavrilyuk and Gouin \(1999\) \[79\]](#), [Gouin and Gavrilyuk \(1999\) \[94\]](#), [Gavrilyuk and Saurel \(2002\) \[81\]](#).

The advantage of the SAP against other method is that the conservative model is obtained from the knowledge of only one scalar function, the Lagrangian of the system L . However, to account for specific effects, such as the microstructure of the flow or sub-scale effects, one needs to introduce additional variables describing the phenomena to be accounted for [Bedford and Drumheller \(1978\) \[8\]](#). For example, to model a bubbly flow, one needs to introduce variables to describe the volume and shape variations of the bubbles and the corresponding energies into the Lagrangian [Gavrilyuk and Saurel \(2002\) \[81\]](#), [Drui et al. \(2019\) \[60\]](#). Nonetheless, if a certain effect is needed to be included, the variational approach permits it to be consistently included in the mass, momentum and energy conservative equations. Still finding an explicit form of the Lagrangian that encompasses any flow topology remains a challenging task.

Last but not least, the dissipative part of the system must be added afterwards by exploiting the second principle of thermodynamics. For barotropic materials, the mixture of the entropy is known, thus the derivation is straightforward. It is still an open question when equipping the fluids with complete equations of state. We want to show how the present formalism clarifies and innovates the entropy closure of the system returned by the SAP.

Assuming a compressible flow is under hydrodynamical equilibrium, each phase flowing at the same speed \mathbf{v} and equipped with a two-parameter equation of state, the general closure given to the Lagrangian is

$$L = \frac{1}{2} \rho \|\mathbf{v}\|^2 - e(s, \rho, y_{(j,k)}, \alpha_{(k)}), \quad (2.45)$$

where ρ is the averaged density of the flow, $\rho = 1/v$, e is the internal energy of the mixture and mass and volume fraction constraints hold $\alpha_1 + \alpha_2 = 1$, $y_{(j),1} + y_{(j),2} = 1$.

The SAP yields the momentum equations together with the assumed constraints imposed on the flow. The latter are always composed at least of the mass conservation, which seems natural, but also of constraints regarding the dissipation process. Two approaches have been investigated in the literature, assuming either mixture entropy conservation or partial entropy conservation, and we will employ each of these constraints to illustrate first how the mathematical structure is impacted by the non-ideal effects of the thermodynamics, and how the present formalism gives an alternative for the entropy closure of the system of PDE.

2.1.6.2 IMPACT OF THE NON-IDEAL EFFECTS ON THE MATHEMATICAL WAVE STRUCTURE

Under total mass ρ , partial mass $y_{j,k}$ and total entropy s conservations, we obtain the following system of equations $\forall (j, k) \in \mathcal{N}_s(k) \times \{1, 2\}$,

$$\partial_t \rho + \nabla \cdot [\rho \mathbf{v}] = 0, \quad (2.46a)$$

$$D_t y_{j,k} = 0, \quad (2.46b)$$

$$\partial_t (\rho \mathbf{v}) + \nabla \cdot [\rho \mathbf{v}^t \mathbf{v} + \rho^2 \partial_\rho e] = 0, \quad (2.46c)$$

$$D_t s = 0, \quad (2.46d)$$

$$\rho \partial_{\alpha_k} e = 0. \quad (2.46e)$$

Conducting a single dimensional mathematical analysis on this system shows that the spectrum is $\{v, v \pm a\}$, with $a^2 = \partial_\rho(\rho^2 \partial_\rho e)$ the mixture sound speed. So far, no hypothesis has been done on the thermodynamics of the mixture. To simplify the following derivation, we will assume thermal equilibrium of the fluids, such that the Gibbs equation (2.17a) reads

$$de = -T ds - \sum_{k \in \mathcal{N}_s(k)} p_k d(v_k y_k) + \sum_{k \in \mathcal{N}_f} \sum_{j \in \mathcal{N}_s(k)} G_{j,k} dy_{j,k}. \quad (2.47)$$

Expliciting the partial derivative involved in the term $\rho^2 \partial_\rho e(\zeta)$ in the momentum equation and using the fact that the mapping $(s, \rho, y_{(j,k)}, \alpha_{(k)}) \mapsto \zeta$ is a one-to-one mapping under the two mass and volume fraction constraints,

$$\rho^2 \partial_\rho e = \rho^2 \frac{\partial e}{\partial \rho} \Big|_{y_{(j,k)}, s, \alpha_{(k)}} = - \frac{\partial e}{\partial v} \Big|_{y_{(j,k)}, s, \alpha_{(k)}} = - \sum_{k \in \mathcal{N}_f} \frac{\partial v_k y_k}{\partial v} \frac{\partial e}{\partial v_k y_k} \Big|_{s, v_{k'} y_{k'}, y_{(j,k)}}. \quad (2.48)$$

Since $\partial v_k y_k / \partial v = \alpha_k$, from Equation (2.47), we obtain

$$\rho^2 \partial_\rho e = \sum_{k \in \mathcal{N}_f} \alpha_k [p_k(\zeta_k) + \Delta p_k(\zeta)]. \quad (2.49)$$

Thus, the mixture sound speed reads

$$a^2 = -v^2 \partial_v \left(\sum_{k \in \mathcal{N}_f} \alpha_k [p_k(\zeta_k) + \Delta p_k(\zeta)] \right) \Big|_s. \quad (2.50)$$

Hence, we clearly see how the mixing part of the pressure laws, $\Delta p_k(\zeta)$, impacts the mathematical wave structures of any two-phase flow model. The formalism of the previous section brings out the direct link between thermodynamics and system modeling.

2.1.6.3 THE INTEREST OF THE GIBBS EQUATION HIERARCHY UNDER PARTIAL ENTROPY CONSTRAINTS

In the previous paragraph, we have not highlighted the fact that the Stationary Action Principle fails at generating a closed system of equations when constraining the mixture entropy, since we can not retrieve the partial entropy equations without further hypothesis.

On specific flows, such as quantum fluids, it is reasonable to assume that the mixture entropy s is convected along one of the two components trajectory [Landau and Lifshitz \(1987\) \[207\]](#), and identifying $s = s_1, s_2 = 0$ closes the system. In [Gouin and Ruggeri \(2009\) \[95\]](#), the authors assumed that the mixture is weakly out of equilibrium ($|\mathbf{v}_d| \ll 1$). Considering this last assumption, they introduced an averaged temperature T and after some calculations (the reader may refer to their work), thanks to a postulated mixture Gibbs equation, they obtain a evolution equation for each partial entropy.

Another solution to close the system of equations consists in constraining the partial entropies rather than the mixture entropy. The partial entropy are then assumed to be advected

$$D_t s_k = 0 \quad (2.51)$$

as in [Gouin and Gavriljuk \(1999\) \[94\]](#). These entropy closures are very accomodating since we can infer from them the phase internal energy transport equations given a Gibbs equation for each phase, and thus the system of equations is closed. Nevertheless, these constraints are questionable in the sense that they seem to prohibit any interaction between the fluids and prevent a thermodynamics relaxation of the phases, which must be added *a posteriori* by exploiting the second thermodynamics principle and postulating relaxation source terms.

However, from the hierarchy of Gibbs equations derived in [Section 2.1.5.1](#), we can revisit the entropy closure and propose an original approach to derive both the mixture entropy and its evolution equation for any system obtained through the Stationary Action Principle where the partial entropies are constrained as in Equation (2.51). Given the definition of the mixture entropy, taking its material derivative yields

$$D_t s(\zeta) = \sum_{k \in \mathcal{N}_f} \left(D_t y_k [s_k(\zeta_k) + \Delta s(\zeta)] + y_k [D_t s_k(\zeta_k) + D_t \Delta s(\zeta)] \right) = \sum_{k \in \mathcal{N}_f} y_k D_t \Delta s_k(\zeta), \quad (2.52a)$$

which leads to the following evolution equation for the mixture entropy

$$D_t s(\zeta) = \sum_{k \in \mathcal{N}_f} y_k \sum_{l \in \mathcal{N}_f} \left(\tilde{\partial}_{T_l}(\Delta s_k) + \tilde{\partial}_{v_k y_k}(\Delta s_k) \right). \quad (2.52b)$$

In Equation (2.52), the unknowns are only the partial derivatives of the mixing part of the entropy, since the SAP together with the set of constraints have returned evolution equations for the density, the velocity, the volume fraction, the pulsation and the interfacial density area. On the top of this equation, one needs to consider the constraint imposed by the hypothesis of two Gibbs equations, as shown in [Section 2.1.5.1](#). From this set of equations, we should be able to propose a closure for the mixing part of the entropy.

2.1.7 SHEDDING SOME LIGHTS ON IDENTIFIED SYSTEMS OF THE LITERATURE WITH NON-IDEAL EFFECTS

Some approaches commonly encountered in the literature to account for non-ideal effects consist either modifying directly the system of partial differentiating equations by adding terms in the pressure law, or extending the definition of a thermodynamics potentials such as the energy, the entropy or the Gibbs free energy. Nonetheless, in light of the formalism introduced in this contribution, we see that such approaches can result in an inconsistency between the system and the associated thermodynamics since accounting for non-ideal effect in two-phase flow modeling can potentially impact both the model and the thermodynamics.

We propose here to revisit these attempts and obtain the natural definitions of the thermodynamics variables associated to the extended pressure laws employed together with an eligible pressure law compatible with the extended thermodynamics variables proposed by the modellers.

2.1.7.1 STAGNATION PRESSURE IN A DISPERSED PHASE

Sainsaulieu has found a way to reestablish the hyperbolicity of his two-phase flow model for dispersed flow, by adding a pressure term, function of the volume fraction [Sainsaulieu \(1995\) \[189\]](#) in the momentum equation of the dispersed phase

$$\nabla \cdot [p_2 + \theta_0(1 - \alpha_2)^\delta] \quad (2.53)$$

where θ_0 is a constant related to the stagnation pressure of the gas on each liquid droplet and $\delta = 4/3$. However, he has not verified if this alteration of the pressure law could have an impact on the thermodynamics.

Let us see if this new pressure law has an impact on the thermodynamics. In this case, we identify the pressure law $\Delta p_2 = \theta_0 \alpha_2^\delta$. From Equations (2.25a) and Equations (2.27a), we have

$$\Delta s_1(\zeta) = \Delta s_2(\zeta) = \Delta e_1(\zeta) = 0, \quad \Delta e_2(\zeta) = \frac{1}{y_2} \alpha_2 (1 - \alpha_2)^\delta \int_0^{+\infty} \theta_0 d\tau. \quad (2.54)$$

As we see, the behaviour of the parameter θ_0 in the limit of *Perfect Gas mixture* is yet inconsistent, the formalism now suggests a dependency with respect to either the specific volume of the dispersed phase or of the total specific volume to bound the integral of θ_0 . If we assume it is the case, then, while this pressure correction does not change the definition of the mixing entropy, it does change the energy of the system.

As we see, the formalism brings out conditions on the form of the pressure laws helping in system modeling and yields the correct thermodynamics associated to the extended system of equations.

2.1.7.2 OSMOTIC PRESSURE IN A SOLUTE/SOLVENT MIXTURE

In solute/solvent mixture, the osmotic pressure accounts for solute concentration disequilibrium and occurs in the case of semi-permeable membrane for example. This colligative property (ie proportional to the mass fraction of the solute) adds up to the phasic pressure. In [Guazzelli and Pouliquen \(2018\) \[98\]](#), the authors investigate dense granular suspensions and

relate a force due to the particles pushing on the wall, inducing in turn a pressure on the fluid. They compare this particle pressure to the osmotic pressure.

Let us consider a mono-species solute, referred as phase 2, in a solvent, phase 1, at thermal equilibrium. In the case of an ideal mixture of solute and solvent, the osmotic pressure is described by the van't Hoff equation whereby we retrieve the classic pressure of a Perfect Gas

$$p_2^{VH} = \frac{y_2}{v} r_2 T = \alpha_2 \rho_2 r_2 T = \alpha_2 p_2^{PG}, \quad (2.55)$$

with r_2 the solvent specific gas constant, p_2^{PG} the solvent pressure following an Perfect Gas EOS. The solution is said ideal in the sense the solute-solvent, solvent-solvent, and solute-solute interactions are all equivalent. Osmotic pressure in real solution is given by a power series expansion in $\frac{y_2}{v}$,

$$p_2(\zeta_2) + \Delta p_2(\zeta) = \frac{y_2}{v} r_2 T \left(1 + \sum_{n=1}^{+\infty} \frac{A_n(T) y_2^n}{v^n} \right) \quad (2.56)$$

where A_n are the virial coefficients defined in the limit of infinitely dilute solvent, whereby the unique non-ideal interactions accounted for are between a single solute particle with the solvent [McMillan and Mayer \(1945\) \[157\]](#). The mixing pressure term is thus equal to

$$\Delta p_2(\zeta) = r_2 T \sum_{n=1}^{+\infty} \frac{A_n(T) y_2^{n+1}}{v^{n+1}}. \quad (2.57)$$

Any solvent-solvent interactions should be accounted for at a phase-level, ie in the EOS chosen for the solvent phase.

We can now derive the mixing terms in the thermodynamics of the solute, using Equations (2.41),

$$\Delta e_2 = -\alpha_2 \sum_{n=1}^{+\infty} r_2 \frac{y_2^n}{n v^n} T^2 \partial_T (A_n(T)), \quad (2.58a)$$

$$\Delta s_2 = -\alpha_2 \sum_{n=1}^{+\infty} r_2 \frac{y_2^n}{n v^n} T^2 \partial_T (T A_n(T)), \quad (2.58b)$$

$$\Delta g_2 = \alpha_2 \sum_{n=1}^{+\infty} r_2 \frac{n+1}{n} \frac{y_2^n}{v^n} T A_n(T). \quad (2.58c)$$

and $\Delta e_1 = 0$, $\Delta s_1 = 0$, $\Delta g_1 = 0$. The temperature at which $A_1(T) = 0$ is called the Flory T -temperature, and represents the theoretical temperature at which an infinite molecular weight solute just precipitates from solution and a negative value of $A_1(T)$ indicates a good solvent in the sense the interactions between solute particles are repulsive, leading to a dilute solution.

In [Lhuillier \(1995\) \[135\]](#), the author proposes to include non-ideal effects in the thermodynamics of particle suspensions through the thermodynamics potential g , the free enthalpy of the mixture, by adding an unknown mixing term Δg . The extended potential leads to an extended entropy equation, into which are injected the postulated mass, momentum and energy equations of the mixture. From the second-principle of thermodynamics, the source terms of the entropy equations are closed so as to induce entropy production rate. The author proposes

the identification of a force as a osmotic pressure gradient, the osmotic pressure being defined as

$$\rho_k(1 - y_k)^2 \frac{\partial \Delta g / (1 - y_k)}{\partial (1 - y_k)}. \quad (2.59)$$

Assuming $\Delta g = y_2 \Delta g_2$, with Δg_2 given by Equation (2.58c), Equation (2.59) yields the following pressure

$$\frac{\rho_1 \alpha_2}{\rho} r_2 T \sum_{n=1}^{+\infty} \frac{A_n(T)(n+1)y_2^{n+1}}{v^{n+1}}, \quad (2.60)$$

which differs slightly from Δp_2 given by Equation (2.57). Hence we see here the interest of the present formalism. It includes non-ideal effects directly through the pressure law, which might be more adequate for physics modeling, or at least complementary, than inferring the form of the free enthalpy of a multi-fluid mixture.

2.1.7.3 MODIFICATION OF THE THERMODYNAMICS POTENTIALS

Introduced in the context of deflagration-to-detonation modeling [Baer and Nunziato \(1986\) \[5\]](#), [Bdzil et al. \(1999\) \[7\]](#), [Saurel et al. \(2003\) \[191\]](#), and then used more generally in [Gallouët et al. \(2004\) \[78\]](#), convex functions with respect to the volume fractions can be added to the phase entropies to account for phase compaction. The mixing entropy reads

$$s(\zeta) = \sum_k y_k (s_k(\zeta_k) - \varphi_k(\alpha_k)). \quad (2.61)$$

Nevertheless, so far in the literature, no explicit expressions of these functions have been proposed, except the constrain $\varphi_1(\alpha_1) = \varphi_2(\alpha_2)$ introduced in [Gallouët et al. \(2004\) \[78\]](#) to obtain a supplementary conservative equation. In [Cordesse and Massot \(2020\) \[41\]](#), new closure are proposed for these function, such as $\varphi_k = r_k \ln(\alpha_k)$, with r_k the specific gas constant of fluid k , which is identified as an ideal combinatory entropy due to spatial rearrangement of the phases in multiple configurations. In [Cordesse and Massot \(2020\) \[41\]](#), the autors have shown that such extension of the entropy questioned the classical closures of the interfacial quantities of the Baer-Nunziato model [Baer and Nunziato \(1986\) \[5\]](#), suggesting that there was an incompatibility between the model and an extended thermodynamics.

From the Gibbs equation (2.17a), we identify the partial derivative of the entropy in the variable set ξ ,

$$\partial_{(v_l y_l)}(s(\xi)) = \frac{p_l}{T_l} \implies \partial_{(v_l y_l)}(y_l s_l(\xi_l)) - \sum_k y_k (\partial_{(v_l y_l)}(\varphi_k(\alpha_k))) = \frac{p_l(\xi_l)}{T_l} + \frac{\Delta p_l(\xi)}{T_l}. \quad (2.62)$$

Recalling s_l and p_l are both 0-homogeneous, we have $y_l s_l(\xi_l) = (\xi_l)$ and $p_l(\xi_l) = p_l^o(\xi_l)$. The isolated phase Gibbs equation (2.15a) infers $\partial_{(v_l y_l)}(y_l s_l(\xi_l)) = p_l(\xi_l)/T_l$. Thus, the previous implication simplifies into

$$\partial_{(v_l y_l)}(s(\xi)) = \frac{p_l}{T_l} \implies \sum_k y_k (-\partial_{(v_l y_l)}(\varphi_k(\alpha_k))) = \frac{\alpha_k'}{v} \sum_k y_k (\varphi_k'(\alpha_k)(-1)^{k+l+1}) = \frac{\Delta p_l(\xi)}{T_l}, \quad (2.63)$$

and leads to the two pressures laws identifications

$$\frac{\Delta p_1}{T_1} = \frac{\alpha_2}{v} [y_2 \varphi'_2(\alpha_2) - y_1 \varphi'_1(\alpha_1)], \quad \frac{\Delta p_2}{T_2} = \frac{\alpha_1}{v} [y_1 \varphi'_1(\alpha_1) - y_2 \varphi'_2(\alpha_2)]. \quad (2.64a)$$

It explains why the compaction pressure has been introduced in some two-phase flow modeling such as in the Baer-Nunziato model where the granular pressure is defined as the sum of the flow pressure and a compaction pressure. Remarkably, phase compaction is not associated with any energetic phenomena since $\Delta e = 0$.

In the particular case of ideal combinatory entropies, $y_k \varphi'_k = v p_k^{PG} / T_k$. It can be seen as a strict rearrangement of the phases increasing the entropy. Such ideal combinatory entropy is found in dispersed flow whereby the inclusions can be rearranged in multiple configurations [Lhuillier et al. \(2013\) \[139\]](#). The associated pressure laws take the form

$$\frac{\Delta p_1}{T_1} = \alpha_2 \left[\frac{p_2^{PG}}{T_2} - \frac{p_1^{PG}}{T_1} \right], \quad \frac{\Delta p_2}{T_2} = \alpha_1 \left[\frac{p_1^{PG}}{T_1} - \frac{p_2^{PG}}{T_2} \right], \quad (2.65a)$$

which directly impact the momentum and energy equations of the investigated system as well as its spectrum. It does not, however change anything on the question of convexity of the entropy, which in this particular case Equation (2.61), remains non-strictly convex.

2.1.7.4 INTERFACE THERMODYNAMICS IN BUBBLY FLOW

In most two-phase flow modeling, the interfacial density area is not an independant variable with its own transport equations, thus the general Gibbs equation including interfacial density area (2.37a) fails at providing a transport equation of the entropy s since $D_t \Sigma_{k,k'}$ is not known.

Nonetheless, in a bubbly flow under given assumptions, the total derivative of the interfacial density area can be expressed in terms of derivatives of other variables of the set ζ circumventing the lack of transport equation for the interfacial density area to provide in the end the transport equation of the entropy accounting for effects related to the interfacial density area.

We first need to express the total derivative of $d(\Sigma_{1,2}v)$ in terms of total derivatives of other variables of the set ζ . In any case, if phase $k = 2$ is the mono-dispersed phase, we naturally have the relation $\Sigma_{1,2} = 3\alpha_2/R$, but depending on the flow configuration we can either assume, (A1) constant radius inclusions, (A2) a constant mass density number of inclusions, n/M , and (A3) a constant volumic density number of inclusions, n/V .

The interfacial density area and the volume fraction of the dispersed phase take the form,

$$\Sigma_{1,2} = \frac{n}{V} 4\pi R^2, \quad \alpha_2 = \frac{n}{V} \frac{4}{3} \pi R^3, \quad (2.66)$$

where n is the number of inclusions, V the volume of the mixture, R the radius of the mono-dispersed inclusions. Taking the ratio of these two equations gives

$$\Sigma_{1,2} = \frac{3}{R} \alpha_2, \quad (2.67)$$

valid without any further assumptions. In the first case, (A1), we have

$$d(\Sigma_{1,2}) = \frac{3}{R}d\alpha_2, \quad d(\Sigma_{1,2}v) = d\left(\frac{3}{R}\alpha_2v\right) = \frac{3}{R}d(v_2y_2). \quad (2.68)$$

In the second case, (A2), noticing that

$$d(\Sigma_{1,2}v) = \frac{n}{M}8\pi R dR, \quad d(\alpha_2v) = \frac{n}{M}4\pi R^2 dR, \quad (2.69)$$

we obtain

$$d(\Sigma_{1,2}v) = \frac{2}{R}d(\alpha_2v) = \frac{2}{R}d(v_2y_2). \quad (2.70)$$

Finally, in the last case, (A3), observing that

$$d(\Sigma_{1,2}) = \frac{n}{V}8\pi R dR, \quad d(\alpha_2) = \frac{n}{V}4\pi R^2 dR, \quad (2.71)$$

we obtain

$$d(\Sigma_{1,2}) = \frac{2}{R}d(\alpha_2) = \frac{2}{R}\left(\frac{\alpha_1}{v}d(v_2y_2) - \frac{\alpha_2}{v}d(v_1y_1)\right), \quad (2.72)$$

which, combined with the fact that $dv = d(v_2y_2) + d(v_1y_1)$ gives

$$d(\Sigma_{1,2}v) = \frac{1}{R}(2 + \alpha_2)d(y_2v_2) + \frac{\alpha_2}{R}d(y_1v_1). \quad (2.73)$$

Each case leads thus to a different expression relating the total derivative of the interfacial density to the other variables derivative that we summarize hereafter

$$(A1) \ d\Sigma_{1,2} = \frac{3}{R}d\alpha_2, \quad (A2) \ d(\Sigma_{1,2}v) = \frac{2}{R}d(\alpha_2v), \quad (A3) \ d\Sigma_{1,2} = \frac{2}{R}d\alpha_2, \quad (2.74)$$

which leads naturally to the following closure

$$(A1) \ d(\Sigma_{1,2}v) = \frac{3}{R}d(v_2y_2), \quad (2.75a)$$

$$(A2) \ d(\Sigma_{1,2}v) = \frac{2}{R}d(v_2y_2), \quad (2.75b)$$

$$(A3) \ d(\Sigma_{1,2}v) = \frac{1}{R}(2 + \alpha_2)d(y_2v_2) + \frac{\alpha_2}{R}d(y_1v_1). \quad (2.75c)$$

Remark 15. In the case (A3), a constant volumic density number, n/V , Equation (2.74) corresponds to the first variation of the surface applied to a spherical surface deforming only normal to its surface (see for example [Chow et al. \(2006\) \[27\]](#)).

To simplify the further derivations, we assume thermal equilibrium and two mono-species fluids. Injecting Equations (2.75a) into the Gibbs relation (2.17a) yields

$$Tds(\zeta) = de_k(\zeta) + \left(p_1(\zeta) - F_{1,2}^\Sigma \frac{\partial(\Sigma_{1,2}v)}{\partial(v_1y_1)}\right) d(v_1y_1) + \left(p_2(\zeta) - F_{1,2}^\Sigma \frac{\partial(\Sigma_{1,2}v)}{\partial(v_2y_2)}\right) d(v_2y_2) - \sum_{k=1}^2 G_k(\zeta) dy_k. \quad (2.76)$$

To make use of the preceding equations, we introduce extended quantities for the pressures

$$\tilde{p}_1(\zeta) = p_1(\zeta) - F_{1,2}^\Sigma \frac{\partial(\Sigma_{1,2}v)}{\partial(v_1y_1)}, \quad \tilde{p}_2(\zeta) = p_2(\zeta) - F_{1,2}^\Sigma \frac{\partial(\Sigma_{1,2}v)}{\partial(v_2y_2)}. \quad (2.77)$$

We now assume the two pressure laws for p_1 and p_2

$$p_1(\zeta) = p_1(\zeta_k), \quad p_2(\zeta) = p_2(\zeta_k) \quad (2.78)$$

whereby we consider no mixing effect between the two phases, as if they were non miscible and we identify the interfacial density area potential as the surface tension coefficient σ in $N.m^{-1}$, which dependencies will be discussed later on.

Equation (2.78) yields $\tilde{p}_k(\zeta) = p_k(\zeta_k) + \Delta p_k(\zeta)$ with

$$(A1) \quad \Delta p_1 = 0, \quad \Delta p_2 = -\sigma \frac{3}{R}, \quad (2.79a)$$

$$(A2) \quad \Delta p_1 = 0, \quad \Delta p_2 = -\sigma \frac{2}{R}, \quad (2.79b)$$

$$(A3) \quad \Delta p_1 = -\sigma \frac{\alpha_2}{R}, \quad \Delta p_2 = -\sigma \frac{1}{R}(2 + \alpha_2). \quad (2.79c)$$

We recognise the Laplace law in the case (A2). To integrate the pressure laws and obtain the thermodynamics variables using the definitions at thermal equilibrium Equations (2.41), we need to explicit the dependency of R with respect to the variables $v_{(k)}y_{(k)}$. For the constant density number of inclusions per unit of mass, case (A2), we define the constant $C_2 = (4\pi/3 n/M)^{1/3}$, such that

$$(A2) \quad \Delta p_1 = 0, \quad \Delta p_2 = -\sigma \frac{2C_2}{(v_2y_2)^{1/3}}. \quad (2.80a)$$

For the constant density number of inclusions per unit of volume, we introduce the constant $C_3 = (4\pi/3 n/V)^{1/3}$, such that

$$(A3) \quad \Delta p_1 = -\sigma C_3 \alpha_2^{2/3}, \quad \Delta p_2 = -\sigma C_3 (2 + \alpha_2) \alpha_2^{-1/3}. \quad (2.80b)$$

The thermodynamics quantities obtained are as follows, for (A1)

$$\Delta e_1(\zeta) = 0, \quad \Delta s_1(\zeta) = 0, \quad \Delta g_1(\zeta) = 0, \quad (2.81a)$$

$$\Delta e_2(\zeta) = \frac{3}{R} \frac{v_2}{v} \int_0^{+\infty} T^2 \frac{\tilde{\partial}}{\partial T} \left(\frac{\sigma}{T} \right) d\tau, \quad \Delta s_2(\zeta) = \frac{3}{R} \frac{v_2}{v} \int_0^{+\infty} \tilde{\partial}_T(\sigma) d\tau, \quad \Delta g_2(\zeta) = 0, \quad (2.81b)$$

and for (A2), we obtain

$$\Delta e_1(\zeta) = 0, \quad \Delta s_1(\zeta) = 0, \quad \Delta g_1(\zeta) = 0, \quad (2.82a)$$

$$\Delta e_2(\zeta) = 2C_2 \frac{v_2}{v} \int_0^{+\infty} T^2 \frac{\tilde{\partial}}{\partial T} \left(\frac{\sigma}{T} \right) (v_2y_2)^{-\frac{1}{3}} d\tau, \quad (2.82b)$$

$$\Delta s_2(\zeta) = 2C_2 \frac{v_2}{v} \int_0^{+\infty} \tilde{\partial}_T(\sigma) (v_2y_2)^{-\frac{1}{3}} d\tau, \quad (2.82c)$$

$$\Delta g_2(\zeta) = 0. \quad (2.82d)$$

and for (A3), we obtain

$$\Delta e_1(\zeta) = C_3 \alpha_2^{2/3} \frac{v_1}{v} \int_0^{+\infty} T^2 \frac{\tilde{\partial}}{\partial T} \left(\frac{\sigma}{T} \right) d\tau, \quad (2.83a)$$

$$\Delta s_1(\zeta) = C_3 \alpha_2^{2/3} \frac{v_1}{v} \int_0^{+\infty} \tilde{\partial}_T(\sigma) d\tau, \quad (2.83b)$$

$$\Delta g_1(\zeta) = 0, \quad (2.83c)$$

$$\Delta e_2(\zeta) = C_3 (2 + \alpha_2) \alpha_2^{1/3} \frac{v_2}{v} \int_0^{+\infty} T^2 \frac{\tilde{\partial}}{\partial T} \left(\frac{\sigma}{T} \right) d\tau, \quad (2.83d)$$

$$\Delta s_2(\zeta) = C_3 (2 + \alpha_2) \alpha_2^{1/3} \frac{v_2}{v} \int_0^{+\infty} \tilde{\partial}_T(\sigma) d\tau, \quad (2.83e)$$

$$\Delta g_2(\zeta) = 0. \quad (2.83f)$$

To conclude, in light of the above results, we see that the flow configuration has a significant impact on the associated thermodynamics potentials.

Discussion on the surface tension coefficient Even if it is quite common to assume the surface tension coefficient to be purely a function of the temperature T , it is in fact not the case as shown in the work of [Jamet \(\) \[111\]](#), where the author shows that $\sigma \approx (\rho_2 - \rho_1)^3$. It seems consistent with the asymptotic limit $\tau \mapsto +\infty$, corresponding to the *Perfect Gas mixture* state, where there are no more molecular interactions, thus there should be no more surface tension.

2.1.8 CONCLUSION

In the present contribution, we have proposed a formalism to build the thermodynamics of a multi-component multi-fluid mixture accounting for non-ideal effects. This thermodynamics has been conceived to equip reduced-order models obtained through an averaging process, thus relying on a threshold length scale. This theory has been motivated regarding the limitations of common approaches encountered in the literature to account for non-ideal effects. They generally consist in either modifying directly the system of equations by adding terms in the pressure law, or extending the definition of a thermodynamics potential such as the energy, the entropy or the Gibbs free energy potentially leading to some level of inconsistency between the system and the associated thermodynamics.

We first have devoted efforts to recover the property of extensivity of the mixture entropy through a well-chosen set of variables involving both bulk and geometric quantities characterizing the geometry of the interface at subscale. We have leveraged from some specific geometrical configuration of separated phases and disperse phase flow where the subscale geometry can be fully characterized in order to prove the extensivity of the entropy.

Then, by postulating a single Gibbs equation for the mixture we have inferred the entropy of the system and exhibited compatibility closures as well as symmetry conditions among the thermodynamics potentials and postulated pressure laws including non-ideal effects. The derivation of all thermodynamics potential has relied on the definition of a reference ideal state and well-chosen integration paths, leading to a natural decomposition of each thermodynamics potential, allowing to properly identify the role played by the mixing terms from the pressure law to the potentials.

Furthermore, we have underlined some of the key implications of the formalism on multi-phase flow modeling. First we have drawn a hierarchy based on three level of interaction of the fluids, from fully coupled multi-fluid mixture allowing for non-ideal effects to non-interacting multi-fluid flow where each phase is isolated from one another preventing any interaction. Secondly, we have demonstrated the fact that the formalism is sufficiently generic to add any supplementary variables to the thermodynamics, provided that the variable bears extensivity. It thus allows for instance to enrich the description of the interface, which makes it very convenient for multi-fluid flow modeling. Then, we have revisited the thermodynamics constraints employed in the framework of the Stationary Action Principle to show how the presence of non-ideal effects impact the mathematical structure and wave propagation of the resulting systems. Finally, we have shed some light on identified systems in the two-phase flow multi-fluid literature, where non-ideal effects are to be found, and to propose a unified point of view, which has the potential to alleviate the classical pitfall of lack of convexity of the standard multi-fluid models entropy, thermodynamics formalism and hyperbolicity.

Further developments would consist in trying to propose a strictly convex entropy, with the associated pressure laws, and see if it permits to symmetrize in the sense of Godunov-Mock two-phase flow systems such as the Baer-Nunziato [Cordesse and Massot \(2020\) \[41\]](#). We would also like to introduce new thermodynamics variables such as velocity fluctuations or supplementary geometric variables to propose a compatible thermodynamics to dual scale two-phase flow modeling [Cordesse et al. \(2020\) \[34\]](#) and make the link with the two very interesting papers of Lhuillier [Lhuillier \(1985\) \[136\]](#), [Lhuillier \(1995\) \[135\]](#).

APPENDIX 2.A ISOTHERMAL THERMODYNAMICS

Given a multi-fluid mixture described by the set of variable ζ , assuming thermal equilibrium, the Gibbs equation (2.37a) takes now the following form

$$Tds(\zeta) = de_k(\zeta) + \sum_{k \in \mathcal{N}_s(k)} p_k(\zeta) d(v_k y_k) - \sum_{k \in \mathcal{N}_f} \sum_{j \in \mathcal{N}_s(k)} G_{j,k}(\zeta) dy_{j,k} - \sum_{(k < k') \in \mathcal{N}_f^2} F_{k,k'}^\Sigma(\zeta) d(\Sigma_{k,k'} v).$$

The total derivative of e , in terms of ζ , reads

$$de(\zeta) = \tilde{\partial}_T(e) dT + \sum_{k \in \mathcal{N}_f} \tilde{\partial}_{v_k y_k}(e) d(v_k y_k) + \sum_{k \in \mathcal{N}_f} \sum_{j \in \mathcal{N}_s(k)} \tilde{\partial}_{y_{j,k}}(e) dy_{j,k} + \sum_{(k < k') \in \mathcal{N}_f^2} \tilde{\partial}_{\Sigma_{k,k'} v}(e) d(\Sigma_{k,k'} v).$$

Injecting it into the fundamental thermodynamics differential leads to

$$ds(\zeta) = \frac{\tilde{\partial}_T e}{T} dT + \sum_{k \in \mathcal{N}_f} \frac{p_k + \tilde{\partial}_{v_k y_k}(e)}{T} d(v_k y_k) + \sum_{k \in \mathcal{N}_f} \sum_{j \in \mathcal{N}_s(k)} \frac{\tilde{\partial}_{y_{j,k}}(e) - G_{j,k}}{T} dy_{j,k} \\ + \sum_{(k < k') \in \mathcal{N}_f^2} \frac{\tilde{\partial}_{\Sigma_{k,k'} v}(e) - F_{k,k'}^\Sigma}{T} d(\Sigma_{k,k'} v).$$

Thanks to the Euler theorem, the mixture entropy per unit of mass $s(\zeta)$ is

$$Ts(\zeta) = e(\zeta) + \sum_{k \in \mathcal{N}_f} p_k(\zeta) v_k y_k - \sum_{k \in \mathcal{N}_f} \sum_{j \in \mathcal{N}_s(k)} G_{j,k}(\zeta) y_{j,k} - \sum_{(k < k') \in \mathcal{N}_f^2} F_{k,k'}^\Sigma \Sigma_{k,k'} v,$$

with $G_{j,k}(\zeta)$ the mixture gibbs potential and $F_{k,k'}^\Sigma(\zeta)$ the interfacial density area potential defined by

$$G_{j,k}(\zeta) = \tilde{\partial}_{y_{j,k}}(e(\zeta) - Ts(\zeta)), \quad F_{k,k'}^\Sigma(\zeta) = \tilde{\partial}_{(\Sigma_{k,k'} v)}(e(\zeta) - Ts(\zeta)).$$

Furthermore, we identify the following compatibility closures

$$p_k(\zeta) = \tilde{\partial}_{v_k y_k}(Ts(\zeta) - e(\zeta)), \quad \tilde{\partial}_{v_k y_k}(e(\zeta)) = T^2 \frac{\tilde{\partial}}{\partial T} \left(\frac{p_k(\zeta)}{T} \right),$$

and a symmetry condition

$$\tilde{\partial}_{v_l y_l}(p_k(\zeta)) = \tilde{\partial}_{v_k y_k}(p_l(\zeta)).$$

APPENDIX 2.B RECOVERING THE MIXTURE ENTROPY EXTENSIVITY

2.B.1 FROM SUBSYSTEMS TO MANY FLUID

Considering a volume $\Delta V \sim \ell_p^3$ big enough to harbour a vast number of particle and small enough for an homogeneous particle population thermodynamics to be expected, the entropy S of this system writes classically

$$S(\Delta\xi) = k_B \ln(\Omega(\Delta\xi)), \quad (2.85)$$

which maximize the entropy of a system of given extensive thermodynamical variables $\Delta\xi$. When these thermodynamical variables are only known through a given probability function $p = (p_1, \dots, p_i, \dots)$ linked with the family of thermodynamical variables $\Delta_i\xi$, the extension is straight forward and leads to the expression

$$\Delta S(p) = -k_B \sum_i p_i \ln p_i + \sum_i p_i S(\Delta_i\xi), \quad (2.86)$$

which exhibit a mixing entropy added to a mean entropy. As stated in section 2.1.3, in the field of multifluid thermodynamics, the spinodal decomposition of the mixture is considered a given so each isolated fluid is modelled through its own thermodynamics, hence its own entropy functional S_k . It seems also interesting to exhibit specifically the fluid-belonging property of each thermodynamical states $\Delta_i\xi$, hence splitting the state-index i into two indexes k, j , the first being related to the fluid, the second to the thermodynamical state of the fluid. The probability function p would now be noted $p = (p_{1,1}, p_{2,1}, \dots, p_{n_f,1}, \dots)$ and the entropy of the Δ -system would be related to the entropy functional modelling each fluid

$$\Delta S(p) = -k_B \sum_{k,j} p_{k,j} \ln p_{k,j} + \sum_{k,j} p_{k,j} S_k(\Delta_{k,j}\xi). \quad (2.87)$$

The probability p_k for the system to belong to a given fluid k may also be explicitly written as

$$p_k = \sum_j p_{k,j}, \quad (2.88)$$

leading to the conditional state probability $p_{k \rightarrow j} = p_{k,j}/p_k$, and the following expression for entropy

$$\Delta S(p) = -k_B \sum_k p_k \ln p_k + \sum_k p_k \sum_j p_{k \rightarrow j} [S_k(\Delta_{k,j}\xi) - k_B \ln p_{k \rightarrow j}]. \quad (2.89)$$

The description of volume containing a vast number N_Δ of Δ volume is obtained through the proposal of a $p = (p^{(k,j)}_{n \in N_\Delta})$ describing the probability to realise the configuration $(k, j)_{n \in N_\Delta}$. For each m -indexed Δ -volume, a probability function may be recovered as

$$p_{k,j}^m = \sum_{(k,j)_{n \in N_\Delta} | (k,j)_m} p^{(k,j)}_n, \quad (2.90)$$

and the related conditional probability writes $p^{(k,j)}_{n \in N_\Delta} | (k,j)_m = p^{(k,j)}_{n \in N_\Delta} / p_{k,j}^m$. The entropy of the collection of subsystems now writes

$$S(p) = -k_B \sum_{(k,j)_{n \in N_\Delta}} p^{(k,j)}_n \ln p^{(k,j)}_n + \sum_m \sum_{k,j} p_{k,j}^m S_k(\Delta_{k,j}\xi), \quad (2.91)$$

and, in the particular case of independent Δ volume, that is to say when $p^{(k,j)}_{n \in N_\Delta} = p_{k_1, j_1} \times \dots \times p_{k_{N_\Delta}, j_{N_\Delta}}$ for a given ($p_{fluid, j}$) probability function, entropy extensivity is recovered since

$$S(p) = \sum_m \left[\sum_{k,j} p_{k,j} S_k(\Delta_{k,j} \xi) \right] - k_B \sum_m \left[\sum_{k,j} p_{k,j} \ln p_{k,j} \right] \quad (2.92a)$$

$$= N_\Delta \Delta S(p) . \quad (2.92b)$$

Introducing the fluid conditional state probability $p_{k \rightarrow j}$, then mean Δ volume state variables are independent of the specific Δ volume and obtained from whole volume average by

$$\xi_k / N_\Delta \equiv \Delta_k \xi = p_k \sum_j p_{k \rightarrow j} \Delta_{k,j} \xi , \quad (2.93a)$$

$$V_k / N_\Delta \equiv \Delta_k V = p_k \Delta V , \quad (2.93b)$$

associated with the Δ entropy

$$\Delta S(p) = -k_B \sum_k p_k \ln p_k + \sum_k p_k \sum_j p_{k \rightarrow j} [S_k(\Delta_{k,j} \xi) - k_B \ln p_{k,j}] , \quad (2.93c)$$

$$= -k_B \sum_k p_k \ln p_k + \sum_k p_k \Delta_k S(p) . \quad (2.93d)$$

Constrained entropy maximization may be performed independently on each fluid, fluid occupation p_k probability being taken as granted, and yields

$$p_{k \rightarrow j} = \exp((S_k(\Delta_{k,j} \xi) - \beta_k \cdot \Delta_{k,j} \xi) / k_B) / Z_k \quad (2.94a)$$

$$Z_k = \sum_j \exp((S_k(\Delta_{k,j} \xi) - \beta_k \cdot \Delta_{k,j} \xi) / k_B) , \quad (2.94b)$$

β_k being the vector of Lagrange multiplier with 0 on the ΔV coordinate. The mean Δ volume state variables writes

$$\Delta_k \xi = -p_k \partial_{\beta_k} \ln Z_k , \quad (2.95)$$

allowing the determination of each Lagrange multiplier. The distribution of thermodynamical states in fluid k is then centered around the state $\Delta_k \xi(\beta_k)$ defined by

$$\partial_\xi S_k(\Delta_k \xi(\beta_k)) = \beta_k , \quad (2.96)$$

for coordinates other than the ΔV one. The fluid occupation probability p_k is to be determined either by given fluid volumes V_k or by Δ entropy constrained maximization. Either way, the average $\mathcal{S}_{k,l}$ interfacial area separating fluids k and l is closely linked to the fluid occupation probabilities through the relation

$$\mathcal{S}_{k,l} \propto N_\Delta p_k p_l \Delta \Sigma , \quad (2.97)$$

the interfacial element $\Delta \Sigma$ depending of the paving of the euclidian space performed by the Δ volumes. For instance, in the case of a simple cubic Δ volume pattern, each subvolume sharing its six faces with another Δ volume, the mean $\Delta \mathcal{S}_{k,l}$ may be evaluated by

$$\Delta \mathcal{S}_{k,l} = p_k p_l 6 (\Delta V)^{2/3} . \quad (2.98)$$

This evaluation is obviously crude but still lead to mean interfacial area extensivity.

One limitation of the independant subvolume hypothesis is that the interfacial interface $\mathcal{S}_{k,l}$ is then directly linked with the fluid occupation probabilities p_k and hence to the volume fractions α_k . This major drawback is to be overturned by considering spatially correlated subvolume probabilities. The main difficulty is then to preserve entropy extensivity which requires finite range spatial correlation as illustrated in the following simplified example.

Considering a maximal correlation range ΔN , the probability p may be formally split as

$$p_{(k,j)_{n \in N_\Delta}} = \sum_{\Delta N} p_{\Delta N} \left[p_{(k,j)_{n \in \Delta N_1}} \times \cdots \times p_{(k,j)_{n \in \Delta N_{N_\Delta/\Delta N}}} \right], \quad (2.99)$$

where $p_{\Delta N} = 1/\Delta N$ is the position probability of the ΔN pattern grid, $p_{(k,j)_{n \in \Delta N}}$ is the pattern probability function and periodicity is assumed. Entropy now writes

$$S(p) = k_B \ln \Delta N - k_B N_\Delta / \Delta N \sum_{(k,j)_{n \in \Delta N}} p_{(k,j)_n} \ln p_{(k,j)_n} + N_\Delta / \Delta N \sum_m \sum_{k,j} p_{k,j}^m S_k(\Delta_{k,j}\xi), \quad (2.100)$$

where $p_{k,j}^m = p_{(k,j)_{n \in \Delta N}} / p_{(k,j)_{n \in \Delta N} | (k,j)_m}$ is the probability of the m -indexed subvolume of the pattern to bear a $\Delta_{k,j}\xi$ thermodynamical state and extensivity is recovered for $\Delta N \ll N_\Delta$. It should be noted that the independant subvolume assumption described above correspond to the limit case $\Delta N = 1$. A formal derivation for a gliding correlation pattern is yet to be developed, but it is expected that the condition stated on the pattern range will still be needed to recover extensivity.

To be more specific about what may be understood as a $p_{(k,j)_{n \in \Delta N}}$ pattern, it may be represented as a family of configurational Dirach function $\delta_c \left((k,j)_{n \in \Delta N} = X_c \in (\mathcal{N}_f, \mathbb{N})^{\Delta N} \right)$ describing for instances droplets, flat interfaces, inclusions of specific shape, even homogeneous states, ponderated by the probability of occurence p_c

$$p_{(k,j)_{n \in \Delta N}} = \sum_c p_c \delta_c. \quad (2.101)$$

The mean interfacial area is then no longer solely linked to the volume fractions, since, introducing $\mathcal{S}_{k,l,c}$ and $V_{k,c}$ respectively the k, l - interfacial area and k -fluid volume of pattern c , we have the following relations

$$\mathcal{S}_{k,l} = N_\Delta / \Delta N \sum_c p_c \mathcal{S}_{k,l,c}, \quad (2.102a)$$

$$V_k = N_\Delta / \Delta N \sum_c p_c V_{k,c}, \quad (2.102b)$$

so that the knowledge of the independent variables $\mathcal{S}_{k,l}$ and V_k brings information on the pattern probability function through the configuration probability occurrence p_c . The latter begin true when other configuration specific variables are considered.

It must be underlined here that the pattern probability function $p_{(k,j)_{n \in \Delta N}}$ does not need to be unique on the whole volume to insure entropy extensivity, since extensivity may be recovered on lower dimensional manifolds complying with the periodical condition compatible

with the different zone where different pattern probability function applies. More explicitly, if a given x -axis is chosen such that for n -indexed subvolumes below a given x coordinate, a $p_{(k,j)n \in \Delta N}^-$ applies and $p_{(k,j)n \in \Delta N}^+$ applies for n -indexed subvolumes above this coordinate, extensivity of entropy may still be recovered considering y, z extension of the system volume. Figures 2.3 and 2.4 illustrate these different cases.

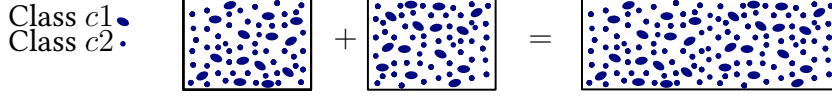


FIGURE 2.3: Illustration of the entropy extensivity in an unique pattern configuration.

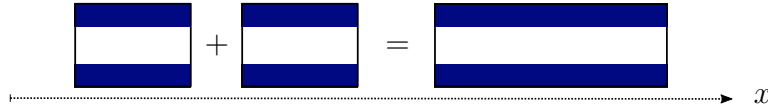


FIGURE 2.4: Illustration of the entropy extensivity in low-dimensional configurations.

2.B.2 FROM MANY FLUID TO MULTI FLUID

In order to regain the conciseness of a multifluid formulation, an expression of entropy as a function of a few fluid-specific thermodynamical variable is needed. To obtain such an expression, a Taylor extension of the homogenous fluid entropy function S_k is introduced in expression (2.100). Considering the $p_{(k,j)n \in \Delta N}$ pattern probability function and the related $p_{k,j}^m$ state probabilities, the macroscopic mean state variables writes

$$\xi_k = N_{\Delta}/\Delta N \sum_m \sum_{k,j} p_{k,j}^m \Delta_{k,j} \xi, \quad (2.103a)$$

$$V_k = N_{\Delta}/\Delta N \sum_m \sum_{k,j} p_{k,j}^m \Delta V. \quad (2.103b)$$

Introducing ξ_k^a the a order central moment of the $\Delta_{k,j} \xi$ random variable

$$\xi_k^a = \sum_m \sum_{k,j} p_{k,j}^m \otimes^a (\Delta_{k,j} \xi - \xi_k \Delta V/V_k), \quad (2.104)$$

the expansion of the ξ_k 1-homogeneous fluid model entropy function S_k in expression (2.100) lead to the following formulation

$$S(p) = \sum_k S_k(\xi_k) + N_{\Delta} \Delta V / \Delta N \sum_k \sum_{a>1} \frac{1}{a!} \partial_{\xi^a} S_k(\xi_k/V_k) : \xi_k^a - k_B N_{\Delta} / \Delta N \sum_{(k,j)n \in \Delta n} p_{(k,j)n} \ln p_{(k,j)n} \quad (2.105a)$$

$$S(p) = S^{\text{hom}} + S^{\text{het}}(p) + S^{\text{mix}}(p). \quad (2.105b)$$

The entropy of the mixture of fluids may thus be divided into three separated contributions, the first being the entropy of homogeneous fluid juxtaposition S^{hom}

$$S^{\text{hom}} = \sum_k S_k(\xi_k), \quad (2.106)$$

which depend solely of the mean thermodynamical states ξ_k . Thanks to the central limit theorems, these mean states are almost certain in the thermodynamical limit $\Delta N \ll N_\Delta$, so the formal dependance with respect to p may be dropped. The second contribution S^{het} takes into account for each fluid the heterogeneity of each pattern or each c configuration. This contribution writes

$$S^{\text{het}}(p) = N_\Delta \Delta V / \Delta N \sum_k \sum_{a>1} \frac{1}{a!} \partial_{\xi_k^a} S_k(\xi_k / V_k) : \xi_k^a, \quad (2.107)$$

and may be divided into fluid contributions. The third contribution S^{mix} does not depends of fluid modelisation and resumes to

$$S^{\text{mix}}(p) = -k_B N_\Delta / \Delta N \sum_{(k,j)_{n \in \Delta_n}} p_{(k,j)_n} \ln p_{(k,j)_n}. \quad (2.108)$$

Generally, this contribution is not related to any of the fluid, but when the pattern probability function reflect fluid specific configurations, for instance droplets of different sizes of a specific fluid into another, it may be attributed to this specific fluid.

Dealing with pattern probability function is not satisfactory from a modelling point of view and in the following these entropy and entropy contribution will be approximated by entropy fonctionnal of fluid variables.

DERIVATION OF TWO-SCALE KINEMATICS AND CAPILLARY TWO-PHASE FLOW MODEL TO DESCRIBE THE INTERFACE DYNAMICS

3

In this [Chapter 3](#), relying on a probability density function, we depart from a geometric approach of the interface and propose a multi-scale rendering of the interface without any postulate on its location nor its shape. This novel multi-scale modelling tool is thus not relying on any two-phase flow topology assumption and seems to bridge the diverse approaches, in particular diffuse and sharp interface models, to describe multi-fluid flow.

From the pdf, we recover classic geometric variables as well as a natural decomposition into a filtered and fluctuating contributions. Based on these quantities, we extend the definition of the Lagrangian describing the barotropic two-phase flow medium adding dual-scale kinetic and potential contributions to account for small-scale kinematics and surface tension. The Stationary Action Principle returns a system of PDE showing a coupling between large and small scales.

One small-scale modelling is detailed in the core of the Chapter, another is detailed in the ESAIM proceeding attached in the Appendix section. The former models pulsating inclusions, the latter oscillating inclusions. Two subsequent systems are obtained using barotropic fluids. Further extension to a two-parameter equation of state is proposed for the first model to account for compressible and thermal effect of the flow.

Turbulence is of major importance in interface modelling, since speed fluctuations contribute directly to the surface deformation. Since it is already hard enough to tackle in the simplified case of isolated inclusions, full two-way coupling of the carrier phase and the dispersed phase are still current reasearch area. In all our study, we discard turbulence, but it could naturally be added to the present accounted effects.

This Chapter is the results of three proceedings, [Cordesse et al. \(2020\) \[37\]](#), [Cordesse et al. \(2019\) \[40\]](#), [Cordesse et al. \(2019\) \[33\]](#) and an article [Cordesse et al. \(2020\) \[34\]](#) submitted to the *International Journal of Multiphase Flow*.

3.1	Review of surface description in two-phase flow modelling	141
3.1.1	What is a two-phase flow interface ?	141
3.1.2	Review of existing modelling approach of a two-phase interface	141
3.1.3	Review of existing models based on a surface approach of the interface	142
3.1.3.1	Interface tracking or capturing models	143
3.1.3.2	Diffuse interface models	143

	3.1.3.3	Surface density function	144
	3.1.3.4	Dispersed flow	145
	3.1.3.5	Mean and Gauss curvatures	145
	3.1.3.6	Interfacial closures	146
	3.1.3.7	Scale separation	146
	3.1.4	Going somewhere else with diffuse interface models	147
3.2		Two-scale description of an interface by means of a pdf	148
	3.2.1	Definition of the pdf	148
	3.2.2	Interfacial area density	148
	3.2.3	Two-scale interface description	149
3.3		Deriving a two-scale two-phase interface model	151
	3.3.1	Two-phase medium kinetic energy	151
	3.3.2	Two-phase medium interfacial energy	152
	3.3.3	Lagrangian energy of the two-phase system	152
	3.3.4	Hamilton's stationnary action principle	152
	3.3.5	Final form of the system	155
	3.3.6	Dissipation	156
	3.3.7	A hierarchy of models	157
3.4		Extending the two-scale two-phase interface model to a complete EOS	159
	3.4.1	Stationary Action principle	159
	3.4.2	Final form of the system	162
	3.4.3	Dissipation	163
		Appendices	165
3.A		Normal perturbation of a regular closed surface	165
3.B		A diffuse interface approach for disperse two-phase flows involving dual-scale kinematics of droplet deformation based on geometrical variables	166
	3.B.1	Oscillating inclusion subscale modelling	168
		3.B.1.1 Oscillating inclusion literature review	168
		3.B.1.2 Analytical energy balance of an isolated oscillating inclusion	168
		3.B.1.3 Direct Numerical Simulation Comparison and Validation	170
	3.B.2	Two-scale kinematics Two-phase flow model	173
		3.B.2.1 Hypotheses related to the small scale kinematics	174
		3.B.2.2 Lagrangian energy of the two-phase system	175
		3.B.2.3 Extremization of the action	176
		3.B.2.4 Companion Conservation Equation	177
		3.B.2.5 Final system	177
		3.B.2.6 Dissipation	178
		3.B.2.7 Properties of the system	180
	3.B.3	Conclusion	180
	3.B.4	Appendices	181
		3.B.4.1 Energy analytical calculation of a deformed droplet	181
		3.B.4.2 Approximation of the droplet deformation	181
		3.B.4.3 Kinetic energy	183
		3.B.4.4 Potential energy	185
		3.B.4.5 Mean curvature	186

3.1 REVIEW OF SURFACE DESCRIPTION IN TWO-PHASE FLOW MODELLING

3.1.1 WHAT IS A TWO-PHASE FLOW INTERFACE ?

The main difficulty of two-phase flow modelling with respect to single-phase flow modelling lies in the presence of an interface, whose definition is not clear but impacts significantly the final model. For instance, let us consider a liquid droplet in atmospheric air on a solid wall as depicted on [Figure 3.1](#). The meniscus caused by surface tension observed at macro-

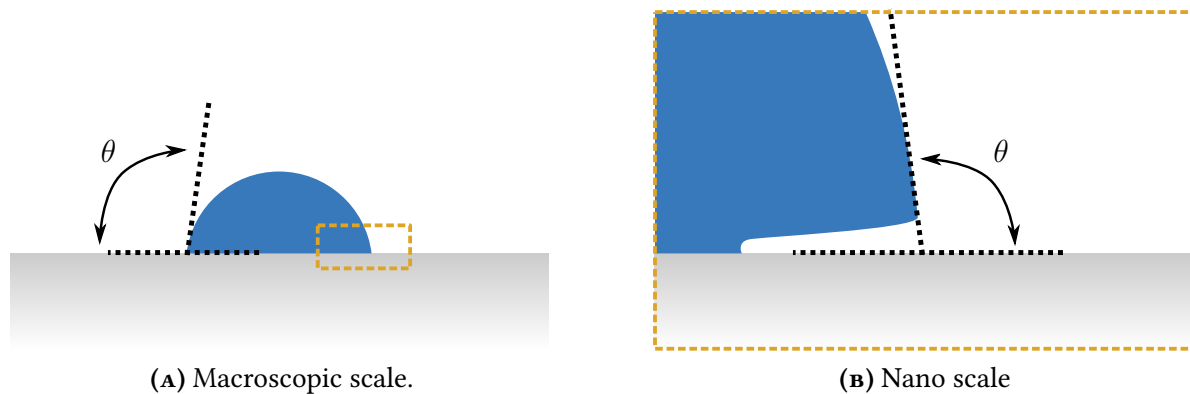


FIGURE 3.1: Meniscus of a partial wetting droplet on a wall observed on two different length scales, with θ the contact angle.

scopic scale [Figure 3.1a](#) takes a very different aspect when zooming at a nano scale [Figure 3.1b](#) [Jawurek \(1969\) \[113\]](#), [Kim and Buongiorno \(2011\) \[119\]](#), [Guion et al. \(2018\) \[99\]](#). This simple example depicts the scale dependency of an interface representation.

3.1.2 REVIEW OF EXISTING MODELLING APPROACH OF A TWO-PHASE INTERFACE

Although it seems unclear how to mathematically define a two-phase interface, many approaches have been proposed in the literature which split between kinetics and continuum mechanics modelling and various length scales at which the interface is described.

In a kinetic approach, the length scale at which we observe the interface is a few Angstrom, allowing to distinguish each molecule. The two-phase flow is described by three regions, two homogeneous regions and one heterogeneous region, in which strong variation in terms of species concentration locate the interfacial region (see [Frenkel \(1946\) \[72\]](#) for instance).

Continuum mechanics approach relies a continuous description of fluids, the smallest element being a fluid particle, large compared to the mean free path but small with respect to any characteristic macroscopic length scale of the flow. Fluid particles gather a large amount of molecules allowing for a statistical treatment of the parcel. In this framework, several interface representation are proposed. We will illustrate the main conceptual differences relying on one simple two-phase flow example, water flowing in an open canal. From a macroscopic point of view, we genuinely visualize a water-air interface.

- Full-spectrum single fluid approach: retaining the continuum mechanics assumption, we can zoom on the water-air interface, up to the characteristic length scale of a particle fluid, which corresponds to a few Angstroms. At this scale, we can again model the two-phase flow as a single multi-component multi-phase flow, with transient zones where the concentration changes drastically from water to air. This has led to the development of thermodynamics accounting for phase transition through the Van der Waals equation of state [Van der Waals \(1894\) \[215\]](#) and extended through the inclusion of the gradients of composition quantities as thermodynamics internal variables to describe capillary effects [Korteweg, D.J. \(1901\) \[121\]](#), [Cahn and Hilliard \(1958\) \[16\]](#). Some examples of these models can be found in [Gouin \(1987\) \[92\]](#), [Jamet et al. \(2001\) \[112\]](#).
- Using a discontinuous approach employed by DNS: if we zoom out from the water-air interface, the interface will appear as a sharp discontinuity separating two fluids, air and water. It has led to assume the interface as a surface separating two fluids, which is the underlying assumption of all DNS. The two fluids do not coexist, each of them is a pure single, potentially multi-species, fluid. We will refer this approach as *sharp DNS* see for instance [Glimm et al. \(1998\) \[88\]](#), [Tryggvason et al. \(2001\) \[213\]](#). Nevertheless, as treating a discontinuity may result in mathematical difficulties, the sharp interface has been artificially spread, bringing on phase field models such as in [Lamorgese et al. \(2011\) \[126\]](#). We emphasize that this artificial thickness of the interface seen as a surface separating two fluids is by nature different from the spreading resulting from the previous microscopic approaches either in a kinetic or a continuum framework.
- Using an averaging process: if we apply an averaging statistical treatment on the water-air two-phase flow, we lose the notion of a sharp discontinuity separating two fluids, both fluids coexist everywhere instead. We obtain a mixing of fluids, which is usually referred as a multi-fluid. The notion of interface is then retrieved by looking at the volume fraction variable, α_k , whose strong variation may be interpreted as the interface locus. The Baer-Nunziato models and all the hierarchy of diffuse interface models introduced in [Chapter 1](#) belong to this category of models, see [Ishii \(1975\) \[110\]](#), [Drew \(1983\) \[57\]](#), [Baer and Nunziato \(1986\) \[5\]](#). The ambiguity of these models lies in the fact that the interface is still initially considered as a discontinuity described by $X_k(\mathbf{x}, t)$ the compact support phase function (see [Section 1.1.1](#)). Again the spreading of the interface due to the averaging process is strictly different in nature to the artificial spreading of some DNS approaches or of the previous models.

Remark 16. *In this thesis, the term diffuse interface model refers to the multi-fluids models obtained from an averaging process. We underline they are no established nomenclature to identify each of the introduced models, leading sometimes to confusion. A synthesis of the methods is proposed in [Prosperetti and Tryggvason \(2007\) \[179\]](#) for instance.*

3.1.3 REVIEW OF EXISTING MODELS BASED ON A SURFACE APPROACH OF THE INTERFACE

We propose to review briefly the exhaustive work proposed in the literature for the models introduced herein before, which rely on the strong conceptual assumption that an interface is a surface. We consider thus only DNS and averaging models and see how the interface is solved. We will pay attention to distinguish the models from the numerical methods employed, but models and numerical methods are often intertwined with each other.

3.1.3.1 INTERFACE TRACKING OR CAPTURING MODELS

DNS relies on models that solve precisely the interface locus by either tracking its position from its initial position during the whole time simulation or capturing and then reconstructing its position at all time by transporting an indicator function. We refer them as *tracking* and *capturing methods*.

The *tracking methods* propose an explicit representation of the interface, either with a deforming mesh molding the interface or in a Lagrangian way with tracking marker particles on the interface, originated as the so called Marker and Cell (MAC) method [Harlow and Welch \(1965\)](#) [102]. Several variants based on moving/stationary dual/single meshes have then appeared like the Front-Tracking method [Tryggvason et al. \(2001\)](#) [213] where the unsteady Navier–Stokes equations are solved on a fixed grid and the interface is tracked explicitly by connected marker points. One of the major drawbacks of these methods is the mass conservation issues and the remeshing or tracker remapping any time the interface deforms significantly.

Capturing methods are distributed in two main classes, the *Volume of Fluid* (VOF) and the *Level Set*, both implicitly representing the interface through an advected marker function. *Level Set method*, introduced in [Osher and Sethian \(1988\)](#) [169], is based on the convection of a distance function, whose zero determines the interface location. It naturally offers an accurate representation of the normal of the interface and its curvature, since both stem from the gradient of the distance function defined everywhere in the flow. *VOF methods* [Hirt and Nichols \(1981\)](#) [108] capture the interface through the transport of the liquid volume fraction, whose sharp variations from 0 to 1 locates precisely the interface. The major difference with VOF method lays thus in the smooth variation of the Level Set function across the interface, increasing its robustness. Nevertheless Level Set does not intrinsically ensure mass conservation, lacking a discrete mass conservation equation, even if techniques have made improvement on this point by modifying the definition of the level set function. On the contrary, *VOF methods* guaranty the mass conservation since it provides a discrete mass conservation equation. The interface is then obtained through a geometric reconstruction with originally a Simple Line Interface Calculation (SLIC) [Noh and Woodward \(1976\)](#) [166] replaced later by a Piecewise Linear Interface Calculation (PLIC) technique [Debar \(1974\)](#) [46]. Several coupling methods emerged to combine advantages of both methods such as the Coupled Level Set VOF (CLSVOF) [Sussman and Puckett \(2000\)](#) [206].

While these methods of surface capturing method have been employed primitively with one-phase incompressible Navier-Stokes equations for DNS, there are extended to model compressible two-phase flow [Kuila et al. \(2015\)](#) [123], [Duret et al. \(2018\)](#) [63], as already mentioned in the general introduction of the thesis.

3.1.3.2 DIFFUSE INTERFACE MODELS

Concerning *diffuse interface models*, while they offer a hierarchy of models with respect to the level of thermodynamical and hydrodynamical equilibrium among the phases, they provide a poor description of the interface dynamics, limited to the transport of a volume fraction of one phase indicating the volume ratio of the phases in each computational cells. In separated phase, the gradient of the volume fraction is a good indicator of the normal to the interface and thus of the local curvature. Nonetheless, as soon as sub-scale surface phenomena occur, the volume fraction prediction smooths out all the details of the flow and its gradient can no longer

provide meaningful information regarding the topology of the interface. It has stimulated the inclusion of supplementary geometric variables in multi-fluid flow models.

3.1.3.3 SURFACE DENSITY FUNCTION

The first supplementary variable to be solved in the flow was the surface density function, which is easily conceivable when the interface is seen as a surface.

Early conceptual definitions of the surface density function were introduced in turbulent single phase flows as in the work of Marble and Broadwell (1977) [151], where he defined an Eulerian fluid variable $\Sigma(\mathbf{x}, t)$ specifying the flame surface area per unit volume, together with an empirical transport equation

$$D_t \Sigma = \text{Sc} \nabla \cdot (D \nabla \Sigma) + \epsilon \Sigma - \left(\sum_j \frac{V_{j,D}}{\alpha_j} \right), \quad (3.1)$$

with $V_{j,D}$ the volume consumption rate of fuel species j by unit flame area, D turbulent diffusivity, ϵ local scalar mean strain rate and Sc Schmidt number. The material derivative of the surface density function is thus the sum of the turbulent diffusion, the increase of flame density by local strain rate of the mean motion and the flame shortening mechanism in which adjacent flame can annihilate each other.

Pope (1988) [174] first developed a probabilistic description of the surface properties. In particular, he introduced a mathematical expression of the geometric quantities, such as the expected surface density area defined as

$$\Sigma(\mathbf{x}, t) = \langle \Sigma'(\mathbf{x}, t) \rangle \quad (3.2)$$

with $\langle \bullet \rangle$ the surface average operator. The quantity $\Sigma'(\mathbf{x}, t)$, called the fine-grained surface-to-volume ratio, is defined by

$$\Sigma'(\mathbf{x}, t) = \int_{S(u,v)} \delta(\mathbf{x} - \mathbf{X}(u, v, t)) |\partial_u \mathbf{X} \times \partial_v \mathbf{X}| du dv, \quad (3.3)$$

where \mathbf{X} is the surface point coordinates with u, v local coordinates parametrizing the surface, and $A = |\partial_u \mathbf{X} \times \partial_v \mathbf{X}|$ is the local surface area. Then, he introduced the surface density function defined by

$$f(\mathbf{x}, t, \varphi) = \int_{S(u,v)} \langle G \rangle du dv, \quad (3.4)$$

with the distribution $G(\mathbf{x}, t, u, v, \varphi) = \delta(\varphi' - \varphi(t, u, v)) \delta(\mathbf{x} - \mathbf{X}(t, u, v)) A(u, v)$ where φ is any surface quantity. Finally, through the postulation of a transport equation for f , he derived a transport equation for Σ , which takes the form

$$\partial_t \Sigma + \nabla \cdot (\mathbf{v}_s \Sigma) = \epsilon \Sigma, \quad (3.5)$$

where \mathbf{v}_s is the surface mean velocity and ϵ the surface mean stretching rate, both to be modelled.

Following this pioneering work, several models for the flame surface density have been devised for reactive single phase flow, focusing on the definition of the stretching rate, for

example for turbulent premixed combustion [Cant et al. \(1991\) \[18\]](#), or more general derivation for combustion purposes in [Candel and Poinso \(1990\) \[17\]](#).

In the two-phase flow community, the surface density area has been introduced in the framework of ensemble averaging of an indicator function in [Kataoka et al. \(1986\) \[117\]](#). Given a function φ , if the zero of this function locates the two-phase flow interface, $\varphi(t, \mathbf{x}) = 0$, then the local instant interfacial area concentration is given by

$$\Sigma(t, \mathbf{x}) = \langle \|\nabla\varphi(t, \mathbf{x})\| \delta(\varphi(t, \mathbf{x})) \rangle, \quad (3.6)$$

or equivalently, using the indicator function X_k introduced in [Chapter 1](#) for two-phase flow averaging,

$$\Sigma(t, \mathbf{x}) = \langle \|\nabla X_k(t, \mathbf{x})\| \rangle. \quad (3.7)$$

Both definition are shown to be equivalent by defining $X_1 = \mathcal{H}(\varphi(t, \mathbf{x}))$ for instance. A transport equation has been derived later on in [Drew \(1990\) \[56\]](#) and takes the form

$$\partial_t \Sigma + \nabla \cdot (\langle \mathbf{v}_I \rangle \Sigma) = \langle \mathbf{v}_I H \nabla X_k \cdot \mathbf{n}_k \rangle \quad (3.8)$$

with a new definition of the average interfacial velocity $\langle \mathbf{v}_I \rangle = \langle \mathbf{v}_I \nabla X_k \cdot \mathbf{n}_k \rangle / \Sigma$. For dispersed two-phase flow, the instantaneous local interfacial area concentration can be specialized in

$$\Sigma(t, \mathbf{x}) = \sum_{\alpha=1, N} \langle \delta(\|\mathbf{x} - \mathbf{r}_\alpha\| - \Sigma_\alpha) \rangle, \quad (3.9)$$

where \mathbf{r}_α is the radial vector of the inclusion α , N the total number of inclusions, and Σ_α the surface density area of inclusion α . Interestingly, in [Equation \(3.6\)](#) we sum the interfacial area contained in a given volume, whereas in [Equation \(3.9\)](#), the surface of all particles whose center is in the given volume is summed up. These two approaches are found compatible in [Lhuillier et al. \(2000\) \[137\]](#).

3.1.3.4 DISPERSED FLOW

For dispersed flow, the instantaneous local interfacial area concentration is also introduced as a particular moment of the distribution function of the particles,

$$\Sigma(t, \mathbf{x}) = \int_{\xi \in \Omega} A(\xi) f(t, \mathbf{x}, \xi) d\xi \quad (3.10)$$

with ξ the phase vector function of some geometrical properties such as diameter or curvatures. The interface is thus defined as the total surface of a collection of objets. A review of these different approaches can be found in [Delhaye \(2001\) \[48\]](#) and more recently in [Morel \(2015\) \[162\]](#).

3.1.3.5 MEAN AND GAUSS CURVATURES

In [Drew \(1990\) \[56\]](#), the author supplemented the description of the interface by equations on the mean Gauss $\langle G \rangle$ and mean Mean curvature, $\langle H \rangle$, added at the top of the surface area evolution equation [\(3.8\)](#). They read

$$\begin{aligned} \partial_t (\langle H \rangle \Sigma) + \nabla \cdot (\langle \mathbf{v}_I \rangle \langle H \rangle \Sigma) = & - \nabla \cdot (\langle \mathbf{v}_I - \langle \mathbf{v}_I \rangle \rangle H \nabla X_k \cdot \mathbf{n}_k) \\ & - (\langle H \rangle^2 - \langle G \rangle) \langle \mathbf{v}_I \nabla X_k \cdot \mathbf{n}_k \rangle + \Sigma \mathbf{S}_H \end{aligned} \quad (3.11a)$$

$$\begin{aligned} \partial_t(\langle G \rangle \Sigma) + \nabla \cdot (\langle \mathbf{v}_I \rangle \langle G \rangle \Sigma) = & - \nabla \cdot (\langle \mathbf{v}_I - \langle \mathbf{v}_I \rangle \rangle G \nabla X_k \cdot \mathbf{n}_k) \\ & - \langle H \rangle \langle G \rangle \langle \mathbf{v}_I \nabla X_k \cdot \mathbf{n}_k \rangle / \Sigma + \Sigma \mathbf{S}_G \end{aligned} \quad (3.11b)$$

where \mathbf{S}_H and \mathbf{S}_G are the sources terms of the related quantities, to be modelled. We notice the presence of the fluctuating interfacial velocity, $\mathbf{v}_I - \langle \mathbf{v}_I \rangle$, also found in the source terms \mathbf{S}_H and \mathbf{S}_G suggesting to either close or transport this quantity, thus the need of turbulence modelling.

Recently in [Essadki et al. \(2019\) \[67\]](#), a Surface Density Function (SDF) is introduced within a phase space composed of the mean and Gauss curvatures and the interfacial velocity. Doing so, the authors finally link the statistics of a local description of the interface through geometrical variables with the SDF and the statistical description of isolated objects through the classical number density function (NDF) in the appropriate phase space. In particular, in the case of dispersed phase flows, fractional moments of a NDF returns the same geometrical quantities as the SDF moments used to describe the polydispersity of the droplets [Essadki et al. \(2016\) \[66\]](#), [Essadki et al. \(2018\) \[68\]](#).

3.1.3.6 INTERFACIAL CLOSURES

The transport equations of the geometric quantities contain many unclosed terms. In particular, there is the averaged interfacial velocity $\langle \mathbf{v}_I \rangle$ for which we already have seen some closure in [Chapter 1](#). Then, the fluctuating interfacial velocity is of great importance and implies the need of turbulence modelling.

3.1.3.7 SCALE SEPARATION

Since complex two-phase flow such as atomization process involve a large spectrum of length scale and DNS are still unreachable for industrial application, reduced-order models offering accurate description of all scales phenomena are very appealing.

For single phase flow, the scale separation is related to the velocity fluctuation amplitudes. Given a characteristic length scale, RANS techniques model entirely the turbulent scales below this reference length. Large Eddy simulations (LES) at least rely on a cascade process to infer the sub-grid dynamics of the flow from the resolved scale down to the Kolmogorov scale of the flow, under which all the turbulent kinetic energy is dissipated into heat. Thus, they outperform RANS.

For two-phase flow, RANS and LES are not directly applicable since velocity fluctuations are compounded by interface fluctuations and both phenomena interact. Furthermore, there are no smallest length scale for interfacial fluctuations, which would dictate dissipation, such as the Kolmogorov scale for turbulence. Indeed, the interface thickness can tend towards zero when a ligament stretches for instance.

RANS and LES have thus been adapted to two-phase flow turbulence modelling relying on a single characteristic separation length scale for both velocity and interfacial fluctuations. It implies to model the sub-scale turbulence, the sub-scale interfacial fluctuations and the dissipation as well as terms accounting for the two-way coupling of these phenomena. An exhaustive list of models and their comparisons can be found in [Klein et al. \(2019\) \[120\]](#). They all rely on filtered single-fluid conservation equations combined with a VOF or Level-Set method. We detail hereafter some of them.

The Volume Averaged-VOF (VA-VOF) method [Wörner et al. \(2001\) \[222\]](#) proposes a local algebraic model for the relative velocity to represent the influence of velocity fluctuations close to the interface. Then, the LES Large Eddy and Interface Simulation (LEIS) [Liovic and Lakehal \(2012\) \[141\]](#) adds a closure of the sub-scale surface tension term.

In the Interfaces and Subgrid Scales (ISS) model [Toutant et al. \(2008\) \[211\]](#), the interface geometry is fully resolved through a combined Front-Tracking and VOF methods and the unresolved scales of the two-way coupling phenomena between interfaces and turbulence are integrated into subgrid models. Furthermore, the Sub-Grid Surface Dynamics (SGSD) [Herrmann \(2013\) \[106\]](#) solves on an auxiliary refined grid, the sub-grid dynamics of the interface using a refined level set. It allows for an exact closure of the unclosed surface tension force term in the Navier–Stokes equations by explicitly filtering the fully resolved immiscible interface. Numerically, a refined Local Surface Grid approach is used, which solves the advection equation of a level set on a highly resolved mesh using a dual narrow-band approach, while the Navier-Stokes equations are solved on a coarser mesh. In [Herrmann \(2015\) \[107\]](#), the model is expanded to include the effects of sub-filter turbulent velocity fluctuations.

3.1.4 GOING SOMEWHERE ELSE WITH DIFFUSE INTERFACE MODELS

Dual-scale approaches for two-phase flow introduced in the previous paragraph are attached to a sharp representation of the interface. Hence such approach are not directly applicable to the diffuse interface models, whereby the representation of the interface is diffused. Recent advances are based on supplementary evolution equations of large and small scale interfacial density areas proposed in the work of [M Devassy et al. \(2015\) \[148\]](#). This approach is very appealing, but no mathematical formalism allowing for solid and consistent interface scale separation exists.

3.2 TWO-SCALE DESCRIPTION OF AN INTERFACE BY MEANS OF A PDF

Two-scale description of the interface are yet specialized to the way the interface is described, and previous review has shown progress mainly for methods relying on a local instantaneous geometric representation of the interface, where fluids are separated by sharp surfaces. Nevertheless this approach seems restrictive and does not apply to diffuse interface models.

3.2.1 DEFINITION OF THE PDF

We propose here to depart from the above lines by proposing a direct definition of the two-phase interface that does not rely on the filtering of an instantaneous model. We suppose given a Probability Density Function (PDF) f as follows

$$f : (\mathbf{x}', t', \varphi', H') \in \mathbb{R}^d \times [0, +\infty) \times \mathbb{R} \times \mathbb{R} \mapsto f \in [0, 1], \quad (3.12)$$

such that $f(\mathbf{x}', t', \varphi', H') d\mathbf{x}' dt' d\varphi' dH'$ the probability that at the space-time location (\mathbf{x}', t') , the two-phase interface can be described by a level set function that takes the value φ' and that the mean curvature field has the value H' . When $\varphi' > 0$ (resp. $\varphi' < 0$) we will consider that the fluid is the component $k = 1$ (res. $k = 0$). In our representation, The PDF f contains all the information that describes the two-phase interface. In this sense, the two-phase interface is an object that can be characterized through geometrical informations with a certain amount of reliability instead of averaged surfaces.

We can now define the following geometric fields

$$\varphi(\mathbf{x}, t) = \int \varphi' f(\mathbf{x}, t, \varphi', H') d\varphi' dH', \quad (3.13)$$

$$H(\mathbf{x}, t) = \int H' f(\mathbf{x}, t, \varphi', H') d\varphi' dH'. \quad (3.14)$$

The field φ can be considered as a "most probable level set" function that can be associated with the two-phase interface. It yields the definition of a surface $\{\varphi = 0\}$ that can be considered as the "most probable surface" that characterizes the two-phase interface. Following the same lines, $H(\mathbf{x}, t)$ is the most probable value of the mean curvature at (\mathbf{x}, t) for the two-phase interface.

Thanks to f we can also propose a definition for fields that are common in the literature to characterize a two-phase medium: we can define a field α as follows

$$\alpha(\mathbf{x}, t) = \int_{\varphi' > 0} f(\mathbf{x}, t, \varphi', H') d\varphi' dH', \quad (3.15)$$

where α is consistent with the average probability that the fluid 1 is present at (\mathbf{x}, t) . For the sake of consistency with the standard terms, we shall also (abusively) refer to α as a volume fraction or a void fraction.

3.2.2 INTERFACIAL AREA DENSITY

Now consider a characteristic length $\ell > 0$ and a family of mollifier functions θ_ℓ , if we note $\mathcal{B}_\ell(\mathbf{x}) = \{\mathbf{x}' \in \mathbb{R}^d / |\mathbf{x}' - \mathbf{x}| < \ell\}$, then we can define the density of interfacial area Σ by

$$\Sigma(\mathbf{x}, t) = \int_{\varphi' > 0} H' f(\mathbf{x}', t, \varphi', H') \theta_\ell(\mathbf{x} - \mathbf{x}') d\mathbf{x}' d\varphi' dH'. \quad (3.16)$$

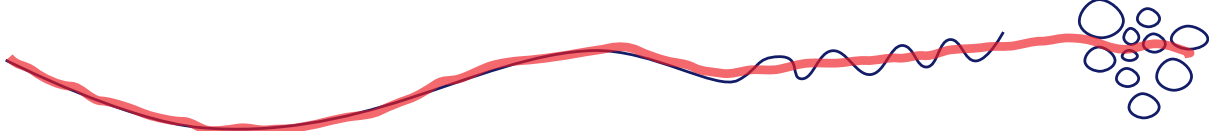


FIGURE 3.2: Representation of an interface and the most probable surface (red color) provided by the most probable level set function φ .

The value $\Sigma(\mathbf{x}, t)$ then represents the most probable area value for the interface within $\mathcal{B}_\ell(\mathbf{x})$ at instant t .

We can note that the classic definition of an interface by means of a infinitely thin surface is a particular case of our PDF characterization of a two-phase flow. Indeed, if one considers that the interface is a surface $\{\bar{\varphi} = 0\}$ where $\bar{\varphi}$ is a given level set function, then one can define

$$f(\mathbf{x}', t', \varphi', H') = \delta(\varphi' - \bar{\varphi}(\mathbf{x}', t')) \delta\left(H' - \operatorname{div}\left[\frac{\nabla\bar{\varphi}(\mathbf{x}', t')}{|\nabla\bar{\varphi}(\mathbf{x}', t')|}\right]\right)$$

An interesting feature of the two-phase interface definition by means of f that can be observed is that there can be conflicts between the information provided by f . Consider for example the situation depicted at [Figure 3.2](#). On the left of the picture, the interface has only large scale variations and the most probable level set function φ provides a reasonable representation of the interface, in this region the value of H and $\operatorname{div}(\nabla\varphi/|\nabla\varphi|)$ probably quite similar. Past the center of the image, the interface starts to wiggle. The function φ will provide a reasonable definition of a mean position of the interface, however H will start to disagree with the value of $\operatorname{div}(\nabla\varphi/|\nabla\varphi|)$. At the far right of the picture where the flow is dispersed, φ will yield a position of the interface that is not coherent with the small scale interfaces of the flow and the value of H will be much larger than $\operatorname{div}(\nabla\varphi/|\nabla\varphi|)$. In this sense one can see that this mismatch between φ and H allows to detect regions where the interface develops characteristic across multiple scales. In the next section we will see how to use f to describe the properties of the interface across two different scales.

3.2.3 TWO-SCALE INTERFACE DESCRIPTION

In this section we will see how f can be useful tool for discriminating scales in the properties of an interface. In order to distinguish between small and large scales we introduce a characteristic cut-off length $\ell_c > 0$ such that $\ell > \ell_c$. (resp. $\ell < \ell_c$) corresponds to large scale (resp. small scales) features of the flow. By considering a ball \mathcal{B} of radius $\ell_c/2$, we associate to this scale separation a threshold mean curvature value $H_{\max} = 2/\ell_c$ that corresponds to curvature of \mathcal{B} and a threshold interfacial area value $\Sigma_{\min} = 6/\ell_c = \operatorname{area}(\mathcal{B})/\operatorname{volume}(\mathcal{B})$. Given a PDF description of the interface f we can introduce a new PDF f_c that will only describe large scale features of the interface. We propose to define f_c as follows

$$f_c(\mathbf{x}, t, \varphi, H) = \mathbb{1}_{[0, H_{\max}]}(H) \int f(\mathbf{x}', t, \varphi, H) \theta_{\ell_c}(\mathbf{x} - \mathbf{x}') d\mathbf{x}', \quad (3.17)$$

where $\mathbb{1}_{\mathcal{D}}$ is the characteristic function of the set \mathcal{D} . Using this new large scale PDF, we can define an associated most probable level set φ_c , an associated most probable mean curvature

H_c and an associated void fraction α_c by setting

$$\varphi_c(\mathbf{x}, t) = \int \varphi' f_c(\mathbf{x}, t, \varphi', H') d\varphi' dH', \quad (3.18a)$$

$$H_c(\mathbf{x}, t) = \int H' f_c(\mathbf{x}, t, \varphi', H') d\varphi' dH', \quad (3.18b)$$

$$\alpha_c(\mathbf{x}, t) = \int_{\varphi' > 0} f_c(\mathbf{x}, t, \varphi', H') d\varphi' dH'. \quad (3.18c)$$

Now, the features of the interface can be describe by a PDF f_c related to large scales and a PDF $(f - f_c)$ related to small scales. This scale decomposition now extends naturally to fields associated with the interface as follows

$$\alpha = \alpha_c + \tilde{\alpha}, \quad \tilde{\alpha}(\mathbf{x}, t) = \int_{\varphi' > 0} (f - f_c)(\mathbf{x}, t, \varphi', H') d\varphi' dH', \quad (3.19a)$$

$$H = H_c + \tilde{H}, \quad \tilde{H}(\mathbf{x}, t) = \int H' (f - f_c)(\mathbf{x}, t, \varphi', H') d\varphi' dH', \quad (3.19b)$$

$$\Sigma = \Sigma_c + \tilde{\Sigma}, \quad \tilde{\Sigma}(\mathbf{x}, t) = \int_{\varphi' > 0} H' (f - f_c)(\mathbf{x}', t, \varphi', H') \theta_\ell(\mathbf{x} - \mathbf{x}') d\mathbf{x}' d\varphi' dH'. \quad (3.19c)$$

In this section we have formally defined parameters that allow to characterize a two-phase interface across two different scales. We will now use these parameters to build a two-phase model.

3.3 DERIVING A TWO-SCALE TWO-PHASE INTERFACE MODEL

We now turn to the derivation of a two-phase model by following similar lines as in [Drui et al. \(2019\) \[60\]](#) we will choose a set of parameters that characterize our two-phase medium and we will build an associated Lagrangian energy L .

For the sake of simplicity, we will consider that there is an equilibrium of bulk velocities between both fluids $\mathbf{v}_1 = \mathbf{v}_2 = \mathbf{v}$. Let Y be the mass fraction of fluid 1 and ρ be the density of the medium. We will also suppose that the flow is barotropic and we assume the system is equipped with a specific bulk barotropic potential energy e of the form

$$e = e(\rho, Y, \alpha). \quad (3.20)$$

3.3.1 TWO-PHASE MEDIUM KINETIC ENERGY

We start by considering the kinetic energy of the medium. First we equip the system with a large scale kinetic energy \mathcal{K} with the classic definition $\mathcal{K} = \rho \|\mathbf{v}\|^2/2$. We now wish to add a small scale kinematic energy to the system. This task is not straightforward as it requires first to propose a small scale kinematic for the system.

We consider the interface at a small scale: we suppose that the only possible small scale motion of the interface is small displacement normal to the interface. At (\mathbf{x}, t) we suppose that the most probable small displacement amplitude is $h(\mathbf{x}, t)$. The variation of this small scale displacement will modify the interfacial area, the mean curvature and the void fraction at (\mathbf{x}, t) . We postulate that there is a geometric constraint that connects $h, \tilde{\Sigma}, H$ and $\tilde{\alpha}$: if δb is an infinitesimal variation of $b \in \{h, \tilde{\Sigma}, H, \tilde{\alpha}\}$, we assume that

$$\delta \tilde{\Sigma} = -2H\tilde{\Sigma}\delta h, \quad \delta \tilde{\alpha} = \tilde{\Sigma}\delta h. \quad (3.21)$$

The relations (3.21) are motivated by simple geometric argument analogous to Weyl's tube formula that is presented in [Appendix 3.A](#). These hypotheses suggest to impose

$$D_t \tilde{\Sigma} = -2H\tilde{\Sigma}D_t h, \quad D_t \tilde{\alpha} = \tilde{\Sigma}D_t h, \quad (3.22)$$

where $D_t \cdot = \partial_t \cdot + \mathbf{v}^T \nabla \cdot$ is the material derivative. So as to complete the definition of the small kinematic, we postulate two additional relations: first, we suppose that evolution of the void fraction for the large scales are purely driven by material transport. This boils down to assume that

$$D_t \alpha_c = 0 \quad \text{or equivalently} \quad D_t \alpha = D_t \tilde{\alpha}. \quad (3.23)$$

Second, we assume that the mean curvature field is passively advected, in other words the evolution of H reads

$$D_t H = 0. \quad (3.24)$$

We now sum up the evolution equations that define the small scale kinematics

$$D_t \tilde{\Sigma} = -2H\tilde{\Sigma}D_t h, \quad D_t \alpha = \tilde{\Sigma}D_t h, \quad D_t \alpha = D_t \tilde{\alpha}, \quad D_t H = 0. \quad (3.25)$$

In agreement with our hypotheses, the only small scale motion that are involved in our model are due to the small displacement h of the interface. We choose thus to equip our model with a small scale kinetic energy \mathcal{K}_i defined by

$$\mathcal{K}_i = \frac{1}{2}m(D_t h)^2, \quad (3.26)$$

where the coefficient $m > 0$ has the dimension of a mass.

3.3.2 TWO-PHASE MEDIUM INTERFACIAL ENERGY

We now turn to the definition of interfacial energy \mathcal{U}_i . Following a classic approach, we suppose that an infinitesimal variation of interface energy $\delta\mathcal{U}_i$ is proportional to the variation of the surface area (see Young (1995) [223]).

If one considers that the interface can be accurately described at the large scale then the density of area variation is given by $\delta(\|\nabla\alpha_c\|)$. In the case the interface features are characterized by the small scales, then the density of area variation is given by $\delta\tilde{\Sigma}$. If one notes σ the capillarity coefficient of the medium, this suggests to set for the interfacial energy $-\sigma\|\nabla\alpha_c\|$ when the large scale of the interface are dominant and $-\sigma\tilde{\Sigma}$ in the region where the interface features are mostly small scales. In order to account for this scale change, we use the variable H to determine whether large scale or small are dominant: we define

$$\sigma_c(H) = \begin{cases} \sigma, & \text{if } H \leq H_{\max} \\ 0, & \text{if } H > H_{\max} \end{cases}, \quad \tilde{\sigma}(H) = \begin{cases} \sigma, & \text{if } H > H_{\max} \\ 0, & \text{if } H \leq H_{\max} \end{cases} \quad (3.27)$$

Then we can say that $-\sigma_c(H)\|\nabla\alpha_c\|$ (resp. $-\tilde{\sigma}(H)\tilde{\Sigma}$) will account for the large scale (resp. small scale) interfacial energy in the whole domain. Finally, we remark that in region where large scale interface features are dominant, it is reasonable to claim that $\|\nabla\alpha_c\| \simeq \|\nabla\alpha\|$, and we thus choose for the two-scale interfacial energy to set

$$\mathcal{U}_i = -\sigma_c(H)\|\nabla\alpha\| - \tilde{\sigma}(H)\tilde{\Sigma}. \quad (3.28)$$

3.3.3 LAGRANGIAN ENERGY OF THE TWO-PHASE SYSTEM

Now that we have defined a bulk potential energy, the kinetic and interfacial energies for both small and large scales, we can consider the following Lagrangian energy for the system

$$L = \frac{1}{2}\rho\|\mathbf{v}\|^2 + \frac{1}{2}m(D_t h)^2 - \sigma_c(H)\|\nabla\alpha\| - \tilde{\sigma}(H)\tilde{\Sigma} - \rho e(\rho, Y, \alpha).$$

Using (3.25), we see that the small scale kinetic energy also reads $\mathcal{K}_i = \frac{1}{2}m(D_t\alpha)^2/\tilde{\Sigma}^2$, which allows to discard the variable h from the expression of L . We thus finally obtain

$$L(\rho, \mathbf{v}, Y, \alpha, \nabla\alpha, D_t\alpha, H, \tilde{\Sigma}) = \frac{1}{2}\rho\|\mathbf{v}\|^2 + \frac{1}{2}m\frac{(D_t\alpha)^2}{\tilde{\Sigma}^2} - \sigma_c(H)\|\nabla\alpha\| - \tilde{\sigma}(H)\tilde{\Sigma} - \rho e(\rho, Y, \alpha). \quad (3.29)$$

3.3.4 HAMILTON'S STATIONNARY ACTION PRINCIPLE

Following classic lines (see Chapter 1, we consider the motion of a portion of medium that occupies the volume $\mathcal{B}(t)$ for $t \in [t_0, t_1]$. We note $(t, \mathbf{X}) \mapsto \varphi^L(t, \mathbf{X})$ the position of at instant t of a fluid particle that was initially located at \mathbf{X} and set $\Omega = \{(t, \varphi^L(t, \mathbf{X})) \mid \mathbf{X} \in \mathcal{B}(t_0), t \in [t_0, t_1]\}$. We consider a transformation of the medium that defined by the fields $(t, \mathbf{x}) \mapsto (\rho, \mathbf{v}, Y, \alpha, H, \tilde{\Sigma})$ and the mapping $(t, \mathbf{X}) \mapsto \varphi^L(t, \mathbf{X})$ that verifies the small scale kinematics hypotheses (3.26) and the mass conservation equations

$$\partial_t \rho + \operatorname{div}(\rho \mathbf{v}) = 0, \quad \partial_t(\rho Y) + \operatorname{div}(\rho Y \mathbf{v}) = 0. \quad (3.30)$$

We now consider a family of transformations medium $(t, \mathbf{x}, \lambda) \mapsto (\rho_\lambda, \mathbf{v}_\lambda, Y_\lambda, \alpha_\lambda, H_\lambda, \tilde{\Sigma}_\lambda)$ and $(t, \mathbf{X}, \lambda) \mapsto \varphi_\lambda^L(t, \mathbf{X}, \lambda)$ that are parameterized by $\lambda \in [0, 1]$. We note $\Omega_\lambda = \{(t, \varphi_\lambda^L(t, \mathbf{X}, \lambda)) \mid \mathbf{X} \in \mathcal{B}(t_0), t \in [t_0, t_1], \lambda \in [0, 1]\}$ and we suppose that these fields also verify the small scale kinematics hypotheses (3.26) and the mass conservation equations, that is to say

$$D_t \Sigma_\lambda + 2H_\lambda D_t \alpha_\lambda = 0, \quad D_t H_\lambda = 0, \quad (3.31a)$$

$$\partial_t \rho_\lambda + \operatorname{div}(\rho_\lambda \mathbf{v}_\lambda) = 0, \quad \partial_t(\rho_\lambda Y_\lambda) + \operatorname{div}(\rho_\lambda Y_\lambda \mathbf{v}_\lambda) = 0, \quad (3.31b)$$

supplemented with the classic boundary constraints

$$(\rho_\lambda, Y_\lambda, \alpha_\lambda, \Sigma_\lambda, H_\lambda)(t, \mathbf{x}, \lambda = 0, 1) = (\rho, Y, \alpha, \Sigma, H)(t, \mathbf{x}) \quad \lambda = 0, 1, \quad (3.32a)$$

$$\varphi_\lambda^L(\mathbf{X}, t, \lambda = 0, 1) = \varphi^L(\mathbf{X}, t), \quad \lambda = 0, 1 \quad (3.32b)$$

$$(\rho_\lambda, Y_\lambda, \alpha_\lambda, \Sigma_\lambda, H_\lambda)(t, \mathbf{x}, \lambda) = (\rho, Y, \alpha, \Sigma, H)(t, \mathbf{x}), \quad (t, \mathbf{x}) \in \partial\Omega_\lambda \quad (3.32c)$$

$$\varphi_\lambda^L(\mathbf{X}, t, \lambda) = \varphi^L(\mathbf{X}, t), \quad (t, \mathbf{X}) \in \partial([t_0, t_1] \times \mathcal{B}(t_0)). \quad (3.32d)$$

Following standard lines, this family of transformation yields a family of infinitesimal transformations defined by

$$\delta_\lambda \varphi(t, \varphi^L(t, \mathbf{X})) = \left(\frac{\partial \varphi_\lambda^L}{\partial \lambda} \right)_{t, \mathbf{X}}(t, \mathbf{X}, \lambda = 0), \quad (3.33a)$$

$$\delta_\lambda b(t, \mathbf{x}) = \left(\frac{\partial b_\lambda}{\partial \lambda} \right)_{t, \mathbf{x}}(t, \mathbf{x}, \lambda = 0), \quad (3.33b)$$

for $b \in \{\rho, Y, \alpha, \tilde{\Sigma}, H\}$.

Applying (3.33) with the constraints (3.31) allows to express following relations between the infinitesimal variations

$$\delta_\lambda \rho = -\operatorname{div}(\rho \delta_\lambda \varphi), \quad \delta_\lambda \mathbf{v} = D_t(\delta_\lambda \varphi) - (\delta_\lambda \varphi^T \nabla) \mathbf{v}, \quad \delta_\lambda b = -\delta_\lambda \varphi^T \nabla b, \quad b \in \{Y, H\}, \quad (3.34a)$$

$$\delta_\lambda \Sigma = -2H \delta_\lambda \alpha - (\nabla \Sigma^T \delta_\lambda + 2H \nabla \alpha^T) \delta_\lambda \varphi. \quad (3.34b)$$

Let us now define the Hamiltonian action \mathcal{A} associated with family of transformations $(t, \mathbf{x}, \lambda) \mapsto (\rho_\lambda, Y_\lambda, \alpha_\lambda, \Sigma_\lambda, H_\lambda)$ and $(t, \mathbf{X}, \lambda) \mapsto \varphi_\lambda^L$ by setting

$$\mathcal{A}(\lambda) = \int_{\Omega_\lambda} L(\rho_\lambda, \mathbf{v}_\lambda, Y_\lambda, \alpha_\lambda, \nabla \alpha_\lambda, D_t \alpha_\lambda, H_\lambda, \tilde{\Sigma}_\lambda) \, d\mathbf{x} dt. \quad (3.35)$$

The Stationary Action Principle states that a physical transformation of the system verifies

$$\frac{d\mathcal{A}}{d\lambda}(0) = 0. \quad (3.36)$$

which will yield the motion equations of the flow. We introduce the following notations

$$\mathbf{K}^T = \left(\frac{\partial L}{\partial \mathbf{v}} \right), \quad \mathbf{D}^T = \left(\frac{\partial L}{\partial \nabla \alpha} \right), \quad M = \left(\frac{\partial L}{\partial D_t \alpha} \right), \quad L + L^* = \rho \left(\frac{\partial L}{\partial \rho} \right). \quad (3.37)$$

Relation (3.36) reads

$$\int_{\Omega} \left([L + L^*] \delta \rho + \mathbf{K}^T \delta \mathbf{v} + \frac{\partial L}{\partial Y} \delta Y + \frac{\partial L}{\partial \alpha} \delta \alpha + \frac{\partial L}{\partial H} \delta H + \frac{\partial L}{\partial \tilde{\Sigma}} \delta \tilde{\Sigma} + M \delta (D_t \alpha) + \mathbf{D} \delta (\nabla \alpha) \right) d\mathbf{x} dt = 0. \quad (3.38)$$

We follow standards lines: taking into account (3.34), (3.32c) and (3.32d), after thorough calculations relation (3.38) provides

$$0 = \int_{\Omega} \left\{ \left[-\rho D_t(\mathbf{K}/\rho) + \nabla L^* + \left(\frac{\partial L}{\partial \alpha} - \rho D_t(M/\rho) - 2H \frac{\partial L}{\partial \tilde{\Sigma}} \right) \nabla \alpha + (\mathbf{D}^T \nabla) \nabla \alpha \right]^T \delta_{\lambda} \varphi + \left(\frac{\partial L}{\partial \alpha} - \rho D_t(M/\rho) - 2H \frac{\partial L}{\partial \tilde{\Sigma}} - \operatorname{div}(\mathbf{D}) \right) \delta_{\lambda} \alpha \right\} d\mathbf{x} dt,$$

for any $\delta_{\lambda} \varphi$ and $\delta_{\lambda} \alpha$. This implies that

$$\rho D_t(\mathbf{K}/\rho) = \nabla L^* + \left(\frac{\partial L}{\partial \alpha} - \rho D_t(M/\rho) - 2H \frac{\partial L}{\partial \tilde{\Sigma}} \right) \nabla \alpha + (\mathbf{D}^T \nabla) \nabla \alpha, \quad (3.39a)$$

$$\rho D_t(M/\rho) = \frac{\partial L}{\partial \alpha} - 2H \frac{\partial L}{\partial \tilde{\Sigma}} - \operatorname{div}(\mathbf{D}). \quad (3.39b)$$

By using (3.39b), equation (3.39a) also reads

$$\rho D_t(\mathbf{K}/\rho) = \nabla L^* + \operatorname{div}(\nabla \alpha \otimes \mathbf{D}). \quad (3.40)$$

Finally, by gathering the mass conservation equations (3.30), the small scale kinematics equations (3.25) and the evolution equations derived by the stationary action principle, we see that the full system that governs our two-phase model is

$$\partial_t \rho + \operatorname{div}(\rho \mathbf{v}) = 0, \quad (3.41a)$$

$$\partial_t(\rho Y) + \operatorname{div}(\rho Y \mathbf{v}) = 0, \quad (3.41b)$$

$$\rho D_t(\mathbf{K}/\rho) - \nabla L^* - \operatorname{div}(\nabla \alpha \otimes \mathbf{D}) = 0, \quad (3.41c)$$

$$\rho D_t(M/\rho) - \frac{\partial L}{\partial \alpha} + 2H \frac{\partial L}{\partial \tilde{\Sigma}} + \operatorname{div}(\mathbf{D}) = 0, \quad (3.41d)$$

$$D_t \tilde{\Sigma} + 2H D_t \alpha = 0, \quad (3.41e)$$

$$D_t \alpha - D_t \tilde{\alpha} = 0, \quad (3.41f)$$

$$D_t H = 0. \quad (3.41g)$$

Manipulating the two evolution equations (3.39a) and (3.39b), we obtain

$$\rho D_t \left(\frac{1}{\rho} (L - \mathbf{K}^t \mathbf{v} - M D_t \alpha) \right) + \nabla \cdot [(L^* + \nabla \alpha \otimes \mathbf{D}) \mathbf{v} - D_t \alpha \mathbf{D}] = 0. \quad (3.42)$$

Defining a total energy ρE as

$$\rho E = \mathbf{K}^t \mathbf{v} + M D_t \alpha - L, \quad (3.43)$$

Equation (3.42) yields a supplementary conservative equation on ρE

$$\partial_t(\rho E) + \nabla \cdot [E - (L^* + \nabla \alpha \otimes \mathbf{D}) \mathbf{v} + D_t \alpha \mathbf{D}] = 0. \quad (3.44)$$

3.3.5 FINAL FORM OF THE SYSTEM

In order to express the system of equations of our model in a more natural way, we start by making explicit the derivative of L defined by (3.29). We have

$$\frac{\partial L}{\partial \Sigma} = -\tilde{\sigma} - m \frac{(D_t \alpha)^2}{\tilde{\Sigma}^3}, \quad \frac{\partial L}{\partial \alpha} = -\rho \frac{\partial e}{\partial \alpha}, \quad \mathbf{K} = \rho \mathbf{v}, \quad (3.45a)$$

$$M = \frac{m}{\tilde{\Sigma}^2} D_t \alpha, \quad \mathbf{D} = -\sigma_c \frac{\nabla \alpha}{\|\nabla \alpha\|}, \quad \frac{\partial L}{\partial \rho} = \frac{\|\mathbf{v}\|^2}{2} - \rho \frac{\partial e}{\partial \rho} - e, \quad (3.45b)$$

$$L^* = -\rho^2 \frac{\partial e}{\partial \rho} + \sigma_c(H) \|\nabla \alpha\| + \tilde{\sigma}(H) \tilde{\Sigma} - \frac{1}{2} m \frac{(D_t \alpha)^2}{\tilde{\Sigma}^2}. \quad (3.45c)$$

We define the pressure p of the two-phase flow medium by

$$p = \rho^2 \frac{\partial e}{\partial \rho}, \quad (3.46)$$

and introduce an auxiliary variable, ω , defined similarly as in Drui et al. (2019) [60], and a coefficient, ν ,

$$\rho Y \omega = D_t \alpha, \quad \nu(\tilde{\Sigma}) = \frac{m}{\tilde{\Sigma}^2}. \quad (3.47)$$

Injecting these relations into Equations (3.41), we obtain the system

$$\partial_t \rho + \operatorname{div}(\rho \mathbf{v}) = 0, \quad (3.48a)$$

$$\partial_t(\rho Y) + \operatorname{div}(\rho Y \mathbf{v}) = 0, \quad (3.48b)$$

$$\rho D_t \mathbf{v} + \nabla \mathcal{P} + \operatorname{div} \left(\sigma_c(H) \frac{\nabla \alpha \otimes \nabla \alpha}{\|\nabla \alpha\|} \right) = \mathbf{0}, \quad (3.48c)$$

$$D_t \alpha - \rho Y \omega = 0, \quad (3.48d)$$

$$D_t \omega + \frac{1}{Y \nu} \frac{\partial e}{\partial \alpha} - 2H \frac{1}{2} \frac{\nu'}{\nu} \rho Y \omega^2 - \frac{1}{\rho Y \nu} \left(2H \tilde{\sigma}(H) + \operatorname{div} \left(\sigma_c(H) \frac{\nabla \alpha}{\|\nabla \alpha\|} \right) \right) = 0, \quad (3.48e)$$

$$D_t \tilde{\Sigma} + 2H \rho Y \omega = 0, \quad (3.48f)$$

$$D_t \alpha - D_t \tilde{\alpha} = 0, \quad (3.48g)$$

$$D_t H = 0. \quad (3.48h)$$

with the extended pressure $\mathcal{P} = -L^* = p + \nu(\rho Y \omega)^2/2 - \tilde{\sigma}(H) \tilde{\Sigma} - \sigma_c(H) \|\nabla \alpha\|$. The supplementary conservative equation on the total energy E reads

$$\partial_t(\rho E) + \nabla \cdot \left[\rho E + \left(\mathcal{P} + \sigma_c(H) \frac{\nabla \alpha \otimes \nabla \alpha}{\|\nabla \alpha\|} \right) \mathbf{v} - D_t \alpha \sigma_c \frac{\nabla \alpha}{\|\nabla \alpha\|} \right] = 0, \quad (3.49)$$

with

$$\rho E(\rho, Y, \mathbf{v}, \alpha, \omega, \tilde{\Sigma}, H) = \frac{1}{2} \rho \|\mathbf{v}\|^2 + \frac{1}{2} m \frac{(D_t \alpha)^2}{\tilde{\Sigma}^2} + \sigma_c(H) \|\nabla \alpha\| + \tilde{\sigma}(H) \tilde{\Sigma} + \rho e(\rho, Y, \alpha). \quad (3.50)$$

The Stationary Action Principle does not account for irreversible process. Thus, system (3.48) is purely non-dissipative. Based on the second principle of thermodynamics, we can define an entropy of the system and build the dissipation.

3.3.6 DISSIPATION

The flow being barotropic, we assume the total energy to be a mathematical entropy of the system,

$$\rho s(\rho, Y, \mathbf{v}, \alpha, \omega, \tilde{\Sigma}, H) = \rho E. \quad (3.51)$$

Following the lines of [Drui et al. \(2019\) \[60\]](#), we seek an entropy flux \mathbf{G} to determine a new transport equation for ω allowing for dissipation, such that

$$\rho D_t s + \nabla \cdot \mathbf{G} \leq 0, \quad (3.52)$$

or equivalently, noticing that $D_t Y = D_t H = 0$,

$$\begin{aligned} \nabla \cdot \mathbf{G} + \rho \frac{\partial s}{\partial \rho} D_t \rho + \rho \left(\frac{\partial s}{\partial \mathbf{v}} \right)^t D_t \mathbf{v} + \rho \frac{\partial s}{\partial \alpha} D_t \alpha \\ + \rho \frac{\partial s}{\partial (\nabla \alpha)} D_t (\nabla \alpha) + \rho \frac{\partial s}{\partial \omega} D_t \omega + \rho \frac{\partial s}{\partial \tilde{\Sigma}} D_t \tilde{\Sigma} \leq 0. \end{aligned} \quad (3.53)$$

Most of the material derivatives are easily obtained from system [\(3.48\)](#),

$$D_t \rho = -\rho \nabla \cdot \mathbf{v}, \quad D_t (\nabla \alpha) = \nabla (D_t \alpha) - \nabla \mathbf{v} \nabla \alpha, \quad (3.54a)$$

and the partial derivatives read

$$\frac{\partial s}{\partial \rho} = \frac{\nu}{2} Y^2 \omega^2 - \frac{\sigma_c \|\nabla \alpha\|}{\rho^2} - \frac{\tilde{\sigma} \tilde{\Sigma}}{\rho^2} + \frac{\partial e}{\partial \rho}, \quad \frac{\partial s}{\partial \mathbf{v}} = \mathbf{v}, \quad \frac{\partial s}{\partial \alpha} = \frac{\partial e}{\partial \alpha}, \quad \rho \frac{\partial s}{\partial (\nabla \alpha)} = -\mathbf{D}, \quad (3.54b)$$

$$\rho \frac{\partial s}{\partial \tilde{\Sigma}} = \tilde{\sigma} + \frac{1}{2} \nu' (\rho Y \omega)^2. \quad (3.54c)$$

Injecting [\(3.54\)](#) into [\(3.53\)](#), we obtain

$$\begin{aligned} \nabla \cdot [\mathbf{G} - (\mathcal{P} - \mathbf{D} \otimes \|\nabla \alpha\|) \mathbf{v} - D_t \alpha \mathbf{D}] \\ + \rho Y \omega \left(\nu \rho Y D_t \omega + \rho \frac{\partial e}{\partial \alpha} - 2H \frac{1}{2} \nu' (\rho Y \omega)^2 - 2H \tilde{\sigma} + \nabla \cdot \mathbf{D} \right) \leq 0. \end{aligned} \quad (3.55)$$

A simple closure consists in equating

$$\mathbf{G} = (\mathcal{P} - \mathbf{D} \otimes \|\nabla \alpha\|) \mathbf{v} - D_t \alpha \mathbf{D}, \quad (3.56)$$

which is consistent with the conservative equation on the total energy [\(3.49\)](#), and introducing a coefficient ϵ_α such that

$$-\epsilon_\alpha \rho Y \omega = \nu \rho Y D_t \omega + \rho \frac{\partial e}{\partial \alpha} - 2H \frac{1}{2} \nu' (\rho Y \omega)^2 - 2H \tilde{\sigma} + \nabla \cdot \mathbf{D}. \quad (3.57)$$

Thus, the equation on the entropy takes the conservative part of the total energy supplemented by a dissipative source term. We finally obtain a new equation for ω that takes the form

$$D_t \omega + \frac{\epsilon_\alpha}{\nu} \omega + \frac{1}{Y \nu} \frac{\partial L}{\partial \alpha} - 2H \frac{1}{2} \frac{\nu'}{\nu} \rho Y \omega^2 - \frac{1}{\rho Y \nu} \left(2H \tilde{\sigma}(H) + \operatorname{div} \left(\sigma_c(H) \frac{\nabla \alpha}{\|\nabla \alpha\|} \right) \right) = 0. \quad (3.58)$$

To close the investigated system, we need to specify the thermodynamics of the mixture. We propose to decompose the barotropic potential energy of the mixture as the phase barotropic potential energy mass averaged and a mixing term

$$e(\rho, Y, \alpha) = \sum_{k=1,2} y_k e_k(\rho_k) + \Delta e(\alpha), \quad (3.59)$$

where $\alpha_2 = 1 - \alpha$, $y_2 = 1 - Y$ and ρ_k is the fluid density, related to the volume fraction and the mass fraction by the relation $y_k = \alpha_k \rho_k / \rho$. The mixing term Δe accounts for phase interaction and could depend on supplementary variables. We further assume that the phase internal energies verify the Gibbs equation. Thus, the partial pressure p_k are defined by $p_k = \rho_k^2 \partial_{\rho_k} e_k$, and

$$\rho^2 \frac{\partial e}{\partial \rho} = \sum_{k=1,2} \alpha_k p_k, \quad \rho \frac{\partial e}{\partial \alpha} = p_d + \rho \Delta e', \quad (3.60)$$

with $p_d = p_2 - p_1$. We obtain the final form of the system, equipped with a dissipative part,

$$\partial_t \rho + \operatorname{div}(\rho \mathbf{v}) = 0, \quad (3.61a)$$

$$\partial_t(\rho Y) + \operatorname{div}(\rho Y \mathbf{v}) = 0, \quad (3.61b)$$

$$\rho D_t \mathbf{v} + \nabla \mathcal{P} + \operatorname{div} \left(\sigma_c(H) \frac{\nabla \alpha \otimes \nabla \alpha}{\|\nabla \alpha\|} \right) = \mathbf{0}, \quad (3.61c)$$

$$D_t \alpha - \rho Y \omega = 0, \quad (3.61d)$$

$$D_t \omega + \frac{\epsilon_\alpha}{\nu} \omega - H \frac{\nu'}{\nu} \rho Y \omega^2 + \frac{1}{\rho Y \nu} \left(p_d + \rho \Delta e' - 2H \tilde{\sigma}(H) - \operatorname{div} \left(\sigma_c(H) \frac{\nabla \alpha}{\|\nabla \alpha\|} \right) \right) = 0, \quad (3.61e)$$

$$D_t \tilde{\Sigma} + 2H \rho Y \omega = 0, \quad (3.61f)$$

$$D_t \alpha - D_t \tilde{\alpha} = 0, \quad (3.61g)$$

$$D_t H = 0, \quad (3.61h)$$

$$\partial_t(\rho E) + \nabla \cdot \left[\rho E + \left(\mathcal{P} + \sigma_c(H) \frac{\nabla \alpha \otimes \nabla \alpha}{\|\nabla \alpha\|} \right) \mathbf{v} - D_t \alpha \sigma_c \frac{\nabla \alpha}{\|\nabla \alpha\|} \right] = 0, \quad (3.61i)$$

with the extended pressure $\mathcal{P} = -L^* = p + \nu(\rho Y \omega)^2/2 - \tilde{\sigma}(H) \tilde{\Sigma} - \sigma_c(H) \|\nabla \alpha\|$.

3.3.7 A HIERARCHY OF MODELS

System (3.61) is a generalization of the system found in [Drui et al. \(2019\) \[60\]](#). The coefficients ϵ_α and ν are identified in the case of disperse flow thanks to a comparison with the Rayleigh-Plesset equation. The coefficient ϵ_α introduced in the dissipation evaluation is referred *microviscosity* and is related to damping of the inclusion pulsations, whereas ν is called *micro-inertia* and is indeed connected to the inertial effects of the pulsating inclusion interface.

As proposed in [Drui et al. \(2019\) \[60\]](#), System (3.61) yields a hierarchy of models by taking the asymptotic limits of zero μ micro-viscosity $\epsilon_\alpha \rightarrow 0$ and zero *micro-inertia* $\nu \rightarrow 0$.

In the limit $\nu \rightarrow 0$ with a fixed ϵ_α , the sub-scale momentum equation (3.61e) returns,

$$\rho Y \omega = -\frac{1}{\epsilon_\alpha} \left(p_d + \rho \Delta e' - 2H \tilde{\sigma}(H) - \operatorname{div} \left(\sigma_c(H) \frac{\nabla \alpha}{\|\nabla \alpha\|} \right) \right). \quad (3.62)$$

The micro-inertia free model obtained in the limit $\nu \rightarrow 0$ of System (3.61) thus reads

$$\partial_t \rho + \operatorname{div}(\rho \mathbf{v}) = 0, \quad (3.63a)$$

$$\partial_t(\rho Y) + \operatorname{div}(\rho Y \mathbf{v}) = 0, \quad (3.63b)$$

$$\rho D_t \mathbf{v} + \nabla \mathcal{P} + \operatorname{div} \left(\sigma_c(H) \frac{\nabla \alpha \otimes \nabla \alpha}{\|\nabla \alpha\|} \right) = \mathbf{0}, \quad (3.63c)$$

$$D_t \alpha + \frac{1}{\epsilon_\alpha} \left(p_d + \rho \Delta e' - 2H \tilde{\sigma}(H) - \operatorname{div} \left(\sigma_c(H) \frac{\nabla \alpha}{\|\nabla \alpha\|} \right) \right) = 0, \quad (3.63d)$$

$$D_t \tilde{\Sigma} - \frac{2H}{\epsilon_\alpha} \left(p_d + \rho \Delta e' - 2H \tilde{\sigma}(H) - \operatorname{div} \left(\sigma_c(H) \frac{\nabla \alpha}{\|\nabla \alpha\|} \right) \right) = 0, \quad (3.63e)$$

$$D_t \alpha - D_t \tilde{\alpha} = 0, \quad (3.63f)$$

$$D_t H = 0, \quad (3.63g)$$

$$\partial_t(\rho E) + \nabla \cdot \left[\rho E + \left(\mathcal{P} + \sigma_c(H) \frac{\nabla \alpha \otimes \nabla \alpha}{\|\nabla \alpha\|} \right) \mathbf{v} - D_t \alpha \sigma_c \frac{\nabla \alpha}{\|\nabla \alpha\|} \right] = 0, \quad (3.63h)$$

with the extended pressure $\mathcal{P} = p - \tilde{\sigma}(H) \tilde{\Sigma} - \sigma_c(H) \|\nabla \alpha\|$.

As mentioned in [Section 1.1.3.2 of Chapter 1](#), the SAP provides a closed model in the particular case of barotropic flow since the mixture entropy is known.

3.4 EXTENDING THE TWO-SCALE TWO-PHASE INTERFACE MODEL TO A COMPLETE EOS

Since we are aiming at describing two-phase flow compressibility and thermal effects in our applications, we have to extend the previous model of [Section 3.3](#) derived in the framework of barotropic flow by equipping each fluid with a two-parameter equation of state.

Let us assume that the flow can be fully characterized by $(t, \mathbf{x}) \mapsto \eta$ with

$$\eta = (\rho, \mathbf{v}, y_{j,k}, s_k, \alpha, \tilde{\Sigma}, H) \quad (3.64)$$

where ρ is the mixture density defined as $\rho = \alpha\rho_1 + (1-\alpha)\rho_2$, α is the volume fraction of phase $k = 1, 2$, ρ_k the density of phase k , $y_{j,k}$ is the mass fraction of species $j \in \mathcal{N}_s(k)$ of phase k , s_k the entropy per unit of mass of phase k , $\tilde{\Sigma}$ the small-scale interfacial density area, H the mean curvature. The flow is equivalently described by $\mathbf{x} \mapsto (y_{j,k}, s_k, \alpha, \tilde{\Sigma}, H)$ and $(t, \mathbf{X}) \mapsto \varphi^L$ if φ^L complies with the mass conservation equation.

The Lagrangian of the system is defined as in the previous [Section 3.3](#),

$$L(\eta) = \frac{1}{2}\rho\|\mathbf{v}\|^2 + \frac{1}{2}m\frac{(D_t\alpha)^2}{\tilde{\Sigma}^2} - \sigma_c(H)\|\nabla\alpha\| - \tilde{\sigma}(H)\tilde{\Sigma} - \rho e(\eta). \quad (3.65)$$

In the following, we assume to simplify calculations that the surface tension coefficients are both constant. The internal energy e of the mixture is expressed as

$$e(\eta) = \sum_{j \in \mathcal{N}_s(k)} y_{j,k} e_k \left(\frac{y_{j,k}\rho}{\alpha_k}, s_k \right) + \Delta e(\eta). \quad (3.66)$$

where the first term of the RHS corresponds to the internal energy of each phase in a pure state and the second term accounts for mixing effects as in [Chapter 2](#).

Since the Stationary Action principle does not permit to recover an entropy equation for each phase when setting a constraint on the mixture entropy, as seen in [Section 1.2](#) of [Chapter 1](#), we propose to set a constraint on each specific entropy s_k such that

$$D_t s_k = 0. \quad (3.67)$$

The mixture entropy s is defined as

$$s(\eta) = \sum_{j \in \mathcal{N}_s(k)} y_{j,k} s_k \left(\frac{y_{j,k}\rho}{\alpha_k}, e_k \right) + \Delta s(\eta). \quad (3.68)$$

3.4.1 STATIONARY ACTION PRINCIPLE

For a given transformation of the medium $\mathbf{x} \mapsto (y_{j,k}, s_k, \alpha, \tilde{\Sigma}, H)$ and $(t, \mathbf{X}) \mapsto \varphi^L$, let $(t, \mathbf{x}, \lambda) \mapsto \eta_\lambda$ and $(t, \mathbf{X}, \lambda) \mapsto \varphi_\lambda^L$ be a family of medium transformations parametrized by $\lambda \in [0, 1]$. We note $\tilde{\Omega}(\lambda) = \{(t, \varphi_\lambda^L(t, \mathbf{X}, \lambda)) | \mathbf{X} \in \mathcal{B}(t_0), t \in [t_0, t_1]\}$ and we require these fields to satisfy constraints pertaining to mass conservation and partial entropy conservation

$$\partial_t \rho_\lambda + \nabla \cdot (\rho_\lambda \mathbf{v}_\lambda) = 0, \quad \partial_t (\rho_\lambda y_{j,k,\lambda}) + \nabla \cdot (\rho_\lambda y_{j,k,\lambda} \mathbf{v}_\lambda) = 0, \quad D_t s_{k,\lambda} = 0, \quad (3.69)$$

supplemented by constraints regarding the topology evolution

$$D_t \tilde{\Sigma}_\lambda + 2H_\lambda \tilde{\Sigma}_\lambda D_t h_\lambda = 0, \quad D_t \alpha_\lambda - \tilde{\Sigma}_\lambda D_t h_\lambda = 0, \quad D_t H_\lambda = 0, \quad (3.70)$$

which can be recast

$$D_t (\tilde{\Sigma}_\lambda + 2H_\lambda \alpha_\lambda) = 0, \quad D_t \alpha_\lambda - \tilde{\Sigma}_\lambda D_t h_\lambda = 0, \quad D_t H_\lambda = 0, \quad (3.71)$$

and finally classic boundary constraints

$$(y_{j,k,\lambda}, s_{k,\lambda}, \alpha_\lambda, \tilde{\Sigma}_\lambda, H_\lambda)(t, \mathbf{x}, \lambda = 0, 1) = (y_{j,k}, s_k, \alpha, \tilde{\Sigma}, H)(t, \mathbf{x}), \quad (3.72a)$$

$$\varphi_\lambda^L(\mathbf{X}, t, \lambda = 0, 1) = \varphi^L(\mathbf{X}, t), \quad (3.72b)$$

$$(y_{j,k,\lambda}, s_{k,\lambda}, \alpha_\lambda, \tilde{\Sigma}_\lambda, H_\lambda)(t, \mathbf{x}, \lambda)|_{(t,\mathbf{x}) \in \partial \tilde{\Omega}(\lambda)} = (y_{j,k}, s_k, \alpha, \tilde{\Sigma}, H)(t, \mathbf{x}), \quad (3.72c)$$

$$\varphi_\lambda^L(\mathbf{X}, t, \lambda)|_{(t,\mathbf{X}) \in \partial([t_0, t_1] \times \mathcal{B}(t_0))} = \varphi^L(\mathbf{X}, t). \quad (3.72d)$$

Following standard lines, this family of transformation yields a family of infinitesimal transformations defined as follows

$$\delta_\lambda \varphi_\lambda(t, \varphi^L(t, \mathbf{X})) = \left(\frac{\partial \varphi_\lambda^L}{\partial \lambda} \right)_{t, \mathbf{X}} (t, \mathbf{X}, \lambda = 0), \quad (3.73a)$$

$$\delta_\lambda b(t, \mathbf{x}) = \left(\frac{\partial b}{\partial \lambda} \right)_{t, \mathbf{x}} (t, \mathbf{x}, \lambda = 0), \quad (3.73b)$$

for $b \in \eta$. Let us now define the Hamiltonian action \mathcal{A} associated with Ω for the family of transformations $(t, \mathbf{x}, \lambda) \mapsto (y_{j,k,\lambda}, s_{k,\lambda}, \alpha_\lambda, \tilde{\Sigma}_\lambda, H_\lambda)$ and $(t, \mathbf{X}, \lambda) \mapsto \varphi_\lambda^L$

$$\mathcal{A}(\lambda) = \int_{\tilde{\Omega}(\lambda)} L(\rho_\lambda, y_{j,k,\lambda}, \mathbf{v}_\lambda, s_{k,\lambda}, \alpha_\lambda, D_t \alpha_\lambda, \nabla \alpha_\lambda, \tilde{\Sigma}_\lambda, H_\lambda) \, d\mathbf{x} dt. \quad (3.74)$$

Applying (3.73b) with the constraints (3.69) (3.70) allows to express following relations between the infinitesimal variations

$$\delta_\lambda \rho = -\nabla \cdot (\rho \delta_\lambda \varphi_\lambda), \quad \delta_\lambda b = -\delta_\lambda \varphi_\lambda^T \nabla b, \quad b \in \{y_{j,k}, s_k, H\}, \quad (3.75a)$$

$$\delta_\lambda \mathbf{v} = D_t (\delta_\lambda \varphi_\lambda) - (\delta_\lambda \varphi_\lambda^T \nabla) \mathbf{v}, \quad (3.75b)$$

$$\delta_\lambda \tilde{\Sigma} = -2H \delta_\lambda \alpha - \nabla \tilde{\Sigma}^T \delta_\lambda \varphi_\lambda - 2H \nabla \alpha^T \delta_\lambda \varphi_\lambda. \quad (3.75c)$$

The Least Action Principle states that a physical transformation of the system verifies

$$\frac{d\mathcal{A}}{d\lambda} = 0. \quad (3.76)$$

Relation (3.76) will provide the motion equations of the flow. We introduce the following notations

$$\mathbf{K}^T = \left(\frac{\partial L}{\partial \mathbf{v}} \right), \quad \mathbf{D} = \left(\frac{\partial L}{\partial \nabla \alpha} \right), \quad M = \left(\frac{\partial L}{\partial D_t \alpha} \right), \quad L + L^* = \rho \left(\frac{\partial L}{\partial \rho} \right). \quad (3.77)$$

In order to obtain a set of partial differential equations, we need to express $d\mathcal{A}/d\lambda$. Using definition (3.74) we can write

$$\partial_\lambda \mathcal{A}(0) = \partial_\lambda \mathcal{A}_\rho + \sum_{b|D_t b=0} \partial_\lambda \mathcal{A}_b + \partial_\lambda \mathcal{A}_v + \partial_\lambda \mathcal{A}_\alpha + \partial_\lambda \mathcal{A}_{D_t \alpha} + \partial_\lambda \mathcal{A}_{\nabla \alpha} + \partial_\lambda \mathcal{A}_{\tilde{\Sigma}} \quad (3.78)$$

where

$$\partial_\lambda \mathcal{A}_\rho = \int_{\tilde{\Omega}(\lambda)} \delta_\lambda \boldsymbol{\varphi}_\lambda^T \left(\nabla L^* + \sum_{b|b \neq \rho} \nabla b \partial_b L \right) d\mathbf{x}dt, \quad (3.79a)$$

$$\partial_\lambda \mathcal{A}_b = \int_{\tilde{\Omega}(\lambda)} -\delta_\lambda \boldsymbol{\varphi}_\lambda^T \partial_b L \nabla b d\mathbf{x}dt, \quad (3.79b)$$

$$\partial_\lambda \mathcal{A}_v = \int_{\tilde{\Omega}(\lambda)} -\delta_\lambda \boldsymbol{\varphi}_\lambda^T (\partial_t \mathbf{K} + \nabla \cdot [\mathbf{K} \otimes \mathbf{v}] + \nabla \mathbf{v} \mathbf{K}) d\mathbf{x}dt, \quad (3.79c)$$

$$\partial_\lambda \mathcal{A}_\alpha = \int_{\tilde{\Omega}(\lambda)} \partial_\alpha L \delta_\lambda \alpha d\mathbf{x}dt, \quad (3.79d)$$

$$\begin{aligned} \partial_\lambda \mathcal{A}_{D_t \alpha} = \int_{\tilde{\Omega}(\lambda)} & - \left[(\partial_t M + \nabla \cdot [M \mathbf{v}]) \delta_\lambda \alpha + \delta_\lambda \boldsymbol{\varphi}_\lambda^T (\partial_t M + \nabla \cdot [M \mathbf{v}]) \nabla \alpha \right. \\ & \left. + \delta_\lambda \boldsymbol{\varphi}_\lambda^T M \nabla (D_t \alpha) \right] d\mathbf{x}dt, \end{aligned} \quad (3.79e)$$

$$\partial_\lambda \mathcal{A}_{\tilde{\Sigma}} = \int_{\tilde{\Omega}(\lambda)} -2H \partial_{\tilde{\Sigma}} L \delta_\lambda \alpha d\mathbf{x}dt + \int_{\tilde{\Omega}(\lambda)} -\delta_\lambda \boldsymbol{\varphi}_\lambda^T (\nabla \tilde{\Sigma} + 2H \nabla \alpha) \partial_{\tilde{\Sigma}} L d\mathbf{x}dt, \quad (3.79f)$$

$$\partial_\lambda \mathcal{A}_{\nabla \alpha} = \int_{\tilde{\Omega}(\lambda)} -\nabla \cdot \mathbf{D} \delta_\lambda \alpha d\mathbf{x}dt \quad (3.79g)$$

Recasting relations (3.75) into (3.78) provides

$$\int_{\Omega(0)} [\mathbf{A}^T \delta \boldsymbol{\varphi}_\lambda + \mathbf{B} \delta \alpha] d\mathbf{x}dt = 0, \quad (3.80a)$$

with

$$\mathbf{A} = -\partial_t \mathbf{K} - \nabla \cdot [\mathbf{K} \otimes \mathbf{v}] + \nabla L^* + \mathbf{B} \nabla \alpha + \nabla \cdot [\nabla \alpha \otimes \mathbf{D}], \quad (3.80b)$$

$$\mathbf{B} = \partial_\alpha L - \partial_t M - \nabla \cdot [M \mathbf{v}] - 2H \partial_{\tilde{\Sigma}} L - \nabla \cdot \mathbf{D} \quad (3.80c)$$

We can conclude that the Least Action Principles applied to the Lagrangian energy defined by (3.65) yields the following equations of motion

$$\mathbf{A}^T = \mathbf{0}, \quad B = 0, \quad (3.81)$$

such that we obtain two momentum equations,

$$\partial_t \mathbf{K} + \nabla \cdot [\mathbf{K} \otimes \mathbf{v}] - \nabla L^* - \nabla \cdot [\nabla \alpha \otimes \mathbf{D}] = 0, \quad (3.82a)$$

$$\partial_t M + \nabla \cdot [M \mathbf{v}] + 2H \partial_{\tilde{\Sigma}} L - \partial_\alpha L + \nabla \cdot \mathbf{D} = 0, \quad (3.82b)$$

and after some manipulations, a supplementary conservative equation on the total energy of the system

$$\partial_t (\rho E) + \nabla \cdot [\rho E - (L^* + \nabla \alpha \otimes \mathbf{D}) \mathbf{v} + D_t \alpha \mathbf{D}] = 0, \quad (3.83)$$

with $\rho E = \mathbf{K}^T \mathbf{v} + M D_t \alpha - L$. From the definition of the Lagrangian of our system, we have

$$\mathbf{K} = \rho \mathbf{v}, \quad \mathbf{D} = -\sigma_c \frac{\nabla \alpha}{\|\nabla \alpha\|}, \quad M = m \frac{D_t \alpha}{\tilde{\Sigma}^2}, \quad (3.84a)$$

$$L^* = -\rho^2 \partial_\rho e(\eta) - \frac{1}{2} m \frac{(D_t \alpha)^2}{\tilde{\Sigma}^2} + \sigma_c \|\nabla \alpha\| + \tilde{\sigma} \tilde{\Sigma}, \quad (3.84b)$$

$$\partial_{\tilde{\Sigma}} L = -m \frac{(D_t \alpha)^2}{\tilde{\Sigma}^3} - \tilde{\sigma} - \rho \partial_{\tilde{\Sigma}} e(\eta), \quad \partial_\alpha L = -\rho \partial_\alpha e(\eta), \quad (3.84c)$$

and

$$\rho E = \frac{1}{2} \rho \|\mathbf{v}\|^2 + \rho e + \frac{1}{2} m \frac{(D_t \alpha)^2}{\tilde{\Sigma}^2} + \sigma_c \|\nabla \alpha\| + \tilde{\sigma} \tilde{\Sigma}. \quad (3.84d)$$

Therefore we obtain the two following momentum equations

$$\partial_t(\rho \mathbf{v}) + \nabla \cdot \left[\rho \mathbf{v} \otimes \mathbf{v} + \sigma_c \frac{\nabla \alpha \otimes \nabla \alpha}{\|\nabla \alpha\|} \right] + \nabla \cdot \left[\rho^2 \partial_\rho e + \frac{m}{2} \frac{(D_t \alpha)^2}{\tilde{\Sigma}^2} - \tilde{\sigma} \tilde{\Sigma} - \sigma_c \|\nabla \alpha\| \right] = 0, \quad (3.85a)$$

$$\begin{aligned} \partial_t \left(m \frac{D_t \alpha}{\tilde{\Sigma}^2} \right) + \nabla \cdot \left[m \frac{D_t \alpha}{\tilde{\Sigma}^2} \mathbf{v} \right] + \rho \partial_\alpha e - \nabla \cdot \left[\sigma_c \frac{\nabla \alpha}{\|\nabla \alpha\|} \right] \\ - 2H \left(\tilde{\sigma} + \rho \partial_{\tilde{\Sigma}} e + m \frac{(D_t \alpha)^2}{\tilde{\Sigma}^3} \right) = 0, \end{aligned} \quad (3.85b)$$

and the energy conservation equation

$$\begin{aligned} \partial_t(\rho E) + \nabla \cdot \left[\rho E + \left(\rho^2 \partial_\rho e(\eta) + \frac{1}{2} m \frac{(D_t \alpha)^2}{\tilde{\Sigma}^2} - \sigma_c \|\nabla \alpha\| - \tilde{\sigma} \tilde{\Sigma} + \sigma_c \frac{\nabla \alpha \otimes \nabla \alpha}{\|\nabla \alpha\|} \right) \mathbf{v} \right. \\ \left. - D_t \alpha \sigma_c \frac{\nabla \alpha}{\|\nabla \alpha\|} \right] = 0. \end{aligned} \quad (3.85c)$$

The last term of the left hand side of Equation (3.85c) corresponds to a coupling effect of the volume fraction evolution equation and the large scale capillary effect. In more classic compressible two-phase flow model accounting for large scale capillary effects, such as in [Perigaud and Saurel \(2005\) \[173\]](#), this effect can not appear since $D_t \alpha = 0$. In a sense, the present energy equation (3.85c) degenerates towards classic energy equations whenever $D_t \alpha = 0$.

3.4.2 FINAL FORM OF THE SYSTEM

To go further, we need to close the partial derivatives of the internal energy e . To simplify the approach, we assume that each phase obeys a Gibbs equation,

$$T_k ds_k = de_k - p_k / \rho_k^2 d\rho_k. \quad (3.86)$$

Remark 17. Assuming that the phase Gibbs equation holds implies some constraints on the mixing terms and the transport equations as we have seen in [Chapter 2](#).

Thus, from the Definition (3.66) of the energy e , we obtain

$$\rho^2 \partial_\rho e = \alpha p_1 + (1 - \alpha) p_2 + \rho^2 \partial_\rho \Delta e, \quad \rho \partial_\alpha e = p_2 - p_1 + \rho \partial_\alpha \Delta e, \quad \partial_{\tilde{\Sigma}} e = \partial_{\tilde{\Sigma}} \Delta e. \quad (3.87)$$

We define p the pressure of the two-phase medium by

$$p = \alpha p_1 + (1 - \alpha) p_2, \quad (3.88)$$

and introduce an auxiliary variable, ω , defined similarly as in Druj (2017) [59], and a coefficient, ν , by

$$\rho Y \omega = D_t \alpha, \quad \nu(\tilde{\Sigma}) = \frac{m}{\tilde{\Sigma}^2}, \quad (3.89)$$

with $Y = \sum_{j \in \mathcal{N}_s(1)} y_{j,k}$. Injecting these relations into Equations (3.85), one obtains the system

$$\partial_t \rho + \operatorname{div}(\rho \mathbf{v}) = 0, \quad (3.90a)$$

$$\partial_t(\rho y_{j,k}) + \operatorname{div}(\rho y_{j,k} \mathbf{v}) = 0, \quad (3.90b)$$

$$\rho D_t \mathbf{v} + \nabla \mathcal{P} + \operatorname{div} \left(\sigma_c(H) \frac{\nabla \alpha \otimes \nabla \alpha}{\|\nabla \alpha\|} \right) = \mathbf{0}, \quad (3.90c)$$

$$D_t s_k = 0, \quad (3.90d)$$

$$D_t \alpha - \rho Y \omega = 0, \quad (3.90e)$$

$$D_t \omega - H \frac{\nu'}{\nu} \rho Y \omega^2 + \frac{1}{\rho Y \nu} \left(p_d + \rho \partial_\alpha \Delta e - 2H \left(\tilde{\sigma} + \rho \frac{\partial \Delta e}{\partial \tilde{\Sigma}} \right) - \operatorname{div} \left(\sigma_c(H) \frac{\nabla \alpha}{\|\nabla \alpha\|} \right) \right) = 0, \quad (3.90f)$$

$$D_t \tilde{\Sigma} + 2H \rho Y \omega = 0, \quad (3.90g)$$

$$D_t \alpha - D_t \tilde{\alpha} = 0, \quad (3.90h)$$

$$D_t H = 0. \quad (3.90i)$$

with $\mathcal{P} = p + \rho^2 \partial_\rho \Delta e + \nu(\rho Y \omega)^2 / 2 - \sigma_c(H) \|\nabla \alpha\| - \tilde{\sigma}(H) \tilde{\Sigma}$, and a supplementary conservative equation on the total energy of the system $\rho E = \rho \|\mathbf{v}\|^2 / 2 + \rho e + \nu(\rho Y \omega)^2 + \sigma_c(H) \|\nabla \alpha\| + \tilde{\sigma}(H) \tilde{\Sigma}$,

$$\partial_t(\rho E) + \nabla \cdot \left[\rho E \mathbf{v} + \left(\mathcal{P} + \sigma_c(H) \frac{\nabla \alpha \otimes \nabla \alpha}{\|\nabla \alpha\|} \right) \mathbf{v} - \rho Y \omega \sigma_c(H) \frac{\nabla \alpha}{\|\nabla \alpha\|} \right] = 0. \quad (3.90j)$$

3.4.3 DISSIPATION

As opposed to the simplified framework of barotropic flow, for which the entropy is equal to the total energy, for two-parameter equations of state, we do not know the mixture entropy. Consequently we can no more express the partial derivatives of the entropy and proceed as in Section 3.3.6 to sign the source terms of the entropy equation.

In the following, we give some hints on an original approach to derive both the mixture entropy and its evolution equation for any system obtained through the Stationary Action Principle where the partial entropies were constrained as in Equation (3.67). Given the general definition of the mixture entropy, taking the material derivative Equation (3.68) yields,

$$D_t s = D_t \Delta s(\eta, \omega), \quad (3.91)$$

or equivalently, recalling that $D_t Y = D_t H = D_t s_k = 0$,

$$D_t s = \frac{\partial \Delta s}{\partial \rho} D_t \rho + \left(\frac{\partial \Delta s}{\partial \mathbf{v}} \right)^t D_t \mathbf{v} + \frac{\partial \Delta s}{\partial \alpha} D_t \alpha + \frac{\partial \Delta s}{\partial \omega} D_t \omega + \frac{\partial \Delta s}{\partial \tilde{\Sigma}} D_t \tilde{\Sigma}. \quad (3.92)$$

In Equation (3.92), the unknowns are only the partial derivatives of the mixing part of the entropy, since the SAP together with the set of constraints have returned evolution equations for the density, the velocity, the volume fraction, the pulsation and the interfacial density area. On the top of this equation, one needs to consider the constraint imposed by the hypothesis of two Gibbs equations, as shown in Chapter 2. From this set of equations, we should be able to propose a closure for the mixing part of the entropy.

To conclude this chapter, we would like to emphasize how strongly related the two-scale two-phase flow model are to the geometric constraints. Here, we have modelled the sub-scale topology of the flow as pulsating inclusions. As part of my PhD, we also have worked on another sub-scale closure considering ellipsoidal inclusions oscillating around a spherical shape. The new model has led to a publication Cordesse et al. (2019) [33] and the reader may refer to it in Appendix 3.B.

APPENDIX 3.A NORMAL PERTURBATION OF A REGULAR CLOSED SURFACE

Let \mathcal{D} be an open subset of \mathbb{R}^2 and I be an interval of \mathbb{R} . Consider a regular closed surface \mathcal{S} defined by the mapping $(u, v) \in \mathcal{D} \mapsto \mathcal{M}(u, v) \in \mathbb{R}^3$. We note $\mathbf{n}(u, v) \in \mathbb{R}^3$ the unit outward normal to \mathcal{S} at the point $\mathcal{M}(u, v) \in \mathcal{S}$. Let us now consider a family of surfaces $\mathcal{S}(h) = \{\mathcal{M}(u, v) + h \mathbf{n}(u, v) \in \mathbb{R}^3 \mid (u, v) \in \mathcal{D}\}$ parametrized by $h \in I$ where \mathcal{M} is a smooth mapping as depicted in Figure 3.3. Following [97], one can show that

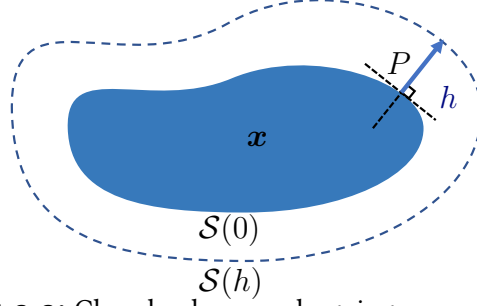


FIGURE 3.3: Closed volume undergoing normal variation

$$\text{meas}[\mathcal{S}(h)] = \text{meas}[\mathcal{S}(0)] - 2h \int_{P \in \mathcal{S}} H^{\text{loc}}(P) dP + O(h^2), \quad (3.93)$$

where dP is the standard surface measure defined over \mathcal{S} and $H^{\text{loc}}(P)$ is the mean curvature of \mathcal{S} at the point $P \in \mathcal{S}$. Let us define the average mean curvature $H_{\mathcal{S}}^{\text{loc}}$ of $\text{meas}(\mathcal{S})$ by

$$H_{\mathcal{S}}^{\text{loc}} = \frac{\int_{P \in \mathcal{S}} H^{\text{loc}}(P) dP}{\text{meas}[\mathcal{S}]}.$$

From (3.93) one deduces that

$$\frac{d}{dh}(\text{meas}[\mathcal{S}(h)]) = -2H_{\mathcal{S}}^{\text{loc}} \text{meas}[\mathcal{S}]. \quad (3.94)$$

Equation (3.93) is also referred as the first variation of the surface in Chow et al. (2006) [27]. The definition of the mean curvature varies among communities, letting the factor 2 sometimes vanish. We refer to the case of a spherical inclusion of radius R and define the mean curvature as the inverse of the radius, $H_{\mathcal{S}}^{\text{loc}} = 1/R$. Evaluating the surface variation of the sphere after a normal perturbation h gives

$$\frac{\mathcal{S}(h) - \mathcal{S}(0)}{h} = 8\pi R + O(h) = \frac{2}{R} 4\pi R^2 + O(h) = 2H_{\mathcal{S}}^{\text{loc}} \mathcal{S} + O(h). \quad (3.95)$$

Dividing by the reference volume and taking the limit $h \mapsto 0$ yields (3.94).

Injecting the definition of the average mean curvature into (3.93) and integrating over the normal variation h gives

$$\int_0^h \text{meas}[\mathcal{S}(h)] dh = \text{meas}[\mathcal{S}(0)] \int_0^h dh - 2H_{\mathcal{S}}^{\text{loc}} \int_0^h h dh + \int_0^h O(h^2) dh, \quad (3.96a)$$

$$V(h) = V(0)h + O(h^2). \quad (3.96b)$$

Taking the limit $h \mapsto 0$ provides the first variation of the volume

$$\frac{d}{dh}(V(h)) = \text{meas}[\mathcal{S}]. \quad (3.97)$$

APPENDIX 3.B A DIFFUSE INTERFACE APPROACH FOR DISPERSE TWO-PHASE FLOWS INVOLVING DUAL-SCALE KINEMATICS OF DROPLET DEFORMATION BASED ON GEOMETRICAL VARIABLES

ABSTRACT

The purpose of this contribution is to derive a reduced-order two-phase flow model including interface subscale modeling through geometrical variables based on Stationary Action Principle (SAP) and Second Principle of Thermodynamics in the spirit of [Drui et al. \(2019\) \[60\]](#), [Cordes et al. \(2020\) \[39\]](#). The derivation is conducted in the disperse phase regime for the sake of clarity but the resulting paradigm can be used in a more general framework. One key issue is the definition of the proper potential and kinetic energies in the Lagrangian of the system based on geometrical variables (Interface area density, mean and Gauss curvatures...), which will drive the subscale kinematics and dissipation, and their coupling with large scales of the flow. While [Drui et al. \(2019\) \[60\]](#) relied on bubble pulsation, that is normal deformation of the interface with shape preservation related to pressure changes, we aim here at tackling inclusion deformation at constant volume, thus describing self-sustained oscillations. In order to identify the proper energies, we use Direct Numerical Simulations (DNS) of oscillating droplets using ARCHER code and recently developed library, Mercur(v)e, for mean geometrical variable evaluation and analysis preserving topological invariants. This study is combined with historical analytical studies conducted in the small perturbation regime and shows that the proper potential energy is related to the surface difference compared to the spherical minimal surface. A geometrical quasi-invariant is also identified and a natural definition of subscale momentum is proposed. The set of Partial Differential Equations (PDEs) including the conservation equations as well as dissipation source terms are eventually derived leading to an original two-scale diffuse interface model involving geometrical variables.

INTRODUCTION

The simulation of two-phase flows in many industrial processes requires to account for physical phenomena that operate over a large range of different scales. For example, in the case of jet atomization in sub-critical conditions, the interface between the liquid and the gas experiences a dramatic change of topology from a separate-phase flow regime to a disperse flow regime. Although Direct Numerical Simulations (DNS) have provided impressive results in this field [Shinjo and Umemura \(2010\) \[201\]](#), [Desjardins et al. \(2013\) \[51\]](#), [Ling et al. \(2015\) \[140\]](#), [Zandian et al. \(2018\) \[225\]](#), they remain too costly in terms of computing resources to be applied in an industrial context or conduct parametrical studies. Therefore, the derivation of averaged models is still an important question and it has to cope with the predictive modeling of small scales of interfacial flows, which can not be resolved. Several authors have proposed various means to enrich these *reduced-order models* by introducing additional flow parameters that are reminiscent of small scale features that cannot be described by the bulk variables such as the density of interfacial area [M Devassy et al. \(2015\) \[148\]](#), or local curvature of the interface to account for small scale dynamics connected to capillary effects [Herrmann \(2013\) \[106\]](#). Works in this direction are also found in [Drui \(2017\) \[59\]](#), [Drui et al. \(2019\) \[60\]](#) where a unified model accounting for micro-inertia and micro-viscosity associated to bubble pulsation is proposed.

In this paper, we propose to focus on the coupling in a disperse flow between small and large scales through the kinematics description by revisiting the approach proposed in [Druil et al. \(2019\) \[60\]](#), [Cordesse et al. \(2020\) \[39\]](#) in a different physical setting.

More specifically, we propose to study means to supplement the bulk velocity that allows to represent large scale motions with additional parameters that describe small scale properties of the interface. Such approach relies on several hypotheses related to the evolution of the small scale features of the interface. The first assumption concerns the choice of kinetic and potential energies associated with the small scale motion. The second assumption deals with the connections between the small scale parameters. A set of constraints expressed by Partial Differential Equations (PDEs) has been proposed in [Cordesse et al. \(2020\) \[39\]](#) by considering that small scale perturbations behave in the same way as small amplitude motions along the normal to the interface.

In this contribution, we propose to examine a complementary type of small scale motions by considering ellipsoidal deformed droplets oscillating around a spherical shape. An analytic study of this problem has been achieved in [Chandrasekhar \(1981\) \[22\]](#) thanks to a harmonic analysis based on the work of Taylor and was also reproduced in [O'Rourke and Amsden \(1987\) \[167\]](#) about the well-known TAB model for secondary break-up. More recently, [Herrmann \(2013\) \[106\]](#) considered a harmonic oscillator involving another set of variables, including mean curvature. Revisiting the theory allows to show that the various approaches are equivalent in the limit of small perturbations but we aim at deriving a model valid with large deformations. We thus need to propose the proper set of kinetic and potential energies related to the droplet deformations and the proper variables in order to describe such physics. We propose to rely on a DNS of a single droplet performed with the code ARCHER and a post-processing library `Mercur(v)e`, which is designed for mean geometrical variable evaluation and analysis preserving topological invariants. The results of this simulation suggest a specific choice for both the constraints to be applied on the small scale dynamics and the small scale kinetic and potential energies defined as function of the proper variable, which is the surface variation compared to the spherical minimal surface of the inclusions. The system of PDEs is eventually derived and involves both large scale and small scales dynamics as well as their coupling through convection and dissipation.

The paper is organized as follows: we first briefly recall the main results obtained by an harmonic analysis of the motion of an ellipsoidal droplet performed in [Chandrasekhar \(1981\) \[22\]](#) in the limit of an infinitely small perturbation and extend the derivations to obtain analytical expressions for several geometric variables involved in the dynamics beyond the kinetic energy and the potential energy. We then introduce the DNS results obtained with the code ARCHER and post-processed by the library `Mercur(v)e` in order to estimate the evolution of geometric variables and associated potential energies. We identify the proper variable for the potential energy to remain harmonic in the large deformation regime, thus identifying the best candidate to use the SAP. Finally, we propose a new set of PDEs that relates parameters accounting for small scale motion of the interface and the new form of potential and kinetic energies. The proposed form of the equations and identification of the various contribution in the Lagrangian naturally allow to separate the properties of the interface between large scales and small scales in the two-phase system. This is a specific case of a more general approach where a systematic framework is proposed in order to conduct such a study in the general case of separated and disperse phases [Cordesse et al. \(2020\) \[34\]](#). Thanks to the Stationary Action Principle, we obtain a set of evolution equations for the medium without dissipation

that enables us to assess the hyperbolic behaviour of the system. Eventually, we show that this system of equations can be complemented with a mathematical entropy evolution equation that is compatible with the Second Principle of Thermodynamics. This helps bringing up additional terms to the system that account for internal dissipation mechanisms.

3.B.1 OSCILLATING INCLUSION SUBSCALE MODELLING

3.B.1.1 OSCILLATING INCLUSION LITERATURE REVIEW

In [Taylor \(2011\) \[208\]](#), Sir G.I. Taylor studied secondary breakup through droplet deformation under a non-homogeneous pressure field and surface tension. He noticed an oscillating phenomena among the droplets, which he saw as an important source of dissipation for the system. This phenomenon leads to a higher pressure difference than expected before breakup of the droplets, as the energy from the pressure wave gets converted into mechanical oscillating energy and thus is rapidly dissipated. He concluded that in order to get a satisfactory model of secondary breakup, the frequency of the incoming pressure waves should be compared to the oscillating frequency of the droplets since some frequencies may trigger droplet oscillation rather than breakup.

Later on, in [Chandrasekhar \(1981\) \[22\]](#), S. Chandrasekhar considered an object with a deformation around its original spherical shape governed by a spherical harmonic function. He solved the velocity field inside a spherical droplet that is only subjected to its own weight, and then drew a formal analogy with a droplet experiencing surface tension. The exact resolution of the velocity field is conducted through solving Laplace's equation using the potential nature of gravity, and using Kelvin's formulas in the limite of small displacements. In this approach, the key variable leading to a harmonic oscillation is the amplitude of the spherical harmonic function, the frequency of oscillation being related to the characteristics of the spherical harmonic perturbation and droplet physical parameters. The derivations were extended for bubbles in [Prosperetti \(1980\) \[180\]](#) and the reader is referred to [Lalanne et al. \(2013\) \[124\]](#) for a more modern view on the literature on which we will come back later.

3.B.1.2 ANALYTICAL ENERGY BALANCE OF AN ISOLATED OSCILLATING INCLUSION

The analytic derivation of the flow field arising in a droplet of radius R , oscillating due to capillarity, the surface tension coefficient of which is denoted σ , may be found in [Chandrasekhar \(1981\) \[22\]](#), [Lamb \(1945\) \[125\]](#) and we briefly recall here some of the main results.

In the limit of small initial perturbations and considering one deformed incompressible spherical inclusion, the governing equations can be linearized as

$$\rho \partial_t \mathbf{v} = -\nabla p - \mu \nabla \wedge (\nabla \wedge \mathbf{v}) , \quad (3.98)$$

$$\nabla \cdot \mathbf{v} = 0 , \quad (3.99)$$

leading to the harmonic pressure field $\Delta p = 0$.

Under the assumption that the initial surface deformation of the droplet is described by spherical harmonic functions Y_l^m , the flow field may be explicitly calculated as a harmonic function of time for both inviscid and viscous cases and thus yields the evolution of kinetic \mathcal{K} and potential \mathcal{U} energies per unit of volume during the oscillation of the droplet.

We choose to focus on a small axisymmetric ellipsoidal perturbation with of non-dimensionalized magnitude $\eta \ll 1$ ($\eta = p/q - 1$, where p and q are the large and small axis of the ellipse - see Appendix 3.B.4.1), which is applied to a spherical liquid droplet. Thus, the initial perturbation surface function of r/R may be approximated by the Y_2^0 spherical harmonic, as detailed in Appendix 3.B.4.1. It leads to the following expression for the kinetic and potential energies per unit of volume

$$\mathcal{K} = \frac{8}{45} \sigma \Sigma_0 \eta^2 \sin^2 \left(\sqrt{\frac{8\sigma}{\rho R^3}} t \right), \quad (3.100)$$

$$\mathcal{U} = \frac{8}{45} \sigma \Sigma_0 \eta^2 \cos^2 \left(\sqrt{\frac{8\sigma}{\rho R^3}} t \right), \quad (3.101)$$

where the reference interfacial density area Σ_0 is defined as the reference surface $\mathcal{S}_0 = 4\pi R^2$ divided by the volume V of interest (which will be the volume of the simulation in the DNS configuration). It is then clear that the potential energy, in this limit, is a harmonic function, reaching zero every time a spherical shape is recovered, the frequency of which is clearly identified and coherent with various contributions in the literature. Let us underline that the system naturally admits an invariant quantity in the limit of small perturbations $\Sigma + 3 \langle H \rangle \alpha = 0$ (see Appendix 3.B.4.1 - bracket notation is dropped in it), where $\alpha = V_0/V$ is a constant, $V_0 = 4\pi R^3/3$, Σ is the surface area density and $\langle H \rangle$ the surface averaged mean curvature of the droplet. However, at this level, the key issue is the functional dependency of the potential energy since several quantities are harmonic oscillators in the limit of small perturbations.

Indeed, in the asymptotic case of small deformations, two expressions are eligible for the potential energy of the oscillating droplet. The first is directly related to the excess surface of the perturbed droplet and reads:

$$\mathcal{U} = \sigma (\Sigma - \Sigma_0), \quad (3.102)$$

the second one is, following Herrmann [Herrmann \(2013\) \[106\]](#), related to the surface averaged mean curvature $\langle H \rangle$ of the droplet and reads

$$\mathcal{U} = \sigma \Sigma_0 (\langle H \rangle - H_0) / H_0, \quad (3.103)$$

where Σ and $\langle H \rangle$ expressions are given in Appendix 3.B.4.1 and where $H_0 = -1/R$.

Furthermore, in [O'Rourke and Amsden \(1987\) \[167\]](#), a harmonic oscillator model was derived providing a new modeling strategy called TAB (for *Taylor Analogy Breakup*). This model allows for a better handling of secondary breakup through modeling high Weber number spherical droplets as ellipsoids with axisymmetric forms, a framework closely related to our problem. The key parameter in this approach leading to harmonic oscillations is the displacement of the equator of the droplet from its equilibrium position noted x .

In the following, a DNS-based study will be conducted in order to discriminate what should be the proper variable underlying the definition of the potential energy, keeping in mind that several variables are harmonic functions in the limit of small displacement, but we aim at defining a subscale model relying on an oscillator that is valid beyond the regime of infinitely small perturbations.

3.B.1.3 DIRECT NUMERICAL SIMULATION COMPARISON AND VALIDATION

The PhD of R. Di Battista [Di Battista et al. \(2019\) \[54\]](#) at CMAP laboratory proposes a methodology to perform post-processing of DNS simulations exploiting geometrical properties of the interface between two phases. In particular, a library called `Mercur(v)e` has been developed and allows the characterization of two-phase interface geometrical features thanks to a triangulation of the interface and the calculation of geometrical properties from the discretized surface, while preserving topological and geometrical invariants of the considered objects. We rely on this tools to study droplet pulsation or collisions. We propose in this work to apply the same methodology in order to investigate small axisymmetric ellipsoidal deformations of a liquid droplet in order to gain insight on the evolution of the droplet geometrical features. Therefore, we will first perform DNS simulations of the axisymmetric ellipsoidal deformation of a spherical droplet with ARCHER and then use `Mercur(v)e` to compute its geometrical features.

Two-phase Interface Model and Discretization Strategy of the code ARCHER The code ARCHER is developed at the CORIA laboratory. It has been successfully used for simulating the atomization of a liquid-jet under a realistic diesel injection configuration [Ménard et al. \(2007\) \[158\]](#). The two-phase medium considered in ARCHER is composed by two incompressible fluids separated by a sharp interface. The position of the interface and the description of its geometrical characteristics is ensured by a Coupled Level Set/Volume of Fluid (CLSVOF) method: a Level Set function is used for evaluating the normal and the curvature of the interface while the Volume of Fluid approach ensures the mass conservation of each component. A key element of the numerical strategy implemented in ARCHER relies on solving a Poisson equation for the dynamic pressure that is performed using a MultiGrid preconditioned Conjugate Gradient algorithm (MGCG) [Zhang \(1996\) \[227\]](#) coupled with a Ghost-Fluid method [Fedkiw et al. \(1999\) \[69\]](#) to take into account the pressure jump due to the presence of surface tension. The time-integration is performed with a second-order Runge-Kutta scheme. For more information about the ARCHER solver, we refer the reader to [Ménard et al. \(2007\) \[158\]](#), [Duret et al. \(2012\) \[64\]](#), [Canu et al. \(2018\) \[20\]](#), [Vaudor et al. \(2017\) \[216\]](#).

Interface triangulation and geometrical properties estimation in `Mercur(v)e` `Mercur(v)e` library takes as input the volumetric Level-Set field provided by ARCHER and performs an iso-contouring procedure using a Marching Cube approach [Lorensen and Cline \(1987\) \[145\]](#), [Schroeder et al. \(2015\) \[198\]](#), generating a triangulated and discretized representation of the interface. For each vertex of the triangles composing the discretized interface, geometrical properties are estimated as *1-ring surface-averaged quantities* as presented in [Meyer et al. \(2003\) \[159\]](#), where the *1-ring* is a portion of surface around a vertex that is equivalent to a Voronoi region if the triangles composing it are non-pathological. For pathological cases an error-bounding fix is possible. This computational approach guarantees the conservation of the Gauss-Bonnet theorem in discrete form. For more information the reader can refer to [Di Battista et al. \(2019\) \[54\]](#), [Essadki et al. \(2019\) \[67\]](#).

Direct Numerical Simulation configuration The computational domain is a box of dimension $40 \times 40 \times 40 \mu\text{m}$ that is discretized over a regular Cartesian grid with 128 points per dimension leading to a total of 2 097 152 computational nodes. Symmetric boundary conditions are imposed on each face of the domain. The kinematic viscosity of the fluid is set to $\nu = 1.7\text{e}-8 \text{ m s}^{-2}$. We consider as initial condition a deformed droplet with an axisymmetric

ellipsoidal shape that will evolve due to surface tension effects: the initial shape is defined thanks to the zero-level of a Level Set such that the semi-major axis p over semi-minor axis q ratio is $p/q = (1.08, 1.15)$ and such that the volume of the droplet is $\frac{4}{3}\pi R^3$ with $R = 10\ \mu\text{m}$. The computational load for a single run is $1280\ h.CPU$ which represents $20\ h$ of computation over $64\ CPU$. We have chosen two deformation amplitudes, one will still be in the small perturbation limit leading to harmonic oscillations of most of the considered quantities, while the second will allow to go beyond this regime and discriminate the proper variables.

Figure 3.4 shows the initial Level-Set volumetric field and the triangulated interface obtained with Mercur(v)e.

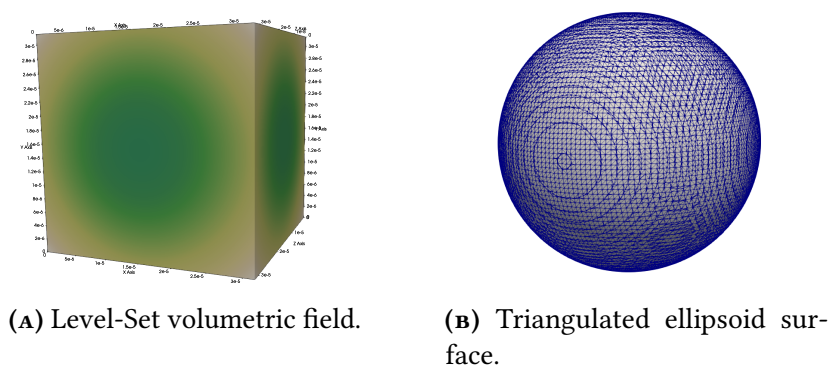


FIGURE 3.4: The initial configuration of the ellipsoidal droplet.

Results One period T of evolution of the droplet deformation is shown in Figure 3.5. At

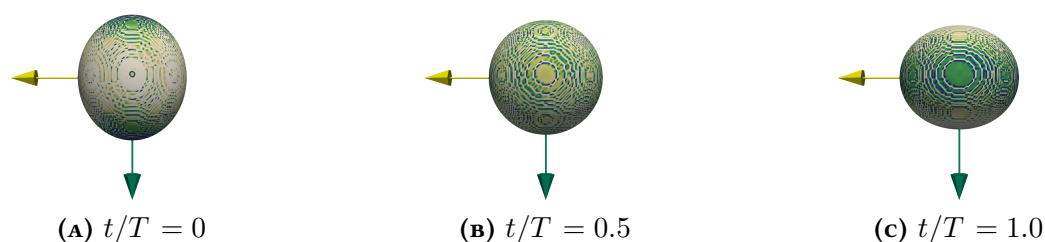


FIGURE 3.5: One period T of evolution of the deformed droplet. The colormap maps values of the Gauss curvature from low to high.

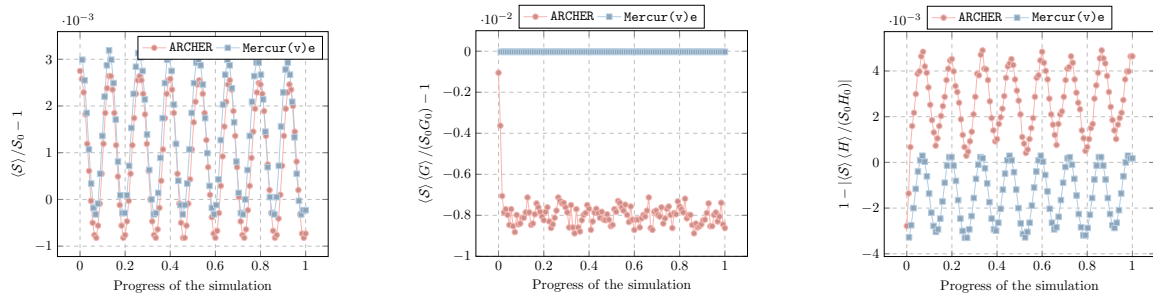
$t/T = 0$, Figure 3.5a, the droplet is initially at a prolate state. Due to capillarity, the droplet potential energy starts to be converted into kinetic energy such that the droplet reaches a spherical shape in Figure 3.5b, and then continues to deform such that at $t/T = 1.0$, Figure 3.5c, the droplet is in an oblate configuration.

We now investigate the evolution of geometric quantities over the whole simulation time and integrated over the surface of the droplet for two different initialization of the deformed droplet, $p/q = 1.08$ and $p/q = 1.15$ which correspond to $\eta = 0.08$ and $\eta = 0.15$.

Figures 3.6b and 3.7b display the relative mean Gauss curvature ratio, with S_0G_0 the integral of the Gauss curvature over the spherical droplet, $S_0G_0 = 4\pi$. It is found to be constant

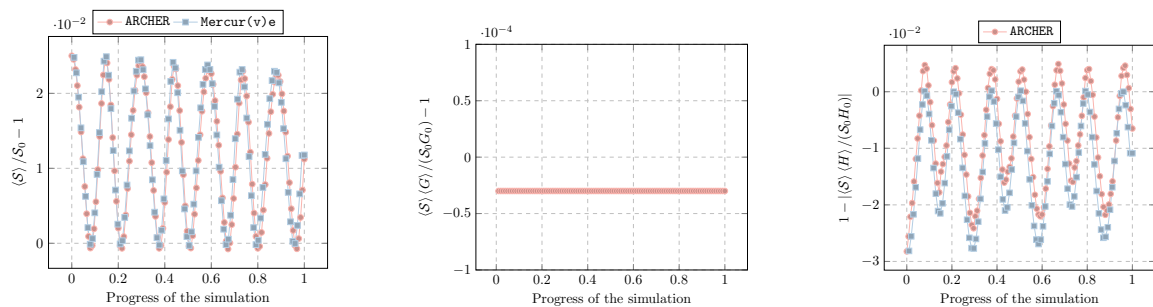
and close to zero with three orders of magnitude less than the amplitudes of the other quantities. This result was expected since from the Gauss-Bonnet theorem, $\langle G \rangle$ is a topological invariant, but it attests the reliability of the post-processing library Mercur(v)e. Let us underline from the various evaluations, that it is essential to use the Mercur(v)e library for two reasons : 1- we can guarantee the proper evaluation of the topological invariant through a discrete verification of the Gauss-Bonnet theorem, 2- the level of error obtained from the library compared to the evaluation conducted in ARCHER directly from the Level-Set function is much lower and it is essential in this configuration of small perturbation in order to draw some firm conclusions from the investigation. Depending on the cases, since the references quantities used for the relative quantity ratio are exact characteristics of the sphere, mainly functions of its radius, we can have a slight shift in the quantities represented as observed in Figures 3.6a and 3.6c. It is due to the level set formulation and to its discretization on the proposed grid, which is not guaranteed to preserve exactly the volume V_0 or the surface S_0 of the sphere.

Figures 3.6a and 3.7a show the relative surface ratio evolution over the simulation time, with $S_0 = 4\pi R^2$ the theoretical surface of the droplet when reaching a spherical shape. As we can see, once the droplets is left unconstrained in its perturbed configuration, its surface evolves as a harmonic oscillator, as well as the mean curvature, even if we can detect a small departure from harmonic oscillations. This is the reason why we have provided a second case, with larger amplitude, where this departure is more pronounced.



(A) Relative surface ratio. (B) Relative surface averaged Gauss curvature ratio. (C) Relative surface averaged Mean curvature ratio.

FIGURE 3.6: Evolution of the geometrical properties ($p/q = 1.08$).



(A) Relative surface ratio. (B) Relative surface averaged Gauss curvature ratio. (C) Relative surface averaged Mean curvature ratio.

FIGURE 3.7: Evolution of the geometrical properties ($p/q = 1.15$).

Actually, as plotted in [Figure 3.7c](#), the relative mean Mean curvature does not show the same behavior for a larger deformation. The integral of the Mean curvature of the droplet at its spherical state divided by the surface reads $H_0 = -1/R$. Two non-identical periodic peaks are clearly visible, suggesting the surface averaged mean curvature is not harmonic, thus disqualifying the potential energy expressed in terms of $\langle H \rangle$ as the proper harmonic oscillator. It confirms that the energy term associated to the "loss of sphericity" expressed in terms of the interfacial density area $\sigma(\Sigma - \Sigma_0)$ is reliably representing the underlying harmonic oscillation phenomenon as observed in [Figure 3.7a](#). This is also coherent with what has been observed numerically and experimentally for bubbles [Lalanne et al. \(2013\) \[124\]](#), where the harmonic oscillation behavior is very robust, even within the framework of large deformations, an essential feature of the model we aim at building.

Eventually, [Figure 3.8](#) emphasizes the volume conservation over time of the deformed droplet by plotting the relative volume ratio where V_0 is the volume of the droplet when reaching its spherical shape, $V_0 = 4/3\pi R^3$. Again, the order of magnitude is 3 times less than

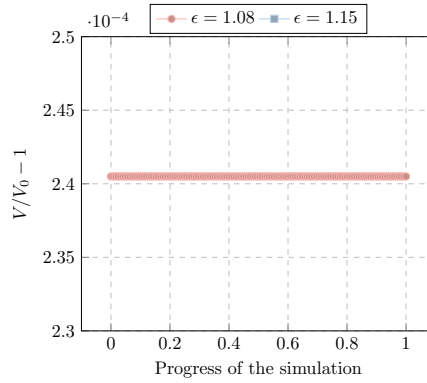


FIGURE 3.8: Relative volume ratio conservation.

the amplitude of the surface, and similar to the relative ratio of the mean Gauss curvature. These residuals quantify the error made by the post-processing library.

As mentioned before and relying on an analytical derivation presented in [Appendix 3.B.4.1](#), we have identified a quasi-invariant quantity, holding exactly in the limit of small perturbations: $I = \Sigma + 3 \langle H \rangle \alpha$. In [Figure 3.9](#), we plot the corresponding extensive quantity over the simulation time obtained with the DNS.

[Figure 3.9](#) highlights the level of invariance of the quantity $I = \Sigma + 3 \langle H \rangle \alpha$, even for a larger perturbation, $p/q = 0.15$, allowing its applicability only for relatively slight perturbations from the equilibrium spherical configuration.

3.B.2 TWO-SCALE KINEMATICS TWO-PHASE FLOW MODEL

We will now follow the lines proposed in [Gavrilyuk and Saurel \(2002\) \[81\]](#), [Drui et al. \(2019\) \[60\]](#) for instance in order to elaborate a two-phase model that accounts for both large scale kinematics and small scale kinematics using the results of [section 3.B.1](#).

We consider two compressible fluids $k = 1, 2$. Each of them is equipped with a barotropic

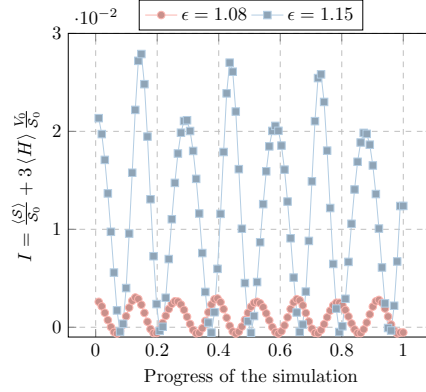


FIGURE 3.9: Time evolution of the relative geometrical quasi-invariant

equation of state (EOS) defined by $\rho_k \mapsto f_k(\rho_k)$, where f_k and ρ_k are respectively the specific barotropic energy and the density of the fluid k . The partial pressure p_k and the sound velocity a_k of the component k are defined by $p_k = \rho_k^2 (df_k/d\rho_k)$, $a_k^2 = dp_k/d\rho_k$.

We suppose that there is a large scale kinematic equilibrium in the sense that both fluid k have the same bulk velocity \mathbf{v} . We note α_k the volume fraction of the fluid k and we suppose that two-component medium to be immiscible so that we have $\alpha_1 + \alpha_2 = 1$. The density ρ of the overall medium is defined by $\rho = \alpha_1\rho_1 + \alpha_2\rho_2$ and the mass fraction y_k of the fluid k verifies $\rho y_k = \alpha_k\rho_k$. We set $\alpha = \alpha_1 = 1 - \alpha_2$ and $Y = y_1 = 1 - y_2$. We also suppose that two additional parameters pertaining to the geometry of the interface are defined on the whole computational domain: $(\mathbf{x}, t) \mapsto \Sigma$ and $(\mathbf{x}, t) \mapsto H$ that respectively denotes the density of interfacial area and the mean curvature of the interface.

3.B.2.1 HYPOTHESES RELATED TO THE SMALL SCALE KINEMATICS

As the droplets are deforming, the variation of their surface, the mean curvature and the volume are connected. In our case, the deformation of the inclusion is expressed by the variations of the parameters Σ , H and α , so that the variations of the latter shall not be independent. In [Cordesse et al. \(2020\) \[39\]](#), the authors considered a single surface modified by a small displacement $\mathbf{n}\delta h$ oriented along the normal \mathbf{n} of interface. In that case, the infinitesimal variations $\delta\Sigma$, δH and $\delta\alpha$ verify¹

$$\delta\Sigma = -2H\Sigma h, \quad \delta\alpha = \Sigma\delta h.$$

As in [Cordesse et al. \(2020\) \[39\]](#), [Cordesse et al. \(2019\) \[40\]](#), this suggested to assume that

$$D_t\Sigma + 2HD_t\alpha = 0. \quad (3.104)$$

If the variations of H along the streamlines can be neglected, that is to say $D_tH = 0$, then one obtains $D_t(\Sigma + 2H\alpha) = 0$, which means that $\Sigma + 2H\alpha$ remains constant along the streamlines.

In the present configuration, the deformations are no more normal to the interface, preventing the use of above geometric constraints. Furthermore in agreement with the volume conservation showed in [Figure 3.8](#), we suppose that the small scale motion of the droplets is

¹For sake of simplicity, from now on, we drop the surface averaging operator $\langle \cdot \rangle$.

incompressible. As a consequence, if no breakup occurs, the volume of each droplet remains constant. It first implies that $D_t\alpha = 0$, but also that the volumetric density number of the droplet is constant, allowing us to apply the results of Section 3.B.1 valid for a single droplet to a spray of droplets. We thus propose to consider that the small scale kinematics of the droplets is now constrained by the relations

$$D_t(\Sigma + 3H\alpha) = 0, \quad D_t\alpha = 0. \quad (3.105)$$

Thanks to the results of the previous section 3.B.1.3, we can single out parameters that show the oscillating behavior of the system and parameters that are invariant during the small scale motion. According to Figures 3.6 and 3.7, the oscillating profile obtained for the density of interfacial area Σ suggests to drive the motion of the small scale using Σ . We express this choice in the definition of our system by considering a small scale kinetic energy \mathcal{K} and a potential energy pertaining to small scale capillary effects \mathcal{U} as follows

$$\mathcal{K} = \frac{1}{2}\nu_\Sigma(D_t\Sigma)^2, \quad \mathcal{U} = \sigma\Sigma, \quad (3.106)$$

where $\nu_\Sigma = \nu_\Sigma(\Sigma) > 0$ and the capillarity coefficient $\sigma > 0$ is supposed to be constant.

3.B.2.2 LAGRANGIAN ENERGY OF THE TWO-PHASE SYSTEM

We proceed following Druil et al. (2019) [60], Cordesse et al. (2020) [39] by postulating a Lagrangian energy L associated with our system. This energy is the difference between the kinetic energy of the system and the potential energy. Concerning the kinetic energy, we simply add the classic kinetic energy associated with the bulk kinematic $\frac{1}{2}\rho\|\mathbf{v}\|^2$ and the small scale kinetic energy \mathcal{K} . We assume that the medium is equipped with a specific bulk potential energy of the form $f(\rho, Y, \alpha)$. This suggests to postulate the following form for L

$$L = \frac{1}{2}\rho\|\mathbf{v}\|^2 + \frac{1}{2}\nu_\Sigma(D_t\Sigma)^2 - \sigma\Sigma - \rho f(\rho, Y, \alpha) \quad (3.107)$$

Following the lines of Druil et al. (2019) [60], Cordesse et al. (2020) [39], we consider the motion of a portion of medium that occupies the volume $\mathcal{B}(t)$ for $t \in [t_0, t_1]$. We note $(t, \mathbf{X}) \mapsto \varphi^L(t, \mathbf{X})$ the position of at instant t of a fluid particle that was initially located at \mathbf{X} and set $\Omega = \{(t, \varphi^L(t, \mathbf{X})) \mid \mathbf{X} \in \mathcal{B}(t_0), t \in [t_0, t_1]\}$. We consider a transformation of the medium that defined by the fields $(t, \mathbf{x}) \mapsto (\rho, \mathbf{v}, Y, \alpha, H, \Sigma)$ and the mapping $(t, \mathbf{X}) \mapsto \varphi^L(t, \mathbf{X})$ that verifies the small scale kinematics (3.105) hypotheses and the mass conservation equations

$$\partial_t\rho + \operatorname{div}(\rho\mathbf{v}) = 0, \quad \partial_t(\rho Y) + \operatorname{div}(\rho Y\mathbf{v}) = 0. \quad (3.108)$$

We now consider a family of transformations medium $(t, \mathbf{x}, \lambda) \mapsto (\rho_\lambda, \mathbf{v}_\lambda, Y_\lambda, \alpha_\lambda, H_\lambda, \Sigma_\lambda)$ and $(t, \mathbf{X}, \lambda) \mapsto \varphi_\lambda^L(t, \mathbf{X}, \lambda)$ that are parameterized by $\lambda \in [0, 1]$. We note $\Omega_\lambda = \{(t, \varphi_\lambda^L(t, \mathbf{X}, \lambda)) \mid \mathbf{X} \in \mathcal{B}(t_0), t \in [t_0, t_1], \lambda \in [0, 1]\}$ and we suppose that these fields also verify the small scale kinematics hypotheses (3.105) and the mass conservation equations, that is to say

$$D_t\Sigma_\lambda + 3\alpha_\lambda D_t H_\lambda = 0, \quad D_t\alpha_\lambda = 0, \quad (3.109a)$$

$$\partial_t\rho_\lambda + \operatorname{div}(\rho_\lambda\mathbf{v}_\lambda) = 0, \quad \partial_t(\rho_\lambda Y_\lambda) + \operatorname{div}(\rho_\lambda Y_\lambda\mathbf{v}_\lambda) = 0, \quad (3.109b)$$

supplemented with the classic boundary constraints

$$(\rho_\lambda, Y_\lambda, \alpha_\lambda, \Sigma_\lambda, H_\lambda)(t, \mathbf{x}, \lambda = 0, 1) = (\rho, Y, \alpha, \Sigma, H)(t, \mathbf{x}) \quad \lambda = 0, 1, \quad (3.110a)$$

$$\varphi_\lambda^L(\mathbf{X}, t, \lambda = 0, 1) = \varphi^L(\mathbf{X}, t), \quad \lambda = 0, 1 \quad (3.110b)$$

$$(\rho_\lambda, Y_\lambda, \alpha_\lambda, \Sigma_\lambda, H_\lambda)(t, \mathbf{x}, \lambda) = (\rho, Y, \alpha, \Sigma, H)(t, \mathbf{x}), \quad (t, \mathbf{x}) \in \partial\Omega_\lambda \quad (3.110c)$$

$$\varphi_\lambda^L(\mathbf{X}, t, \lambda) = \varphi^L(\mathbf{X}, t), \quad (t, \mathbf{X}) \in \partial([t_0, t_1] \times \mathcal{B}(t_0)). \quad (3.110d)$$

Following standard lines, this family of transformation yields a family of infinitesimal transformations defined by

$$\delta_\lambda \varphi(t, \varphi^L(t, \mathbf{X})) = \left(\frac{\partial \varphi_\lambda^L}{\partial \lambda} \right)_{t, \mathbf{X}} (t, \mathbf{X}, \lambda = 0), \quad (3.111a)$$

$$\delta_\lambda b(t, \mathbf{x}) = \left(\frac{\partial b_\lambda}{\partial \lambda} \right)_{t, \mathbf{x}} (t, \mathbf{x}, \lambda = 0), \quad (3.111b)$$

for $b \in \{\rho, Y, \alpha, \Sigma, H\}$. Applying (3.111) with the constraints (3.109) allows to express following relations between the infinitesimal variations

$$\delta_\lambda \rho = -\operatorname{div}(\rho \delta_\lambda \varphi), \quad \delta_\lambda \mathbf{v} = D_t(\delta_\lambda \varphi) - (\delta_\lambda \varphi^T \nabla) \mathbf{v}, \quad \delta_\lambda b = -\delta_\lambda \varphi^T \nabla b, \quad b \in \{Y, \alpha\}, \quad (3.112a)$$

$$\delta_\lambda H = -\delta_\lambda \Sigma / (3\alpha) - (\nabla \Sigma^T / (3\alpha) + \nabla H^T) \delta_\lambda \varphi. \quad (3.112b)$$

3.B.2.3 EXTREMIZATION OF THE ACTION

Let us now define the Hamiltonian action \mathcal{A} associated with the family of transformations $(t, \mathbf{x}, \lambda) \mapsto (\rho_\lambda, Y_\lambda, \alpha_\lambda, \Sigma_\lambda)$ and $(t, \mathbf{X}, \lambda) \mapsto \varphi_\lambda^L$ by setting

$$\mathcal{A}(\lambda) = \int_{\Omega_\lambda} L(\rho_\lambda, \mathbf{v}_\lambda, Y_\lambda, \alpha_\lambda, D_t \Sigma_\lambda, \Sigma_\lambda) d\mathbf{x} dt. \quad (3.113)$$

The Least Action Principle states that a physical transformation of the system verifies

$$\frac{d\mathcal{A}}{d\lambda}(0) = 0. \quad (3.114)$$

which will yield the motion equations of the flow. We introduce the following notations

$$\mathbf{K}^T = \left(\frac{\partial L}{\partial \mathbf{v}} \right), \quad N = \left(\frac{\partial L}{\partial D_t \Sigma} \right), \quad L + L^* = \rho \left(\frac{\partial L}{\partial \rho} \right). \quad (3.115)$$

Relation (3.114) reads

$$\int_\Omega \left([L + L^*] \delta \rho + \mathbf{K}^T \delta \mathbf{v} + \frac{\partial L}{\partial Y} \delta Y + \frac{\partial L}{\partial \alpha} \delta \alpha + \frac{\partial L}{\partial \Sigma} \delta \Sigma + N \delta(D_t \Sigma) \right) d\mathbf{x} dt = 0. \quad (3.116)$$

We follow standards lines: taking into account (3.112), (3.110c) and (3.110d), after thorough calculations relation (3.116) provides

$$0 = \int_\Omega \left\{ \left[-\rho D_t(\mathbf{K}/\rho) + \nabla L^* + \left(\frac{\partial L}{\partial \Sigma} - \rho D_t(N/\rho) \right) \nabla \Sigma \right]^T \delta_\lambda \varphi + \left(\frac{\partial L}{\partial \Sigma} - \rho D_t(N/\rho) \right) \delta_\lambda \Sigma \right\} d\mathbf{x} dt,$$

for any $\delta_\lambda \varphi$ and $\delta_\lambda \alpha$. It implies that

$$\rho D_t(\mathbf{K}/\rho) = \nabla L^*, \quad (3.117a)$$

$$\rho D_t(N/\rho) = \frac{\partial L}{\partial \Sigma}. \quad (3.117b)$$

Finally, by gathering the mass conservation equations (3.108), the small scale kinematics equations (3.105) and the evolution equations derived by the stationary action principle, we see that the full system that governs our two-phase model is

$$\partial_t \rho + \operatorname{div}(\rho \mathbf{v}) = 0, \quad (3.118a)$$

$$\partial_t(\rho Y) + \operatorname{div}(\rho Y \mathbf{v}) = 0 \quad (3.118b)$$

$$\rho D_t(\mathbf{K}/\rho) - \nabla L^* = 0 \quad (3.118c)$$

$$\rho D_t(N/\rho) - \frac{\partial L}{\partial \Sigma} = 0 \quad (3.118d)$$

$$D_t \Sigma + 3\alpha D_t H = 0, \quad (3.118e)$$

$$D_t \alpha = 0. \quad (3.118f)$$

3.B.2.4 COMPANION CONSERVATION EQUATION

Manipulating evolution equations (3.117a) and (3.117b), we obtain

$$\rho D_t \left(\frac{1}{\rho} (L - \mathbf{K}^t \mathbf{v} - N D_t \Sigma) \right) + \nabla \cdot (L^* \mathbf{v}) = 0. \quad (3.119)$$

Defining a total energy ρE as

$$\rho E = \mathbf{K}^t \mathbf{v} + N D_t \Sigma - L, \quad (3.120)$$

Equation (3.119) yields a supplementary conservative equation on ρE

$$\partial_t(\rho E) + \nabla \cdot (\rho E \mathbf{v} - L^* \mathbf{v}) = 0. \quad (3.121)$$

3.B.2.5 FINAL SYSTEM

In order to express the system of equations of our model in a more natural way, we start by making explicit the derivative of L defined by (3.107). We have

$$\frac{\partial L}{\partial \Sigma} = -\sigma + \frac{1}{2} \nu'_\Sigma(\Sigma) (D_t \Sigma)^2, \quad \frac{\partial L}{\partial \alpha} = -\rho \frac{\partial f}{\partial \alpha}, \quad \mathbf{K} = \rho \mathbf{v}, \quad (3.122a)$$

$$N = \nu_\Sigma(\Sigma) D_t \Sigma, \quad \frac{\partial L}{\partial \rho} = \frac{|\mathbf{v}|^2}{2} - \rho \frac{\partial f}{\partial \rho} - f, \quad (3.122b)$$

$$L^* = -\rho^2 \frac{\partial f}{\partial \rho} + \sigma \Sigma - \frac{1}{2} \nu_\Sigma(\Sigma) (D_t \Sigma)^2. \quad (3.122c)$$

We define the pressure p of the two-phase flow medium by

$$p = \rho^2 \frac{\partial f}{\partial \rho}, \quad (3.123)$$

and introduce new variable ω_Σ that accounts for the pulsation effects by setting

$$\rho Y \omega_\Sigma = D_t \Sigma. \quad (3.124)$$

Injecting these relations into Equations (3.118), we obtain the system

$$\partial_t \rho + \operatorname{div}(\rho \mathbf{v}) = 0, \quad (3.125a)$$

$$\partial_t(\rho Y) + \operatorname{div}(\rho Y \mathbf{v}) = 0, \quad (3.125b)$$

$$\rho D_t \mathbf{v} + \nabla \mathcal{P} = \mathbf{0}, \quad (3.125c)$$

$$D_t \Sigma - \rho Y \omega_\Sigma = 0. \quad (3.125d)$$

$$D_t \omega_\Sigma + \frac{1}{Y \rho \nu_\Sigma} \sigma + \frac{1}{2} \frac{\nu'_\Sigma}{\nu_\Sigma} \rho Y \omega_\Sigma^2 + \frac{1}{\rho Y \nu_\Sigma} = 0, \quad (3.125e)$$

$$D_t \alpha = 0, \quad (3.125f)$$

$$D_t H + \frac{1}{3\alpha} \rho Y \omega_\Sigma = 0, \quad (3.125g)$$

with the extended pressure $\mathcal{P} = -L^* = p + \frac{1}{2} \nu_\Sigma (\rho Y \omega_\Sigma)^2 - \sigma \Sigma$. The supplementary conservative equation on the total energy E reads

$$\partial_t(\rho E) + \nabla \cdot (\rho E \mathbf{v} + \mathcal{P} \mathbf{v}) = 0, \quad (3.126)$$

with

$$\rho E(\rho, Y, \mathbf{v}, \alpha, \omega, \Sigma) = \frac{1}{2} \rho |\mathbf{v}|^2 + \frac{1}{2} \nu_\Sigma (D_t \Sigma)^2 + \sigma \Sigma + \rho f(\rho, Y, \alpha). \quad (3.127)$$

The Least Action Principle does not account for irreversible process. Thus, system (3.125) is purely non-dissipative. We shall propose in the next section additional terms that account for inner dissipation processes that are compatible with the Second Principle of Thermodynamics.

3.B.2.6 DISSIPATION

Following the lines of [Drui et al. \(2019\) \[60\]](#), we seek an entropy flux \mathbf{G} and additional terms in the evolution equation of ω_Σ and α so that we can obtain an evolution equation for E of the form

$$\rho D_t E + \nabla \cdot \mathbf{G} \leq 0, \quad (3.128)$$

or equivalently, noticing that $D_t Y = 0$,

$$\nabla \cdot \mathbf{G} + \rho \frac{\partial E}{\partial \rho} D_t \rho + \rho \left(\frac{\partial E}{\partial \mathbf{v}} \right)^t D_t \mathbf{v} + \rho \frac{\partial E}{\partial \alpha} D_t \alpha + \rho \frac{\partial E}{\partial \omega_\Sigma} D_t \omega_\Sigma + \rho \frac{\partial E}{\partial \Sigma} D_t \Sigma \leq 0. \quad (3.129)$$

Accounting for the mass conservation and the following partial derivatives of E

$$\frac{\partial E}{\partial \rho} = \frac{\nu_\Sigma}{2} (Y \omega_\Sigma)^2 - \frac{\sigma \Sigma}{\rho^2} + \frac{\partial f}{\partial \rho}, \quad \frac{\partial E}{\partial \mathbf{v}} = \mathbf{v}, \quad \frac{\partial E}{\partial \alpha} = \frac{\partial f}{\partial \alpha}, \quad \rho \frac{\partial E}{\partial \Sigma} = \sigma + \frac{1}{2} \nu'_\Sigma (\rho Y \omega_\Sigma)^2, \quad (3.130)$$

by injecting into (3.129), we obtain

$$\nabla \cdot [\mathbf{G} - \mathcal{P} \mathbf{v}] + \left(\rho \frac{\partial f}{\partial \alpha} \right) D_t \alpha + \rho Y \omega_\Sigma \left(\nu_\Sigma \rho Y D_t \omega_\Sigma + \sigma + \frac{1}{2} \nu'_\Sigma (\rho Y \omega_\Sigma)^2 \right) \leq 0. \quad (3.131)$$

A simple closure consists in choosing

$$\mathbf{G} = \mathcal{P}\mathbf{v} \quad (3.132)$$

and setting

$$-\epsilon_\Sigma \rho Y \omega_\Sigma = \nu_\Sigma \rho Y D_t \omega_\Sigma + \sigma + \frac{1}{2} \nu'_\Sigma (\rho Y \omega_\Sigma)^2, \quad D_t \alpha = -\mu \rho \frac{\partial f}{\partial \alpha}, \quad (3.133)$$

where ϵ_Σ and μ are both positive coefficients.

We finally obtain a new equation for ω_Σ and α that takes the form

$$D_t \omega_\Sigma + \frac{\epsilon_\Sigma}{\nu_\Sigma} \omega_\Sigma + \frac{1}{Y \rho \nu_\Sigma} \sigma + \frac{1}{2} \frac{\nu'_\Sigma}{\nu_\Sigma} \rho Y \omega_\Sigma^2 = 0, \quad (3.134)$$

$$D_t \alpha + \mu \rho \frac{\partial f}{\partial \alpha} = 0. \quad (3.135)$$

To close the investigated system, we need to specify the thermodynamics of the mixture. We propose to choose the medium barotropic energy as follows

$$f(\rho, Y, \alpha) = \sum_{k=1,2} y_k f_k(\rho_k) + \Delta f(\alpha), \quad (3.136)$$

where Δf is a mixing energy that accounts for phase interaction. We further assume that the phase barotropic potential energies verify the Gibbs equation. In this case, we obtain

$$\rho^2 \frac{\partial f}{\partial \rho} = \sum_{k=1,2} \alpha_k p_k, \quad \rho \frac{\partial f}{\partial \alpha} = p_2 - p_1 + \rho \Delta f'. \quad (3.137)$$

By noticing that the velocity evolution equation can be expressed as a conservation equation for the momentum $\rho \mathbf{v}$, the overall system equipped with its dissipative part reads

$$\partial_t \rho + \operatorname{div}(\rho \mathbf{v}) = 0, \quad (3.138a)$$

$$\partial_t(\rho Y) + \operatorname{div}(\rho Y \mathbf{v}) = 0, \quad (3.138b)$$

$$\rho D_t \mathbf{v} + \nabla \mathcal{P} = \mathbf{0}, \quad (3.138c)$$

$$D_t \alpha - \mu(p_2 - p_1 + \rho \Delta f') = 0, \quad (3.138d)$$

$$D_t \omega_\Sigma + \frac{\epsilon_\Sigma}{\nu_\Sigma} \omega_\Sigma + \frac{1}{Y \rho \nu_\Sigma} \sigma + \frac{1}{2} \frac{\nu'_\Sigma}{\nu_\Sigma} \rho Y \omega_\Sigma^2 = 0, \quad (3.138e)$$

$$D_t \Sigma - \rho Y \omega_\Sigma = 0, \quad (3.138f)$$

$$D_t H + \frac{1}{3\alpha} \rho Y \omega_\Sigma = 0. \quad (3.138g)$$

Let us underline that the dissipation coefficients can both be interpreted as a micro-viscosity for the pressure relaxation in this spray configuration along the lines of [Drui et al. \(2019\) \[60\]](#) and, in the same manner, the oscillation micro-viscosity ϵ_Σ can be related to the classical dissipation process of a single droplet oscillation described for example in [O'Rourke and Amsden \(1987\) \[167\]](#), [Chandrasekhar \(1981\) \[22\]](#).

3.B.2.7 PROPERTIES OF THE SYSTEM

Considering smooth solutions for one-dimensional problem, the pure convective part of (3.138) is obtained by canceling the source terms and reads

$$\partial_t \mathbf{u} + \mathbf{A}(\mathbf{u}) \partial_x \mathbf{u} = \mathbf{0}, \quad \mathbf{u}^T = (\rho, v, Y, \alpha, \omega_\Sigma, H, \Sigma), \quad (3.139a)$$

$$\mathbf{A} = \begin{bmatrix} v & \rho & 0 & 0 & 0 & 0 & 0 \\ \frac{1}{\rho} \partial_\rho \mathcal{P} & v & \frac{1}{\rho} \partial_Y \mathcal{P} & \frac{1}{\rho} \partial_\alpha \mathcal{P} & \frac{1}{\rho} \partial_{\omega_\Sigma} \mathcal{P} & \frac{1}{\rho} \partial_H \mathcal{P} & \frac{1}{\rho} \partial_\Sigma \mathcal{P} \\ 0 & 0 & v & 0 & 0 & 0 & 0 \\ 0 & 0 & 0 & v & 0 & 0 & 0 \\ 0 & 0 & 0 & 0 & v & 0 & 0 \\ 0 & 0 & 0 & 0 & 0 & v & 0 \\ 0 & 0 & 0 & 0 & 0 & 0 & v \end{bmatrix}. \quad (3.139b)$$

The eigenvalues of the matrix \mathbf{A} are v (five times) and $v \pm a$, where $a^2 = \partial_\rho \mathcal{P}$. If one notes a_k is sound velocity of the pure material k , in the case of the classic choice (3.136), this yields the classic definition $a^2 = Y a_1^2 + (1 - Y) a_2^2$, which ensures that (3.139a) is hyperbolic.

The definition (3.127) provides the system (3.138) with a companion inequality (3.128) that can be considered as an entropy inequality associated as it reads

$$\frac{\partial \rho E}{\partial t} + \nabla \cdot (\rho E \mathbf{v} + \mathbf{G}) \leq 0.$$

Moreover, depending on the modeling choices for f , Δf and ν_Σ , one can ensure that $[\rho Y, \rho(1 - Y), \rho v, \alpha, \rho Y \omega_\Sigma, \Sigma, H] \mapsto \rho E$ is a (not strictly) convex function. A possible choice that enables convexity would be to use the classic definition (3.136) with a convex function $\alpha \mapsto \Delta f$ and $\nu_\Sigma > 0$ a constant.

3.B.3 CONCLUSION

In the present work, we have recalled and extended the analytical study of Chandrasekhar (1981) [22] within the framework of a spherical liquid droplet subject to an axisymmetric ellipsoidal deformation. We have in particular verified that the system is experiencing a harmonic oscillator behavior with identified frequency and potential damping and have shown that in the small perturbation limit, several candidate in terms of small scale variables can be envisioned since most of the variable experience a quasi-harmonic dynamics in that limit.

In order to discriminate the proper variables, we have conducted a series of DNS configurations with variable deformation amplitudes relying on the code ARCHER for high-fidelity simulations. The evolution of the geometrical characteristics of the droplet surface have been analyzed thanks to a post-processing library Mercur (v) e introduced in Di Battista et al. (2019) [54]. The proper and accurate evaluation of the geometrical properties of the deformed spherical droplet have shown that the excess surface are density is the eligible variable to relate accurately the harmonic oscillation of the droplet in a large range of amplitudes and thus offer a clear picture on what should be the functional dependency of the potential energy, as well as kinetic energy in order to describe the small scale.

Then following the lines of Drui et al. (2019) [60], Cordesse et al. (2020) [39], we have proposed a model for disperse flow that can account for small scale oscillations of the liquid inclusions by accounting for small scale kinematics and small scale surface tension effects

based on the interfacial density area. One key of the derivation is the constraints on the geometric variables. The hypotheses, holding exactly in the limit of the small perturbation, were analyzed through our DNS results and validated. The extension of the present study to large scale and small scale capillarity is the subject of our current research and is conducted in [Cordesse et al. \(2020\) \[34\]](#).

ACKNOWLEDGEMENT

The support of the French Government Space Agency (CNES) and the French Aerospace Lab (ONERA) through a PhD grant for P.Cordesse is gratefully acknowledged. We also thank the PhD grant of Ruben Di Battista from École polytechnique and the Direction générale de l'Armement (DGA). Simulations have been successfully conducted using the ARCHER code of CORIA laboratory.

3.B.4 APPENDICES

3.B.4.1 ENERGY ANALYTICAL CALCULATION OF A DEFORMED DROPLET

We detail here the analytical calculation of the deformed droplet dynamics. We first show that the ellipsoidal deformation of the droplet may be approximated by a single spherical harmonic. The analytical study of Chandrasekhar [Chandrasekhar \(1981\) \[22\]](#) then allows the determination of the evolution of the kinetic energy of the droplet during its oscillations. The integration of the droplet oscillating surface and mean curvature lead to a surface energy expression displaying expected energy conservation properties.

3.B.4.2 APPROXIMATION OF THE DROPLET DEFORMATION

In the following, we consider that the initial droplet deformation is described by an ellipsoid of e_z symmetry axis as shown on [Figure 3.10a](#). The deformed surface is then entirely given

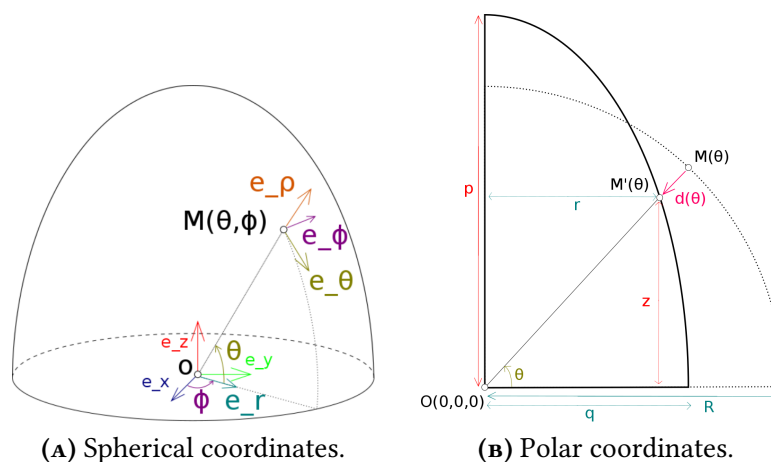


FIGURE 3.10: Spherical and polar coordinate system for the upper half deformed droplet.

by its semi-major axis p and its semi-minor axis q and may be described in cylindrical (z, r, ϕ)

(see Figure 3.10b) through the equations

$$\forall(\theta', \phi) \in [0, \pi] \times [0, 2\pi], \quad \begin{cases} z = p \sin \theta', \\ r = q \cos \theta', \\ \phi = \phi, \end{cases}$$

where the θ' parameter does not necessarily reduce to the θ spherical coordinate. In the following, colatitude will be written $\vartheta = \pi/2 - \theta$ and the ellipsoid aspect ratio $\epsilon = p/q$.

We can describe the ellipsoid as a deformed sphere of equivalent volume and radius R . Considering the following relationship between the θ' parameter and the θ coordinate,

$$\tan \theta = \frac{z}{r} = \epsilon \tan \theta',$$

and reducing the range of parameter θ' to $\theta' \in [0, \pi/2]$ thanks to system's symmetry, the deformation $\mathbf{d}(\theta)$ may be expressed as

$$\begin{aligned} \mathbf{d}(\theta) &= \mathbf{M}\mathbf{M}'(\theta), \\ &= (q \cos \theta' - R \cos \theta)\mathbf{e}_r + (p \sin \theta' - R \sin \theta)\mathbf{e}_z, \\ &= R \left[\left(\frac{q}{R} \frac{\epsilon}{\sqrt{\epsilon^2 + \tan^2 \theta}} - \cos \theta \right) \mathbf{e}_r + \left(\frac{p}{R} \frac{\tan \theta}{\sqrt{\epsilon^2 + \tan^2 \theta}} - \sin \theta \right) \mathbf{e}_z \right]. \end{aligned}$$

Denoting $\bar{X} = X/R$ the scaling by droplet radius R , the deformation reduces to

$$\bar{\mathbf{d}}(\theta) = \frac{1}{\cos \theta \sqrt{\epsilon^2 + \tan^2 \theta}} (\bar{q}\epsilon - \cos \theta \sqrt{\epsilon^2 + \tan^2 \theta}) \mathbf{e}_\varrho,$$

where ϱ is the radial coordinate in the spherical coordinate system and \mathbf{e}_ϱ is defined as $\mathbf{e}_\varrho = \mathbf{e}_r + \tan \theta \mathbf{e}_z$. For small deformations, the ellipsoid remains close to a sphere and the aspect ratio may be expanded as

$$\epsilon = 1 + \bar{\eta}.$$

For now we suppose $\bar{\eta}$ of small maximal amplitude η with no hypothesis concerning its time dependence. The Taylor expansion of the θ dependance of $\bar{\mathbf{d}}$ writes

$$\cos(\theta) \sqrt{\epsilon^2 + \tan^2 \theta} = \cos \theta \sqrt{2\bar{\eta} + \bar{\eta}^2 + 1/\cos^2 \theta} \underset{\eta \rightarrow 0}{=} 1 + \bar{\eta} \cos^2 \theta + \frac{\bar{\eta}^2}{2} \cos^2 \theta \sin^2 \theta + o(\eta^2).$$

Under the hypothesis of incompressible liquid, the volume of the deformed sphere must remains equal to the volume of the sphere, inducing

$$\frac{4}{3}\pi R^3 = \frac{4}{3}\pi p q^2 \Leftrightarrow \bar{q}\epsilon \underset{\eta \rightarrow 0}{=} 1 + \frac{2}{3}\bar{\eta} - \frac{\bar{\eta}^2}{9} + o(\eta^2).$$

As a consequence, the expression of deformation $\mathbf{d}(\theta)$ may be expanded with respect to the droplet perturbation η as

$$\begin{aligned} \bar{\mathbf{d}}(\theta) &\underset{\eta \rightarrow 0}{=} \frac{1 + \frac{2}{3}\bar{\eta} - \frac{\bar{\eta}^2}{9} - (1 + \bar{\eta} \cos^2 \theta + \frac{\bar{\eta}^2}{2} \cos^2 \theta \sin^2 \theta) + o(\eta^2)}{1 + \bar{\eta} \cos^2 \theta + \frac{\bar{\eta}^2}{2} \cos^2 \theta \sin^2 \theta + o(\eta^2)} \mathbf{e}_\varrho, \\ &\underset{\eta \rightarrow 0}{=} \bar{\eta} \left(\frac{3 \sin^2 \theta - 1}{3} + \bar{\eta} \frac{27 \sin^4 \theta - 33 \sin^2 \theta + 4}{18} \right) \mathbf{e}_\varrho + o(\eta^2). \end{aligned}$$

Expressing the deformation with respect to the colatitude ϑ yields

$$\begin{aligned}\bar{\mathbf{d}}(\vartheta) &\underset{\eta \rightarrow 0}{=} \bar{\eta} \left(\frac{3 \cos^2 \vartheta - 1}{3} + \bar{\eta} \frac{27 \cos^4 \vartheta - 33 \cos^2 \vartheta + 4}{18} \right) \mathbf{e}_\varrho + \mathbf{o}(\eta^2), \\ &\underset{\eta \rightarrow 0}{=} \frac{2\bar{\eta}}{3} \frac{3 \cos^2 \vartheta - 1}{2} \mathbf{e}_\varrho + \mathbf{o}(\eta), \\ &\underset{\eta \rightarrow 0}{=} \frac{2\bar{\eta}}{3} Y_2(\vartheta) \mathbf{e}_\varrho + \mathbf{o}(\eta),\end{aligned}$$

where Y_2 represents the spherical harmonic Y_2^0 . The initial condition of the weakly deformed ellipsoid droplet is thus similar to the analytical framework developed in Chandrasekhar (1981) [22] such as similar dynamics can be expected asymptotically.

Approximating the $\bar{\eta}$ volume-preserving ellipsoidal perturbation by the $2\bar{\eta}Y_2/3$ spherical harmonic rises the question of volume conservation. Indeed, performing the exact integration on a $2\bar{\eta}Y_2/3$ perturbed droplet lead to the following result

$$\begin{aligned}\int_0^{2\pi} \int_0^\pi \int_0^{R+2\bar{\eta}Y_2(\vartheta)/3} \varrho^2 \sin \vartheta d\varrho d\vartheta d\phi &= 2\pi R^3 \int_0^\pi \frac{(1 + \bar{\eta}(3 \cos^2 \vartheta - 1)/3)^3}{3} \sin \vartheta d\vartheta, \\ &= \frac{4}{3}\pi R^3 \left(1 + \frac{4}{15}\bar{\eta}^2 + \frac{16}{945}\bar{\eta}^3 \right).\end{aligned}$$

Volume conservation is only valid at first order in the perturbation η - this comes as no surprise given the linearisation - and thus must be, if necessary, enforced *a posteriori*. This will be done by imposing a spherical radius of the deformed sphere R_d slightly smaller than the reference R ,

$$R^3 = R_d^3 \left(1 + \frac{4}{15}\bar{\eta}^2 + \frac{16}{945}\bar{\eta}^3 \right) \Rightarrow R_d \underset{\eta \rightarrow 0}{=} R \left(1 - \frac{4}{45}\bar{\eta}^2 \right) + o(\bar{\eta}^2)$$

This leads to the volume preserving $2\bar{\eta}Y_2/3$ expression for the deformed surface

$$r(\vartheta, t) = R \left(1 + \frac{4}{15}\bar{\eta}^2 + \frac{16}{945}\bar{\eta}^3 \right)^{-1/3} \left(1 + \frac{2}{3}Y_2(\vartheta)\bar{\eta} \right),$$

which remains equivalent to the ellipsoidal perturbation at first η order

$$r(\vartheta, t) \underset{\eta \rightarrow 0}{=} R \left(1 + \frac{2\bar{\eta}}{3}Y_2(\vartheta) \right) + o(\eta).$$

This approximation is compared to the reference sphere and the exact ellipsoid on Figure 3.11.

3.B.4.3 KINETIC ENERGY

Approximating the initial ellipsoidal droplet by a sphere perturbed by an Y_2 spherical harmonic allows the use of the analytical expressions developed by Chandrasekhar Chandrasekhar (1981) [22] which are briefly recalled hereafter.

In the case of weakly spherical harmonic deformed bubble of non-viscous fluid of density ρ in a vacuum force-free surroundings only subject to capillarity effects with capillarity

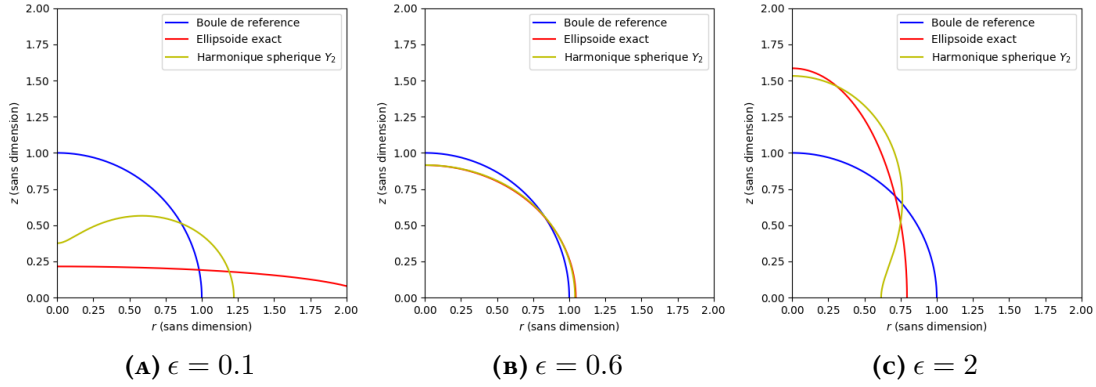


FIGURE 3.11: Numerical approximation of the ellipsoid in the $(O, \mathbf{e}_r, \mathbf{e}_z)$ plane for different aspect ratios.

coefficient σ , the linearized equation of fluid dynamics can be explicitly solved and yields the following surface tension induced oscillations

$$\begin{aligned} \mathbf{v}_{\varrho,l} &= -\sqrt{\frac{\sigma}{\rho} l(l-1)(l+2) R^{3/2-l-2}} A \varrho^{l-1} Y_l \sin(\omega_l t), \\ \mathbf{v}_{\vartheta,l} &= -\sqrt{\frac{\sigma}{l\rho} (l-1)(l+2) R^{3/2-l-2}} A \frac{\partial Y_l}{\partial \vartheta} \sin(\omega_l t), \\ \mathbf{v}_{\phi,l} &= 0, \end{aligned}$$

compatible with the given radial deformation $r(\vartheta, t) = R + AY_l(\vartheta) \cos(\omega_l t)$. Each chosen spherical harmonic Y_l then selects a precise pulsation given by the relation

$$\omega_l^2 = l(l-1)(l+2) \frac{\sigma}{\rho R^3}.$$

In the case of the ellipsoid surface approximation, the spherical harmonic Y_2 is of special interest and yields

$$\omega_2 = \omega = \sqrt{\frac{8\sigma}{\rho R^3}},$$

and we will suppose $\bar{\eta} = \eta \cos(\omega t)$ to comply with Chandrasekar's hypothesis set so that the surface deformation will satisfy

$$r(\vartheta, t) \underset{\eta \rightarrow 0}{=} R \left(1 + \frac{2\eta}{3} Y_2(\vartheta) \cos(\omega t) \right) + o(\eta).$$

The corresponding droplet dynamics is then given by the relation

$$\mathbf{v}(\varrho, \vartheta, t) = \eta \sqrt{\frac{2\sigma}{\rho R^3}} \varrho \left(2 \frac{1 - 3 \cos^2 \vartheta}{3} \mathbf{e}_\varrho + \sin(2\vartheta) \mathbf{e}_\vartheta \right) \sin(\omega t).$$

Writing $\tilde{\eta} = \eta \sin(\omega t)$ and $\mathcal{S}_0 = 4\pi R^2$, we can integrate the velocity field to obtain the kinetic energy

$$E_k(t) = \frac{1}{2} \int_0^{2\pi} \int_0^\pi \int_0^{r(\vartheta,t)} \rho \mathbf{v}^2 d\varrho d\vartheta d\phi \underset{\eta \rightarrow 0}{=} \frac{8}{45} \sigma \mathcal{S}_0 \tilde{\eta}^2 + o(\eta^2),$$

or, with the time dependency made explicit

$$E_k(t) \underset{\eta \rightarrow 0}{=} \frac{8}{45} \eta^2 \sigma \mathcal{S}_0 \sin^2 \left(t \sqrt{\frac{8\sigma}{\rho R^3}} \right) + o(\eta^2).$$

3.B.4.4 POTENTIAL ENERGY

The dynamics of the oscillating droplet is obtained by Chandrasekhar by considering the Laplace pressure given by the deformation as a boundary condition for the pressure field. Our purpose is here to underline the energy balance between the kinetic energy E_k and the surface energy E_p of the oscillating droplet. In order to do so, the $2\eta Y_2/3$ perturbed droplet surface is evaluated as a function of time. Care must be taken that the expression of the perturbation has to be expanded to second η order to yield consistent results. Let us consider the second order corrected deformation

$$r(\vartheta, t) = R \left(1 - \frac{4}{45} \bar{\eta}^2 \right) \left(1 + \frac{3 \cos^2 \vartheta - 1}{3} \bar{\eta} \right),$$

with $\bar{\eta} = \eta \cos(\omega t)$. The corresponding mathematical surface is then given by the function

$$\mathbf{f}(\vartheta, \phi, t) = r(\vartheta, t) \mathbf{e}_\varrho = r(\vartheta, t) \begin{pmatrix} \sin \vartheta \cos \phi \\ \sin \vartheta \sin \phi \\ \cos \vartheta \end{pmatrix},$$

and leads to the following expression for a small surface element

$$\|\partial_\vartheta \mathbf{f} \times \partial_\phi \mathbf{f}\| = r \sin \vartheta \sqrt{(\partial_\vartheta r \cos \vartheta - r \sin \vartheta)^2 + (\partial_\vartheta r \sin \vartheta + r \cos \vartheta)^2} = r^2 \sin \vartheta \sqrt{1 + \left(\frac{\partial_\vartheta r}{r} \right)^2}.$$

Using the second order compatible deformation expression of r , the second order of the surface element writes

$$r^2 \sin \vartheta \sqrt{1 + \left(\frac{\partial_\vartheta r}{r} \right)^2} = R^2 \left(1 + \frac{2}{3} \bar{\eta} (3 \cos^2 \vartheta - 1) + \bar{\eta}^2 \left(-\frac{1}{15} + \frac{4}{3} \cos^2 \vartheta - \cos^4 \vartheta \right) \right) + o(\eta^2)$$

The complete surface area of the oscillating droplet is obtained thanks to an analytic integration of surface elements which yields

$$\mathcal{S}(t) = \int_0^{2\pi} \int_0^\pi \|\partial_\vartheta \mathbf{f} \times \partial_\phi \mathbf{f}\| d\vartheta d\phi \underset{\eta \rightarrow 0}{=} \mathcal{S}_0 \left(1 + \frac{8}{45} \eta^2 \cos^2(\omega t) \right) + o(\eta^2).$$

The potential energy $E_p = \sigma(\mathcal{S} - \mathcal{S}_0)$ corresponding to the excess surface with respect to the minimal surface \mathcal{S}_0 then writes

$$E_p(t) \underset{\eta \rightarrow 0}{=} \frac{8}{45} \eta^2 \sigma \mathcal{S}_0 \cos^2 \left(t \sqrt{\frac{8\sigma}{\rho R^3}} \right) + o(\eta^2),$$

which balances exactly the kinetic energy.

3.B.4.5 MEAN CURVATURE

In the case of droplet oscillation due to the surface tension effect, a natural parameter is the local mean curvature which gives birth to the Laplace pressure driving the fluid motion. In the derivation of Chandrasekhar, this Laplace pressure is imposed as a compatible boundary condition for the pressure field. In some studies, see Herrmann [Herrmann \(2013\) \[106\]](#), the local mean curvature is used as a parameter describing the interface non-equilibrium and giving birth to a spring-like force putting the interface into motion.

In the following, we detail the expression of local mean curvature in the case of a volume-preserving $2\bar{\eta}Y_2/3$ perturbation. In the case of a surface of revolution, the local curvature is given by the general formula

$$H = \frac{1}{2R \left(1 - \frac{4}{45}\bar{\eta}^2\right)} \left(\frac{r''z' - z''r'}{\left((r')^2 + (z')^2\right)^{\frac{3}{2}}} - \frac{z'}{r \left((r')^2 + (z')^2\right)^{\frac{1}{2}}} \right),$$

where the volume preserving correction is factorized to ease the computation, so that the surface coordinate in cylindrical coordinate may be directly used in the expressions. They and their derivatives write

$$\begin{aligned} z &= \left(1 + \frac{2}{3}\bar{\eta}Y_2\right) \cos \vartheta, & r &= \left(1 + \frac{2}{3}\bar{\eta}Y_2\right) \sin \vartheta, \\ z' &= -\left(1 + \frac{2}{3}\bar{\eta}Y_2\right) \sin \vartheta + \frac{2}{3}\bar{\eta}Y_2' \cos \vartheta, & r' &= \left(1 + \frac{2}{3}\bar{\eta}Y_2\right) \cos \vartheta + \frac{2}{3}\bar{\eta}Y_2' \sin \vartheta, \\ z'' &= -\left(1 + \frac{2}{3}\bar{\eta}(Y_2 - Y_2'')\right) \cos \vartheta - \frac{4}{3}\bar{\eta}Y_2' \sin \vartheta, & r'' &= -\left(1 + \frac{2}{3}\bar{\eta}(Y_2 - Y_2'')\right) \sin \vartheta + \frac{4}{3}\bar{\eta}Y_2' \cos \vartheta. \end{aligned}$$

The different terms needed in the local mean curvature expression may be detailed as follows

$$(z')^2 + (r')^2 = 1 + \frac{4}{3}\bar{\eta}Y_2 + \frac{4}{9}\bar{\eta}^2 \left((Y_2)^2 + (Y_2')^2\right),$$

and

$$r''z' - z''r' = 1 + \frac{2}{3}\bar{\eta}(2Y_2 - Y_2'') + \frac{4}{9}\bar{\eta}^2 \left((Y_2)^2 + 2(Y_2')^2 - Y_2Y_2''\right),$$

so that the local mean curvature of the volume-preserved $2\bar{\eta}Y_2/3$ perturbation is given by

$$H = \frac{1}{2R \left(1 - \frac{4}{45}\bar{\eta}^2\right)} \left(\frac{2 + \frac{2}{3}\bar{\eta}(4Y_2 - Y_2'') + \frac{4}{9}\bar{\eta}^2 \left(2(Y_2)^2 + 3(Y_2')^2 - Y_2Y_2''\right)}{\left(1 + \frac{4}{3}\bar{\eta}Y_2 + \frac{4}{9}\bar{\eta}^2 \left((Y_2)^2 + (Y_2')^2\right)\right)^{\frac{3}{2}}} - \frac{\frac{2}{3}\bar{\eta}Y_2' \cos \vartheta}{\left(1 + \frac{2}{3}\bar{\eta}Y_2\right) \sin \vartheta \left(1 + \frac{4}{3}\bar{\eta}Y_2 + \frac{4}{9}\bar{\eta}^2 \left((Y_2)^2 + (Y_2')^2\right)\right)^{\frac{1}{2}}} \right).$$

The η second order expansion of the local curvature thus takes the form

$$\begin{aligned} H &\underset{\eta \rightarrow 0}{=} \frac{1}{R} \left(1 - \frac{\bar{\eta}}{3} \left(2Y_2 + Y_2' \frac{\cos \vartheta}{\sin \vartheta} + Y_2''\right) + \frac{4\bar{\eta}^2}{9} \left(\frac{1}{5} + Y_2^2 + Y_2Y_2' \frac{\cos \vartheta}{\sin \vartheta} + Y_2Y_2''\right)\right) + o(\eta^2), \\ &\underset{\eta \rightarrow 0}{=} \frac{1}{R} \left(1 + \frac{2}{3}\bar{\eta} \left(3 \cos^2 \vartheta - 1\right) + \bar{\eta}^2 \left(-\frac{7}{15} + \frac{10}{3} \cos^2 \vartheta - 5 \cos^4 \vartheta\right)\right) + o(\eta^2), \end{aligned}$$

so that, multiplying with the perturbed surface element, leads to the integrand

$$\|\partial_\vartheta \mathbf{f} \times \partial_\phi \mathbf{f}\| H(\vartheta) \underset{\eta \rightarrow 0}{=} R \left(1 + \frac{4}{3} \bar{\eta} (3 \cos^2 \vartheta - 1) + \bar{\eta}^2 \left(-2 \cos^4 \vartheta + 2 \cos^2 \vartheta - \frac{4}{45} \right) \right) + o(\eta^2).$$

The integral of local mean curvature on the perturbed surface writes

$$\int_0^{2\pi} \int_0^\pi \|\partial_\vartheta \mathbf{f} \times \partial_\phi \mathbf{f}\| H(\vartheta) d\vartheta d\phi = 4\pi R \left(1 + \frac{8}{45} \eta^2 \cos^2(\omega t) \right) + o(\eta^2),$$

so that the global mean curvature H may be splitted into a reference curvature $H_0 = 1/R$ and an oscillating term

$$H = H_0 + \frac{8}{45R} \eta^2 \cos^2 \left(t \sqrt{\frac{8\sigma}{\rho R^3}} \right) + o(\eta^2).$$

Considering the potential energy derived in terms of the surface, an expression of potential energy in terms of the Mean curvature both complying to the analytical results of Chandrasekhar and the H -based approach of Herrmann [Herrmann \(2013\) \[106\]](#) would thus write,

$$E_p(t) = \sigma S_0 R (H - H_0).$$

IMPLEMENTATION OF A FINITE VOLUME NUMERICAL STRATEGY FOR THE DUAL-SCALE TWO-PHASE FLOW MODEL

4

In this [Chapter 4](#), we propose a numerical strategy to implement the dual-scale two-phase flow model derived in the previous [Chapter 3](#).

In the first section, we make supplementary assumptions on the thermodynamics and neglect the pulsation to alleviate some difficulties related to the original model and obtain a primary block, from which we derive an asymptotic system when assuming instantaneous pressure relaxation. We proceed then to the mathematical analysis of the homogeneous form of the primary block. In order to include the large scale capillary terms in the mathematical analysis, we add a supplementary equation on the volume fraction gradient. The model is found to be weakly hyperbolic. We then present a splitting strategy leading to three sub-models corresponding respectively to the hydrodynamics and acoustics convection, then the large and small capillary fluxes and finally the relaxation procedure, and proceed to their mathematical analysis. Later on, we detail the numerical method applied on each sub-system based on a Finite Volume discretization.

Then, we address the framework whereby the new model has been implemented. Benefitting from the Generalized Eulerian Solver (GES) architecture of the industrial CFD code CEDRE, it has allowed a fast and elaborate implementation.

Finally we proceed to a numerical verification of the implemented model by reproducing classic one and two dimensional test cases selected to test Euler and large scale capillary fluxes as well as the pressure relaxation. The results attest the reliability of the splitting strategy.

4.1	Selection of numerical schemes for the two-scale two-phase flow model	191
4.1.1	Simplified system to be implemented as a primary block	191
4.1.1.1	Thermodynamics closure	191
4.1.1.2	Micro-inertia free	192
4.1.1.3	Geometric variables	193
4.1.1.4	Final system of equations	194
4.1.2	Mathematical analysis of the models	195
4.1.2.1	Operator splitting	197
4.1.3	Numerical method	199
4.1.3.1	First sub-system: euler flux with HLLC Solver	201
4.1.3.2	Second sub-system: capillary flux	204
4.1.3.3	Third sub-system: pressure relaxation procedure	205

	4.1.3.4	Second-order extension	207
	4.1.3.5	Summary of the numerical procedure	207
4.2		CEDRE Implementation of the two-scale two-phase flow model	208
4.3		Numerical verification of the two-scale two-phase flow model	210
	4.3.1	Verification tests of the Euler flux and the relaxation procedure	210
	4.3.1.1	Pure interface advection	210
	4.3.1.2	Water-air shock tube with moderate density ratio	211
	4.3.1.3	Water-air shock tube with high density ratio	211
	4.3.1.4	Two-phase flow problem: comparison with the <i>five equation</i> model	212
	4.3.2	Verification tests of the capillary flux	218
	4.3.2.1	Static capillary effects	218
	4.3.2.2	Dynamic capillary effects: oscillating ellipsoidal drop	220
	4.3.2.3	Dynamic capillary effects: uniform velocity flow	222
	4.3.2.4	Dynamic capillary effects: water shock interaction	223
	4.3.3	Verifications tests on the new geometric terms	226
		Appendices	230
4.A		Model Analysis	230
	4.A.1	Euler with capillary flux	230
	4.A.2	Sub-system 1: Euler system	230
	4.A.3	Sub-system 2: Capillary system	231
4.B		Energy equations	233

4.1 SELECTION OF NUMERICAL SCHEMES FOR THE TWO-SCALE TWO-PHASE FLOW MODEL

System (3.90) equipped with a 2-parameter equation of state for each phase, defined in Chapter 3 departs from the six-equation model with instantaneous pressure relaxation originally proposed in Saurel et al. (2009) [195] and revisited with phasic total energy equations in Pelanti and Shyue (2014) [172] by considering transport equations for the partial entropies and two novel ingredients, 1) mixing thermodynamics, 2) dual-scale effects with geometric variables.

In order to assess our model, we will first aim at verifying its common part with already validated models. Therefore, we first proceed with the simplification of our model and a selection of the best adequate equations.

4.1.1 SIMPLIFIED SYSTEM TO BE IMPLEMENTED AS A PRIMARY BLOCK

4.1.1.1 THERMODYNAMICS CLOSURE

We will neglect the mixing terms of the thermodynamics in System (3.90) and any mass transfer between the phases. We recall that we assumed a Gibbs equation for each phase,

$$T_k ds_k = de_k + p_k dv_k. \quad (4.1)$$

Since we neglect entirely the mixing terms together with assuming a Gibbs equation for each phase, it implies we consider the phases isolated from each other as seen in Chapter 2. System (3.90) reduces to

$$\partial_t \rho + \operatorname{div}(\rho \mathbf{v}) = 0, \quad (4.2a)$$

$$\partial_t(\rho y_{j,k}) + \nabla \cdot (\rho y_{j,k} \mathbf{v}) = 0, \quad (4.2b)$$

$$\rho D_t \mathbf{v} + \nabla \mathcal{P} + \nabla \cdot \left(\sigma_c(H) \frac{\nabla \alpha \otimes \nabla \alpha}{\|\nabla \alpha\|} \right) = \mathbf{0}, \quad (4.2c)$$

$$D_t s_k = 0, \quad (4.2d)$$

$$D_t \alpha - \rho Y \omega = 0, \quad (4.2e)$$

$$D_t \omega - H \frac{\nu'}{\nu} \rho Y \omega^2 + \frac{1}{\rho Y \nu} \left[p_d - 2H \tilde{\sigma} - \nabla \cdot \left(\sigma_c(H) \frac{\nabla \alpha}{\|\nabla \alpha\|} \right) \right] = 0, \quad (4.2f)$$

$$D_t \tilde{\Sigma} + 2H \rho Y \omega = 0, \quad (4.2g)$$

$$D_t \alpha - D_t \tilde{\alpha} = 0, \quad (4.2h)$$

$$D_t H = 0. \quad (4.2i)$$

with $\mathcal{P} = p + \nu(\rho Y \omega)^2/2 - \sigma_c(H)\|\nabla \alpha\| - \tilde{\sigma}(H)\tilde{\Sigma}$. In System (4.2), ρ is the mixture density, \mathbf{v} the hydrodynamical velocity, $y_{j,k}$ the mass fraction of species j of phase k , p the acoustic pressure, ν the micro inertia, Y the mass fraction of fluid $k = 1$, ω the pulsation, σ_c and $\tilde{\sigma}$ respectively the filtered and fluctuating surface tension coefficients, α the volume fraction of phase $k = 1$, $\tilde{\Sigma}$ the fluctuating interfacial density area, s_k the phasic entropy per unit of volume, ν' the derivative of ν with respect to $\tilde{\Sigma}$, $p_d = p_2 - p_1$, H the Mean curvature, α the volume fraction of phase $k = 1$ and $\tilde{\alpha}$ its fluctuating part.

4.1.1.2 MICRO-INERTIA FREE

In the asymptotic limit of no micro-inertia, $\nu \mapsto 0$, the pulsation equation (4.2f) yields,

$$p_2 - p_1 - \kappa_c(\alpha) - 2H\tilde{\sigma} = 0 \quad (4.3)$$

where we have introduced the local curvature κ_c defined by $\kappa_c(\alpha_k) = \nabla \cdot [\sigma_c \nabla \alpha_k / \|\nabla \alpha_k\|]$. Noticing that the limit of the term in the momentum equation depending on the pulsation is

$$\lim_{\nu \rightarrow 0} \frac{1}{2} \nu (\rho Y \omega)^2 = 0, \quad (4.4)$$

we obtain the following system

$$\partial_t \rho + \operatorname{div}(\rho \mathbf{v}) = 0, \quad (4.5a)$$

$$\partial_t(\rho y_{j,k}) + \nabla \cdot (\rho y_{j,k} \mathbf{v}) = 0, \quad (4.5b)$$

$$\rho D_t \mathbf{v} + \nabla \cdot [p \mathcal{I}_d - \tilde{\sigma}(H) \tilde{\Sigma} \mathcal{I}_d - \Omega] = \mathbf{0}, \quad (4.5c)$$

$$D_t s_k = 0, \quad (4.5d)$$

$$D_t \omega = 0, \quad (4.5e)$$

$$p_2 - p_1 - \kappa_c(\alpha) - 2H\tilde{\sigma} = 0, \quad (4.5f)$$

$$D_t \tilde{\Sigma} + 2H D_t \alpha = 0, \quad (4.5g)$$

$$D_t \alpha - D_t \tilde{\alpha} = 0, \quad (4.5h)$$

$$D_t H = 0, \quad (4.5i)$$

where \mathcal{I}_d is the identity matrix and Ω is the large scale capillary symmetric tensor $\Omega = \sigma_c \|\nabla \alpha\| \mathcal{I}_d - \sigma_c \nabla \alpha \otimes \nabla \alpha / \|\nabla \alpha\|$.

Pressure equality when discarding capillary effects

Equation (4.5f) is the local Laplace law which states that the pressure jump must equal all capillary effects. Here, we both account for small and large scale surface tension. When neglecting the capillary effects, we obtain the pressure equality

$$p_2 - p_1 = 0. \quad (4.6)$$

When assuming barotropic fluids, Equation (4.6) becomes an equation on the volume fraction only, and in [Chanteperdrix et al. \(2002\) \[23\]](#), they proved the uniqueness of the solution $\alpha^* \in [0, 1]$. For smooth solutions, taking the material derivative of the pressure equation (4.6),

$$D_t p_2 - D_t p_1 = 0,$$

and recalling that $D_t s_k = 0$, yields the following pressure evolution equations

$$D_t p_k = \left. \frac{\partial p_k}{\partial \rho_k} \right|_{s_k} D_t \rho_k + \left. \frac{\partial p_k}{\partial s_k} \right|_{\rho_k} D_t s_k = a_k^2 D_t \rho_k, \quad (4.7)$$

Then, from the mass conservation equation (4.5a), we have

$$D_t \rho_k = -\rho_k \nabla \cdot \mathbf{v} - \frac{\rho_k}{\alpha_k} D_t \alpha_k.$$

Injecting both results in the derived pressure equation provides the following volume fraction evolution equation

$$D_t \alpha_k = \frac{\rho_{k'} a_{k'}^2 - \rho_k a_k^2}{\sum_{l=1}^2 \rho_l a_l^2 / \alpha_l} \quad (4.8)$$

where $k' = k + 1$ [2], the phasic sound speed is defined as $a_k^2 = dp_k(\rho_k)/d\rho_k$. This results extends for two-parameter equations of state as found in [Murrone and Guillard \(2005\) \[164\]](#), provided the pressure equality is supplemented with the transport of the partial entropies, $D_t s_k = 0$. In this case, the phasic sound speed is defined as $a_k^2 = \partial p_k(\rho_k, s_k) / \partial \rho_k|_{s_k}$.

Equation (4.8) describes a pressure relaxation process whereby the volume of each fluid adapts to ensure pressure equilibrium in the mixture. Besides, the non-conservative term is the zeroth-order term obtained when relaxing instantaneously the pressures and the velocities of the seven equation model as shown in [Section 1.1.4](#). Therefore, many authors such as in [Saurel and Abgrall \(1999\) \[190\]](#), replace the non-conservative term by a relaxation term impacting both the volume fraction and the energies, as mentioned in [Section 1.1.1.3](#), leading to a new transport equation for the volume fraction,

$$D_t \alpha_k = \mu(p_k - p_{k'}). \quad (4.9)$$

Pressure equality when accounting for capillary effects

When accounting for capillary effects, the transport equation obtained from the algebraic constrain (4.5f) takes the form

$$D_t \alpha_k = \frac{\rho_{k'} a_{k'}^2 - \rho_k a_k^2}{\sum_{l=1}^2 \rho_l a_l^2 / \alpha_l} + D_t [\kappa_c(\alpha_k)], \quad (4.10)$$

since $D_t H = 0$. The material derivative of the local curvature complexifies the numerical implementation and therefore, we propose to transform the Laplace equation into an extended pressure relaxation term, such that we obtain

$$D_t \alpha_k = \mu [p_k - p_{k'} + \kappa_c(\alpha_k) - 2H\tilde{\sigma}]. \quad (4.11)$$

Locally, the relaxation process ensures the Laplace equation. It implies a local pressure jump whenever the local curvature obtained through the volume fraction gradient is not null, thus causing some difficulties in pure fluid zones. This problem will be addressed later on.

4.1.1.3 GEOMETRIC VARIABLES

Since the fluctuating volume fraction $\tilde{\alpha}$ transport equation equals that of the total volume fraction α and since $\tilde{\alpha}$ is not present in any terms of System (4.5), we remove its transport equation (4.5h).

4.1.1.4 FINAL SYSTEM OF EQUATIONS

From the previous paragraph, we obtain a first simplified model $(\mathcal{S})_\mu^{s_k}$,

$$(\mathcal{S})_\mu^{s_k} \left\{ \begin{array}{l} \partial_t(\rho) + \nabla \cdot (\rho \mathbf{v}) = 0, \\ D_t y_{j,k} = 0, \\ \rho D_t \mathbf{v} + \nabla \cdot [p \mathcal{I}_d - \tilde{\sigma}(H) \tilde{\Sigma} \mathcal{I}_d - \Omega] = \mathbf{0}, \\ D_t s_k = 0, \\ D_t \omega = 0, \\ D_t H = 0, \\ D_t \tilde{\Sigma} = 2H \mu [p_k - p_{k'} + \kappa_c(\alpha_k) - 2H \tilde{\sigma}], \\ D_t \alpha_k = \mu [p_k - p_{k'} + \kappa_c(\alpha_k) - 2H \tilde{\sigma}], \end{array} \right. \quad (4.12)$$

solved with the two constitutive equations of state, $p_k = p_k(\rho_k, s_k)$ and where the pressure p writes $p = \sum_{k=1}^2 \alpha_k p_k$. System $(\mathcal{S})_\mu^{s_k}$ is similar to the *six equation* model proposed originally in [Saurel et al. \(2009\) \[195\]](#) and revisited in [Pelanti and Shyue \(2014\) \[172\]](#), but they use the interfacial pressure p_I in the relaxation pressure terms instead in our case of the fluid pressure and have a relaxation pressure term for the partial entropies as well whereas we do not.

Since in our applications, the pressure is expected to relax instantaneously, we are only interested in the asymptotic limit $\mu \mapsto \infty$, leading to the system $(\mathcal{S})_{\mu \rightarrow \infty}^{s_k}$,

$$(\mathcal{S})_{\mu \rightarrow \infty}^{s_k} \left\{ \begin{array}{l} \partial_t(\rho) + \nabla \cdot [\rho \mathbf{v}] = 0, \\ D_t y_{j,k} = 0, \\ \rho D_t \mathbf{v} + \nabla \cdot (p \mathcal{I}_d - \tilde{\sigma}(H) \tilde{\Sigma} \mathcal{I}_d - \Omega) = 0, \\ D_t s_k = 0, \\ D_t \omega = 0, \\ D_t H = 0, \\ p_k - p_{k'} + \kappa_c(\alpha_k) - 2H \tilde{\sigma} = 0, \end{array} \right. \quad (4.13)$$

with the two constitutive equations of state, $p_k = p_k(\rho_k, s_k)$ and an algebraic equation defining a unique volume fraction α_k^* and a unique interfacial density area, $\tilde{\Sigma}^*$, at pressure equilibrium when $p_k - p_{k'} + \kappa_c(\alpha_k) - 2H \tilde{\sigma} = 0$. Alternatively, the algebraic constraint could be replaced by an equation on the volume fraction, as discussed previously, namely by Equation (4.10), such that we obtain

$$(\mathcal{S}^*)_{\mu \rightarrow \infty}^{s_k} \left\{ \begin{array}{l} \partial_t(\rho) + \nabla \cdot [\rho \mathbf{v}] = 0, \\ D_t y_{j,k} = 0, \\ \rho D_t \mathbf{v} + \nabla \cdot (p \mathcal{I}_d - \tilde{\sigma}(H) \tilde{\Sigma} \mathcal{I}_d - \Omega) = \mathbf{0}, \\ D_t s_k = 0, \\ D_t \omega = 0, \\ D_t H = 0, \\ D_t \tilde{\Sigma} = 2H D_t \alpha_k, \\ D_t \alpha_k = \frac{\rho_{k'} a_{k'}^2 - \rho_k a_k^2}{\sum_{l=1}^2 \rho_l a_l^2 / \alpha_l} + D_t(\kappa_c(\alpha_k)). \end{array} \right. \quad (4.14)$$

$(\mathcal{S}^*)_{\mu \rightarrow \infty}^{s_k}$ clearly appears as a direct extension of the *five equation* model of [Kapila et al. \(2001\) \[115\]](#), [Murrone and Guillard \(2005\) \[164\]](#).

4.1.2 MATHEMATICAL ANALYSIS OF THE MODELS

The mathematical analysis should be conducted on both $(\mathcal{S})_{\mu}^{s_k}$ and $(\mathcal{S})_{\mu \rightarrow \infty}^{s_k}$ or alternatively on $(\mathcal{S}^*)_{\mu \rightarrow \infty}^{s_k}$. Studying the mathematical properties of the asymptotic model $(\mathcal{S})_{\mu \rightarrow \infty}^{s_k}$ implies to account for the Laplace law in the calculation, which is not trivial at all. Even if we use $(\mathcal{S}^*)_{\mu \rightarrow \infty}^{s_k}$, we have no equation on the local curvature, nor on the gradient of the volume fraction to pursue the analysis. A solution would be to assume a constant local curvature and get rid of the transport of κ_c . Then, analyzing only the first-order terms of the system would lead to the same conclusions as for the *five equation* model and one can refer to [Murrone and Guillard \(2005\) \[164\]](#) for instance. The system is found hyperbolic with three distinct real eigenvalues

$$v, v \pm a_W, \quad (4.15)$$

where a_W is the Wallis sound speed of the mixture, defined as

$$\frac{1}{\rho a_W^2} = \sum_{k=1}^2 \frac{\alpha_k}{\rho_k a_k^2}. \quad (4.16)$$

Since one of the main advances of the current work is to account for capillary effects, we would like to keep the second order terms in the mathematical analysis. As proposed in [Schmidmayer et al. \(2017\) \[197\]](#), we could introduce a supplementary equation on the gradient of the volume fraction, which could be derived from the equation on the volume fraction, but this is rather fastidious in the asymptotic model.

Therefore, we propose to study the mathematical properties of the homogeneous form of the system of equations $(\mathcal{S})_{\mu}^{s_k}$, that we note $(\mathcal{S})_{\mu=0}^{s_k}$ and can be written

$$(\mathcal{S})_{\mu=0}^{s_k} \left\{ \begin{array}{l} \partial_t(\rho) + \nabla \cdot [\rho \mathbf{v}] = 0, \\ D_t y_{j,k} = 0, \\ \rho D_t \mathbf{v} + \nabla \cdot (p \mathcal{I}_d - \tilde{\sigma}(H) \tilde{\Sigma} \mathcal{I}_d - \Omega) = 0, \\ D_t s_k = 0, \\ D_t \omega = 0, \\ D_t H = 0, \\ D_t \tilde{\Sigma} = 0, \\ D_t \alpha_k = 0, \end{array} \right. \quad (4.17)$$

Accounting for both first-order terms and second-order capillary terms is then possible by deriving a supplementary equation on the gradient of the volume fraction. Since in this case, the equation on the volume fraction takes the form

$$D_t \alpha_k = 0, \quad (4.18)$$

a simple equation on the volume fraction gradient is obtained

$$\partial_t \nabla \alpha_k + \nabla (\mathbf{v} \cdot \nabla \alpha_k) = 0 \Leftrightarrow D_t (\nabla \alpha_k) + \nabla \mathbf{v}^T \nabla \alpha_k = 0, \quad (4.19)$$

the latter considered now as a supplementary independent variable for the analysis of the system $(\mathcal{S})_{\mu=0}^{s_k}$. Due to the rotational invariance of System (4.17), we can analyze its homogeneous form in a single direction. We will drop the fluid subscript of the volume fraction considering as in Chapter 3 that $\alpha = \alpha_1$. It has no impact on the capillary tensor due to its symmetry. Introducing the components of the speed $\mathbf{v} = (v_{x_1}, v_{x_2}, v_{x_3})^t$ and of the volume fraction gradient $\nabla\alpha = (\partial_{x_1}\alpha, \partial_{x_2}\alpha, \partial_{x_3}\alpha)^t$, the projection of System (4.17) with the supplementary equation (4.19) along the first direction x_1 yields

$$(\mathcal{S})_{\mu=0}^{s_k} \left\{ \begin{array}{l} \partial_t(\rho) + \partial_{x_1}(\rho v_{x_1}) = 0, \\ \partial_t(y_{j,k}) + v_{x_1}\partial_{x_1}(y_{j,k}) = 0, \\ \rho\partial_t(v_{x_1}) + \rho v_{x_1}\partial_{x_1}(v_{x_1}) + \partial_{x_1}(\mathcal{P}) + \sum_{i=1,3} \frac{\partial\Omega_{11}}{\partial(\partial_{x_i}\alpha)} \partial_{x_i}\alpha = 0, \\ \rho\partial_t(v_{x_2}) + \rho v_{x_1}\partial_{x_1}(v_{x_2}) + \sum_{i=1,3} \frac{\partial\Omega_{12}}{\partial(\partial_{x_i}\alpha)} \partial_{x_i}\alpha = 0, \\ \rho\partial_t(v_{x_3}) + \rho v_{x_1}\partial_{x_1}(v_{x_3}) + \sum_{i=1,3} \frac{\partial\Omega_{13}}{\partial(\partial_{x_i}\alpha)} \partial_{x_i}\alpha = 0, \\ \partial_t(s_k) + v_{x_1}\partial_{x_1}(s_k) = 0, \\ \partial_t(\omega) + v_{x_1}\partial_{x_1}(\omega) = 0, \\ \partial_t(H) + v_{x_1}\partial_{x_1}(H) = 0, \\ \partial_t(\tilde{\Sigma}) + v_{x_1}\partial_{x_1}(\tilde{\Sigma}) = 0, \\ \partial_t(\alpha) + v_{x_1}\partial_{x_1}(\alpha) = 0, \\ \partial_t(\partial_{x_1}\alpha) + v_{x_1}\partial_{x_1}(\partial_{x_1}\alpha) + \sum_{i=1,3} \partial_{x_i}(\alpha) \frac{\partial v_{x_i}}{\partial x_1} = 0, \\ \partial_t(\partial_{x_2}\alpha) + v_{x_1}\partial_{x_1}(\partial_{x_2}\alpha) = 0, \\ \partial_t(\partial_{x_3}\alpha) + v_{x_1}\partial_{x_1}(\partial_{x_3}\alpha) = 0, \end{array} \right. \quad (4.20)$$

where

$$\Omega = \sigma_c \|\nabla\alpha\| \mathcal{I}_d - \sigma_c \nabla\alpha \otimes \nabla\alpha / \|\nabla\alpha\| \quad (4.21a)$$

$$= \frac{\sigma_c}{\|\nabla\alpha\|} \begin{pmatrix} (\partial_{x_2}\alpha)^2 + (\partial_{x_3}\alpha)^2 & -(\partial_{x_1}\alpha)(\partial_{x_2}\alpha) & -(\partial_{x_1}\alpha)(\partial_{x_3}\alpha) \\ \text{sym} & (\partial_{x_1}\alpha)^2 + (\partial_{x_3}\alpha)^2 & -(\partial_{x_2}\alpha)(\partial_{x_3}\alpha) \\ \text{sym} & \text{sym} & (\partial_{x_1}\alpha)^2 + (\partial_{x_2}\alpha)^2 \end{pmatrix} \quad (4.21b)$$

The extended pressure \mathcal{P} has been reintroduced to shorten the equations and writes $\mathcal{P} = p - \tilde{\sigma}\tilde{\Sigma}$.

Remark 18. For the equations on the gradient of the volume fraction, we have taken advantage of the property of the curl of the gradient of any scalar $\nabla \times \nabla\alpha = 0$, see Schmidmayer et al. (2017) [197].

The quasi-linear form of this first-order system of partial differential equations can be expressed using primitive variables. We group all transported quantities into the variable ψ , such that $\psi \in \{y_{j,k}, s_k, \alpha, \omega, H, \tilde{\Sigma}, \partial_{x_2}\alpha, \partial_{x_3}\alpha\}$. Noting $\mathbf{u} = (\rho, v_{x_1}, v_{x_2}, v_{x_3}, \partial_{x_1}\alpha, \psi)^t$, the system (4.20) takes the form

$$\partial_t \mathbf{u} + \mathcal{A}(\mathbf{u}) \partial_x \mathbf{u} = \mathbf{0}, \quad (4.22a)$$

$$\mathcal{A} = \begin{pmatrix} v_{x_1} & \rho & 0 & 0 & 0 & 0 \\ \frac{1}{\rho} \partial_\rho \mathcal{P} & v_{x_1} & 0 & 0 & \frac{1}{\rho} \frac{\partial \Omega_{11}}{\partial (\partial_{x_1} \alpha)} & \frac{1}{\rho} \partial_\psi \left(\mathcal{P} + \frac{\partial \Omega_{11}}{\partial \psi} \right) \\ 0 & 0 & v_{x_1} & 0 & \frac{1}{\rho} \frac{\partial \Omega_{12}}{\partial (\partial_{x_1} \alpha)} & \frac{1}{\rho} \frac{\partial \Omega_{12}}{\partial \psi} \\ 0 & 0 & 0 & v_{x_1} & \frac{1}{\rho} \frac{\partial \Omega_{13}}{\partial (\partial_{x_1} \alpha)} & \frac{1}{\rho} \frac{\partial \Omega_{13}}{\partial \psi} \\ 0 & \partial_{x_1} \alpha & \partial_{x_2} \alpha & \partial_{x_3} \alpha & v_{x_1} & 0 \\ 0 & 0 & 0 & 0 & 0 & v_{x_1} \end{pmatrix} \quad (4.22b)$$

Referring to Appendix 4.A, the spectrum of \mathcal{A} is composed of 14 real eigenvalues, among which five are distinct,

$$v, v \pm a_+, v \pm a_-, \quad (4.23a)$$

with

$$a_\pm^2 = \frac{1}{2} \left(\epsilon_{x_1} \mathcal{E}_c^l + \rho \partial_\rho \mathcal{P} \pm \sqrt{(\epsilon_{x_1} \mathcal{E}_c^l + \rho \partial_\rho \mathcal{P})^2 + 4\rho \epsilon_{x_1} \mathcal{E}_c^l \partial_\rho \mathcal{P}} \right) \quad (4.23b)$$

and $\epsilon_{x_1} = 1 - \left((\mathcal{E}_c^l)_{x_1} / \mathcal{E}_c^l \right)^2 \in [0, 1]$, $(\mathcal{E}_c^l)_{x_1} = \sigma_c \partial_{x_1} \alpha$ and $\mathcal{E}_c^l = \sigma_c \|\nabla \alpha\|$. However, the eigenvectors associated to the spectrum of \mathcal{A} do not generate a free family. Thus, the system is only weakly hyperbolic.

4.1.2.1 OPERATOR SPLITTING

To numerically solve system $(\mathcal{S})_\mu^{sk}$ in the limit $\mu \mapsto \infty$, we propose a splitting of operators between the euler flux, the capillarity flux and the relaxation terms. The method is in the same spirit of Schmidmayer et al. (2017) [197]. Therefore, $(\mathcal{S})_\mu^{sk}$ splits into three sub-systems.

Sub-system 1:

The first sub-system includes the Euler fluxes and takes the form

$$(\mathcal{S}_1)_\mu^{sk} \left\{ \begin{array}{l} \partial_t(\rho) + \nabla \cdot [\rho \mathbf{v}] = 0, \\ D_t y_{j,k} = 0, \\ \rho D_t \mathbf{v} + \nabla(\alpha_1 p_1 + \alpha_2 p_2) = \mathbf{0}, \\ D_t s_k = 0, \\ D_t \omega = 0, \\ D_t H = 0, \\ D_t \tilde{\Sigma} = 0, \\ D_t \alpha = 0, \\ \partial_t(\partial_{x_1} \alpha) + \mathbf{v} \cdot \nabla(\partial_{x_1} \alpha) + \partial_{x_1} v_{x_1} \partial_{x_1} \alpha = 0, \\ \partial_t(\partial_{x_2} \alpha) + \mathbf{v} \cdot \nabla(\partial_{x_2} \alpha) + \partial_{x_2} v_{x_1} \partial_{x_2} \alpha = 0, \\ \partial_t(\partial_{x_3} \alpha) + \mathbf{v} \cdot \nabla(\partial_{x_3} \alpha) + \partial_{x_3} v_{x_1} \partial_{x_3} \alpha = 0, \end{array} \right. \quad (4.24)$$

Because of rotation invariance, the mathematical study of smooth solutions can be done using the quasi-linear form of this first-order system of partial differential equations in a single dimension with the set of variables $\mathbf{u} = (\rho, v, \partial_{x_1} \alpha, \varphi)^t$ with $\varphi \in \{y_{j,k}, s_k, \omega, \tilde{\Sigma}, H, \alpha, \partial_{x_2} \alpha, \partial_{x_3} \alpha\}$

such that $D_t\varphi = 0$. Referring to Appendix 4.A.2, System (4.24) is hyperbolic, and the spectrum is composed of three real distinct eigenvalues

$$v, v \pm a_F, \quad (4.25a)$$

where a_F is the Frozen sound speed of the mixture defined as

$$a_F^2 = \sum_{k=1}^2 y_k a_k^2, \quad \text{with } a_k^2 = \left. \frac{\partial p_k}{\partial \rho_k} \right|_{s_k}. \quad (4.25b)$$

Sub-system 2:

The second sub-system accounts for small and large scale capillary fluxes and is defined by

$$(\mathcal{S}_{\text{II}})_{\mu}^{s_k} \left\{ \begin{array}{l} \partial_t \rho = 0, \\ \partial_t y_{j,k} = 0, \\ \rho \partial_t \mathbf{v} + \nabla \cdot [\tilde{\sigma} \tilde{\Sigma} \mathcal{I}_d - \Omega] = \mathbf{0}, \\ \partial_t s_k = 0, \\ \partial_t \omega = 0, \\ \partial_t H = 0, \\ \partial_t \tilde{\Sigma} = 0, \\ \partial_t \alpha = 0, \\ \partial_t (\partial_{x_1} \alpha) + \partial_{x_1} v_{x_2} \partial_{x_2} \alpha + \partial_{x_1} v_{x_3} \partial_{x_3} \alpha = 0, \\ \partial_t (\partial_{x_2} \alpha) + \partial_{x_2} v_{x_1} \partial_{x_1} \alpha + \partial_{x_2} v_{x_3} \partial_{x_3} \alpha = 0, \\ \partial_t (\partial_{x_3} \alpha) + \partial_{x_3} v_{x_1} \partial_{x_1} \alpha + \partial_{x_3} v_{x_2} \partial_{x_2} \alpha = 0, \end{array} \right. \quad (4.26)$$

Using the same arguments as for the previous system, the one-dimensional analysis of System (4.26) detailed in Section 4.A.3 shows that the system is weakly hyperbolic with three distinct eigenvalues given by

$$0, \pm \epsilon_{x_1} \sqrt{\frac{\mathcal{E}_c^l}{\rho}}. \quad (4.27)$$

Sub-system 3:

The third sub-system contains the relaxation sources terms and takes the form

$$(\mathcal{S}_{\text{III}})_{\mu}^{s_k} \left\{ \begin{array}{l} \partial_t \rho = 0, \\ \partial_t y_{j,k} = 0, \\ \partial_t \mathbf{v} = \mathbf{0}, \\ \partial_t s_k = 0, \\ \partial_t \omega = 0, \\ \partial_t H = 0, \\ \partial_t \tilde{\Sigma} = -2H \mu (p_1 - p_2 + \kappa_c(\alpha) - 2H\tilde{\sigma}), \\ \partial_t \alpha = \mu (p_1 - p_2 + \kappa_c(\alpha) - 2H\tilde{\sigma}), \\ \partial_t \nabla \alpha = \mathbf{0}, \end{array} \right. \quad (4.28)$$

where we have not included any relaxation on the volume fraction gradient equations by simplification and also because we will never numerically transport the gradients. Future

works could consist in taking the relaxation into account for such variables. $(\mathcal{S}_{\text{III}})_{\mu}^{s_k}$ in the limit $\mu \mapsto \infty$ describes a relaxation procedure, which is very similar to the one proposed in [Miller and Puckett \(1996\) \[160\]](#), [Saurel et al. \(2009\) \[195\]](#), and will be described in the next section.

4.1.3 NUMERICAL METHOD

The Stationary Action Principle returns naturally transport equations for the partial entropies. However, it is known that due to the non-linearity between the entropy and the pressure, using the partial entropies fails at preserving a uniform pressure and velocity flow. A simplified example is given in [Appendix 4.B](#). We thus propose to replace the entropy equations with the internal energy equations. Using the Gibbs equation, and assuming it still holds in non-equilibrium flows in the frame moving with the local hydrodynamic velocity \mathbf{v} , we have

$$T_k D_t s_k = D_t e_k - \frac{p_k}{\rho_k^2} D_t \rho_k, \quad (4.29)$$

which, after some manipulations, yields

$$\alpha_k \rho_k T_k D_t s_k = \alpha_k \rho_k D_t e_k + \alpha_k p_k \nabla \cdot \mathbf{v} + p_k D_t \alpha_k. \quad (4.30)$$

Reinjecting the transport equation for the partial entropy and the volume fraction, we obtain the transport equation of the partial internal energy

$$\partial_t(\alpha_k \rho_k e_k) + \nabla \cdot (\alpha_k \rho_k e_k \mathbf{v}) - \alpha_k p_k \nabla \cdot \mathbf{v} = -p_k D_t \alpha_k. \quad (4.31)$$

Nonetheless, the partial internal energy equations contain non-conservative terms, which prevent the strict conservation of the total energy due to the loss of Rankine-Hugoniot jump condition when solving the Riemann problem. In [Saurel et al. \(2009\) \[195\]](#), the authors propose to use the total energy equation as a corrector of the internal energy equations. We propose to use the same strategy and add the supplementary conservative equation on the total energy equation as a corrector for the numerical errors obtained on the internal energies due to the non-conservative terms in their equations. In [Chapter 3](#), the Stationary Action Principle has returned a total energy evolution equation (3.85c). We propose to neglect the coupling term between the volume fraction evolution equation and the large capillary effects to simplify the approach. Since we have also taken the asymptotic limit of the micro inertia $\nu \lim 0$, and neglected mixing terms of the mixture energy and entropy, the total energy equation takes the form

$$\partial_t(\rho E) + \nabla \cdot \left[\rho E + \left(p - \sigma_c \|\nabla \alpha\| - \tilde{\sigma} \tilde{\Sigma} + \sigma_c \frac{\nabla \alpha \otimes \nabla \alpha}{\|\nabla \alpha\|} \right) \mathbf{v} \right] = 0. \quad (4.32)$$

Furthermore, the supplementary equation on the gradient of the volume fraction was only a mathematical artifact to operate a second-order analysis of the system. We will not solve these transport equations. Finally, we will always privilege conservative equations to obtain Rankine-Hugoniot jump conditions for the Riemann problem we are about to solve.

Therefore, the system to be implemented is noted $(\mathcal{S})_\mu^{e_k}$ and takes the form

$$(\mathcal{S})_\mu^{e_k} \left\{ \begin{array}{l} \partial_t(\rho) + \nabla \cdot [\rho \mathbf{v}] = 0, \\ \partial_t(\rho y_{j,k}) + \nabla \cdot [\rho y_{j,k} \mathbf{v}] = 0, \\ \partial_t(\rho \mathbf{v}) + \nabla \cdot [\rho \mathbf{v} \otimes \mathbf{v} + p \mathcal{I}_d - \tilde{\sigma} \tilde{\Sigma} - \Omega] = 0, \\ \partial_t(\alpha_k \rho_k e_k) + \nabla \cdot [\alpha_k \rho_k e_k \mathbf{v}] - \alpha_k p_k \nabla \cdot \mathbf{v} = -\mu p_k (p_k - p_{k'} + \kappa_c(\alpha_k) - 2H\tilde{\sigma}), \\ \partial_t(\rho E) + \nabla \cdot [\rho E + (p - \tilde{\sigma} \tilde{\Sigma} - \Omega) \mathbf{v}] = 0, \\ \partial_t(\omega) + \nabla \cdot [\omega \mathbf{v}] - \omega \nabla \cdot \mathbf{v} = 0, \\ \partial_t(\rho H) + \nabla \cdot [\rho H \mathbf{v}] = 0, \\ \partial_t(\rho \tilde{\Sigma}) + \nabla \cdot [\rho \tilde{\Sigma} \mathbf{v}] = -2H \mu (p_k - p_{k'} + \kappa_c(\alpha_k) - 2H\tilde{\sigma}), \\ \partial_t(\alpha_k) + \nabla \cdot [\alpha_k \mathbf{v}] - \alpha_k \nabla \cdot \mathbf{v} = \mu (p_k - p_{k'} + \kappa_c(\alpha_k) - 2H\tilde{\sigma}), \end{array} \right. \quad (4.33)$$

with the total pressure $p = \alpha_1 p_1 + \alpha_2 p_2$, the large scale capillary tensor $\Omega = \sigma_c \|\nabla \alpha_k\| \mathcal{I}_d - \sigma_c \nabla \alpha_k \otimes \nabla \alpha_k$, the total energy $\rho E = \rho \|\mathbf{v}\|^2/2 + \rho e + \sigma_c \|\nabla \alpha\| + \tilde{\sigma} \tilde{\Sigma}$, the mixture internal energy $e = y_1 e_1 + y_2 e_2$, the local curvature $\kappa_c(\alpha_k) = \nabla \cdot [\sigma_c \nabla \alpha_k]$ and the two constitutive equations of state $p_k = p_k(\rho_k, e_k)$. The notation $\nabla \alpha$ corresponds to the normalized volume fraction gradient $\nabla \alpha_k = \nabla \alpha_k / \|\nabla \alpha_k\|$. We reformulate and rearrange the system in terms of conservative, non-conservative and relaxation sources terms to obtain a matrix formulation,

$$\partial_t \mathbf{q} + \nabla \cdot [\mathbf{f}^e(\mathbf{q}) + \mathbf{f}^c(\mathbf{q})] + \mathbf{n}(\mathbf{q}) \nabla \cdot \mathbf{v} = \frac{\mathbf{r}(\mathbf{q})}{\epsilon^p}, \quad (4.34a)$$

with

$$\mathbf{q} = \begin{pmatrix} \rho \\ \rho \mathbf{v} \\ \rho E \\ \omega \\ \rho \tilde{\Sigma} \\ \rho H \\ \rho y_{j,k} \\ \alpha_k \\ \alpha_k \rho_k e_k \end{pmatrix}, \quad \mathbf{f}^e(\mathbf{q}) = \begin{pmatrix} \rho \mathbf{v} \\ \rho \mathbf{v} \otimes \mathbf{v} + p \\ (\rho E + p) \mathbf{v} \\ \omega \mathbf{v} \\ \rho \tilde{\Sigma} \mathbf{v} \\ \rho H \mathbf{v} \\ \rho y_{j,k} \mathbf{v} \\ \alpha_k \mathbf{v} \\ \alpha_k \rho_k e_k \mathbf{v} \end{pmatrix}, \quad \mathbf{f}^c(\mathbf{q}) = - \begin{pmatrix} 0 \\ \tilde{\sigma} \tilde{\Sigma} + \Omega \\ (\tilde{\sigma} \tilde{\Sigma} + \Omega) \mathbf{v} \\ 0 \\ 0 \\ 0 \\ 0 \\ 0 \\ 0 \end{pmatrix}, \quad \mathbf{n}(\mathbf{q}) = \begin{pmatrix} 0 \\ 0 \\ 0 \\ -\omega \\ 0 \\ 0 \\ 0 \\ -\alpha_k \\ -\alpha_k p_k \end{pmatrix}, \quad (4.34b)$$

$$\frac{\mathbf{r}(\mathbf{q})}{\epsilon^p} = \begin{pmatrix} 0 \\ 0 \\ 0 \\ 0 \\ -2H(\Delta p_k + \kappa_c(\alpha_k) - 2H\tilde{\sigma}) \\ 0 \\ 0 \\ \Delta p_k + \kappa_c(\alpha_k) - 2H\tilde{\sigma} \\ -p_k(\Delta p_k + \kappa_c(\alpha_k) - 2H\tilde{\sigma}) \end{pmatrix}, \quad (4.34c)$$

where we have replaced the relaxation coefficient μ by its inverse $\epsilon^p = 1/\mu$, and $\Delta p_k = p_k - p_{k'}$. We have rearranged the order of the variables to have a first subset of mixing and geometric

quantities $(\rho, \rho \mathbf{v}, \rho E, \omega, \rho \tilde{\Sigma}, \rho H)$ and then a subset of fluid variables $(\rho y_{j,k}, \alpha_k, \alpha_k \rho_k e_k)$ with $k = 1, 2$.

Thus, the Lie-splitting operation will consist in solving first the Euler fluxes with the non-conservative terms,

$$(\mathcal{S}_I)_\mu^{e_k} \left\{ \partial_t \mathbf{q} + \nabla \cdot [\mathbf{f}^e(\mathbf{q})] + \mathbf{n}(\mathbf{q}) \nabla \cdot \mathbf{v} = 0, \right. \quad (4.35)$$

with a HLLC solver. Then, we will solve the capillary fluxes,

$$(\mathcal{S}_{II})_\mu^{e_k} \left\{ \partial_t \mathbf{q} + \nabla \cdot [\mathbf{f}^c(\mathbf{q})] = 0, \right. \quad (4.36)$$

with a simple arithmetic average solver. Finally we will proceed to the pressure relaxation procedure using a Newton algorithm to solve

$$(\mathcal{S}_{III})_\mu^{e_k} \left\{ \partial_t \mathbf{q} = \frac{\mathbf{r}(\mathbf{q})}{\epsilon^p}, \right. \quad (4.37)$$

in the limit $\epsilon^p \mapsto 0$.

We propose a Finite Volume discretization method. It implies the resolution of a local Riemann problem at each interface seen as a discontinuity between two referring states, namely \mathbf{q}_L on the left side and \mathbf{q}_R on the right side. To cope with strong discontinuities faced in two phases flows, Godunov-type schemes are based on solutions to local Riemann problems to evaluate inter-cell fluxes. Exact Riemann solver are costly, hard to implement for system of PDE with non-conservative terms and can lack some robustness, which is our primary concern keeping in mind the targeted challenging industrial applications. Therefore we will adopt approximate Riemann solvers.

In the following we present the first-order version of the scheme for sake of simplicity, and extension to second-order is detailed hereinafter. Whenever we will use a first-order scheme for space discretization, we will also adopt an Euler explicit temporal scheme.

4.1.3.1 FIRST SUB-SYSTEM: EULER FLUX WITH HLLC SOLVER

Among the approximate Riemann solvers, the HLLC solver of [Toro et al. \(1994\)](#) [210] seems adequate for the problem since the investigated system $(\mathcal{S}_I)_\mu^{e_k}$ has only three distinct waves. It is also known to be robust for flows with high gradients or strong discontinuities, which we will encounter in the targeted applications.

Integrating System (4.35) over a given cell control volume \mathcal{V}_i leads to

$$\int_{\mathcal{V}_i} \partial_t \mathbf{q} \, dV = - \int_{\mathcal{V}_i} \nabla \cdot \mathbf{f}^e(\mathbf{q}) \, dV - \int_{\mathcal{V}_i} \mathbf{n}(\mathbf{q}) \nabla \cdot \mathbf{v} \, dV. \quad (4.38)$$

Following the cell centered Finite volume approach, we evaluate the variables at the center of the cell, such that

$$\mathcal{V}_i \mathbf{q}_i \approx \int_{\mathcal{V}_i} \mathbf{q} \, dV, \quad (4.39)$$

where \mathcal{V}_i is the volume of cell i , \mathbf{q}_i is the set of variables \mathbf{q} evaluated at the center of the cell i . We then assume $\mathbf{n}(\mathbf{q})$ constant in the cell. Given polyhedral cells, applying the Green-Ostrogradski theorem we obtain

$$\mathcal{V}_i \partial_t \mathbf{q}_i = - \sum_{j \in N_S^i} \int_{S_{ij}} \mathbf{f}^e(\mathbf{q}) \cdot \mathbf{n}_{ij} dS - \mathbf{n}(\mathbf{q}_i) \sum_{j \in N_S^i} \int_{S_{ij}} \mathbf{v} \cdot \mathbf{n}_{ij} dS, \quad (4.40)$$

with S_{ij} the area of the face j of cell i , N_S^i the set of face indexes of cell i , \mathbf{n}_{ij} the normal vector to the face j pointing outward the cell i to the neighbor cell j . We finally associate the physical flux \mathbf{f}^e with a numerical flux, ϕ^e , in order to approximate the flux integral over each face j of cell i ,

$$S_{ij} \phi^e(\mathbf{q}_i, \mathbf{q}_j, \mathbf{n}_{ij}) \approx \int_{S_{ij}} \mathbf{f}^e(\mathbf{q}) \cdot \mathbf{n}_{ij} dS, \quad (4.41)$$

and we obtain the finite volume formulation

$$\mathcal{V}_i \partial_t \mathbf{q}_i = - \sum_{j \in N_S^i} S_{ij} [\phi^e(\mathbf{q}_i, \mathbf{q}_j, \mathbf{n}_{ij}) + \mathbf{n}(\mathbf{q}_i) v_{ij}], \quad (4.42)$$

with $v_{ij} = \mathbf{v} \cdot \mathbf{n}_{ij}$ the normal velocity at the face j of cell i to be modelled.

We now proceed to the evaluation of the numerical flux ϕ^e and the normal velocity v_{ij} using the HLLC solver. Assuming the left and right waves S_L, S_R known (Figure 4.1), the

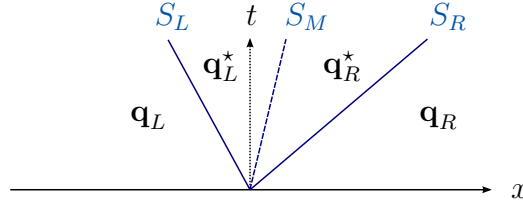


FIGURE 4.1: Representation of the local Riemann problem in the HLLC frame at face j of cell i .

Rankine-Hugoniot jump conditions are applied on each genuinely non-linear waves S_L, S_R for each conservative variables, such that $\forall q \in (\rho, \rho \mathbf{v}, \rho E, \rho \tilde{\Sigma}, \rho H, \rho y_{j,k})$,

$$S_K q_K^* - \mathbf{f}^e(q_K^*) = S_K q_K - \mathbf{f}^e(q_K), \quad \text{with } K = L, R. \quad (4.43)$$

The linearly degenerated wave defines a contact discontinuity, for which p and v are Riemann invariants (see Section 4.A.2), such that

$$p_L^* = p_R^* = p^*, \quad v_{n,L}^* = v_{n,R}^* = S_M, \quad (4.44a)$$

where $v_n = v_{ij}$ is the component of the velocity normal to the interface. Since $(s_k, \omega, \tilde{\Sigma}, H, \alpha)$ are Riemann invariants of the shock and rarefaction waves, these quantities stay continuous across these waves such that

$$(s_k)_K^* = (s_k)_K, \quad \omega_K^* = \omega_K, \quad \tilde{\Sigma}_K^* = \tilde{\Sigma}_K, \quad H_K^* = H_K, \quad \alpha_K^* = \alpha_K, \quad (4.45)$$

with $K = L, R$. Manipulating Equations (4.43) leads to

$$p^* - p_K = \rho_K (S_K - v_{n,K}) (S_M - v_{n,K}). \quad (4.46)$$

Combining the two equations obtained for $K = L$ and $K = R$ from Equation (4.46) into Equations (4.43) gives an expression for S_M ,

$$S_M = \frac{p_L - p_R + \rho_L v_{n,L}(v_{n,L} - S_L) + \rho_R v_{n,R}(S_R - v_{n,R})}{\rho_L(v_{n,L} - S_L) + \rho_R(S_R - v_{n,R})}. \quad (4.47)$$

Concerning the non-conservative variables, (ρ_k, p_k, e_k) , we need to circumvent the absence of Rankine-Hugoniot jump condition. Noticing that the quantity $(\alpha_k \rho_k)$ is conserved across the genuinely non-linear waves, we determine $(\rho_k)_K^*$ thanks to

$$(\rho_k)_K^* = (\alpha_k \rho_k)_K^* / (\alpha_k)_K^*, \quad (4.48)$$

where $(\alpha_k \rho_k)_K^*$ can also be obtained from Rankine-Hugoniot jump conditions as in Equation (4.43).

Then, as a first approach, since the shock and the rarefaction waves are isentropic, the phasic entropies s_k being Riemann invariants, we could exploit the relation $(s_k)_K^* = s_k^*$ such that the total derivative of each fluid pressure p_k yields

$$dp_k = a_k^2 d\rho_k, \quad (4.49)$$

leading to a first estimate of the fluid pressures p_k in the star regions

$$(p_k)_K^* = (p_k)_K + (a_k)_K^2 [(\rho_k)_K^* - (\rho_k)_K]. \quad (4.50)$$

Nevertheless, in Saurel et al. (2007) [193], the authors demonstrate that using this closure is not compatible with the total energy conservation. Instead, since we are not solving the partial entropies but the internal energies, we can also use the fact that across the isentropic waves,

$$de_k + p_k d(1/\rho_k) = 0, \quad (4.51)$$

and integrate it, such that

$$(e_k)_K^* = (e_k)_K - \tilde{p} \left[\frac{1}{(\rho_k)_K^*} - \frac{1}{(\rho_k)_K} \right], \quad (4.52)$$

with \tilde{p} a pressure estimate, which, constrained by the total mass conservation, is found in Saurel et al. (2007) [193] to be equal to

$$\tilde{p} = \frac{p^* + p_K}{2}. \quad (4.53)$$

We obtain then an estimate of each phasic pressure, which depends on the equation of state and reads for example for the Stiffened Gas equation of state,

$$(p_k)_K^* = [(p_k)_K + p_k^\infty] \frac{(\gamma_k - 1)(\rho_k)_K - (\gamma_k + 1)(\rho_k)_K^*}{(\gamma_k - 1)(\rho_k)_K^* - (\gamma_k + 1)(\rho_k)_K}, \quad (4.54)$$

and the fluid internal energies are readily obtained with the equation of state, $(e_k)_K^* = e_k [(\rho_k)_K^*, (p_k)_K^*]$. To sum up, the intermediate states of the Riemann problem in a condensed form are

$$\mathbf{q}_K^* = \frac{v_{n,K} - S_K}{S_M - S_K} \begin{pmatrix} \rho_K \\ \rho_K [\mathbf{v}_K + (S_M - v_{n,K})\mathbf{n}] \\ \rho_K \left[E_K + \frac{p_K v_{n,K} - S_M}{\rho_K v_{n,K} - S_K} + (S_M - v_{n,K})S_M \right] \\ 0 \\ \rho_K \tilde{\Sigma}_K \\ \rho_K H_K \\ \rho_K (y_{j,k})_K \\ 0 \\ \rho_K e_k [(p_k)_K^*, (\rho_k)_K^*] \end{pmatrix} + \begin{pmatrix} 0 \\ 0 \\ 0 \\ \omega_K \\ 0 \\ 0 \\ 0 \\ \alpha_K \\ 0 \end{pmatrix}, \text{ with } K = L, R. \quad (4.55)$$

The numerical conservative flux at the interface is given as follows

$$\phi^e(\mathbf{q}_i, \mathbf{q}_j, \mathbf{n}_{ij}) = \begin{cases} \mathbf{f}_L^e \hat{=} \mathbf{f}^e(\mathbf{q}_L) & \text{if } S_L > 0, \\ (\mathbf{f}_L^e)^* \hat{=} \mathbf{f}^e(\mathbf{q}_L^*) & \text{if } S_L < 0 \text{ and } S_M > 0, \\ (\mathbf{f}_R^e)^* \hat{=} \mathbf{f}^e(\mathbf{q}_R^*) & \text{if } S_M < 0 \text{ and } S_R > 0, \\ \mathbf{f}_R^e \hat{=} \mathbf{f}^e(\mathbf{q}_R) & \text{if } S_R > 0. \end{cases}, \quad (4.56)$$

and the non-conservative terms are evaluated as

$$\mathbf{n}(\mathbf{q}_i)v_{ij} = \begin{cases} \mathbf{n}_L \hat{=} \mathbf{n}(\mathbf{q}_i)v_{n,L} & \text{if } S_L > 0, \\ \mathbf{n}_L^* \hat{=} \mathbf{n}(\mathbf{q}_i)S_M & \text{if } S_L < 0 \text{ and } S_M > 0, \\ \mathbf{n}_R^* \hat{=} \mathbf{n}(\mathbf{q}_i)S_M & \text{if } S_M < 0 \text{ and } S_R > 0, \\ \mathbf{n}_R \hat{=} \mathbf{n}(\mathbf{q}_i)v_{n,R} & \text{if } S_R > 0. \end{cases} \quad (4.57)$$

We propose a compact form for each flux,

$$\phi^e = \frac{\mathbf{f}_L^e + \mathbf{f}_R^e}{2} + \frac{\epsilon_L + \epsilon_R}{2} \frac{\mathbf{f}_L^e - \mathbf{f}_R^e}{2} + \frac{\epsilon_R - \epsilon_L}{2} \left[S_L \frac{\mathbf{q}_L^* - \mathbf{q}_L}{2} + S_R \frac{\mathbf{q}_R^* - \mathbf{q}_R}{2} + \epsilon_M S_M \frac{\mathbf{q}_L^* - \mathbf{q}_R^*}{2} \right], \quad (4.58a)$$

$$\mathbf{n} = \left(\frac{1}{2} - \frac{\epsilon_L - \epsilon_R}{4} \right) [\mathbf{n}_L + \mathbf{n}_R] + \frac{\epsilon_L + \epsilon_R}{4} [\mathbf{n}_L - \mathbf{n}_R] + \frac{\epsilon_M - \epsilon_L}{2} \mathbf{n}_L^* + \frac{\epsilon_R - \epsilon_M}{2} \mathbf{n}_R^* \quad (4.58b)$$

where ϵ_K is the sign of the wave speed S_K , $K = L, R, M$ and equals unity if the wave speed is null.

The only pending task is to estimate the smallest and largest wave speeds, S_L and S_R . Davis (1988) [43] gives a simple estimate in the monophasic configuration, that we propose to adapt to the present model. It leads to the following estimates

$$S_L = \min(v_{n,L} - a_L, v_{n,R} - a_R), \quad (4.59a)$$

$$S_R = \min(v_{n,L} + a_L, v_{n,R} + a_R). \quad (4.59b)$$

4.1.3.2 SECOND SUB-SYSTEM: CAPILLARY FLUX

Large scale capillarity terms are discretized in the conservative formulation rather than as source terms. Integrating System (4.36) in a given cell and applying the same approach as for

the Euler flux leads to

$$\mathcal{V}_i \partial_t \mathbf{q}_i = - \sum_{j \in N_S^i} \mathcal{S}_{ij} \phi^c(\mathbf{q}_i, \mathbf{q}_j, \mathbf{n}_{ij}), \quad (4.60)$$

with ϕ^c the numerical flux associated to the physical flux \mathbf{f}^c . Only the momentum and the total energy are modified by the capillary fluxes. We obtain

$$\mathcal{V}_i \partial_t (\rho \mathbf{v})_i = \sum_{j \in N_S^i} \left(\mathcal{S}_{ij} \sigma_c \|\nabla \alpha_{ij}\| \left[\mathbf{n}_{ij} - (\overline{\nabla \alpha_{ij}} \cdot \mathbf{n}_{ij}) \nabla \alpha_{ij} \right] + \mathcal{S}_{ij} \tilde{\sigma} \tilde{\Sigma}_{ij} \mathbf{n}_{ij} \right), \quad (4.61)$$

$$\mathcal{V}_i \partial_t (\rho E)_i = \sum_{j \in N_S^i} \left(\mathcal{S}_{ij} \sigma_c \|\nabla \alpha_{ij}\| \left[\mathbf{n}_{ij} - (\overline{\nabla \alpha_{ij}} \cdot \mathbf{n}_{ij}) \nabla \alpha_{ij} \right] \cdot \mathbf{v}_{ij} + \mathcal{S}_{ij} \tilde{\sigma} \tilde{\Sigma}_{ij} \mathbf{n}_{ij} \cdot \mathbf{v}_{ij} \right), \quad (4.62)$$

where $\nabla \alpha_{ij}$, $\tilde{\Sigma}_{ij}$ and \mathbf{v}_{ij} are respectively the volume fraction gradient, the interfacial density area and the velocity, each of them evaluated on the face \mathcal{S}_{ij} by an approximation.

If we were solving the equations on the gradient of the volume fraction, we could use a HLLC solver since the spectrum of the associated jacobian of system $(\mathcal{S}_{\parallel})_{\mu}^{e_k}$ is composed of three distinct waves (Equation (4.27)). However, for the sake of simplicity and CPU saving, we will not implement the equations on the volume fraction gradient and therefore, we propose to use the arithmetic cell averaging to define the interfacial quantities. If not mistaken, it is also the solution adopted in Schmidmayer et al. (2017) [197].

Finally, all the quantities involved in this second sub-system are updated after the integration of the first sub-system.

4.1.3.3 THIRD SUB-SYSTEM: PRESSURE RELAXATION PROCEDURE

After the integration of the two preceding fluxes, we want to instantaneously relax the pressures. The procedure is very similar to the one proposed in Miller and Puckett (1996) [160], Saurel et al. (2009) [195]. We will recall the main steps here.

Neglecting the local and mean curvature

The algebraic equation of System $(\mathcal{S})_{\mu \rightarrow \infty}^{s_k}$ imposing the pressure equality when neglecting the local curvature and the mean curvature reads

$$p_2(\rho_2, e_2) - p_1(\rho_1, e_1) = 0. \quad (4.63)$$

Looking at system (4.37), the relaxation procedure will maintain ρ , \mathbf{v} , E , ω , H , $y_{j,k}$ constant, while e_k , ρ_k , p_k , α_k , $\tilde{\Sigma}$ will change. As shown in the case of Stiffened Gas equations of state in Saurel et al. (2009) [195], Equation (4.63) is an equation on the volume fraction α_k and there is a unique solution, α_k^* . We can use a Newton algorithm to find it. Assuming $\alpha = \alpha_1 = 1 - \alpha_2$, an estimate of α is given by the convergence of the series

$$\alpha^{n+1} = \alpha^n - \frac{p_1^n - p_2^n}{\left(\frac{dp_1}{d\alpha}\right)^n + \left(\frac{dp_2}{d(1-\alpha)}\right)^n}. \quad (4.64)$$

The partial derivatives of the pressure are

$$\frac{dp_k}{d\alpha_k} = -\frac{\rho y_k}{\alpha_k^2} \frac{\partial p_k}{\partial \rho_k} \Big|_{e_k} + \frac{\partial p_k}{\partial e_k} \Big|_{\rho_k} \frac{de_k}{d\alpha_k}. \quad (4.65)$$

The two derivatives $\left. \frac{\partial p_k}{\partial \rho_k} \right|_{e_k}$ and $\left. \frac{\partial p_k}{\partial e_k} \right|_{\rho_k}$ are evaluated according to the EOS and a discrete approximation leads to

$$\frac{de_k}{d\alpha_k} \approx \frac{e_k^{n+1} - e_k^n}{\alpha_k^{n+1} - \alpha_k^n}. \quad (4.66)$$

Recalling that the conservative internal energy equations can also be expressed as

$$\partial_t \alpha_k \rho_k e_k = -p_k \partial_t \alpha_k, \quad (4.67)$$

and that $\alpha_k \rho_k$ remains constant, the discrete approximation leads to

$$\frac{de_k}{d\alpha_k} \approx \frac{\widetilde{p}_k}{(\alpha_k \rho_k)^0}, \quad (4.68)$$

where \widetilde{p}_k is an estimator of the fluid pressure, taken as the mixing pressure p^n . At each iteration of the Newton algorithm, the fluid pressures p_k and the internal energies e_k are updated as well as the fluctuating interfacial density area,

$$\widetilde{\Sigma}^{n+1} = \widetilde{\Sigma}^n - 2(H)^0 (\alpha^{n+1} - \alpha^n). \quad (4.69)$$

A threshold, defined for each partial pressure as

$$\frac{|p_k^{n+1} - p_k^n|}{p_k^n} \ll 1, \quad (4.70)$$

stops the algorithm once verified. It is to be noticed that numerical difficulties may occur during the algorithm due to too large volume fraction steps, $\alpha^{n+1} - \alpha^n$, incompatible with the linear approximation of the update (4.64) leading to extrapolations in thermodynamics regions where the equations of state used are not valid. Limiting the volume change such as in [Miller and Puckett \(1996\)](#) [160] prevents such issues. At the end of the procedure we obtain the updated quantities α^* , ρ_k^* and $\widetilde{\Sigma}^*$ as well as the equilibrium pressure.

Including the local and mean curvature

When keeping the local and mean curvature, the Laplace equation, $p_1 - p_2 + \kappa_c(\alpha) - 2H\tilde{\sigma} = 0$ becomes a second-order ODE on the volume fraction. As a first approach, one can assume the local and mean curvature constant during relaxation, thus, introducing the modified pressure $\tilde{p}_2 = p_2 - \kappa_c(\alpha) + 2H\tilde{\sigma}$, the equation to solve is

$$p_1 - \tilde{p}_2 = 0, \quad (4.71)$$

and the procedure remains identical as in the previous paragraph.

Total energy correction

Since the internal energy equations contain non-conservative terms, their integration leads to numerical errors, which directly impact the pressures and the temperatures recalculated from the internal energies. To circumvent this problem, in [Saurel et al. \(2009\)](#) [195], the authors propose a reinitialization step whereby the equilibrium pressure is recalculated from the mixing internal energy derived from the mixing total energy. Then, the new equilibrium

pressure together with the updated partial densities ρ_k yields corrected internal energies. We have thus adapted this method to our present model including capillary terms. The equation

$$\left(\rho E - \frac{1}{2}\rho\|\mathbf{v}\|^2 - \sigma_c\|\nabla\alpha\|\right)^0 = \rho e = \sum_{k=1}^2 (\alpha_k \rho_k)^0 e_k(p, \rho_k^*), \quad (4.72)$$

has a unique unknown p to be determined using the value of the variables before relaxation, $\rho^0, E^0, \mathbf{v}^0, \nabla\alpha^0, (\alpha_k \rho_k)^0$ and the updated densities obtained through the Newton algorithm ρ_k^* . This equation can be solved using an other Newton algorithm or, for simple EOS, we can derive an expression of the corrected pressure. For instance, the Stiffened Gas EOS leads to

$$p = \frac{\left(\rho E - \frac{1}{2}\rho\|\mathbf{v}\|^2 - \sigma_c\|\nabla\alpha\|\right)^0 - \sum_{k=1}^2 \frac{\alpha_k^* \gamma_k p_k^\infty}{\gamma_k - 1}}{\sum_{k=1}^2 \frac{\alpha_k^*}{\gamma_k - 1}}. \quad (4.73)$$

Each internal energy is then reevaluated using this new equilibrium pressure p and the partial density ρ_k^* . This procedure guarantees the conservation of the total energy.

4.1.3.4 SECOND-ORDER EXTENSION

Second-order extension is achieved using a second-order Runge-Kutta scheme for the time discretization of each sub-system together with a multislope MUSCL second-order space discretization [Le Touze et al. \(2014\) \[133\]](#). The technique consists in computing two dedicated slopes for each face of each mesh cell. It uses the vertex neighbors and ensures the L^∞ norm stability on the scalar advection. The interpolated variables are composed of mixing quantities $(\mathbf{v}, \omega, \tilde{\Sigma}, H)$ and fluid variables $(\alpha_k, \rho_k \bar{y}_{j,k}, p_k)$. We recall that $\bar{y}_{j,k}$ is the mass fraction of species j of fluid k with respect to the fluid mass and not the mixture mass, such that $\bar{y}_{j,k} = y_{j,k}/y_k$ (see [Chapter 2](#)). The second-order spatial discretization is combined with a second-order Runge-Kutta scheme for the time integration.

4.1.3.5 SUMMARY OF THE NUMERICAL PROCEDURE

The numerical methods based on the splitting procedure can be summarized as follows:

- We first integrate the Euler flux using a HLLC solver and update all the variables.
- Then we compute the capillary flux using an arithmetic average to estimate both the volume fraction gradient and the interfacial density area at each cell interface and update all the variables.
- Then we use the pressure relaxation to estimate the relaxed volume fraction α_k^* and partial densities ρ_k^* .
- Finally, the energy correction leads to a final equilibrium pressure p which is then used together with ρ_k^* to correct the partial internal energies e_k through the EOS.

4.2 CEDRE IMPLEMENTATION OF THE TWO-SCALE TWO-PHASE FLOW MODEL

In order to test the numerical method described in the previous [Section 4.1.3](#), we have implemented it in the industrial CFD code CEDRE developed at ONERA, a multiphysics computational fluid dynamics software working on general unstructured meshes and organized as a set of solvers [Refloch et al. \(2011\) \[184\]](#), [Gaillard et al. \(2016\) \[76\]](#).

Instead of building from scratch a new solver, the strategy retained by ONERA for the past few years consists in upgrading the CHARME solver towards a Generalized Eulerian Solver (GES) in order to factorize the numerical development of the existing and future Eulerian systems of PDE which could be implemented in CEDRE. These range from the multi-species Navier-Stokes equations historically solved in CHARME solver, to the Eulerian disperse phase models including the KBMM, as well as all the elements of the diffuse interface model hierarchy.

The GES aims at maximizing the factorization of the programming architecture and any action which would be duplicated in other solvers otherwise. In particular, the GES offers a backbone composed of the numerical flux pre and post-processing, the space and time discretization methods, pre and post-processing libraries, and specific features such as the dynamic meshes. Any task dedicated to a specific solver is confined at low-level as for instance the definition of the initial and boundary conditions, the variable mappings, numerical flux schemes, thermodynamics equations of state and source terms.

Not only does the GES allow for a significant code rationalization, while offering a larger panel of physical models, but it eases its maintenance and its evolution. Furthermore, the generalized approach benefits from a better management of coupling phenomena since we can treat through splitting operators different systems of PDE in the same unique solver. It is more adequate than coupling solvers through source terms, the latter method being limited whenever one needs to account for strong two-way coupling.

This thesis has leveraged from this rich framework developed by CEDRE programming team. The new two-scale two-phase flow model has thus been implemented in the GES and constitutes the first physical model to be implemented in it besides the multi-species Navier-Stokes equations. Implementing this model into the GES rather than in a new specific solver was challenging and more demanding but at the end, we have taken full advantage of all the existing GES generic features.

Helped by one member of the CEDRE developer team, Clément Le Touze, we successfully implemented the new system in approximately a single month proving the effectiveness of the general approach. It was then followed by few months of debugging, improvements of specific parts such as the numerical flux and the relaxation procedure and continuous integration and verification.

For the implementation of the first multi-fluid model in CEDRE, major efforts have been devoted to

- build a multi-fluid data structure with any arbitrary entries encompassing the existing multi-species mono-fluid data structure,

- define the sets of primitive and conservative variables and their mappings,
- implement and validate two numerical fluxes, euler fluxes and capillary fluxes,
- implement and validate of a new type of source terms, the pressure relaxation with energy correction,
- extend the splitting method to encompass flux splitting,
- adjust the boundary and initial conditions,
- upgrade to second-order multi-slope,
- implement the equations involving the geometric variables.

Finally, we have carried out a continuous integration and testing through several verification test cases, whose results are presented in the next section.

4.3 NUMERICAL VERIFICATION OF THE TWO-SCALE TWO-PHASE FLOW MODEL

4.3.1 VERIFICATION TESTS OF THE EULER FLUX AND THE RELAXATION PROCEDURE

In the following, we want to verify the implementation of the first sub-system and the relaxation procedure by going through classical tube shock problems found in the literature. We will use two Stiffened Gas equations of state to mimick air and liquid properties. The pressure laws are

$$p_k = \rho_k(\gamma_k - 1)e_k - \gamma_k p_k^\infty, \begin{cases} \text{Air} : \gamma_1 = 1.4, p_1^\infty = 0, c_{v,1} = 1000, \\ \text{Water} : \gamma_2 = 4.4, p_2^\infty = 6.8 \cdot 10^8, c_{v,2} = 4180, \end{cases} \quad (4.74)$$

with γ_k the fluid isentropic coefficient, p_k^∞ the residual pressure at zero temperature accounting for attractive effects guaranteeing the cohesion of matter for liquids or solids in Pa . The internal energy is defined as

$$e_k = c_{v,k} T_k \frac{p_k + \gamma_k p_k^\infty}{p_k + p_k^\infty}, \quad (4.75)$$

where $c_{v,k}$ is the calorific heat at constant volume in $J/kg/K$.

4.3.1.1 PURE INTERFACE ADVECTION

The first test case proposed is a one-dimensional water-air interface advection in a $x = 1 m$ long tube. The interface is initially at the location $x = 0.5 m$, separating two nearly pure fluids, on the left side air, with a density $\rho_1 = 10 kg/m^3$, and on the right side water, with a density $\rho_2 = 1000 kg/m^3$, both including a residual fraction of the other phase, $\epsilon = 10^{-8}$. Each fluid flows at uniform pressure $p^0 = 10^5 Pa$ and uniform velocity $v^0 = 100 m/s$. [Table 4.1](#) summarizes the test case data.

TABLE 4.1: Initial state of advection case with $\rho_1 = 10 kg.m^{-3}$, $\rho_2 = 1000 kg.m^{-3}$, $\epsilon = 10^{-8}$.

x	$\alpha_1 [-]$	$v [m/s]$	$p_1 [Pa]$	$p_2 [Pa]$
$0 \leq x < 0.5$	ϵ	100	10^5	10^5
$0.5 \leq x \leq 1$	$1 - \epsilon$			

The simulation is performed on a 1000 cell mesh, with a CFL number of $\nu_{\text{CFL}} = 0.8$, a second-order HLLC solver with the multislope MUSCL method equipped with the hybrid limiter [Le Touze et al. \(2014\) \[133\]](#) and a second-order Runge-Kutta method. The results are shown at the simulation time $t_{\text{sim}} = 229 \mu m$ in [Figure 4.2](#).

[Figure 4.2](#) shows a very good agreement with [Saurel et al. \(2009\) \[195\]](#). As discussed previously, a pressure and velocity uniform flow must remain uniform. As shown on [Figures 4.2c](#) and [4.2d](#), the maximum relative error of the fluid pressures and of the velocity is respectively of the order 10^{-9} for the water pressure and 10^{-13} for the velocity. Whereas the velocity error

is close to the machine epsilon, the water pressure tends to oscillate around the target pressure. These errors reduce to machine epsilon when increasing the compressibility of the water by diminishing p_2^∞ . We explain these minor errors by accumulating rounding errors when computing the fluid pressure from the internal fluid energy and vice versa. We conclude that the implementation of the model preserves constant velocity and pressure profiles.

4.3.1.2 WATER-AIR SHOCK TUBE WITH MODERATE DENSITY RATIO

The second test case is a water-air shock tube of $x = 4\text{ m}$ length. The interface lying at $x = 0.7\text{ m}$ separates highly pressurized nearly pure water, $p_2 = 10^9\text{ Pa}$, on the left side of the tube, from a nearly pure air at atmospheric pressure $p_1 = 10^5\text{ Pa}$ at the right side of the tube. The whole mixture is initially at rest. This pressure discontinuity can be solved using an exact Riemann solver for the Euler equations. The density ratio is set to 200 with $\rho_1 = 50\text{ kg/m}^3$ and $\rho_2 = 1000\text{ kg/m}^3$. The residual volume fraction is set to $\epsilon = 10^{-8}$. The fluid properties are summarized in [Table 4.2](#).

TABLE 4.2: Initial state of shock tube case with $\rho_1 = 50\text{ kg.m}^{-3}$, $\rho_2 = 1000\text{ kg.m}^{-3}$, $\epsilon = 10^{-8}$.

x	$\alpha_1 [-]$	$v [m/s]$	$p_1 [Pa]$	$p_2 [Pa]$
$-2 \leq x < 0.75$	ϵ	0	10^9	10^9
$0.75 \leq x \leq 2$	$1 - \epsilon$		10^5	10^5

We have used a second-order HLLC solver with the multislope MUSCL method equipped with the hybrid limiter [Le Touze et al. \(2014\) \[133\]](#) and a second-order Runge-Kutta method, on a 1000 cell grid and the CFL number is set to $\nu_{\text{CFL}} = 0.3$. The solution is plotted in [Figure 4.3](#) at time $t_{\text{sim}} = 900\text{ }\mu\text{s}$ together with the exact solution obtained by solving the Riemann problem on the Euler equations.

[Figure 4.3](#) displays the fluid pressures p_k , the velocity v , the volume fractions α_k , the mixture density ρ , the fluid temperatures T_k and the Mach number defined by the ratio of the velocity to the frozen speed of sound v/a_F . [Figure 4.3](#) shows an excellent agreement with respect to the exact solution for each quantity. We point out the fact that [Section 4.3.1.2](#) displays the fluid temperatures averaged by the volume fraction, $\alpha_1 T_1 + \alpha_2 T_2$. It agrees with the exact temperature.

4.3.1.3 WATER-AIR SHOCK TUBE WITH HIGH DENSITY RATIO

The third test case is another water-air shock tube of $x = 1\text{ m}$ length. The interface lying at $x = 0.75\text{ m}$ separates highly pressurized nearly pure water, $p_2 = 10^9\text{ Pa}$, on the left side of the tube, from a nearly pure air at atmospheric pressure $p_1 = 10^5\text{ Pa}$ on the right side. The whole mixture is initially at rest. This pressure discontinuity can still be solved using an exact Riemann solver for the Euler equations. This time, the density ratio is increased up to 1000, making this test case relatively extreme. As a consequence, the residual volume fraction is increased to $\epsilon = 10^{-6}$ as summarized in [Table 4.3](#).

Again, we have used the second-order HLLC solver on a 1000 cell grid but have lowered the CFL number to $\nu_{\text{CFL}} = 0.1$. The solution is plotted in [Figure 4.4](#) at time $t_{\text{sim}} = 240\text{ }\mu\text{s}$.

TABLE 4.3: Initial state of shock tube case with $\rho_1 = 1 \text{ kg.m}^{-3}$, $\rho_2 = 1000 \text{ kg.m}^{-3}$, $\epsilon = 10^{-6}$.

x	$\alpha_1 [-]$	$v [m/s]$	$p_1 [Pa]$	$p_2 [Pa]$
$0 \leq x < 0.75$	ϵ	0	10^9	10^9
$0.75 \leq x \leq 1$	$1 - \epsilon$		10^5	10^5

In [Figure 4.4a](#), where we have plotted the pressures, the right log axis reveals a small oscillation of the computed pressures between the rarefaction wave and the contact discontinuity. In this quasi-pure liquid zone, the pressure fails at remaining completely constant. For the temperatures depicted in [Section 4.3.1.3](#), we see excellent an agreement of the fluid temperatures with the exact temperature in the respective pure fluid zones. Defining an averaged temperature with the volume fractions as we proposed in [Section 4.3.1.2](#) is not appropriate in the present case, the residual volume fraction being not small enough to prevent the temperature of the residual phase to have an impact on the average temperature. In overall, the results still show a very good agreement with the exact solution, attesting the accuracy and robustness of the numerical solver.

4.3.1.4 TWO-PHASE FLOW PROBLEM: COMPARISON WITH THE FIVE EQUATION MODEL

So far we have only investigated separated phases. We thus propose to consider fluid mixtures. Given a 1 m long shock tube composed of a mixture of water and air with a composition and pressure discontinuity at the location $x = 0.7 \text{ m}$. The left hand side is highly pressurized, $p = 10^9$, and the gas is preponderant, $\alpha_1 = 0.8$, while the right hand side is at ambient pressure and the liquid dominates with $\alpha_1 = 0.2$. Both phase are thus simultaneously present in a non-negligible amount everywhere. We keep the high density ratio $\rho_2/\rho_1 = 1000$. The initial state is summarized in [Table 4.4](#).

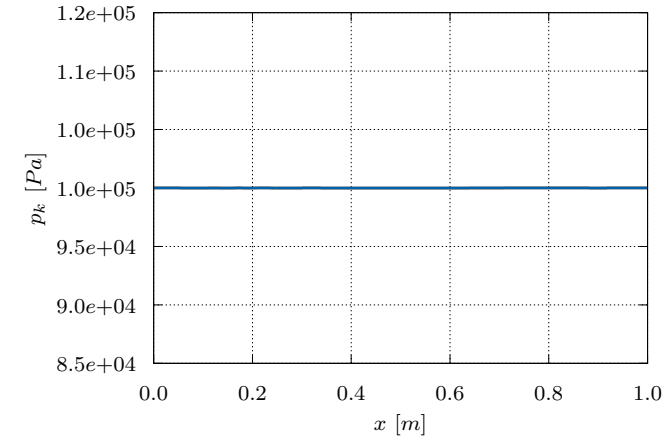
TABLE 4.4: Initial state of water-air mixture with a pressure discontinuity and with $\rho_1 = 1 \text{ kg.m}^{-3}$, $\rho_2 = 1000 \text{ kg.m}^{-3}$, $\epsilon = 10^{-6}$.

x	$\alpha_1 [-]$	$v [m/s]$	$p_1 [Pa]$	$p_2 [Pa]$
$0 \leq x \leq 0.7$	0.2	0	10^9	10^9
$0.7 \leq x \leq 1$	0.8		10^5	10^5

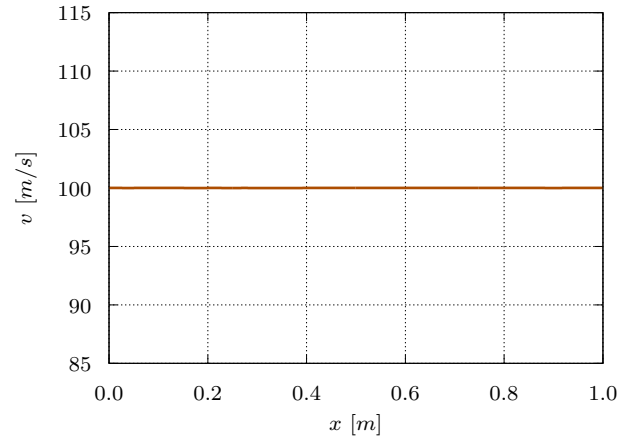
Since the Exact Riemann solver using the Euler equations is not valid in mixing regions, we propose to compare the outcomes of the simulation with the results obtained with the *five equation* model studied in [Murrone and Guillard \(2005\) \[164\]](#), from which this test case is inspired. We have used the first-order HLLC solver on a 1000 cell grid with a CFL number of $\nu_{\text{CFL}} = 0.8$ and a Euler explicit temporal integration scheme, corresponding to the settings of [Murrone and Guillard \(2005\) \[164\]](#). The results are shown in [Figure 4.5](#).

The results perfectly match between our instantaneously relaxed *six equation* model and the *five equation* model. Interestingly enough, [Figure 4.5f](#) compares the Mach numbers of both systems of equations. In the *five equation* model, the mixture sound speed is the Wallis or Wood sound speed a_w [Wood \(1930\) \[220\]](#), [Wallis \(1969\) \[218\]](#), whereas for the present model, it is the

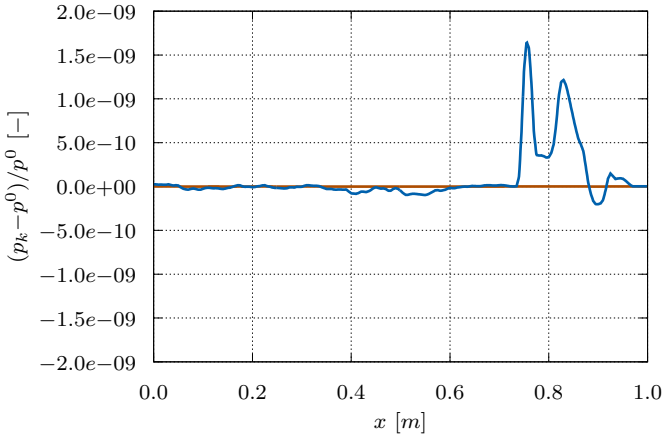
frozen sound speed a_F . Since the velocities are the same as depicted in [Figures 4.5b](#) and [4.5f](#) reveals a twice as large speed of sound for the *six equation* model as for the *five equation* model.



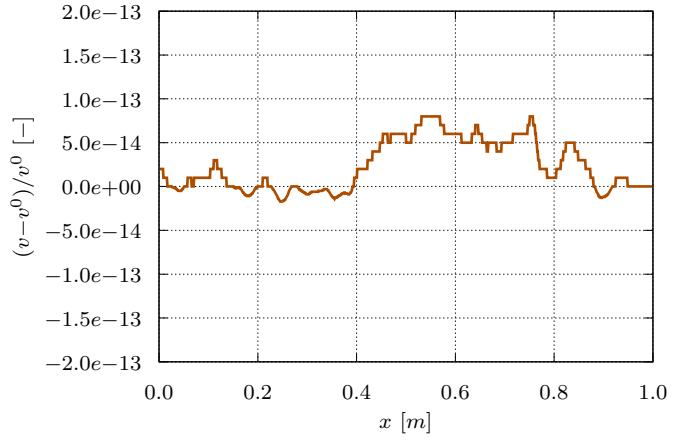
(A) — p_1 , — p_2 , $p^0 = 10^5 Pa$.



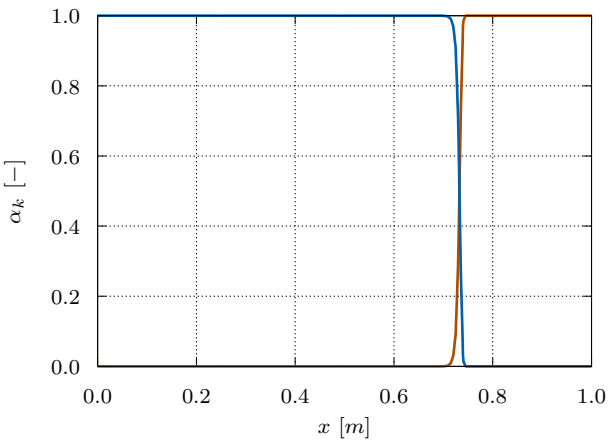
(B) — v , $v^0 = 100 m/s$.



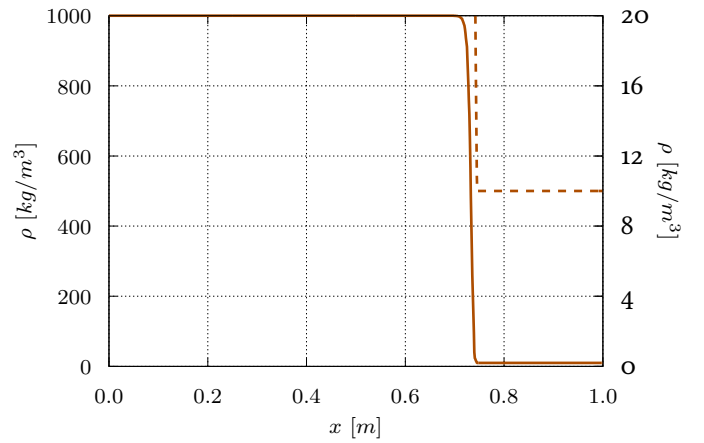
(C) — p_1 , — p_2 , $p^0 = 10^5 Pa$.



(D) — v , $v^0 = 100 m/s$.

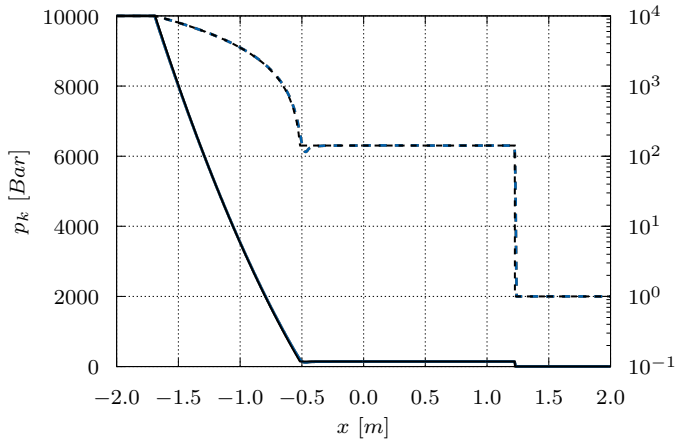


(E) — α_1 , — α_2 .

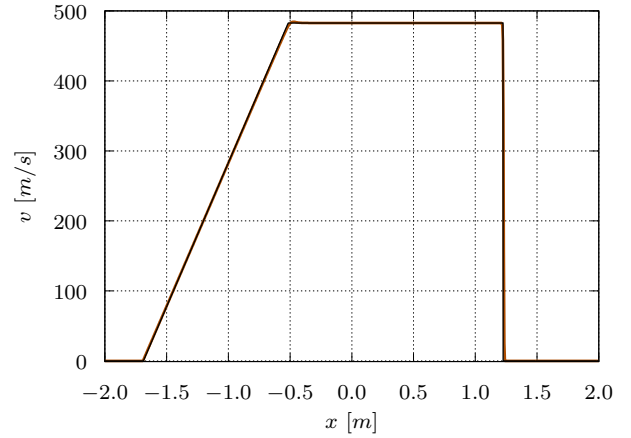


(F) Left axis — ρ . Right axis - - - ρ .

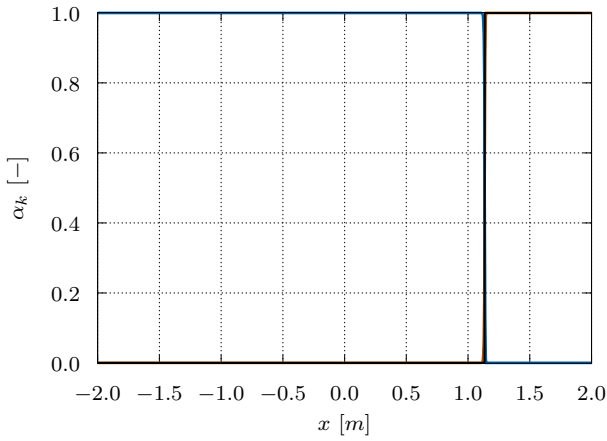
FIGURE 4.2: Case 1: water-air interface advection computed on a 1000 cell grid using a second-order HLLC solver at $\nu_{\text{CFL}} = 0.8$. Results are shown at time $t_{\text{sim}} = 229 \mu s$.



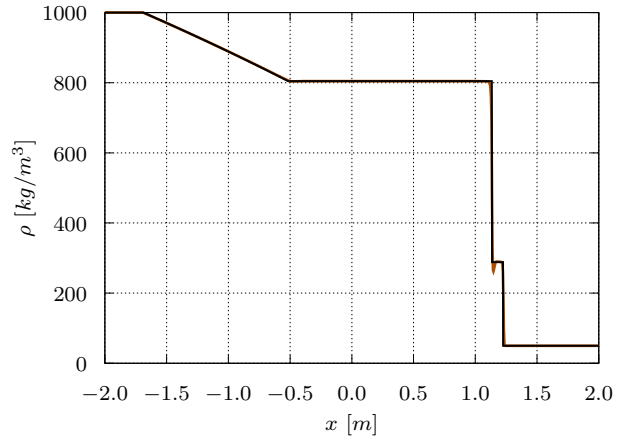
(A) Left axis: — p_1 , — p_2 , — p exact.
Right log axis: - - - p_1 , - - - p_2 , - - - p exact.



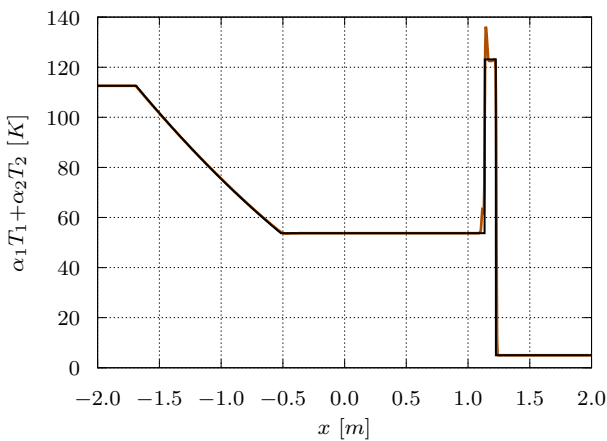
(B) — v , — v exact.



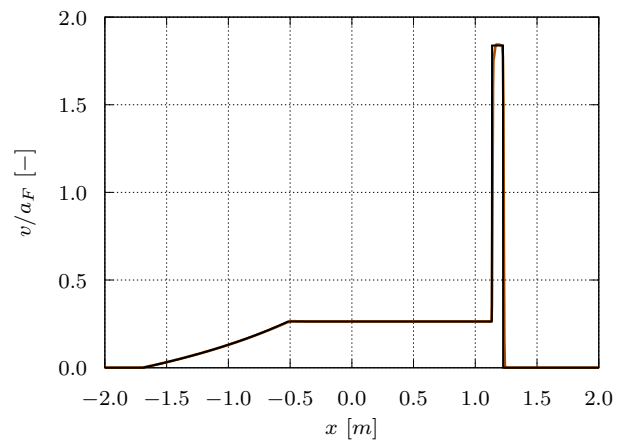
(C) — α_1 , — α_2 , — α_1 exact.



(D) — ρ , — ρ exact.

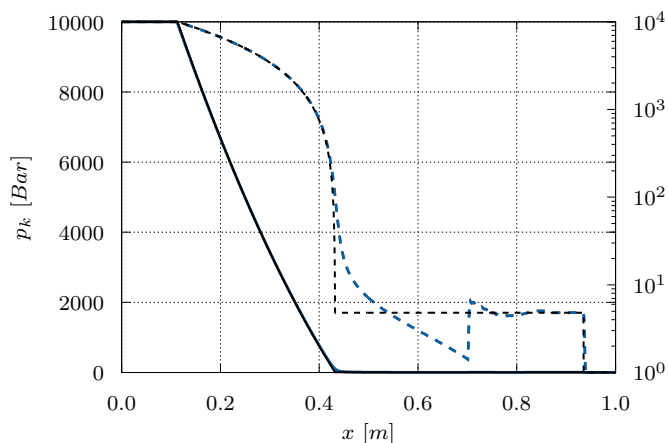


(E) — $\alpha_1 T_1 + \alpha_2 T_2$, — T exact.

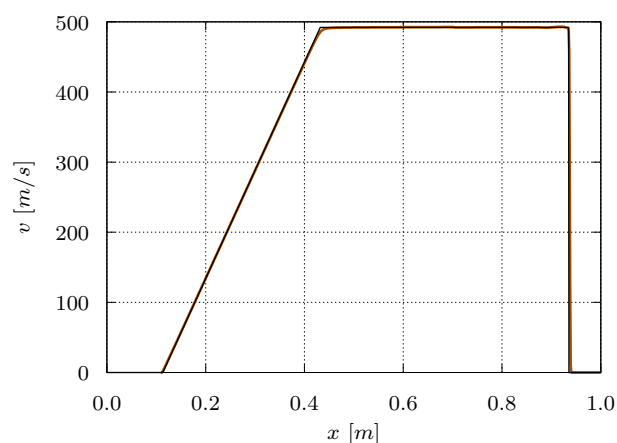


(F) — v/a_F , — v/a exact.

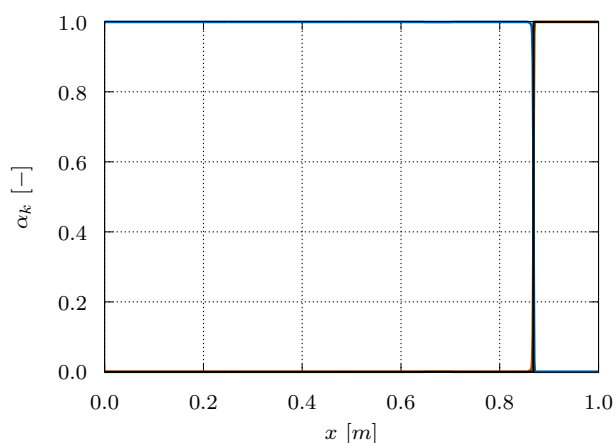
FIGURE 4.3: Case 2: water-air pressure discontinuity with moderate density ratio computed on a 1000 cell grid using a second-order HLLC solver at $\nu_{\text{CFL}} = 0.6$. Results are shown at time $t_{\text{sim}} = 900 \mu\text{m}$.



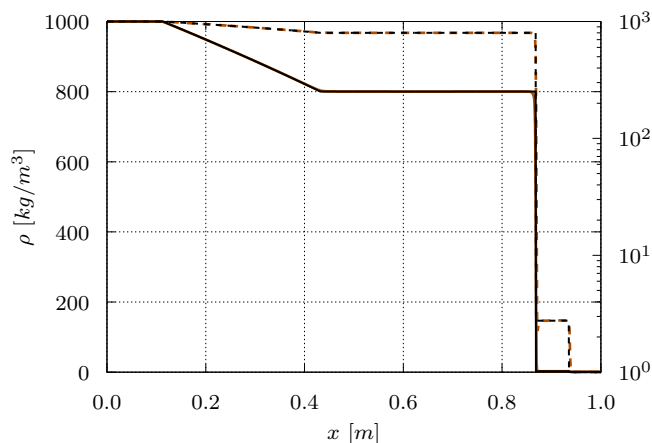
(A) Left axis: — p_1 , — p_2 , — p exact.
Right log axis: - - - p_1 , - - - p_2 , - - - p exact.



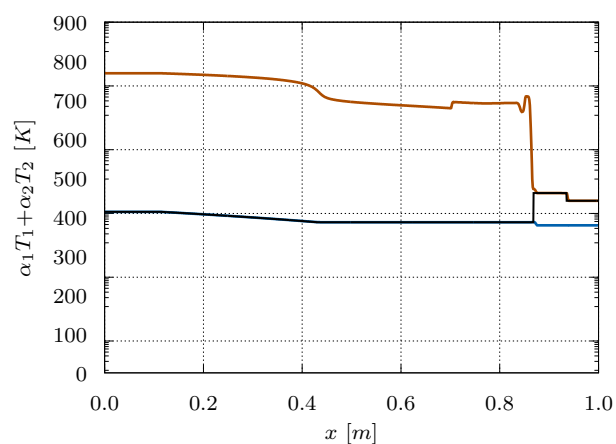
(B) — v , — v exact.



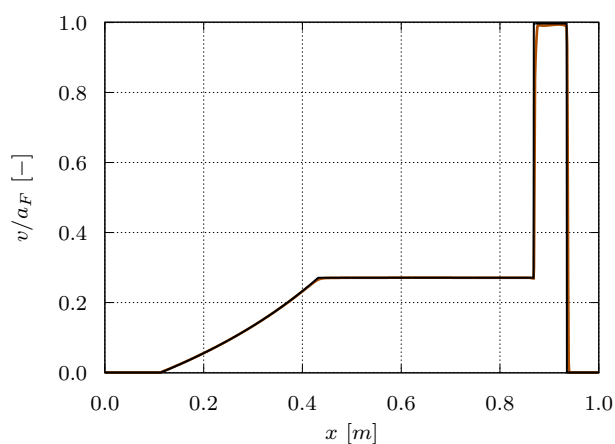
(C) — α_1 , — α_2 , — α_1 exact.



(D) Left axis — ρ , — ρ exact. Right log axis
- - - ρ , - - - ρ exact.

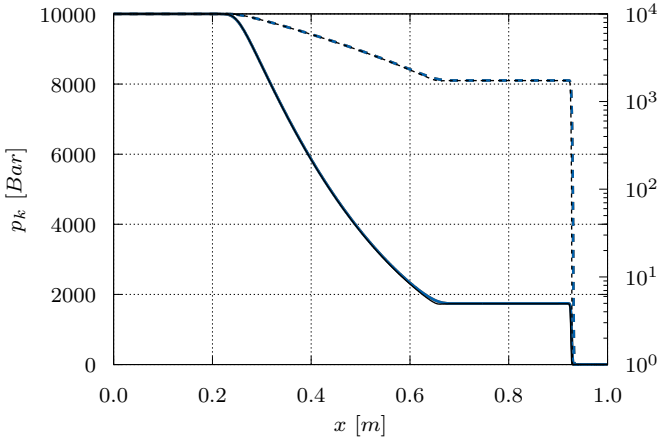


(E) — T_1 , — T_2 , — T exact.

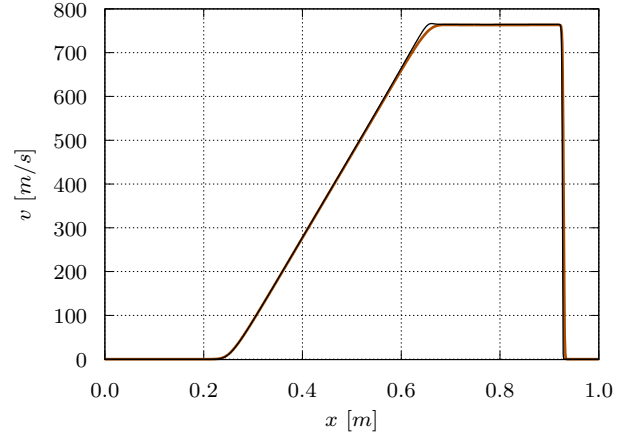


(F) — v/a_F , — v/a exact.

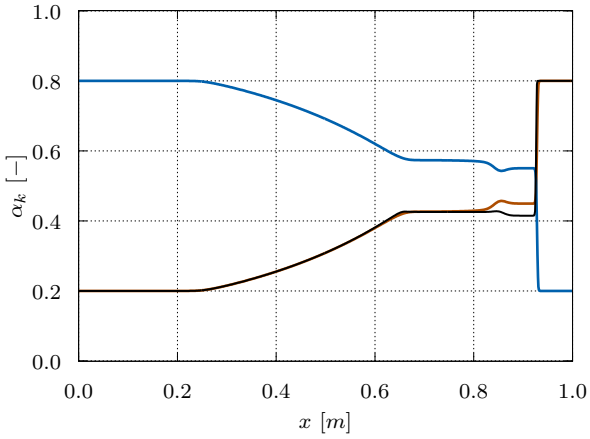
FIGURE 4.4: Case 3: water-air pressure discontinuity with high density ratio computed on a 1000 cell grid using a second-order HLLC solver at $\nu_{\text{CFL}} = 0.1$. Results are shown at time $t_{\text{sim}} = 240 \mu\text{m}$.



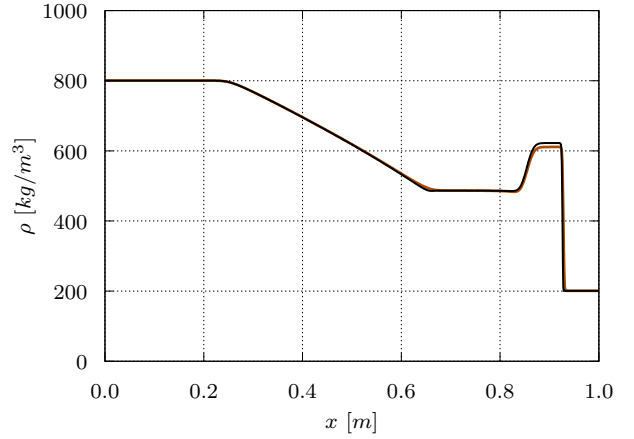
(A) Left axis: — p_1 , — p_2 , — p_{5eq} .
Right log axis: - - - p_1 , - - - p_2 , - - - p_{5eq} .



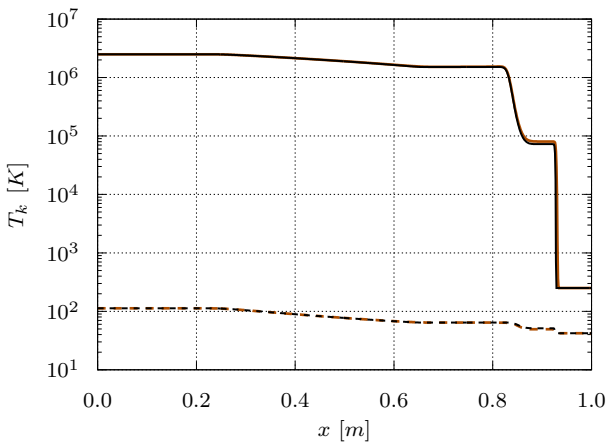
(B) — v , — v_{5eq} .



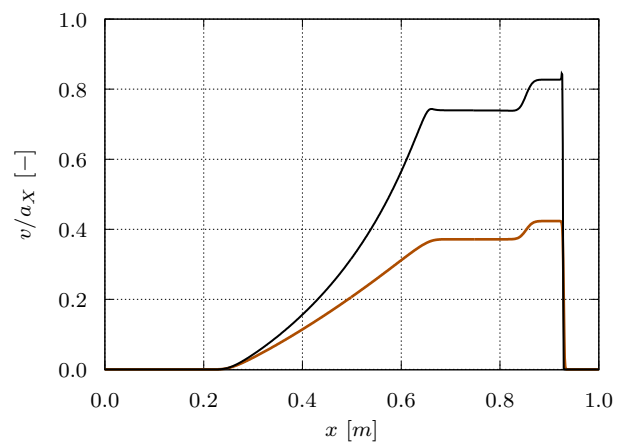
(C) — α_1 , — α_2 , — α_1_{5eq} .



(D) Left axis — ρ , — ρ_{5eq} .



(E) — T_1 , — T_2 , — T_1_{5eq} , - - - T_2_{5eq} .



(F) — v/a_F , — v/a_W_{5eq} .

FIGURE 4.5: Case 4: water-air mixture with a pressure discontinuity computed on a 1000 cell grid using a first-order HLLC solver at $\nu_{CFL} = 0.8$. Results are shown at time $t_{sim} = 200 \mu m$.

4.3.2 VERIFICATION TESTS OF THE CAPILLARY FLUX

4.3.2.1 STATIC CAPILLARY EFFECTS

The first capillary test case consists in starting with a circular liquid column initialized at the same pressure as the surrounding air and observe the effect of the capillarity to recover and maintain over time the Laplace pressure jump. We consider a steady liquid column with a radius of $R = 0.15 \text{ m}$ in a $0.75 \times 0.75 \text{ m}^2$ rectangle of air at rest. The pressure is homogeneous over the whole domain. The boundaries are all slippery wall. [Table 4.5](#) summarizes the initial state and the fluid properties.

TABLE 4.5: Initial state of the 2D case with $\rho_1 = 1 \text{ kg.m}^{-3}$, $\rho_2 = 1000 \text{ kg.m}^{-3}$, $\epsilon = 10^{-6}$, $\sigma_c = 800 \text{ N/m}$.

Region	$\alpha_1 [-]$	$v [\text{m/s}]$	$p_k [\text{Pa}]$
In column	ϵ	0	10^5
Out of column	$1 - \epsilon$		

We have run the simulation over $t_{sim} = 2 \text{ s}$ with the time and space second-order methods presented in [Section 4.1.3.2](#) on a 120×120 cartesian grid with a CFL number of $\nu_{CFL} = 0.1$.

In [Figure 4.6](#) we display the initial and final liquid volume fraction isoline $\alpha_2 = 0.5$ over the theoretical column position, colored in green. As expected, in [Figure 4.6](#) the shift of the

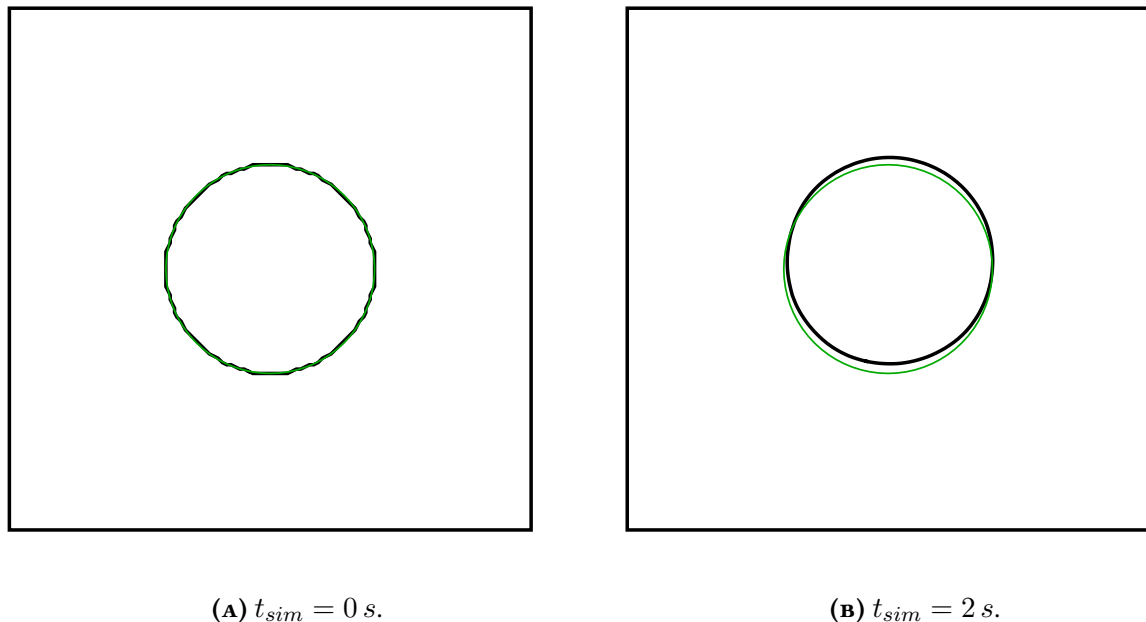


FIGURE 4.6: Instantaneous liquid volume fraction iso-contour, $\alpha_2 = 0.5$, — numerical and — theoretical, over time with the second-order splitting method.

column position is visually very limited after 2 s attesting the good implementation of the capillary fluxes. Nevertheless, the iso-contour is not perfectly superimposed to the theoretical

position. This effect is related to the pressure currents occurring at the liquid interface due to numerical errors.

To go further into the analysis, we define the relative pressure error, ξ_p , as

$$\xi_p = \frac{|[p_{sim}] - [p_{theo}]|}{[p_{theo}]}, \quad (4.76)$$

with $[p_{sim}]$ and $[p_{theo}]$ the numerical and theoretical pressure jumps between the ambient air and the water inside the column. The numerical pressure jump is defined as the discrete weighed average,

$$[p_{sim}] = \frac{\sum_{i \in N_{cell}} (p_2)_i (\alpha_2)_i}{\sum_{i \in N_{cell}} (\alpha_2)_i} - \frac{\sum_{i \in N_{cell}} (p_1)_i (\alpha_1)_i}{\sum_{i \in N_{cell}} (\alpha_1)_i}, \quad (4.77)$$

with N_{cell} the set of cell indexes, and computed with a threshold on each volume fraction, $\alpha_k \geq 0.99$. The theoretical jump is defined as

$$[p_{theo}] = \sigma_c \sqrt{\frac{\pi}{\sum_{i \in N_{cell}} (\alpha_2)_i \mathcal{S}_i}}. \quad (4.78)$$

where \mathcal{S}_i is the surface area of cell i . In [Figure 4.7](#), we plot the numerical and theoretical pressure jump over time along with the relative pressure error ξ_p . At the beginning of the simulation,

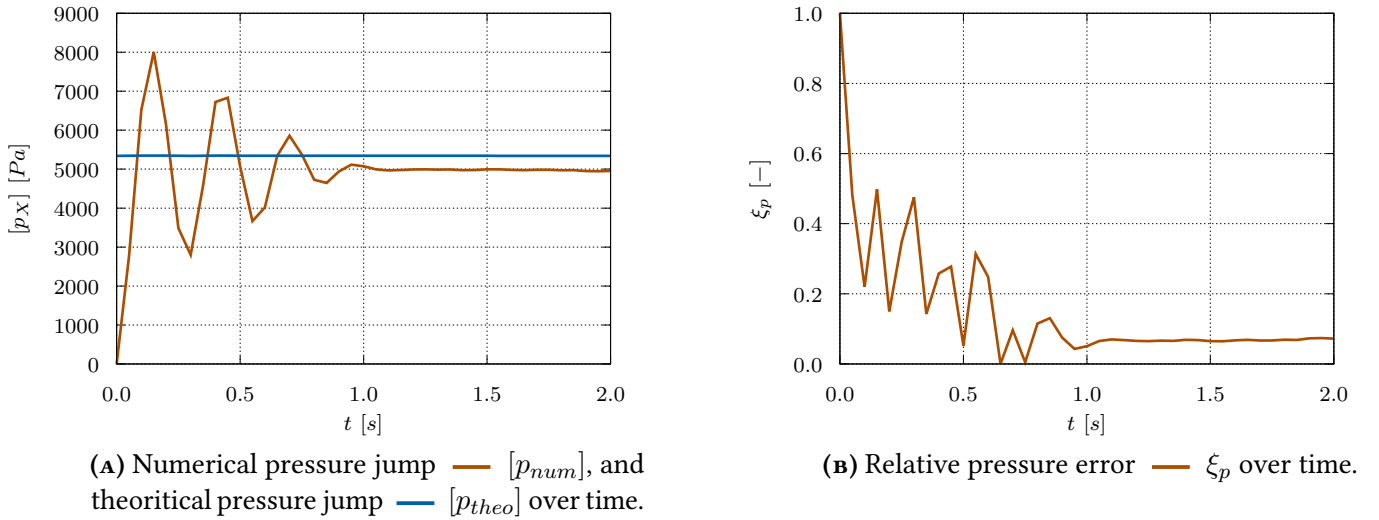


FIGURE 4.7: Static capillary effect case: analysis of the instantaneous pressure jump.

since the pressure is uniform, the numerical pressure jump is null. Then, a transient regime is observed with an oscillating pressure jump which eventually converges after approximately $t_{sim} = 1 \text{ ms}$. The relative pressure error ξ_p reduces over time and reaches 7.1%. The origin of this error is probably linked to the parasitic currents.

[Figure 4.8](#) displays four instants of the function, $(1 + \alpha_2^2) \ln(\|\nabla \rho\|)$, a modified mixture density gradient. This variable is adapted to capture spread values of the mixture density gradient norm. At $t_{sim} = 0 \text{ s}$, in [Figure 4.8a](#), the liquid column is initialized at the center of the box. The interface is spread over approximately two cells leading to a very sharp density

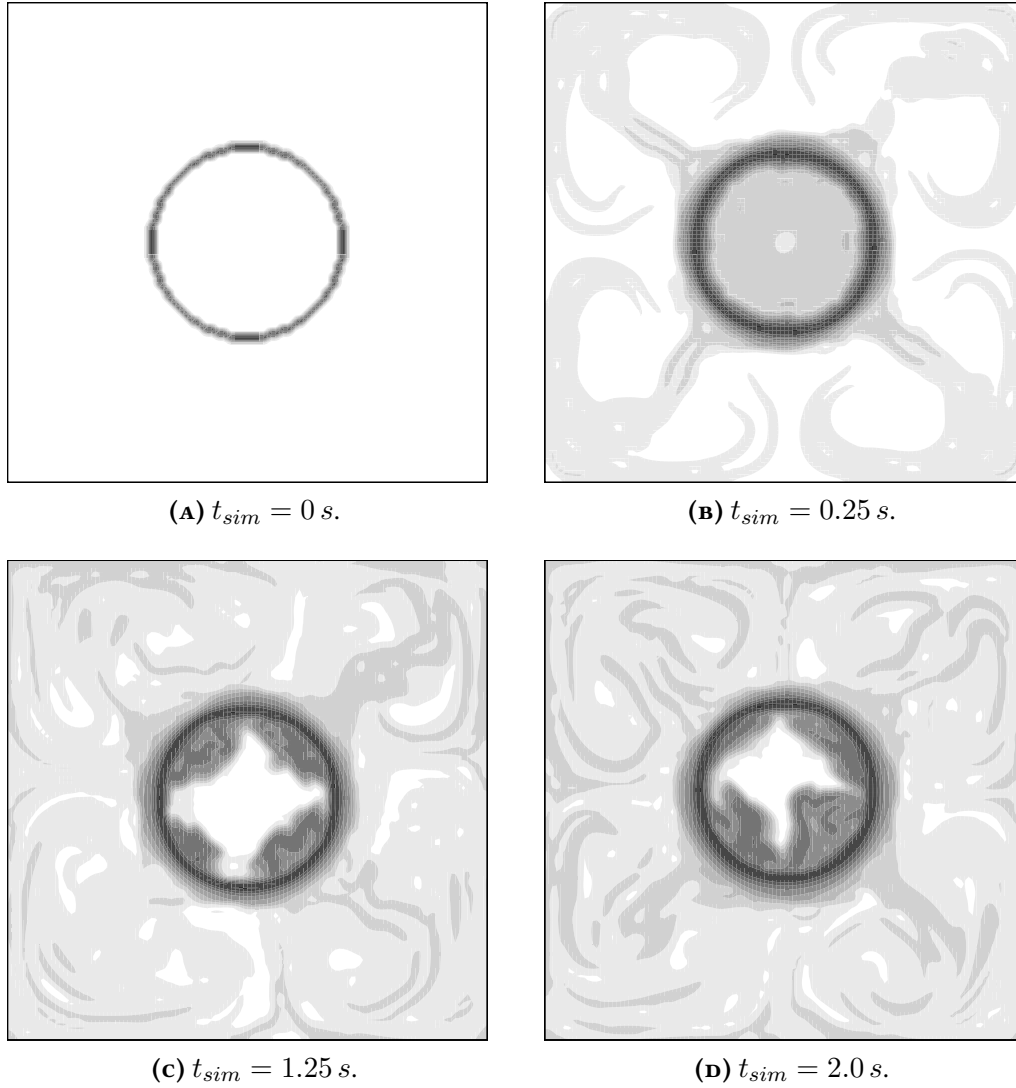


FIGURE 4.8: Schlieren contour of mixture density, $(1 + \alpha_2^2) \ln(\|\nabla\rho\|) \in [1, 23]$ at four given simulation times.

gradient at the column perimeter. At $t_{sim} = 0.25 s$, in [Figure 4.8b](#), we observe four symmetric branches reflecting on the wall, creating eight zones of recirculation of the flow. These branches are due to the pressure adjustment operated by the capillary fluxes in the liquid column to establish the Laplace pressure jump. The situation remains quite symmetric over more than 1 s, see [Figure 4.8c](#), but eventually it disymmetrizes due to numerical errors as shown on the last time step ([Figure 4.8d](#)), with a up-ward shift already observed in [Figure 4.6](#).

4.3.2.2 DYNAMIC CAPILLARY EFFECTS: OSCILLATING ELLIPSOIDAL DROP

This test case is inspired from [Perigaud and Saurel \(2005\) \[173\]](#). We propose to analyze the oscillation of an ellipsoidal drop due to the surface tension acting upon it. We initialize an ellipsoidal liquid droplet with the following equation

$$\frac{(x - 0.5)^2}{0.2^2} + \frac{(y - 0.5)^2}{0.12^2} = 1, \quad (4.79)$$

at ambient pressure $p_2 = 1 \text{ bar}$ in a uniform gas at rest at ambient pressure, $p_1 = 1 \text{ bar}$. The phase densities are $\rho_2 = 100 \text{ kg/m}^3$ and $\rho_1 = 1 \text{ kg/m}^3$ and the surface tension coefficient is set artificially to $\sigma_c = 340 \text{ N/m}$ to enhance the surface tension force. [Table 4.6](#) summarizes the fluid parameters.

TABLE 4.6: Initial state of 2D case with $\rho_1 = 1 \text{ kg.m}^{-3}$, $\rho_2 = 100 \text{ kg.m}^{-3}$, $\epsilon = 10^{-6}$, $\sigma_c = 340 \text{ N/m}$.

Region	$\alpha_1 [-]$	$v [\text{m/s}]$	$p_k [\text{Pa}]$
In drop	ϵ	0	10^5
Out of drop	$1 - \epsilon$		

The computational domain is a square of 1 m long edge, and the mesh contains 111×111 cells. The boundaries are set to subsonic outflow. We use a second-order HLLC MUSCL solver with a Van-Leer limiter combined with a second-order Rung-Kutta time integration scheme. The CFL number is set to $\nu_{\text{CFL}} = 0.1$. Due to surface tension, the drop starts to move from its ellipsoidal shape to a spherical shape, and so on as depicted qualitatively in [Figure 4.9](#) where volume fraction contours are drawn at specific time steps for which the kinetic energy is either maximal or minimal. More quantitatively, [Figure 4.10](#) displays the time evolution of the space

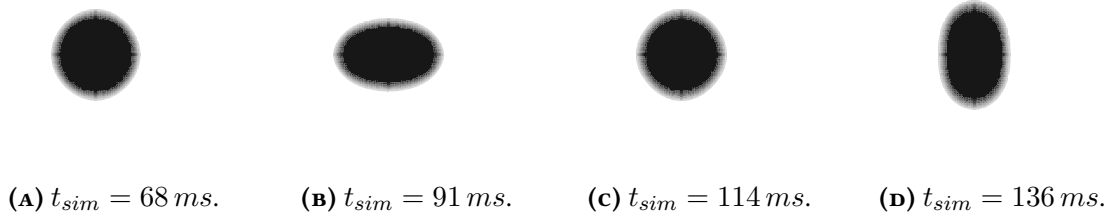


FIGURE 4.9: Case 5: instantaneous liquid volume fraction α_2 at four successive averaged kinetic energy extrema, $\alpha_2 \in [0.1, 1]$.

averaged kinetic energy of the mixture, $\mathcal{K} = \rho \|\mathbf{v}\|^2/2$, against the space averaged large scale capillary energy, $\mathcal{E}_c^l = \sigma_c \|\nabla \alpha\|$, from which we have withdrawn the minimum of \mathcal{E}_c^l which corresponds to the potential energy of the sphere. Both volume averages are evaluated on the whole domain.

As shown in [Figure 4.10](#), the initial large scale capillary energy of the ellipsoidal droplet is converted into kinetic energy, the latter being maximal when the droplet reaches a circular shape, and then diminishes while the droplet recovers an ellipsoidal shape. We clearly observe that the energies are out-of-phase attesting the oscillatory movement of the drop. The oscillating period of the drop corresponds to two oscillating periods of the energies. Using a Fourier transform in the interval $t_{\text{sim}} \in [0.1, 0.5] \text{ s}$, we find

$$T = 88.5 \text{ ms.} \quad (4.80)$$

We also notice a decrease of the energies overtime even though no viscosity is accounted for. This is due to the numerical dissipation. As recalled in [Perigaud and Saurel \(2005\) \[173\]](#), an

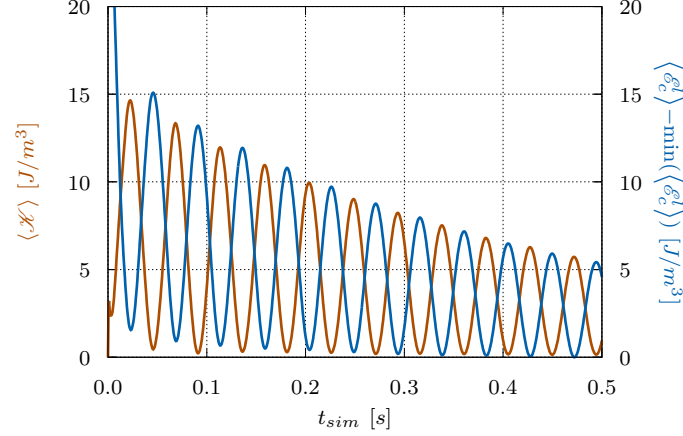


FIGURE 4.10: Case 5: Space averaged kinetic energy and large scale capillary energy of an oscillating ellipsoidal droplet computed on a 111×111 mesh grid using a second-order HLLC solver at $\nu_{\text{CFL}} = 0.1$. $\min(\langle \mathcal{E}_c^l \rangle) = 3.29 \cdot 10^2 \text{ J/m}^3$.

analytical expression of the oscillating period of a liquid droplet surrounded by a gas has been proposed in [Fyfe et al. \(1988\) \[75\]](#) based on the modified Rayleigh formula [Rayleigh \(1879\) \[182\]](#),

$$T = \sqrt{\frac{4\pi^2(\rho_1 + \rho_2)R^3}{(o^3 - o)\sigma_c}} \quad (4.81)$$

with o the oscillation mode and R the drop radius at rest. In the present configuration, the oscillation mode is 2 and the numerical time averaged radius of the drop, defined as

$$R = \sqrt{\frac{\sum_{i \in N_{\text{cell}}} (\alpha_2)_i \mathcal{S}_i}{\pi}} \quad (4.82)$$

and evaluated in the regions where $(\alpha_2)_i \geq 0.99$, is $R = 155 \text{ mm}$. The theoretical period is thus 85.0 ms which leads to a relative error of 4.1%. Therefore, this test case validates the dynamics and static large scale capillary effects.

4.3.2.3 DYNAMIC CAPILLARY EFFECTS: UNIFORM VELOCITY FLOW

In this test case inspired from [Schmidmayer et al. \(2017\) \[197\]](#), we investigate a cylindrical liquid column initialized with a correct pressure jump in a uniform velocity flow sketched in [Figure 4.11](#). The surface tension should maintain the pressure jump.

The column is initialized with a radius $R = 0.15 \text{ m}$ at the pressure $p_2 = p_1 + \sigma/R$ moving at the velocity $\mathbf{v} = 50 \text{ m/s}$ in ambient air contained in a $2.25 \times 0.75 \text{ m}^2$ box. The column center is initially located at 0.375 m from the inlet boundary. The initial and boundary conditions are summarized in [Table 4.7](#).

The inflow [①](#) injects air flowing at speed $v = 50 \text{ m/s}$ at pressure $p = 1 \text{ bar}$. The outflows [①](#) impose the pressure $p = 1 \text{ bar}$ to the flow. The simulation time is $t_{\text{sim}} = 300 \text{ ms}$ and we employ the time and space second-order numerical method described in [section 4.1.3](#) at $\nu_{\text{CFL}} = 0.2$ on a cartesian grid 360×120 .

In [Figure 4.12](#), we plot Schlieren contours of the variable $(1 + \alpha_2^2) \ln(\|\nabla \rho\|)$ at the initial instant $t_{\text{sim}} = 0 \text{ ms}$ and final instant $t_{\text{sim}} = 300 \text{ ms}$. The theoretical expected position of the

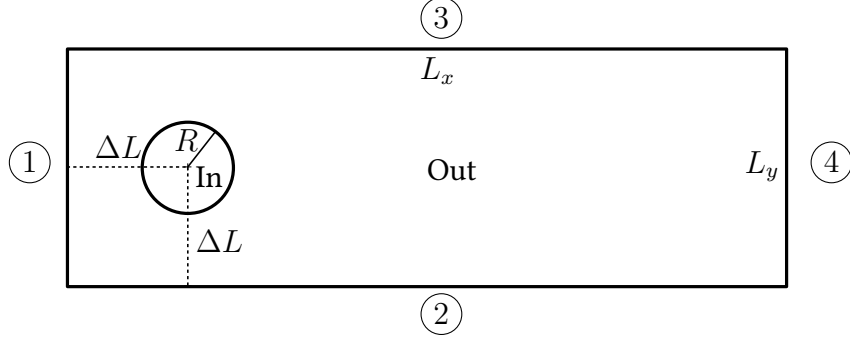


FIGURE 4.11: Test case configuration and initial boundary conditions: $L_x = 2.25 \text{ m}$, $L_y = 0.75 \text{ m}$, $\Delta L = 0.375 \text{ m}$, $R = 0.15 \text{ m}$, (1) inflow, (2)(3)(4) outflows.

TABLE 4.7: Initial state of 2D case with $\rho_1 = 1 \text{ kg.m}^{-3}$, $\rho_2 = 1000 \text{ kg.m}^{-3}$, $\epsilon = 10^{-6}$, $\sigma_c = 800 \text{ N/m}$.

Region / Boundary	$\alpha_1 [-]$	$v [\text{m/s}]$	$p_k [\text{Pa}]$
In column	ϵ	50	105333
Out of column	$1 - \epsilon$	50	10^5
Inflow	$1 - \epsilon$	50	10^5
Outflow	—	—	10^5

column center is drawn in green color for each simulation time. In the present case, the mass barycenter of the column should reach the location $x = 1.875 \text{ m}$. While in [Figure 4.12a](#), the

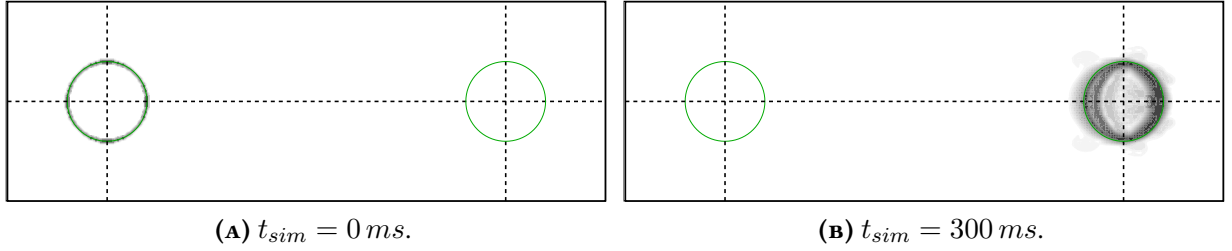


FIGURE 4.12: Schlieren contour of mixture density, $(1 + \alpha_2^2) \ln (\|\nabla \rho\|) \in 1 \text{ --- } 23$.

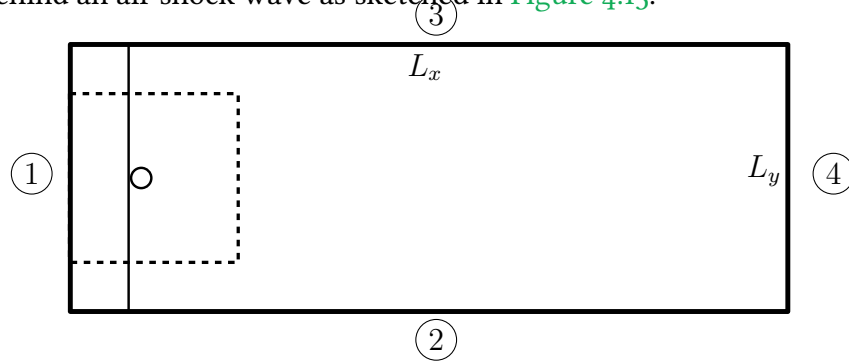
density gradient is sharp and localized on the cylinder perimeter, after $t_{sim} = 300 \text{ ms}$, [Figure 4.12b](#) shows the spreading of the density gradient due to numerical diffusion. Nevertheless, the center of the column matches the theoretical position.

The mean time averaged relative pressure error obtained is $\xi_p = 8.0\%$ attesting the ability of the implemented model to solve accurately 2D advection test cases.

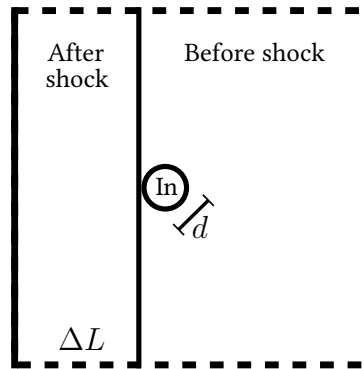
4.3.2.4 DYNAMIC CAPILLARY EFFECTS: WATER SHOCK INTERACTION

The final test case proposed is an air shock impacting a liquid column. The main interface dynamics is first driven by hydrodynamical effects but eventually, after the shock has passed the column, the shape of the interface evolution is impacted by the capillary effects.

The present configuration reproduces the experiments of [Igra and Takayama \(2001\) \[109\]](#). We initialize in a $220 \times 85.5 \text{ mm}^2$ domain a cylindrical liquid column of diameter $d = 6.4 \text{ mm}$, placed just behind an air shock wave as sketched in [Figure 4.13](#).



(A) Sketch of the whole computational domain.



(B) Zoom on the liquid column.

FIGURE 4.13: Sketch of the configuration with $d = 6.4 \text{ mm}$, $\Delta L = 16.8 \text{ mm}$, $L_x = 220 \text{ mm}$, $L_y = 85.5 \text{ mm}$.

Before the shock, the liquid column is in standstill air at atmospheric pressure $p = 101325 \text{ Pa}$. The normal shock induces the following pressure and density jumps

$$\frac{(p_k)_a}{(p_k)_b} = \frac{2\gamma_k M^2 - (\gamma_k - 1)}{\gamma_k + 1}, \quad \frac{(\rho_k)_a}{(\rho_k)_b} = \frac{(\gamma_k + 1)M^2}{(\gamma_k - 1)M^2 + 2}, \quad (4.83)$$

where a stands for conditions after shock and b before shock. The shocked air Mach number used in [Igra and Takayama \(2001\) \[109\]](#) is $M = 1.3$. The Weber number evaluated with the gas density and the velocity in the shocked gas as $We_1 = \rho_1 v^2 d / \sigma_c$ takes the value $We_1 = 3690$. The required velocity of the shock is thus $v = 151 \text{ m/s}$. The fluid properties in each region are summarized in [Table 4.8](#).

Concerning the boundary conditions shown on [Figure 4.13](#), the west side of the domain, ①, is an inlet flow at supercritical conditions where the shock air state is imposed. Since the simulation time does not exceed $t_{sim} = 1.2 \text{ ms}$, the shock does not reach the outlet. Therefore ④ is a subsonic outflow where the atmospheric pressure is imposed. The boundaries ②, ③ are also set to subsonic outflow. All these conditions have been chosen to reproduce the same test case as in [Igra and Takayama \(2001\) \[109\]](#) which has been also numerically investigated by [Schmidmayer et al. \(2017\) \[197\]](#).

TABLE 4.8: Initial state of shock wave case $\epsilon = 10^{-6}$, $\sigma_c = 7.20 \cdot 10^{-2} N/m$.

Region	$\alpha_1 [-]$	$v [m/s]$	$p_k [Pa]$	ρ_1	ρ_2
In column	ϵ	0	101347.5	1.200	1000
Before shock	$1 - \epsilon$	0	101325	1.200	1000
After shock	$1 - \epsilon$	151	182892	1.819	1000

As analyzed in Igra and Takayama (2001) [109] there are four stages to be expected in this test case which starts when the shock wave impinges the liquid column at $t_{sim} = 0 \mu s$.

- $0 \lesssim t_{sim} \lesssim 25 \mu s$: the shock wave impinges upon the liquid column, creating a reflecting shock wave propagating in the opposite direction and a transmitted wave into the liquid, while the incident wave continues to move symmetrically around the column. Rapidly two Mach stems form on each side of the column, in the gas. The transmitted wave reaches the rear of the liquid column and reflects, creating a decompression wave leading to cavitation at the rear of the liquid column. The first stage finishes when the two stems collapse at the rear of the liquid column and the first instability on the interface occurs.
- $25 \lesssim t_{sim} \lesssim 300 \mu s$: the liquid column starts to deform, but the degree of deformation is still small, and progressively elongates in the lateral direction until the first strippings on both sides of the liquid column appear generating micro-mists.
- $300 \lesssim t_{sim} \lesssim 1200 \mu s$: the micro-mists expand in the re-circulations zones created by two counter-rotating vortices at the rear of the liquid column whose size significantly decreases.
- $t_{sim} \gtrsim 1200 \mu s$: the water column starts to break-up.

In Figure 4.14, a time lapse of mixture density gradient in the zoomed region shown in Figure 4.13b is proposed from $t_{sim} = 0 \mu s$ to $t_{sim} = 55 \mu s$.

In Figure 4.14a, the shock wave impinges upon the liquid column. In Figure 4.14b, the left normal shock wave is the reflecting shock propagating in the opposite direction. The incident wave is moving symmetrically around the liquid column and two Mach stems have formed on each side of the column, in the gas. In Figure 4.14c, the two stems collapse at the rear of the liquid column. It is the end of the first stage.

As depicted in Figures 4.14d to 4.14f, the liquid column starts to deform slightly from the rear, corresponding to the second stage.

Figure 4.15 emphasizes the high fidelity of the numerical results by comparing two instants with experimental Schlieren images taken from Igra and Takayama (2001) [109].

The simulation has been successfully conducted until $t_{sim} = 1.2 ms$. Nevertheless, no non-reflecting subsonic outflow boundary conditions are yet implemented in CEDRE for the present model. Therefore, shock waves have reflected on all the limits, perturbing the liquid column in the next phases. Figure 4.16 still underline the good agreement between the simulation and the experimental Schlieren image during the second phase, when the liquid column progressively

elongates in the lateral direction until the first stripping on both sides of the liquid column appear generating micro-mists.

4.3.3 VERIFICATIONS TESTS ON THE NEW GEOMETRIC TERMS

A demonstrative test case might be included in this section if time allows.

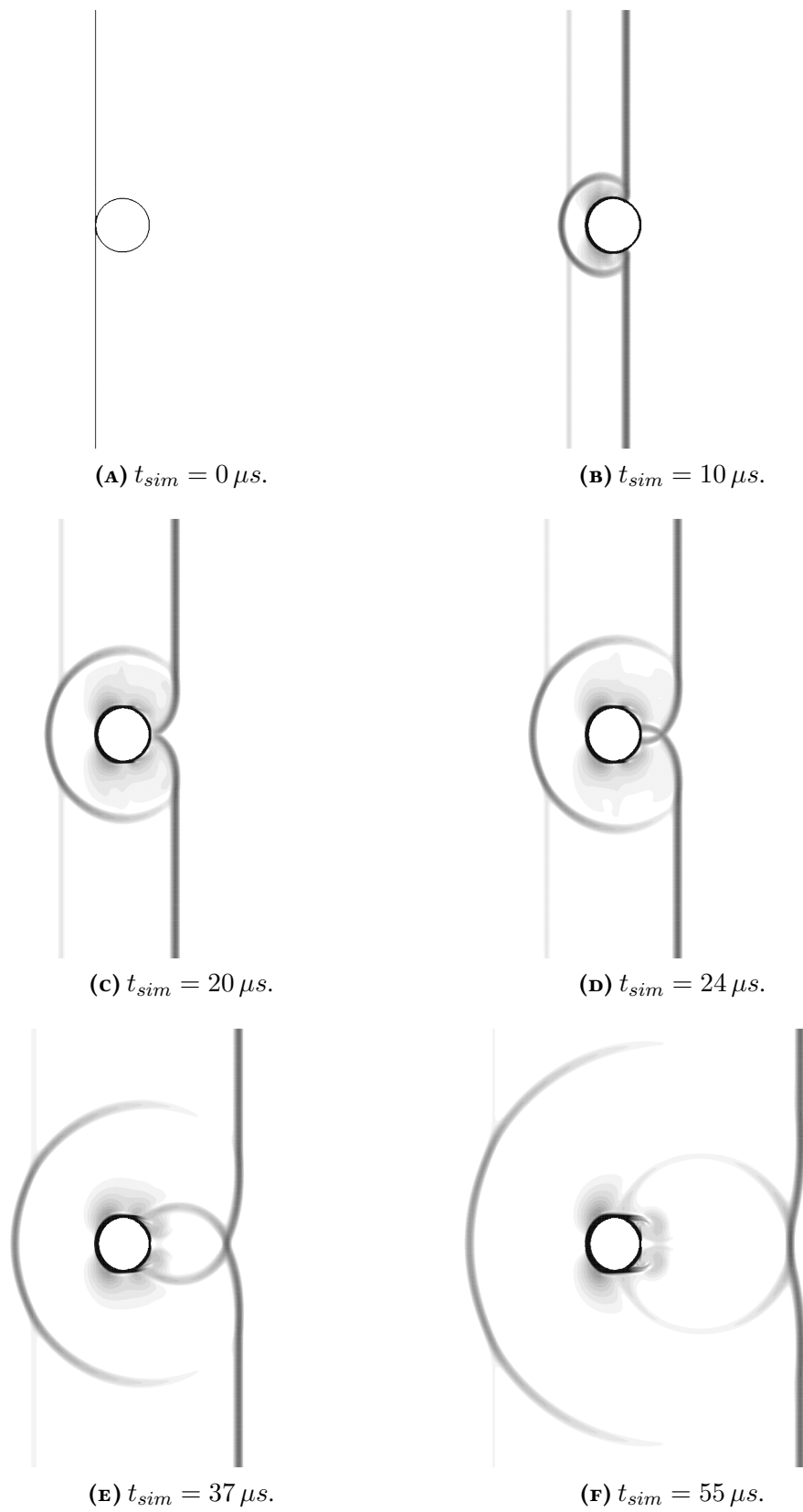
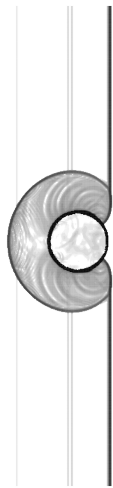
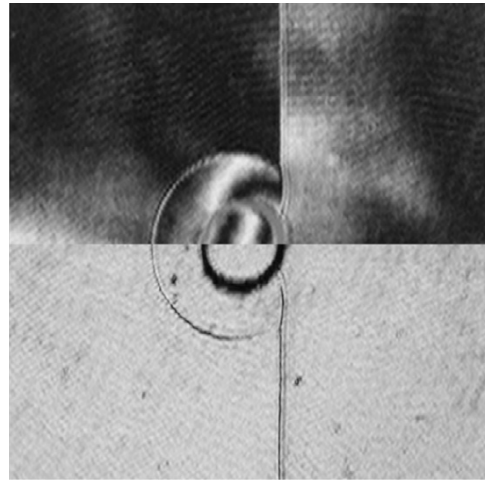


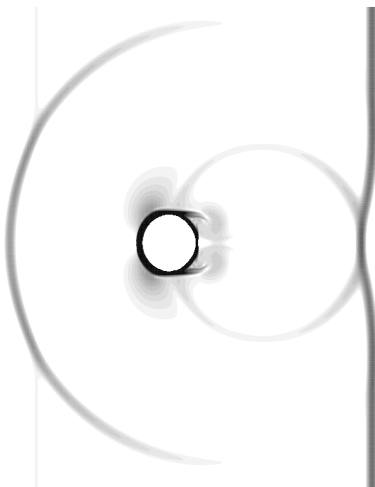
FIGURE 4.14: Schlieren contour of mixture density, $\|\nabla\rho\| \in 10 \text{ --- } 8 \cdot 10^3$ at a given simulation time.



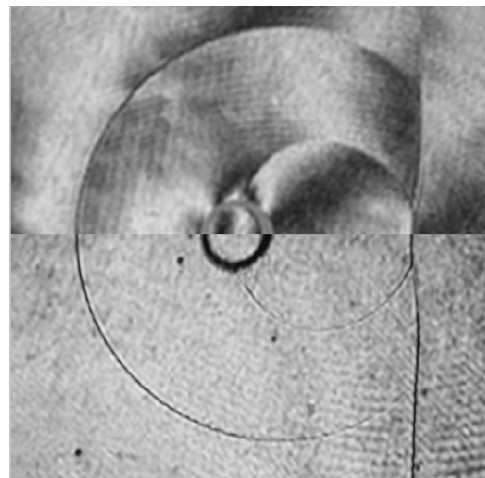
(A) $t_{sim} = 15 \mu s$.



(B) Expe $t_{sim} = 15 \mu s$.



(C) $t_{sim} = 55 \mu s$.



(D) Expe $t_{sim} = 55 \mu s$.

FIGURE 4.15: Comparison of Schlieren contour of mixture density between numerical and experimental results Igra and Takayama (2001) [109] at two given simulation times.

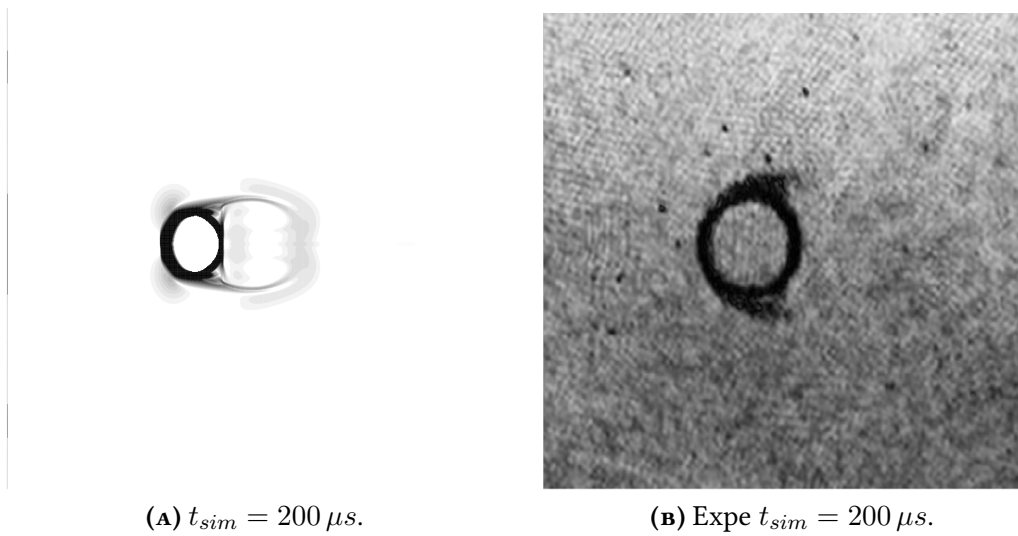


FIGURE 4.16: Comparison of Schlieren contour of mixture density between numerical and experimental results [Igra and Takayama \(2001\)](#) [109] at $t_{sim} = 200 \mu s.$

APPENDIX 4.A MODEL ANALYSIS

4.A.1 EULER WITH CAPILLARY FLUX

Deriving the spectrum of $\mathcal{A}(\mathbf{u})$ of System (4.22) leads to

$$\begin{aligned} \det\{\mathcal{A}(\mathbf{u}) - \lambda \mathcal{I}_d\} &= (v_{x_1} - \lambda)^9 \times \det \begin{pmatrix} v_{x_1} - \lambda & \rho & 0 & 0 & 0 \\ \frac{1}{\rho} \partial_\rho \mathcal{P} & v_{x_1} - \lambda & 0 & 0 & \frac{1}{\rho} \frac{\partial \Omega_{11}}{\partial (\partial_{x_1} \alpha)} \\ 0 & 0 & v_{x_1} - \lambda & 0 & \frac{1}{\rho} \frac{\partial \Omega_{12}}{\partial (\partial_{x_1} \alpha)} \\ 0 & 0 & 0 & v_{x_1} - \lambda & \frac{1}{\rho} \frac{\partial \Omega_{13}}{\partial (\partial_{x_1} \alpha)} \\ 0 & \partial_{x_1} \alpha & \partial_{x_2} \alpha & \partial_{x_3} \alpha & v_{x_1} - \lambda \end{pmatrix} \\ &= (v_{x_1} - \lambda)^{10} \left((v_{x_1} - \lambda)^4 + B(v_{x_1} - \lambda)^2 + C \right) \end{aligned}$$

with

$$\begin{aligned} B &= -\frac{1}{\rho} \left((\partial_{x_1} \alpha) \frac{\partial \Omega_{11}}{\partial (\partial_{x_1} \alpha)} + (\partial_{x_2} \alpha) \frac{\partial \Omega_{12}}{\partial (\partial_{x_1} \alpha)} + (\partial_{x_3} \alpha) \frac{\partial \Omega_{13}}{\partial (\partial_{x_1} \alpha)} \right) - \partial_\rho \mathcal{P} \\ C &= \frac{1}{\rho} \partial_\rho \mathcal{P} \left((\partial_{x_2} \alpha) \frac{\partial \Omega_{12}}{\partial (\partial_{x_1} \alpha)} + (\partial_{x_3} \alpha) \frac{\partial \Omega_{13}}{\partial (\partial_{x_1} \alpha)} \right), \end{aligned}$$

and $\alpha = \alpha_1 = 1 - \alpha_2$. Working out the partial derivatives of the Ω terms

$$\frac{\partial \Omega_{1i}}{\partial (\partial_{x_1} \alpha)} = -\frac{\sigma_c \partial_{x_i} \alpha}{\|\nabla \alpha\|^3} \left(\|\nabla \alpha\|^2 - (\partial_{x_1} \alpha)^2 \right), \text{ for } i = 1, 3,$$

we propose to introduce $\epsilon_{x_1} = 1 - \left((\mathcal{E}_c^l)_{x_1} / \mathcal{E}_c^l \right)^2 \in [0, 1]$ with $(\mathcal{E}_c^l)_{x_1} = \sigma_c \partial_{x_1} \alpha$ and $\mathcal{E}_c^l = \sigma_c \|\nabla \alpha\|$ the capillary energy. We obtain

$$B = \frac{1}{\rho} \epsilon_{x_1} \mathcal{E}_c^l - \partial_\rho \mathcal{P}, \quad C = -\frac{1}{\rho} \epsilon_{x_1}^2 \mathcal{E}_c^l \partial_\rho \mathcal{P}.$$

Defining $X = (v_{x_1} - \lambda)^2$, we need to solve a second order polynomial equation. Manipulating the discriminant $\Delta = B^2 - 4C$, we have

$$\Delta \geq \left(\frac{1}{\rho} \epsilon_{x_1} \mathcal{E}_c^l + \partial_\rho \mathcal{P} \right)^2 \geq 0.$$

Thus, the roots a_\pm^2 are all real and take the form

$$a_\pm^2 = \frac{1}{2} \left(\epsilon_{x_1} \mathcal{E}_c^l + \rho \partial_\rho \mathcal{P} \pm \sqrt{(\epsilon_{x_1} \mathcal{E}_c^l + \rho \partial_\rho \mathcal{P})^2 + 4\rho \epsilon_{x_1} \mathcal{E}_c^l \partial_\rho \mathcal{P}} \right)$$

and finally the spectrum of $\mathcal{A}(\mathbf{u})$ is obtained. We could also prove that the system is weakly hyperbolic using the same arguments as in [Schmidmayer et al. \(2017\) \[197\]](#).

4.A.2 SUB-SYSTEM 1: EULER SYSTEM

Assuming $\alpha_1 = \alpha = 1 - \alpha_2$, System (4.24) writes in its quasi linear form and a one-dimensional framework,

$$\partial_t \mathbf{u} + \mathcal{A}(\mathbf{u}) \partial_x \mathbf{u} = 0, \quad (4.84)$$

where $\mathbf{u} = (\rho, v_{x_1}, \partial_{x_1}\alpha, \varphi)^t$ with $\varphi \in \{y_{j,k}, v_{x_2}, v_{x_3}, s_k, \omega, \Sigma, H, \alpha, \partial_{x_2}\alpha, \partial_{x_3}\alpha\}$, such that $D_t\varphi = 0$, and $\mathcal{A}(\mathbf{u})$ takes the form

$$\mathcal{A}(\mathbf{u}) = \begin{pmatrix} v_{x_1} & \rho & 0 & 0 \\ \frac{1}{\rho}\partial_\rho\mathcal{P} & v_{x_1} & 0 & \frac{1}{\rho}\partial_\varphi\mathcal{P} \\ 0 & \partial_{x_1}\alpha & v_{x_1} & 0 \\ 0 & 0 & 0 & v_{x_1} \end{pmatrix}. \quad (4.85)$$

with $\mathcal{P} = \alpha_1 p_1 + \alpha_2 p_2$. Spectrum analysis of $\mathcal{A}(\mathbf{u})$ yields 4 real eigenvalues

$$v_{x_1}, v_{x_1}, v_{x_1} \pm a \text{ with } a^2 = \partial_\rho\mathcal{P}. \quad (4.86a)$$

The right eigenvectors are

$$\lambda_1 = v_{x_1}, \quad \mathbf{r}_1 = (0, 0, 1, 0)^t, \quad (4.86b)$$

$$\lambda_2 = v_{x_1}, \quad \mathbf{r}_2 = (\partial_\varphi\mathcal{P}, 0, 0, -a^2)^t, \quad (4.86c)$$

$$\lambda_{3,4} = v_{x_1} \pm a, \quad \mathbf{r}_{3,4} = \left(1, \pm \frac{a}{\rho}, \pm \frac{\partial_{x_1}\alpha}{\rho}, 0\right)^t. \quad (4.86d)$$

The family of vectors $(\mathbf{r}_1, \mathbf{r}_2, \mathbf{r}_3, \mathbf{r}_4)$ is a basis of \mathbb{R}^4 , thus the system is strictly hyperbolic. Furthermore, we obtain the following Riemann invariants

$$\lambda_{1,2} = v_{x_1}, \quad \{\mathcal{P}, v\}, \quad (4.86e)$$

$$\lambda_{3,4} = v_{x_1} \pm a, \quad \left\{ \varphi, v_{x_1} \mp \int \frac{a}{\rho} d\rho, \partial_{x_1}\alpha \mp \int \frac{\partial_{x_1}\alpha}{\rho} d\rho \right\}. \quad (4.86f)$$

4.A.3 SUB-SYSTEM 2: CAPILLARY SYSTEM

Assuming $\alpha_1 = \alpha = 1 - \alpha_2$, the quasi-linear form in a one-dimensional framework of System (4.26) takes the form

$$\partial_t \mathbf{u} + \mathcal{A}(\mathbf{u}) \partial_x \mathbf{u} = 0, \quad (4.87)$$

where $\mathbf{u} = (v_{x_1}, v_{x_2}, v_{x_3}, \partial_{x_1}\alpha, \varphi)^t$ with $\varphi \in \{\rho, y_{j,k}, s_k, \omega, \Sigma, H, \alpha, \partial_{x_2}\alpha, \partial_{x_3}\alpha\}$ such that $\partial_t\varphi = 0$, and $\mathcal{A}(\mathbf{u})$ takes the form

$$\mathcal{A}(\mathbf{u}) = \begin{pmatrix} 0 & 0 & 0 & \frac{1}{\rho} \frac{\partial\Omega_{11}}{\partial(\partial_{x_1}\alpha)} & \frac{1}{\rho} \frac{\partial\Omega_{11}}{\partial\varphi} \\ 0 & 0 & 0 & \frac{1}{\rho} \frac{\partial\Omega_{12}}{\partial(\partial_{x_1}\alpha)} & \frac{1}{\rho} \frac{\partial\Omega_{12}}{\partial\varphi} \\ 0 & 0 & 0 & \frac{1}{\rho} \frac{\partial\Omega_{13}}{\partial(\partial_{x_1}\alpha)} & \frac{1}{\rho} \frac{\partial\Omega_{13}}{\partial\varphi} \\ 0 & \partial_{x_2}\alpha & \partial_{x_3}\alpha & 0 & 0 \\ 0 & 0 & 0 & 0 & 0 \end{pmatrix}. \quad (4.88)$$

Deriving the spectrum of $\mathcal{A}(\mathbf{u})$ of System (4.26) gives

$$\begin{aligned} 0 = \det\{\mathcal{A}(\mathbf{u}) - \lambda \mathcal{I}_d\} &= -\lambda \times \det \begin{pmatrix} -\lambda & 0 & 0 & \frac{1}{\rho} \frac{\partial\Omega_{11}}{\partial(\partial_{x_1}\alpha)} \\ 0 & -\lambda & 0 & \frac{1}{\rho} \frac{\partial\Omega_{12}}{\partial(\partial_{x_1}\alpha)} \\ 0 & 0 & -\lambda & \frac{1}{\rho} \frac{\partial\Omega_{13}}{\partial(\partial_{x_1}\alpha)} \\ 0 & \partial_{x_2}\alpha & \partial_{x_3}\alpha & -\lambda \end{pmatrix} \\ &= \lambda^3 (\lambda^2 - \tilde{B}) \end{aligned}$$

with

$$\tilde{B} = -\frac{1}{\rho} \left((\partial_{x_2} \alpha) \frac{\partial \Omega_{12}}{\partial(\partial_{x_1} \alpha)} + (\partial_{x_3} \alpha) \frac{\partial \Omega_{13}}{\partial(\partial_{x_1} \alpha)} \right).$$

Using the same notations introduced in [Section 4.A.1](#), we obtain

$$\tilde{B} = \frac{1}{\rho} \epsilon_{x_1}^2 \mathcal{E}_c^l \geq 0,$$

and finally the spectrum of $\mathcal{A}(\mathbf{u})$ is obtained,

$$0, \pm \epsilon_{x_1} \sqrt{\frac{\mathcal{E}_c^l}{\rho}}$$

We could also prove that the system remains weakly hyperbolic using the same arguments as in [Schmidmayer et al. \(2017\) \[197\]](#).

APPENDIX 4.B ENERGY EQUATIONS

The Stationary Action Principle returns naturally transport equations for the partial entropies. However, due to the non-linearity between the entropy and the pressure, using the partial entropies fails at advecting an uniform pressure and velocity flow without instabilities.

Far from being an exhaustive analysis of the problem, we propose to illustrate the non-preservation of pressure uniformity by considering a very simplified Riemann problem at an interface where the flow is supersonic, flowing from the left cell to the right cell at speed v_o , normal to the interface, and at uniform pressure p_o as depicted in Figure 4.17. We want

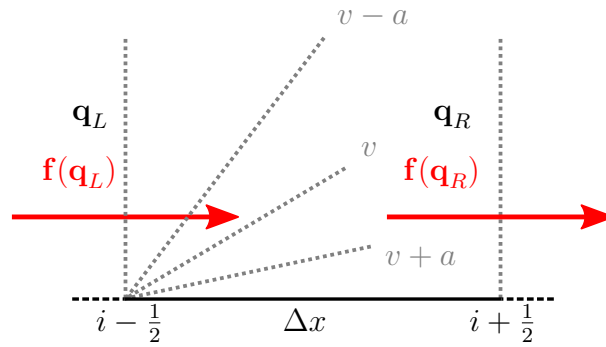


FIGURE 4.17: Scheme of a uniform flow in a Δx -width cell at t^n .

to evaluate the state in the cell i at the next time step $t^{n+1} = t^n + \Delta t$. At uniform pressure and velocity, neglecting capillarity effects and assuming mono-species fluids, the investigated system in one-dimensional framework reduces to

$$\partial_t \begin{pmatrix} \rho \\ \rho y_k \\ \rho v \\ \omega \\ \alpha_k \\ \rho s_k \\ \rho \Sigma \\ \rho H \end{pmatrix} + \partial_x \begin{pmatrix} \rho v \\ \rho y_k v \\ \rho v^2 + p \\ \omega v \\ \alpha_k v \\ \rho s_k v \\ \rho \Sigma v \\ \rho H v \end{pmatrix} = 0. \quad (4.89)$$

At time t^{n+1} , using a Finite Volume approach, the conservative variables inside the cell are updated by an upwind first-order Godunov scheme, leading to

$$\begin{aligned} \mathbf{q}_i^{n+1} &= \mathbf{q}_i^n + \frac{\Delta t}{\Delta x} [\mathbf{f}_{i+\frac{1}{2}} - \mathbf{f}_{i-\frac{1}{2}}] \\ \implies \mathbf{q}_R^{n+1} &= \mathbf{q}_R^n + \frac{\Delta t}{\Delta x} [\mathbf{f}(\mathbf{q}_R) - \mathbf{f}(\mathbf{q}_L)]. \end{aligned} \quad (4.90)$$

Since we only seek the updated state \mathbf{q}_R^{n+1} , we will drop its subscript. Introducing the convec-

tive CFL number ν_{CFL} , Equation (4.90) takes the form

$$\begin{pmatrix} \rho^{n+1} \\ (\rho y_k)^{n+1} \\ (\rho v)^{n+1} \\ \omega^{n+1} \\ \alpha^{n+1} \\ (\rho s_k)^{n+1} \\ (\rho \Sigma)^{n+1} \\ (\rho H)^{n+1} \end{pmatrix} = \begin{pmatrix} \rho_R \\ \rho_R (y_k)_R \\ \rho_R v_o \\ \omega_R \\ (\alpha_k)_R \\ \rho_R (s_k)_R \\ \rho_R \Sigma_R \\ \rho_R H_R \end{pmatrix} - \nu_{\text{CFL}} \begin{pmatrix} \rho_R - \rho_L \\ \rho_R (y_k)_R - \rho_L (y_k)_L \\ (\rho_R - \rho_L) v_o \\ \omega_R - \omega_L \\ (\alpha_k)_R - (\alpha_k)_L \\ \rho_R (s_k)_R - \rho_L (s_k)_L \\ \rho_R \Sigma_R - \rho_L \Sigma_L \\ \rho_R H_R - \rho_L H_L \end{pmatrix}, \quad (4.91)$$

with $\nu_{\text{CFL}} = \Delta t v_o / \Delta x$ the convective Courant Friedrich Lewy number. Manipulating the discrete equations, we can evaluate the update of each variable,

$$\rho^{n+1} = (1 - \nu_{\text{CFL}}) \rho_R + \nu_{\text{CFL}} \rho_L, \quad (4.92a)$$

$$y_k^{n+1} = \frac{(\rho y_k)^{n+1}}{\rho^{n+1}} = \frac{(1 - \nu_{\text{CFL}}) \rho_R (y_k)_R + \nu_{\text{CFL}} \rho_L (y_k)_L}{(1 - \nu_{\text{CFL}}) \rho_R + \nu_{\text{CFL}} \rho_L}, \quad (4.92b)$$

$$v^{n+1} = \frac{(\rho v)^{n+1}}{\rho^{n+1}} = v_o, \quad (4.92c)$$

$$s_k^{n+1} = \frac{(\rho s_k)^{n+1}}{\rho^{n+1}} = \frac{(1 - \nu_{\text{CFL}}) \rho_R (s_k)_R + \nu_{\text{CFL}} \rho_L (s_k)_L}{(1 - \nu_{\text{CFL}}) \rho_R + \nu_{\text{CFL}} \rho_L}, \quad (4.92d)$$

$$\alpha_k^{n+1} = (1 - \nu_{\text{CFL}}) (\alpha_k)_R + \nu_{\text{CFL}} (\alpha_k)_L, \quad (4.92e)$$

$$\omega^{n+1} = (1 - \nu_{\text{CFL}}) \omega_R + \nu_{\text{CFL}} \omega_L, \quad (4.92f)$$

$$\Sigma^{n+1} = \frac{(\rho \Sigma)^{n+1}}{\rho^{n+1}} = \frac{(1 - \nu_{\text{CFL}}) \rho_R \Sigma_R + \nu_{\text{CFL}} \rho_L \Sigma_L}{(1 - \nu_{\text{CFL}}) \rho_R + \nu_{\text{CFL}} \rho_L}, \quad (4.92g)$$

$$H^{n+1} = \frac{(\rho H)^{n+1}}{\rho^{n+1}} = \frac{(1 - \nu_{\text{CFL}}) \rho_R H_R + \nu_{\text{CFL}} \rho_L H_L}{(1 - \nu_{\text{CFL}}) \rho_R + \nu_{\text{CFL}} \rho_L}. \quad (4.92h)$$

Thus, we have immediately that the flow remains at the same speed v_o . To obtain the pressure update, we need first to compute the partial densities. Recalling that $\rho_k^{n+1} = \rho^{n+1} y_k^{n+1} / \alpha_k^{n+1}$, we have

$$\rho_k^{n+1} = \frac{(1 - \nu_{\text{CFL}}) \rho_R (y_k)_R + \nu_{\text{CFL}} \rho_L (y_k)_L}{(1 - \nu_{\text{CFL}}) (\alpha_k)_R + \nu_{\text{CFL}} (\alpha_k)_L} = \frac{(1 - \nu_{\text{CFL}}) (\alpha_k)_R (\rho_k)_R + \nu_{\text{CFL}} (\alpha_k)_L (\rho_k)_L}{(1 - \nu_{\text{CFL}}) (\alpha_k)_R + \nu_{\text{CFL}} (\alpha_k)_L}. \quad (4.93)$$

From any two-parameter equations of state, we can now compute the updated pressure and temperatures in the investigated cell, p^{n+1} and T^{n+1} . General derivation could be done from partial derivatives evaluation using the Gibbs equations assumed for each phase. However, for sake of clarity and simplicity, we will use the Perfect Gas equation of state. The pressure in terms of entropy and density writes

$$p_k^{n+1} = (\rho_k^{n+1})^{\gamma_k} \exp\left(\frac{s_k^{n+1}}{c_{v,k}}\right) \quad (4.94)$$

Reinjecting above expressions, and replacing the partial densities in Equation (4.93) by temperatures through the EOS leads to

$$\frac{p_k^{n+1}}{p_o} = \left[\frac{(1 - \nu_{\text{CFL}}) (\alpha_k)_R / T_{k,R} + \nu_{\text{CFL}} (\alpha_k)_L / T_{k,L}}{(1 - \nu_{\text{CFL}}) (\alpha_k)_R + \nu_{\text{CFL}} (\alpha_k)_L} \right]^{\gamma_k} (T_{k,R})^{\gamma_k \hat{\rho}_R} (T_{k,L})^{\gamma_k \hat{\rho}_L}, \quad (4.95)$$

with $\hat{\rho}_R = (1 - \nu_{\text{CFL}})\rho_R/((1 - \nu_{\text{CFL}})\rho_R + \nu_{\text{CFL}}\rho_L)$ and $\hat{\rho}_L = \nu_{\text{CFL}}\rho_L/((1 - \nu_{\text{CFL}})\rho_R + \nu_{\text{CFL}}\rho_L)$.

For further simplification, we can impose the time step Δt such that the CFL number equals $\nu_{\text{CFL}} = \rho_R/(\rho_R + \rho_L)$ as well as the initial continuity of the volume fraction, $(\alpha_k)_R = (\alpha_k)_L = (\alpha_k)_o$. Noticing that $\hat{\rho}_R = \hat{\rho}_L = 1/2$, the previous equation reduces to

$$\frac{p_k^{n+1}}{p_o} = \left[\frac{1}{2} \frac{(T_{k,R} + T_{k,L})}{\sqrt{T_{k,R}T_{k,L}}} \right]^{\gamma_k}. \quad (4.96)$$

Interestingly, the fluid pressure variation is a function of the temperature arithmetic and geometric means. Thus, the only possibility to guarantee the flow to maintain a uniform pressure is to allow no fluid temperature jump, otherwise pressure oscillations will occur. This effect is one of the main drawback of the four equation model, as detailed in [Le Touze \(2015\)](#) [132]. This side-effect comes from the non-linearity of the partial entropy with respect to the fluid pressure as seen for instance for the Perfect Gas EOS in Equation (4.94). Transporting then the partial entropy does not numerically permit to maintain a pressure continuity.

Since the internal energy is linearly proportional to the fluid pressure, we propose to trade the partial entropy equation for the partial internal energy equation.

Using the Gibbs equation, and assuming it still holds in non-equilibrium flows in the frame moving with the local hydrodynamic velocity \mathbf{v} , we have

$$T_k D_t s_k = D_t e_k - \frac{p_k}{\rho_k^2} D_t \rho_k, \quad (4.97)$$

which, after some manipulations, yields

$$\alpha_k \rho_k T_k D_t s_k = \alpha_k \rho_k D_t e_k + \alpha_k p_k \nabla \cdot \mathbf{v} + p_k D_t \alpha_k. \quad (4.98)$$

Reinjecting the transport equation for the partial entropy and the volume fraction, we obtain the transport equation of the partial internal energy.

Going back to the example, if we no more transport the partial entropy, but the partial internal energy, the entropy update Equation (4.92d) is replaced by the internal energy update,

$$e_k^{n+1} = (1 - \nu_{\text{CFL}})(e_k)_R + \nu_{\text{CFL}}(e_k)_L, \quad (4.99)$$

Unfortunately, still in the particular case $\nu_{\text{CFL}} = 1/2$ and for a Perfect Gas equation of state, it leads to a pressure jump

$$\frac{p_k^{n+1}}{p_o} = \frac{1}{4} \frac{(\rho_k)_R + (\rho_k)_L}{(\rho_k)_R (\rho_k)_L}, \quad (4.100)$$

because the internal energy is not linearly related to the pressure, but to the ratio p_k/ρ_k . It is only if we transport $\alpha_k \rho_k e_k$, for which the transport equation reads

$$\partial_t(\alpha_k \rho_k e_k) + \nabla \cdot (\alpha_k \rho_k e_k \mathbf{v}) - \alpha_k p_k \nabla \cdot \mathbf{v} = 0, \quad (4.101)$$

and the update for the initially uniform flow becomes,

$$(\alpha_k \rho_k e_k)^{n+1} = (1 - \nu_{\text{CFL}})(\alpha_k)_R (\rho_k)_R (e_k)_R + \nu_{\text{CFL}}(\alpha_k)_L (\rho_k)_L (e_k)_L \quad (4.102)$$

and since $\rho_k e_k = p_k c_{v,k} / \gamma_k$, we obtain

$$\frac{p_k^{n+1}}{p_o} = \frac{(1 - \nu_{\text{CFL}})(\alpha_k)_R + \nu_{\text{CFL}}(\alpha_k)_L}{\alpha_k^{n+1}} = 1. \quad (4.103)$$

Thus, the pressure and velocity uniform flow remains uniform and the model, using the transport equation on $\alpha_k \rho_k e_k$ does not lead to pressure oscillations, showing greater benefits compared to the four equation model. Thus, we will replace the entropy equations by the equations on the internal energies.

NUMERICAL SIMULATIONS TO COMPARE AND VALIDATE REDUCED-ORDER MODEL HIERARCHY

5

Whereas direct numerical simulation (DNS) have reached a high level of description in the field of atomization processes, they are not yet able to cope with industrial needs since they lack resolution and are too costly. Predictive simulations relying on reduced-order modeling have become mandatory for applications ranging from combustion processes such as cryotechnic to aeronautic combustion chamber liquid injection, to biological, industrial deposition processes, coating and agricultural sprays. Two-fluid models provide a good basis in order to conduct such simulations, even if recent advances allow to refine subscale modeling using geometrical variables in order to reach a unified model including separate phases and disperse phase descriptions based on high order moment methods. Such models must be resolved using dedicated numerical methods and still lack assessment of their predictive capabilities.

Chapter 5 is firstly dedicated to qualitatively and quantitatively compare some elements of the hierarchy of diffuse interface models on a challenging configuration, a single-injector in cryogenic operating conditions. The investigated models are the single-velocity single-pressure and two-velocity two-pressure models, both coupled or not with a KBMM element. This study has been performed as a demonstration of feasibility rather than validation on experimental results.

Secondly, in Chapter 5, we constitute and investigate a first building block of a hierarchy of test-cases designed to be amenable to DNS while close enough to industrial configurations, for which we propose a comparison of two-fluid compressible simulations with DNS data-bases. Two test-cases are proposed, both air-assisted water atomizations. The first element uses a coaxial injector, the other a planar liquid sheet injector. Qualitative and quantitative comparisons with DNS allow us to study strength and weaknesses of the reduced-order modeling and numerical approach in this specific configuration and set a framework for more refined models since they already provide a very interesting level of comparison on averaged quantities. It has also led to a better understanding of the main conceptual differences between the two modelling approaches.

Chapter 5 is the results of three proceedings, Cordesse et al. (2018) [36], Murrone et al. (2018) [163], Cordesse et al. (2019) [38], a technical report Cordesse et al. (2020) [37] and finally, an article Cordesse et al. (2019) [42] submitted to the journal Flow, Turbulence and Combustion (FTaC) as meriting inclusion in the Special Issue of FTaC, to comprise around 15 papers, selected from a total of the 118 papers that were presented orally at the ICMF 2019 conference.



5.1	Qualitative comparison of a hierarchy of diffuse interface model with and without atomization	239
5.1.1	Numerical strategy: coupling a DIM with a KBMM element	239
5.1.2	Description of the configuration	241
5.1.3	Case 1: five-equation model with and without atomization	242
5.1.4	Case 2: five-equation model and instantaneously relaxed seven-equation model without atomization	244
5.1.5	Case 3: instantaneously relaxed seven-equation model and non-instantaneously relaxed seven-equation model with atomization	245
5.2	Validation strategy of reduced-order two-fluid flow models based on a hierarchy of direct numerical simulations	247
5.2.1	Numerical methods employed	248
5.2.1.1	CEDRE (SEQUOIA) Solver	248
5.2.1.2	ARCHER Solver	249
5.2.2	First test case: an air-assisted water atomization using a coaxial injector	249
5.2.2.1	Description of the LEGI experiment	250
5.2.2.2	Numerical set-up	251
5.2.2.3	Qualitative comparison	252
5.2.2.4	Quantitative comparison	253
5.2.3	Second test case: an air-assisted water atomization using a flat injector	254
5.2.3.1	Description of the configuration	254
5.2.3.2	Identification of the DNS region of validity	259
5.2.3.3	Evaluation of the atomization global characteristics of both numerical approaches	260
5.2.3.4	Statistical analysis	263
5.2.4	Conclusion	272

5.1 QUALITATIVE COMPARISON OF A HIERARCHY OF DIFFUSE INTERFACE MODEL WITH AND WITHOUT ATOMIZATION

In previous works [Le Touze \(2015\) \[132\]](#), [Murrone, A. and Le Touze, C. \(2019\) \[165\]](#), a coupling strategy between a four-equation diffuse interface model and an Eulerian kinetic model for the spray has been investigated and applied to the simulation of the MASCOTTE test facility on the 10-bar operating point corresponding to cryogenic rocket engines under transient operating conditions. In the present work, we focus on the improvement of the diffuse interface model for the simulation of separated two-phase flow in coaxial cryogenic injector in order to realize the same coupling strategy. We thus have employed enhanced elements of the hierarchy of diffuse interface models introduced in [Section 1.1.4](#), namely the *five-equation model (5eq)* with a single pressure and a single velocity, the *instantaneously relaxed seven-equation model (IR7eq)* with two pressures and two velocities instantaneously relaxed, and the *non-instantaneously relaxed seven-equation model (NIR7eq)* with two pressures and two velocities, which are not instantaneously relaxed.

On the way to validation of the numerical results with experimental data, the primary interest of this section is to attest the robustness of the numerical method and the feasibility of performing numerical simulations on challenging real configurations such as on a single cryogenic injector. Therefore, we have increased difficulties one step at a time: first by increasing the disequilibrium accounted for by the diffuse interface model, then by activating the coupling of the DIM with a KBMM element via atomization and pseudo-coalescence source terms. Doing so, we can study the impact of the models and the coupling on quantities of interest such as the liquid core length, its dynamics, the sharpness of the interface and the velocities at the interface. Furthermore, as we have chosen operating conditions as close as possible to a real configuration, the present study lays the groundwork for a future investigation into the level of predictiveness of each model.

5.1.1 NUMERICAL STRATEGY: COUPLING A DIM WITH A KBMM ELEMENT

We shortly introduce the numerical strategy used to perform the simulations. Two models are used: a two-phase flow model based on diffuse interface methods and a multi-fluid model derived by Kinetic Based Moment Methods. They are two-way coupled.

The diffuse interface models, already introduced in [Section 1.1.4](#), write in a quasi-linear form

$$\partial_t \mathbf{q} + \mathcal{A}(\mathbf{q}) \partial_x \mathbf{q} = \mathbf{r}(\mathbf{q}) + \mathbf{S}_{se/sp} \quad (5.1)$$

with the set of quasi conservative variables writing $\mathbf{q} = (\alpha_2, \mathbf{q}_2, \mathbf{q}_1)^t$, $\mathbf{q}_k = (\alpha_k \rho_k, \alpha_k \rho_k \mathbf{v}_k, \alpha_k \rho_k E_k)$ for the *seven-equation* model, and $\mathbf{q} = (\alpha_2, \alpha_2 \rho_2, \alpha_1 \rho_1, \rho \mathbf{v}, \rho E)^t$ for the *five-equation* model. The conservative fluxes $\mathbf{f}(\mathbf{q})$ and the non-conservative fluxes $\mathcal{N}(\mathbf{q})$ defining the matrix $\mathcal{A}(\mathbf{q})$ depend on the DIM and are not recalled here.

A two-parameter equation of state associated with a Gibbs law will be used for each fluid hereafter. Mass transfer between the two phases is neglected. The source term $\mathbf{S}_{se/sp}$ contains all the interactions between the DIM and the KBMM. It includes the atomization of the liquid

phase into droplets and the pseudo coalescence of the droplets into the liquid phase, the drag force of the gas acting upon the droplets using the correlation of Schiller-Naumann and the conducto-convective heat transfer at the surface of the droplet using the Abramzon-Sirignano model.

To obtain the relaxed pressure of the *five-equation* model, one needs to solve a simple ordinary differential equation (ODE). Since the characteristic time is taken to be infinitely small, the problem reduces to apply an iterative procedure as a Newton method to solve a second order equation and obtained a single equilibrium pressure. Detailed of the equation can be found in [Furfaro and Saurel \(2015\)](#) [74]. As for the velocities, since we want to account for finite relaxation time, the associated ODE takes the form

$$d_t \mathbf{v}_d - \frac{A^o}{\epsilon_v} \mathbf{v}_d = 0, \text{ with } A^o = \frac{\rho^o}{\alpha_l^o \rho_l^o \alpha_g^o \rho_g^o}, \quad (5.2)$$

where \mathbf{v}_d is the slip velocity vector, ϵ_v is the characteristic relaxation time, superscript o denotes the state before relaxation, α_k, ρ_k denote respectively the volume fraction and the partial density of the liquid phase, $k = l$, and the gas phase, $k = g$, and ρ is the mixture density, $\rho = \alpha_l \rho_l + \alpha_g \rho_g$. A first numerical approach is to fix a remaining slip velocity ratio target at each computational time step Δt , $\mathbf{v}_d(\Delta t)$. It defines the characteristic relaxing time as

$$\frac{\epsilon_v}{A^o} = \ln \left(\frac{\|\mathbf{v}_d(\Delta t)\|}{\|\mathbf{v}_d^o\|} \right) \Delta t. \quad (5.3)$$

An instantaneous velocity relaxation is in practice also possible and manipulating the ODE leads to a unique relaxed velocity, which is the mass weighted average of the two velocities before relaxing.

It would have been possible to choose one of the best KBMM element such as a multi-fluid modelling using a continuous discretization of the droplet size through sections, which has been validated on evaporating polydisperse sprays [Sibra et al. \(2017\)](#) [202]. Nevertheless since our primary concern is to increase the disequilibrium in the interface diffuse model, for sake of simplicity, a simple KBMM element has been chosen: a multi-fluid modelling with sampling methods [Laurent and Massot \(2001\)](#) [130] and monokinetic and monotemperature assumptions. Evaporation and coalescence of the droplets are neglected, thus only one sample of droplet is needed to attest the success of the coupling strategy of the two models. The system of equation is weekly hyperbolic [De Chaisemartin et al. \(2009\)](#) [44] and writes for one class

$$\partial_t \mathbf{q}_d + \partial_x \mathbf{f}_d(\mathbf{q}_d) = \mathbf{S}_{sp/se} \quad (5.4)$$

where the set of variables are $\mathbf{q}_d = (n_d, \alpha_d \rho_d, \alpha_d \rho_d \mathbf{v}_d, \alpha_d \rho_d e_d)^t$ the conservative fluxes $\mathbf{f}_d(\mathbf{q}_d) = (n_d \mathbf{v}_d, \alpha_d \rho_d \mathbf{v}_d, \alpha_d \rho_d \mathbf{v}_d^2, \alpha_d \rho_d e_d \mathbf{v}_d)^t$, and the coupling source term $\mathbf{S}_{sp/se}$. The quantity n_d is the number of droplets, ρ_d the liquid density depending only on the temperature, \mathbf{v}_d the droplet velocity, e_d the droplet internal energy. To be conservative, the coupling source terms of Equation (5.1) and Equation (5.4) must balance out each other.

Each model is implemented in a specific solver of CEDRE, SEQUOIA for the diffuse interface model and SPIREE for the KBMM element. Both are two-way coupled through the source terms $\mathbf{S}_{sp/se}$ and $\mathbf{S}_{se/sp}$ exchanged at every time step. A Lie splitting technique is used resulting in the following system of equations

$$\mathbf{q}^{n+1} = \left[\mathbf{S}_{se/sp} \frac{\mathbf{r}^v}{\epsilon_u} \right]^{\Delta t} \frac{\mathbf{r}^p}{\epsilon_p} \mathcal{H}_{\mathbf{q}}^{\Delta t}(\mathbf{q}^n) \quad \mathbf{q}_d^{n+1} = \left[\mathbf{S}_{sp/se} \right]^{\Delta t} \mathcal{H}_{\mathbf{q}_d}^{\Delta t}(\mathbf{q}_d^n) \quad (5.5)$$

The hyperbolic operators $\mathcal{H}_{\mathbf{q}}^{\Delta t}$ and $\mathcal{H}_{\mathbf{q}_d}^{\Delta t}$ corresponding to convection of the two-phase model and the dispersed model respectively, are calculated using a HLLC approximate Riemann solver, and a Pressureless Gas Dynamics exact Riemann solver respectively [Boileau et al. \(2016\) \[14\]](#). Then relaxation operators and source terms are applied in the order showed in Equation (5.5) to define the new states \mathbf{q}^{n+1} and \mathbf{q}_d^{n+1} of the conservative variables.

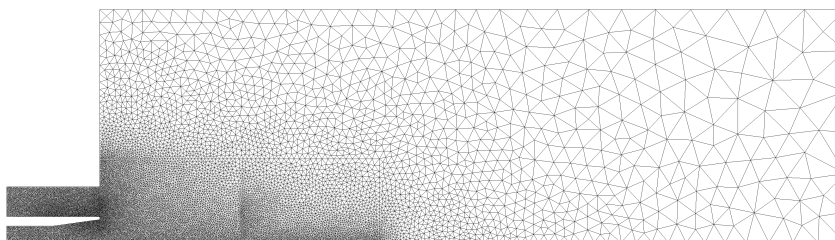
The atomization of the liquid phase and the pseudo-coalescence of the liquid droplets accounted in the coupling source terms are based on two key parameters, a frequency and an efficiency, both different for the atomization and pseudo-coalescence. These parameters are functions of quantities quantifying the shear stress intensity. For single velocity two-phase flow models or instantaneously relaxed two-velocities two-phase flow models, these parameters depend on the velocity gradient or the vortex. Expressions can be found in [Le Touze \(2015\) \[132\]](#) for instance. In the present work, thanks to the finite velocity relaxation, we have revisited the definition of these parameters making full use of the existence of two velocities to track regions with high shear stress. Hence they depend on the slip velocity v_d .

5.1.2 DESCRIPTION OF THE CONFIGURATION

The configuration choice meets several criteria. First, the geometry mimics the experimental Mascotte test-bench [Habiballah et al. \(1997\) \[101\]](#), [Vingert et al. \(1999\) \[217\]](#), a representation of a cryogenic rocket engine combustion chamber. It adopts a unique co-axial injector of liquid oxygen $O_2 (l)$ circumscribed by gaseous hydrogen $H_2 (g)$. Second, it must offer three dimensions in space to capture the dynamics of the jet. However, the computational time should not be too heavy to conduct numerical tests and validations. Hence, only a portion $\theta \in [0, \pi/3]$ of the cylindrical chamber is meshed making use of the symmetric axis of the cylinder preventing the liquid jet to flap.



(A) Global overview of the geometry of the chamber.



(B) 2D section of the mesh.

FIGURE 5.1: Geometry and mesh of the configuration.

As seen in [Figure 5.1](#), the mesh is refined inside the injector and at its exit where the liquid core flows in order to capture the interface dynamics. The mesh size is around a million tetra cells. The injector lip of length L^{lip} is meshed by four cells at the minimum mesh size Δx_{min} . Walls are set to adiabatic slip boundaries, the variables $(\rho_k, v_k, T_k, \alpha_k)$ define the inlets, the outlet is subsonic thus only the pressure is imposed at p^∞ . [Table 5.1](#) summarizes key values of the configuration.

TABLE 5.1: Physical parameters of the configuration.

$J = \frac{\rho_1 v_1^2}{\rho_2 v_2^2}$	T_1/T_2	Gas	Liquid	$L^{\text{lip}}/\Delta x_{\text{min}}$	p^∞	ϵ_α
~ 3	~ 3	$H_{2(g)}$	$O_{2(l)}$	4	10 bar	10^{-6}

The numerical simulations have been conducted as follows: first, the oxygen and the hydrogen have been injected with a ramp-up until $t_{\text{sim}} = t_{\text{sim}}(0)$ the operating point using the *5eq* with no coupling. Then, the simulation has run approximately ten times the characteristic convective time of the liquid core $t_{\text{conv}} = 4.5 \text{ ms}$. At this point, designated $t_{\text{sim}}(1) = 65 \text{ ms}$, starts the comparisons of the models. We thus have relaunched the simulations from this initial state with the various models.

5.1.3 CASE 1: FIVE-EQUATION MODEL WITH AND WITHOUT ATOMIZATION

We have selected first the five-equation model, which can be obtained by velocity and pressure relaxation of the 7 equation model. As opposed to the four equation model offering a single temperature, the two temperatures of the five-equation model provide an accurate description of the liquid temperature and is able to avoid spurious pressure oscillations of the four equation model due to mixing of hot gas with cold liquid in the diffuse interface. Far from validation with experiments results, we want to show the enhancement of the coupling strategy with the 5 equation interface diffuse model.

The law state for the liquid oxygen takes into account the liquid compressibility and reads

$$\rho_l(T_l, p_l) = \frac{1}{v_0} \frac{1 + \beta_0(p_l - p_0)}{1 + \alpha_0(T_l - T_0)}, \quad (5.6)$$

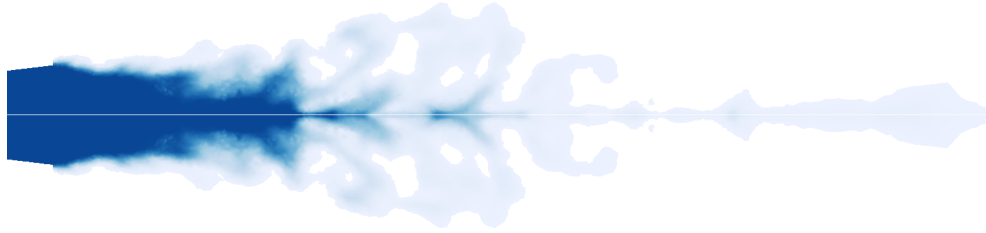
with the reference pressure $p_0 = 10 \text{ bar}$, the reference temperature $T_0 = 85 \text{ K}$, the reference specific volume $v_0 = 8.54 \cdot 10^{-3} \text{ m}^3/\text{kg}$, the two parameters $\beta_0 = 1.71 \cdot 10^{-9}$ and $\alpha_0 = 4.12 \cdot 10^{-3}$ and the calorific heat at constant volume is $c_{v,l} = 951 \text{ J/kg/K}$.

For the gas, we use a Perfect Gas equation of state and the pressure law takes the form

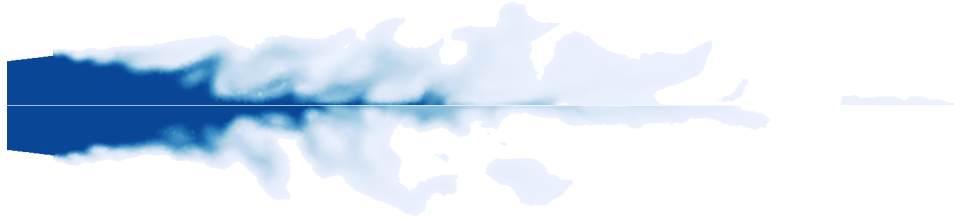
$$p_g = \rho_g(\gamma_g - 1)e_g, \quad e_g = c_{v,g}T_g, \quad (5.7)$$

with $\gamma_g = 1.4$ and $c_{v,g} = 1000 \text{ J/kg/K}$.


In [Figure 5.2](#), we present two instantaneous iso-values field of the volume fraction at times $t_{\text{sim}} = 65 \text{ ms}$ and $t_{\text{sim}} = 74 \text{ ms}$. This time interval corresponds to twice the characteristic convection time of the liquid core, $t_{\text{conv}} = 4.5 \text{ ms}$. We compare results obtained with atomization (upper side of the axis) and without atomization (lower side of the axis).



(A) *5eq* with atomization (top), *5eq* (down), $t_{sim} = t_{sim}(1)$.



(B) *5eq* with atomization (top), *5eq* (down), $t_{sim} = t_{sim}(1) + 2t_{conv}$.

FIGURE 5.2: Comparison of the instantaneous liquid volume fraction α_2 , on a slice at $\theta=\pi/6$ – $\alpha_2=1.0$  0.01.

The capacity of the coupling strategy is illustrated in [Figure 5.3](#). We present an instantaneous visualization of the volume fraction of the liquid jet (iso-surface) as well as the volume fraction of liquid droplets α_d generated by atomization. The physical time simulated corresponds to $t_{sim} = t_{sim}(1) + 2t_{conv} = 74 \text{ ms}$.

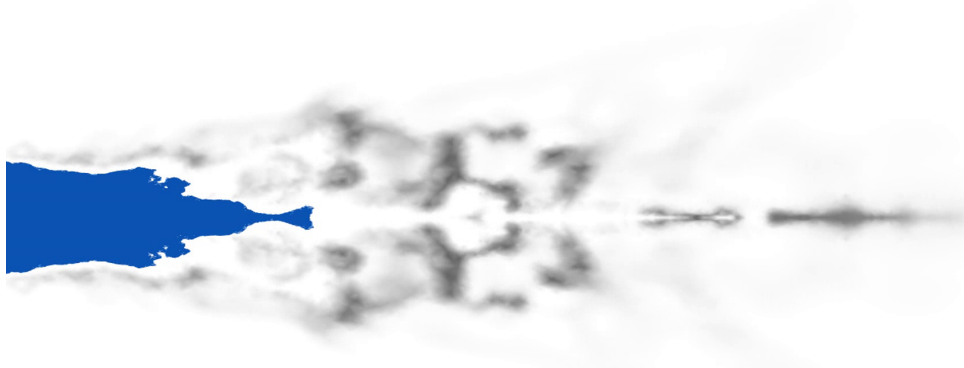



FIGURE 5.3: Instantaneous visualization of the liquid volume fraction iso-surface $\alpha_l = 0.99$ (blue), and volume fraction of liquid droplets α_d generated by atomization, α_d low  high, for the *5eq* with atomization at $t_{sim} = t_{sim}(1) + 2t_{conv}$, on the slice at $\theta=\pi/6$.

Moreover, we give quantitative results of the length of the liquid core, L_{lc} . [Figure 5.4](#) analyzes the liquid core length thanks to iso-values of liquid volume fraction between 0.95 ± 0.04 . The length of the liquid core renormalized by the injector diameter, $d_{inj} = 5 \text{ mm}$, is plotted over two characteristic convection times of the liquid core starting from $t_{sim} = t_{sim}(1)$, together with its time average $\langle L_{lc} \rangle$. We notice instabilities along the axial direction. Compari-

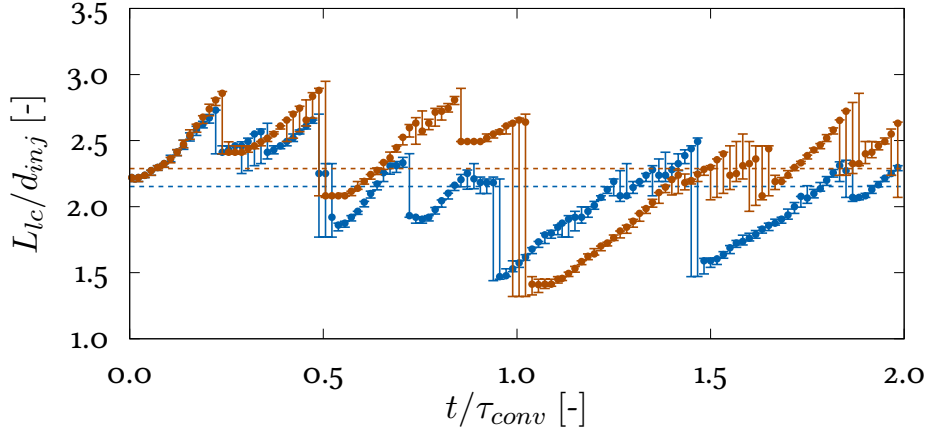


FIGURE 5.4: Model influence on the liquid core length L_{lc} over time and its time average $\langle L_{lc} \rangle$ at isovalue $\alpha_2=0.95\pm 0.04$. $5eq$ $\color{blue}{\bullet-\bullet}$ L_{lc} , $\color{blue}{- -}$ $\langle L_{lc} \rangle$ and $5eq$ with atomization: $\color{orange}{\bullet-\bullet}$ L_{lc} , $\color{orange}{- -}$ $\langle L_{lc} \rangle$.

son is made for the simulations with and without atomization. The length of the liquid core is very similar when taking into account or not for atomization, implying that the atomization procedure does not impact the liquid core length.

This new level of modelling allows us to perform accurate and robust simulations with a correct description of thermal transfer in the interface between liquid and gas because of the two temperatures of the five-equation model. Moreover, the five-equation model has been coupled with a spray kinetic solver following the fully Eulerian strategy proposed in previous works at ONERA. Hence, the atomization process has been taken into account and we have performed a difficult simulation showing very promising results.

5.1.4 CASE 2: FIVE-EQUATION MODEL AND INSTANTANEOUSLY RELAXED SEVEN-EQUATION MODEL WITHOUT ATOMIZATION

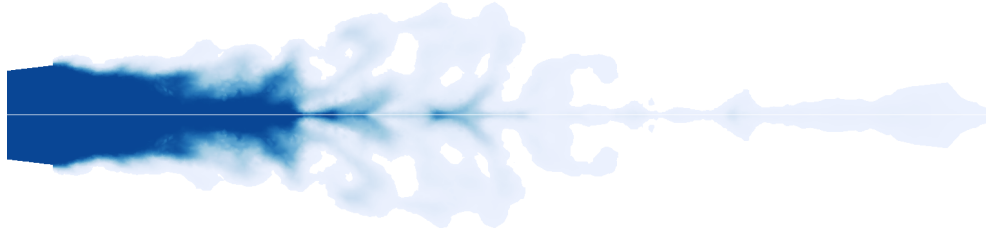
This second case aims at comparing the $5eq$ with the $IR7eq$. The difference emphasized by the mathematical study done in [Section 1.1.4](#) lies on the presence or not of zeroth-order terms of characteristic relaxation parameter in the volume fraction equation. Therefore we mainly focus on the volume fraction.

[Figure 5.5](#) compares qualitatively the liquid core obtained after two convection times, $t_{conv} = 4.5\text{ ms}$, the simulation time starting at $t_{sim}(1) = 65\text{ ms}$.

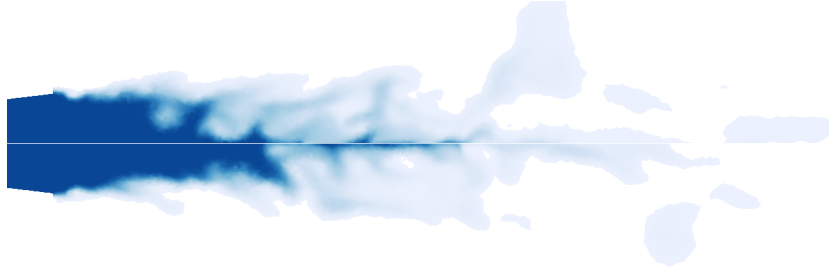
Looking at the bottom [Figure 5.5b](#), the outlook of the interface above and below the axis looks quite unchanged at first sight. Both models capture the disruption of the interface due to high-shear stress sparking ligaments. The interface seems less diffused in the region close to the liquid injector outlet for the $IR7eq$.

The length of the liquid core, L_{lc} , made dimensionless by the diameter of the O_2 (l) injector outlet, d_{inj} , is plotted over time scaled by t_{conv} in [Figure 5.6](#) along with its time average $\langle L_{lc} \rangle$.

The oscillations of the liquid core length reveal a pulsating movement along the axial direction. Even after $2t_{conv}$, the behaviour of the liquid core is similar for the two models. Only the average length over time $\langle L_{lc} \rangle$ for the $IR7eq$ is 15% greater than for the $5eq$. It can be



(A) *5eq* (top), *IR7eq* (down), $t_{sim} = t_{sim}(1)$.



(B) *5eq* (top), *IR7eq* (bottom), $t_{sim} = t_{sim}(1) + 2t_{conv}$.

FIGURE 5.5: Comparison of the instantaneous liquid volume fraction α_2 on a slice at $\theta=\pi/6 - \alpha_2=1.0$ 0.01.

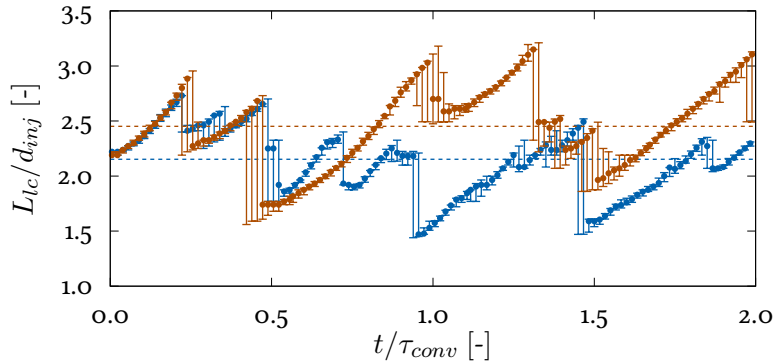


FIGURE 5.6: Model influence on the liquid core length L_{lc} over time and its time average $\langle L_{lc} \rangle$ at isovalue $\alpha_2=0.95\pm 0.04$. *5eq*: \bullet L_{lc} , $--$ $\langle L_{lc} \rangle$ and *IR7eq*: \bullet L_{lc} , $--$ $\langle L_{lc} \rangle$.

interpreted as a quantitative argument attesting of a less-diffusive interface in the case of the *IR7eq*. Nevertheless, putting aside the dissimilarities on the volume fraction, the *IR7eq* does not offer significant improvement compared to the *5eq*.

5.1.5 CASE 3: INSTANTANEOUSLY RELAXED SEVEN-EQUATION MODEL AND NON-INSTANTANEOUSLY RELAXED SEVEN-EQUATION MODEL WITH ATOMIZATION

To better describe the flow in the region close to the interface, it is necessary to increase the disequilibrium of the phases. In the present configuration, a strong velocity gradient occurs at the interface, and the ratio of kinetic energy, $M = (\rho_g v_g^2) / (\rho_l v_l^2)$, is about 3. Physically, the liquid is expected to be accelerated by the gas, but not instantaneously. Therefore it is physically wrong to assume an instantaneous relaxation time for the velocities of the phase.

The same comment can be done on the temperatures. So far in the literature [Saurel and Pantano \(2018\) \[194\]](#), it has been achieved to allow the phases to have their own temperature but always have a common velocity using for example the *5eq*. Even when the *7eq. model* has been used, it was always with an instantaneous relaxation time of the velocities mainly due to numerical difficulties [Furfaro and Saurel \(2015\) \[74\]](#) or the absence of a physical closure for the velocity relaxation parameter. In such case, the *7eq. model* lacks of interest in practice compared to the *5eq*. In this section, we have successfully conducted a simulation of jet atomization with a *non-instantaneously relaxed seven-equation model* with the numerical closure described in [Section 5.1.1](#), with a 10% remaining slip velocity ratio target at each computational time step.

The simulation has run for $2.5 t_{conv}$ attesting the success of the implementation. [Figure 5.7](#) presents the volume fraction of liquid droplets α_d and the norm of the slip velocity of the two-phase flow model $\|\mathbf{v}_d\|$.

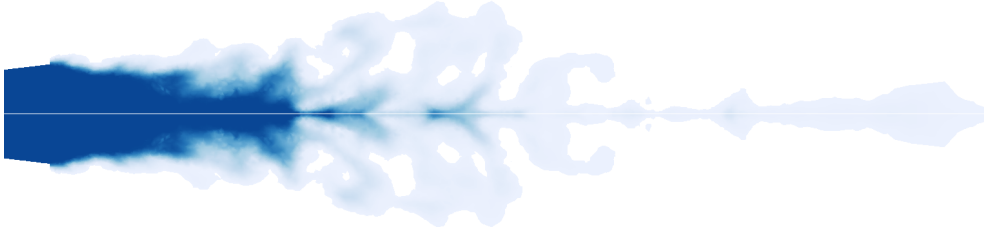


FIGURE 5.7: *NIR7eq* with atomization at $t_{sim} = 2.5 t_{conv}$ on the slice at $\theta = \pi/6$ – blue isovolume of $\alpha_2 = 0.99$, volume fraction of droplets α_d , slip velocity norm $\|\mathbf{v}_d\|$.

The slip velocity is highly concentrated in the interface region, on the so-to-say "gaseous side", where atomization occurs. It permits to give to the atomized liquid droplets the speed of the liquid phase. It is a major gain of accuracy as long as the characteristic time of velocity relaxation is physically well-defined. At the present time, the characteristic time is finite and constant, but it will be revisited in future works to match physical reality.

Finally, a comparison between the *IR7eq* and no coupling and the *NIR7eq* with atomization is proposed hereafter. The reason why the former was not coupled with atomization is due to the fact that the atomization source term $S_{se/sp}$ depends on the existence of a slip velocity \mathbf{v}_d . Nevertheless comparing these two models helps us to verify that the activation of the atomization does not destroy the liquid core. [Figure 5.8](#) compares qualitatively the liquid interface after $1.5 t_{conv}$ simulation time.


Interestingly, the appearance is similar for the two models meaning the atomization process does not interfere with the liquid core, which is what was expected based on the choice of the efficiency coefficients of S_{atom} and S_{coal} . Furthermore the length of the liquid core L_{lc} is also very similar up to the point that the two models show the same time averaged length as emphasized in [Figure 5.9](#).



(A) Atomized *NIR7eq* (top), *IR7eq* (bottom), at $t_{sim}=t_{sim}(1)$.



(B) Atomized *NIR7eq* (top), *IR7eq* (bottom), at $t_{sim}=t_{sim}(1)+1.5t_{conv}$.

FIGURE 5.8: Comparison of the instantaneous liquid volume fraction α_2 , on a slice at $\theta=\pi/6$ – $\alpha_2=1.0$  0.01.

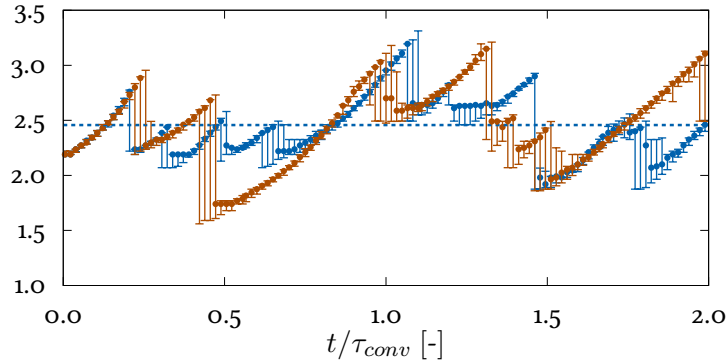


FIGURE 5.9: Model influence on the liquid core length L_{lc} over time and its time average $\langle L_{lc} \rangle$ at isovalue $\alpha_2=0.95\pm 0.04$. *NIR7eq* with atomization $\color{blue}\bullet\text{---} L_{lc}$, $\color{blue}\text{---} \langle L_{lc} \rangle$ and *IR7eq* $\color{orange}\bullet\text{---} L_{lc}$, $\color{orange}\text{---} \langle L_{lc} \rangle$.

5.2 VALIDATION STRATEGY OF REDUCED-ORDER TWO-FLUID FLOW MODELS BASED ON A HIERARCHY OF DIRECT NUMERICAL SIMULATIONS

As seen in the preceding section, diffuse interface models were compared on a challenging real sub-critical cryogenic configuration to prove first their capabilities but also to give a first broad comparison. Nonetheless the limited extend of the comparisons has nourished the need of building a validation strategy to assess the predictivness of those reduced-order models.

As a result, while the mathematical properties of these Eulerian models have been investigated in the previous chapters and are still under current investigations, even the most basic element of the hierarchy of models, that is the Baer-Nunziato model, gives rise to numerical challenges. Since the applications we are seeking are characterized by strong gradients and discontinuities, thus need also to be assessed numerically to highlight their promising predic-

tiveness before being widely deployed in the industry. Even if we eventually want to perform a numerical simulation of the primary atomization by using a Kinetic-Based-Moment Methods (KBMM) modelling the dispersed flow as in [Sibra et al. \(2017\) \[202\]](#) coupled with a hierarchy of diffuse interface models describing the separated phases and the mixed zone, we only focus on the Baer-Nunziato *seven-equation model*. The latter constitutes a very good first candidate for reduced-order simulations and numerical strategy before tackling more recent and refined models and coupling strategies.

Therefore, a hierarchy of specific test cases aiming at reproducing real engine configurations has been selected and reproduced with DNS in order to build an assessment tool to validate sophisticated reduced-order models such as the *seven-equation model*. In [Cordesse et al. \(2020\) \[37\]](#), we have started with an air-assisted water atomization using a coaxial injector, which in addition provides experimental results from the LEGI test bench. The comparison has shown good agreements in terms of liquid core length and important CPU gains between the *seven-equation model* implemented in the CEDRE code and the DNS results obtained with the ARCHER code. It has also shown the limits of diffuse interface models to capture complex liquid structures such as ligaments, rings or deformed droplets and encourages to add a sub-scale description of the interface dynamics through geometric variables such as the interfacial area density, the mean and Gaussian curvatures as proposed in [Cordesse et al. \(2020\) \[39\]](#).

In [Cordesse et al. \(2019\) \[38\]](#), [Cordesse et al. \(2019\) \[42\]](#), we proposed a complementary second test case, an air-assisted water atomization using this time a planar injector rather than a co-axial injector. This planar injector reproduces in terms of Weber and Reynolds numbers the liquid sheet flowing out a swirling atomizer used in agricultural applications [Belhadeff et al. \(2012\) \[11\]](#), $Re_L = 1.5 \cdot 10^3$ and $We_R = 4.0 \cdot 10^2$ and $p = 1 \text{ bar}$. The Reynolds and Weber numbers are also typical of the mid-range aeronautical engines. As we will see, this test case offers also an atomization regime, which makes it complementary with the first test case in order to eventually validate our reduced-order models on a cryogenic coaxial injection.

5.2.1 NUMERICAL METHODS EMPLOYED

5.2.1.1 CEDRE (SEQUOIA) SOLVER

The numerical methods employed to solve the Baer-Nunziato model are implemented in the solver SEQUOIA of the CFD software CEDRE. We do not couple the DIM with a KBBM element as it was done in [Section 5.1](#).

A Strang splitting technique is applied on a multi-slope HLLC with hybrid limiter solver [Furfaro and Saurel \(2015\) \[74\]](#), [Le Touze et al. \(2014\) \[133\]](#) to achieve a time-space second-order accuracy on the discretized equations. The issue encountered when discretizing the non-conservative terms is tackled in [Furfaro and Saurel \(2015\) \[74\]](#) by assuming (1) the interfacial quantities p_I and v_I to be local constants in the Riemann problem, (2) the volume fraction to vary only across the interfacial contact discontinuity v_I . As a result, the non conservative terms vanish, v_I and p_I are determined locally by Discrete Equation Method (DEM) [Saurel et al. \(2003\) \[191\]](#) at each time step and stay constant during the update. Thus, phases are decoupled, the system splits into two conservative sub-systems to which we apply the multi-slope HLLC with hybrid limiter solver.

Depending on the application, the relaxations are assumed either instantaneous or finite

in time. In the present test case, it is reasonable to assume an instantaneous pressure relaxation but one needs to consider a finite velocity relaxation since the interface dynamics is mainly driven by the shear stress induced by a high velocity difference between the phases at the injection.

As already mentioned in [Section 5.1.1](#), to obtain the relaxed pressures, one needs to solve a simple ordinary differential equation (ODE) through a Newton algorithm. As for the velocities, in the present simulation, we have been using the finite velocity relaxation by proposing a closure, which consists in letting at each time step 10% of the relative velocity. This closure is not based on physical considerations and will be revisited in future works.

5.2.1.2 ARCHER SOLVER

As for the DNS, we have used the High-Performance-Computing code ARCHER developed at the CORIA laboratory. It was one of the first code worldwide, undertaking the simulation of liquid-jet atomization under a realistic diesel injection configuration [Ménard et al. \(2007\) \[158\]](#). It solves on a Cartesian mesh the one-fluid formulation of the incompressible Navier-Stokes equation, viz.

$$\partial_t(\rho\mathbf{v}) + \nabla \cdot (\rho\mathbf{v} \otimes \mathbf{v}) = -\nabla p + \nabla \cdot (2\mu\mathbf{T}) + \mathbf{f} + \sigma H\delta_s\mathbf{n} \quad (5.8)$$

where \mathbf{v} is the hydrodynamical velocity vector, p is the pressure field, \mathbf{T} the strain rate tensor, \mathbf{f} a source term, μ the dynamic viscosity, ρ the density, σ the surface tension, \mathbf{n} the unit normal vector to the liquid-gas interface, H its mean curvature and δ_s is the Dirac function characterizing the locations of the liquid gas interface. For solving Equation (5.8), the convective term is written in conservative form and solved using the improved Rudman technique presented in [Vaudor et al. \(2017\) \[216\]](#). The latter allows mass and momentum to be transported in a consistent manner thereby enabling flows with large liquid/gas density ratios to be simulated accurately. The viscosity term is computed following the method presented by [Sussman et al. \(2007\) \[205\]](#). To ensure incompressibility of the velocity field, a Poisson equation is solved. The latter is solved using a MultiGrid preconditioned Conjugate Gradient algorithm (MGCG) [Zhang \(1996\) \[227\]](#) coupled with a Ghost-Fluid method [Fedkiw et al. \(1999\) \[69\]](#) to take into account the pressure jump due to the presence of surface tension.

For transporting the interface, use is made of a coupled Level Set and volume-of-fluid (CLSVOF) solver, in which the Level Set function accurately describes the geometric features of the interface (its normal and curvature) and the VOF function ensures mass conservation. The mixture density is calculated from the VOF (or liquid volume fraction) as $\rho = \rho_l\alpha_l + \rho_g(1 - \alpha_l)$. The dynamic viscosity used (μ_l or μ_g) depends on the sign of the Level Set function. In mixed cells, a specific treatment is performed to evaluate the dynamic viscosity, following the procedure of [Sussman et al. \(2007\) \[205\]](#). The temporal integration is performed through a second-order Runge-Kutta scheme. For more information about the ARCHER solver, the reader can refer to e.g. [Ménard et al. \(2007\) \[158\]](#), [Duret et al. \(2012\) \[64\]](#), [Canu et al. \(2018\) \[20\]](#), [Vaudor et al. \(2017\) \[216\]](#).

5.2.2 FIRST TEST CASE: AN AIR-ASSISTED WATER ATOMIZATION USING A COAXIAL INJECTOR

As part of the validation strategy, the hierarchy of direct numerical simulation test cases starts with an air-assisted water atomization with a coaxial injector and results are presented

hereafter.

The injector at Geophysic and industrial flow laboratory (LEGI) has been the subject of several experiments [Rehab et al. \(1997\) \[185\]](#), [Lasheras and Hopfinger \(2000\) \[128\]](#), [Marmottant and Villermaux \(2002\) \[154\]](#), [Delon et al. \(2018\) \[49\]](#) covering a large range of flow conditions and thus offers experimental data to assess numerical simulations. The present simulations reproduce the experiments conducted by [Delon et al. \(2013\) \[50\]](#), whose results of interests for our study are presented in [Vaudor et al. \(2017\) \[216\]](#) along with the numerical results obtained with ARCHER.

5.2.2.1 DESCRIPTION OF THE LEGI EXPERIMENT

[Figure 5.10](#) renders the simulation configuration which is identical to the experiment of [Delon et al. \(2013\) \[50\]](#) and indicates the velocity profiles at the injector outlets measured experimentally.

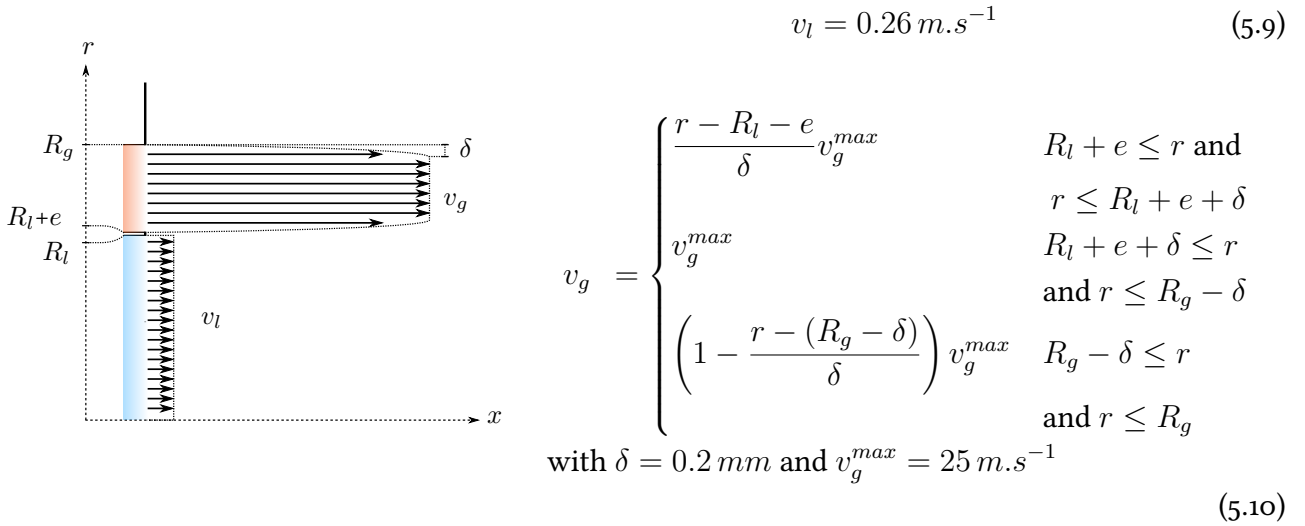


FIGURE 5.10: Injector schematic and velocity profiles.

The inside diameter measures $d_l = 7,6 \text{ mm}$, the outside diameter $d_g = 11,4 \text{ mm}$, the lip length $e = 0.2 \text{ mm}$. The gas velocity profile v_g given in Equation (5.10) models the boundary layer measured experimentally with δ the boundary layer thickness and v_g^{max} the maximum gas velocity.

The fluid properties, type, density ρ , capillarity coefficient σ and viscosity coefficient μ of each fluid are summarized in [Table 5.2](#).

TABLE 5.2: Physical properties of water and air.

	Phase	$\rho \text{ (kg.m}^{-3}\text{)}$	$\sigma \text{ (N.m}^{-1}\text{)}$	$\mu \text{ (1e}^{-5}\text{ Pa.s)}$
Liquid (<i>l</i>)	<i>H</i> ₂ <i>O</i>	1000	0.0072	1002
Gas (<i>g</i>)	<i>Air</i>	1.226		17.8

Let us define and compute the following flow parameters. Re_l is the liquid Reynolds number, Re_g is the gas Reynolds number, M the momentum flux ratio, We_l the liquid Weber Number, We_g the gas Weber Number and We the aerodynamic Weber number. They are defined as follows

$$Re_l = \frac{\rho_l v_l d_l}{\mu_L} = 1972, Re_g = \frac{\rho_g v_g (d_g - d_l - 2e)}{\mu_G} = 5854, M = \frac{\rho_g v_g^2}{\rho_l v_l^2} = 11, \quad (5.11a)$$

$$We_l = \frac{\rho_l v_l^2 d_l}{\sigma} = 7, We_g = \frac{\rho_g v_g^2 (d_g - d_l - 2e)}{\sigma} = 36, We = \frac{\rho_g v_g^2 d_l}{\sigma} = 81. \quad (5.11b)$$

The Weber numbers are relatively high, inferring the surface tension should not play a crucial role in the dynamics of the flow. For the present configuration, there exists a break-up regime map established by [Lasheras and Hopfinger \(2000\)](#) [128], reported in [Figure 5.11](#). The red dot

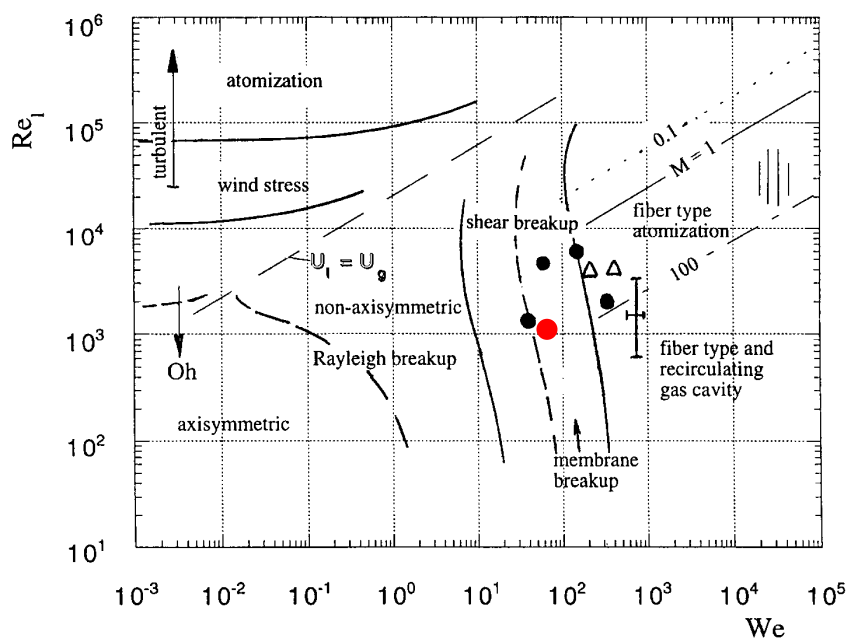


FIGURE 5.11: Break-up regimes in the parameter spaces $Re_l - We$ [Lasheras and Hopfinger \(2000\)](#) [128] - LEGI ●

of coordinates ($Re_l = 1972, We = 81$) locates the investigated flow in the shear breakup zone in [Figure 5.11](#). We should not expect atomization of the liquid jet and therefore the atomization is not activated in CEDRE.

5.2.2.2 NUMERICAL SET-UP

The ARCHER simulations are performed on a Cartesian mesh $1024 \times 512 \times 512$ with a cell size equal to $\Delta x = 6.68 \cdot 10^{-5}$, so a total of 806 millions of faces whereas CEDRE mesh is composed of 278 978 tetrahedral cells. The mesh is composed of 563 116 faces.

To be comparable to the DNS, two difficulties must be tackled. Firstly, the DNS uses an incompressible solver meaning the acoustic is not solved and thus does not interact with the liquid jet and the density remains constant. Secondly, the boundary conditions imposed on the wall of the DNS box do not let any flow backwards such that no wall effect acts upon the liquid

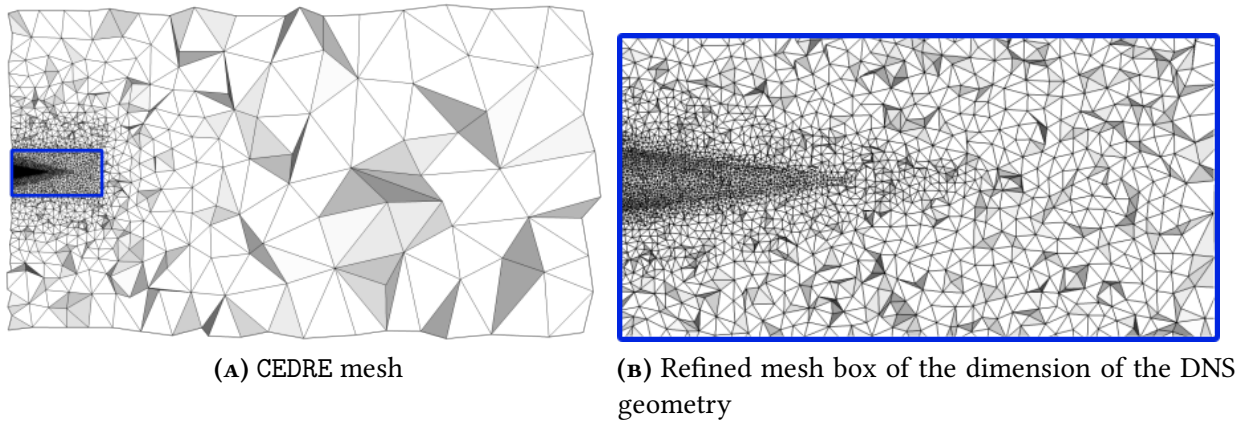


FIGURE 5.12: CEDRE mesh of the configuration

core. Therefore, to eliminate reflected acoustic waves and wall effect on the liquid jet, we have designed an outer box with a coarsening mesh as shown in [Figure 5.12](#). The smallest cell is located at the lip of the injector and measures $\Delta x = 2.0 \cdot 10^{-4} \text{ m}$. As for the thermodynamics, CEDRE uses two Stiffened-Gas equations of state and thus the temperature of the phases has been modified to obtain the same initial pressure and density conditions as in [Table 5.2](#).

The simulation information is summarized in [Table 5.3](#). Remarkably, when considering

TABLE 5.3: Simulation costs

	Simu Time (<i>s</i>)	N_{proc}	Total CPU (<i>h</i>)
CEDRE	0.160	420	$2.14 \cdot 10^4$
ARCHER	0.500	8192	10^7

the same simulation time, the total CPU is 150 times greater than for ARCHER than for CEDRE.

5.2.2.3 QUALITATIVE COMPARISON

We propose to compare the liquid jet obtained with ARCHER and CEDRE at given simulation time. The Level Set function of the DNS permits an exact reconstruction of the interface whereas for the diffuse interface model, the interface lays in the region where the volume fraction varies from $\alpha \approx 0$ to $\alpha \approx 1$. Consequently, in [Figure 5.13](#) we have superimposed the solved interface of the DNS to a volume rendering of the liquid volume fraction and a single liquid volume fraction isosurface. We distinguish two regions: close to the injector, on the first half of the DNS box, the diffuse interface model is able to match accordingly to the DNS results. In this region, the mesh used by CEDRE prevents the interface to diffuse too much for the diffuse interface model and the interface of the DNS lays in the volume rendering of the liquid volume fraction of CEDRE. On the second half of the DNS box, where the DNS shows complex liquid structures such as rings, droplets and ligaments, the diffuse interface model is not able to capture these effects since the mesh is coarsened and the volume fraction alone is not sufficient to describe such complex interface dynamics. Nevertheless, the *seven equation model* diffusion zone accords well with the DNS, the red cloud which corresponds to a low liquid volume fraction is limited to the zones where liquid elements of the DNS exist.

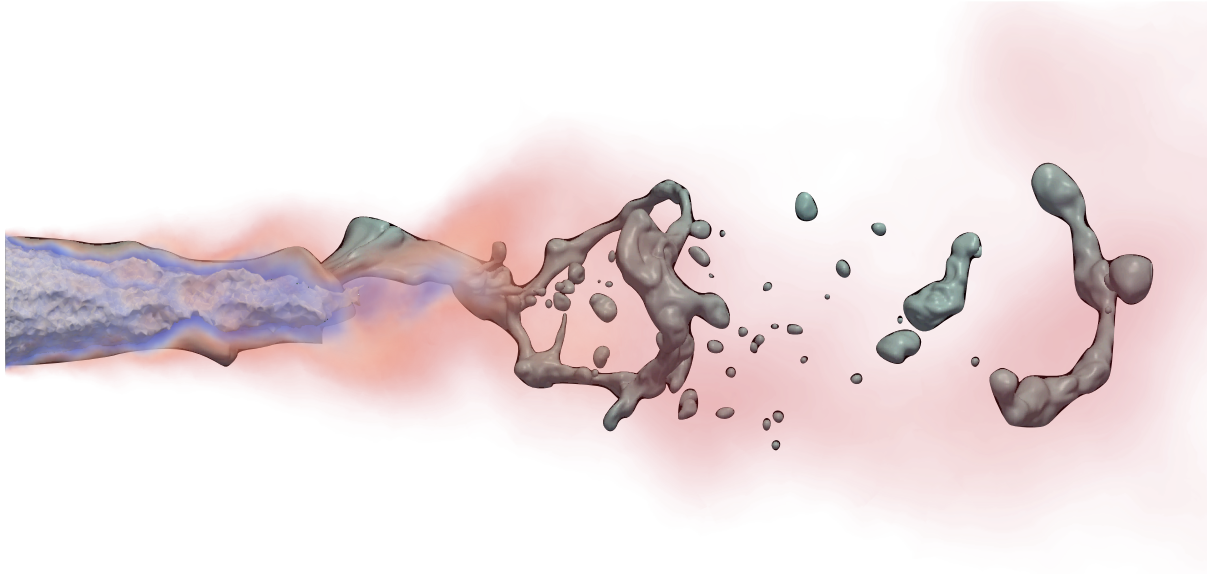



FIGURE 5.13: Instantaneous liquid core comparison. CEDRE: volume rendering of the liquid volume fraction, α_l high  low, grey isosurface $\alpha_l = 0.99$. ARCHER: Grey isovolume of liquid volume fraction $\alpha_l = 1$

This comparison gives an interesting interpretation of the diffuse interface models. The volume fraction is not enough to reconstruct the whole dynamics of the interface but attests the presence or the absence of liquid.

5.2.2.4 QUANTITATIVE COMPARISON

The liquid core is defined as the region of the liquid jet that is always occupied by liquid. To obtain it, a time-averaging of the liquid volume fraction is needed. To compare the liquid core obtained with CEDRE, we need to eliminate the transient phase during which the liquid jet is not established. Figure 5.14 plots the instantaneous liquid jet length L_{lc} over time for several α_l .

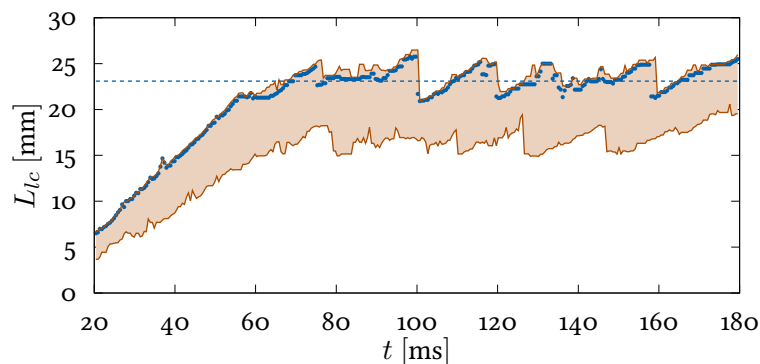


FIGURE 5.14: Instantaneous liquid jet length L_{lc} over time at iso-value $\alpha_2 \in [0.91, 1 - 2\epsilon]$, \bullet iso-value $\alpha_2 = 0.99$, --- $\alpha_2 = 1 - 2\epsilon$ (bottom) and $\alpha_2 = 0.91$ (top), --- $\langle L_{lc}(\alpha_2 = 0.99) \rangle$ for $t > 60 \text{ ms}$, $\hat{O}\epsilon = 1e - 6$.

For $t > 60 \text{ ms}$ the liquid jet length starts to oscillate around a time averaged value which equals $\langle L_{lc}(\alpha_2 = 0.99) \rangle = 23 \text{ mm}$. We then computed the time average liquid volume fraction

between $t_{sim} \in [60, 160]$ *ms* to obtain the liquid core shown in [Figure 5.15](#). The liquid core of

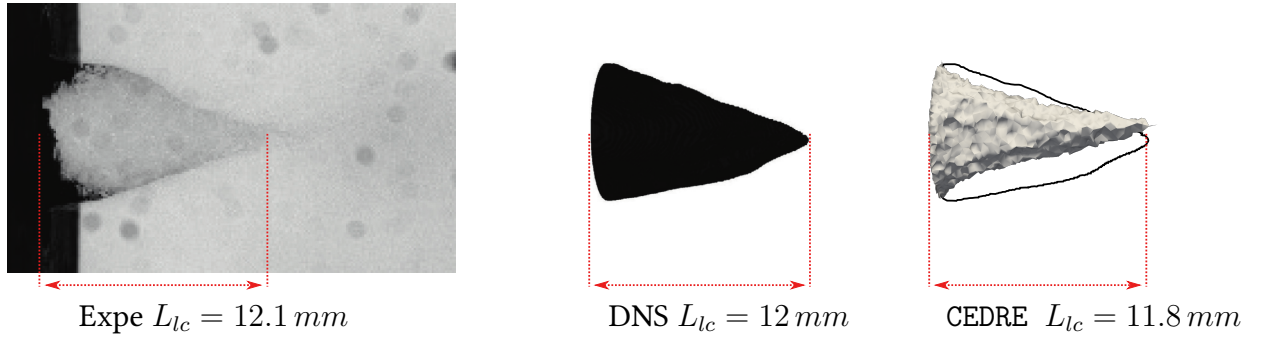


FIGURE 5.15: Liquid core comparison - from left to right: experiment, DNS, CEDRE and DNS. CEDRE liquid core is the isovolume at $\langle \alpha_l \rangle = 1 - 2\epsilon$, with $\langle \alpha_l \rangle$ the time averaged liquid volume fraction and $\epsilon = 1e-6$ residual volume fraction.

the diffuse interface model was identified as the isovolume of $\alpha_l = 1 - 2\epsilon$, where $\epsilon = 1e-6$ is the residual volume fraction. The reason for not choosing $\alpha_l = 1 - \epsilon$ holds to the fact that due to numerical diffusion in a unstructured mesh and mesh interpolation, the volume fraction in single phase region does not stay at the initial value $\alpha_k = 1 - \epsilon$.

Experimental, DNS and CEDRE values show the same trend. We also could have compared the angle of the spray, but for the diffuse interface model, the result depends highly on the threshold chosen for the liquid volume fraction.

5.2.3 SECOND TEST CASE: AN AIR-ASSISTED WATER ATOMIZATION USING A FLAT INJECTOR

5.2.3.1 DESCRIPTION OF THE CONFIGURATION

We propose in this subsection the study of the atomization of an air-assisted flat liquid sheet at high Reynolds and Weber number. The reason for choosing this test case is twofold: first it makes a complementary test case to the air-assisted coaxial atomization analyzed in the previous subsection in terms of injection type while still offering an atomized regime, second while the Reynolds and Weber numbers are farther away from cryogenic applications, they still are typical from the mid-range aeronautical engines.

Assisted liquid sheet atomization Atomization of air-assisted flat liquid sheets have been widely experimentally investigated such as in [Lozano et al. \(2001\) \[147\]](#), [Carvalho et al. \(2002\) \[21\]](#) and [Dumouchel \(2008\) \[61\]](#). The behavior of such flow is mainly driven by several parameters. The ratio of the norm of the gas velocity and the liquid velocity, v_g/v_l , and the momentum flux ratio M are predominant to determine the breakup regime. Then the width of liquid injection, d_l and the relative gaseous Weber number, We_R , influence also the breakup length, the breakup frequency and the liquid sheet vibrating frequency [Dumouchel \(2008\) \[61\]](#). Other flow parameters, that are used for liquid atomization of cylindrical jet can be adapted as well, such as the liquid Reynolds number, Re_l and the liquid Weber Number, We_l .

However, they are less important for air-blast atomizer because, for high momentum ratio M , the effect of the dynamics of the liquid jet is very low. The atomization process is then mostly

driven by the shear that is induced by high gas velocity with respect to the liquid velocity. On the contrary, the dynamics of the gaseous flow is determinant in particular in the vicinity of liquid-gas layer. Thus, the gas longitudinal velocity profile normal to the issued liquid-gas surface is determinant for the development of the first instabilities [Lozano et al. \(2001\) \[147\]](#). For experiments, it is of primary importance to characterize the gas boundary layer that depends on the geometry of the air-blast injector upstream of the injection location. From these initial Kelvin-Helmholtz-types of instability, if the liquid thickness is small, a coupling occurs between instabilities on both sides of the liquid sheet leading to the flag effect. From this feature shared by most of liquid sheet atomization systems based on air blast, several processes are involved in the disintegration of the liquid sheet. For instance, the liquid sheet flapping induce variation of the liquid thickness. In the stretched part, this thinness can induce perforation of the liquid sheet leading to the emergence of a hole surrounded by a liquid rim. The accumulation of liquid within these rims or in other part of the liquid sheet under the effect of surface tension can create ligaments, which are finally destabilized by Raleigh-Plateau-types of instability. In many industrial applications, to reach high injection rate with an efficient atomization, the flow conditions are such that turbulence is induced at least in the gas flow. The turbulent nature of the two-phase flow complicates then the previously described instabilities adding a transient stretching effect and a possible collision between liquid elements. This is where the numerical simulation of the entire flow is supposed to help the design of injection systems. Accordingly, the numerical test case has been designed to be as close as possible of these typical conditions. The limitation comes from the mesh resolution that should be fine enough to capture most of these phenomena.

To design the appropriate test case we refer to previous study that have classified break-up mechanism with respect to velocity ratio ([Lozano et al. \(2001\) \[147\]](#), [Carvalho et al. \(2002\) \[21\]](#)). At low speed ratio, the liquid sheet oscillates with a potential low amplitude growth of the liquid core. Moreover the atomization happens following streamwise and spanwise ligament break-up and the spray angle is particularly low. It is called the *cellular breakup regime*. This regime would be very challenging for computation requiring a very long computational domain together with high mesh resolution to capture the decreasing liquid thickness. Then at medium ratio, vorticity becomes more important and the breakup is controlled by streamwise structure of liquid detaching from the principal liquid core. The high amplitude of the sinusoidal wave induces a high spray angle. This is the *streamwise ligaments breakup* [Stapper and Samuelsen \(1990\) \[204\]](#). Finally, very high v_g/v_l brings to a complete and immediate disintegration of the liquid sheet. In [Dumouchel \(2008\) \[61\]](#), the authors also observed that high relative velocity usually leads to strong sinusoidal oscillations of the liquid flow inducing an high spray angle and short sheet breakup length, called *flag-effect* [Dumouchel \(2008\) \[61\]](#).

These last two observations indicate that a high velocity ratio is suitable to promote an efficient atomization with a quite large spray angle in order to reduce the required length of the computational domain. High velocity ratio also increase the momentum ratio which is beneficial to reduce the liquid core length at least in cylindrical liquid jet atomization [Lasheras et al. \(1998\) \[129\]](#), [Porcheron et al. \(2002\) \[175\]](#), [Leroux et al. \(2007\) \[134\]](#). In addition, having high velocity and momentum ratio will lead to simulation that is closer to most industrial application. The limitation comes from the turbulence that leads to smaller length scale as the Reynolds increasing. Similarly, it is expected that the final droplet sizes decrease as the velocity ratio increases leading to higher Weber number. It has been chosen not to inject turbulent fluctuations of velocity at the inlet, though this may seem less realistic for real applications,

it allows to more deterministic comparison between numerical approaches and postpones slightly the creation of smallest length scales. Finally, the density ratio has to be high enough to ensure a realistic representation of a liquid and a gas phase that is typically of a thousandth for air and liquid water at atmospheric pressure. However, less is the density ratio less is the interaction between phases again leading to a less efficient atomization. At least, in engines very often the gas is pressurized leading to density ratio of the order of a hundredth. Based on these principles, the present configuration has been set by adjusting flow parameters in order to promote a fast atomization, limit the liquid core penetration and having a density ratio realistic for aircraft engines. A reasonably high momentum $M = 18.7$ is obtained with a moderately high speed ratio, $v_g/v_l = 43$ and a density ratio $\rho_g/\rho_l = 1/100$. To reduce the role played by the surface tension, since it is not solved by the diffuse interface model, we have chosen a high relative gaseous Weber number, $We_R = 403$. As we will see in the results, we obtain a regime resembling the *streamwise ligaments breakup*, with a short liquid core, ligaments and an atomized spray.

Geometry and description of various meshes The simulated domain described in [Figure 5.16a](#) shows the boundary conditions of the simulation. ① is the liquid injection plan, ②

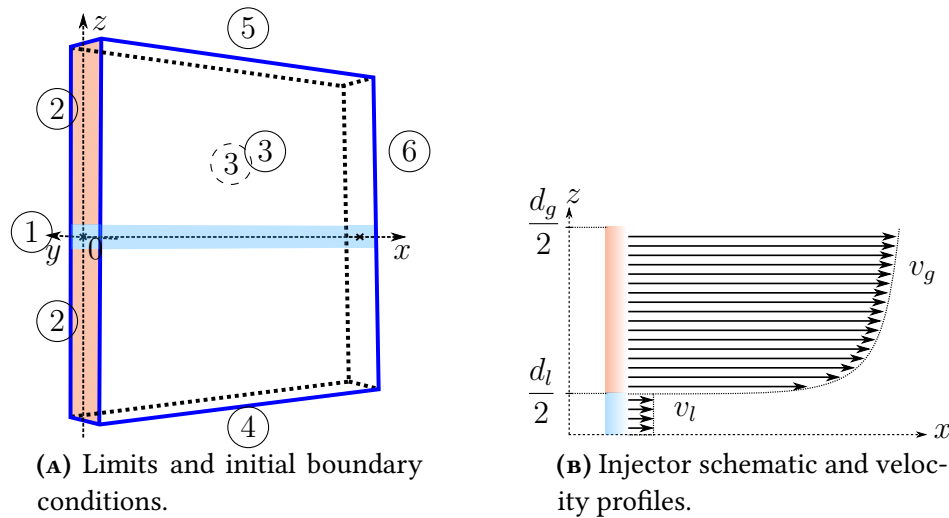


FIGURE 5.16: Geometry, limits and boundary conditions of the configuration.

is the gas injection plan, ③ and ③̄ are periodic planes, ④, ⑤ and ⑥ are outflow plans. The liquid injection height, d_l , the gas injection height, d_g , the x-y-z length of the box, L_x, L_y, L_z , are given in [Table 5.4](#).

[Figure 5.16b](#) defines the velocity profile of the gas and the liquid, which are symmetric with respect to the x-axis and y-invariant. The gas velocity profile v_g given in Equation (5.12) is typical for turbulent pipe flow [Schlichting \(1979\) \[196\]](#).

$$v_g = v_g^{avg} \frac{7}{6} \left(\frac{2|z| - d_l}{d_g - d_l} \right)^{\frac{1}{6}} + v_l. \quad (5.12)$$

The average gas velocity v_g^{avg} is 65 m/s . An offset equal to $v_l = 1.5 \text{ m/s}$ ensures the continuity of the velocity profile at the injection plan. The domain is initially filled with a liquid sheet in the x-y plan, as thick as the liquid slit as shown in [Figure 5.16a](#). [Table 5.4b](#) states the fluid properties in terms of density ρ , surface tension coefficient, σ , and viscosity, μ .

TABLE 5.4: Dimensions and physical properties of the configuration.

(A) Dimensions					
units	d_l	d_g	L_x	L_y	L_z
(mm)	1	16	16	4	16

(B) Fluids physical properties				
Phase	ρ (kg/m ³)	p (MPa)	σ (N/m)	μ (Pa.s)
Liquid	100	0.1	0.01	0.0001
Gas	1	0.1	0.01	0.0001

The ARCHER simulations are performed on a Cartesian mesh $512 \times 128 \times 512$ with a cell size equal to $\Delta x = 3.125 \cdot 10^{-5} m$, so a total of 101M faces, 33.6M cells and 32 cells in the liquid slit. In terms of degrees of freedom, which is defined as the product of the number of variables solved and the number of cells, ARCHER solves 42.0M. CEDRE simulations have been performed on two meshes composed of tetrahedral cells. The first, referred later on as CEDRE (MR), proposes a medium refinement level with 148k faces, 71.7k cells and 788k degrees of freedom, and the second, referred later on as CEDRE (HR), a high refinement level with 1.11M faces, 546k cells, thus 6.01M degrees of freedom. CEDRE (MR) has only 10 cells in the slit, while CEDRE (HR) has 20 cells. The data are summarized in [Table 5.5](#). In terms of degrees of freedom,

TABLE 5.5: Mesh statistics of the three simulations.

	Face number	Cell number	$\min(\Delta x)/d_l$
CEDRE (MR)	0.148M	71.7k	10
CEDRE (HR)	1.11M	546k	20
ARCHER	101M	33.6M	32

there is a factor 7.6 between the two CEDRE simulations, and similar factor, 7.0, between the high refined CEDRE simulation and the DNS. The three simulations all together encompass thus a large level of refinements.

In order to compare the results of the DNS to the results obtained with CEDRE, one must consider the fact that the DNS solver is incompressible, thus there is no acoustic impacting the liquid sheet and its density is constant. To restrain the acoustic role in the CEDRE compressible solver, we have enlarged the computational domain by a factor 5 in the x and z direction and meshed it with a very coarse mesh to avoid any reflecting waves as shown in [Figure 5.17](#). The minimum cell size is located along the liquid slit as one notices on [Figure 5.17b](#).

Furthermore the use of a compressible thermodynamics in CEDRE through the Stiffened-Gas equation of state makes it impossible to maintain the liquid density constant. The temperature of the phases have been modified to obtain the same initial pressure and density conditions as in [Table 5.4b](#) and in practice, the liquid density almost stays constant as shown on [Figure 5.18](#).

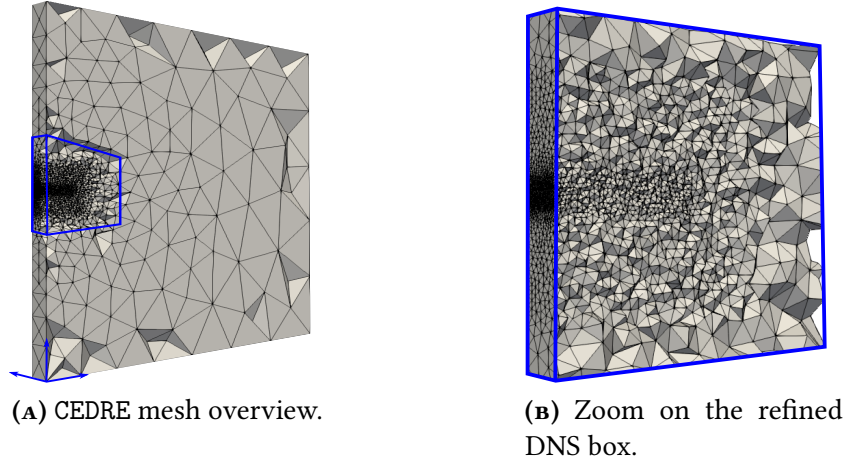


FIGURE 5.17: Clip of the CEDRE mesh on the plane $y = 0$ but keeping whole elements.

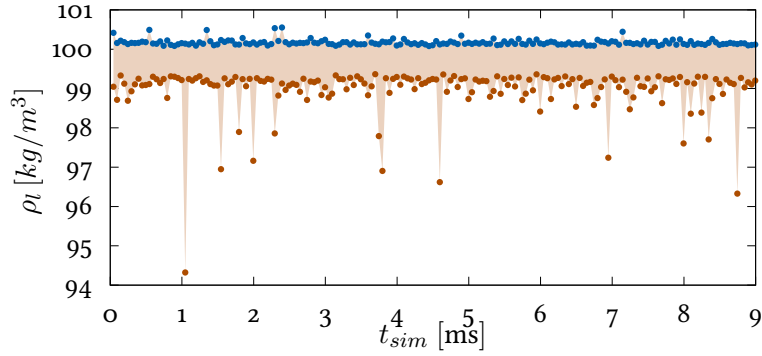


FIGURE 5.18: CEDRE (MR) instantaneous liquid density ρ_l over time, ● maximum value, ● minimum value.

The convection time t_{conv} of the system is defined as $t_{conv} = L_x/v_l$. The liquid is quickly accelerated and flows at an averaged speed of $v_l \approx 15 \text{ m/s}$ at $x = 3 \text{ mm}$ as we will see in the results in [Figure 5.28c](#). Hence the convection time approximately equals $t_{conv} \approx 1 \text{ ms}$. The minimum simulation time of the three simulations is 8 ms , which corresponds to approximately height convective times, yielding a priori satisfying statistical convergence for each simulation. The simulation information are summarized in [Table 5.6](#). The total CPU cost is defined as

TABLE 5.6: Simulation time and costs comparisons.

	Total t_{sim}	CPU cost for $t_{sim} = 9 \text{ ms}$ [h]	Degrees of freedom
CEDRE (MR)	18	$8.54 \cdot 10^3$	0.788M
CEDRE (HR)	10.5	$69.3 \cdot 10^3$	6.01M
ARCHER	14	$245 \cdot 10^3$	42.0M

the product of the number of processors, N_{proc} , times the computational time for a given simulation time, t_{sim} . The three simulations have not run in overall the same amount of simulation time, due to time, resource and statistical convergence constraints. Therefore, only partial comparison in terms of CPU costs can be proposed. For $t_{sim} = 9 \text{ ms}$, we see that

ARCHER is 3.5 times more costly than CEDRE (HR), the latter being 8.1 times more costly than CEDRE (MR). However, as we will see in the results, time simulation needed to gain statistical convergence differs from one simulation to another. In overall CEDRE offers quicker stastical convergence than ARCHER with a significant reduction of degrees of freedom, highlighting again the interest of reduced-order model simulations for industrial configurations.

Before moving on to the analyses and discussions of the results obtained with the DNS and the diffuse interface model, [Figure 5.19](#) offers a global overview of the simulations performed with ARCHER and CEDRE. On the left hand side of [Figure 5.19](#), we have drawn a volume rendering of the liquid volume fraction α_l obtained with the CEDRE (HR) simulation. On the right hand side is shown the level set solved by ARCHER, indicating the position of the interface.

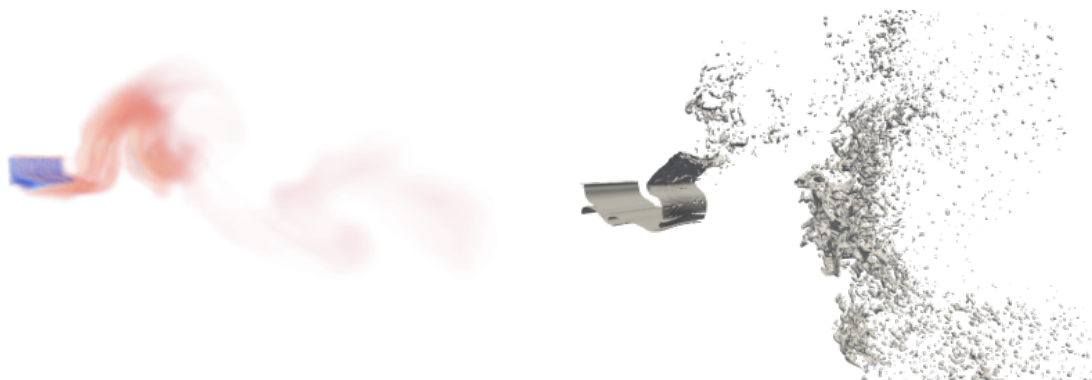



FIGURE 5.19: Instantaneous overview of the simulations: volume rendering of the liquid volume fraction, α_l high  low (CEDRE (HR) - left) and level set in grey (ARCHER - right).

We propose now a qualitative and quantitative comparison of the results of the simulations performed with CEDRE and ARCHER in order to, first, understand the behavior of each numerical method, second, emphasize the main conceptual differences between them and, finally, evaluate to which extent CEDRE reduced order model is predictive and why is it departing from the DNS results.

This section is organized as follows: we start by assessing the DNS reliability to identify the most relevant region where the DNS can stand as a trustworthy benchmark. Then, we provide a comparison of the atomization global characteristics obtained by each simulation through the volume fraction time evolution and averaging. We further detail the comparison with statistical analyses of the flow through first and second order moments based on the liquid volume fraction and velocities.

5.2.3.2 IDENTIFICATION OF THE DNS REGION OF VALIDITY

Since the DNS results have to be reliable to assess the predictiveness of the reduced order model, an analysis of the IRQ_K criterion described in [Anez et al. \(2019\) \[4\]](#) is first performed. This indicator, based on the mean curvature, has been used in several studies to assess the quality of the resolution [Canu et al. \(2019\) \[19\]](#). The main advantage of this criterion is to evaluate the quality of complex configuration simulations, such as the present one, without running the simulation with several levels of mesh resolution to achieve a proper mesh convergence study. This criterion is defined as $IRQ_K = 1/(\Delta x^2 H)$, where Δx is the grid size and H the mean curvature. This criterion highlights the under-resolved regions of the simulation

where its value diminishes. For instance, a droplet described with 4 mesh cells along its radius has an $IRQ_K = 2$. Therefore, the lower the IRQ, the lower the resolution of the liquid (or gas) structure highlighted. Note that the threshold value of 2 chosen here is arbitrary and the user is expected to choose a value that is the most adequate to a given simulation. Instead of investigating the individual IRQ_K for each structure, the IRQ_K PDF can be studied to obtain a better picture of the resolution level of the overall simulation.

In this work, the IRQ_K is extracted from two specific regions of the jet: in the main liquid core, where the criterion should behave perfectly since most wrinkling of the interface is expected to be captured, and in the most critical secondary atomization region, where liquid structures encounter fragmentation/breakup processes that can lead to under-resolved liquid structures. These two regions of interest are illustrated in [Figures 5.20a](#) and [5.20b](#).

The PDF of IRQ_K , shown in [Figures 5.20c](#) and [5.20d](#), gives useful information about the quality of the simulation. In the first region of the liquid sheet, most of the IRQ values of the PDF (around 95%) are located beyond the critical zone of low IRQ, $IRQ_K \in [-2 : 2]$, as shown in [Figure 5.20c](#): this range is indicated by two red dotted lines in the figure. As expected, the resolution is sufficient here to describe the main physical phenomena such as instabilities on the liquid surface and the flapping mechanism. However, in the second region, the PDF is compressed close to the critical IRQ_K zone, hence only around 60% of the interface is well resolved ([Figure 5.20d](#)). It indicates that the DNS results should be taken with caution for large x^* . This can be explained by the production of droplets of small scale due to atomization of the flapping sheet. Note that this kind of simulations at high Weber and Reynolds numbers are quite challenging in term of computational costs, explaining the difficulty to reach higher IRQ in the most atomized or dispersed region. Besides, we specifically have chosen two different regions with opposite behavior to assess the pertinence of the criterion.

Consequently, the DNS appears sufficiently trustworthy until the jet become more dispersed, due to the presence of very small droplets. In addition, in the present work, CEDRE simulation has not been coupled with any specialized reduced-order model, such as KBMM, to better describe the dispersed flow. It is unlikely the diffuse interface model alone will capture properly this part of the flow. The whole analysis will therefore be conducted in the zone $x^* \in [0 - 4]$ along the streamwise axis.

5.2.3.3 EVALUATION OF THE ATOMIZATION GLOBAL CHARACTERISTICS OF BOTH NUMERICAL APPROACHES

To begin with, we would like to evaluate broadly the macroscopic features of the investigated flow. We first analyze the time evolution of the liquid volume fraction in order to reveal the expected flag effect mentioned in [Section 5.2.3.1](#). Then we interest ourselves to the liquid core penetration as it is usually a key feature measured in experiments.

Time evolution [Figure 5.21](#) shows the temporal evolution of the liquid volume fraction obtained with the interface capturing technique (left) and the diffuse interface model (right). The time-frame starts at a given simulation time $t_{sim} = t_0$ with a δt frame rate and stops after nine iterations.

In the first place some inherent properties linked to these numerical methods are clearly observable: results obtained with the CLSVOF method exhibit a sharp interface between liquid

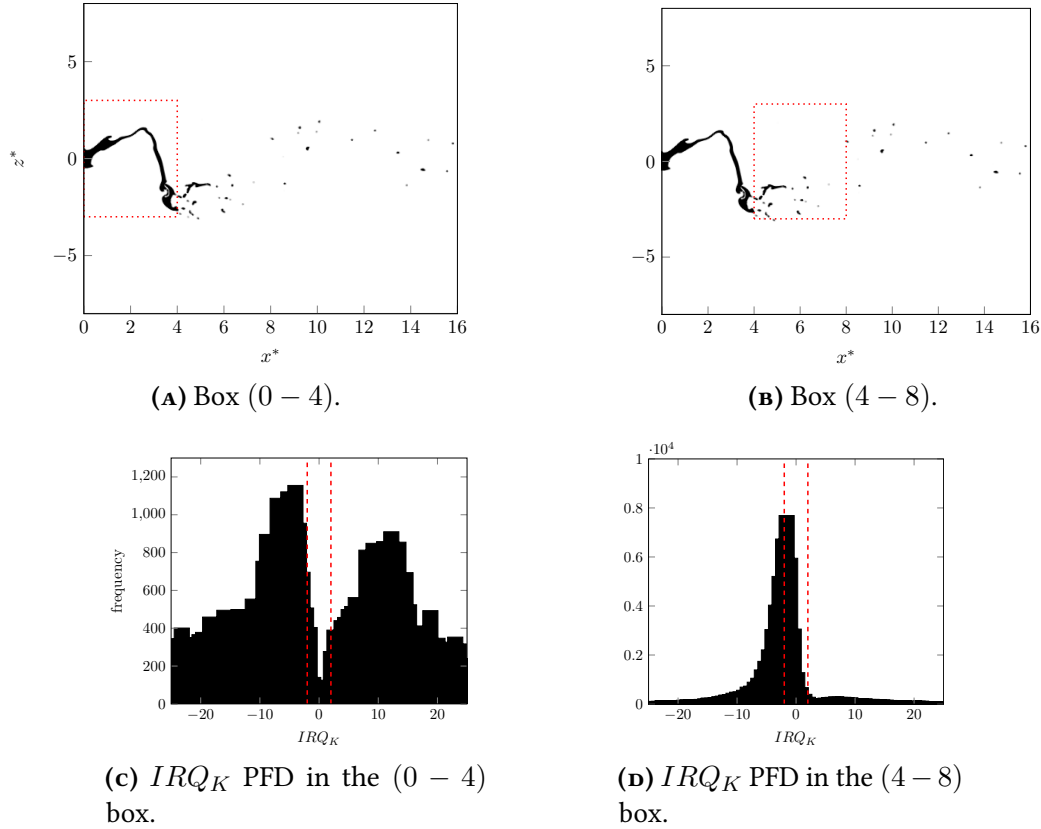


FIGURE 5.20: IRQ_k PDF analysis at time $t = 12\text{ ms}$ (bottom), in two regions identified by the red dashed rectangles drawn on the plan $y^* = 0$ showing liquid volume fraction α_l (top).

and gas, i.e. a one cell transition between $\alpha_l = 0$ or $\alpha_l = 1$ at the interface. On the contrary, the liquid volume fraction obtained with the seven equation model allows a wide range of α_l to be found across the interface. Consequently, a smooth transition between liquid and gas can be observed.

When comparing the instantaneous snapshots, the local representation of the interface is clearly different due to the intrinsic modeling gap between a sharp and a diffuse interface modeling. Nevertheless, these differences are less obvious when considering that the diffuse interface approach may be interpreted in terms of some statistical probability to find the liquid phase, i.e. 0.5 value of liquid volume fraction does not actually mean that there is actually 50% of liquid phase and gas phase but that pure liquid may be found there with a probability of 50%.

Focusing on large scale motions, [Figure 5.21](#) reveals a sinusoidal flapping. Measuring this flapping frequency could be done by Fourier transform of a signal characteristic of the flapping varying over time. However, while this procedure is conducted in experiments since operators can record the signal in time for a large number of flapping, it is nonetheless hardly applicable to the present numerical simulations including only few flapping events. Instead, we have chosen an arbitrary initial time t_0 at which both simulations are synchronized. The global flapping evolution of both numerical approaches are much the same inferring that, despite the different representation of the interface, the liquid sheet flapping frequency is similar. One may have also noticed at the end of [Figure 5.21](#), that both simulations exhibit a transient regime

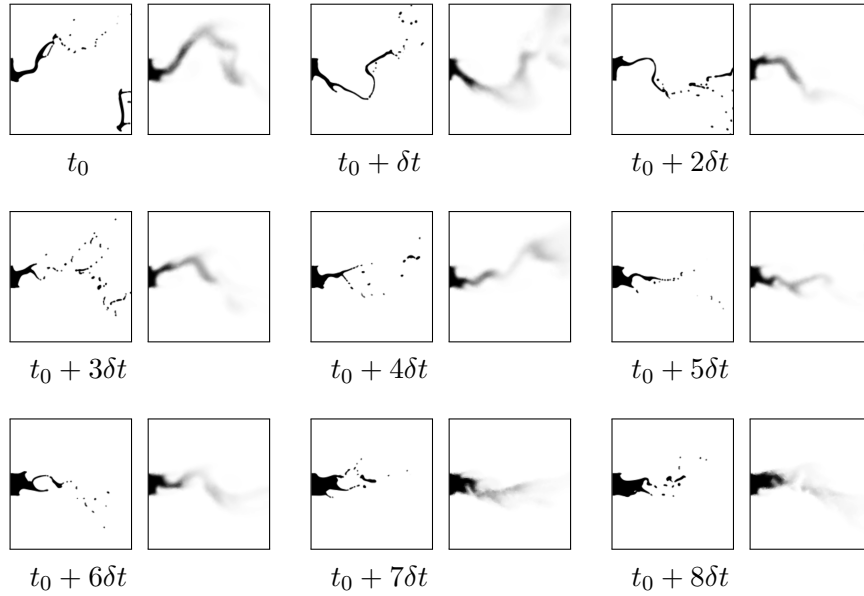



FIGURE 5.21: Time lapse of liquid volume fraction near the injector, $\alpha_l = 0$ . Left: ARCHER, right: CEDRE. We define t_0 as the starting time and δt as the time step.

during which we observe compaction of the thin flapping liquid sheet starting to be thicker and shorter. Then the liquid sheet stretches again at the very end of the time-lapse for both simulations.

Liquid core penetration One key quantity in the study of liquid injection is the liquid penetration length. For transient injection, for which no liquid is initially present, the liquid spray grows from the injector outlet and penetrates into the chamber. The liquid core penetration length is then easily obtained at the first break-up event. Since the present case focuses on the established state of the flow, we cannot monitor such event. Worst, the flow has undergone multiple break-ups through time and the spray has reached the outlet of the computational domain. Experimentally, some apparatus may give a picture of the spray with high contrast between a zone where the spray is present and a zone where there is nearly no liquid and average it over time. Since this procedure is hard to apply on numerical simulations, we choose to study the time averaged liquid volume fraction, $\langle \alpha_l \rangle_t$, along the streamwise direction (x -axis) in [Figure 5.22](#).

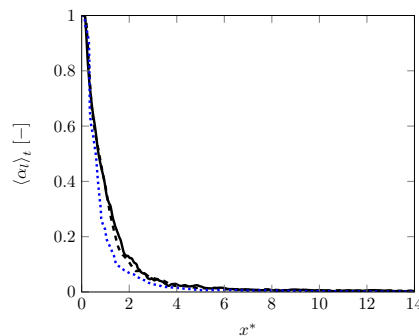


FIGURE 5.22: Averaged liquid volume fraction $\langle \alpha \rangle_t$ along streamwise axis. — ARCHER, - - - CEDRE (HR), - - - CEDRE (MR).

The liquid profile along the axis obtained by the DNS ranges from unity close to the injector slit towards zero further downstream, once atomization and dispersion have occurred. The high resolution profile CEDRE (HR) of the diffuse interface model matches nicely the DNS data. It is a noticeable result that despite of the difference on the representation of the interface the evolution of the liquid concentration is accurately captured. The CEDRE (MR) profile on the contrary shows a certain discrepancy with the reference DNS result. This suggests a correlation with the mesh resolution, which can be explained as follows: the diffuse interface approach integrates a part of the interface statistics by representing the phase transition by a smooth function rather than by a discontinuity as for the DNS. The diffuse interface model contains thus an underlying averaging procedure related to the mesh resolution, causing the observed discrepancy with the medium refined mesh.

Discussion on small-scale representations Turbulence is intrinsically impossible to be reproduced and thus to be predicted locally in space and time by simulations. Accordingly, only statistical characteristics of turbulent flows can be predicted. With this in mind, DNS simulation has the meaning of a numerical procedure that can be used directly without any modeling assumptions to generate flow samples having the same statistical characteristics as the real investigated flow, such as the averaged velocity. DNS instantaneous results can not be considered as the true realization of the flow, but rather possible realizations. Our understanding of turbulence in liquid-gas flow and in particular for this test case is not complete, but it may be a reasonable hypothesis that the unpredictable characteristics are present. It is even possible that the complex interaction between phases across the interface enforce the unpredictability of the exact flow. Thus, it is possible to expect that a small perturbation of the DNS can lead to a significant position change of some droplets later on.

On the contrary, as explained in [Figure 5.21](#), the diffuse interface model makes explicit this non-determination of the interface real position by estimating the probability of the interface presence in each cell. The diffuse interface approach is then potentially representing correctly the real flow, but it is highly relying on the closure of the models, such as the velocity relaxation time introduced in Equation (5.2) or the interfacial pressure and speed.

To conclude, on these preliminary comparisons, while the two models show a very different representation of small-scales due to the distinct interface modeling, large-scale motions seems reasonably in good agreements and sufficient to recover global features of the atomization process such as liquid penetration and spray angle.

Beyond the global characteristic of the atomization, numerical simulations give also access to more complete data set of results. In particular, for this established flow, the time averaging procedure provides local statistics of the flow. The following part is thus dedicated to statistical analysis of results obtained by diffuse interface method compared to the reference DNS data. To ensure a fair comparison the domain is limited to the well-resolved part $\langle 0, 4 \rangle$.

5.2.3.4 STATISTICAL ANALYSIS

To push further the comparison of the simulations, we now provide statistical analyses of the flow. The first paragraph evaluates first-order moments with the time averaged liquid volume fraction and the time averaged hydrodynamical velocity components. Then, the second paragraph discusses about the second-order moments obtained from the liquid volume fraction and velocity fluctuations.

First-order moments: Time averaged liquid volume fraction Isolines of the time averaged liquid volume fraction $\langle \alpha \rangle_t$ with its spatial evolution on the $y^* = 0$ plane are drawn in Figure 5.23. The averaging time is $t_{sim} = 9 \text{ ms}$. The axis are non-dimensionalized with respect d_l , the thickness of the liquid injector slit.

A good agreement is observed in both methods: the isolines almost match each other and contours of liquid volume fraction are similar. However, the isolines extend a bit further along the x -axis for the DNS than those of the diffuse interface model. This effect is probably due to the numerical dissipation, since the DNS mesh is about four time refined in each direction compared to CEDRE (HR) mesh. The isolines extend slightly more for the DNS case, by a small margin due. Interestingly, from the lower value of isolines, we can clearly see qualitatively the spray angle of the simulations. The angle is a little wider for the DNS confirming that DNS is more subjected to *dispersion* than the diffuse interface model. This effect is nearly noticeable from the HR diffused interface simulation but clearly visible from the MR simulation.

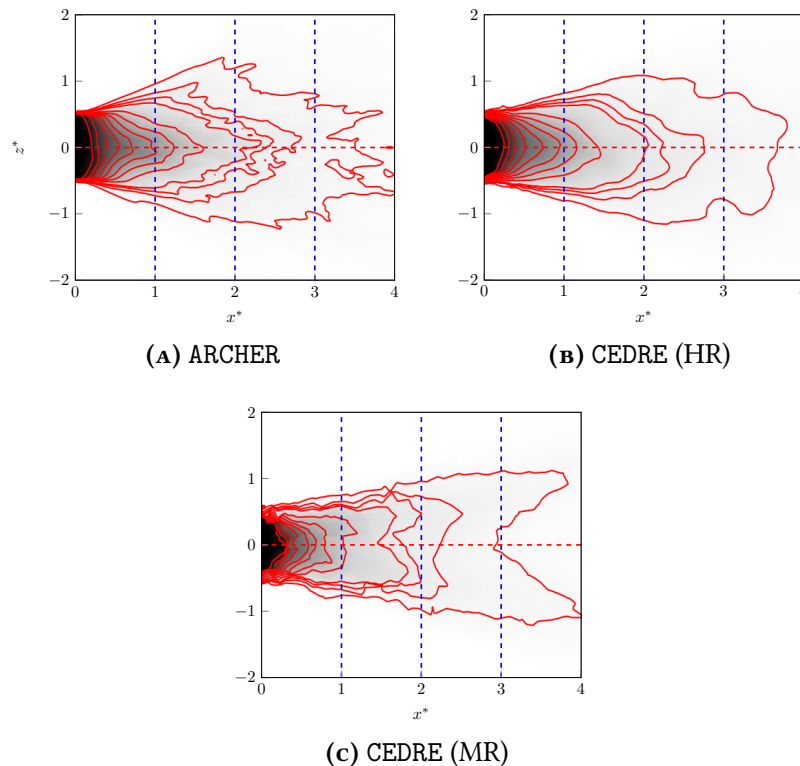



FIGURE 5.23: Averaged liquid volume fraction isolines $\langle \alpha_l \rangle_t = 0.1$  1, dashed located at $x^* \in \{1, 2, 3\}$ and $y^* = 0$. Reader must take care to the fact that the $\langle \alpha_l \rangle_t$ range is different for the three slices.

Time averaged liquid volume fraction profiles along the transverse direction (z) are depicted for different x positions in Figure 5.24. The positions of transverse profiles are shown on Figure 5.23. Again, the diffuse interface model is very close to the DNS reference simulation, but confirms the slightly higher dispersion in the reference DNS, visible at least on the CEDRE (MR) case. These comparisons suggest that the seven equation model is able to better capture the liquid phase dispersion in this specific atomization process than the DNS. This surprising result may again be due to the mesh resolution, which is higher for the DNS independently of the method use to represent the interface. Another possible explanation, involving this time the representation of the interface, could be that droplets formed during the atomization pro-

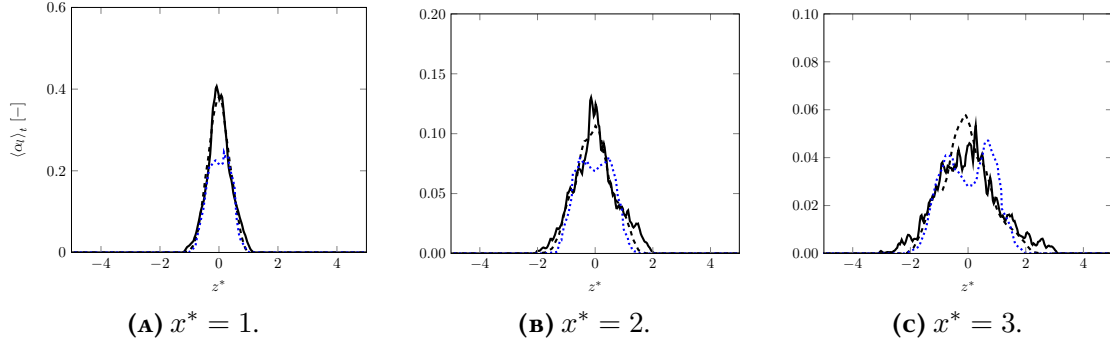


FIGURE 5.24: Averaged liquid volume fraction $\langle \alpha \rangle_t$ along Figure 5.23 dashed lines. — ARCHER, - - - CEDRE (HR), ···· CEDRE (MR).

cess are thrown away by the flapping motion of the liquid sheet. Once they are ejected, they have a relative transverse velocity component with respect to the surrounding gas phase. The relaxation of this slip velocity has not the same mechanism in the DNS that aims at solving the force acting at the liquid surface, whereas the diffuse interface models it (see Equation (5.2)). The correct resolution of these forces by the DNS depends on the mesh resolution, hence is difficult to achieve for droplets having a radius of the order of the mesh resolution. This may lead to these slight differences on the dispersion, the DNS approach estimating a longer time of relaxation than the diffused interface approach.

As a concluding remark, in future work, we could characterize the relaxation time of the velocity relaxation based on the dispersion observed in the results to close the diffuse interface model.

First-order moments: Mean velocities Time averaged transverse velocity contours are illustrated in the $y^* = 0$ plane in Figure 5.25 for both formalisms.

Initial velocity profiles are very similar in the range $x^* \in [0 : 1]$. Then $\langle v_z \rangle_t$ tends to spread vertically in the DNS, whereas in the diffuse interface model the transverse velocity remains closer to the $z^* = 0$ axis. The same behavior was observed in the previous paragraph for the liquid volume fraction. Velocities maximum and minimum are, to some degree, higher in the DNS, which is not surprising since some numerical diffusion is expected to happen on the coarser mesh used for the seven equation model computation. In the DNS, $\langle v_z \rangle_t$ velocities display a sharp variation along the $z^* = 0$ axis, when $z^* > 0$ $\langle v_z \rangle_t$ is negative otherwise $\langle v_z \rangle_t$ is positive. On the contrary, the diffuse interface model lets a slight interaction between positive and negative velocities on the $z^* = 0$ axis, the transition being smooth.

Transverse velocity profiles are shown in Figure 5.26 for different locations. For $z^* > 0$, profiles of the DNS and the seven equation model are similar in terms of values and slope. Although, for negative value of z^* , a discrepancy is found at $z^* = -2$. In the DNS, the velocity is rising when further progressing in the x axis, whereas in the diffuse interface model the velocity decreases. This gap could eventually be filled by integrating along the y axis to gain statistical convergence.

Similar comparisons are performed on the time averaged streamwise velocity, $\langle v_x \rangle_t$, in Figure 5.27. An excellent agreement is observed with respect to the diffuse interface model

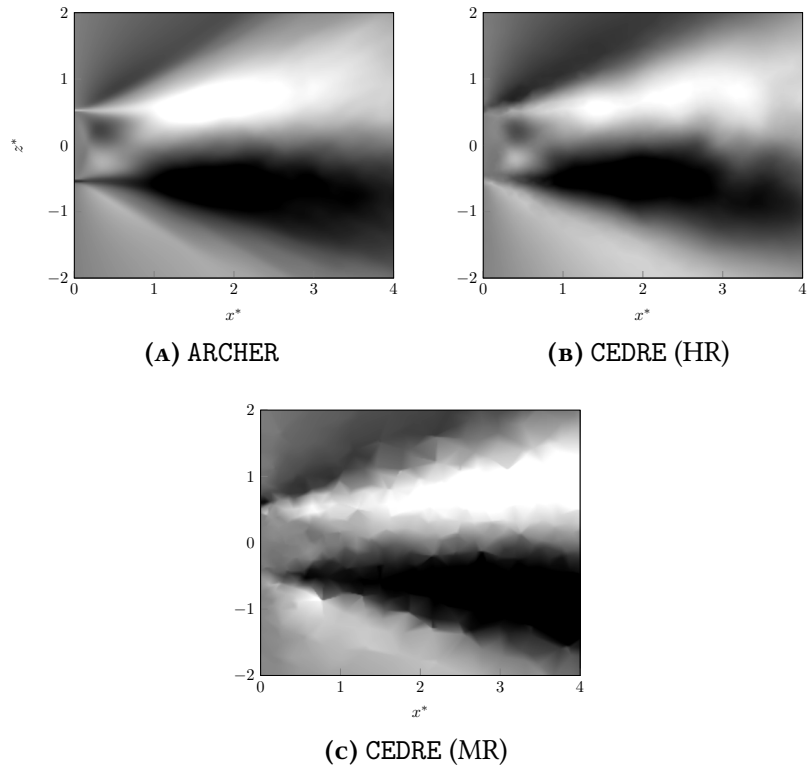



FIGURE 5.25: Averaged transverse velocity $\langle v_z \rangle_t = -3$  3 m/s at $y^* = 0$.

results. Again, the intensity of the velocity is slightly smaller due to numerical dissipation inherent to the diffuse interface model. This is confirmed by analyzing the velocity profiles at different locations shown in [Figure 5.28](#).

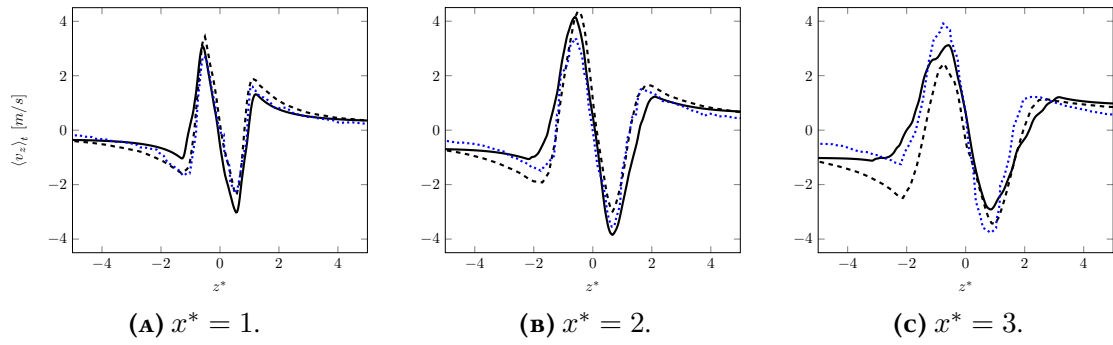


FIGURE 5.26: Averaged transverse velocity $\langle v_z \rangle_t$ along Figure 5.23 dashed lines. — ARCHER, - - - CEDRE (HR), ···· CEDRE (MR).

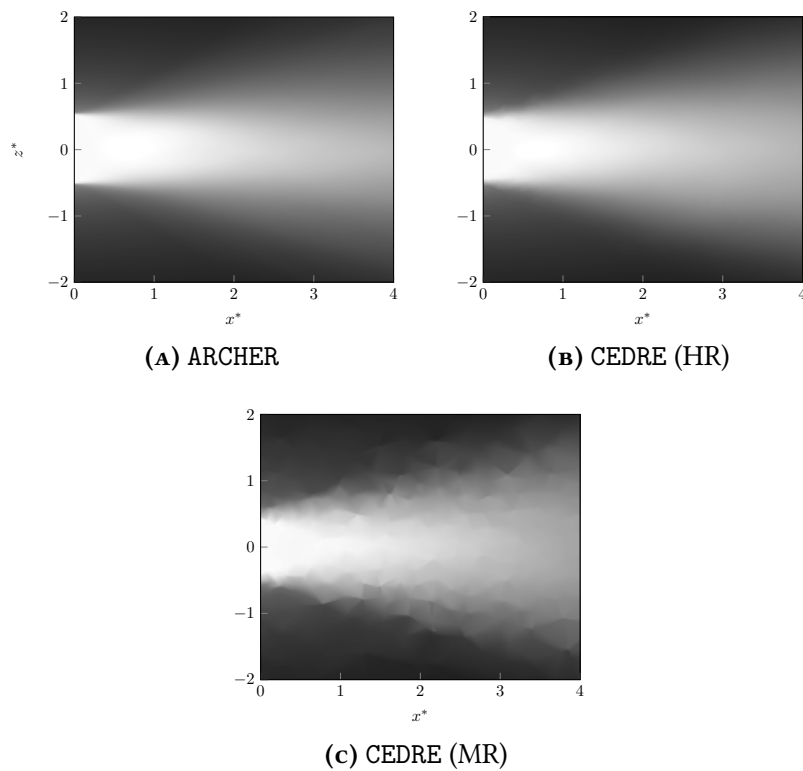



FIGURE 5.27: Averaged axial velocity $\langle v_x \rangle_t = 0$  70 m/s at $y^* = 0$.

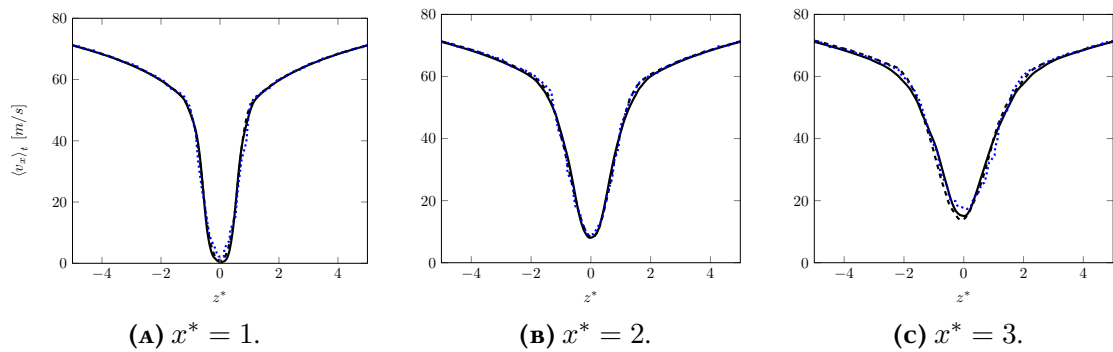


FIGURE 5.28: Averaged axial velocity $\langle v_x \rangle_t$ along Figure 5.23 dashed lines. — ARCHER, - - - CEDRE (HR), ···· CEDRE (MR).

The next paragraph is dedicated to the study of turbulent statistics through the analysis of the second order moments of the flow using the liquid volume fraction and velocity components fluctuations.

Second-order moments: Mean components of the Reynolds stress tensor To study more deeply statistic of the flow, we have computed the second order moments based on the liquid volume fraction and velocity fields. Three kind of second order moment emanate from these quantities: the liquid volume fraction variance, $\overline{\tilde{\alpha}_l \tilde{\alpha}_l}$, nine components of the Reynolds stress tensor, $\overline{v'_i v'_j}$, and the three components of the liquid turbulent flux $\overline{\tilde{\alpha}_l v'_i}$.

The analysis of the Reynolds stress tensor allows a validation of the turbulence characteristics observed in the diffuse interface model. [Figure 5.29](#) shows the averaged transverse Reynolds stress tensor component $\langle v'_z v'_z \rangle$ contour in the $y^* = 0$ plane. Turbulence inten-

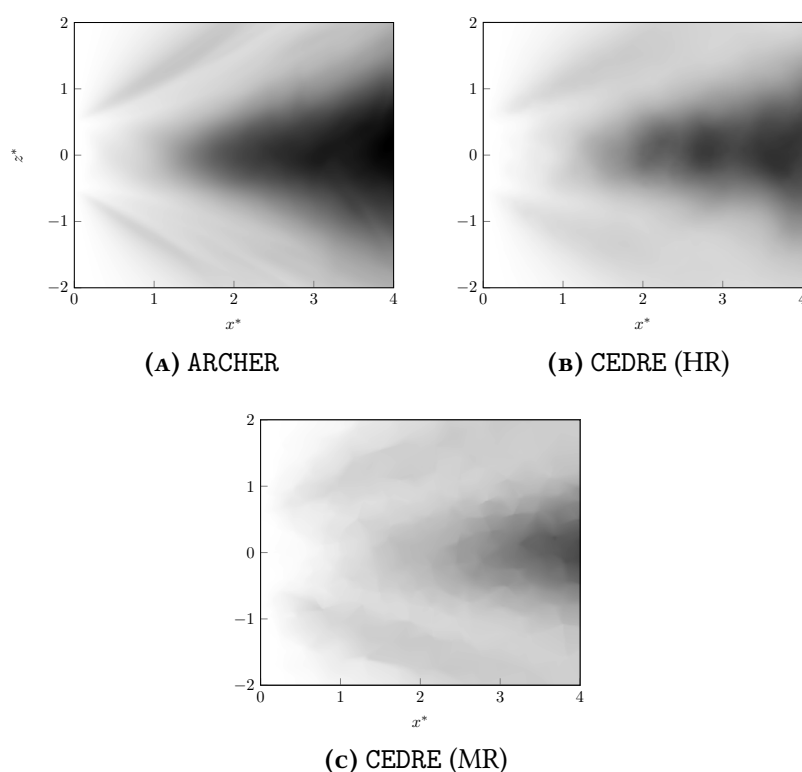



FIGURE 5.29: Transverse Reynolds stress tensor component $\langle v'_z v'_z \rangle_t = 0$  $350 \text{ m}^2/\text{s}^2$ at $y^* = 0$.

sity is higher downstream in both formalisms. Again, the intensity obtained with the seven equation model is slightly smaller but the overall results are close to the one obtained with the DNS.

[Figure 5.30](#) illustrates the transverse Reynolds stress tensor component for different locations in the streamwise direction. As mentioned before, the maximum turbulence intensity is lower than the DNS but the trend of the curve are very similar in both methods, confirming the ability of the diffuse interface model to represent the fluctuating velocities.

The same analysis is performed on the longitudinal Reynolds stress component $\langle v'_x v'_x \rangle$, shown in [Figure 5.31](#). Here, some differences are observed: turbulent intensity in the DNS

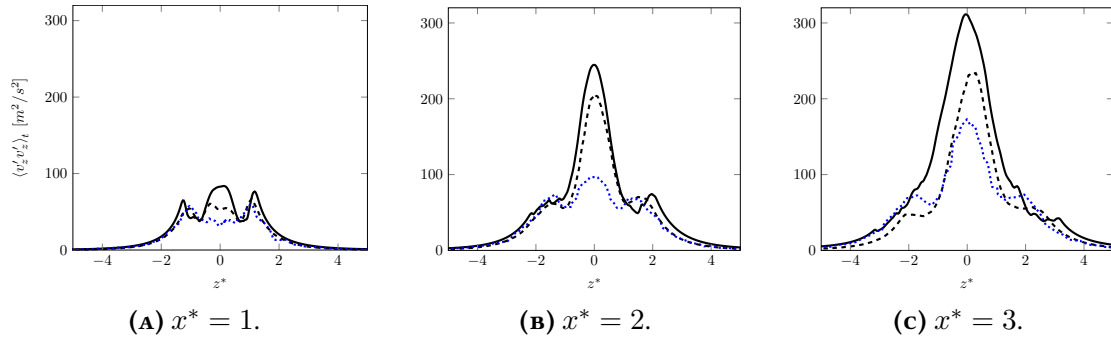


FIGURE 5.30: Transverse Reynolds stress tensor component $\langle v'_z v'_z \rangle_t$ along Figure 5.23 dashed lines. — ARCHER, ---- CEDRE (HR), CEDRE (MR).

is higher, but also more spread vertically compared to the results obtained with the diffuse interface model, for which the turbulence fluctuations are located closer to the main axis.

Concerning transverse Reynolds stress tensor profiles along the z -axis shown in Figure 5.32, an overall good agreement is found between the DNS and the diffuse interface model results. Nevertheless, a peak of turbulent intensity is found in the $x^* = 3$ profile around $z^* = 2$

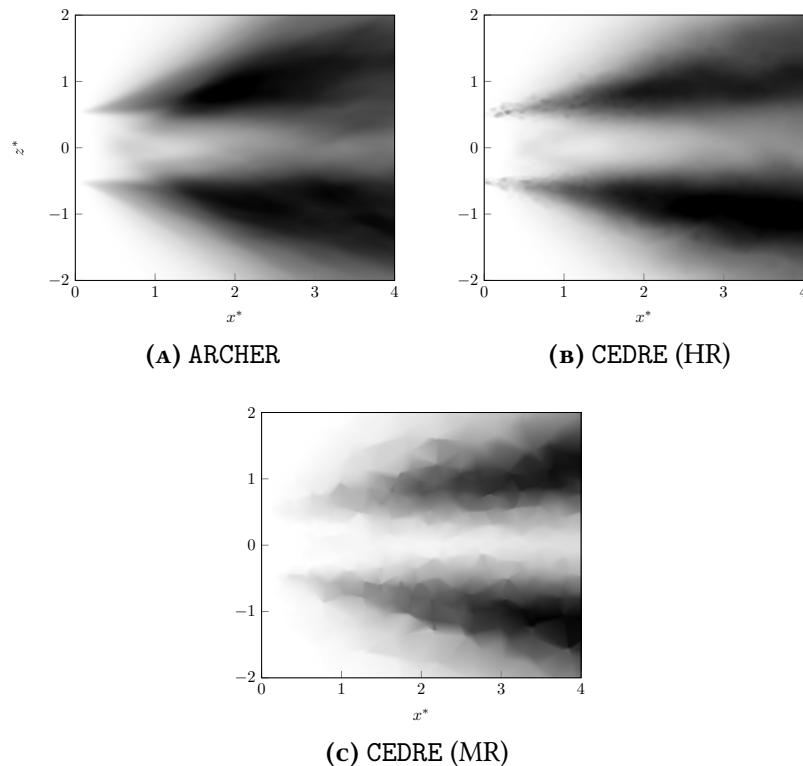


FIGURE 5.31: Longitudinal Reynolds stress tensor component $\langle v'_x v'_x \rangle_t$. $\langle v'_x v'_x \rangle_t \in [0 m^2/s^2, 300 m^2/s^2]$

in the CEDRE results. As mentioned previously, the flow seems to expand downstream in the seven equation model results.

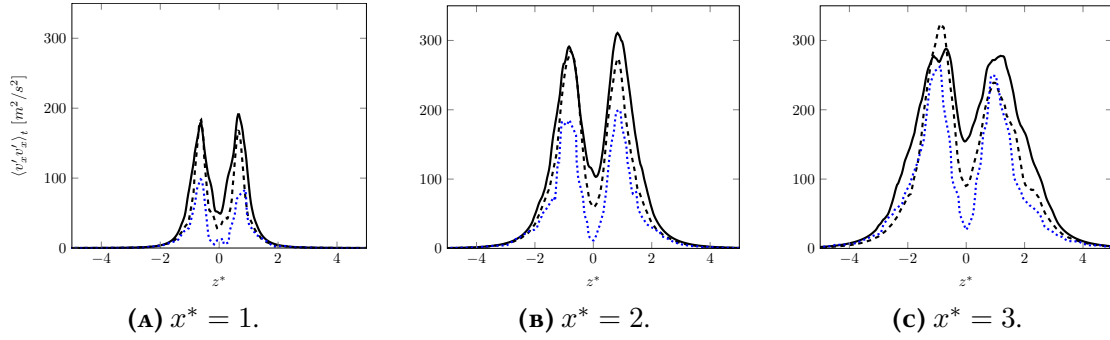


FIGURE 5.32: Longitudinal Reynolds stress tensor component $\langle v'_x v'_x \rangle_t$ along Figure 5.23 dashed lines. — ARCHER, - - - CEDRE (HR), ···· CEDRE (MR).

Second-order moments: Transversal turbulent liquid flux The turbulent liquid flux $\langle \tilde{\alpha}_l v'_z \rangle_t$ represents the transport of the liquid volume fraction induced by velocity fluctuations. This quantity is important for atomization modeling Anez et al. (2019) [4], where this term is usually modelled with a turbulent viscosity approach.

Using the plane $y^* = 0$ as in previous paragraphs, $\langle \tilde{\alpha}_l v'_z \rangle_t$ contours are summarized in Figures 5.33 and 5.34.

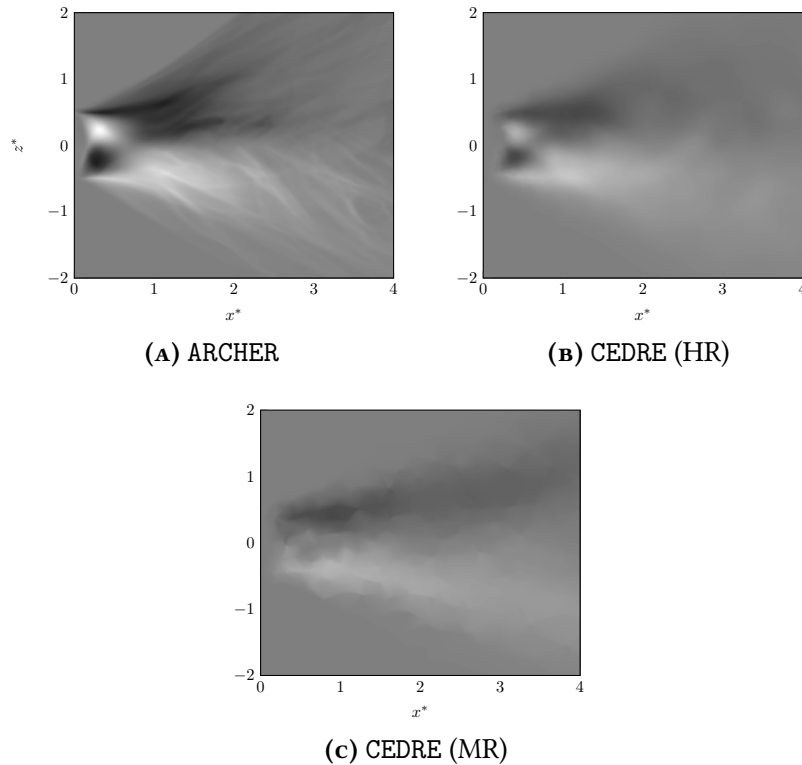
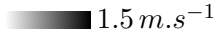


FIGURE 5.33: Transversal turbulent liquid flux tensor component $\langle \tilde{\alpha}_l v'_z \rangle_t = -1.5$  $1.5 m \cdot s^{-1}$ at $y^* = 0$.

This variable behavior combines the effects pointed out earlier on the liquid volume fraction and the transverse velocity fluctuation: the turbulent liquid flux is more spread in the DNS case due to the higher spray angle. The turbulent liquid flux intensity is lower in the

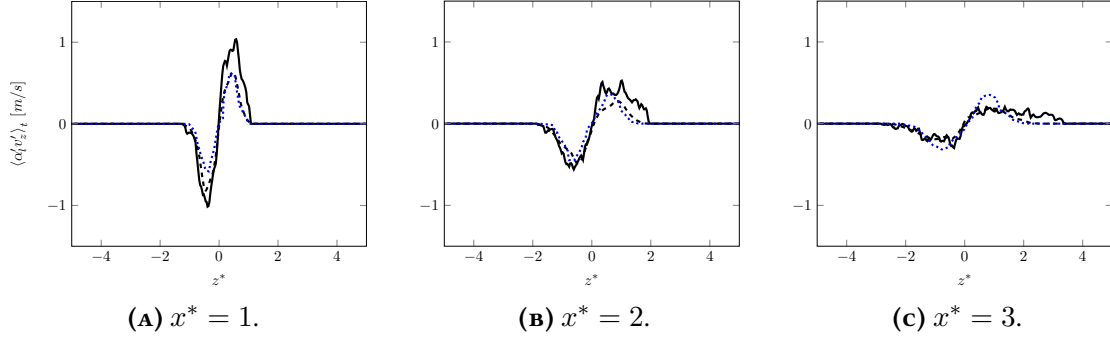


FIGURE 5.34: Transversal liquid flux tensor component $\langle \tilde{\alpha}_l v'_z \rangle_t$ along Figure 5.23 dashed lines. — ARCHER, CEDRE (HR), - - - - CEDRE (MR).

seven equation model. These results confirms that the liquid dispersion is higher in the DNS results.

Discussion on second-order moments The second-order moment statistics exhibit some differences between both numerical approaches that are most probably related to the different representation of the small scale features of the flows, and more particularly to the representation of the liquid-gas transition as already attested with the global feature flow comparison at the beginning of the section.

In addition, it can be pointed out that it is more difficult to achieve the statistical convergence, as shown by remaining fluctuations in all the second-order moment figures. To show the effect of small scale structure on the second-order fluctuations, let us first consider the variance of the liquid volume fraction, defined as

$$\overline{\tilde{\alpha}_l \tilde{\alpha}_l} = \overline{\alpha_l \alpha_l} - \overline{\alpha_l} \overline{\alpha_l}. \quad (5.13)$$

Since locally there can either be liquid or gas, the admissible values of α_l are only one and zero respectively, thus the probability density function $P(\alpha_l) = (1 - \overline{\alpha_l})\delta(\vec{x}) + \overline{\alpha_l}\delta(\vec{x})$ yielding

$$\overline{\tilde{\alpha}_l \tilde{\alpha}_l} = \overline{\alpha_l} - \overline{\alpha_l} \overline{\alpha_l} = \overline{\alpha_l}(1 - \overline{\alpha_l}). \quad (5.14)$$

The sharp interface representation of the interface preserves this feature as shown in Figure 5.19, since the product $\overline{\alpha_l}(1 - \overline{\alpha_l})$ is always null, whereas the diffuse interface model gives necessarily lower resolved variance level since $\overline{\alpha_l}(1 - \overline{\alpha_l})$ is not null in zones where the interface has been diffused (see Figure 5.21), yielding a lower variance. This variance gap has not disappeared in the diffuse interface approach. If the construction of the diffuse interface approach is based for instance on some probability to find the liquid, the same statistical approach induces that a certain amount of variance is related to this probability, this part is somehow included as a model and hidden at the resolved scale.

Furthermore, the turbulent liquid flux includes also this kind of effect, by considering at one location and time there can be only liquid and gas. It can be shown that

$$\overline{\tilde{\alpha}_l v'} = \overline{\alpha_l}(1 - \overline{\alpha_l})(\overline{v_l} - \overline{v_g}) = \overline{\tilde{\alpha}_l \tilde{\alpha}_l}(\overline{v_l} - \overline{v_g}). \quad (5.15)$$

Thus, the turbulent liquid flux is related to the variance and the difference of velocity between phases. Since the resolved part of the diffuse interface underestimates the variance, it penalizes

the turbulent liquid flux. Here again, it is due to the fact that second-order moments are sensitive to the small-scales feature of the flow.

On the same line not all the features of the flow are perfectly represented by the sharp interface approach (DNS), since for low mesh resolution the precision on the determination of the interface position will decrease leading to other kind of numerical artefacts. For low resolution, the methods that preserve the sharp interface transition to keep also the total amount of each phase forces somehow the phase inclusion to remain at the resolution level. This has been shown on [Figure 5.20d](#), for the low resolution part of the simulation, an accumulation of surface that has a curvature related to Δx appears showing that the numerical method start to limit the atomization process to preserve droplet that can be captured with the present mesh resolution.

Finally, the implication of the reduction of variance can also be demonstrated for Reynolds stress correlation, as an example the same PDF of α_l implies

$$\overline{v'v'} = \overline{\alpha_l} \overline{v'_l v'_l} + (1 - \overline{\alpha_l}) \overline{v'_g v'_g} + \overline{\alpha'_l \alpha'_l} (\overline{v_l} - \overline{v_g})^2. \quad (5.16)$$

The Reynolds stress contains three contributions: a part in the liquid phase, a part in a gas phase and a last part due to the velocity difference between gas and liquid. This last contribution is proportional to the variance of α_l . Thus the under estimation of the variance by the diffuse interface approach reduces also the Reynolds stress. This effect can be observed on [Figure 5.32](#) and it is more pronounced for the MR case than for the HR case.

To conclude this discussion, the fact that the diffuse interface model underestimates the variance does not mean that the diffuse interface model produces wrong result, but that a part of second-order moments is included in the statistical representation of the transition between the gas and liquid.

5.2.4 CONCLUSION

In the present section, we have proposed to pursue the evaluation of reduced-order models to perform predictive simulations of the primary atomization in engines ranging from cryotechnic to aeronautic applications. As a baseline comparator, we have relied on the DNS results of a hierarchy of specific test-cases.

The original test-case consisted in an air-assisted water atomization using a coaxial injector with experimental results from the LEGI test bench [Cordesse et al. \(2020\) \[37\]](#). If not exhaustive at all, the comparison has showed at least good agreements of macroscopic quantities and important CPU gains between the *seven-equation model* implemented in the CEDRE code and the DNS results from the ARCHER code. It has also emphasized the limits of diffuse interface models to capture complex liquid structures such as ligaments, rings or deformed droplets and encourages to add a sub-scale description of the interface dynamics through geometric variables such as the interfacial area density, the mean and Gaussian curvatures.

For the planar injector, we have provided a deeper qualitative and quantitative comparison of the results of simulations performed with CEDRE for the diffuse interface reduced-order model and ARCHER for the DNS. We have first assessed the DNS reliability through the use of the IRQ criterion to identify the most relevant region where the DNS can stand as a trustworthy benchmark. Then, we have provided a comparison of the atomization global characteristics

obtained by each simulations through the volume fraction time evolution and spatial mean penetration of the liquid core. These preliminary comparisons have shown that, while the two models show a different representation of small-scales due to the distinct interface modeling, large-scale motions seems in reasonably good agreement and sufficient to recover global features of the atomization process such as liquid penetration and spray angle. We have further detailed the comparison with statistical analyses of the flow through first and second-order moments based on the liquid volume fraction and velocities limited to the well-resolved part $\langle 0, 4d_i \rangle$ of the computational domain. The first-order moments have brought out a slightly higher dispersion of the reference DNS than the diffuse interface model resolution and tend to indicate that enough resolution is essential for the latter model. The second-order moments have confirmed the liquid higher dispersion for the DNS. We finally have analyzed why the diffuse interface model underestimates the variance and emphasized that it does not mean that the diffuse interface model produces wrong result, but that a part of second-order moments may be included in the representation of the transition between the gas and liquid. To summarize, we have understood the behavior of each numerical method and identified the main conceptual differences between them.

The comparison has finally shown good agreements, together with an important CPU gains between the *seven-equation model* implemented in the CEDRE code and the DNS results from the ARCHER code.

The diverging modeling of the small-scale between the two approaches has brought out the need to examine in future works the underlying averaging process coming from the diffuse interface modeling, which is linked to the mesh resolution and produces numerical dissipation leading to a lost of amplitude of the fields. It also suggests to add a sub-scale description of the interface dynamics through geometric variables such as the interfacial area density, the mean and Gaussian curvatures as proposed in [Cordesse et al. \(2020\) \[39\]](#).

CONCLUSION AND PERSPECTIVES

This thesis has lifted several critical barriers to the design and the use of reduced-order models as predictive tools for applications involving off-disequilibrium two-phase flows with complex interface dynamics, such as in jet atomization. Beyond combustion processes as for instance cryogenic rocket engines, for which primary atomization may engender combustion instabilities, jet atomization is involved in a wide panel of industrial and agricultural purposes, from biological sprays to deposition and coating. The large applicability of the present study has been a motivating driver.

Encased in the strategy of ONERA and CNES to perform numerical simulations of the primary atomization from the injection to the combustion of the spray by coupling reduced-order models, this thesis has contributed to two of the main approaches to provide reduced-order models able to deal with jet atomization. Whether it is the method of coupling specific models, each of them suited to a given flow topology, or the method of using a unified model encompassing all the flow topologies of the given application, they both face the same challenge, which consists in accurately describing the *mixed region* where the flow is the most complex due to the high thermodynamics disequilibrium between the phases and the rich interface dynamics. Focusing on the most complex part of the flow, the present thesis naturally contributed to both approach.

Simple reduced-order models such as the multi-species compressible Navier-Stokes have proved their interests, being commonly adopted in the industry [Le Touze \(2015\) \[132\]](#). They also have called for a renewal, in order to account for fluids thermodynamics off-equilibrium in the mixing zones and capture the complex dynamics of the interface especially in the *mixed region*. Nevertheless such improvements are not straightforward and give on to complex problems that we have detailed in the introduction and detailed in the present work.

As such, the outreach of the present work had to rely on a large panel of disciplines, from the mathematical analysis of the models and their derivation tools, the physical modelling and closure of these systems of PDE as well as the associated thermodynamics, to their numerical discretization and implementation in CFD codes for industrial uses. By combining mathematical, physical, thermodynamical and numerical analysis as well as computer science and engineering work in a industrial context, this thesis has led to the following results:

- 1) PDE's analysis: we have extended the existing theory of supplementary conservative equations to system of non-conservation laws. It has brought about entropy supplementary conservative equations for the Baer-Nunziato model together with constraints on the interfacial quantities and the definition of the thermodynamics for non-miscible fluids and also when accounting for some level of mixing of the two phases. This result has been published in [Cordesse and Massot \(2020\) \[41\]](#).

2) Mathematical and physical modelling: we have derived from variational calculus a two-velocity two-pressure two-phase flow model along with an equation on the mixture entropy piloting the relaxation phenomena. We have highlighted how the average interfacial pressure and velocity are closed and the consequences of their closures based on waves types and Riemann invariants. Furthermore relying on a probability density function, we have departed from a geometric approach of the interface and proposed a multi-scale rendering of the interface bridging diffuse and sharp interface models, to describe multi-fluid flow. From the probability density function, we have recovered classic geometric variables as well as a natural decomposition into mean and fluctuating contributions. Based on these quantities, we have extended the definition of the Lagrangian describing the barotropic two-phase flow medium adding dual-scale kinetic and potential contributions to account for small-scale kinematics and surface tension. The SAP has returned a system of PDE showing a coupling between large and small scales. We finally have extended the system to two-parameter equations of state for each phase, leading to a single-velocity two-pressure six-equation model. This work is almost complete and an article is in preparation for submission [Cordesse et al. \(2020\) \[34\]](#).

3) Thermodynamics analysis: we have introduced a formalism to build a multi-fluid thermodynamics, based on a reference state and pressure law, accounting for non-ideal effects. It has highlighted the impact on the mathematical structure of the system derived from the Stationary Action Principle and has given hints on how to recover the phase evolution equations. The work is submitted in [Cordesse et al. \(2020\) \[35\]](#).

4) Numerical strategy: a simplified version of the dual-scale two-phase flow model is obtained, to which we have developed a splitting strategy leading to three sub-systems corresponding respectively to the hydrodynamics and acoustics convection, then the large and small capillary fluxes and finally the relaxation procedure of the pressures, and proceeded to their mathematical analysis. Based on a Finite Volume discretization, we have implemented the new model in the industrial CFD software CEDRE of ONERA to proceed to a numerical verification of the implemented model by reproducing classic one and two dimensional test cases selected to test Euler and large capillary fluxes as well as the pressure relaxation. The results have attested the reliability of the splitting strategy.

5) Numerical simulations: we first have proposed a qualitative and quantitative comparisons of some elements of the hierarchy of diffuse interface models, the single-velocity and single-pressure and two-velocity two-pressure models, with or without coupling with a KBMM element. The numerical simulations have been performed on challenging cryogenic jet atomization configurations as a demonstration of feasibility and a first step towards genuine validation. Then, we have constituted and investigated a first building block of a hierarchy of test-cases designed to be amenable to DNS while close enough to industrial configurations, for which we have proposed a comparison of two-fluid compressible simulations with DNS data-bases. It has led to a better understanding of the main conceptual differences between the two modelling approaches. It has led to the submission of an article [Cordesse et al. \(2019\) \[42\]](#).

As direct continuations of this thesis, we would like to mention

1) PDE analysis:

- The quest of two-phase flow model hyperbolicity was one of the main dormant guidelines of this work. Thanks to the extension of the theory on supplementary conservative

equations to system of non-conservation laws and the formalism of the multi-fluid thermodynamics, we should be able to define a strictly convex mixture entropy consistent with the system of equations and the pressure laws, to recover the entropic symmetrization of two-velocity two-pressure models such as the Baer-Nunziato, leading to generalized source terms.

- Furthermore, an orthogonal decomposition of the entropic variable has been investigated in order to apply the partial symmetrization in the sense of Godunov-Mock proposed in [Forestier and Gavrilyuk \(2011\) \[71\]](#) to a broader class of systems for which the non-conservative terms affect genuinely nonlinear fields. Through this partial symmetrization in the sense of Mock-Godunov, we hope to prove that the non-conservative terms do not impact the eigenvalues of the spectrum, and conditions on the hyperbolicity of the system can be derived.

2) Mathematical and physical modelling:

- The work proposed on the derivation from variational calculus of a two-velocity two-pressure two-phase flow model along with an equation on the mixture entropy piloting the relaxation phenomena should be further investigated, in particular by proposing a method to recover the partial entropy equations.
- Moreover, the dual-scale modelling approach through the stationary action principle has shown great promises. Time constraint has left open this breakthrough, since only primary results were obtained in terms of sub-scale modelling, physical effects and numerical simulations. In particular, pursuing the numerical assessment of the geometric invariants with libraries such as MERCURVE are pursued in Ruben Di Battista's PhD [Di Battista \(2020\) \[53\]](#). Coupling the two subscale modelling proposed, pulsation and oscillation, is also under investigation. Work has to be done to model properly the large and sub-scale energy transfer.
- Later on we will also enrich the physics accounted for, such as including turbulence and diffusion terms. It will be part of next developments at ONERA and CMAP.

3) Thermodynamics analysis:

- The multi-fluid thermodynamics formalism has been built and applied through the SAP, nevertheless not yet used in practice in the implemented system. It must be done in coherence with the subscale closure of the model, meaning we need to add the geometric variables as internal variables and derive the associated thermodynamics.
- In future works, transition to subcritical to transcritical regimes will be examined through additional energy terms that are quadratic gradient function of internal variables characterizing the heterogeneity of the mixture when crossing the interface.
- Mass and heat transfer will be also examined since one of the primary targeted applications is the combustion from jet atomization.

4) Numerical strategy:

- Numerical schemes which would accurately handle the non-conservative terms should bring significant gain of accuracy and probably robustness. Relaxation schemes have already been developed for the Baer-Nunziato model [Coquel et al. \(2014\) \[32\]](#), [Coquel et al. \(2017\) \[29\]](#) and are an interesting lead to investigate.
- In addition, developing implicit-time schemes would reduce simulation time. Improvements in this direction will be carried out at ONERA.
- Finally, an Adaptive Mesh Refinement (AMR) code has been developed at CMAP and Maison de La Simulation, which enables highly parallel computations and high resolution in the interfacial zones. The dual-scale two-phase flow model will be implemented and tested in this code.

5) Numerical simulations:

- The dual-scale two-phase flow model implemented in the GES of CEDRE will be used to conduct simulations on real applications, in particular jet atomizations but also on underwater start-up of a booster at ONERA.
- Furthermore, efforts are already devoted to continue building the hierarchy of test cases amenable by DNS to provide supplementary data for assessing the dual-scale models. It is part of Alberto Remigi's PhD [Remigi \(2021\) \[186\]](#).
- Since the SAP does only return the convective structure of the system, we are also seeking for adequate source terms, in particular, for the interfacial density area evaluation equation. DNS results of this hierarchy of test cases will leverage closures and this work will be conducted in a large collaboration involving ONERA, CORIA and CMAP.

Finally, this work has also given the playground to broaden horizons. We would like to derive a dual-scale two-phase models including non-ideal effects in the thermodynamics, but also velocity off-equilibrium, implying to introduce velocity fluctuations as part of the internal variables of the system as already proposed for dispersed flow in [Lhuillier \(1995\) \[135\]](#). We also think the Stationary Action Principle is able to include dissipative effects and work in this direction has been proposed in [Öttinger \(2005\) \[170\]](#).

BIBLIOGRAPHY

- [1] Ambroso, A. and Chalons C.and Raviart, P.-A. “A Godunov-type method for the seven-equation model of compressible two-phase flow”. *Computers & Fluids*, 54, 67–91, 2012 (cit. on pp. 10, 24).
- [2] Andrianov, N., Saurel, R., and Warnecke, G. “A simple method for compressible multiphase mixtures and interfaces”. *Int. J. Numer. Meth. Fl.*, 41.2, 109–131, 2003. URL: <http://dx.doi.org/10.1002/flid.424> (cit. on pp. 65, 73, 86).
- [3] Andrianov, N. and Warnecke, G. “The Riemann problem for the Baer-Nunziato two-phase flow model”. *J. Comput. Phys.*, 195.2, 434–464, 2004 (cit. on pp. 9, 24).
- [4] Anez, J., Ahmed, A., Hecht, N., Duret, B., Reveillon, J., and Demoulin, F. “Eulerian–Lagrangian spray atomization model coupled with interface capturing method for diesel injectors”. *Int. J. Multiphase Flow*, 113, 325–342, 2019 (cit. on pp. 259, 270).
- [5] Baer, M. R. and Nunziato, J. W. “A two-phase mixture theory for the Deflagration-to-Detonation Transition (DDT) in reactive granular materials”. *Int. J. Multiphase Flow*, 12.6, 861–889, 1986 (cit. on pp. 6 sq., 21 sq., 45, 47, 50, 72 sq., 80, 83, 85, 100 sqq., 107, 127, 142).
- [6] Barros, R. “Conservation laws for one-dimensional shallow water models for one and two-layer flows”. *Math. Models Methods Appl. Sci.*, 31, 119–137, Jan. 2005 (cit. on p. 76).
- [7] Bdzil, J. B., Menikoff, R., Son, S. F., Kapila, A. K., and Stewart, D. S. “Two-phase modeling of deflagration-to-detonation transition in granular materials: A critical examination of modeling issues”. *Phys. Fluids*, 11.2, 378–402, Jan. 1999 (cit. on pp. 44, 73, 83, 85, 102, 127).
- [8] Bedford, A. and Drumheller, D. “A variational theory of immiscible mixtures”. *Arch. Ration. Mech. Anal.*, 68, 37–51, Mar. 1978 (cit. on pp. 48 sq., 122).
- [9] Beijeren, H. V. and Ernst, M. “The modified Enskog equation”. *Physica*, 68.3, 437–456, 1973. URL: <http://www.sciencedirect.com/science/article/pii/0031891473903728> (cit. on pp. 100, 103).
- [10] Beijeren, H. V. and Ernst, M. “The modified Enskog equation for mixtures”. *Physica*, 70.2, 225–242, 1973. URL: <http://www.sciencedirect.com/science/article/pii/0031891473902474> (cit. on pp. 100, 103).
- [11] Belhadef, A., Vallet, A., Amielh, M., and Anselmet, F. “Pressure-swirl atomization: Modeling and experimental approaches”. *Int. J. Multiphase Flow*, 39, 13–20, 2012. URL: <http://www.sciencedirect.com/science/article/pii/S0301932211002096> (cit. on p. 248).
- [12] Bérrest, P. *Calcul des variations Application à la Mécanique et à la Physique*. École polytechnique. 1997 (cit. on p. 55).

- [13] Bissuel, A., Allaire, G., Daumas, L., Barré, S., and Rey, F. “Linearized Navier-Stokes Equations for Aeroacoustics using Stabilized Finite Elements: Boundary Conditions and Industrial Application to Aft-Fan Noise Propagation”. *Computers and Fluids* 2018. URL: <https://hal.archives-ouvertes.fr/hal-01695874> (cit. on pp. 71 sq.).
- [14] Boileau, M., Lagarde, J., Dupif, V., Laurent, F., and Massot, M. “Two-size moment Eulerian multi-fluid method describing the statistical trajectory crossing: modeling and numerical scheme”. *ICMF Proceedings, Firenze, Italy* May 2016. URL: <https://hal.archives-ouvertes.fr/hal-01543507> (cit. on p. 241).
- [15] Bourguignon, J.-P. *Calcul Variationnel*. École polytechnique. 2007 (cit. on pp. 55, 91).
- [16] Cahn, J. W. and Hilliard, J. E. “Free Energy of a Nonuniform System. I. Interfacial Free Energy”. *The Journal of Chemical Physics*, 28.2, 258–267, 1958. eprint: <https://doi.org/10.1063/1.1744102>. URL: <https://doi.org/10.1063/1.1744102> (cit. on pp. 100, 142).
- [17] Candel, S. M. and Poinso, T. J. “Flame Stretch and the Balance Equation for the Flame Area”. *Combust. Sci. Technol.*, 70.1-3, 1–15, 1990. eprint: <https://doi.org/10.1080/00102209008951608>. URL: <https://doi.org/10.1080/00102209008951608> (cit. on p. 145).
- [18] Cant, R., Pope, S., and Bray, K. “Modelling of flamelet surface-to-volume ratio in turbulent premixed combustion”. *Symp. (Int.) Combust.*, 23.1. Twenty-Third Symposium (International) on Combustion, 809–815, 1991. URL: <http://www.sciencedirect.com/science/article/pii/S0082078406803346> (cit. on p. 145).
- [19] Canu, R., Duret, B., Reveillon, J., and Demoulin, F.-X. “A surface resolution criterion for two-phase flows DNS”. *ILASS Europe, 29th Annual Conference on Liquid Atomization and Spray Systems*. 2019 (cit. on p. 259).
- [20] Canu, R., Puggelli, S., Essadki, M., Duret, B., Menard, T., Massot, M., Reveillon, J., and Demoulin, F. “Where does the droplet size distribution come from?” *Int. J. Multiphase Flow*, 107, 230–245, 2018. URL: <http://www.sciencedirect.com/science/article/pii/S0301932218302854> (cit. on pp. 170, 249).
- [21] Carvalho, I., Heitor, M., and Santos, D. “Liquid film disintegration regimes and proposed correlations”. *Int. J. Multiphase Flow*, 28.5, 773–789, 2002 (cit. on pp. 254 sq.).
- [22] Chandrasekhar, S. *Hydrodynamic and Hydromagnetic Stability (International Series of Monographs on Physics)*. Dover Publications, Feb. 1, 1981. 704 pp. URL: <https://www.amazon.com/Hydrodynamic-Hydromagnetic-Stability-International-Monographs/dp/048664071X?SubscriptionId=AKIAIOBINVZYXZQZ2U3A&tag=chimbori05-20&linkCode=xm2&camp=2025&creative=165953&creativeASIN=048664071X> (cit. on pp. 167 sq., 179 sqq., 183).
- [23] Chantepredrix, G., Villedieu, P., and Vila, J. “A compressible model for separated two-phase flows computations”. *ASME Fluid Eng. Div. Summer Meeting 2002*. 2002 (cit. on p. 192).
- [24] Chapman, S. and Cowling, T. G. *The Mathematical Theory of Non-uniform Gases: An Account of the Kinetic Theory of Viscosity, Thermal Conduction and Diffusion in Gases*. ed. by Cambridge. Cambridge University Press, 1970 (cit. on pp. 100, 103).
- [25] Chen, G.-Q. and Levermore C.D. Liu, T.-P. “Hyperbolic Conservation Laws with Stiff Relaxation Terms and Entropy”. *Comm. Pure Appl. Math*, XLVII, 787–830, 1994 (cit. on pp. 91, 94).

- [26] Chen, X., Ma, D., Yang, V., and Popinet, S. “High-Fidelity Simulations Of Impinging Jet Atomization”. *Atomization and Sprays*, 23.12, 1079–1101, 2013 (cit. on pp. 5, 20).
- [27] Chow, B., Lu, P., and Ni, L. *Hamilton’s Ricci Flow (Graduate Studies in Mathematics)*. American Mathematical Society, 2006 (cit. on pp. 129, 165).
- [28] Coquel, F., Gallouët, T., Hérard, J.-M., and Seguin, N. “Closure laws for a two-fluid two-pressure model”. *C.R. Math.*, 334.10, 927–932, 2002. URL: <http://www.sciencedirect.com/science/article/pii/S1631073X0202366X> (cit. on pp. 8, 23, 66 sqq., 73, 81, 83, 85, 90).
- [29] Coquel, F., Hérard, J.-M., and Saleh, K. “A positive and entropy-satisfying finite volume scheme for the Baer-Nunziato model”. *J. Comput. Phys.*, 330, 401–435, 2017 (cit. on pp. 10, 25, 278).
- [30] Coquel, F., Hérard, J.-M., Saleh, K., and Seguin, N. “A class of two-fluid two-phase flow models”. *42nd AIAA Fluid Dynamics Conference and Exhibit*. 2012, 3356 (cit. on p. 101).
- [31] Coquel, F., Hérard, J.-M., Saleh, K., and Seguin, N. “Two properties of two-velocity two-pressure models for two-phase flows”. *Commun. Math. Sci.*, 12, 593–600, 2014. URL: <https://hal.archives-ouvertes.fr/hal-00788902> (cit. on pp. 8, 23, 67, 73).
- [32] Coquel, F., Hérard, J.-M., Saleh, K., and Seguin, N. “A Robust Entropy-Satisfying Finite Volume Scheme for the Isentropic Baer-Nunziato Model”. *ESAIM: Mathematical Modelling and Numerical Analysis*. 42 pages Jan. 2014. URL: <https://hal.archives-ouvertes.fr/hal-00795568> (cit. on pp. 10, 24 sq., 278).
- [33] Cordesse, P., Di Battista, R., Chevalier, Q., Matuszewski, L., Ménard, T., Kokh, S., and Massot, M. “A Diffuse Interface Approach for Disperse Two-phase Flows Involving Dual-scale Kinematics of Droplet Deformation Based on Geometrical Variables”. *submitted to ESAIM: Proceedings and Surveys* 2019 (cit. on pp. 11, 26, 139, 164).
- [34] Cordesse, P., Kokh, S., and Massot, M. “Derivation of a two-phase flow model with two-scale kinematics and surface tension by means of variational calculus”. *in preparation for IJMF* 2020 (cit. on pp. 11, 26, 107, 132, 139, 167, 181, 276).
- [35] Cordesse, P., Matuszewski, L., and Massot, M. “A consistent Multi-Fluid thermodynamics formalism including non-ideal effects and interface geometry : from thermodynamic potentials to pressure law and the impact on multiphase flow modeling”. *submitted to Continuum Mech. Therm.* 2020 (cit. on pp. 11, 26, 59, 97, 99, 276).
- [36] Cordesse, P., Murrone, A., and Massot, M. “Coupling a hierarchy of diffuse interface model with kinetic-based moment methods for spray atomization simulations in cryogenic rocket engines”. *ICLASS 2018 Proceedings*. ICLASS 2018. Chicago, US, 2018. URL: <https://hal.archives-ouvertes.fr/hal-01888477> (cit. on pp. 12, 27, 237).
- [37] Cordesse, P., Murrone, A., Menard, T., and Massot, M. “Comparative study of jet atomization simulations: direct numerical simulations and diffuse interface models coupled with kinetic-based moment methods”. *NASA Summer Program Proceedings*. Nasa Technical Memorandum. NASA Ames Reseach Center, 2020, 1–12. URL: <https://hal.archives-ouvertes.fr/hal-02349534> (cit. on pp. 11 sq., 26 sq., 139, 237, 248, 272).
- [38] Cordesse, P., Murrone, A., Ménard, T., and Massot, M. “Validation strategy of reduced-order two-fluid flow models based on a hierarchy of direct numerical simulations”. *ICMF 2019 Proceedings*. 10th International Conference on Multiphase Flow. Rio de Janeiro, Brazil, May 19–24, 2019. URL: <https://hal.archives-ouvertes.fr/hal-02194973> (cit. on pp. 12, 27, 237, 248).

- [39] Cordesse, P., Di Battista, R., Drui, F., Kokh, S., and Massot, M. “Derivation of a Two-Phase Flow Model with Two-Scale Kinematics, Geometric Variables and Surface Tension Using Variational Calculus”. *NASA Summer Program Proceedings*. Nasa Technical Memorandum. NASA Ames Reseach Center, 2020, 1–12. URL: <https://hal.archives-ouvertes.fr/hal-02336996> (cit. on pp. 166 sq., 174 sq., 180, 248, 273).
- [40] Cordesse, P., Di Battista, R., Kokh, S., and Massot, M. “Derivation of a two-phase flow model with two-scale kinematics and surface tension by means of variational calculus”. *ICMF 2019 Proceedings*. 10th International Conference on Multiphase Flow. Rio de Janeiro, Brazil, May 19–24, 2019. URL: <https://hal.archives-ouvertes.fr/hal-02194951> (cit. on pp. 11, 26, 139, 174).
- [41] Cordesse, P. and Massot, M. “Entropy supplementary conservation law for non-linear systems of PDEs with non-conservative terms: application to the modelling and analysis of complex fluid flows using computer algebra”. *In Press, Commun. Math. Sci.* 2020. URL: <https://hal.archives-ouvertes.fr/hal-01978949> (cit. on pp. 11, 26, 38, 71, 101, 107, 119, 127, 132, 275).
- [42] Cordesse, P., Remigi, A., Duret, B., MURRONE, A., Ménard, T., Demoulin, F.-X., and Massot, M. “Validation strategy of reduced-order two-fluid flow models based on a hierarchy of direct numerical simulations”. submitted to FTaC. Nov. 2019. URL: <https://hal.archives-ouvertes.fr/hal-02350200> (cit. on pp. 12, 27, 237, 248, 276).
- [43] Davis, S. F. “Simplified Second-Order Godunov-Type Methods”. *SIAM J. Sci. Stat. Comput.*, 9.3, 445–473, May 1988. URL: <https://doi.org/10.1137/0909030> (cit. on p. 204).
- [44] De Chaisemartin, S., Fréret, L., Kah, D., Laurent, F., Fox, R., Reveillon, J., and Massot, M. “Eulerian models for turbulent spray combustion with polydispersity and droplet crossing”. *Comptes Rendus Mécanique*, 337.6, 438–448, 2009. URL: <http://www.sciencedirect.com/science/article/pii/S1631072109000801> (cit. on p. 240).
- [45] De lorenzo, M. “Modelling and numerical simulation of metastable two-phase flows”. Theses. Université Paris-Saclay, May 2018. URL: <https://pastel.archives-ouvertes.fr/tel-01889103> (cit. on pp. 8, 23, 53).
- [46] Debar, R. “Fundamentals of the KRAKEN code. [Eulerian hydrodynamics code for compressible nonviscous flow of several fluids in two-dimensional (axially symmetric) region]”. *Technical Report UCIR-760* 1974. URL: <https://ci.nii.ac.jp/naid/10006079211/en/> (cit. on p. 143).
- [47] Deledicque, V. and Papalexandris, M. V. “An Exact Riemann Solver for Compressible Two-phase Flow Models Containing Non-conservative Products”. *J. Comput. Phys.*, 222.1, 217–245, Mar. 2007. URL: <http://dx.doi.org/10.1016/j.jcp.2006.07.025> (cit. on pp. 9, 24).
- [48] Delhayé, J.-M. “Some issues related to the modeling of interfacial areas in gas–liquid flows I. The conceptual issues”. *Comptes Rendus de l’Académie des Sciences - Series IIB - Mechanics*, 329.5, 397–410, 2001. URL: <http://www.sciencedirect.com/science/article/pii/S1620774201013472> (cit. on p. 145).
- [49] Delon, A., Cartellier, A. H., and Matas, J.-P. “Flapping instability of a liquid jet”. *Physical Review Fluids*, 3.4 Apr. 2018. URL: <https://hal.archives-ouvertes.fr/hal-01761377> (cit. on p. 250).

- [50] Delon, A., Matas, J.-P., and Cartellier, A. “Flapping instability of a liquid jet”. *8th International Conference on Multiphase Flow, ICMF 2013, Jeju, Korea, May 26 - 31, 2013*. South Korea, May 2013, ICMF2013–586. URL: <https://hal.archives-ouvertes.fr/hal-00937742> (cit. on pp. 6, 20, 250).
- [51] Desjardins, O., McCaslin, J., Owkes, M., and Brady, P. “Direct Numerical and Large-Eddy Simulation of primary atomization in complex geometries”. *Atomization Sprays*, 23.11, 1001–1048, 2013 (cit. on pp. 5, 20, 166).
- [52] Després, B. and Dubois, F. *Systèmes hyperboliques de lois de conservation: application à la dynamique des gaz*. Mathématiques appliquées. Ecole polytechnique, 2005. URL: <https://books.google.fr/books?id=OUoPoT4B4rIC> (cit. on p. 75).
- [53] Di Battista, R. “Towards a Unified Eulerian Modeling Framework for Two-Phase Flow: Geometrical Subscale Phenomena and Associated Highly-Scalable Numerical Methods”. PhD thesis. Université de Paris-Saclay — École polytechnique, 2020 (cit. on p. 277).
- [54] Di Battista, R., Bermejo-Moreno, I., Ménard, T., de Chaisemartin, S., and Massot, M. “Post-Processing of Two-Phase DNS Simulations Exploiting Geometrical Features and Topological Invariants to Extract Flow Statistics and Droplets Number Density”. *ICMF Proceedings*. International Conference on Multiphase Flow. Rio de Janeiro, May 19–24, 2019. URL: <https://hal.archives-ouvertes.fr/hal-02345825v1> (cit. on pp. 170, 180).
- [55] Diu, B., Lederer, D., and Roulet, B. *Elements de Physique statistique*. Hermann, 1996 (cit. on p. 103).
- [56] Drew, D. “Evolution of Geometric Statistics”. *SIAM J. Appl. Math.*, 50.3, 649–666, 1990. eprint: <https://doi.org/10.1137/0150038>. URL: <https://doi.org/10.1137/0150038> (cit. on p. 145).
- [57] Drew, D. “Mathematical Modeling of Two-Phase Flow”. *Annu. Rev. Fluid Mech.*, 15, 291–291, 1983 (cit. on pp. 6, 21, 43, 45, 73, 100, 142).
- [58] Drew, D. and Passman, S. L. *Theory of Multicomponent Fluids*. vol. 135. Applied Mathematical Sciences. Springer, 1998 (cit. on p. 64).
- [59] Drui, F. “Eulerian modeling and simulations of separated and disperse two-phase flows : development of a unified modeling approach and associated numerical methods for highly parallel computations”. <https://tel.archives-ouvertes.fr/tel-01618320>. PhD Thesis. Université Paris-Saclay, July 2017 (cit. on pp. 6 sq., 21, 53, 163, 166).
- [60] Drui, F., Larat, A., Kokh, S., and Massot, M. “Small-scale kinematics of two-phase flows: identifying relaxation processes in separated- and disperse-phase flow models”. *J. Fluid Mech.*, 876, 326–355, 2019 (cit. on pp. 6 sq., 21, 52 sq., 72, 100 sqq., 122, 151, 155 sqq., 166 sq., 173, 175, 178 sqq.).
- [61] Dumouchel, C. “On the experimental investigation on primary atomization of liquid streams”. *Exp. Fluids*, 45, 371–422, Sept. 2008 (cit. on pp. 254 sq.).
- [62] Dupif, V. “Eulerian modeling and simulation of two-phase flows in solid rocket motors taking into account size polydispersion and droplet trajectory crossing”. Theses. Université Paris-Saclay, June 2018. URL: <https://tel.archives-ouvertes.fr/tel-01989050> (cit. on pp. 6, 21).

- [63] Duret, B., Canu, R., Reveillon, J., and Demoulin, F. “A pressure based method for vaporizing compressible two-phase flows with interface capturing approach”. *Int. J. Multiphase Flow*, 108, 42–50, 2018. URL: <http://www.sciencedirect.com/science/article/pii/S0301932218302799> (cit. on pp. 5, 19, 143).
- [64] Duret, B., Luret, G., Reveillon, J., Menard, T., Berlemont, A., and Demoulin, F. “DNS analysis of turbulent mixing in two-phase flows”. *Int. J. Multiphase Flow*, 40, 93–105, 2012. URL: <http://www.sciencedirect.com/science/article/pii/S0301932211002448> (cit. on pp. 170, 249).
- [65] Embid, P. and Baer, M. “Mathematical analysis of a two-phase continuum mixture theory”. *Cont. Mech. Therm.*, 4.4, 279–312, 1992 (cit. on pp. 8, 23, 48, 66 sq., 81).
- [66] Essadki, M., De Chaisemartin, S., Massot, M., Laurent, F., Larat, A., and Jay, S. “Adaptive Mesh Refinement and High Order Geometrical Moment Method for the Simulation of Polydisperse Evaporating Sprays”. *Oil & Gas Science and Technologie, Rev. IFP Energies Nouvelles*, 71.5, 25, 2016 (cit. on p. 146).
- [67] Essadki, M., Drui, F., Chaisemartin, S. de, Larat, A., Ménard, T., and Massot, M. “Statistical modeling of the gas-liquid interface using geometrical variables: toward a unified description of the disperse and separated phase flows”. *Int. J. Multiphase Flow*, 120, 204–216, 2019. URL: <https://hal.archives-ouvertes.fr/hal-01615076> (cit. on pp. 7, 21, 101, 146, 170).
- [68] Essadki, M., De Chaisemartin, S., Laurent, F., and Massot, M. “High order moment model for polydisperse evaporating sprays towards interfacial geometry”. *SIAM Journal on Applied Mathematics*, 78.4, 2003–2027, 2018. URL: <https://hal.archives-ouvertes.fr/hal-01355608> (cit. on pp. 7, 21, 146).
- [69] Fedkiw, R. P., Aslam, T., Merriman, B., and Osher, S. “A Non-oscillatory Eulerian Approach to Interfaces in Multimaterial Flows (the Ghost Fluid Method)”. *J. Comput. Phys.*, 152.2, 457–492, 1999. URL: <http://www.sciencedirect.com/science/article/pii/S0021999199962368> (cit. on pp. 5, 19, 170, 249).
- [70] Ferziger, J. H. and Kaper, H. G. *Mathematical theory of transport processes in gases*. North Holland Publishing Company, Amsterdam, 1972 (cit. on p. 72).
- [71] Forestier, A. and Gavriluk, S. “Criterion of hyperbolicity for non-conservative quasi-linear systems admitting a partially convex conservation law”. *Mathematical Methods in the Applied Sciences*, 34, 2148–2158, Nov. 2011 (cit. on pp. 8, 23, 73, 90, 277).
- [72] Frenkel, J. *Kinetic Theory of Liquids*. The Clarendon Press, Oxford, 1946 (cit. on p. 141).
- [73] Friedrichs, K. O. and Lax, P. D. “Systems of Conservation Equations with a Convex Extension”. *Proceedings of the National Academy of Sciences*, 68.8, 1686–1688, 1971. eprint: <http://www.pnas.org/content/68/8/1686.full.pdf>. URL: <http://www.pnas.org/content/68/8/1686> (cit. on pp. 8, 22, 70, 72, 101).
- [74] Furfaro, D. and Saurel, R. “A simple HLLC-type Riemann solver for compressible non-equilibrium two-phase flows”. *Computers & Fluids*, 111, 159–178, 2015 (cit. on pp. 9, 24, 240, 246, 248).
- [75] Fyfe, D., Oran, E., and Fritts, M. “Surface tension and viscosity with lagrangian hydrodynamics on a triangular mesh”. *J. Comput. Phys.*, 76.2, 349–384, 1988. URL: <http://www.sciencedirect.com/science/article/pii/0021999188901477> (cit. on p. 222).

- [76] Gaillard, P., Le Touze, C., Matuszewski, L., and Murrone, A. “Numerical Simulation of Cryogenic Injection in Rocket Engine Combustion Chambers”. *AerospaceLab*, 11, 16, 2016. URL: <https://hal.archives-ouvertes.fr/hal-01369627> (cit. on pp. 7, 21, 72, 208).
- [77] Gaillard, P. “Diffuse interfaces and LOX/H₂ transcritical flames”. Theses. Université Pierre et Marie Curie - Paris VI, Dec. 2015. URL: <https://tel.archives-ouvertes.fr/tel-01308564> (cit. on p. 110).
- [78] Gallouët, T., Hérard, J.-M., and Seguin, N. “Numerical modeling of two-phase flows using the two-fluid two-pressure approach”. *Math. Models Methods Appl. Sci.*, 14.05, 663–700, 2004 (cit. on pp. 8, 10, 23 sq., 66, 69, 73, 81 sq., 85, 90, 102, 127).
- [79] Gavrilyuk, S. and Gouin, H. “A new form of governing equations of fluids arising from Hamilton’s principle”. *Int. J. Eng. Sci.*, 37.12, 1495–1520, 1999. URL: <http://www.sciencedirect.com/science/article/pii/S0020722598001311> (cit. on pp. 50, 122).
- [80] Gavrilyuk, S., Gouin, H., and Perepechko, Y. “A variational principle for two-fluid models”. *Comptes Rendus de l’Académie des Sciences - Series IIB - Mechanics-Physics-Astronomy*, 8.324, 483–490, 1997. eprint: 0802.0609 (physics.class-ph) (cit. on pp. 49, 122).
- [81] Gavrilyuk, S. and Saurel, R. “Mathematical and numerical modeling of two-phase compressible flows with micro-inertia”. *J. Comput. Phys.*, 175.1, 326–360, 2002 (cit. on pp. 50, 52, 62, 72, 101 sq., 122, 173).
- [82] Gavrilyuk, S., Gouin, H., and Perepechko, Y. V. “Hyperbolic Models of Homogeneous Two-Fluid Mixtures”. *Meccanica*, 33.2, 161–175, 1998. URL: <http://dx.doi.org/10.1023/A:1004354528016> (cit. on p. 49).
- [83] Geurst, J. “Variational principles and two-fluid hydrodynamics of bubbly liquid/gas mixtures”. *Physica A*, 135.2, 455–486, 1986. URL: <http://www.sciencedirect.com/science/article/pii/0378437186901548> (cit. on pp. 49, 122).
- [84] Geurst, J. “Virtual mass in two-phase bubbly flow”. *Physica A*, 129.2, 233–261, 1985. URL: <http://www.sciencedirect.com/science/article/pii/0378437185901682> (cit. on pp. 49, 122).
- [85] Giovangigli, V. and Massot, M. “Asymptotic Stability of equilibrium states for multi-component reactive flows”. *Math. Models Methods Appl. Sci.*, 8.2, 251–297, 1998 (cit. on pp. 8, 22, 72, 78, 90, 101).
- [86] Giovangigli, V. and Massot, M. “Entropic structure of multicomponent reactive flows with partial equilibrium reduced chemistry”. *Math. Methods Appl. Sci.*, 27, 739–768, 2004 (cit. on p. 90).
- [87] Giovangigli, V. and Matuszewski, L. “Supercritical fluid thermodynamics from equations of state”. *Physica D*, 241.6, 649–670, 2012. URL: <http://www.sciencedirect.com/science/article/pii/S0167278911003423> (cit. on pp. 100 sq., 110, 112 sq., 115).
- [88] Glimm, J., Graham, M., Grove, J., Li, X., Smith, T., Tan, D., Tangerman, F., and Zhang, Q. “Front tracking in two and three dimensions”. *Computers & Mathematics with Applications*, 35.7, 1–11, Apr. 1998. URL: <https://doi.org/10.1016%2Fs0898-1221%2898%2900028-5> (cit. on p. 142).

- [89] Glimm, J., Grove, J., Li, X., Oh, W., and Sharp, D. “A Critical Analysis of Rayleigh–Taylor Growth Rates”. *Journal of Computational Physics*, 169.2, 652–677, 2001. URL: <http://www.sciencedirect.com/science/article/pii/S0021999100965902> (cit. on pp. 5, 19).
- [90] Godlewski, E. and Raviart, P.-A. *Numerical Approximation of Hyperbolic Systems of Conservation Laws*. Springer, 1996 (cit. on pp. 74 sq.).
- [91] Godunov, S. K. “An Interesting Class of Quasilinear Systems”. *Soviet Math. Dokl.*, 2.3, 947–949, 1961 (cit. on pp. 8, 22, 70, 72).
- [92] Gouin. “Thermodynamic form of the equation of motion for perfect fluids of grade n ”. *Comptes Rendus de l’Academie des Sciences Serie II*, 305.2, 833–83, 1987. URL: [hal-00488912](http://hal.archives-ouvertes.fr/hal-00488912) (cit. on p. 142).
- [93] Gouin, H. “Variational Theory of Mixtures in Continuum Mechanics”. *European Journal of Mechanics - B/Fluids*, 9.5, 469–491, 1990. URL: <https://hal.archives-ouvertes.fr/hal-00306965> (cit. on pp. 49, 52, 91, 122).
- [94] Gouin, H. and Gavrilyuk, S. “Hamilton’s Principle and Rankine-Hugoniot Conditions for General Motions of Mixtures”. *Meccanica, Springer Verlag*, 34.1, 39–47, 1999. URL: <https://hal.archives-ouvertes.fr/hal-00249829> (cit. on pp. 50, 122, 124).
- [95] Gouin, H. and Ruggeri, T. “The Hamilton principle for fluid binary mixtures with two temperatures”. *Bollettino della Unione Matematica Italiana*, 9.2, 403–422, Apr. 2009 (cit. on pp. 50 sqq., 58, 60, 63, 72, 119, 124).
- [96] Graille, B., Magin, T. E., and Massot, M. “Kinetic theory of plasmas: translational energy”. *Math. Models Methods Appl. Sci.*, 19.4, 527–599, 2009 (cit. on pp. 72 sq., 87, 90).
- [97] Gray, A. “An Introduction to Weyl’s Tube Formula”. *Tubes*. Birkhäuser Basel, Basel, 2004, 1–12. URL: https://doi.org/10.1007/978-3-0348-7966-8_1 (cit. on p. 165).
- [98] Guazzelli, E. and Pouliquen, o. “Rheology of dense granular suspensions”. *Journal of Fluid Mechanics*, 852 Oct. 2018. URL: <https://hal.archives-ouvertes.fr/hal-01902053> (cit. on pp. 101, 125).
- [99] Guion, A., Afkhami, S., Zaleski, S., and Buongiorno, J. “Simulations of microlayer formation in nucleate boiling”. *International Journal of Heat and Mass Transfer*, 127, 1271–1284, Dec. 2018. URL: <https://doi.org/10.1016%2Fj.ijheatmasstransfer.2018.06.041> (cit. on p. 141).
- [100] Gujrati, P. D. “Effects of Particle sizes, Non-Isometry and Interactions in Compressible Polymer Mixtures”. *eprint arXiv:cond-mat/0308598* Aug. 2003. eprint: [cond-mat/0308598](https://arxiv.org/abs/cond-mat/0308598) (cit. on p. 101).
- [101] Habiballah, M., Vingert, L., Traineau, J., and Vuillermoz, P. “MASCOTTE : A test bench for cryogenic combustion research.” *47th International astronautical congress*. 1997 (cit. on pp. 3, 17, 241).
- [102] Harlow, F. H. and Welch, J. E. “Numerical Calculation of Time-Dependent Viscous Incompressible Flow of Fluid with Free Surface”. *Phys. Fluids*, 8.12, 2182, 1965 (cit. on pp. 5, 19, 143).
- [103] Harten, A. “On the symmetric form of systems of conservation laws with entropy”. *J. Comput. Phys.*, 49.1, 151–164, 1983. URL: <http://www.sciencedirect.com/science/article/pii/0021999183901183> (cit. on p. 101).

- [104] Harten, A. and Hyman, J. M. “Self adjusting grid methods for one-dimensional hyperbolic conservation laws”. *J. Comput. Phys.*, 50.2, 235–269, 1983 (cit. on pp. 8, 22, 72, 75).
- [105] Hecht, N. “Large eddy simulation for liquid-gas flow : application to atomization”. PhD Thesis. INSA de Rouen, Mar. 2016. URL: <https://tel.archives-ouvertes.fr/tel-01654625> (cit. on pp. 6, 21).
- [106] Herrmann, M. “A sub-grid surface dynamics model for sub-filter surface tension induced interface dynamics”. *Computers & Fluids*, 87. USNCCM Moving Boundaries, 92–101, 2013. URL: <http://www.sciencedirect.com/science/article/pii/S0045793013000637> (cit. on pp. 6 sq., 9, 21, 23, 147, 166 sq., 169, 186 sq.).
- [107] Herrmann, M. “A Dual-Scale LES Subgrid Model for Turbulent Liquid/Gas Phase Interface Dynamics”. *Volume 1: Symposia*. ASME, 2015 (cit. on p. 147).
- [108] Hirt, C. and Nichols, B. “Volume of fluid (VOF) method for the dynamics of free boundaries”. *J. Comput. Phys.*, 39.1, 201–225, Jan. 1981 (cit. on pp. 5, 19, 143).
- [109] Igra, D. and Takayama, K. “A study of shock wave loading on a cylindrical water column”. *Technical Report, Institute of Fluid Science, Tohoku University*, 13, 19–36, Mar. 2001 (cit. on pp. 224 sq., 228 sq.).
- [110] Ishii, M. *Thermo-fluid dynamic theory of two-phase flow*. Eyrolles, 1975 (cit. on pp. 40, 42, 100, 142).
- [111] Jamet, D. “Diffuse interface models in fluid mechanics”. *CEA-Grenoble* (cit. on p. 131).
- [112] Jamet, D., Lebaigue, O., Coutris, N., and Delhayé, J. “The Second Gradient Method for the Direct Numerical Simulation of Liquid–Vapor Flows with Phase Change”. *Journal of Computational Physics*, 169.2, 624–651, May 2001. URL: <https://doi.org/10.1006/Jcp.2000.6692> (cit. on p. 142).
- [113] Jawurek, H. “Simultaneous determination of microlayer geometry and bubble growth in nucleate boiling”. *International Journal of Heat and Mass Transfer*, 12.8, 843–848, Aug. 1969. URL: <https://doi.org/10.1016%2F0017-9310%2869%2990151-3> (cit. on p. 141).
- [114] Jemison, M., Sussman, M., and Arienti, M. “Compressible, multiphase semi-implicit method with moment of fluid interface representation”. *Journal of Computational Physics*, 279, 182–217, 2014. URL: <http://www.sciencedirect.com/science/article/pii/S0021999114006317> (cit. on pp. 5, 19).
- [115] Kapila, A. K., Menikoff, R., Bdzil, J. B., Son, S. F., and Stewart, D. S. “Two-phase modeling of deflagration-to-detonation transition in granular materials: Reduced equations”. *Phys. Fluids*, 13.10, 3002–3024, 2001 (cit. on pp. 7, 22, 54, 100, 195).
- [116] Kapila, A. K., Son, S. F., Bdzil, J. B., Menikoff, R., and Stewart, D. S. “Two-phase modeling of DDT: Structure of the velocity-relaxation zone”. *Phys. Fluids*, 9.12, 3885–3897, 1997. eprint: <https://doi.org/10.1063/1.869488>. URL: <https://doi.org/10.1063/1.869488> (cit. on pp. 73, 83, 85).
- [117] Kataoka, I., Ishii, M., and Serizawa, A. “Local formulation and measurements of interfacial area concentration in two-phase flow”. *Int. J. Multiphase Flow*, 12.4, 505–529, 1986. URL: <http://www.sciencedirect.com/science/article/pii/S0301932286900571> (cit. on p. 145).

- [118] Kawashima, S. and Shizuta, Y. “On the normal form of the symmetric hyperbolic-parabolic systems associated with the conservation laws”. *Tohoku Math. J.*, 40.3, 449–464, 1988. URL: <https://doi.org/10.2748/tmj/1178227986> (cit. on pp. 8, 22, 72, 101).
- [119] Kim, H. and Buongiorno, J. “Detection of liquid–vapor–solid triple contact line in two-phase heat transfer phenomena using high-speed infrared thermometry”. *International Journal of Multiphase Flow*, 37.2, 166–172, Mar. 2011. URL: <https://doi.org/10.1016/j.ijmultiphaseflow.2010.09.010> (cit. on p. 141).
- [120] Klein, M., Ketterl, S., and Hasslberger, J. “Large eddy simulation of multiphase flows using the volume of fluid method: Part 1—Governing equations and a priori analysis”. *Experimental and Computational Multiphase Flow*, 1.2, 130–144, May 2019 (cit. on p. 146).
- [121] Korteweg, D.J. “Sur la forme que prennent les équations de mouvements des fluides si l’on tient compte des forces capillaires par des variations de densité”. *Arch. Néer. Sci. Exactes Sér. II*, 6, 1–24, 1901 (cit. on pp. 100, 142).
- [122] Kružkov, S. N. “First-order quasilinear equations in several independent variables”. *Math. USSR Sb.*, 10.2, 217, 1970. URL: <http://stacks.iop.org/0025-5734/10/i=2/a=A06> (cit. on pp. 8, 22, 72, 101).
- [123] Kuila, S., Sekhar, T. R., and Zeidan, D. “A Robust and accurate Riemann solver for a compressible two-phase flow model”. *Appl. Math. Comput.*, 265, 681–695, 2015. URL: <http://www.sciencedirect.com/science/article/pii/S0096300315007109> (cit. on pp. 5, 19, 143).
- [124] Lalanne, B., Tanguy, S., and Risso, F. “Effect of Rising Motion on the Damped Shape Oscillations of Drops and Bubbles”. *Physics of Fluids*, 25.11, 112107, 2013 (cit. on pp. 168, 173).
- [125] Lamb, S. H. *Hydrodynamics*. Courier Corporation, Jan. 1, 1945. 774 pp. Google Books: [237xDg7T0RkC](https://books.google.com/books?id=237xDg7T0RkC) (cit. on p. 168).
- [126] Lamorgese, A. G., Molin, D., and Mauri, R. “Phase Field Approach to Multiphase Flow Modeling”. *Milan Journal of Mathematics*, 79.2, 597–642, Nov. 2011. URL: <https://doi.org/10.1007%2Fs00032-011-0171-6> (cit. on p. 142).
- [127] Landau, L. and Lifshitz, E. *Mechanics. Vol. 1 (3rd ed.)* ed. by Landau, L. and Lifshitz, E. Third Edition. Butterworth-Heinemann, 1976 (cit. on p. 72).
- [128] Lasheras, J. C. and Hopfinger, E. J. “Liquid Jet Instability and Atomization in a Coaxial Gas Stream”. *Annu. Rev. Fluid Mech.*, 32.1, 275–308, 2000. eprint: <https://doi.org/10.1146/annurev.fluid.32.1.275>. URL: <https://doi.org/10.1146/annurev.fluid.32.1.275> (cit. on pp. 250 sq.).
- [129] Lasheras, J. C., Villermaux, E., and Hopfinger, E. J. “Break-up and atomization of a round water jet by a high-speed annular air jet”. *J. Fluid Mech.*, 357, 351–379, 1998 (cit. on pp. 4, 18, 255).
- [130] Laurent, F. and Massot, M. “Multi-fluid modelling of laminar polydisperse spray flames: origin, assumptions and comparison of sectional and sampling methods”. *Combustion Theory and Modelling*, 5.4, 537–572, 2001. eprint: <https://doi.org/10.1088/1364-7830/5/4/303>. URL: <https://doi.org/10.1088/1364-7830/5/4/303> (cit. on pp. 10, 25, 240).

- [131] Le Métayer, O. and Saurel, R. “The Noble-Abel Stiffened-Gas equation of state”. *Phys. Fluids*, 28.4, 046102, 2016. eprint: <https://doi.org/10.1063/1.4945981>. URL: <https://doi.org/10.1063/1.4945981> (cit. on p. 104).
- [132] Le Touze, C. “Coupling between separated and dispersed two-phase flow models for the simulation of primary atomization in cryogenic combustion”. PhD Thesis. Université Nice Sophia Antipolis, 2015 (cit. on pp. 6 sq., 21 sq., 235, 239, 241, 275).
- [133] Le Touze, C., Murrone, A., and Guillard, H. “Multislope MUSCL method for general unstructured meshes”. *J. Comput. Phys.*, 284, 389–418, 2014 (cit. on pp. 207, 210 sq., 248).
- [134] Leroux, B., Delabroy, O., and Lacas, F. “Experimental study of coaxial atomizers scaling. Part I: dense core zone.” *Atomization Sprays*, 17.5, 381–407, 2007 (cit. on p. 255).
- [135] Lhuillier, D. “From Molecular Mixtures to Suspensions of Particles”. *Journal de Physique II France*, 5.1, 19–36, 1995 (cit. on pp. 101, 120, 126, 132, 278).
- [136] Lhuillier, D. “Phenomenology of inertia effects in a dispersed solid-fluid mixture”. *Int. J. Multiphase Flow*, 11.4, 427–444, 1985 (cit. on p. 132).
- [137] Lhuillier, D., Morel, C., and Delhayé, J.-M. “Bilan d’aire interfaciale dans un mélange diphasique : approche locale vs approche particulière”. *Comptes Rendus de l’Académie des Sciences - Series IIB - Mechanics-Physics-Astronomy*, 328.2, 143–149, 2000. URL: <http://www.sciencedirect.com/science/article/pii/S1287462000001022> (cit. on p. 145).
- [138] Lhuillier, D. *Rappels de Thermodynamique*. tech. rep. Laboratoire de Modélisation en Mécanique, CNRS et Université P. et M. Curie (Paris 6), 2019 (cit. on p. 107).
- [139] Lhuillier, D., Chang, C.-H., and Theofanous, T. G. “On the quest for a hyperbolic effective-field model of disperse flows”. *J. Fluid Mech.*, 731, 184–194, 2013 (cit. on pp. 44, 64, 128).
- [140] Ling, Y., Zaleski, S., and Scardovelli, R. “Multiscale simulation of atomization with small droplets represented by a Lagrangian point-particle model”. *Int. J. Multiphase Flow*, 76, 122–143, 2015. URL: <http://www.sciencedirect.com/science/article/pii/S0301932215001524> (cit. on pp. 5 sq., 20 sq., 166).
- [141] Liovic, P. and Lakehal, D. “Subgrid-scale modelling of surface tension within interface tracking-based Large Eddy and Interface Simulation of 3D interfacial flows”. *Computers & Fluids*, 63, 27–46, June 2012 (cit. on p. 147).
- [142] Liu, T., Khoo, B., and Wang, C. “The ghost fluid method for compressible gas–water simulation”. *Journal of Computational Physics*, 204.1, 193–221, 2005. URL: <http://www.sciencedirect.com/science/article/pii/S0021999104004139> (cit. on pp. 5, 19).
- [143] Liu, T., Khoo, B., and Yeo, K. “Ghost fluid method for strong shock impacting on material interface”. *Journal of Computational Physics*, 190.2, 651–681, 2003. URL: <http://www.sciencedirect.com/science/article/pii/S0021999103003012> (cit. on pp. 5, 19).
- [144] Lochon, H. “Modélisation et simulation d’écoulements transitoires eau-vapeur en approche bi-fluide”. PhD Thesis. Université d’Aix-Marseille, 2016 (cit. on pp. 8, 23, 53, 73, 81, 83).

- [145] Lorensen, W. E. and Cline, H. E. “Marching Cubes: A High Resolution 3D Surface Construction Algorithm”. *ACM Siggraph Computer Graphics*. vol. 21. ACM, 1987, 163–169 (cit. on p. 170).
- [146] Lorenzo, M. D., Lafon, P., Matteo, M. D., Pelanti, M., Seynhaeve, J.-M., and Bartosiewicz, Y. “Homogeneous two-phase flow models and accurate steam-water table look-up method for fast transient simulations”. *International Journal of Multiphase Flow*, 95, 199–219, 2017. URL: <http://www.sciencedirect.com/science/article/pii/S0301932216307236> (cit. on pp. 8, 23).
- [147] Lozano, A., Barreras, F., Hauke, G., and Dopazo, C. “Longitudinal instabilities in an air-blasted liquid sheet”. *J. Fluid Mech.*, 437, 143–173, 2001 (cit. on pp. 254 sq.).
- [148] M Devassy, B., Habchi, C., and Daniel, E. “Atomization modelling of liquid jets using a two-surface-density approach”. *Atomization Spray*, 25.1, 47–80, 2015 (cit. on pp. 7, 9, 21 sqq., 101 sq., 147, 166).
- [149] M Devassy, B. “Atomization Modeling of Liquid Jets using an Eulerian-Eulerian Model and a Surface Density Approach”. PhD thesis. Univ. Aix-Marseille, Jan. 2013 (cit. on pp. 7, 21).
- [150] Magin, T., Graille, B., and Massot, M. “Thermo-chemical dynamics and chemical quasi-equilibrium of plasmas in thermal non-equilibrium”. *Ann. Research Briefs, CTR, Stanford Uni.*, 71–82, 2009 (cit. on pp. 73, 87, 90).
- [151] Marble, F. E. and Broadwell, J. E. “The Coherent Flame Model of Turbulent Chemical Reactions”. *TRW Report 1977* (cit. on p. 144).
- [152] Marble, F. “Dynamics of a gas containing small solid particles”. *Combustion and Propulsion (5th AGARD Colloquium, Pergamon Press)* 1963 (cit. on p. 86).
- [153] Mareschal, M., Blawdziewicz, J., and Piasecki, J. “Local Entropy Production from the Revised Enskog Equation: General Formulation for Inhomogeneous Fluids”. *Phys. Rev. Lett.*, 52, 1169–1172, 14 Apr. 1984. URL: <https://link.aps.org/doi/10.1103/PhysRevLett.52.1169> (cit. on pp. 100, 103).
- [154] Marmottant, P. and Villermaux, E. “Atomisation primaire dans les jets coaxiaux”. *Combustion*, 2. cited By 1, 1–37, 2002 (cit. on p. 250).
- [155] Massot, M. “Singular perturbation analysis for the reduction of complex chemistry in gaseous mixtures using the entropic structure”. *Discrete and Continuous Dynamical Systems-Series B*, 2.3, 433–456, 2002 (cit. on p. 90).
- [156] Mathis, H. “A thermodynamically consistent model of a liquid-vapor fluid with a gas”. working paper or preprint. Oct. 2017. URL: <https://hal.archives-ouvertes.fr/hal-01615591> (cit. on p. 101).
- [157] McMillan, W. G. and Mayer, J. E. “The Statistical Thermodynamics of Multicomponent Systems”. *The Journal of Chemical Physics*, 13.7, 276–305, 1945. eprint: <https://doi.org/10.1063/1.1724036>. URL: <https://doi.org/10.1063/1.1724036> (cit. on p. 126).
- [158] Ménard, T., Tanguy, S., and Berlemont, A. “Coupling level set/VOF/ghost fluid methods: Validation and application to 3D simulation of the primary break-up of a liquid jet”. *Int. J. Multiphase Flow*, 33.5, 510–524, 2007. URL: <http://www.sciencedirect.com/science/article/pii/S0301932206001832> (cit. on pp. 170, 249).

- [159] Meyer, M., Desbrun, M., Schröder, P., and Barr, A. H. “Discrete Differential-Geometry Operators for Triangulated 2-Manifolds”. *Visualization and Mathematics III*. ed. by Hege, H.-C. and Polthier, K. red. by Farin, G., Hege, H.-C., Hoffman, D., Johnson, C. R., and Polthier, K. Springer Berlin Heidelberg, Berlin, Heidelberg, 2003, 35–57. URL: http://link.springer.com/10.1007/978-3-662-05105-4_2 (visited on 06/14/2018) (cit. on p. 170).
- [160] Miller, G. H. and Puckett, E. G. “A High-Order Godunov Method for Multiple Condensed Phases”. *J. Comput. Phys.*, 128.1, 134–164, 1996. URL: <http://www.sciencedirect.com/science/article/pii/S0021999196902004> (cit. on pp. 199, 205 sq.).
- [161] Mock, M. “Systems of conservation laws of mixed type”. *Journal of Differential Equations*, 37.1, 70–88, 1980. URL: <http://www.sciencedirect.com/science/article/pii/0022039680900893> (cit. on pp. 8, 22, 72).
- [162] Morel, C. *Mathematical Modeling of Disperse Two-Phase Flows*. Fluid Mechanics and Its Applications. Springer International Publishing, 2015. URL: <https://books.google.fr/books?id=L7Q0CgAAQBAJ> (cit. on p. 145).
- [163] Murrone, A., Boucher, A., and Cordesse, P. “A five equation model for the simulation of the two-phase flow in cryogenic coaxial injector”. *Space Propulsion 2018 Proceedings*. Space Propulsion 2018. Seville, Spain, 2018. URL: <https://hal.archives-ouvertes.fr/hal-02195012> (cit. on pp. 7, 12, 22, 27, 237).
- [164] Murrone, A. and Guillard, H. “A five equation reduced model for compressible two phase flow problems”. *J. Comput. Phys.*, 202, 664–698, 2005 (cit. on pp. 54, 91, 100, 193, 195, 212).
- [165] Murrone, A. and Le Touze, C. *Eulerian coupling of two-phase flow models for the large eddy simulation of the atomization in cryogenic combustion chamber*. ed. by Array. 2019. URL: <https://doi.org/10.1051/eucass/201911195> (cit. on p. 239).
- [166] Noh, W. F. and Woodward, P. “SLIC (Simple Line Interface Calculation)”. *Proceedings of the Fifth International Conference on Numerical Methods in Fluid Dynamics June 28 – July 2, 1976 Twente University, Enschede*. ed. by Vooren, A. I. van de and Zandbergen, P. J. Springer Berlin Heidelberg, Berlin, Heidelberg, 1976, 330–340 (cit. on p. 143).
- [167] O’Rourke, P. J. and Amsden, A. A. “The Tab Method for Numerical Calculation of Spray Droplet Breakup”. *SAE Technical Paper Series*. SAE International, Nov. 1987 (cit. on pp. 167, 169, 179).
- [168] Olver, P. *Applications of Lie groups to differential equations*. Graduate texts in mathematics. Springer-Verlag, 1986. URL: <https://books.google.fr/books?id=D2APAQAAMAAJ> (cit. on p. 72).
- [169] Osher, S. and Sethian, J. A. “Fronts propagating with curvature-dependent speed: Algorithms based on Hamilton-Jacobi formulations”. *J. Comput. Phys.*, 79.1, 12–49, Nov. 1988 (cit. on pp. 5, 19, 143).
- [170] Öttinger, H. C. *Beyond Equilibrium Thermodynamics*. Wiley-Interscience, 2005 (cit. on p. 278).
- [171] Patureau de Mirand, A., Bahu, J.-M., and Gogdet, O. “Ariane Next, a vision for the next generation of Ariane Launchers”. *Acta Astronautica*, 170, 735–749, 2020. URL: <http://www.sciencedirect.com/science/article/pii/S0094576520300631> (cit. on pp. 1, 16).

- [172] Pelanti, M. and Shyue, K.-M. “A mixture-energy-consistent six-equation two-phase numerical model for fluids with interfaces, cavitation and evaporation waves”. *Journal of Computational Physics*, 259, 331–357, 2014. URL: <http://www.sciencedirect.com/science/article/pii/S0021999113008024> (cit. on pp. 10, 24, 191, 194).
- [173] Perigaud, G. and Saurel, R. “A Compressible Flow Model with Capillary Effects”. *J. Comput. Phys.*, 209.1, 139–178, Oct. 2005. URL: <http://dx.doi.org/10.1016/j.jcp.2005.03.018> (cit. on pp. 162, 220 sq.).
- [174] Pope, S. B. “The evolution of surfaces in turbulence”. *Int. J. Eng. Sci.*, 26, 445–469, 1988 (cit. on p. 144).
- [175] Porcheron, E., Carreau, J.-L., Visage, D. L., and Roger, F. “Effect of injection gas density on coaxial liquid jet atomization”. *Atomization Sprays*, 12.1-3, 209–227, 2002 (cit. on p. 255).
- [176] Powers, J.-M. “Theory of detonation structure for two-phase materials”. PhD Thesis. Illinois Univ., 1988 (cit. on p. 73).
- [177] Powers, J., Stewart, D., and Krier, H. “Theory of two-phase detonation—Part I: Modeling”. *Combust. Flame*, 80.3, 264–279, 1990. URL: <http://www.sciencedirect.com/science/article/pii/001021809090104Y> (cit. on p. 73).
- [178] Prausnitz, J., Lichtenthaler, R., and Azevedo, E. de. *Molecular Thermodynamics of Fluid-Phase Equilibria*. Pearson Education, 1998. URL: <https://books.google.fr/books?id=VSwc1XUmYpCC> (cit. on p. 100).
- [179] Prosperetti, A. and Tryggvason, G. *Computational Methods For Multiphase Flow*. Cambridge University Press, 2007. URL: <https://www.amazon.com/Computational-Methods-Multiphase-Andrea-Prosperetti/dp/0521847648?SubscriptionId=AKIAIOBINVZYXZQZ2U3A&tag=chimbiori05-20&linkCode=xm2&camp=2025&creative=165953&creativeASIN=0521847648> (cit. on p. 142).
- [180] Prosperetti, A. “Free oscillations of drops and bubbles: the initial-value problem”. *J. Fluid Mech.*, 100.02, 333, Sept. 1980 (cit. on p. 168).
- [181] Ransom, V. and Hicks, D. “Hyperbolic two-pressure models for two-phase flow”. *J. Comput. Phys.*, 53.1, 124–151, 1984 (cit. on p. 45).
- [182] Rayleigh, L. “On the Capillary Phenomena of Jets”. *Proc. Roy. Soc. London*, 29, 71–97, 1879. URL: <http://www.jstor.org/stable/113738> (cit. on p. 222).
- [183] Redlich, O. and Kwong, J. N. S. “On the Thermodynamics of Solutions. V. An Equation of State. Fugacities of Gaseous Solutions”. *Chemical Reviews*, 44.1, 233–244, Feb. 1949 (cit. on p. 104).
- [184] Refloch, A., Courbet, B., Murrone, A., Villedieu, P., Laurent, C., Gilbank, P., Troyes, J., Tessé, L., Chaineray, G., Dargaud, J., Quémerais, E., and Vuillot, F. “CEDRE Software”. *Aerospace Lab*, 1.2 Mar. 2011 (cit. on pp. 7, 10, 21, 25, 208).
- [185] Rehab, H., Villermaux, E., and Hopfinger, E. J. “Flow regimes of large-velocity-ratio coaxial jets”. *J. Fluid Mech.*, 345, 357–381, 1997 (cit. on p. 250).
- [186] Remigi, A. “Numerical modeling of an aeronautical injector, from the internal flow to the dispersed spray”. PhD thesis. Université de Rouen Normandie, 2021 (cit. on p. 278).
- [187] Sabat, M. “Eulerian modeling and numerical methods for the description of turbulent polydisperse sprays”. PhD thesis. Université Paris-Saclay, 2016 (cit. on pp. 6, 21).

- [188] Sabat, M., Vié, A., Larat, A., and Massot, M. “Statistical description of turbulent particle-laden flows in the very dilute regime using the anisotropic Gaussian moment method”. *Int. J. Multiphase Flow*, 112, 243–257, 2019. URL: <http://www.sciencedirect.com/science/article/pii/S0301932218301526> (cit. on pp. 7, 21).
- [189] Sainsaulieu, L. “Finite Volume Approximation of Two Phase-Fluid Flows Based on an Approximate Roe-Type Riemann Solver”. *J. Comput. Phys.*, 121.1, 1–28, 1995. URL: <http://www.sciencedirect.com/science/article/pii/S002199918571176X> (cit. on pp. 10, 24, 86, 101 sq., 125).
- [190] Saurel, R. and Abgrall, R. “A Multiphase Godunov Method for Compressible Multifluid and Multiphase Flows”. *J. Comput. Phys.*, 150.2, 435–467, 1999 (cit. on pp. 9 sq., 24, 44 sq., 47, 64 sq., 80, 100, 193).
- [191] Saurel, R., Gavriluk, S., and Renaud, F. “A multiphase model with internal degrees of freedom : application to shock-bubble interaction”. *J. Fluid Mech.*, 495, 283–321, 2003 (cit. on pp. 53, 73, 77, 84, 102, 127, 248).
- [192] Saurel, R. and Le Métayer, O. “A multiphase model for compressible flows with interfaces, shocks, detonation waves and cavitation”. *J. Fluid Mech.*, 431, 239–271, 2001 (cit. on pp. 46, 86).
- [193] Saurel, R., Le Métayer, O., Massoni, J., and Gavriluk, S. “Shock jump relations for multiphase mixtures with stiff mechanical relaxation”. *Shock Waves*, 16.3, 209–232, 2007. URL: <http://dx.doi.org/10.1007/s00193-006-0065-7> (cit. on p. 203).
- [194] Saurel, R. and Pantano, C. “Diffuse-Interface Capturing Methods for Compressible Two-Phase Flows”. *Annu. Rev. Fluid Mech.*, 50.1, 105–130, 2018. eprint: <https://doi.org/10.1146/annurev-fluid-122316-050109> (cit. on p. 246).
- [195] Saurel, R., Petitpas, F., and Berry, R. A. “Simple and efficient relaxation methods for interfaces separating compressible fluids, cavitating flows and shocks in multiphase mixtures”. *J. Comput. Physics*, 228, 1678–1712, 2009 (cit. on pp. 10 sq., 24, 26, 54, 100, 191, 194, 199, 205 sq., 210).
- [196] Schlichting, H. *Boundary - Layer Theory*. McGraw-Hill, 1979 (cit. on p. 256).
- [197] Schmidmayer, K., Petitpas, F., Daniel, E., Favrie, N., and Gavriluk, S. “A model and numerical method for compressible flows with capillary effects”. *J. Comput. Phys.*, 334, 468–496, 2017. URL: <http://www.sciencedirect.com/science/article/pii/S0021999117300116> (cit. on pp. 195 sqq., 205, 222, 224, 230, 232).
- [198] Schroeder, W., Maynard, R., and Geveci, B. “Flying Edges: A High-Performance Scalable Isocontouring Algorithm”. IEEE, Oct. 2015, 33–40. URL: <http://ieeexplore.ieee.org/document/7348069/> (visited on 06/28/2018) (cit. on p. 170).
- [199] Schwendeman, D., Wahle, C., and Kapila, A. “The Riemann problem and a high-resolution Godunov method for a model of compressible two-phase flow”. *J. Comput. Phys.*, 212.2, 490–526, 2006. URL: <http://www.sciencedirect.com/science/article/pii/S002199910500330X> (cit. on pp. 9, 24).
- [200] Serrin, J. “Mathematical Principles of Classical Fluid Mechanics”. *Fluid Dynamics I / Strömungsmechanik I*. ed. by Truesdell, C. Springer Berlin Heidelberg, Berlin, Heidelberg, 1959, 125–263. URL: http://dx.doi.org/10.1007/978-3-642-45914-6_2 (cit. on pp. 48, 72, 122).

- [201] Shinjo, J. and Umemura, A. “Simulation of liquid jet primary breakup: Dynamics of ligament and droplet formation”. *Int. J. Multiphase Flow*, 36.7, 513–532, 2010. URL: <http://www.sciencedirect.com/science/article/pii/S0301932210000637> (cit. on p. 166).
- [202] Sibra, A., Dupays, J., Murrone, A., Laurent, F., and Massot, M. “Simulation of reactive polydisperse sprays strongly coupled to unsteady flows in solid rocket motors: Efficient strategy using Eulerian Multi-Fluid methods”. *J. Comput. Phys.*, 339, 210–246, 2017. URL: <http://www.sciencedirect.com/science/article/pii/S0021999117300967> (cit. on pp. 6, 21, 240, 248).
- [203] Soave, G. “Equilibrium constants from a modified Redlich-Kwong equation of state”. *Chem. Eng. Sci.*, 27, 157–172, 1972 (cit. on p. 104).
- [204] Stapper, B. and Samuelsen, G. “An experimental study of the breakup of a two-dimensional liquid sheet in the presence of co-flow air shear”. *28th Aerospace Sciences Meeting*. 1990, 461 (cit. on p. 255).
- [205] Sussman, M., Smith, K., Hussaini, M., Ohta, M., and Zhi-Wei, R. “A sharp interface method for incompressible two-phase flows”. *J. Comp. Phys.*, 221.2, 469–505, 2007. URL: <http://www.sciencedirect.com/science/article/pii/S0021999106002981> (cit. on p. 249).
- [206] Sussman, M. and Puckett, E. G. “A Coupled Level Set and Volume-of-Fluid Method for Computing 3D and Axisymmetric Incompressible Two-Phase Flows”. *J. Comp. Phys.*, 162.2, 301–337, 2000. URL: <http://www.sciencedirect.com/science/article/pii/S0021999100965379> (cit. on p. 143).
- [207] Landau, L. and Lifshitz, E. *Fluid Mechanics (Second Edition)*. ed. by Landau, L. and Lifshitz, E. Second Edition. Pergamon Press, 1987, ifc2-. URL: <http://www.sciencedirect.com/science/article/pii/B9780080339337500015> (cit. on pp. 46, 51, 124).
- [208] Taylor, G. I. *The Scientific Papers of Sir Geoffrey Ingram Taylor, Volume IV*. Cambridge University Press, May 20, 2011. 652 pp. URL: https://www.ebook.de/de/product/13155226/geoffrey_ingram_taylor_the_scientific_papers_of_sir_geoffrey_ingram_taylor_volume_iv.html (cit. on p. 168).
- [209] Tomar, G., Fuster, D., Zaleski, S., and Popinet, S. “Multiscale simulations of primary atomization”. *Computers & Fluids*, 39.10, 1864–1874, 2010. URL: <http://www.sciencedirect.com/science/article/pii/S0045793010001490> (cit. on pp. 5, 20).
- [210] Toro, E., Spruce, M., and Speares, W. “Restoration of the contact surface in the HLL Riemann solver”. *Shock Waves*, 4.1, 25–34, 1994 (cit. on p. 201).
- [211] Toutant, A., Labourasse, E., Lebaigue, O., and Simonin, O. “DNS of the interaction between a deformable buoyant bubble and a spatially decaying turbulence: A priori tests for LES two-phase flow modelling”. *Computers & Fluids*, 37.7, 877–886, Aug. 2008 (cit. on p. 147).
- [212] Truesdell, C. *Rational Thermodynamics*. 2nd ed. 578. McGraw Hill, 1969 (cit. on pp. 46, 72, 100).
- [213] Tryggvason, G., Bunner, B., Esmaeeli, A., Juric, D., Al-Rawahi, N., Tauber, W., Han, J., Nas, S., and Jan, Y.-J. “A Front-Tracking Method for the Computations of Multiphase Flow”. *J. Comput. Phys.*, 169.2, 708–759, May 2001 (cit. on pp. 5, 19, 142 sq.).

- [214] Tryggvason, G., Scardovelli, R., and Zaleski, S. *Direct Numerical Simulations of Gas–Liquid Multiphase Flows*. Cambridge University Press, 2011 (cit. on pp. 5, 20).
- [215] Van der Waals, J. “Thermodynamische Theorie der Kapillarität unter Voraussetzung stetiger Dichteänderung”. *Z. Phys. Chem*, 13, 657–725, 1894 (cit. on pp. 100, 142).
- [216] Vaudor, G., Ménard, T., Aniszewski, W., Doring, M., and Berlemont, A. “A consistent mass and momentum flux computation method for two phase flows. Application to atomization process”. *Computers & Fluids*, 152 Apr. 2017 (cit. on pp. 5 sq., 20, 41, 170, 249 sq.).
- [217] Vingert, L., Habiballah, M., and Traineau, J. “MASCOTTE: a research facility for high pressure combustion of cryogenic propellants”. *EAC Proceedings, Paris, France 1999* (cit. on pp. 3, 17, 241).
- [218] Wallis, G. B. *One-dimensional two-phase flow*. McGraw-Hill, 1969 (cit. on p. 212).
- [219] Wargnier, Q., Faure, S., Graille, B., Magin, T. E., and Massot, M. “Numerical treatment of the nonconservative product in a multiscale fluid model for plasmas in thermal nonequilibrium: application to solar physics”. submitted <https://hal.archives-ouvertes.fr/hal-01811837>. June 2018. URL: <https://hal.archives-ouvertes.fr/hal-01811837> (cit. on pp. 9, 24, 73).
- [220] Wood, A. *A Textbook of Sound: Being an Account of the Physics of Vibrations with Special Reference to Recent Theoretical and Technical Developments*. G. Bell and Sons Ltd., 1930. URL: <https://books.google.fr/books?id=E7VaAAAAYAAJ> (cit. on p. 212).
- [221] Woods, L. *The thermodynamics of fluid systems*. Clarendon Press, 1975 (cit. on pp. 72, 100).
- [222] Wörner, M., Sabisch, W., Grötzbach, G., and Cacuci, D. “Volume-averaged conservation equations for volume-of-fluid interface tracking”. *Fourth International Conference on Multiphase Flow (ICMF)*. 2001 (cit. on p. 147).
- [223] Young, J. “The fundamental equations of gas-droplet multiphase flow”. *Int. J. Multiphase Flow*, 21.2, 175–191, 1995 (cit. on pp. 105, 152).
- [224] Zamansky, R., Coletti, F., Massot, M., and Mani, A. “Turbulent thermal convection driven by heated inertial particles”. *J. Fluid Mech.*, 809, 390–437, 2016 (cit. on pp. 6, 21).
- [225] Zandian, A., Sirignano, W. A., and Hussain, F. “Understanding liquid-jet atomization cascades via vortex dynamics”. *J. Fluid Mech.*, 843, 293–354, 2018 (cit. on pp. 5, 20, 166).
- [226] Zein, A., Hantke, M., and Warnecke, G. “Modeling phase transition for compressible two-phase flows applied to metastable liquids”. *J. Comput. Phys.*, 229.8, 2964–2998, 2010 (cit. on pp. 9, 24, 54, 100).
- [227] Zhang, J. “Acceleration of five-point red-black Gauss-Seidel in multigrid for Poisson equation”. *Appl. Math. Comput.*, 80.1, 73–93, 1996. URL: <http://www.sciencedirect.com/science/article/pii/0096300395002766> (cit. on pp. 170, 249).